Identification of Biomarkers Associated With the Combination of Immunotherapy and Anti-Angiogenic Drugs in the Treatment of Mesothelioma : Translational Analyses of the PEMBIB Clinical Trial Combining the Anti-PD1 Monoclonal Antibody Embrolizumab and the Anti-Angiogenic Tyrosine Kinase Inhibitor Nintedanib

François-Xavier Danlos

Thèse de doctorat

NNT : 2021UPASL075

université PARIS-SACLAY

Identification of biomarkers associated with the combination of immunotherapy and anti-angiogenic drugs in the treatment of mesothelioma.

Translational analyses of the PEMBIB clinical trial combining the anti-PD1 monoclonal antibody pembrolizumab and the anti-angiogenic tyrosine kinase inhibitor nintedanib.

Identification de biomarqueurs associés à la combinaison d'immunothérapie et d'anti-angiogéniques dans le traitement des mésothéliomes.

Analyses translationnelles de l'essai clinique PEMBIB combinant l'anticorps monoclonal anti-PD1 pembrolizumab et l'inhibiteur de tyrosine kinase anti-angiogénique nintedanib

Thèse de doctorat de l'université Paris-Saclay

École doctorale n° 582, Cancérologie : biologie – médecine – santé (CBMS)
Spécialité de doctorat : Sciences de la vie et de la santé
Unité de recherche : Université Paris-Saclay, Institut Gustave Roussy, Inserm, Immunologie anti-tumorale et immunothérapie des cancers, 94805, Villejuif, France.
Référent : Faculté de médecine

Thèse présentée et soutenue à Paris-Saclay, le 11/10/2021, par

François-Xavier DANLOS

Composition du Jury

Christophe MASSARD PU-PH, Université Paris Saclay	Président
Magali TERME MCU, Université de Paris	Rapporteur & Examinatrice
Christine MENETRIER-CAUX DR, Université de Lyon	Rapporteur & Examinatrice
Françoise GALATEAU-SALLE PU-PH, Université de Lyon	Examinatrice
Gérard ZALCMAN PU-PH, Université de Paris	Examinateur
Arnaud SCHERPEREEL PU-PH, Université de Lille	Examinateur
David PLANCHARD PH, Université Paris Saclay	Examinateur

Direction de la thèse

Aurélien MARABELLE PU-PH, Université Paris Saclay	Directeur de thèse

Aux bons souvenirs de ces années !

Remerciements

Je remercie sincèrement les **membres du Jury,** d'avoir accepté d'évaluer mes travaux et de participer à ma soutenance de thèse. C'est un grand honneur pour moi de pouvoir défendre mon travail devant eux. Leurs travaux ont éclairé et *challengé* beaucoup des observations que j'ai pu réaliser.

Je remercie très spécialement,

Aurélien, qui a su me recevoir, me faire confiance et m'accompagner ;

Laurence Zitvogel, qui m'a accueilli et soutenu dans son Unité de recherche ;

Christophe Massard ;

Jean-Charles Soria.

Je remercie chaleureusement toutes les personnes qui ont été présentes à mes côtés durant ces dernières années, extrêmement enrichissantes. Elles m'ont toutes beaucoup apporté, chacune à leurs manières, et sans effort je grandis de les avoir rencontré :

En premier lieu, l'**Equipe** du LRTI ! Merci, merci, merci ! Je vous remercierais tous personnellement.

Mes co-thésards les plus proches, AGG & JEF, qui m'ont ENORMEMENT appris.
Mathieu & Lambros !
Les U1015^{iens} d'hier et d'aujourd'hui: Lisa, Agathe, Marine, Imran, Gladys, Pierre, Eugénie, Nicolas, Carolina, Yacine, Camille, Cissé, Caroline, Nathalie, Marion, et tous ses autres passionné.es !!!
Les « filles » de l'ENS : Masha, Diane & Félicie.
Les « mecs » de la plateforme (peut-être un peu plus Yann !) et aussi Alexia !
Les collègues du BiGR : Bastien & Marine (Merci pour votre patience).
Celles de l'UGF ! Promis, j'ai réellement fait mon maximum pour être à l'heure.
Les pro de la métabolo : Claudia, Sylvère et Prof Kroemer.
Nathalie et la belle équipe du LIO.
Toute la team PREMIS +++
Miha, ma bro' (quel soutien !!!!!!!).
Jean-Marie, Ariane, Stéphane, Capucine et tous le DITEP: à très très vite !
Marion et Véronique : je suis content de savoir que vous n'êtes pas loin.
Mes références : Profs Benjamin Terrier, Olivier Lambotte et Xavier Mariette.
Vassili Soumelis & son équipe, qui m'ont transmis l'envie de persévérer.
Toutes les personnes qui ont fait grandir ce projet : Matthieu, Camille, Kevin, Aymeric, Andrei, Leonardo, Nicolas, Laetitia, Paul (!) et encore plus ceux que j'oublie.
Le département d'hémato de GR : vous m'avez permis des bouffées « cliniques » d'oxygènes !

Je remercie aussi, ici, mon comité de suivi : Eliane Piaggio, Gaëtane Nocturne & David Boutboul. Rudement efficace.

Un immense MERCI à ma famille, mon frère, mes parents, Sésé, Yéyé & Poapoa, mes amis, qui sont certainement un peu rassurés que mes 15 années d'études se terminent (non 😉 ?).

Mon cœur : Sonia & Auguste.

Table of content

Index of Figures

Index of Tables

Index of Supplementary Figures.

Index of Supplementary Tables

List of Abbreviations.

ASXL1 = Additional sex combs-like 1

AKT = protein kinases B

B = Biphasic

BAP1 = BRCA1 Associated Protein 1

BARD1 = BRCA1 Associated RING Domain 1

BET = Bromodomain and extraterminal

BRCA1 = Breast cancer type 1

CDKN2A = Cyclin Dependent Kinase Inhibitor 2A

C1D1 = Cycle 1 day 1

DCB = Durable clinical benefit

DC = Dendritic cells

DCR = Disease control rate

D-7 = day -7

E = Epithelioid

ECOG = Eastern Cooperative Oncology Group

EED = Embryonic ectoderm development

EZH2 = Enhancer of zeste homolog 2

ERK = Extracellular signal-regulated kinase

E2F = E2 Transcription Factor

FAT1 = FAT Atypical Cadherin 1

FDA = U.S. Food and Drugs Administration

FOXK1 = Forkhead Box K1

GPCR = G protein-coupled receptor

HCF1 = Host cell factor 1

H3K27me3 = tri-methylation of lysine 27 on histone H3

IHC = Immuno-Histo-chemistry

LATS1 = Large tumour suppressor 1

mAb = monoclonal antibody

MAPS = Mesothelioma Avastin Cisplatin Pemetrexed Study (NCT NCT00651456)

MCP1 = Monocyte Chemoattractant protein

MDC = Macrophage Derived Chemokine

MEK = Mitogen-activated protein kinase

MIP = Macrophage Inflammatory Protein.

MST1 = mammalian STE20-like protein kinase 1

mTOR = mechanistic target of rapamycin

NF2 = Neurofibromatosis type 2

Ninte. = nintedanib

OS = Overall survival

PARP = Poly ADP-ribose polymerase

PD = Progressive disease

PD(L)1 = Programmed Death Ligand 1

PI3K = Phosphoinositide 3-kinase

PR = Partial response

PRC2 = Polycomb Repressive Complex 2

RAF= Rapidly accelerated fibrosarcoma

RAS = Rat sarcoma virus

RB1 = Retinoblastoma protein

RTK = Receptor of tyrosine kinases

S = Sarcomatoid

SD = Stable disease

SOC = Standard of care

TAZ = Transcriptional co-activator with PDZ-binding motif

TEAD = Transcriptional enhancer factor

TGFR = Transforming growth factor receptor

TKI = Tyrosine kinase inhibitor.

TNF = Tumor Necrosis Factor.

Treg = regulatory T cells

UICC = International Union against Cancer

VEGFA: Vascular endothelial growth factor A

YAP = Yes associated protein

Synthèse.

L'essai clinique PEMBIB (NCT02856425) est un essai thérapeutique de phase 1 évaluant l'association d'un anticorps monoclonal anti-Programmed-Death 1 (PD-1) avec le nintedanib, un traitement anti-angiogénique inhibiteur de tyrosine kinases. L'objectif de ce travail de thèse était d'identifier des facteurs biologiques sanguins et tumoraux associés à la survenue d'une réponse antitumorale associée aux traitements par pembrolizumab et nintedanib, administrés à des patients atteints de cancer métastatique ou avancé dans cette étude.

Les patients inclus dans l'étude PEMBIB ont été traités les 7 premiers jours par une monothérapie de nintedanib, puis le traitement par pembrolizumab était administré par voie intra-veineuse toutes les 3 semaines. Les patients étudiés dans ce travail de thèse ont été inclus dans deux cohortes différentes de l'essai clinique. Les premiers patients ont été traités dans la cohorte d'escalade de dose, dédiée à la définition de la dose maximale toléré de nintedanib en association au pembrolizumab, utilisé à la dose unique de 200mg en perfusion intra-veineuse toutes les 3 semaines. La première posologie de nintedanib était de 150mg matin et soir, et le palier supérieur était de 200mg matin et soir. Au-delà, les patients ont été traités dans différentes cohortes, dites d'extension, conçues pour évaluer la tolérance et l'efficacité de la combinaison dans différentes indications. Les patients inclus dans la seconde cohorte analysée dans ce travail étaient atteints de mésothéliome pleural non résécable réfractaire à une chimiothérapie, associant un sel de platine et du pemetrexed. Ces patients n'avaient pas été antérieurement traités par une immunothérapie. Des prélèvements sanguins et tumoraux ont été prospectivement collectés pour la réalisation d'analyses ancillaires. Les prélèvements sanguins ont été réalisés avant le début de traitement par nintedanib (J-7), avant la première perfusion de pembrolizumab (C1J1), 8 jours après la première perfusion de pembrolizumab (C1J8) et avant les 2ème et 5ème cycle de traitement (C2J1 et C5J1). Des biopsies tumorales ont été réalisés pendant la période de *screening* (préalablement à l'administration des traitements) et avant le 2ème cycle de traitement.

12 patients ont été traités dans la cohorte d'escalade de dose. La dose maximale administrés de 200mg matin et soir de nintedanib a entrainé la survenue de plusieurs toxicités limitant la dose (essentiellement des toxicités hépatiques). La dose retenue pour les cohortes d'extensions a été de 150mg matin et soir en association au pembrolizumab. Des réponses antitumorales objectives ont été observés chez 3 patients, atteints d'un carcinome thymique, carcinome cervical et carcinome indifférencié du nasopharynx. Les deux patients atteints de mésothéliomes avancés dans cette cohorte ont présenté une progression de leur maladie cancéreuse, sans bénéfice aux traitements. L'analyse des prélèvements sanguins et tumoraux avant le début des traitements ont suggérés que les patients avec un bénéfice durable (absence de progression tumorale avant 6 mois de traitement) présentaient des taux plasmatiques de CXCL10,

CCL22 et Tie2 plus élevés que les patients n'en bénéficiant pas. Après l'initiation des traitements, les patients avec un bénéfice présentaient dans les biopsies réalisées avant la deuxième perfusion de pembrolizumab, un infiltrat immunitaire caractérisé par un ratio lymphocytaire T CD3+ / macrophage CD68+, une infiltration de lymphocyte T FOXP3+ et une expression de PDL-1 sur les cellules tumorales plus importantes que ceux ne bénéficiant pas du traitement.

30 patients ont été inclus dans la cohorte dédiés aux mésothéliomes pleuraux non résécables. Parmi ceux-ci, une patiente est décédée d'une toxicité liée à la combinaison thérapeutique, caractérisée par une atteinte cardiaque et des thromboses veineuses et artérielles. Considérant un bénéfice clinique durable par l'absence de survenue de progression tumorale avant 6 mois, 14 patients (46,6%) ont été considéré avec un bénéfice clinique durable. Parmi eux, 7/29 (24,1%) ont eu une réponse partielle antitumorale objective. Le phénotypage immunitaire des cellules sanguines par cytométrie de flux réalisé avant l'initiation des traitements a montré que les patients bénéficiant des traitements présentaient des proportions de lymphocytes T CD4 de type Th1 et de lymphocytes T CD8+ exprimant l'intégrines CD49a plus importantes que les patients ne bénéficiant pas des traitements. Considérant les taux plasmatiques de chémokines, il n'y avait pas de différence entre les patients considérant les taux de CXCL9, CXCL10 ou CXCL13, antérieurement associée à l'efficacité des anti-PD-1, et après la première perfusion de pembrolizumab, les concentrations plasmatiques de ces chémokines ainsi que celles de PD-1 et PD-L1 solubles ont augmentés significativement, de façon pharmacodynamique, chez tous les patients qu'ils aient bénéficié ou non des traitements. Au niveau intra-tumoral, les analyses de l'infiltration immunitaire par immunohistochimie et par déconvolution à partir de données de séquençage complet des ARN messagers (RNA-seq) n'ont pas montrés de différences entre les patients avec un bénéfice ou non aux traitements, considérant les lymphocytes T et notamment les lymphocytes T CD8+. En revanche, l'expression de PD-L1 évaluée en IHC sur les cellules tumorales était significativement plus élevée chez les patients avec un bénéfice durable. L'infiltration de cellules myéloïdes dendritiques estimée par déconvolution des données RNA-seq était significativement plus élevée chez les patients ayant un bénéfice clinique durable aux traitements. L'analyse des expressions différentielles de gènes issues des données RNA-seq des biopsies tumorales réalisées avant l'initiation des traitements montre que des voies oncogéniques (*E2F* et *cKIT*), la prolifération cellulaire (phase G2M du cycle cellulaire) et la différentiation épithélio-mésenchymateuse étaient amplifiées dans les tumeurs des patients sans bénéfice au traitement. A *contrario*, la transcription des gènes induits par les interférons gamma et de type 1 était diminuée chez ces mêmes patients. L'analyse des exomes tumoraux a permis d'identifier des délétions et des mutations récurrentes chez ces patients, notamment des gènes de *BAP1*, *EP300*, *NF2*, *SETD2*, *CDKN2A* ou encore *TP53*. Les patients avec un bénéfice

durable au traitement semblaient présenter moins de délétion homozygote de CDKN2A que les patients sans bénéfice ; ce qui pourrait être associé à l'augmentation d'expression des gènes transcrit par E2F et la diminution de ceux induits par les interférons de type 1. Une analyse protéique par fluorescence *in situ* par hybridation a permis d'étudier les délétions du segment 21 du bras court du chromosome 9 (9p21) ; responsable des délétions des gènes de *CDKN2A* et des interférons de type 1. Des délétions homozygotes de 9p21 ont été observés chez plusieurs patients (4/18 [22%]), mais uniquement chez ceux sans bénéfice au traitement. Par ailleurs, un score estimant la quantité globale d'altérations du nombres de copies de gènes à partir des données d'exomes tumoraux a montré que les patients sans bénéfice aux traitements en présentent significativement plus que les patients avec un bénéfice durable. Ces altérations étaient positivement corrélées aux taux plasmatiques d'IL6 et d'IL8 circulants et au taux de CCL2 tumoral soluble. Ces cytokines et chémokines étaient plus élevés chez les patients ne bénéficiant pas des traitements et associées à des proportions de polynucléaires neutrophiles et de monocytes inflammatoires circulants.

Ces analyses ont permis d'identifier des caractéristiques individuelles et tumorales associées à l'efficacité ou la résistance aux traitements administrés à des patients atteints de cancer et particulièrement de mésothéliomes pleuraux dans le cadre d'un essai de phase 1. Ces observations sont intéressantes parce qu'elles permettent de souligner des éléments importants associées à l'inefficacité des traitements. Cependant, le faible effectif de patients inclus dans ces études et le nombre limité d'échantillons analysés imposent d'interpréter ces résultats avec précautions: des travaux complémentaires de confirmation sont indispensables pour valider ou infirmer les résultats observés.

Background

Immune checkpoint blockade is undergoing extensive investigation in oncology, and has become a new standard of care in many cancer types, in many clinical situations (1,2). Unlike standard chemotherapy or targeted agents, which act mainly on tumor cells, immune checkpoint blockade act by restoring the immune system's ability to eradicate tumors (3). Results of clinical trials evaluating anti-PD-(L)1 monotherapies have shown meaningful and to promote durable tumor response rates, with overall survival benefits compared to conventional treatments. Remarkable activity has been demonstrated in Renal Cell Carcinoma (RCC), Non-Small Cell Lung Cancer (NSCLC), Head & Neck Squamous Cell Carcinoma (HNSCC), Gastric Cancer (GC), Urothelial Cancer (UC), Triple Negative Breast Cancer (TNBC), non-Hodgkin and Hodgkin Lymphoma (4–11). Thus, trials in many tumor types have validated the relevancy of blocking the PD-1 / PD-L1 pathway in order to unleash specific anti-tumoral $CD8^+$ T cells to eliminate cancer cells and control metastatic disease (12–14). However, a majority of patients still do not respond to immune checkpoint blockade monotherapy. Clinical and fundamental research is required to develop new immunotherapeutic strategies and overcome such primary resistance to immunotherapies in order to improve cancer patients survival (15–18).

One main approach to overcome primary resistance to immune checkpoint blockade should be to promote a normalization of angiogenesis in the tumor and limit the pleiotropic pro-tumoral effects of angiogenic factors (19). Angiogenesis is involved in tumor growth and in the development of metastases (20). Tumors induce blood vessel growth by secreting many angiogenic factors. Vascular Endothelial Growth Factor (VEGF) and its high affinity receptor VEGFR-2 are crucial for the formation of new tumor vessels. In addition, there is preclinical evidence that fibroblast growth factor (FGF) and platelet-derived growth factor (PDGF) and their associated receptors substantially contribute to such tumor angiogenesis (21,22). The VEGF – VEGFR-2 axis, besides promoting angiogenesis, may also be involved in stimulating growth of tumor cells themselves via an autocrine loop (23,24). This is suggested by *in vitro* data and immunohistochemical studies in NSCLC, ovarian carcinoma (OC), colorectal cancer, and also mesothelioma (20). Therefore, suppression of neo angiogenesis via inhibition of the VEGF / VEGFR pathway has become a useful strategy for the treatment of solid cancers (25).

A substantial number of clinical trials with different VEGF and VEGFR inhibitors, in various type of cancers, have demonstrated that this approach can convey clinical benefit, as monotherapy in RCC and HCC as well as in combination therapy with standard chemotherapeutic drugs in NSCLC, CRC, Ovarian Cancer (26–30).

Unresectable pleural mesothelioma is a rare cancer evolved to pleural leaflets, primary induced by asbestos exposure and for which immune checkpoint blockade and anti-angiogenics drugs, in different clinical settings, have shown anti-tumoral efficacy. In this thesis, I will present the biomarkers identified to be associated with the efficacy or resistance to the association of pembrolizumab (an anti-PD-1 monoclonal antibodies) with nintedanib (an anti-angiogenic tyrosine kinase inhibitor); first in an escalation cohort of patients with several cancer type, then in an expansion cohort dedicated to patients with pleural unresectable mesothelioma.

Malignant Mesothelioma, a disease with angiogenesis and immune dysregulation

Malignant Mesothelioma pathophysiology

Malignant mesotheliomas are infrequent and severe cancers arising from mesothelial cells (31). Mesotheliomas have been mainly associated to the environmental and professional exposure to asbestos (32). Our current understanding of the pathophysiology of the disease is that non-degradable asbestos mineral fibers are deposited into mesothelial cells and phagocyted by macrophages, inducing a chronic inflammation *in situ* which could led to the development of malignant mesotheliomas after a long period of clinical latency (33–35). More specifically, mesothelial cells exposed to asbestos undergo an oxidative stress with the generation of reactive oxygen species (ROS) which can lead to DNA mutagenesis and chromosomal damage (33). Just like a damage associated molecular pattern (DAMP) molecule, asbestos fibers can stimulate the NOD-like receptor family pyrin domain containing 3 (NLRP3, or Nalp3) which induces the production of pro-inflammatory cytokines IL1β, IL18 and macrophages recruiting chemokines such as C-C chemokine ligand 2 (CCL2) (36–38). The necrosis of mesothelial cells induced by asbestos fibers leads to the release of high-mobility group box 1 protein (HMGB1) which activates macrophages and stimulates their production of tumor necrosis factor (TNF) (39). Those pro-inflammatory cytokines together with the accumulation of DNA damages contribute to the mesothelial cells transformation and their increased survival, leading to an oncogenesis process (40–43).

Malignant Mesothelioma molecular subtypes

Malignant Mesotheliomas have been classified in three major histologic subtypes with increasing aggressiveness: epithelioid, biphasic and sarcomatoid (median survival of 9-12 months for the first two types and 4 months for the sarcomatoid type) (44,45). International guidelines for the classification of malignant mesotheliomas have recently evolved, integrating new molecular data characterizing mesothelioma cells and taking into account the tumor microenvironment

(46,47). Routine assessments of the loss of BRCA-1 Associated Protein-1 (BAP1), of the homozygous loss of cyclin dependent kinase inhibitor 2A (CDKN2A), and the expression of PD-L1 on tumor cells, have been recommended for clinical practices in several situations (48). The histological type, architectural patterns, cellular and nuclear atypia and the presence of necrosis could also be monitored as they have been shown to be prognostic for the survival of patients with pleural and peritoneal malignant mesotheliomas (49–51).

Malignant Mesothelioma angiogenesis

Malignant mesotheliomas are also characterized by a sustained hypoxia and neo-angiogenesis in their microenvironment. Higher angiogenesis and hypoxia, assessed by micro vessel density and tumor necrosis have been shown to be prognostic for MM patients survival (52–54). There are close interactions between inflammation and angiogenesis, notably mediated by mesothelial cells and macrophages through the production of cytokines and pro-angiogenic factors (55–57). Soluble pro-angiogenic factors such as vascular endothelial growth factors (VEGF)-A, VEGF-C, HIF1α, transforming growth factor (TGF)-β or platelet derived growth factors (PDGF) have been shown to be highly expressed and produced in the mesothelial microenvironment, enhancing the tumor progression through direct and indirect effects (58–62). Besides to pro-angiogenic growth factors, mesothelial cells can take advantage directly from fibroblast growth factors (FGF) or indirectly from tumor-associated fibroblasts which promote cancer cells survival and spreading by epithelial to mesenchymal transition (63–65).

Malignant Mesothelioma immune microenvironment

Human mesothelioma are inflammatory tumors highly infiltrated by T lymphocytes, regulatory T cells and macrophages and less by dendritic cells or B cells (66). Higher PD-L1 expression on tumor cells, higher infiltration by $CD8^+$ T lymphocytes and macrophages were observed in sarcomatoid and biphasic tumors and associated with resistance to platinum-based chemotherapy and shorter overall survival (67–70). A study highlighted that tumors with expression of PD-L1 and sarcomatoid/biphasic tumors presented with higher immune infiltration, and higher infiltration by $CD3^+$ T cells (71). Among $CD4^+$ T cells, $FOXP3^+$ regulatory cells and $PD1^+$ $CD4^+$ T cells were higher in patients with $PDL1^+$ tumors cells, but was associated to lower production of interferon-gamma (IFNγ) by $CD8^+$ T cells and worse prognostic (71,72). Genome wide copy number analyses from MM tumor samples highlighted that in epithelioid histological subtype, higher rate of genomic alteration was associated with lower overall survival but did not correlate with PD-L1 expression, which suggested that tumor cells developed different evasion mechanisms (73).

Over the last decades, few therapeutic innovations have significantly benefited to the treatment and outcome of MMs (**Figure 1**). The advent of immune checkpoint blockade therapy in oncology has recently also revolutionized the standard of care in mesothelioma (1). Indeed, in a randomized phase 3 clinical trial, the combination of anti PD-1 (nivolumab) and anti-CTLA-4 (ipilimumab) monoclonal antibodies improved the median overall survival by 4 months compared to conventional platinum-based chemotherapy with pemetrexed in patients with untreated unresectable pleural mesothelioma (74). Interestingly, the nivolumab + ipilimumab combination immunotherapy generated a similar objective response rate than chemotherapy (n=120/303, 40%; 95% confidence interval [IC] 34-45 and n=129/302, 43%; 95% CI 37.1-45.4, respectively) (74). However, only immune checkpoint blockade therapy obtained complete responses in 5/303 (2%) patients and showed durable remissions with a 2-year duration of response rate of 32% (95% CI 23-41) compared to 8% (95% CI 3-15) with chemotherapy. Overall, those results demonstrated that immune modulation by targeting T-cell checkpoints was superior to conventional cytotoxic chemotherapies for untreated pleural mesothelioma (3).

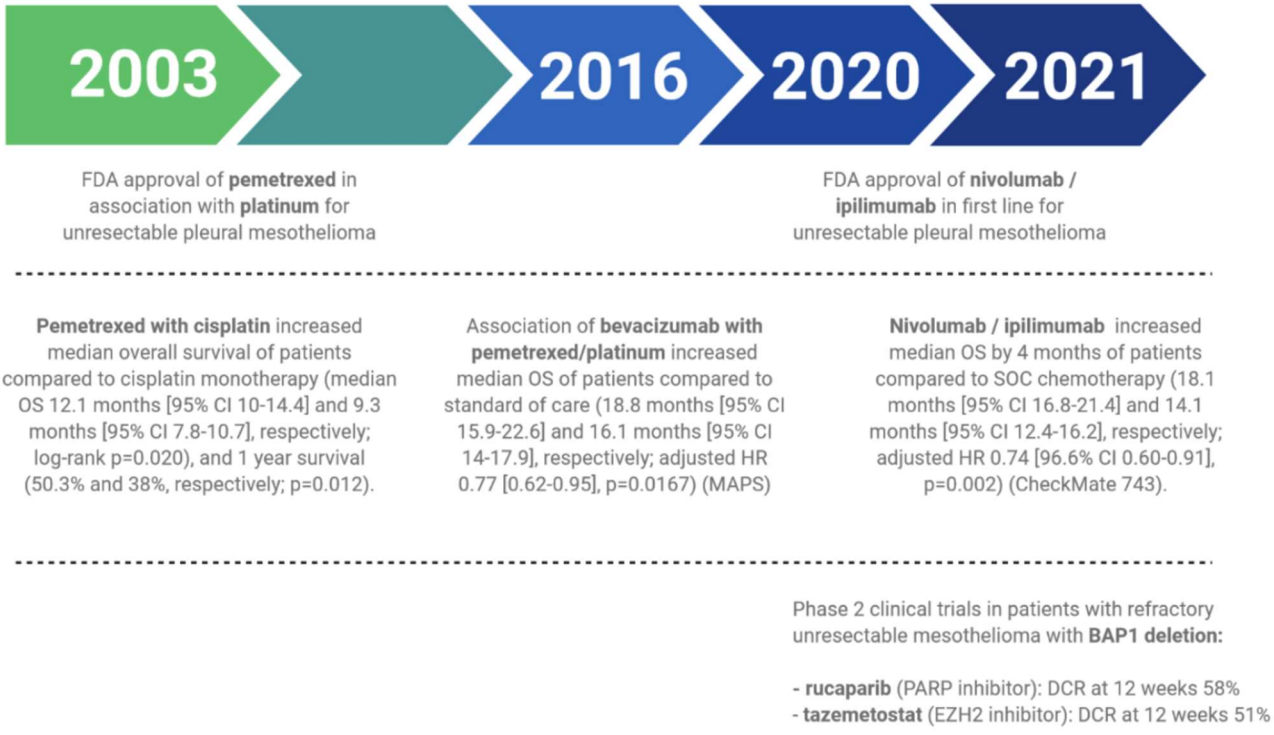

FIGURE 1. KEY STAGES OF SUCCESSFUL DRUG DEVELOPMENT FOR PATIENTS WITH UNRESECTABLE MALIGNANT PLEURAL MESOTHELIOMA.

THREE PHASE 3 CLINICAL TRIALS BROUGHT IMPROVEMENT OF PATIENT'S OVERALL SURVIVAL IN LAST DECADES **(74–76)**.

However, the value of immune checkpoint blockade for patients with unresectable pleural MM who are refractory to platinum-based chemotherapy with pemetrexed has been less successful. Although superior in terms of ORR (22% for pembrolizumab vs 6% for chemotherapy by blinded independent radiological review), anti PD-1 monotherapy could not increase OS and neither progression free survival (PFS) compared to single-agent chemotherapy in a randomized phase 3 clinical trial (77). Interestingly, open-label phase 2 clinical trials suggested that PD-1/PD-L1 blockade monotherapy would be less efficient than combination with anti CTLA-4 monoclonal antibody (78–82). The MAPS2 trial, a non-comparative randomized phase 2 trial for patients with advanced pleural MM refractory to pemetrexed and platinum-based chemotherapy illustrated that disease control rate at 12 weeks tended to be higher with combination than monotherapy (27/54 Pts - 50%; 95% IC [37-63] and 24/54 Pts - 44%; 95% IC [31-58], respectively) (83). Moreover, tumor hyper progression phenomena occurred in 6/59 patients (10%) treated with nivolumab and 2/55 patients (4%) treated with nivolumab and ipilimumab (83).

The FDA has now approved the nivolumab + ipilimumab combination as the standard of care in first line for the treatment of unresectable pleural MM. With this approval in first line and the disappointing results obtained by anti-PD1 monotherapies in second line for platinum-based chemotherapy refractory diseases, there are limited options for patients relapsing or refractory to either checkpoint blockade of chemotherapies. Therefore, novel therapeutic strategies are eagerly needed for patients with MM in situations of primary or secondary resistance to immune checkpoint blockade. Several ongoing clinical trials are evaluating therapeutics combination with immune checkpoint blockade but only few allowed previous treatment by anti PD-1 or anti CTLA-4 monoclonal antibodies (**Table 1**).

	Treatment(s)	Phase	Type of treatment	Post-ICB	NCT
Chemotherapy with ICB	PCT + atezolizumab +/- bevacizumab	3	First line	N/A	NCT03762018
	PCT with durvalumab	3	First Line	N/A	NCT04334759
	Gemcitabine with atezolizumab	2	_	Allowed	NCT04480372
Anti-angiogenic drug with ICB	Ramucirumab with nivolumab	2	mAb anti VEGFR2	Excluded	NCT04287829
	Bevacizumab with atezolizumab	2	mAb anti VEGF-A	N/S	NCT03654833
	Lenvatinib with pembrolizumab	2	Tyrosine kinase inhibitor	Excluded	NCT03502746
	Nintedanib with pembrolizumab	1	Tyrosine kinase inhibitor	Excluded	NCT02856425
Targeted therapy with ICB	Niraparib with dostarlimab	2	PARP inhibitor	Allowed	NCT04940637
	Niraparib with dostarlimab	2	PARP inhibitor	N/S	NCT03654833
	Bemcentinib with pembrolizumab	2	AXL inhibitor	N/S	NCT03654833
	Defactinib with pembrolizumab	½	FAK inhibitor	Excluded	NCT02758587
Anti mesothelin therapy with ICB	LMB-100 + ipilimumab	1	Immunotoxin anti mesothelin	Allowed	NCT04840615
	Anetumab ADC + pembrolizumab	½	ADC anti mesothelin	Excluded	NCT03126630
	iCasp9M28z T-cell + pembrolizumab	½	Autologous T-cell antimesothelin	N/S	NCT02414269
	CRS-207 with pembrolizumab	2	Mesothelin L. monocytogenes	Excluded	NCT03175172
Immune stimula-tory drugs with ICB	THOR-707 with pembrolizumab	2	IL-2 PEGylated	Allowed	NCT04914897
	SO-C101 with pembrolizumab	1	IL-15 superagonist RLI	Allowed	NCT04234113
	DC with pembrolizumab	1	Autologous DC + IL-2	Excluded	NCT03546426
	Galinpepimut-S with nivolumab	1	Targeted Cancer Vaccine	Excluded	NCT04040231
	UV1 with nivolumab + ipilimumab	2	UV1 vaccine + IL-2	Excluded	NCT04300244
	MTG201 with nivolumab	2	Adenovirus	Excluded	NCT04013334
	Naptumomab ADC with durvalumab	1	Fab anti 5T4 x SEA/E-120	Allowed	NCT03983954
ICB Combinations	NGM707 with pembrolizumab	½	Antibody anti ILT2/ILT4	Allowed	NCT04913337
	MK-4830 with pembrolizumab	1	Antibody anti ILT4	Allowed	NCT03564691
	Sym024 with Sym021 (anti PD-1)	1	Antibody anti CD73	Excluded	NCT04672434
	XmAb 20717	1	bispecific Ab aPD-1 x aCTLA-4	Excluded	NCT03517488

TABLE 1. ONGOING CLINICAL TRIALS WITH IMMUNE CHECKPOINT BLOCKADE (ICB) COMBINATION THERAPIES FOR MALIGNANT MESOTHELIOMA.

Interestingly, in the above mentioned randomized phase 3 trial of first line ipilimumab + nivolumab in MM, the therapeutic benefit of immune checkpoint blockade was higher in patients with sarcomatoid/biphasic MM compared to epithelioid MM, and in diseases which expressed more than 1% of PD-L1 on tumor cells (74). Those results highlight the fact that a better understanding of the histological, molecular and microenvironment of MMs should determine the features associated with resistance to immunotherapy. Genomic, transcriptomic, and epigenetic characterization of MM in the last decades brought important knowledge on MM physiopathology (**Figure 2**).

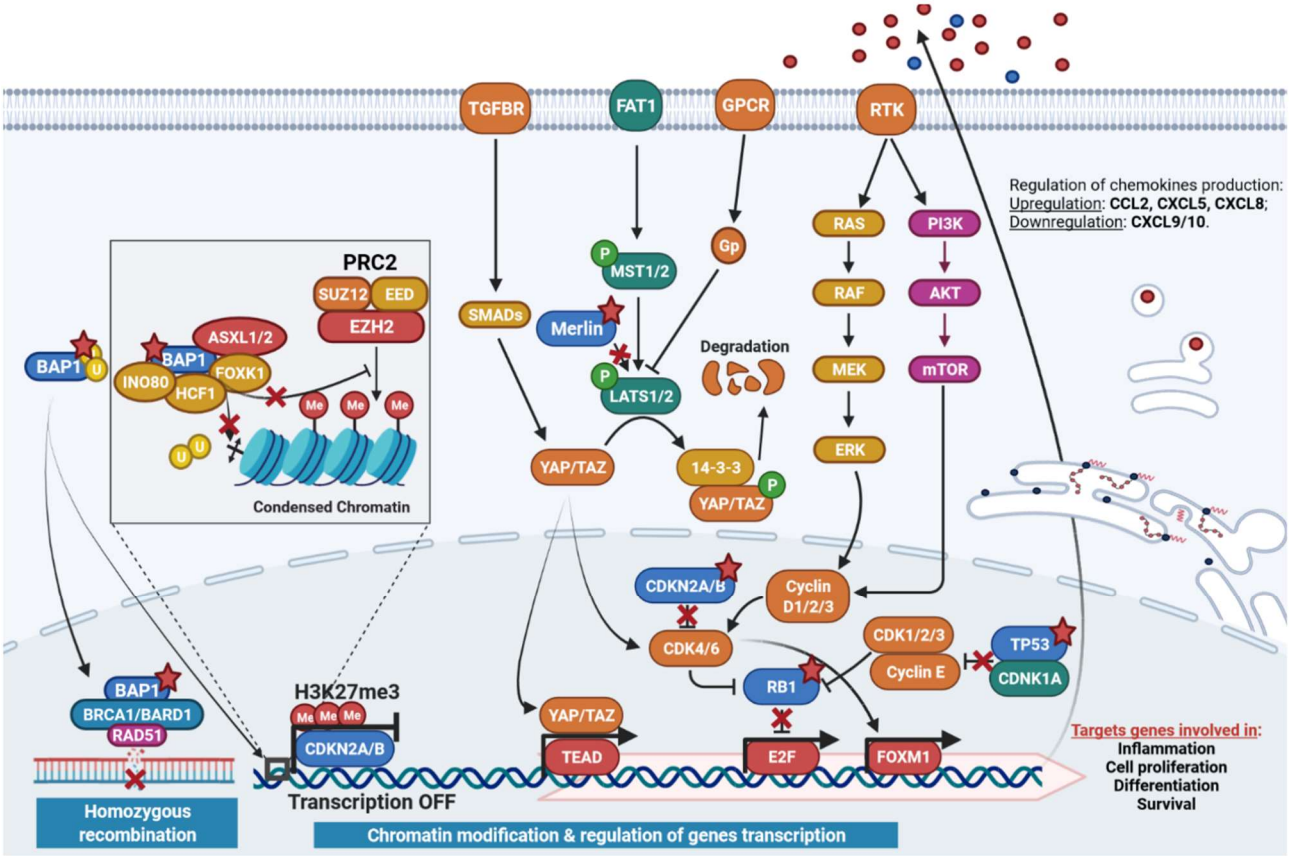

FIGURE 2. MAIN MOLECULAR PATHWAYS AND ALTERATIONS INVOLVED IN MALIGNANT MESOTHELIOMA PATHOPHYSIOLOGY.

RED STARS: PRINCIPAL GENES INVOLVED BY MUTATIONS, DELETION OR EPIGENETIC SILENCING IN MESOTHELIOMA.

Cytogenetic analyses have shown that MM are characterized by frequent deletions of chromosomal segments, such as 3p, 9p and 22q or present with chromosomal monosomies, leading to the loss of several tumor suppressor genes (84–86). The most common cytogenetic abnormality in MM is the homozygous deletion of 9p21 which leads to complete loss of *CDKN2A* gene (87,88). The CDKN2A protein is a powerful inhibitor of the formation of active cyclin D / cyclin-dependent kinases (CDK) 4 and 6 (89,90). *CDKN2A* deletion therefore leads to a strong inhibition of the retinoblastoma protein (RB1) by CDK4/6 proteins, and an upregulation of the transcription of genes that are targeted by E2 factors (E2F)

(Figure 2). Loss of regulation by CDKN2A leads to chronic activation of the CDK4/6-E2F pathway by the mitogen activated protein kinase (MAPK) signaling pathway, secondary to the multiple stimuli from the tumor microenvironment (VEGF, PDGF, FGF, TNF or IL1). Over stimulation of transcription of the E2F target genes leads to cell proliferation (transition of phase G1 to S in cellular cycle, then S to G2 by FOXM1 target transcription) and resistance to apoptosis (**Figure 11**).

Neurofibromin 2 (NF2) is a regulator of the Hippo pathway, an evolutionarily conserved signaling pathway which regulates organ size and maintains tissue homeostasis (91). *NF2* is another tumor suppressor gene frequently lost by mutations or deletion of the chromosomic region 22q (84,92). The *NF2* gene encodes for a protein called Merlin, which controls the "Hippo" pathway. This pathway includes the main cytosolic serine/threonine kinases, mammalian STE20-like protein kinase 1 (MST1/STK4) and MST2/STK3, and the large tumour suppressor 1 (LATS1) and LATS2, which are associated with adaptor proteins (93). These proteins limit the nuclear translocation of the oncoproteins Yes-associated protein (YAP) by phosphorylation and the transcriptional activities of the transcriptional co-activator with PDZ-binding motif (TAZ) (94). Merlin regulates the Hippo pathway through interactions with LATS1/2 and its deletion leads to cell stemness properties, survival and proliferation; notably by interactions between YAP/TAZ, CDK4/RB1 and TP53 (95,96). Signals received from the tumor micro-environment amplify this pathway through activation of the MAPK and TGF/SMADs pathways and a loss of cellular mechano-transduction induced by epithelial to mesenchymal transition (97).

BAP1 loss is another main genomic alteration associated with MM development. To note, germline mutation of *BAP1* have been identified as a hereditary syndrome responsible for familial MM, uveal melanoma and renal carcinoma (98,99). BAP1 is a ubiquitin carboxy-terminal hydrolase, promoting deubiquitylation of itself and other enzymes, and has important function to prevent DNA damages, genomic instability and also regulate gene transcription to control cell survival and proliferation (100,101). *BAP1* loss can be obtained by deletion of 3p21 region or can be inactivated by somatic non-synonymous mutations and post-translational deregulation (86,102,103). Its loss can lead to an accumulation of DNA double strand breaks by destabilization of its binding with BARD1 (102,104). BAP1 participates to the preservation of genome stability, to DNA synthesis and to genes transcription by interaction and deubiquitylation of chromatin remodeling complexes (105–107). BAP1 also interacts with ASXL1 to form a complex which leads to deubiquitinate the histone H2A lysine 119, and to inhibit the polycomb repressive complexe (PRC) 1/2 activity (108). Loss of BAP1 in mice is associated with elevated enhancer of zeste 2 polycomb respressive complex 2 subunit (EZH2), increase of trimethylated histone H3 lysine 27 (H3K27me3) and repression of PRC2 targets transcription (109). Interestingly, CDKN2A gene transcription was shown to be abolished by H3K27 methylation and EZH2 activity and, as a negative retro control, EZH2 activity is promoted by RB1/E2F pathway (110,111).

Whole exome sequencing analyses of MM tumor samples have identified other mutations, particularly in *TP53*, *SETD2*, *SETDB1* or *DDX3X* which are also implicated in cellular cycle, histone methylation and alternative splicing of RNA (103,112,113). Characterization of human MM tumor samples by transcriptomic analyses have shown that the deletions and mutations previously described are associated with dysregulation of concordant pathways, such as Hippo, histone methylation and p53 ones (103) and are correlated with specific immune infiltrates in the tumor microenvironment and impact MM survival (114).

This knowledge on pathophysiological mechanisms implicated in malignant mesothelioma development suggested that immune checkpoint blockade and anti-angiogenic drugs could be an efficient therapeutic strategy to treat patients with these diseases.

Neo-angiogenesis and hypoxia are hallmarks of cancer and targets of distinct therapeutic interventions.

Neo-angiogenesis as a hallmark of cancers.

Neo-angiogenesis and abnormal vasculature development in the tumor microenvironment have been identified since decades as a major hallmark of cancer development (115). Blood vessels in tumors present with an aberrant morphology, characterized by excessive branching, abundant and abnormal ends, discontinuous endothelial cells lining, and defective basement membrane and pericyte coverage (116,117). These features are associated with impaired vascular maturation, poor vessel functionality and incoherent tumor perfusion (118). During tumor progression, angiogenesis is almost always activated leading to persistent sprouting of new vessels that help to sustain expansion of tumor growths (119). Angiogenesis is promoted by signaling proteins that bind to stimulatory or inhibitory cell surface receptors displayed by vascular endothelial cells, which are induced by hypoxia in tumor microenvironment (120). The well-known angiogenesis inducer is vascular endothelial growth factor-A (VEGF-A) (121). The *VEGF-A* gene encodes ligands that are involved in orchestrating new blood vessel growth during embryonic and postnatal development, and then in homeostatic survival of endothelial cells, as well as in physiological and pathological situations in the adult (122). VEGF signals through three receptors of tyrosine kinases (VEGFR-1–3), which are regulated at multiple levels. And VEGF gene expression can by upregulated both by hypoxia and by oncogenic stress signaling (123).

Pro-angiogenic factors can be also produced in the tumor microenvironment by immune cells.

Cancer cells are an important source of VEGF-A and other pro-angiogenic mediators, but immune cells recruited in the tumor microenvironment, such as macrophages, polymorphonuclear cells, NK and B cells, can also be a source of pro-angiogenic factors. Particularly, tumor associated macrophages (TAM) secrete growth factors and inflammatory cytokines that support angiogenesis by promoting endothelial cells survival, activation and proliferation (124). TAMs are an important source of VEGFA in tumors (125). TAM-derived VEGF-A also enhances vascular permeability, thereby facilitating cancer cell intravasation and metastasis (126). Pro-angiogenic factors produced by TAMs include also Placental growth factor (PlGF) and VEGF-C, tumor necrosis factor (TNF), interleukin-1β, (IL-1β), IL-6, CXC-chemokine ligand 8 (CXCL8; also known as IL-8) and fibroblast growth factor 2 (FGF2) (127). A recent subpopulation of circulating blood monocytes can be distinguished from other circulating monocytes by their expression of the angiopoietin receptor TIE2 (also known as TEK) (128). Tie2 expressing monocytes (TEM) have been identified in the peripheral blood of

both humans and mice and are distinct from the previously described circulating endothelial cells or endothelial progenitors' cells that also express TIE2 (129). Macrophages expressing Tie2 are found in human tumors and have also been identified in mice (130). Unlike peripheral blood monocytes, TEM do not express chemokine (C-C motif) receptor 2 (CCR2) and are unlikely to respond to CCL2, suggesting that TEM are recruited to tumors by a mechanism different to that of monocytes that are destined to differentiate into TAM (128). The monocyte attracting chemokines CCL3, CCL5 and CCL8 are also upregulated in tumors, and these could cause recruitment of TEM through chemokine receptors CCR1 or CCR5. However, TEM could also be recruited by the TIE2 ligand, angiopoietin 2, a cytokine abundantly expressed by both hypoxic tumor cells and endothelial cells in tumor blood vessels (131). Angiopoietin 2 may not only help to recruit TEM into tumors but also regulate their release of angiogenesis-modulating, inflammatory and immunosuppressive cytokines (132,133).

Angiogenic factors and hypoxia lead to immunosuppression in the tumor area and inhibit the anti-tumor response.

Circulating immune cells have to interact with endothelial cells from tumor blood vessels in order to infiltrate tumors and develop an efficient anti-tumor immune response (134,135). Leukocytes can adhere to the endothelium and transmigrate across the vessel wall thanks to specific interactions between membrane molecules (136). Angiogenic molecules present in the tumor microenvironment, such as VEGF-A, can control the trafficking of immune cells to the tumor by altering the expression of such adhesion molecules, including the integrin ligands intercellular adhesion molecule 1 (ICAM1) and the vascular cell adhesion protein 1 (VCAM1), on endothelial cells and immune cells (137). Endothelial cells in tumors can also express the immune-checkpoint protein programmed cell death 1 ligand 1 (PD-L1), which binds to PD-1 expressed on T cells and thereby suppresses their anticancer activity (138). In addition, tumors can secrete soluble factors, such as chemokines (CCL2, CCL28, CXCL8 and CXCL12), angiopoietin 2, VEGF, PlGF, and adenosine, which promote the recruitment of immunosuppressive cells (cf **review 1 in annexes** and (139)). These cells include immature dendritic cells (DC), regulatory T cells (Treg), myeloid-derived suppressor cells (MDSCs), and TAM with pro-tumor immunosuppressive phenotypes (140). In turn, through the production of VEGF, angiopoietin 2, IL-10, and TGFβ, these leukocytes collaborate with tumor cells and endothelial cells to promote angiogenesis and both local and systemic immunosuppression (141).

VEGF is also well known to induce immunosuppression (142). VEGF inhibits DC maturation and antigen presentation, limits T cell activation and anti-tumor immune responses (143,144). VEGF directly inhibits $CD8^+$ T cells trafficking, proliferation, and effector functions (145). Moreover, angiopoietin 2 has been shown to promote immunosuppression in

tumors. Angiopoietin 2 leads to the upregulation of adhesion molecules by endothelial cells, increases tumor infiltration by MDSCs or TEM and suppress anti-tumor function of such monocytes derived cells in the tumor microenvironment (132,146).

VEGF-A promotes immunosuppressive function of Antigen Presenting Cells (APC)

Mature DC are key elements of the anti-tumor immune response as they can present tumor-specific antigens on class 1 major histocompatibility complex (MHC) molecules and trigger efficiently $CD8^+$ T-cells cytotoxic immune responses (147). However most tumor infiltrative DCs are immature and impaired in their functions; they promote tumor tolerance rather than tumor immunity (148). VEGF-A affects DC maturation *in vitro* (143,149). A study revealed that VEGF-A can alter the differentiation of monocytes into DC (150). This effect was reversed by an anti-VEGF-A monoclonal antibody (bevacizumab) or by sorafenib, an anti-angiogenic molecule targeting different receptors (VEGFR, PDGFR, and RAF kinases) (150). Accordingly, the proportion of circulating immature DCs in patients with cancer is correlated with the stage of the disease and the level of circulating VEGF-A, and is partially corrected by surgery or anti-VEGF treatment (148,151).

VEGF-A promotes the recruitment and activation of regulatory T-cells (Tregs)

VEGF-A favors the immature phenotype of tumor associated myeloid cells or APC which in turn sustain the development of Tregs, key actors of the tumor immune tolerance. This phenomenon is induced via TGF-β either directly or indirectly (152,153). Moreover, it has been demonstrated that VEGF-A could also directly induce Treg proliferation in patients with cancers in a VEGFR-2 dependent manner (154–156). Higher infiltration of colorectal cancer microenvironment by $VEGFR\text{-}2^+$ Tregs has been correlated with a worst outcome after surgical resection of localized colorectal cancer (157). Bevacizumab, as well as sunitinib, an anti-angiogenic tyrosine kinase inhibitor, were shown to decrease *in vivo* in a murine model the regulatory T cells infiltration of tumors , mostly mediated by an inhibition of Treg proliferation (155). A similar decrease of circulating Treg proliferation was induced by bevacizumab in patients treated for metastatic colorectal carcinoma in combination with 5-fluorouracil and oxaliplatin (FOLFOX) (155).

VEGF-A limits the functions of anti-tumor cytotoxic $CD8^+$ T-cells.

Intra-tumoral hypoxia induces VEGF-A, which promotes intrinsic abilities of tumor cells to resist to cytotoxic T lymphocyte mediated lysis (158). VEGF-A, together with immunosuppressive cytokines, can also induce the expression of Fas-ligand on endothelial cells surface, which induces $CD8^+$ T cells apoptosis and promotes Treg infiltration into tumors (159). Indeed, anti-angiogenic drugs (and notably bevacizumab) have been reported to increase T cell trafficking into the tu-

mor bed. Specifically, bevacizumab has been shown to affect DC priming of T cells through the stimulation of DC maturation and inhibition of myeloid derived suppressor cells (160). Moreover, VEGF-A had direct effects on human VEGFR-2$^+$ CD8$^+$ T cells through NFAT and TOX transcriptional activities and induces T cell exhaustion, with expression of checkpoint molecules such as PD-1, T-cell immunoglobulin mucin-3 (Tim3) or Lymphocyte Activation Gene 3 (LAG3) (145,161). Proliferation of CD8$^+$ T cells after *in vitro* stimulation is limited by VEGF-A through VEGFR-2 expression (162,163).

Development of anti-angiogenic drugs in medical oncology.

Treatments blocking angiogenic pathways in cancers are powerful drugs theoretically acting directly on tumor cells growth and indirectly through inhibition of neo-angiogenesis and increasing immune cells infiltration in the tumor microenvironment. Those treatments have been developed to prevent the interactions between extra-cellular soluble or membranous VEGF with their receptors VEGFR-1/2 and to limit the expression of VEGF/VEGFR intracellular pathways (164). Several agents, including bevacizumab, aflibercept, and ramucirumab, that target the VEGF/VEGFR interactions have been developed and are now approved across several indications. Tyrosine kinase inhibitors targeting the VEGF/VEGFR pathways are numerous and present the particularity to not be exclusively specific of this pathway, and to inhibit other intracellular pathways, such as VEGFR-3, PDGFR-1, Kit, Flt3 and less frequently FGFR, Tie2 or RAF. Although they all aim at inhibiting the angiogenesis, those drugs are not strictly equivalent as described below.

Bevacizumab

Bevacizumab is a humanized monoclonal antibody that targets VEGF-A to prevent its interaction with VEGFR-1 and -2. It was the first targeted antiangiogenic approved for use in oncology (165). Currently approved as combination therapy for first- and second-line treatment of metastatic colorectal cancer (mCRC) and metastatic renal cell carcinoma (mRCC) and for first-line therapy of unresectable, locally advanced, recurrent, or metastatic non-small cell lung cancer (NSCLC). Although an important advance in treatment, the monotherapy of bevacizumab provides only a modest survival benefit, with inconsistent effects in different tumor types. Responses to bevacizumab are often transient, and patients could experience disease progression as an adaptive response to ongoing therapy or following treatment withdrawal (166,167). Early studies with bevacizumab across a variety of cancer types have established a set of adverse events associated with anti-angiogenic treatments, with the most documented toxicity being hypertension (168). The most common adverse events of bevacizumab are epistaxis, headaches, hypertension and proteinuria (169).

Aflibercept

Aflibercept is a fusion protein that consists of VEGF-binding portions from the extracellular domains of human VEGFR-1 and -2 fused to the Fc portion of human immunoglobulin G1 (IgG1) (170). Aflibercept functions as a decoy receptor by neutralizing the available VEGF-A and -B and PlGF and making the ligands unavailable to bind and activate VEGFRs. The ability of aflibercept to bind multiple VEGF ligands should provide a different blockade of angiogenesis compared to bevacizumab. Indicated for patients with mCRC that is resistant to or that has progressed following an oxaliplatin-containing regimen, the approval of aflibercept was based on findings from a phase III trial that when combined with folinic acid, fluorouracil, and irinotecan it significantly improved OS relative to control arm (171). Adverse events of aflibercept were very similar to those seen with bevacizumab.

Ramucirumab

Ramucirumab is a fully humanized IgG1 monoclonal antibody targeting the extracellular domain of VEGFR-2 (172). Ramucirumab had been evaluated as monotherapy and in combination in previously treated patients with advanced gastric cancer, NSCLC and breast cancer (173–175). Furthermore, ramucirumab was well tolerated, with most adverse events occurring at a similar frequency in the ramucirumab and placebo arms.

Tyrosine kinases inhibitors.

Tyrosine kinases exert their functions by transducing extracellular signals into the cells and play a key role in the intra-cellular homeostasis (176). Receptors of tyrosine kinases have an extracellular domain which can bind specific ligands, a single trans-membrane helix, and an intracellular region which contains a protein tyrosine kinase domain (177). The intracellular domain, also called kinase domain, presents with a N-terminal lobe, an adenosine triphosphate (ATP) binding cleft and a C-terminal lobe. Ligands binding to the extracellular domain induces dimerization and allows auto-phosphorylation of the intracellular domains and activation of the receptor's tyrosine kinase (177). Receptors of tyro-sine kinases catalyze the transfer of the phosphates of ATP to the hydroxyl group of tyrosine residues on target pro-teins (178). VEGF, FGF, PDGF, EGF or insulins receptors are part of the tyrosine kinase receptors family.

VEGF-A mediates its effects by binding to its two high-affinity receptors: VEGFR-1 and VEGFR-2. There are at least four members in the PDGF family (PDGF-A, PDGF-B, PDGF-C, and PDGF-D) and they act through PDGFR-α and PDGFR-β (179). Meanwhile, bFGF, belonging to the FGF family, also contributes to angiogenesis (180). Therefore, small tyrosine kinase inhibitory molecules have been developed as anti-angiogenics drugs and have antitumoral efficiency in patients with several cancer types (**Table 2**). These drugs have different inhibition constant (Ki) for kinases, as resumed in **Fig-ure 3** (reproduced from (164), with the authorization of Dr Paul Gougis). These different effects and target inhibitions

for each drug should led to differential effects on tumor growth, angiogenesis but also on immune infiltrates of the tumor microenvironment.

Tyrosine Kinase Inhibitors	Kinase Receptor Inhibition	Indications in Oncology
Sorafenib (181)	VEGFR-1/2/3, PDGFR-β, and c-Kit	RCC, HCC, DTC
Sunitinib (182)	VEGFR-1/2/3, PDGFR-α/β, c-Kit, FLT-3, and Ret	GIST, RCC, PNET
Pazopanib (183)	VEGFR-1/2/3, PDGFR-α/β, and c-Kit	RCC, STS
Axitinib (184)	VEGFR-1/2/3, PDGFR-α/β, and c-Kit	RCC
Regorafenib (185)	VEGFR-1/2/3, PDGFR-α/β, FGFR-1/2, Tie2, and c-Kit	RCC, GIST, HCC
Cabozantinib (186)	VEGFR-1/2/3, c-Kit, c-Met, and FLT-3	MTC, RCC
Nintedanib (187)	VEGFR-1/2/3, PDGFR-α/β, and FGFR-1/2	IPF, NSCLC
Lenvatinib (188)	VEGFR-1/2/3, PDGFR-α/β, FGFR-1/2/3, Ret, and c-Kit	DTC, RCC, HCC
Apatinib (189)	VEGFR-2, c-Kit, and c-Src	GC
Anlotinib (190)	VEGFR-1/2/3, FGFR-1–4, PDGFR-α/β, c-Kit, and Ret	NSCLC

TABLE 2. ANTI-ANGIOGENIC TYROSINE KINASE INHIBITORS WITH THEIR SELECTIVE RECEPTOR INHIBITIONS AND THEIR APPROVED INDICATIONS IN ONCOLOGY.

ABBREVIATIONS: RCC = RENAL CELL CARCINOMA; HCC = HEPATOCELLULAR CARCINOMA; DTC = DIFFERENTIATED THYROID CARCINOMA; GIST = GASTRO-INTESTINAL STROMAL TUMOR; PNET = PANCREATIC NEUROENDOCRINE TUMORS; STS = SOFT TISSUE SARCOMA; MTC = MEDULLARY THYROID CARCINOMA; IPF = IDIOPATHIC PULMONARY FIBROSIS; NSCLC = NON-SMALL CELL LUNG CANCER; GC = GASTRIC CANCER; CRC = COLORECTAL CANCER.

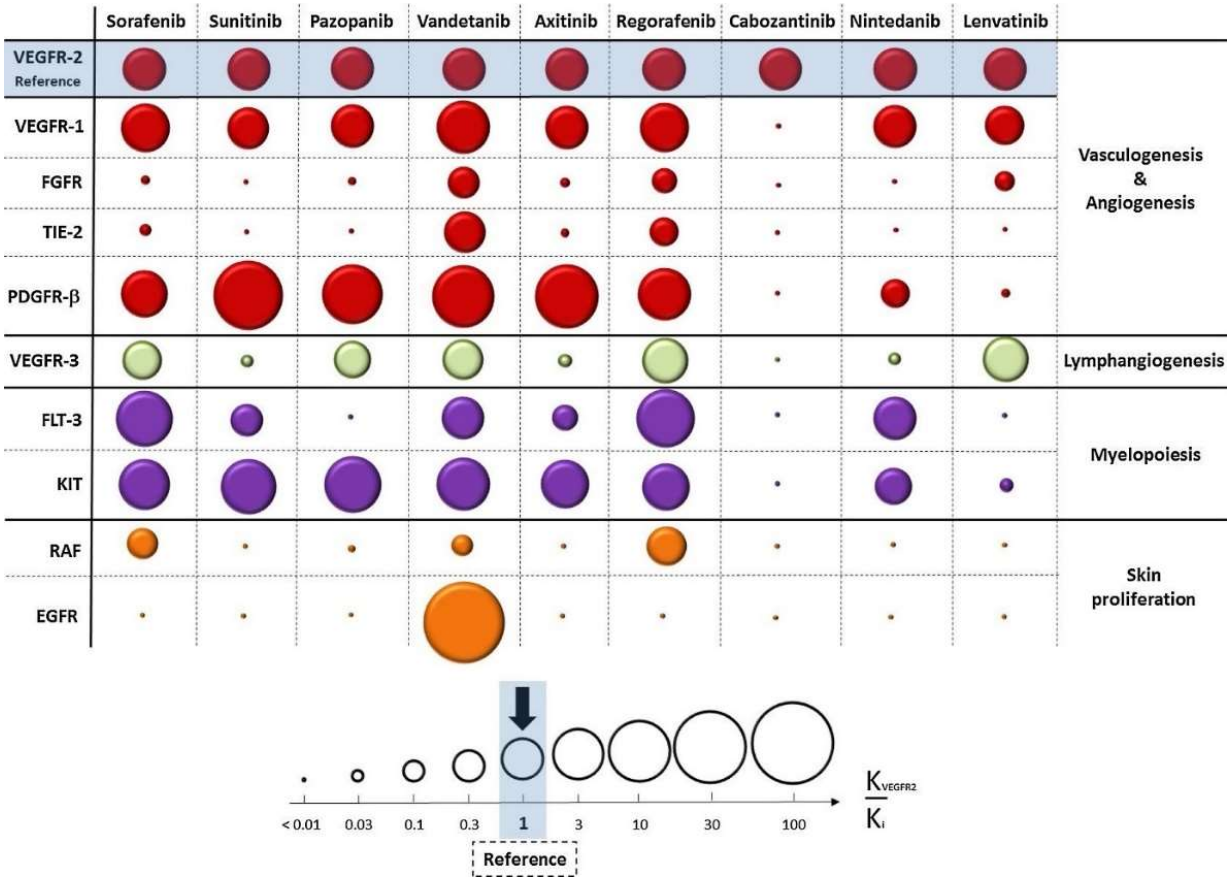

FIGURE 3. COMPARATIVE SPECTRUM OF KINASE INHIBITION FOR KINASES OF INTEREST IN ANGIOGENESIS, FOR ALL APPROVED ANTI-ANGIOGENIC PROTEIN KINASE INHIBITORS, REPRODUCED FROM (164).

Factors associated with the resistance of tumor to anti-angiogenic drugs.

Tumor cells adapt to VEGF blockade and hypoxia by redundancy in angiogenic signaling and activation of compensatory signaling pathways of angiogenesis, summarized in **Figure 4** (reproduced from (18), with the authorization of Dr Mihaela Aldea). Mechanisms of resistance partly implicate redundancy between proangiogenic pathways, strong interaction with stromal cells such as cancer-associated fibroblast and macrophages, pro-inflammatory cytokines induced by secondary hypoxia and stimulation of reactive pathways such as indication of MAP Kinase by increased of apelin.

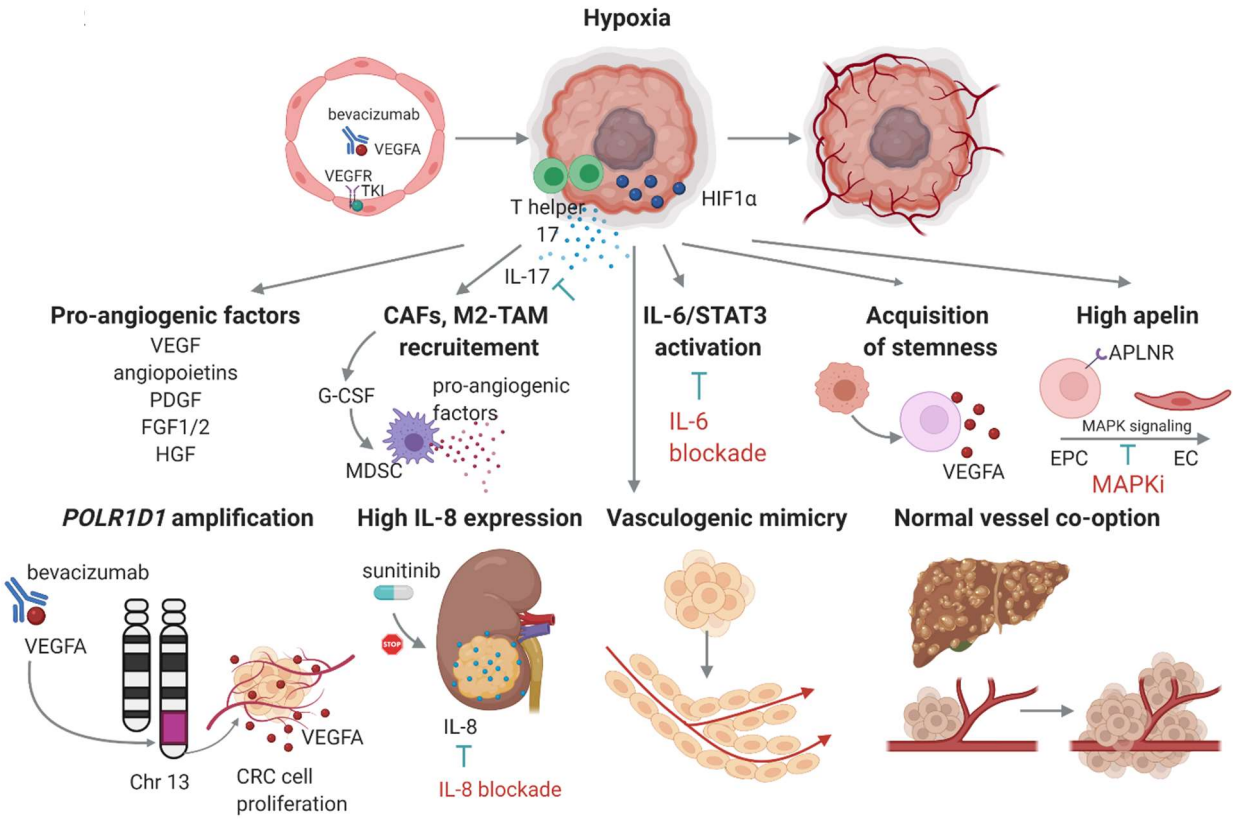

FIGURE 4. POTENTIAL MECHANISMS OF RESISTANCE TO ANTIANGIOGENIC DRUGS AND PROPOSED THERAPEUTIC WAYS TO OVERCOME RESISTANCE (REPRODUCED FROM (18))

ABBREVIATIONS: CHR, CHROMOSOME; CRC, COLORECTAL CANCER; EC, ENDOTHELIAL CELL; EPC, ENDOTHELIAL PROGENITOR CELL; FGF, FIBROBLAST GROWTH FACTOR; HGF, HEPATOCYTE GROWTH FACTOR; IL, INTERLEUKIN; MAPKI, MAPK INHIBITORS; M2-TAM, M2 TUMOR–ASSOCIATED MACROPHAGES; MDSC, MYELOID-DERIVED SUPPRESSOR CELLS; TKI, TYROSINE KINASE INHIBITORS.

Immune checkpoint blockade in onco-immunology.

The immune system, through all its orchestrated and integrated effectors, from innate sensing and response to damage signals from cancer cells up to the adequate adaptive cytotoxic and humoral T and B cells responses, is closely implicated in tumor control and growth (140). By using preclinical studies, the concept of "cancer immunoediting" has described distinct steps leading to efficient immune control of tumor cells vs immune responses facilitating tumor development and metastatic spreading of cancers (191). Several therapeutic strategies dedicated to increase immune responses against tumors were developed to treat patients with advanced cancers. William Coley is considered as a pioneer through intra-tumoral injections of bacteria and bacteria's toxins in patients with unresectable sarcomas (192). Clinical trials evaluating type 1 interferons and IL-2 administrations in patients with advanced melanoma, renal cell carcinoma and hepatocellular carcinoma showed efficiency in patients but their uses had not been generalized to all fields of medical oncology mostly because of their low therapeutic index (i.e. high toxicities and low efficacy) (193–196). Moreover, a better understanding of immune responses from cytotoxic $CD8^+$ T lymphocytes against class 1 major histocompatibility complex (MHC) restricted tumor associated antigens, such as MAGEA1, gp100, Wt1 or Hsp7, led to the development of anti-tumoral vaccination strategies, but again with modest results (197–200). However, these therapeutic strategies did not allow to overcome and explain the *Hellström paradox*: why the cellular infiltrates in tumors and humoral immune responses were inefficient to control tumor growth in patients (201)? The discovery of immune checkpoints such as Cytotoxic T Lymphocyte Associated protein 4 (CTLA-4) and Programmed Death-1 (PD-1) brought stones to the building and allowed the development of a new therapy field in oncology.

Discovery of immune checkpoints: CTLA-4 and PD-1.

The CTLA-4 molecule, belonging to the immunoglobulin family, was discovered in 1987 by the team of Prof. Pierre Golstein at the Marseille-Luminy immunology center (202). The inhibitory properties of CTLA-4 were demonstrated by the scientific teams of Prof. Gordon Freeman, James Allison and Jeffrey Bluestone in the early 1990s (203–205). This costimulatory molecule is expressed on the surface of T lymphocytes after their activation and constitutionally on the surface of regulatory CD4 T lymphocytes. After T cell receptor (TCR) engagement and a costimulatory signal through

CD28, CTLA-4 translocate to the cell surface, where it outcompetes CD28 for binding to critical costimulatory molecules (CD80, CD86) and mediates inhibitory signaling into the T cell, resulting in arrest of both proliferation and activation (206).

The PD-1 receptor is a powerful negative regulator of T cell effector function when engaged by its ligands programmed cell death ligand 1 (PD-L1) and PD-L2, expressed on the surface of cells within a tumor (207,208). Its inhibitory function is mediated by the tyrosine phosphatase SHP-2, which dephosphorylates signaling molecules downstream of the TCR (209). PD-1 has two ligands, PD-L1 (also known as CD274 or B7-H1), which is expressed by numerous cells upon exposure to cytokines, such as interferon gamma, and PD-L2 which has more restricted expression in antigen-presenting cells (209). PD-L1 expression in the tumor microenvironment results in PD-1–mediated T cell exhaustion, inhibiting the antitumor cytotoxic T cell response and is frequently observed in human tumors, independently of histological tumor types (210,211). Exposure of T cells to class 1 MHC / tumor antigen complexes results in reactive PD-L1 expression by target cells, and continuous PD-1 signaling in T cells induces an epigenetic program of T cell exhaustion (212). PD-1 is therefore a negative regulator of preexisting immune responses, which becomes relevant in the biology of immune tolerance to cancer. In the first year of 21st century, Prof James Allison theorized that the blocking of immune checkpoints with antibodies might allow tumor immunotherapy (206).

Clinical development of immune checkpoint blockade for patients with cancers.

First, anti CTLA-4 antibody therapy has been shown to induce durable regression of tumors in animal models (213). The first translation of this therapeutic strategy into humans with ipilimumab, an IgG1 anti-CTLA-4 antibody, was tested in cancer patients in 2000. It led to tumor regressions and were unfrequently associated with adverse events related to tissue specific inflammation (214,215). The most common of these toxicities included colitis, hepatitis, and dermatitis, which could be frequently controlled by corticosteroids. The clinical activity of CTLA-4 blockade was most apparent in patients with advanced metastatic melanoma, with a 15% rate of objective radiographic response that has been durable in some patients for >10 years since stopping therapy (7, 8).

Nivolumab was the first anti PD-1 checkpoint blocker administered into a patient in a phase 1 clinical trial in 2006 (216). Among the 16 patients included, six (37.5%) had objective tumor responses, including patients with melanoma, renal cell carcinoma, and non–small cell lung cancer (NSCLC) (216). The anti–PD-1 antibody pembrolizumab clinical

development began in April 2011 (the antibody was initially called lambrolizumab). The phase 1 clinical trial of pembrolizumab, for patients with melanoma and NSCMC was one of the larger ever conducted in oncology (217,218). FDA approvals of PD-1–blocking antibodies for the treatment of patients with refractory melanoma and advanced NSCLC happened in 2014 and in 2015, respectively. The first anti–PD-L1 antibody approved was atezolizumab for urothelial cancers in 2016, followed by avelumab for Merkel cell carcinoma in 2017.

As opposed to chemotherapies and tumor-targeted therapies, objective tumor responses with those immune-targeted therapies are durable. It was hoped that such immunotherapy could induce long-lasting responses, because of the ability of T cells to maintain memory to their target, and a polyclonal response that the cancer should have trouble escaping. However, a significant proportion (~50%) of patients with partial responses to anti-PD(L)1 monotherapies eventually have their disease relapsing (219).

Anti PD-1 blockade monotherapy has a relatively favorable toxicity profile, with toxicities requiring medical intervention (grades 3 to 4) in the range of 10 to 15% in most series (220). The most common immune related adverse events are fatigue, diarrhea, rash, and pruritus. In a smaller percentage of patients, toxicities are more serious and include several endocrinopathies, in which the immune system infiltrates a hormone producing gland, leading to permanent dysfunction that requires lifelong substitutive hormonal therapy, such as thyroid disorders (10 to 15%), hypophysitis, adrenal gland disorders (1 to 3%), and type 1 diabetes (1%). Serious visceral organ inflammatory toxicities are uncommon (~1%) but can affect any organ, such as lung or heart, leading to life threatening adverse events (221).

Mechanisms of action of anti PD-1 immune checkpoint blockade.

It is believed that patients respond to single-agent anti–PD-1 or anti–PD-L1 therapy because of a preexisting antitumor T cell response: infiltrating T cells engage their TCR through recognition of a tumor antigen, triggering expression of PD-1 on T cells and release of IFN-g, resulting in reactive expression of PD-L1 by cancer-resident cells (222). PD-1 blockade can promote tumor rejection through reactivation of $CD8^+$ T cells, leading to both increased functional activity and frequency (208). Blockade of the PD-1 signaling axis prevents PD-1–mediated attenuation of proximal TCR signaling, allowing for restoration of activity of exhausted CD8 effectors (223). Clinical evidence supports a model in which blockade of the PD-1 signaling axis is most effective in tumors in which an endogenous T-cell response has already been elicited but is suppressed through PD-1 engagement by its ligands PD-L1 and PD-L2 (12,14). Phenotyping of peripheral blood from patients treated with anti–PD-1 antibodies showed an expansion of $PD\text{-}1^+$ $CD8^+$ T cells after treatment infusion (224,225). A study from a neoadjuvant trial of nivolumab in patients with NSCLC showed that anti–

PD-1 therapy enhances neoantigen-specific T-cell responses (226). It is likely that only specific T-cell populations mediate responses to checkpoint blockade therapy. But not all tumor infiltrating T cells in tumor are specific of tumor antigens and certainly only subsets of such reactivated T cells led to an antitumoral responses (227,228). Although PD-1 blockade primarily leads to the expansion of $CD8^+$ T cells, CD4 T cells are required for effective responses (229). In addition to facilitating T-cell memory formation, it is possible that CD4 helper T cells may also enhance antitumor immunity by increasing $CD8^+$ T-cell and antibody entry into peripheral tissue sites, as observed in viral infections (230,231). Recent observations highlighted that coordination in tertiary lymphoid structures of such $CD8^+$ T cells with dendritic cells, $CD4^+$ T cells and B cells in tumor stroma is associated with better outcomes of patients treated with PD-1 blockade for different cancer types (232–234). In another way, blockade of PD-L1 may also derive part of its efficacy from ADCC: Fc receptor binding is important for the efficacy of anti–PD-L1, but not anti–PD-1, for tumor regression in mouse models (235).

Characteristics associated with outcomes of patients treated by immune checkpoint blockade.

Between the two main immune checkpoint blockade classes, anti CTLA-4 and anti PD-1/PD-L1 monoclonal antibodies, most efforts were done to identify tumoral and individual features associated with efficiency of treatment with PD-(L)1 blockers. There are several characteristics associated with the pharmacodynamics of the treatment, the tumor contexture (cancer cells and their stromal microenvironment), and the features of the host.

Immune checkpoint blockers do not have similar pharmacodynamic effects.

Pharmacodynamic effects of immune checkpoint blockade are different between anti CTLA-4 and anti-PD-1 monoclonal antibodies. Different doses of anti CTLA-4 antibodies were used in clinical trials, in monotherapy or in combination with anti PD-1 antibodies. There was a correlation between the concentrations of ipilimumab, its toxicity and its therapeutic efficacy (236,237). On the contrary, the anti-PD1 immunotherapies nivolumab and pembrolizumab efficiencies were not related to their concentration (238). These differences may be due to the biochemical structures of those drugs and their constant fragment of Ig (Fc) isotype and their construct: ipilimumab is an IgG1k, nivolumab is an IgG4 and pembrolizumab is an IgG4k. The IgG1 sequence of ipilimumab is able to link to all Fc gamma receptors (FcGR). The activity of ipilimumab seems to be dependent of linkage of cells with FcGR, such as dendritic cells or macrophages in tumors (239,240). Preclinical studies highlighted that depletion of Tregs constitutively expressing CTLA-4 by antibody

dependent cellular cytotoxicity (ADCC) is one key mechanism of action of anti CTLA-4 antibodies(241,242). Nevertheless, presence of Treg in human tumor is not yet associated with efficacy of anti CTLA-4 antibodies and their mechanism of action remain controversial (243,244). The IgG4 isotype of anti PD-1 monoclonal antibodies have a low affinity to FcGR, except with FcGRI (CD64), and should not promote ADCC. A preclinical study showed that linkage to CD64 could led to anti PD-1 clearance by macrophages in tumors (245). The anti-PD-L1 antibodies atezolizumab and durvalumab are IgG1 antibodies with mutated Fc regions in order to have a low affinity for FcGR and avoid ADCC/ADCP (246). However avelumab has a non-modified IgG1 sequence and can trigger ADCC (247–249). This feature negatively impacts the half life of avelumab and increases its infusion related reactions but do not alter its objective response rate compared to other anti-PD-L1 (250).

<u>High tumor mutational burden is associated with better efficiency of anti PD-1 antibodies.</u>

Recognition of cancer cells by the immune system is believed to be related to the increased tumor mutational burden (TMB) in cancers (222,251). However, not all mutations seem to have the necessary qualities to give rise to robust targets of an antitumor immune responses (252). The processing and presentation by MHC molecules of neoepitopes that result from mutations shapes the landscape of neoantigens recognized by antitumor T cells (253,254). A low preexisting T cell infiltration in tumors may be due to the low immunogenicity of such somatic mutations, therefore not favoring T-cell responses against neoantigens (251). The oncogenic conditions leading to high TMB are associated with a better antitumoral efficiency for patients treated by PD-1 blockade (255). Examples of oncogenic processes leading to high TMB Cancers include:

- Cancers with Micro Satellite-Instability (MSI) secondary to mismatch-repair deficiency (MMrD); those tumors present with a high frequency of insertions and/or deletions (indels) (256);

- Cancers with mutations in the DNA polymerase epsilon (POLE); those tumors are associated with an ultra-mutator phenotype, notably in endometrial tumors (257);

- Cancers with chronic ultraviolet light–induced point mutations such as desmoplastic melanoma (258);

In these cases, response rates are around 50 to 90%. TMB is considered high when the number of mutations per megabase is higher than 10. This threshold is part of the labeling for the approval by the FDA of pembrolizumab for TMB high cancers (259). However, this threshold might not be optimal for all cancers and there is no consensus on the method to measure TMB precisely. Efforts to homogenize the measurement of TMB is mandatory to be really used in real life clinical practice (260).

Preexisting tumor cells expression of PD-L1 is associated with increased efficacy of PD-1 blockade.

The value of PD-L1 expression on tumor and immune cells to predict the efficacy of anti-PD1 was early identified after the fundamental discovery of the molecule (211). It was early studied as a potential markers associated with efficacy of PD-1/PD-L1 blockade (216). As each companies developing an anti PD-1 developed a companion test for immunohistochemistry (IHC) study of PDL1 expression, an effort had been done to homogenize clinical practice (261). In phase 3 clinical trials, the expression of PD-L1 on tumor cells or on both tumor and immune cells in stroma was associated overall with better anti tumoral responses and overall survival of patients receiving anti PD-1 in monotherapy (9,262). However, there are subtle differences across tumor histologies (e.g PD-L1 has predictive value mostly when expressed on cancer cells but not immune cells in NSCLC and vice versa in bladder cancers).

Preexisting tumor infiltration by coordinated adaptive immune response is associated with a better efficacy of PD-1 blockade.

The infiltration of the tumor microenvironment by immune cells and particularly lymphocytes has been known for decades (201). The prognostic value of such infiltration is not similar for each tumor type. In colorectal cancer, the *immunoscore* computing the number of CD3+ and CD8+ cells in the tumor and invasive margins has a better prediction of the patients' prognostic than conventional TNM classification (263,264). However, $CD8^+$ T cells infiltration and PD-L1 expression on tumor cells are higher in sarcomatoid mesothelioma compared to epithelioid subtypes of mesothelioma, but the prognostic of patients is lower (69–71,265). Considering the expected mode of action of PD-1 blockade, its efficacy should be associated with higher infiltration by T cells in the tumor microenvironment. Some cancers display a low level of T cell infiltration into the tumor and other tumors may have higher T cell infiltration but exhausted T cells. Signature methods from transcriptomic analyses of melanoma biopsies from patients treated by PD-1 blockade comfort this idea (266). Moreover, analyses of pre-treatment and on-treatment biopsies samples of patients treated by PD-1 blockade highlighted that preexisting T cell infiltration in tumor and increasing of T cell infiltration and production of chemokines recruiting such immune cells in tumors, were higher in patients who respond to treatment (12,14). Also, special structures gathering immune cells in the tumor microenvironment and known as tertiary lymphoid structures (TLS) have been described in several tumor types (263,267). These structures correspond to the development in non-lymphoid tissues of coordinated structures centered on follicular dendritic cells, appearance of high endothelial venules and lymphoid structures including DC, $CD4^+$ T cells and B cells (268). The degree of organization of such TLS could be different from one tumor to another, between patients but also in a same patient. The presence of TLS and B cells in the tumor microenvironment of melanoma, renal cell carcinoma and sarcoma has been recently associated

with better responses to PD-1 blockade (232–234). The presence of mature TLS was recently associated with improved objective response rates, progression-free survival and overall survival, independently from PD-L1 expression and CD8+ T cell density (269).

The intestinal microbiota influences the efficacy of immune checkpoint blockade.

Studies of gut dysbiosis in mice highlighted the contribution of commensal bacteria on CTLA-4 and PD-L1 blockade effects (270,271). The diversity and composition of the intestinal microbiota seem to play a key role on response to cancer immunotherapy and might have a prognostic value in patients (272–274). Antibiotic-related dysbiosis seem to impair immune checkpoint blockade efficacy in patients across various cancers (275). These studies have highlighted a strong interaction between specific immunogenic bacteria and systemic anti-tumor immune responses. In NSCLC patients, specific $CD4^+$ and $CD8^+$ T cells memory responses toward Akkermansia muciniphila predicted a longer progression-free survival (272). Whereas in melanoma, an enrichment in Faecalibacterium was associated with a higher frequency of cytotoxic $CD8^+$ T cell infiltration in the tumor bed (274). Moreover, the intestinal microbiota composition was recently associated with the occurrence of immune related adverse events upon combination of CTLA-4 and PD-1 blockades (276).

Primary and acquired resistance to immune checkpoint blockade.

Primary resistance to immune checkpoint blockade is unfortunately frequent and has been reported to be driven by genomic and nongenomic mechanisms (18). Defects or alterations in the processes orchestrating tumor–host–microenvironment relationships could be divided into three broad categories, which relate to the cancer cell–intrinsic biology, the impact of this cancer cell on the phenotype of the TME, and the biology of the host. Different aspects of these categories are summarized in **Figure 5** (reproduced from (18), with the agreement of Dr Mihaela Aldea). Primary resistance is defined as progressive disease as the best response to an anti-PD1 therapy (i.e. at first clinical or radiological assessment). It includes the paradoxical phenomenon of hyperprogression where an acceleration of the cancer is seen upon initiation of the blockade of the PD1/PD-L1 axis (277). Secondary or acquired resistance is defined as a cancer progression occurring after an initial response to PD1/PD-L1 blockade therapy. About 50% of patients with an initial RECIST partial tumor response will eventually die of their cancer reprogression (219).

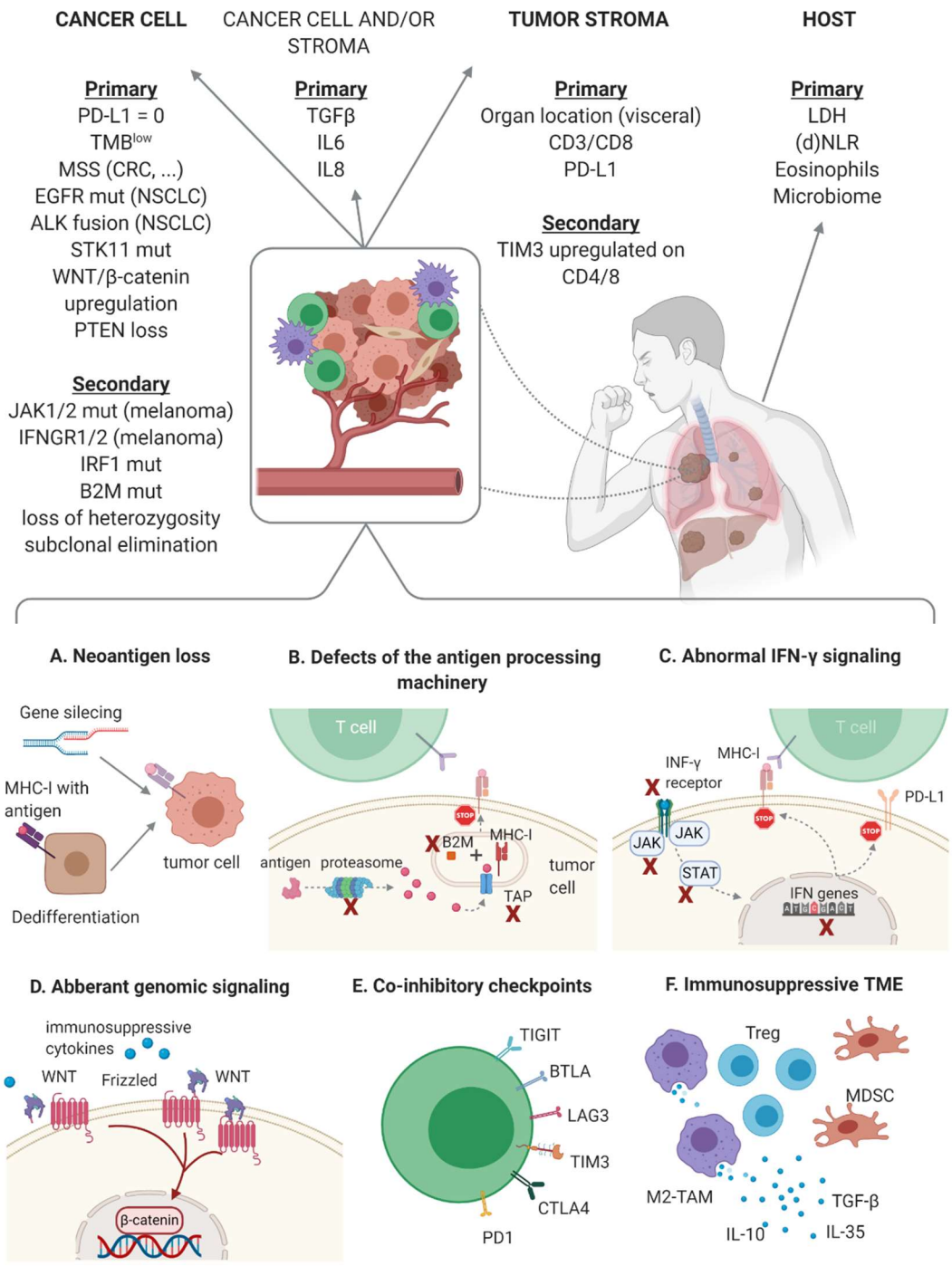

FIGURE 5. MOST COMMONLY DESCRIBED MECHANISMS DRIVING RESISTANCE TO IMMUNOTHERAPY (REPRODUCED FROM (18)).

A, NEOANTIGEN LOSS. B, DEFECTS OF THE ANTIGEN PROCESSING MACHINERY. C, ABNORMAL IFNΓ SIGNALING. D, ABERRANT GENOMIC SIGNALING. E, COINHIBITORY CHECKPOINTS. F, IMMUNOSUPPRESSIVE TME. CRC, COLORECTAL CANCER; IL, INTERLEUKIN; IFNγ, INTERFERON GAMMA; MDSC, MYELOID-DERIVED SUPPRESSOR CELLS; MHC I, MAJOR HISTOCOMPATIBILITY COMPLEX I; M2-TAM, TUMOR-ASSOCIATED MACROPHAGES TYPE 2; MSS, MICROSATELLITE-STABLE; MUT, MUTATION; TREG, REGULATORY T CELLS.

Rationale for anti-PD1 & anti-angiogenic combinations

Both anti-angiogenic treatments and anti-PD1 immune checkpoint blockers have shown monotherapy efficacy in solid tumors. Moreover, comprehensive pre-clinical rationale and clinical results support the hypothesis that anti-VEGF therapy could synergize with checkpoint targeted immunotherapy (19). Fundamental research in the field of cancer angiogenesis has highlighted that an important feature of pro-tumoral abilities of VEGF-A is also to limit the control of cancer cells by the immune system (115). Mechanisms of tumor resistance to both monotherapy strategies could be therefore overcome by the other one.

Anti-VEGF-A anti-angiogenic therapy synergizes with anti-PD-1 immunotherapy

Anti-angiogenic treatment might increase the efficacy of PD-1 blockade, as observed in a murine model, highlighting that such combination could induce both normalization of micro vessel architecture and adaptive immune response in tumors (278). Importantly, VEGFR2 blockade did not seem to interfere with T-cell infiltration and immunological activation induced by PD-1 blockade (278). Simultaneous blockade of PD-1/PD-L1 and VEGF/VEGFR pathways has been shown to induce a synergistic anti-tumor effect in several mouse models (279,280). In patients with untreated metastatic renal cell carcinoma, the association of atezolizumab (an anti PD-L1 monoclonal antibody) with bevacizumab has confirmed that the addition of an anti-angiogenic treatment to immune checkpoint blockade increased immune susceptibility of cancer cells to adaptive immune response (through correction of class 1 MHC expression) and effector $CD8^+$ T cells infiltration (281,282); such as recently in a phase 1 trial, for patients with unresectable peritoneal mesothelioma (283).

Rationale for the association of pembrolizumab with nintedanib.

Both compounds nintedanib, a pan anti-angiogenic TKI, and pembrolizumab, an anti-PD1 monoclonal antibody are being investigated and developed in patients with refractory advanced cancers. Both drugs have proven monotherapy efficacy and the combination of them might be at least additional if not synergistic. Recently, nintedanib was shown to increase CD8+ T cells infiltrates in a mouse model of melanoma and to be synergistic with an anti-PD-1 monoclonal antibody to limit tumor growth (284).

Nintedanib: an anti-angiogenic tyrosine kinases inhibitor

Nintedanib is a potent small molecule belonging to the receptor TKI family. It has inhibitory properties against vascular endothelial growth factor receptor (VEGFR) 1-3, platelet derived growth factor receptor (PDGFR) α/β, and fibroblast growth factor receptor (FGFR) 1-3 (187). At the molecular level, nintedanib inhibits the signaling cascade which mediated angiogenesis by binding to the adenosine 5' triphosphate (ATP) binding pocket of the receptor kinase domain, thus interfering with cross-activation via autophosphorylation of the target receptor homodimers (187). Besides the inhibition of neo angiogenesis, tumor regression may also be achieved by inducing apoptosis of endothelial cells from tumor blood vessel (121). Inhibition of receptor kinases may also interfere with autocrine and paracrine stimulation of tumor angiogenesis via activation loops involving VEGF, PDGF, and FGF.

Kinases	**IC_{50} (nM)***
VEGFR-1	34 +/- 15
VEGFR-2	21 +/- 13
VEGFR-3	13 +/- 10
FGFR-1	69 +/- 70
FGFR-2	37 +/- 2
FGFR-3	108 +/- 41
FGFR-4	610 +/- 117
PDGFR-α	59 +/- 71
PDGFR-β	65 +/- 7
EGFR	>50000
CDK4	>10000
Lck	16 +/- 16

TABLE 3. IN VITRO KINASE INHIBITION PROFILE OF NINTEDANIB.

*Assays performed with ATP concentration at the respective Michaelis constant (Km). This table is a reproduction from one published in *Roth and al. Journal of Medicinal Chemistry, 2015* (187).

In vitro, target receptors are all inhibited by nintedanib at low nanomolar concentrations (cf **Table 3**) (187). In mouse models, nintedanib showed good antitumor efficacy at doses of 50 – 100 mg/kg, leading to a substantial delay of tumor growth or even complete tumor-stasis in xenografts of a broad range of differing human tumor types (285). Histological examination of treated tumors showed a marked reduction of tumor vessel density of approximately 80% (285).

After oral administration, nintedanib is absorbed quickly. Maximum plasma concentrations (Cmax) generally occurs 2 to 4 hours after administration (286). The terminal half-life of nintedanib is in the range of 7 to 19 h. Nintedanib is mainly eliminated via feces. Only 0.7% of total ^{14}C radioactivity was eliminated via the urine. The major metabolites are BIBF-1202 and its glucuronide, which is formed by UGT1A1 (liver and intestine) as well as UGT1A7, UGT1A8 and UGT1A10 (intestine) enzymes (286).

Based on the phase I dose escalation trial of nintedanib, the monotherapy maximum tolerated dose (MTD) was determined at 250 mg bid (i.e twice daily dosing) with a manageable safety profile in advanced cancer patients (287). Based on the overall safety profile, the recommended phase 2 dose (RP2D) for nintedanib as monotherapy is 200 mg bid (287). The predominant adverse events were nausea, diarrhea, vomiting, abdominal pain, and fatigue of mostly low to moderate severity. Dose limiting toxicities (DLT) were mainly limited to reversible hepatic enzyme elevations (AST, ALT, γGT) which increased dose dependently. Most cases occurring at doses of 250 mg and above, and a very low incidence at doses below 200 mg and were reversible after discontinuation of nintedanib treatment (287). All adverse events observed after administration of single doses of nintedanib to healthy volunteers were only of Common Terminology Criteria for Adverse Events (CTCAE) grade 1 severity and fully reversible (286).

Based on phase I trials combining nintedanib with pemetrexed, docetaxel, paclitaxel/carboplatin, or FOLFOX, the recommended dose of nintedanib in combination is 200 mg bid (171,288,289). The pattern of the treatment related adverse events of nintedanib in combinations with chemotherapies was comparable to the adverse event profile of the phase I monotherapy trial. Nintedanib is being investigated in several cancer indications and has been approved by the EMA for the treatment of second line non-squamous NSCLC in combination with docetaxel (290). Additionally, nintedanib is approved for idiopathic pulmonary fibrosis (IPF) in United States of America and European Union (291).

Nintedanib had been evaluated in phase 2 and 3 clinical trials for patients with advanced NSCLC or RCC in combination with chemotherapies. LUME-Lung 1 was an international, randomized, double-blind, phase III trial assessing the efficacy and safety of docetaxel plus nintedanib as second line therapy for non-small-cell lung cancer (NSCLC) (7). LUME-Lung 1 met its primary endpoint by showing a statistically significant improvement of progression free survival (PFS) for all

patients regardless of histology for nintedanib in combination with docetaxel. A significant improvement in overall survival (OS) was demonstrated in patients with adenocarcinoma. LUME-Lung 2 was a multicenter, randomized, double-blind, phase III study of nintedanib plus pemetrexed versus placebo plus pemetrexed in patients with advanced non-squamous NSCLC after failure of first line chemotherapy (292). No safety issues were identified. Even though the study was stopped prematurely, the primary endpoint of this Phase III trial was met; treatment with nintedanib plus pemetrexed resulted in a significant prolongation of PFS compared with placebo plus pemetrexed but there was no improvement in OS in nintedanib-treated patients. Nintedanib 200 mg bid in monotherapy or combination with chemotherapies had an acceptable and manageable safety profile, with no new or unexpected safety findings.

Pembrolizumab: a humanized anti PD-1 monoclonal IgG4–kappa isotype antibody

Pembrolizumab is a highly selective, humanized monoclonal IgG4–kappa isotype antibody against PD-1 (208). The variable region sequences of a very-high-affinity mouse anti-human PD-1 antibody were grafted into a human IgG4 immunoglobulin with a stabilizing S228P Fc alteration (293). The IgG4 immunoglobulin subtype does not promote ADCC or activate complement, thus should avoid cytotoxic effects of the antibody when it binds to the T cells that it is intended to activate (293). The first dose escalation in a phase 1 study involving patients with solid tumors showed that pembrolizumab was safe at the dose levels tested (1 mg per kilogram of body weight, 3 mg per kilogram, and 10 mg per kilogram, administered every 2 weeks) without reaching a maximum tolerated dose (13,294). In addition, clinical responses were observed at all dose levels (13,294). The efficacy of pembrolizumab in melanoma has been subsequently established in a randomized dose comparison Phase 1 trial which demonstrated that pembrolizumab had the same efficacy at 2 and 10mg/kg Q3W with an ORR of 21% in both cohorts (295). Pembrolizumab has also demonstrated superior efficacy to either chemotherapy or ipilimumab (anti-CTLA-4) immunotherapy in metastatic melanoma (296). Pembrolizumab has demonstrated activity with durable tumor responses in NSCLC (217), Hodgkin lymphoma (297), Gastric cancers (298), OC (299), CRC with mismatch repair deficiency (MMRd) (256), mesothelioma (300) and urothelial cancer (301). Anti-PD-1 monoclonal antibody has also shown anti-tumor activity in renal cell carcinoma (10), and hepatocellular carcinoma (302). Pembrolizumab is now approved in the United States of America by the Food & Drug Administration (FDA) and the European Commission granted marketing authorizations for the treatment of patients with many cancer locally advanced or unresectable (2).

Safety issues regarding concomitant blockade of VEGF and PD-1 pathways.

It is of interest to investigate whether the combination of these two treatments is tolerable. Nintedanib has a favorable safety profile, with the main adverse events being diarrhea and liver enzyme elevations. During treatment with pembrolizumab, such as with other anti-PD-1 agents, a unique set of toxicities occur, called immune related adverse events (irAEs) (220). Most reported irAE of pembrolizumab are rash, pruritus, vitiligo, hypothyroidism, arthralgia, diarrhea, and pneumonitis. Most of the time, an efficient management of irAE includes immune checkpoint blockade therapy suspension, associated sometimes to anti-inflammatory corticosteroids (303). But some irAE can be severe, refractory to corticosteroids and deadly (221). Among them myocarditis are infrequent events but leading to death of 50% of patients (61/122 patients) treated by immune checkpoint blockade reported in the VigiBase (WHO's global database of individual case safety reports) (304). These irAEs include colitis, characterized by a mild to moderate but occasionally severe, persistent diarrhea (305). Hepatitis and cholangitis can occur with anti-PD-1 therapy and their incidence could maybe increase when used in combination with anti-angiogenic drugs such as nintedanib (306). Thromboses are not frequently associated with immune checkpoint blockade but several case reports have described such adverse events (307–310). Therefore, an association with an anti-angiogenic drug must lead to pay caution to these events. Even if major clinical adverse events observed after pembrolizumab are distinct from those induced by nintedanib, some overlap may occur, notably diarrhea, nausea, and liver enzyme increase. The incidence of them needs to be carefully monitored.

Conclusion

Although considerable progress has occurred in the field of drug development in oncology, most patients with advanced tumors eventually succumb to their disease (311,312). There is a high need for efficient therapeutic strategies to improve the outcome of patients with advanced cancer. A combination therapy associating pembrolizumab with nintedanib may have the potential to provide significant benefit for patients with solid tumors, by slowing tumor progression and metastasis, restoring normal function of endothelial cells, and promoting anti-tumoral immune response. Ancillary analyses from blood and tumor samples of patients included in such trial should bring important knowledge on real life factors associated with primary resistance to treatment, or efficiency (313).

Thesis objectives

Ancillary analyses of samples from patients included in early development clinical trials can help to discriminate factors associated with tolerability and efficacy of the experimental treatments. These analyses can bring information, which can help future drug developments and build stratification strategies for the treatment of patients with cancers.

The main scientific objective of this thesis work was to identify tumor and blood biomarkers associated with the efficacy or resistance to the combination of pembrolizumab and nintedanib.

This main objective was associated with the following personal correlative objectives:

1. Learn how translational research projects could be built into early phase clinical trials protocols.
2. Become operational with the major techniques used in modern immunology such as multi-color flow cytometry, multiplexed immuno-assays and single cell RNA-seq analysis.
3. Be confronted with the technical challenges of working with fresh, fixed or frozen patient samples collected from blood and tumor.
4. Collaborate with platforms and other research teams in order to perform adequate specialized analyzes (e.g IHC, RNA-seq, WES).
5. Acquire the technical and computational skills (e.g coding with R) which are necessary to compile and analyze big datasets from the results of ancillary analyses, notably when it comes to correlations with clinical outcomes in order to identify biological features associated with primary resistance and/or treatment efficacy.
6. Confront the results obtained from the ancillary analyses to the current scientific knowledge in order to come up with new hypotheses deserving new clinical and translational scientific explorations.
7. Become proficient in the writing of clinico-scientific publications and research grants.

Safety, Recommended Dose and Efficacy Biomarkers for Nintedanib in combination with Pembrolizumab in Patients with Advanced Cancers

Capucine Baldini[1#], François-Xavier Danlos[1,2#], Andreea Varga[1], Matthieu Texier[3], Heloise Halse[4], Severine Mouraud[2], Lydie Cassard[5], Stéphane Champiat[1], Nicolas Signolle[6], Perrine Vuagnat[1,7], Patricia Martin-Romano[1], Jean-Marie Michot[1], Rastislav Bahleda[1], Anas Gazzah[1], Lisa Boselli[5], Delphine Bredel[2], Jonathan Grivel[5], Chifaou Mohamed-Djalim[2], Guillaume Escriou[2], Laetitia Grynszpan[8], Amelie E. Bigorgne[1,4], Saloomeh Rafie[1], Alae Abbassi[1], Vincent Ribrag[1], Sophie Postel-Vinay[1,9], Antoine Hollebecque[1], Sandrine Susini[2], Siham Farhane[1], Aurelien Parpaleix[10], Salim Laghouati[11], Laurence Zitvogel[2], Julien Adam[8,12], Nathalie Chaput[5], Jean-Charles Soria[13], Christophe Massard[1], Aurelien Marabelle[1,2].

# CB and F-XD contributed equally to this work.

Keywords: Phase I, dose escalation, immunotherapy, anti PD-1, anti-angiogenic

AFFILIATIONS

1. Département d'Innovation Thérapeutique et d'Essais Précoces (DITEP), Gustave Roussy, Villejuif, France.
2. INSERM U1015, Gustave Roussy, Villejuif, France.
3. Département de Biostatistiques, Gustave Roussy, Villejuif, France.
4. INSERM U1163, Institut Imagine, Paris, France.
5. Laboratoire d'Immuno-Oncologie (LIO), CNRS-UMS 3655 and INSERM-US23, Gustave Roussy, Villejuif, France.
6. INSERM U981, Department of Experimental Pathology, Gustave Roussy, Université Paris-Sud, Université Paris-Saclay, 94805 Villejuif, France.
7. Département d'Oncologie Médicale, Institut Curie, Paris, France.
8. INSERM UMR 1186, Integrative Tumor Immunology and Immunotherapy, Gustave Roussy, Faculté de Médecine, Université Paris-Sud, Université Paris-Saclay, 94805 Villejuif, France.
9. INSERM U981, Gustave Roussy, Villejuif, France.
10. Service de Promotion des Etudes Cliniques, Gustave Roussy, Villejuif, France.
11. Unité Fonctionnelle de Pharmacovigilance, Villejuif, France.
12. Service d'Anatomo-Pathologie, Hôpital Paris Saint-Joseph, Paris, France.
13. Amgen, Thousand Oaks, CA, USA.

Abstract

Background. We aimed to determine the safety and efficacy of nintedanib, an oral anti-angiogenic tyrosine kinase inhibitor, in combination with pembrolizumab, an anti-PD1 immunotherapy, in patients with advanced solid tumors (PEMBIB trial; NCT02856425).

Methods. In this monocentric phase Ib dose escalation cohort, we evaluated escalating doses of nintedanib (Dose level 1 (DL1) = 150 mg bid [*bis in die*, as twice a day]; DL2 = 200 mg bid, oral delivery) in combination with pembrolizumab (200 mg Q3W, IV). Patients received a 1-week lead-in dose of nintedanib monotherapy prior starting pembrolizumab. The primary objective was to establish the maximum tolerated dose (MTD) of the combination based on dose limiting toxicity (DLT) occurrence during the first 4 weeks. Secondary objectives were to assess the anti-tumor efficacy and to identify the associated immune and angiogenic biomarkers to establish the recommended nintedanib dose for expansion cohorts. Flow cytometry (FC), Immuno-Histo-Chemistry (IHC) and electrochemiluminescence multi-arrays were prospectively performed on baseline & on-treatment tumor and blood samples to identify immune correlates of efficacy.

Results. A total of 12/13 patients enrolled were evaluable for DLT (1 patient withdrew consent prior receiving pembrolizumab). Three patients at 200 mg bid experienced a DLT (grade 3 liver enzymes increase). Four patients developed grade 1-2 immune related adverse events (irAE). Eight patients died because of cancer progression. Median follow-up was 23.7 months (95%CI: 5.55-40.5). Three patients developed a partial response (PR) (ORR=25%) and five patients (42%) had durable clinical benefit (DCB), defined as PR or stable disease (SD) ≥ 6 months. At baseline, patients with DCB had higher plasma levels of Tie2, CXCL10, CCL22 and circulating $CD4^+$ $PD1^+$ $OX40^+$ T cells than patients without DCB. Patients with DCB presented also with more DC-$LAMP^+$ dendritic cells, $CD3^+$ T cells and $FOXP3^+$ Tregs in baseline tumor biopsies. For DCB patients, the nintedanib lead-in monotherapy resulted in higher blood CCL3, Tregs and $CCR4^+$ $CXCR3^+$ $CXCR5^-$ memory CD4 T cells. After the first pembrolizumab infusion, patients with DCB showed lower IL-6, IL-8, IL-27 plasma levels.

Conclusion. Nintedanib 150mg bid is the recommended dose for combination with pembrolizumab and is currently investigated in multiple expansion cohorts. Early tumoral and circulating immune biomarkers were associated with cancer outcome under nintedanib & pembrolizumab therapy.

Trial registration. ClinicalTrials.gov, NCT02856425. Registered August 4, 2016 — Prospectively registered, https://clinicaltrials.gov/ct2/show/NCT02856425?term=PEMBIB&draw=2&rank=1.

Angiogenesis is a key mechanism in tumour growth and development of metastases (20). Tumours induce blood vessel growth (angiogenesis) by secreting growth factors such as the Vascular Endothelial Growth Factor (VEGF), fibroblast growth factor (FGF) and platelet-derived growth factor (PDGF). VEGF and its high affinity receptor VEGFR-2 are crucial for the formation of new tumour vessels (314). In addition, there is preclinical evidence that FGF, PDGF and their associated receptor tyrosine kinases substantially contribute to tumour angiogenesis. The VEGF/VEGFR-2 axis may also generate an autocrine loop which stimulates growth of tumour cells (315). Therefore, suppression of neo-angiogenesis *via* inhibition of VEGFR-2 is a promising and efficient strategy for the treatment of solid tumors (25).

Immune checkpoint blockade is a new treatment strategy undergoing extensive investigation in multiple malignancies. Unlike standard chemotherapy or targeted therapy, the immune checkpoint blockade restores the immune system's capacity to eradicate tumours (316). Antibodies targeting the Programmed Death-1 receptor (PD-1) and its ligand (PD-L1) have been extensively investigated and are still in active development across malignancies and their different lines of treatment (317). Combining anti-angiogenic drugs and anti-PD-(L)1 therapy has recently shown important synergistic results in RCC and HCC (318–320). Indeed, anti-VEGF therapies may enhance anti–PD-(L)1 efficacy by reversing VEGF-mediated immunosuppression and promoting T-cell infiltration in tumours (145,159,281,282,321,322).

Although the combination of anti-angiogenics together with immune checkpoint blockade is becoming an attractive combination for the treatment of many cancers (323), the safety and activity of such combination is depending on the anti-angiogenic molecule tested. For instance, combinations of sunitinib and pazopanib with the anti-PD1 nivolumab were deemed too toxic with more than 70% grade 3/4 treatment related adverse events (324). Therefore, novel anti-angiogenics should be tested in dedicated clinical trials to establish the dose, regimen, safety and activity when used in combination with anti-PD1 immunotherapies (325). Nintedanib is an oral tyrosine kinase receptor inhibitor (TKI) of PDGFRα/β, FGFR1-3, and VEGFR1-3 that has been approved in 2014 by the EMA in combination with docetaxel for the treatment of second line advanced NSCLC.

We aimed to determine for the first time in humans the safety and efficacy of nintedanib, in combination with pembrolizumab, a humanized IgG4 anti-PD1 monoclonal antibody immunotherapy in patients with advanced solid tumors (NCT02856425).

Study design

In this monocentric phase Ib dose escalation cohort (NCT02856425), we evaluated escalating doses of nintedanib (Dose level 1 (DL1) = 150 mg bid, DL2 = 200 mg bid) in combination with IV flat dose of pembrolizumab over 30 minutes (200 mg Q3W). Two dose-levels below the approved regimen of nintedanib (DL-1 & DL-2) could also be tested in case of unacceptable toxicities upon combination with pembrolizumab (**Figure 6A**). Patients received a one-week lead-in course of nintedanib monotherapy prior starting pembrolizumab. The sample size of the dose escalation cohort was conducted according to the rolling 6 design (326). Up to 6 patients evaluable for dose-limiting toxicity (DLT) could be exposed to a dose level. As soon as 3 patients were evaluable for DLT at a given dose level, dose escalation or de-escalation was permitted upon review of the safety data. The protocol was first approved by the Agence Nationale de Sécurité du Médicament (ANSM) on June 24th, 2016 (Ref #160371A-12) and by the Ethical Committee (Comité de Protection des Personnes Ile-de-France 1) on Jul 12th, 2016 (Ref #2016-mai-14236ND). The trial was first posted on clinicaltrials.gov on Aug 4th 2016 (NCT02856425).

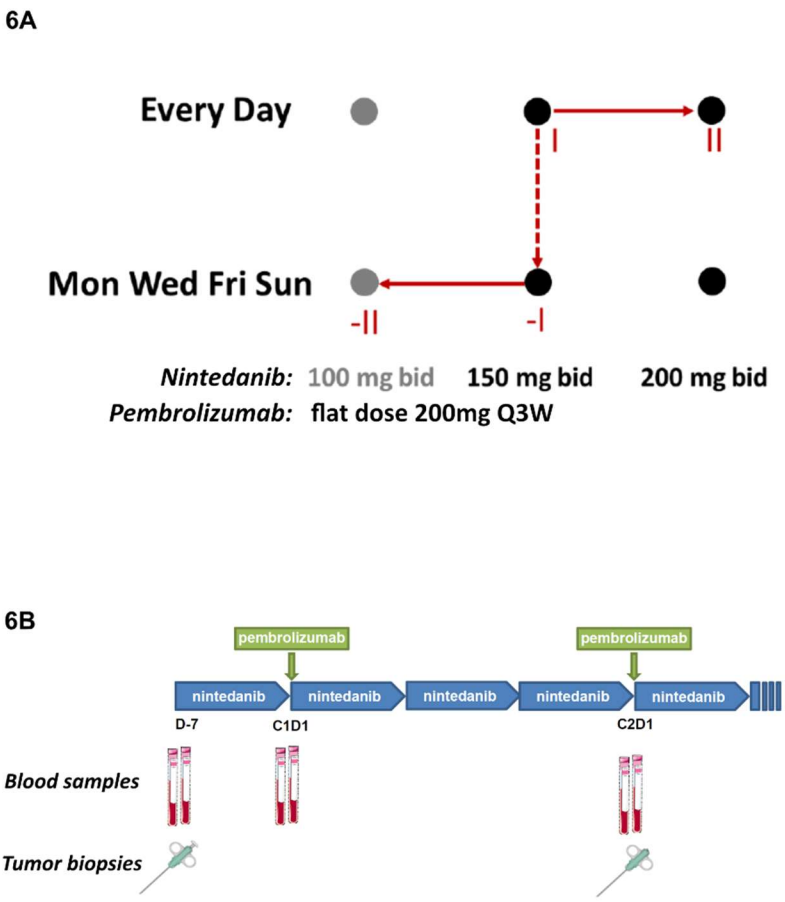

FIGURE 6. DECISION TREE FOR THE NINTEDANIB DOSE ESCALATION (6A) AND THE COLLECTION OF BIOLOGICAL SAMPLES FOR ANCILLARY ANALYSES (6B).

Patients

Eligible patients had advanced, metastatic cancer which progressed after at least one line of standard therapy or were intolerant to standard therapy, naive to immune checkpoint blockade and nintedanib. Additional inclusion criteria included age ≥ 18 years, Eastern Cooperative Oncology Group (ECOG) performance status of 0-1, adequate organ function, measurable disease according to RECIST v1.1, and written informed consent. Key exclusion criteria were radiographic evidence of cavitary tumors, local invasion of major blood vessels and/or at risk for perforation, history of clinically significant hemoptysis within the past 3 months, history of clinically significant hemorrhagic or thromboembolic event in the past 6 months, history of significant cardiovascular diseases, prior treatment with anti PD-(L)1 agents, concurrent steroid medication, history of autoimmune and inflammatory disease. This study was conducted in compliance with the Declaration of Helsinki and the International Ethical Guidelines for Biomedical Research Involving Human Subjects.

Procedures

Screening procedures were performed up to 21 days (D-28) before Day -7 (start of nintedanib). Patients continued treatment until disease progression, undue toxicity, or withdrawal of consent for a maximum duration of 24 months.

Adverse events were graded using National Cancer Institute (NCI) CTCAE Version 4.03. The occurrence of a non-hematological toxicity ≥ CTCAE Grade 3, a hematological toxicity ≥ CTCAE Grade 4, or an inability to resume nintedanib dosing within 7 days of stopping due to treatment related toxicity during the first 4 weeks were considered as a DLT, if judged by the Investigator to be possibly, probably, or related to study drug administration. Tumor evaluation was performed every 6 weeks based on Response Evaluation Criteria in Solid Tumors (RECIST) 1.1 and immune-related RECIST (irRECIST) (327,328). Details about screening exams, Nintedanib dose modification criteria, and other patient management rules are detailed in the protocol of the trial provided in the supplementary information files.

Patients underwent tumor biopsies prior to the beginning of nintedanib and prior to the second injection of pembrolizumab in order to monitor the pharmacodynamic effects of the treatment and to identify biomarkers predictive of efficacy (**Figure 6B**).

Outcomes

The primary objective was to establish the maximal tolerated dose (MTD) of nintedanib in combination with pembrolizumab based on the assessment of DLT occurrence during the first 4 weeks (28 days since C1D1). Secondary objectives were to determine the tolerability and safety of the Recommended Phase 2 Dose (RP2D) of nintedanib combined with

pembrolizumab and to evaluate first anti-tumor activity of this combination in expansion cohorts. The aim of the ancillary studies was to identify predictive biomarkers of efficacy.

Immuno-Histochemistry staining

Multiple chromogenic and one fluorescent multiplex Immuno-Histo-Chemistry (IHC) stainings were performed on each biopsy. The Ventana Discovery Ultra platform was used for both PD-L1 and ICAM1 (DAB) single chromogenic staining, for FOXP3 (Purple)/CD31 (DAB) multiplex and CD3 (Purple)/CD8 (DAB) multiplex chromogenic staining and for a panel combining DC-LAMP (OPAL 620), CD68 (OPAL 570), IDO1 (OPAL 540), CD163 (OPAL 520) and DAPI nuclear staining for the identification of myeloid cells. The multispectral images were captured using the Vectra® microscope tunable filter that shines 35 incremental wave lengths of light from 300 nm to 750 nm. High-powered images were selected by a pathologist, matched to a Hematoxylin and Eosin Staining (HES) to validate tumor-associated tissue. The spectral library was synthesized using the Inform® v2.2 software.

Immune monitoring – Fresh blood immune phenotype.

For each patient, heparinized blood samples (30-40 mL) at day -7 (baseline), C1D1 and C5D1 were collected whenever possible for monitoring circulating immune populations by flow cytometry. Fresh whole blood phenotyping of T-cell migration, T-cell polarization, T-cell activation, Treg function and myeloid cells was performed using 5 specific panels, as previously described (329). Stained cells were acquired using a Gallios Cytometer (Beckman Coulter) and analyzed using Kaluza software (Beckman Coulter).

Cytokine, chemokine and soluble angiogenic factors measurements.

Plasma samples were centrifuged for 15 min at 1,000 g, diluted 1:4, then monitored using the Angiogenesis Panel 1 (human) (Meso Scale Discovery, ref: K151P3S-1), Chemokines Panel 1, Proinflammatory Panel 1, Cytokine Panel 1 (Meso Scale Discovery, ref: K151A9H-1), the ultra-sensitive assay S-plex Human IFNα2a kit (Meso Scale Discovery, ref: K151P3S-1), Human PD-1 and PD-L1 antibody sets (Meso Scale Discovery, ref: F214A-3 & F214C-3, respectively) following manufacturer's instructions. Acquisitions and analyses were performed on a MESO™ QuickPlex SQ120 reader and the MSD's Discovery Workbench 4.0. Each plasma sample was assayed twice with the average value taken as the result.

Statistical analysis and illustrations.

Clinical statistical analysis had been done using the SAS® statistical software version 9.4 (Cary, North Carolina, USA). Calculations and statistical tests for ancillary analyses were performed using R v3.4. Wilcoxon-Mann-Whitney test was used to assess differences between two patient's groups. Data representation was performed with software R v3.3.3

using tidyverse, dplyr, ggplot2 and ggpubr packages. Figure's aesthetics were worked with Affinity Designer® (v1.9.2.1035).

Results.

Safety of nintedanib dose escalation in combination with pembrolizumab

Thirteen patients were enrolled between Nov 24th, 2016, and Jul 24th, 2017, in the dose escalation cohort. Among them, one patient withdrew consent before C1D1. Consequently, 12 patients were evaluable for dose limiting toxicity (DLT). Six patients received nintedanib 150mg bid *per os* (po) and 6 others consecutive patients received nintedanib 200mg bid po. Their clinical characteristics are described in **Table 4**. Patients were treated for different tumor types: cervical cancer (n=2), thymic carcinoma (n=2), mesothelioma (n=2), breast cancer (n=1), colorectal adenocarcinoma (n=1), gastric adenocarcinoma (n=1), clear cell renal carcinoma (n=1), neuroendocrine tumor of the caecum (n=1) and undifferentiated carcinoma of nasopharyngeal type (UCNT) (n=1). All patients received at least one previous line of treatment: chemotherapy (n=12, 100%), immunotherapy (n=1, 8%; intra-tumoral TLR7/8 agonist) and tyrosine kinase inhibitor (n=1, 8%; pazopanib).

	DL1 *Nintedanib 150 mg bid N=6*	DL2 *Nintedanib 200 mg bid N=6*	*Total N=12*
Sex			
Male	3 (50%)	3 (50%)	6 (50%)
Female	3 (50%)	3 (50%)	6 (50%)
Age, Median (range)	62 (43-74)	49 (40-67)	59 (40-74)
ECOG PS			
0	3 (50%)	4 (67%)	7 (58%)
1	3 (50%)	2 (33%)	5 (42%)
Breast cancer	0	1 (17%)	1 (8%)
Cervical cancer	2 (33%)	0	2 (17%)
Colorectal carcinoma dMMR	1 (17%)	0	1 (8%)
Gastric carcinoma	1 (17%)	0	1 (8%)
Renal clear cell carcinoma	1 (17%)	0	1 (8%)
Caecal neuroendocrine carcinoma	0	1 (17%)	1 (8%)
Peritoneal mesothelioma	0	1 (17%)	1 (8%)
Pleural mesothelioma	0	1 (17%)	1 (8%)
Thymic carcinoma	0	2 (33%)	2 (17%)
Nasopharyngeal undifferenciated carcinoma	1 (17%)	0	1 (8%)
Median previous lines of treatment	2 (1-5)	1.5 (1-2)	2 (1-5)
Lung Immune Prognostic Index (LIPI)			
Good	6 (100%)	2 (33%)	8 (67%)
Intermediate	0	4 (67%)	4 (33%)
Poor	0	0	0
GRIm-score			
0-1	6 (100%)	3 (50%)	9 (75%)
2-3	0	3 (50%)	3 (25%)
Median Neutrophil (.10^3/mm^3) (range)	4.45 (3.6-6.1)	3.75 (2-5.4)	4.2 (2.5-6.1)
Median Lymphocytes (.10^3/mm^3) (range)	1.4 (1.2-3.2)	1.1 (0.6-1.4)	1.2 (0.6-3.2)
Median Albumin (g/L) (range)	40 (36-44)	42.5 (35-50)	40.5 (35-50)
Median LDH UI/L (range)	186 (147-245)	288 (154-550)	208 (147-550)
Median CRP (mg/L) (range)	11.1 (5.9-68.2)	17.3 (4.9-49.8)	11.1 (4.9-68.2)

TABLE 4. CLINICAL CHARACTERISTICS OF PATIENTS ENROLLED IN THE DOSE ESCALATION COHORT OF THE PEMBIB PHASE 1B TRIAL.

Patients treated with nintedanib 150 mg bid and 200 mg bid received a median of 9 (range: 4;34) and 3 (range: 2;16) complete cycles, respectively. Dose modifications of nintedanib occurred in 2 patients treated with nintedanib 150 mg bid (33%) and 4 patients (67%) and 200 mg bid, respectively. Three patients experienced dose-limiting toxicities (DLT) at 200 mg bid (nintedanib-related liver toxicities). The MTD of nintedanib with pembrolizumab 200 mg Q3W was 150mg bid, based on dose limiting toxicity (DLT) occurred in this cohort.

All patients presented at least one adverse event associated with one of both drugs. Four of them developed a defined immune related adverse event, a colitis, a nephritis and two thyroiditis (grade 3, 2 & 1 CTCAE v.4.03, respectively). Superior mesenteric artery occlusion was observed in one patient, concomitantly of a grade 3 colitis, confirmed by biopsies, and a thrombus on catheter in superior vena cava. These events were related to both nintedanib and pembrolizumab. One patient had an acute grade 4 pneumonitis related to *Streptococcus pneumoniae* infection, not related to the experimental combination. Listing of adverse events related to treatments are reported in **Table 5**.

	Grade 1-2	Grade 3
Fatigue	2 (17%)	0
Diarrhea	10 (83%)	0
Hypertension	1 (8%)	0
Venous thromboembolism	0	1 (8%)
Cutaneous rash	4 (33%)	0
Alanine aminotransferase increased	9 (75%)	4 (33%)
Aspartate aminotransferase increased	6 (50%)	3 (25%)
Colitis	0	1 (8%)
Creatinin increase	1 (8%)	0
Dyspnea	1 (8%)	0
Abdominal pain	3 (25%)	0
Decreased appetite	2 (17%)	0
Headache	1 (8%)	0
Hearing impairment	1 (8%)	0
Hyperthyroidism	1 (8%)	0
Hypothyroidism	3 (25%)	0
Mucositis	1 (8%)	0
Nausea	5 (42%)	0
Vomiting	6 (50%)	0
Nervous system disorder	1 (8%)	0
Peripheral motor neuropathy	1 (8%)	0
Platelet count decreased	2 (17%)	0
Renal and urinary disorder	1 (8%)	0
Supraventricular tachycardia	1 (8%)	0
Weight loss	1 (8%)	0
GGT increased	1 (8%)	0

TABLE 5. SUMMARY OF ALL ADVERSE EVENTS REPORTED BY INVESTIGATORS IN PATIENTS TREATED BY NINTEDANIB + PEMBROLIZUMAB (DOSE ESCALATION).

Median follow up of the patients was 23.7 months (95% Confidence interval: [5.55; 40.5]). The best objective response was PR for 3 patients (25%), SD for 4 patients (33%) and a primary PD for 5 patients (42%) (Summarized in waterfall plot, **Figure 7A**). Two patients with stable disease did not develop a tumor progression during follow up (**Figure 7B**). Best responses were achieved at cycle 3 in most cases (58%). Five patients were alive at the end of the follow up period (**Figures 7C**). Median Overall Survival was 16.3 months (95% Confidence Interval: [4.34; Not Reached]). Survival rates were 75% (95% CI: [46.8-91]), 64% (95% CI: [35.7-85.4]) and 32% (95% CI: [11.8-62.6]) at 6, 12 and 24 months, respectively. Eight patients died because of cancer progression and no treatment-related deaths were observed.

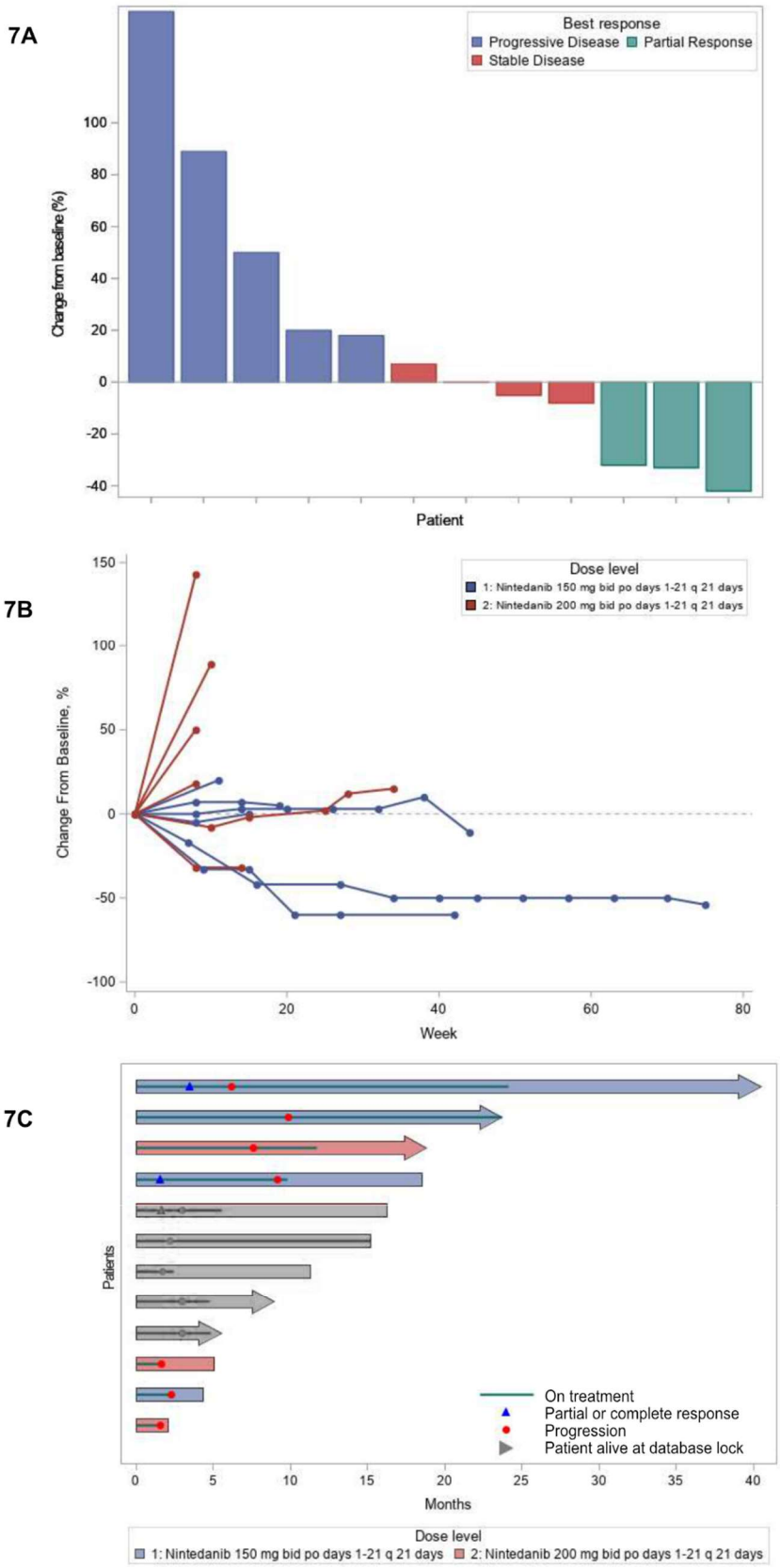

FIGURE 7. CANCER OUTCOMES IN THE DOSE ESCALATION COHORT OF THE PEMBIB TRIAL: WATERFALL PLOT (7A), SPIDER PLOT (7B) AND SWIMMER PLOT (7C).

Preexisting immune & angiogenic characteristics were associated with antitumoral response upon immune checkpoint blockade in combination with antiangiogenic therapy.

Patients with durable clinical benefit (DCB) defined as objective partial response or stable disease for at least 6 months after the beginning of treatment, presented higher CXCL10, CCL22/Macrophage-Derived Chemokine (MDC) and soluble Tie2 plasma levels before initiation of treatment than patients without DCB (**Figure 8A**). Flow cytometry analyses on fresh whole blood highlighted that $CD4^+$ $PD1^+$ $OX40^+$ and $CD4^+$ $\alpha4\beta7^+$ among total $CD4^+$ T cells were more present in patients with DCB than patients without DCB (**Figure 8B**). IHC analyses on pre-treatment tumor biopsies highlighted that patient who developed DCB tended to have higher immune infiltration characterized by higher percentage of $PDL1^+$ tumor cells, and higher densities of $CD3^+$ T cells, $FOXP3^+$ cells and $DCLAMP^+$ dendritic cells than patients without DCB after treatment (**Figure 8C**).

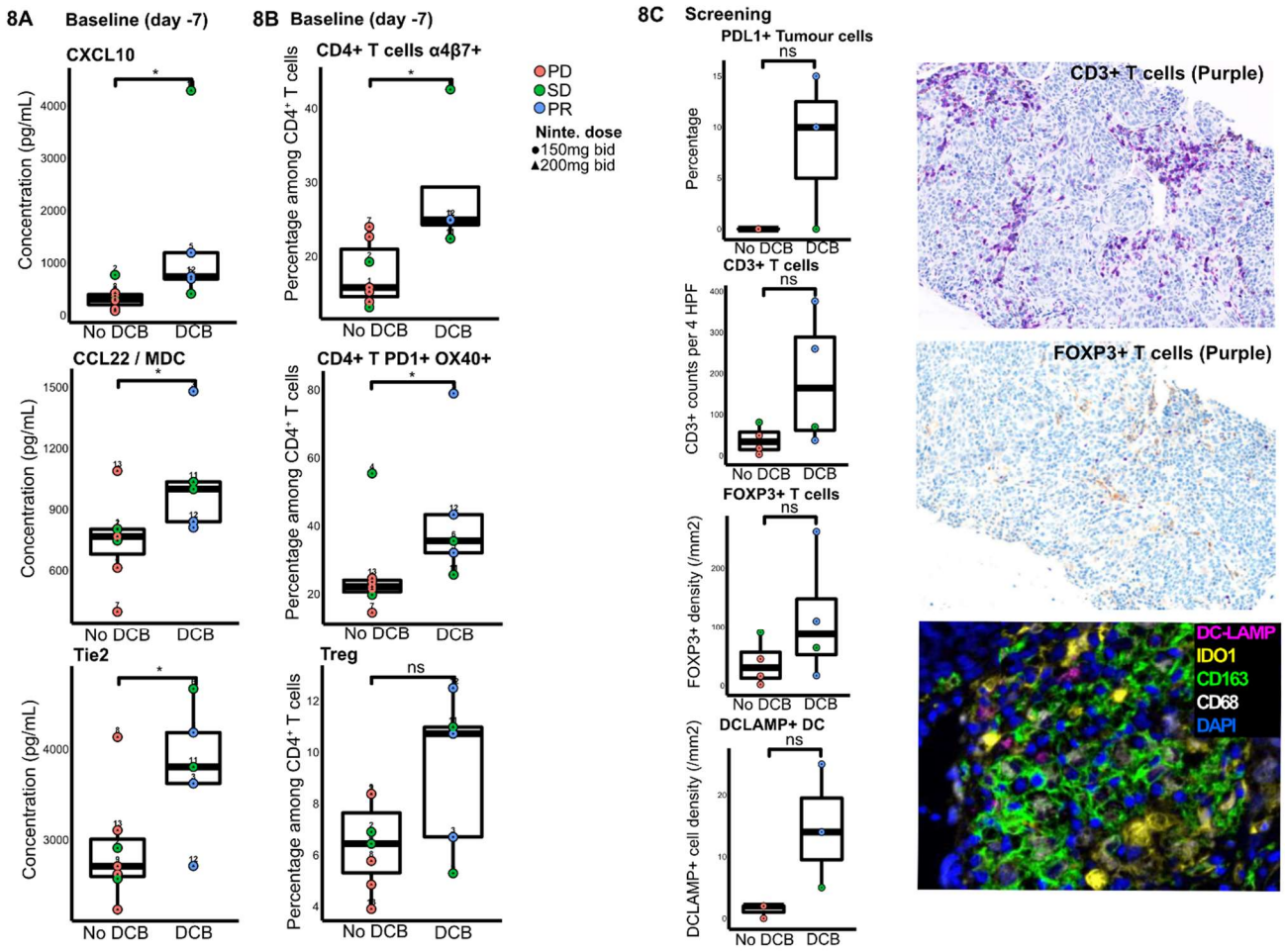

FIGURE 8. INCREASED TUMOR IMMUNE CELL INFILTRATION IN PATIENTS WITH DURABLE CLINICAL BENEFIT BEFORE INITIATION OF THE NINTEDANIB AND PEMBROLIZUMAB ASSOCIATION (DOSE ESCALATION).

8A. CXCL10, CCL22 AND SOLUBLE TIE PLASMA LEVELS WERE SIGNIFICANTLY HIGHER IN PATIENTS WITH DCB (1464PG/ML [RANGE: 409.8-4290.5], 1032.8PG/ML [RANGE: 810.5-1479.9] AND 3796.6PG/ML [RANGE: 2710.9-4665.6], RESPECTIVELY) THAN PATIENTS WITHOUT DCB (334.7PG/ML [RANGE: 81.1-767.6], 745.2PG/ML [RANGE: 396.8-1088.5] AND 2896.5PG/ML [RANGE: 2230.4-4132.7]) (WILCOXON RANK SUM TEST; P=0.03, P=0.03 AND P=0.04, RESPECTIVELY). 8B. THE PERCENTAGE OF A4B7+ CD4+ AND PD1+ OX40+ CD4+ CELLS AMONG TOTAL CIRCULATING CD4+ T CELLS WAS SIGNIFICANTLY HIGHER IN PATIENTS WITH DCB (28.7% [RANGE: 22.4-42.6] AND 43.1% [RANGE: 25.6-78.9], RESPECTIVELY) THAN WITHOUT DCB (17.7% [RANGE: 13.1-23.9] AND 25.9% [RANGE: 14.5-55.4]) (WILCOXON RANK SUM TEST; P=0.024 AND P=0.03, RESPECTIVELY). 8C. PATIENTS WITH PR HAD PD-L1 EXPRESSION ON TUMOR CELLS AND IMMUNE INFILTRATION IN TUMOR STROMA, CHARACTERIZED BY IHC (WILCOXON RANK SUM TEST; NON-SIGNIFICANT).

Specific angiogenic and immune changes occurring during nintedanib lead-in monotherapy could favor primary resistance to immune checkpoint blockade efficiency.

During the first week of the clinical trial, patients received nintedanib monotherapy. The comparison of soluble factors in plasma and phenotype of fresh blood circulating lymphocytes between day - 7 and C1D1 allowed the identification of changes associated with DCB to treatment which could be induced by the lead-in nintedanib monotherapy. Placental Growth Factor (PlGF) and VEGF-D plasma levels increased significantly between day -7 and C1D1 only in patients without DCB (**Figure 9A; Supplementary Figure 1**), although other soluble angiogenic factors levels remained stable. In parallel, plasma levels of CCL3 / MIP-1α (Macrophage Inflammatory Protein 1-Alpha), another ligand for CCR4 with CCL22/MDC, tended to increase in patients with DCB and was significantly higher before pembrolizumab infusion in patients with DCB compared to patients without DCB (**Figure 9B**). Also, patients who benefited from treatment had a higher percentage of circulating conventional CCR4$^+$ CXCR3$^+$ helper memory T cells and Tregs than patients without DCB (**Figure 9C**).

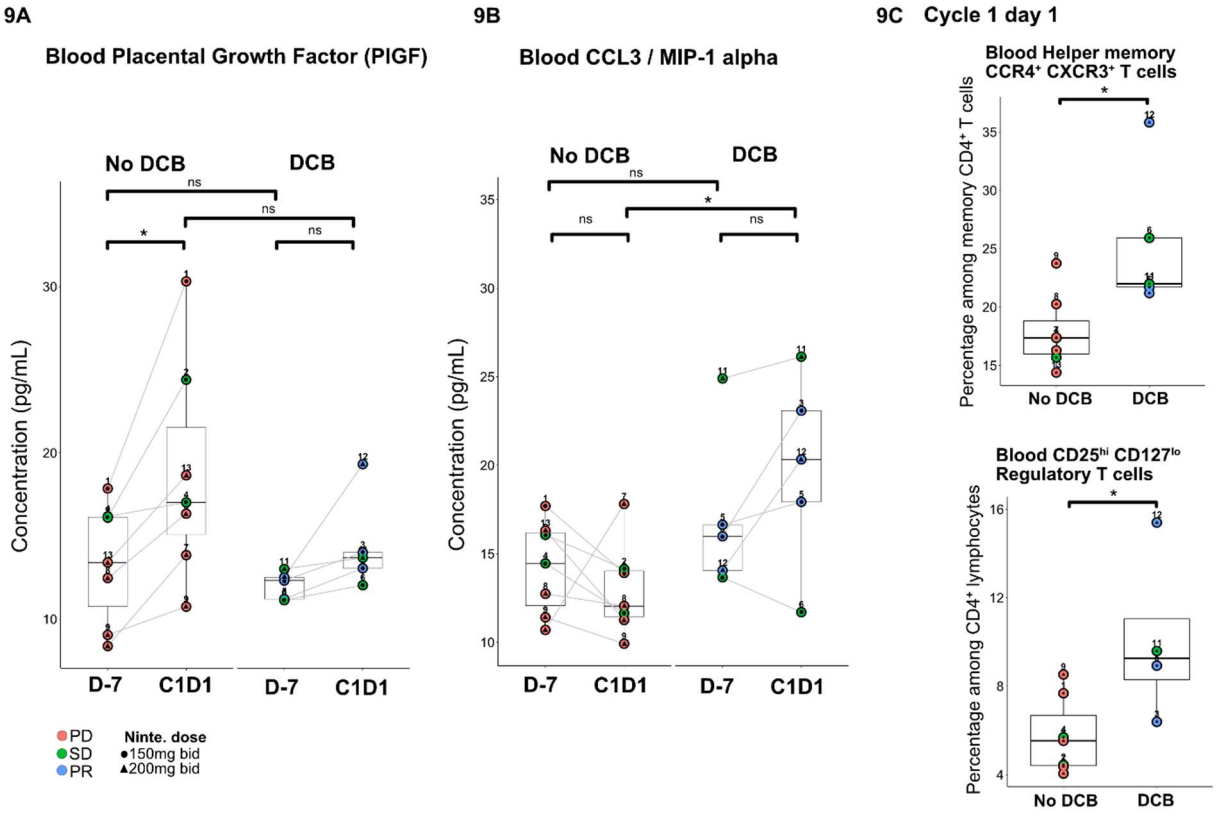

FIGURE 9. INCREASED OF CIRCULATING SOLUBLE PLGF, CCL3 AND INCREASE IN SPECIFIC T CELLS SUBSETS DURING LEAD-IN NINTEDANIB MONOTHERAPY ASSOCIATED TO CLINICAL OUTCOMES (DOSE ESCALATION).

9A. PLASMA RATE OF PLACENTAL GROWTH FACTOR (PLGF) INCREASED IN PATIENTS WITHOUT DCB BETWEEN D-7 (13.4PG/ML [RANGE: 8.4-17.9]) AND C1D1 (18.8PG/ML [RANGE: 10.8-30.3]) (PAIRED WILCOXON SIGNED RANK TEST; P=0.015). 9B. PLASMA RATE OF CCL3 WERE HIGHER IN PATIENTS WITH DCB (19.8PG/ML [RANGE: 11.7-26.1]) THAN WITHOUT DCB (12.9PG/ML [RANGE: 9.9-17.8]) AFTER 7 DAYS OF NINTEDANIB MONOTHERAPY (NON-PARAMETRIC WILCOXON RANK SUM TEST; P=0.03). 9C. PERCENTAGE OF BLOOD CCR4$^+$ CXCR3$^+$ T CELLS AMONG EFFECTOR MEMORY CD4+ T CELLS AND CD25^{HIGH} CD127^{LOW} TREGS AMONG TOTAL CD4+ T LYMPHOCYTES WERE HIGHER AT C1D1 IN PATIENTS WITH DCB (25.3% [RANGE: 21.2-35.8] AND 10% [RANGE: 6.4-15.4], RESPECTIVELY) THAN THOSE WITHOUT DCB (17.9% [RANGE: 14.4-23.8] AND 5.8% [RANGE: 4.1-8.5], RESPECTIVELY) (NON-PARAMETRIC WILCOXON RANK SUM TEST; P=0.017 AND P=0.024, RESPECTIVELY).

Early inflammatory changes occurring after immune checkpoint blockade were associated with resistance to treatment and progressive disease.

Early inflammatory changes were observed in plasma of patients without DCB as opposed to patients with DCB. Before the second pembrolizumab infusion, patients without DCB presented an increasing plasmatic rate of TNF, compared to paired pre-pembrolizumab plasma (**Figure 10A**), and also for CCL3, CCL4, IL-18, IL-10, IL-22 and VEGF-D (**Supplementary Figure 2**). Patients without DCB also had higher plasmatic rate of inflammatory cytokines such as IL-6, IL-27 and CXCL8 than patients with DCB at C2D1 (**Figure 10B**). IHC performed on tumor biopsies done before C2D1, showed that percentages of $PDL1^+$ tumor cells, ratio of $CD3^+$ on $CD163^+$ cells and density of $FOXP3^+$ cells were significantly higher in patients with DCB than without DCB (**Figure 10C**). Tumor densities of $CD68^+$ and $CD163^+$ cells were not different in C2D1 biopsies (**Supplementary Figure 3**); neither those of DC-$LAMP^+$, $IDO1^+$, $ICAM1^+$ or $CD31^+$ cells (data not shown).

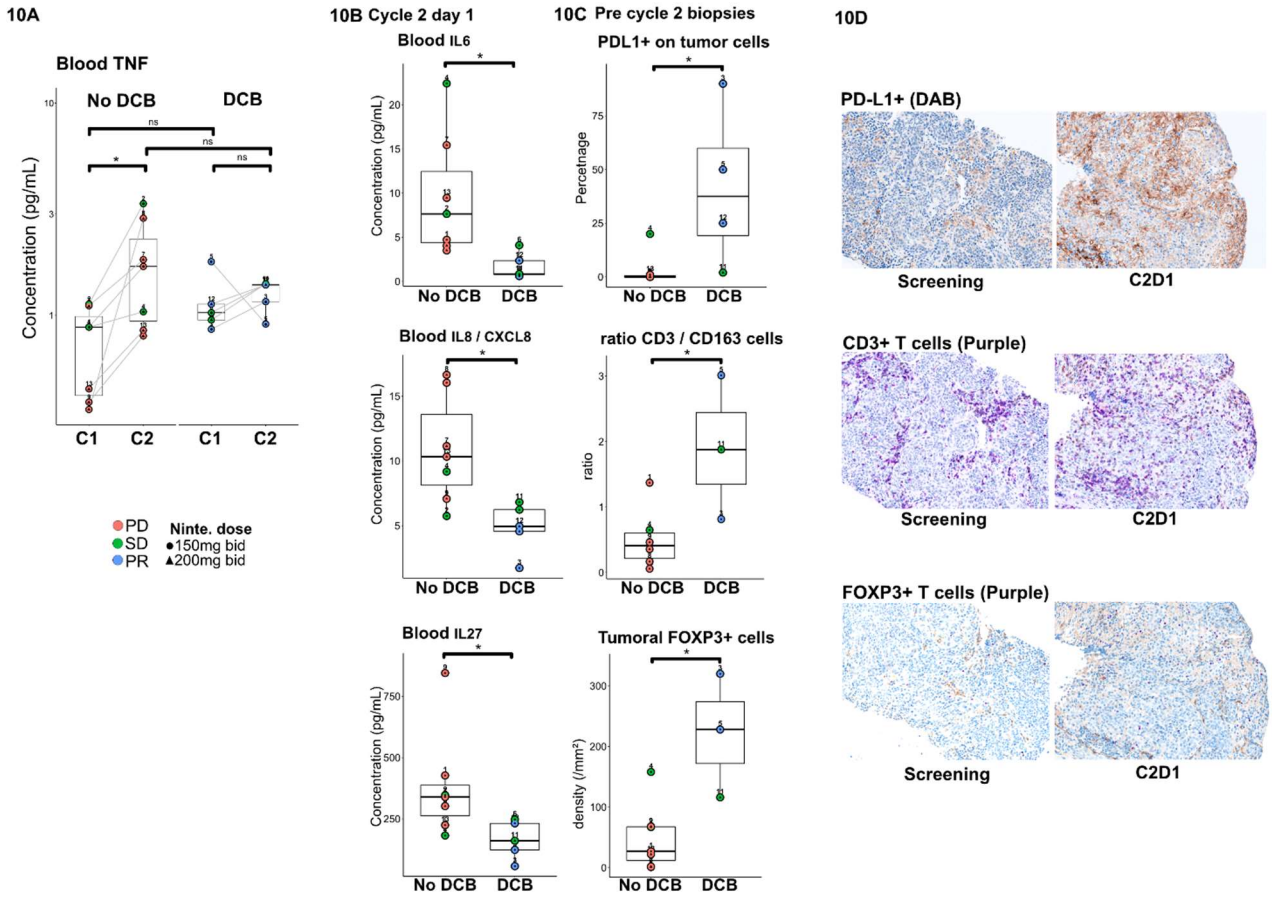

FIGURE 10. AFTER PEMBROLIZUMAB INFUSION, IN ASSOCIATION WITH NINTEDANIB TREATMENT, CIRCULATING AND TUMOR MICROENVIRONMENT CHANGES WERE ASSOCIATED WITH DISCTINCT CLINICAL OUTCOMES (DOSE ESCALATION).

10A. PLASMA LEVELS OF SOLUBLE TNF INCREASED IN PATIENTS WITHOUT DCB BETWEEN C1D1 (0.7PG/ML [RANGE: 0.4-1.1]) AND C2D1 (1.8PG/ML [RANGE: 0.8-3.4]) (PAIRED WILCOXON SIGNED RANK TEST; P=0.015) INSTEAD OF IN PATIENTS WITH DCB. 10B. PLASMA RATE OF IL6, IL8 AND IL27 WERE SIGNIFICANTLY HIGHER AT C2D1 IN PATIENTS WITHOUT DCB (9.6PG/ML [RANGE: 3.5-22.4], 10.8PG/ML [RANGE: 5.8-16.7] AND 380.9PG/ML [RANGE: 181.8-845.2] , RESPECTIVELY) THAN THOSE WITH DCB (1.7PG/ML [RANGE: 0.6-4.14], 4.9PG/ML [RANGE: 1.7-6.8] AND 163.9PG/ML [RANGE: 56.6-247.4], RESPECTIVELY) (NON-PARAMETRIC WILCOXON RANK SUM TEST; P=0.01, P=0.01 AND P=0.03, RESPECTIVELY). 10C. PERCENTAGE OF PDL1+ TUMOR CELLS, RATIO OF CD3+ PER CD163+ CELLS AND FOXP3+ CELLS DENSITY IN BIOPSIES OF PATIENTS WITH DCB (41.8% [RANGE: 2-90], 1.9 [RANGE: 0.8-3] AND 221/MM^2 [RANGE: 116-320], RESPECTIVELY) WAS HIGHER THAN PATIENTS WITHOUT DCB (3% [RANGE: 0-20], 0.5 [RANGE: 0.06-1.4] AND 49/MM^2 [RANGE: 1-158], RESPECTIVELY) AT C2D1 (NON-PARAMETRIC WILCOXON RANK SUM TEST; P=0.009, P=0.047 AND P=0.03, RESPECTIVELY). 10D. ILLUSTRATION OF INCREASED EXPRESSION OF PDL1 AT TUMOR CELL'S SURFACE, CD3+ AND FOXP3+ T CELLS INFILTRATION IN TUMOR MICROENVIRONMENT OBSERVED WITH IHC ANALYSIS (PATIENT #3).

This phase 1b dose escalation cohort showed that the toxicity of the nintedanib and pembrolizumab combination was manageable and consistent with the safety profile of each drug and did not seem to generate higher toxicity than the cumulative impact of each compound. The RP2D for the combination was defined as nintedanib 150mg bid and flat dose of pembrolizumab 200mg IV and is currently being investigated in multiple expansion cohorts The main toxicity of this combination therapy was liver enzymes increase, which is consistent with other combination of immune checkpoint inhibitors and antiangiogenic TKIs. The incidence of drug-related grade 3 liver enzymes elevation was 33% for alanine aminotransferase and 25% for aspartate aminotransferase in our study. Other combinations of anti PD-1 monoclonal antibody and antiangiogenic TKI reported variable liver toxicity: nivolumab/sunitinib, nivolumab/pazopanib, pembrolizumab/pazopanib and pembrolizumab/axitinib reported 18%, 20%, 60-70% and 8% of grade 3–4 elevated alanine aminotransferase, respectively (6,324,330). In the dose escalation trial of nintedanib monotherapy, the DLTs were grade 3 or 4 liver enzyme elevations (2-5%), all reversible upon drug interruption (287). The adverse events reported in this study seem to be mostly related to nintedanib, but programmed death 1 blockade could possibly enhance the on-target off-tumor side effects of the TKIs. The observed levels of immune related adverse events such as colitis (8%), nephritis (8%) and thyroiditis (25%) were in line with the expected irAE associated with pembrolizumab monotherapy. Thromboses were observed in two patients: one with superior mesenteric artery thrombus and both with thrombus on catheter in superior vena cava. These adverse events could be related to the combination of antiangiogenic TKI with immune checkpoint blockade and not to nintedanib alone. These two patients with thromboses obtained a durable clinical benefit (SD and PR, respectively during at least 6 months). Overall, the antitumor activity of the combination tested was promising with an ORR of 25% in this all-comer cohort and will be confirmed in the expansion cohorts of the study.

Baseline ancillary analyses highlighted those patients who developed DCB to this anti-angiogenic / ICB combination presented with both preexisting immune and angiogenic features. Higher expression of CXCL10 and immune infiltrate in biopsies were previously associated with ICB monotherapy efficiency in different tumor types (12,331). It was interesting to observe that soluble Tie2 was higher in plasma of patients with DCB. Tie2 is the receptor of angiopoietin-2, expressed at surface of endothelial cells but also circulating monocytes (332). Studies highlighted that Tie2 production and membrane shedding are increased by hypoxia and induced by VEGF (333). Here, Tie2 plasmatic rate could be a witness of hypoxia occurring in the tumor of patients who benefited from the treatment.

After seven days of nintedanib monotherapy, quick changes were observed in patients who benefited from the treatment. Although those could be spontaneous changes favored by different tumor changes, their rapid evolution suggest

that they could be induced by nintedanib. Particularly, the increase of plasmatic CCL3/MIP-1α in patients with DCB could be a consequence of tumor hypoxia on chemokine production (334). At baseline, a higher Tie2 plasmatic rate, along with higher proportions of circulating Tregs, and conventional helper memory T cells which co-expressed CCR4 and CXCR3 (receptors of CCL22/MDC, CCL3/MIP-1α and CXCL10 respectively) were also predictive of DCB. Blood Tregs constitutively express CCR4 on their surface (335). CCL22 production by tumor cells was identified as a mechanism of immune escape in breast cancer, through $CCR4^+$ Treg recruitment in the tumor microenvironment (TME), induced by IFNγ exposure (336,337). These observations led to the development of CCR4 antagonists as antitumoral immunotherapy (338,339). Our results suggest that Treg recruitment in the TME was associated with a higher infiltration of immune cells, particularly DC-$LAMP^+$ dendritic cells and T cells, associated with a pre-existing anti-tumoral immune response, sensitive to immune checkpoint blockade.

However, patients without DCB developed others significant changes after one week of nintedanib monotherapy. They seemed to present an increasing plasma rate of PlGF as of patients with DCB. This soluble angiogenic factor was recently implicated in interactions between angiogenesis, Th17 polarization of $CD4^+$ T cells and autoimmunity (340). This observation should be associated with changes induced further by anti PD-1 blockade. Patients with tumor progression and resistance to treatment presented then with an increasing plasma rate of IL17A and TNF after the first infusion of pembrolizumab, in comparison to patients with DCB. Patients without DCB had also a higher plasma rate of IL-6, IL-8/CXCL8 and IL-27 at C2D1 than patients who had benefited from treatment. Increased rates of both IL-6 and IL-8/CXCL8 have been described to be associated with resistance to anti-PD1 blockade monotherapy (341,342). Of note, the baseline plasma rates of these cytokines were not significantly different between patients with or without DCB outcome.

Conclusion

Nintedanib 150mg bid is the RP2D for combination with pembrolizumab and is being currently investigated in multiple expansion cohorts. Early immune biomarkers in the tumor and in the blood were associated with the efficacy of the nintedanib + pembrolizumab combination therapy. Our biological findings at baseline and during the early phases of treatment, associated significantly with the clinical benefit to treatment or to primary tumor progression, suggesting that patients could be selected on their tumor biology rather than their cancer histology in order to benefit from such anti-angiogenic and immune targeted therapies.

Supplementary Figures.

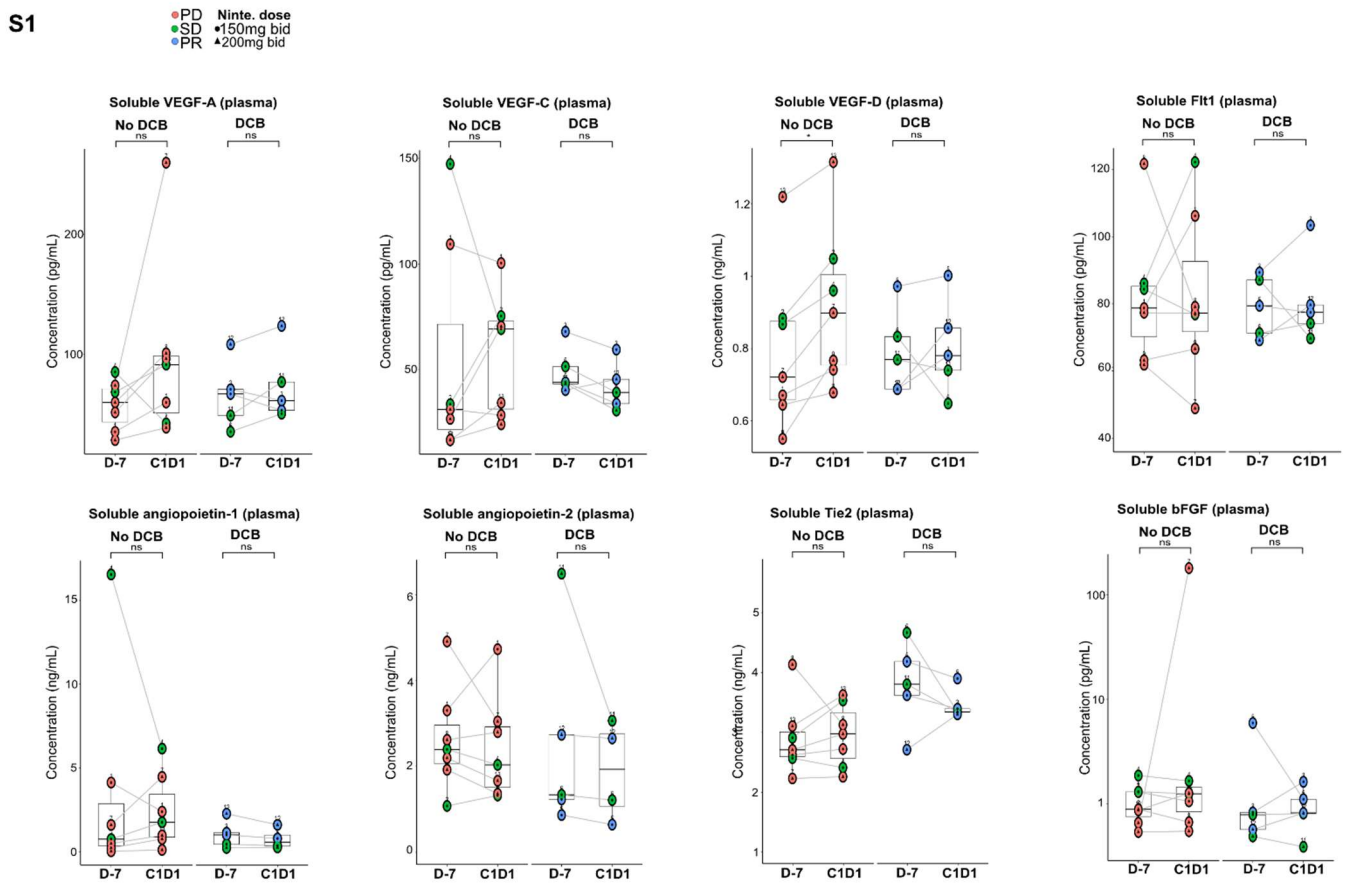

SUPPLEMENTARY FIGURE 1. EVOLUTION OF PLASMA SOLUBLE ANGIOGENIC FACTORS DURING LEAD-IN NINTEDANIB MONOTHERAPY (DOSE ESCALATION).

TESTS WERE PAIRED WILCOXON SIGNED RANK TEST (PAIRED SAMPLES) (REPRESENTATION OF P-VALUE: NS >0.05, * ≤ 0.05).

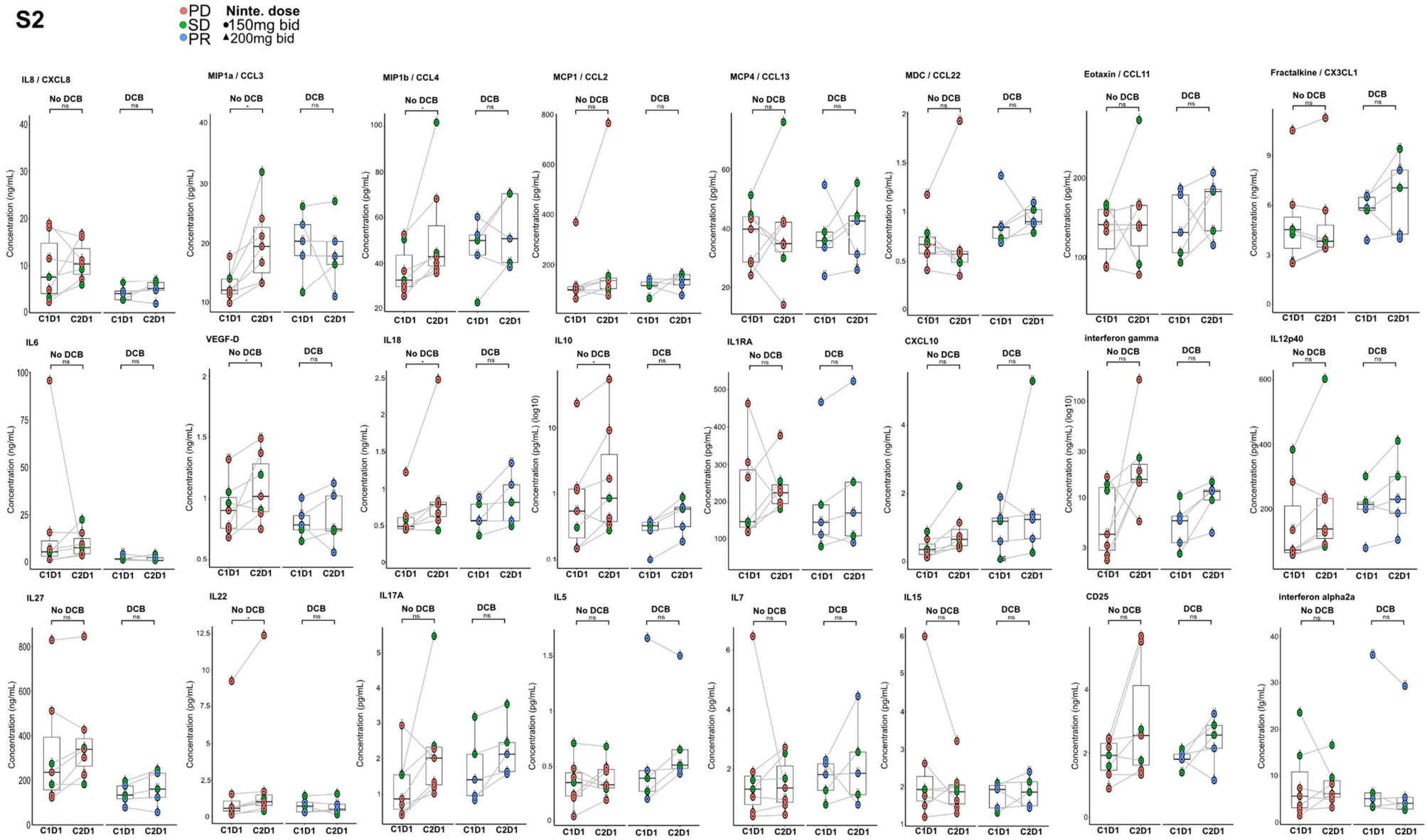

SUPPLEMENTARY FIGURE 2. EVOLUTION OF PLASMA SOLUBLE CYTOKINES AFTER THE FIRST INFUSION OF PEMBROLIZUMAB (DOSE ESCALATION).

TESTS WERE PAIRED WILCOXON SIGNED RANK TEST (PAIRED SAMPLES) (REPRESENTATION OF P-VALUE: NS >0.05, * ≤ 0.05).

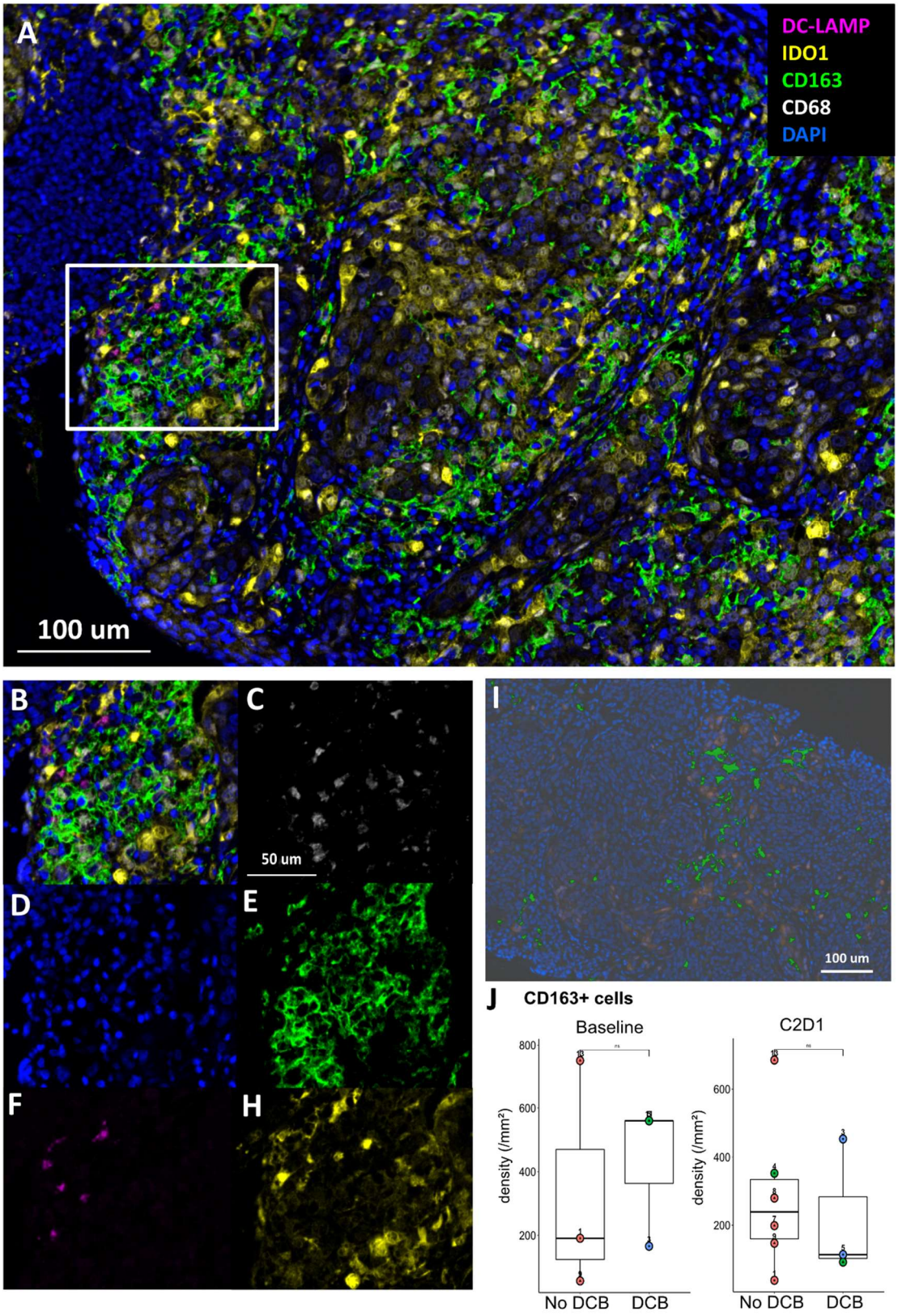

SUPPLEMENTARY FIGURE 3. ILLUSTRATION OF MULTIPLEX CHROMOGENIC STAINING DEDICATED TO MYELOID CELLS.

3A. REPRESENTATIVE IMAGE DISPLAYS A 500UMX669UM IMAGE AFTER MULTISPECTRAL IMAGING AND SPECTRAL UNMIXING (MERGED IMAGE). 3B. ALL MARKERS. 3C. CD68 (PSEUDOCOLOURED WHITE). 3D. DAPI NUCLEAR MARKER (PSEUDOCOLOURED BLUE). 3E. CD163 (PSEUDOCOLOURED GREEN). 3F. DC-LAMP (PSEUDOCOLOURED MAGENTA). 3G. IDO1 (PSEUDOCOLOURED YELLOW). 3H. CD163 MEASUREMENT WAS UNDERTAKEN USING INFORM V2.2 SOFTWARE SEGMENTATION BY PIXEL-BASED THRESHOLD. 3I. $CD163^{+}$ DENSITY IN BIOPSIES OF PATIENTS WITH DCB OR WITHOUT DCB AT BASELINE AND C2D1 WERE NOT SIGNIFICANTLY DIFFERENT (WILCOXON RANK-SUM TEST).

Somatic Copy Number Alterations are associated with inflammation and primary resistance to pembrolizumab plus nintedanib in patients with advanced mesotheliomas .

Francois-Xavier Danlos[1,2,3], Capucine Baldini[1], Matthieu Texier[4], Andreea Varga[1], Audrey Rabeau[5], Bastien Job[6], Kevin Mulder[2,3], Andrei Iurchenko[7], Severine Mouraud[2], Lydie Cassard[8], Yuna Blum[9], Stéphane Champiat[1], Diane Letourneur[2,10], Delphine Bredel[2], Sandrine Susini[2], Aurelien Parpaleix[11], Cedric Parlavecchio[11], Lambros Tselikas[2,3,12], Jean-Eudes Fahrner[2], Anne-Gaelle Goubet[2,3], Mathieu Rouanne[2,3], Saloomeh Rafie[1], Alae Abbassi[1], Ines Kasraoui[12], Marie Breckler[13], Siham Farhane[1], Samy Ammari[12], Salim Laghouati[14], Anas Gazzah[1], Ludovic Lacroix[15], Benjamin Besse[16], Nathalie Droin[13], Marc Deloger[6], Sophie Cotteret[17], Julien Adam[18], Sergei Nikolaev[7], Florent Ginhoux[2], Camille Bleriot[2], Laurence Zitvogel[2,3], Nathalie Chaput[8,19], Christophe Massard[1], Jean-Charles Soria[20], Gomez Roca Carlos[5], Gerard Zalcman[21], David Planchard[16], Aurelien Marabelle[1,2,3].

Affiliations:

1. Département d'Innovation Thérapeutique et d'Essais Précoces (DITEP), Gustave Roussy, Villejuif, France.
2. INSERM U1015, Gustave Roussy, Villejuif, France.
3. Faculté de Médecine, Université Paris Saclay, Kremlin-Bicetre, France
4. Département de Biostatistiques, Gustave Roussy, Villejuif, France.
5. Institut Universitaire Oncologie Thoracique, CHU Larrey, Toulouse, France.
6. Département de Bioinformatique, CNRS-UMS 3655 and INSERM-US23, Gustave Roussy, Villejuif, France.
7. INSERM U981, Cancer Genomics Lab, Gustave Roussy, Villejuif, France.
8. Laboratoire d'Immuno-Oncologie (LIO), CNRS-UMS 3655 and INSERM-US23, Gustave Roussy, Villejuif, France.
9. IGDR / CNRS UMR6290, Gene Expression and Oncogenesis, Faculté de Médecine, Rennes, France.
10. Ecole Normale Supérieure, Université de Lyon, Lyon, France.
11. Service de Promotion des Etudes Cliniques, Gustave Roussy, Villejuif, France.
12. Département de radiologie, Villejuif, France.
13. Unité de Génomique Fonctionnelle, CNRS-UMS 3655 and INSERM-US23, Villejuif, France.
14. Unité Fonctionnelle de Pharmacovigilance, Villejuif, France.
15. Département de Biologie et Pathologie médicales, Plateforme de Biopathologie Moléculaire, CNRS-UMS 3655 and INSERM-US23, Villejuif, France.
16. Département de Médecine Oncologique, Gustave Roussy, Villejuif, France.

17. Laboratoire de cytogénétique, Gustave Roussy, Villejuif, France.

18. Service d'Anatomo-Pathologie, Hopital Paris Saint-Joseph, Paris, France.

19. Faculté de Pharmacie, Université Paris Saclay, Chatenay Malabry, France

20. Amgen, Thousand Oaks, CA, USA.

21. Service de pneumologie, Hopital Bichat, APHP, Université de Paris, Paris, France.

Abstract.

Background: the PEMBIB study (NCT02856425) is a multi-cohort Phase Ib trial evaluating the safety and efficacy of the combination of an anti-angiogenic tyrosine kinase inhibitor (nintedanib) with an anti-PD1 immunotherapy (pembrolizumab). Here we report the results from an expansion cohort dedicated to patients with unresectable malignant mesothelioma, refractory to a first line platinum-based chemotherapy. Ancillary analyses were performed to identify biomarkers associated with efficacy or primary resistance.

Methods: Patients with unresectable mesothelioma relapsing after at least one line of platinum-based chemotherapy were treated with a combination of oral nintedanib (150mg BID) & IV pembrolizumab (200mg Q3W), with a 7 days nintedanib lead-in preceding pembrolizumab initiation. Immune cells, cytokines, chemokines & soluble factors were prospectively measured in baseline and on-treatment fresh tumor biopsies & blood samples by flow cytometry and multiplexed immuno-assays. RNA-sequencing and whole exome sequencing were run on tumor samples, single cell RNAseq on blood samples.

Results: 30 patients received at least one infusion of pembrolizumab combined with oral nintedanib. Median age of patients was 68 years old (38-85) and 86% had epithelioid mesothelioma. The most frequent adverse events (AE) (grades 1-3) related to the combination were liver enzymes increase, fatigue, nausea, and diarrhea. Four (13.3%) patients developed grade 3-5 immune- related AE. Patients died of cancer progression (n=14), myocarditis with thrombo-embolic event (n=1) and COVID-19 (n=1). Median follow-up was 14.8 months (95%CI [9.70-18.2]). Best objective response rates (BOR) were Partial Response (PR; n=7/29; 24.1%), Stable Disease (SD; n=17/29; 58.6%) and Progressive Disease (PD; n=5/29; 17.2%). Disease Control Rate (DCR; defined as PR + SD) was 68.4% and 46.6% at 12 and 24 weeks, respectively.

Patients with durable clinical benefit (DCB), without progressive disease before 6 months, had significantly higher percentages of PDL1 expression on tumor cells and higher CD8+ T cells infiltrate in tumor biopsies, evaluated by flow cytometry at screening. Upon treatment, soluble plasma rate of CXCL9 and CXCL13 as well as tumor immune infiltrates estimated by deconvolution of tumor biopsies RNA-seq increased in all patients independently from clinical benefit. Transcriptomic estimates of NK cells, T cells and myeloid dendritic cells infiltrates in baseline and C2D1 tumors biopsies were higher in patients with DCB. Pre & on-treatment IL6 and IL8 levels in tumor biopsies supernatant & blood plasma were higher among patients with early progression. Gene Set Enrichment Analyses on RNA-seq from screening tumor biopsies found an enrichment in E2F, MYC and KRAS gene pathways and lower expression of type 1 interferon signature in patients with early progressive disease than those with clinical benefit. Aneuploidy, or tumor somatic copy number

alteration, was higher in patients without DCB and positively correlated with inflammatory and immunosuppressive pattern.

Conclusion: Pembrolizumab and nintedanib combination provided valuable therapeutic benefits for patients with refractory to chemotherapy unresectable mesothelioma, with a BOR of 24% and a DCR of 47% at 6 months. Mesothelioma tumors that are refractory to immunotherapy display higher aneuploidy at baseline, which is positively associated with tumor stroma and systemic inflammatory patterns and recruitment of immunosuppressive inflammatory innate cells in tumors.

KEY WORDS: pembrolizumab, nintedanib, angiogenesis, PD-1 blockade, platinum-based chemotherapy refractory, unresectable pleural mesothelioma, aneuploidy, inflammation, monocyte.

Unresectable malignant mesothelioma (MM) is a peculiar cancer, developed from pleural linings, upon chronic airways inhalation of environmental silicate mineral such as asbestos (343). Chronic exposure to asbestos microparticles leads to pleural inflammation, recruitment of inflammatory macrophages, development of an immunosuppressive pro tumoral microenvironment, constitution of pathological neoangiogenesis with hypoxia and eventually pleural cells malignant transformation (344).

Targeting the tumor microenvironment (TME) with immune checkpoint blockers or antiangiogenic drugs, has shown significant activity in several metastatic cancers. Angiogenesis contributes to tumor growth and the development of metastases but the modulation of neo-angiogenesis via inhibition of the VEGF/VEGFR pathway has shown anti-tumor activity in several human solid cancers (345). Also, blocking immune checkpoints with antagonistic monoclonal antibodies targeting Programmed death-1 receptor (PD-1) and its ligand (PD-L1) have been extensively investigated in the recent past and are still in active development across malignancies (1). Combining anti-angiogenic drugs and anti-PD-(L)1 antibodies has recently shown important synergistic results in RCC and HCC (318–320). Indeed, anti-VEGF therapies may enhance anti PD-1/PD-L1 efficacy by reversing VEGF-mediated immunosuppression and promote T-cell infiltration in tumors (19). Both anti-angiogenic and immune checkpoint blockers have shown activity in advanced pleural mesothelioma. Bevacizumab, an IgG1 monoclonal antibody targeting VEGFA, in association with platinum-based regimen chemotherapy, increases the overall survival of patients with untreated unresectable pleural mesothelioma, compared to chemotherapy alone (75). Moreover, the combination of both anti PD-1 and anti CTLA-4 monoclonal antibodies significantly improves the survival of patients with untreated unresectable pleural mesothelioma, compared to standard of care chemotherapy (74).

We aimed to determine the safety and efficacy of nintedanib, an oral triple receptor tyrosine kinase inhibitor (TKI) of PDGFRα/β, FGFR1-3, and VEGFR1-3, in combination with pembrolizumab, a humanized IgG4 anti-PD1 monoclonal antibody in patients with unresectable mesothelioma naïve to immunotherapy, previously treated by at least one line of platinum-based chemotherapy regimen (NCT02856425).

Study design

In this expansion cohort of the phase Ib clinical trial PEMBIB (NCT02856425), we evaluated the association of nintedanib (150 mg BID) in combination with IV flat dose of pembrolizumab 200 mg over 30 minutes Q3W. The posology of nintedanib was first determined in a dose escalation cohort, which showed that nintedanib at 150mg BID was better tolerated than 200mg BID, and subsequently selected for the expansion cohorts. Of note, patients received a one-week lead-in course of nintedanib monotherapy prior to starting pembrolizumab. The protocol was first approved by the Agence Nationale de Sécurité du Médicament (ANSM) on June 24th 2016 (Ref #160371A-12). The protocol was also approved by the Ethical Committee (Comité de Protection des Personnes Ile de France 1) on Jul 12th 2016 (Ref #2016-mai-14236ND). The trial was first posted on clinicaltrials.gov on Aug 4th 2016 (NCT02856425).

Patients

Eligible patients had advanced pleural mesothelioma who progressed after at least one line of standard therapy, naïve to immune checkpoint blockade and nintedanib. Additional inclusion criteria included age ≥ 18 years, Eastern Cooperative Oncology Group (ECOG) performance status of 0-1, adequate organ function, measurable disease according to RECIST v1.1 criteria, and written informed consent. Key exclusion criteria were radiographic evidence of cavitary tumors, local invasion of major blood vessels and/or at risk for perforation, history of clinically significant hemoptysis within the past 3 months, history of clinically significant hemorrhagic or thromboembolic event in the past 6 months, history of significant cardiovascular diseases, prior treatment with nintedanib and anti PD-(L)1 agents, concurrent steroid medication, history of autoimmune and inflammatory disease. This study was conducted in compliance with the Declaration of Helsinki and the International Ethical Guidelines for Biomedical Research Involving Human Subjects.

Procedures

Screening procedures were performed up to 21 days (D-28) before Day -7 (start of nintedanib). Patients continued treatment until disease progression, undue toxicity, withdrawal of consent or for a maximum duration of 24 months. Adverse events were graded using National Cancer Institute (NCI) CTCAE Version 4.03. Tumor responses were evaluated every 6 weeks based on Response Evaluation Criteria in Solid Tumors (RECIST) 1.1 (327,328).

Outcomes

The objectives of the trial were to determine the tolerability and safety of oral nintedanib 150mg BID combined with IV pembrolizumab 200mg Q3W and to evaluate the first efficacy signals with RECIST 1.1 best objective response rate (BOR), progression free survival (PFS), overall survival (OS) of this combination in a dedicated cohort of advanced MM. The aim of the ancillary studies was to identify predictive biomarkers of efficacy or resistance to this combination therapy.

Analyses of tumor infiltrating immune cells from biopsies by flow cytometry

Fine-needle biopsy samples from tumoral lesions were immediately placed into 1ml of NaCl 0.9%. After a minimum of 30 minutes of incubation, the supernatant of fresh tumor biopsies in 0,9% NaCl was collected and frozen at -80°C and biopsies were mechanically dissociated with the top of a 2ml syringe plunger in a wet 70µm filter placed at the top of a 50ml centrifuge tube. Isolated cells were washed by centrifugation and re-suspended in NaCl 0.9% for cell surface staining protocol. Cells were stained with anti-CD3/BUV395 (clone UCHT1; ref. 563546, BD Biosciences), anti CD4/BUV496 (clone SK3, ref. 564651, BD Biosciences), anti CD45/BUV805 (clone HI30, ref. 612891, BD Biosciences), anti PD1/BV421 (clone MIH4, ref. 564323, BD Biosciences), anti OX40/BV650 (clone ACT35, ref. 563658, BD Biosciences), anti CD39/FITC (clone TU66, ref. 561444, BD Biosciences), anti HLA-DR/PerCP5.5 (clone G46-6, ref. 551764, BD Biosciences), anti CTLA4/PE (clone BNI3, ref. 555853, BD Biosciences), anti 41BB/PECF594 (clone 4B4-1, ref. 309826, BD Biosciences), anti CD25/PECy7 (clone B1.49.9, ref. A52882, Beckmann Coulter), anti TIGIT/APC (clone MBSA43, ref. 17-9500-41, Biolegend), anti HLA-ABC/AF700 (clone W6/32, ref. 311438, Biolegend), anti CD8/APC-H7 (clone SK1, ref. 560179, BD Biosciences) and Zombie Aqua™ Fixable Viability (ref. 423101, Biolegend). CTLA-4 was first stained at 37°C for 20min before others surface antibodies were added and incubated at 4°C for 15 min. Then, cells were washed two times and acquired on an 18-colors flow cytometer BD Fortessa X20 (BD Biosciences). Data were acquired in FCS 3.0 format and analyzed with KALUZA software version 2.1.

Immune monitoring – Fresh blood immune phenotype

For every patient, heparinized blood samples (30-40 mL) at day -7 (baseline), C1D1 and C5D1 were collected whenever possible for monitoring circulating immune populations by flow cytometry. Fresh whole blood phenotyping of T-cell migration, T-cell polarization, T-cell activation, Treg function and myeloid cells was performed using 5 specific panels, as previously described (329). Stained cells were acquired using a Gallios Cytometer (Beckman Coulter) and analyzed using Kaluza software (Beckman Coulter).

Cytokine, chemokine and soluble angiogenic factors measurements

Serum IL6 quantification was performed with Siemens Atellica IM1600 and Atellica IM Interleukin-6 kit (Siemens Healthineers, Saint-Denis, France) validated by Gustave Roussy accredited diagnostic laboratory. Quantification method validation was performed according to ISO15189 recommendation. The quantification range covers from 2.7 (limit of quantification) to 5500 pg/ml. Any quantification batches included 3 levels of internal quality control analysis.

Frozen plasma and frozen tumor biopsy supernatants were subsequently thawed, centrifuged for 15 min at 1,000 g, then titrated using Bio-Plex Pro™ Human Chemokine Panel (40-Plex, ref. 171AK99MR2, Bio-rad), Angiogenesis Panel 1 (human) (ref. K151P3S-1, Meso Scale Discovery), Human PD-1 and PD-L1 antibody sets (ref. F214A-3 & F214C-3, Meso Scale Discovery) following manufacturer's instructions. Each plasma sample was run twice with the average value of the doublet taken as the result. Acquisitions were done on Bio-Plex 200TM System and MESO™ QuickPlex SQ120 readers. Raw data from Meso Scale Discovery's kit were analyzed with MSD's Discovery Workbench 4.0.

Immuno-Histo-Chemistry staining

Immuno-Histo-Chemistry (IHC) chromogenic staining were performed on formalin fixed paraffin embedded (FFPE) tumor biopsies. PD-L1 (DAB) single chromogenic staining were performed using the Ventana Benchmark Ultra platform. CD3 (Purple)/CD8 (DAB) multiplex and CD20 (DAB) chromogenic staining were performed using the Ventana Discovery Ultra platform. Images were selected by a Pathologist, Hematoxylin and Eosin (HES) stained slides were used to validate that FFPE tumor locks were tumor-associated tissue.

Whole-transcriptome RNA-seq

Integrity (RNA Integrity Score≥7.0) of RNA extracted from frozen tumoral biopsies was checked on the Agilent 2100 Bioanalyzer (Agilent) and quantity was determined using NanoDrop (Thermofisher Scientific). SureSelect Automated Strand Specific RNA Library Preparation Kit was used according to the manufacturer's instructions with the Bravo Platform. Briefly, 50 to 200ng of total RNA sample was used for poly-A mRNA selection using oligo (dT) beads and subjected to thermal mRNA fragmentation. The fragmented mRNA samples were used for cDNA synthesis and were further converted into double stranded DNA using the reagents supplied in the kit, and the resulting dsDNA was used for library preparation. The final libraries were bar-coded, purified, pooled together in equal concentrations and processed for paired-end 2x100 sequencing on Novaseq-6000 sequencer (Illumina) at Gustave Roussy.

Bulk Tumor RNA-seq analyses

The QC and analysis pipeline was based on Love et al, powered by SnakeMake (346,347). Quality controls were performed on raw FastQ files with FastQC v0.11.9. Reads trimming for low 3' terminal base quality and removing of adapter sequences was performed using fastp v0.20.1. Sample contamination was assessed with FastqScreen v0.14.0. Quality reports were gathered with MultiQC v1.9 (348). Abundance estimation was performed with Salmon v1.4.0, using 100 bootstraps and the GenCode v34 annotations, corresponding to the GRCh38 genome build (349). Aggregation was performed with the tximport package, and differential gene analysis was performed with DESeq2, with a formula design taking care of the sample effect when sample pairs (Screening/C2J1) were taken into consideration (350)**.** Deconvolution of immune cell fractions from bulk RNA sequencing data was done with immunedeconv package (351)**.** Gene set enrichment and overall representation analyses (GSEA/ORA) were performed with the clusterProfiler package v4.0.2, against the MsigDb collections, the Disease Ontology, and the KEGG, CellMarker and MeSH databases (352). For quality control, the variance stabilizing transformation (vst) normalization from DESeq2 was applied on raw counts. Of note, RNA-seq data from baseline biopsies without tumor cells were not integrated in the analyses, and the data from baseline pleural biopsy of patient #23, who had a peritoneal progression before 6 months, was considered in the "DCB" group because of a primary and persistent complete response of pleural lesions (**Supplementary figure 4**).

Tumoral and germline whole exome sequencing (WES)

50 to 200 ng of genomic DNA was extracted from frozen tumor biopsies with the Covaris E220 system (LGC Genomics / Kbioscience). DNA fragments were end-repaired, extended with an 'A' base on the 3' end, ligated with paired-end adaptors with the Bravo Platform (Agilent) and amplified (ten cycles). Exome-containing adaptor-ligated libraries were hybridized for 40 h with biotinylated oligo RNA baits using SureSelect Clinical Research 2 (Agilent), and enriched with streptavidin-conjugated magnetic beads. The final libraries were indexed, pooled and sequenced using the onboard cluster method, as paired-end sequencing (2x100 bp reads) on Illumina NovaSeq-6000 sequencer at Gustave Roussy.

Whole exome sequencing analyses

Identification of mutations and individual somatic copy number alteration were done with following methods. Reads were mapped using BWA-MEM (v0.7.12) software (353) to the GRCh37 human reference genome and then we used the standard GATK best practice pipeline (354) to process the samples and call somatic genetic variants. PCR duplicates were removed and base quality score recalibrated using MarkDuplicates and BaseRecalibrator tools which a part of the GATK package (355). Somatic SNVs and INDELs were called and filtered using GATK tools Mutect2, FilterMutectCalls and

FilterByOrientationBias and annotated with oncotator (356). SCNAs calling was done with FACETS software using only regions with at least 20 reads coverage in both tumor and normal samples (357). Quality controls of FASTQ and mapping were done with FASTQC, samtools (v1.9), GATK HSmetrics and multiqc (348,358,359). The processing steps were combined in a pipeline built with snakemake (360). Somatic mutations with PASS flag from GATK Mutect2 were additionally filtered to have at least 1 supporting reads from each strand and 3 reads in total. We used then MAF annotator to find oncogenic mutations from OncoKB database and visualized them as an oncoplot with the *maftools* R package (361). Tumor mutational burden of the samples was calculated in accordance with the guidelines proposed by the "Friends of Cancer Research TMB Harmonization Project" (260).

Identification of copy-number anomalies were performed using EaCoN v0.3.6 (https://github.com/gustaveroussy/EaCoN) on R v3.6.2. Per-patient paired samples were analyzed using tumoral samples as test, and genomic DNA from PBMCs used as reference, for each pair. GATK-recalibrated BAM files were transformed to the mpileup format using Rsamtools v2.8.0, ignoring replicates and secondary alignments (362). Log2ratio (L2R) data, mpileup profiles were binned to windows of 50 nt in median (depending on the capture BED information), and bins with a total depth < 20 were discarded. Using a pre-generated track of GC% content in bins, those with a value <20% or > 80 were identified as outliers. L2R depths was computed for each bin, and linearly imputed for GC% outliers. L2R was then normalized for GC% using a local regression. To generate the BAF data, any non-reference sequences in the mpileups were identified and their depth quantified (363). SNP variants supported by less than 3 reads and/or for which the total depth was below 20 were discarded. All SNP variants in the test sample with a reference frequency below 33% were discarded. The bivariate (L2R and BAF) data were then segmented, evaluated for their allele-specific absolute copy-number, as well as ploidy and tumor cellularity, using ASCAT v2.5.2.

Single cells RNA-seq analyses of peripheral blood mononuclear cells (PBMC)

Frozen PBMC from pre-treatment (time point "day -7") samples of patients (n=10) and healthy controls (n=2) were thawed in "Medium" constituted by RPMI Medium 1640 (ref. 61870-010, Life Technologies Limited) with 10% decomplemented HyClone™ Fetal Bovine Serum (FBS) (ref. 12389802, Thermo Fisher), 1% Penicillin/Streptomycin and 1% Sodium Pyruvate (ref. 11360-039, Life Technologies Limited). Viable cells enrichment was done by negative selection with magnetic beads (Dead Cell Removal Kit™; ref. 130-090-101, Miltenyi Biotec) following manufacturer's instructions. Cells were suspended at 1.10^6 cells/mL in PBS.

For the Rhapsody experiment, all the process was done by following manufacturer's (BD Biosciences) protocol. 7,239 cells were captured in a single run with 12 barcoded samples pooled together. The sample was processed according to BD mRNA targeted and sample tag library preparation with the BD Rhapsody Immune response (Human) amplification kit. Samples were then subjected to an indexed paired-end sequencing run of 2x151 cycles on an Illumina HiSeq 4000 system (Illumina, San Diego, CA, USA) with 20% PhiX spike in. Targeted transcriptomics Fastq files were processed via the standard Rhapsody analysis pipeline (BD Biosciences)) per the manufacturer's recommendations. First, R1 and R2 reads are filtered for high-quality reads, dropping reads too short (less than 66 bases for R1 and 64 bases for R2) or have a base quality score of less than 20. R1 reads are annotated to identify cell label sequences and unique molecular identifiers (UMIs), and R2 reads are mapped to the respective reference sequences using Bowtie2. Finally, all passing R1 and R2 reads are combined and annotated to the respective molecules. For quality control of the reads, recursive substation error correction (RSEC) and distribution-based error correction (DBEC) were applied, which manufacturer-developed algorithms are correcting for PCR and sequencing errors. For determining putative cells (which will contain many more reads than noise cell labels), a filtering algorithm takes the number of DBEC-corrected reads into account, calculating the minimum second derivative along with the cumulative reads as the cut-off point. Finally, the expression matrix was obtained from the DBEC-adjusted molecule counts in a CSV format. A cell is determined as a singlet if the minimum read count of a single sample tag is above the threshold of 75%. A cell is classified as a multiplet if the cell exceeds the threshold for more than one sample tag. A cell that does not meet the threshold is labelled as undetermined. Both multiplets and undetermined cells were excluded from the analysis as described below.

For downstream analysis, Seurat V4 was used (364). Counts were normalized, and PCA analysis was performed. Using these variable features, a UMAP was generated. Clustering was performed using SNN nearest-neighbour analysis. Differentially expressed genes were identified by a threshold of FDR below 0.05 and logFC below -0.25 or above 0.25.

Analyses of peripheral blood mononuclear cells by flow cytometry

Frozen PBMC from pre-treatment (time points "day -7" [n=19]) samples of patients and healthy controls (n=3) were thawed in "Medium" (see above). Cells were suspended at 1.10^6 cells/mL in PBS with 2% Bovine Serum Albumin (ref. A7030-100G, Sigma) and 2mM EDTA (ref. 15575-038, Invitrogen) (PBS+). Five hundred thousand cells were washed and suspended in 200mL of PBS+. Fcγ-receptors blocking was done adding 5uL Human TruStain FcX™ (ref. 422302, Biolegend), 10min at 4°c then cells were stained with anti CD3/BUV396 (clone UCHT1, ref. 563546, BD Biosciences), anti HLA-DR/BUV737 (clone G46-6, ref. 748339, BD Biosciences), anti CD45/BUV805 (clone HI30, ref. 612891, BD Biosci-

ences), anti CD16/BV421 (clone 3G8, ref. 302038, Biolegend), anti CCR2/BV650 (clone LS132.1D9, ref. 747849, BD Biosciences), anti CD32/BV711 (clone FLI8.26, ref. 564839, BD Biosciences), anti CD14/BV785 (clone M5E2, ref. 301839, Biolegend), anti CD163/AF647 (clone GHI/61, ref. 562669, BD Biosciences), anti TREM1/FITC (clone REA213, ref. 130-101-040, Miltenyi Biotec), anti Tie2/PE (clone 83715, ref. FAB3131P, R&D systems), anti Tim3/PECF594 (clone 7D3, ref. 565560, BD Biosciences) and 7AAD (ref. 559925, BD Biosciences), at room temperature during 15 minutes. Then, cells were washed two times and acquired on flow cytometer BD Fortessa X20 (BD Biosciences). Data were acquired in FCS 3.0 format and analyzed with KALUZA software version 2.1.

Statistical analysis and illustrations

Clinical statistical analysis has been done using the SAS® statistical software version 9.4 (Cary, North Carolina, USA). Calculations and statistical tests for ancillary analyses were performed using R v3.4. Wilcoxon-Mann-Whitney test was used to assess differences between two patient's groups. Data representation and analyses was performed with software R v3.3.3 using tidyverse, dplyr, ggplot2, ggpubr, complexheatmap, survival and atable packages. Figure's aesthetics were worked with Affinity Designer® (v1.9.2.1035).

Tolerability of pembrolizumab with nintedanib for patients with advanced pleural mesothelioma, naive to immuno-therapy and refractory to platinum-based chemotherapy.

32 patients were enrolled between October 10th, 2017, and April 11th, 2019, in the mesothelioma expansion cohort of the trial: two patients were screen failed because of exclusion criteria and 30 patients were included in the trial. Patients' characteristics are described in **Table 6**. They were mainly male (n=20/30, 67%), with a median age of 69 years old (standard-deviation [SD] 11 years). The enrolled MM were advanced tumors involving the pleura, with metastatic peritoneal carcinosis in 2/30 cases (6.7%) and were all refractory to platinum-regimen based chemotherapy. The number of previous lines of treatment were 1, 2 and ≥3 for 23/30 (77%), 5/30 (17%) and 2/30 (6.7%) of the patients, respectively. Previous treatment with bevacizumab, associated with platinum and pemetrexed, was reported for 12/30 (40%). Of note, a patient (#40) was treated efficiently in fourth line by an EZH2 inhibitor for a year before developing a tumor progression and be enrolled in this trial.

Dose modifications and/or scheduling modifications occurred in 12/29 (41%), and 4/29 (14%) patients because of adverse events associated with nintedanib and pembrolizumab, respectively. Adverse events were reported in **Table 7**. The most frequent adverse events (AE) (grades 1-3) related to the combination were diarrhea, fatigue, nausea and liver enzymes elevation. Twelve (40%) and 3/30 (10%) patients developed grade 3/4/5 treatment- and immune- related adverse events respectively (colitis with pneumonitis [n=1] and myocarditis [n=2], grade 3, 4 and 5, respectively). Two patients developed arterial thrombosis (acute coronaropathy [n=2] and mesenteric ischemia [n=1]). Patients died because of cancer progression (n=14/30, 46.7%), myocarditis with mesenteric thrombosis (n=1/30, 3.3%) and COVID-19 (n=1/30, 3.3%).

	Total (n=30)
Female Male	10 (33%) 20 (67%)
Mean age, years [SD]	69 [11]
Body mass index, kg/m², mean [SD]	25 [4.9]
ECOG performans status 0 1	 9 (30%) 20 (67%)
Histology subtypes Epithelioid Biphasic Sarcomatoid	 25 (83%) 4 (13%) 1 (3.3%)
TNM UICC (v.8) III IV Missing	 16 (53%) 8 (27%) 6 (20%)
Previous systemic anticancer treatment 1 2 ≥3	 23 (77%) 5 (17%) 2 (6.7%)
Previous treatment with Bevacizumab No Yes	 18 (60%) 12 (40%)
BAP1 expression status (IHC) Loss Normal Not done Missing	 9 (30%) 3 (10%) 12 (40%) 6 (20%)
PDL1 expression on tumor cells (IHC), mean [SD]	4.1 [9.5]
Median leucocytes (.10^3/mm^3) (range)	8.55 (3.6-15)
Neutrophils to lymphocytes ratio, mean [SD]	4.5 [1.9]
Median LDH (UI/L) (range)	187.5 (130-622)
Median Albumin (g/L) (range)	39 (29-46)
Median CRP (mg/L) (range)	37.8 (2.4-171.5)
Median IL6 (pg/mL) (range)	6.7 (0.8-62)

TABLE 6. BASELINE CHARACTERISTICS OF PATIENTS INCLUDED IN THE EXPANSION COHORT DEDICATED TO NAÏVE TO IMMUNOTHERAPY, REFRACTORY TO PLATINUM BASED CHEMOTHERAPY ADVANCED MESOTHELIOMA.

	Grade 1-2	Grade 3	Grade 4	Grade 5
Alanine aminotransferase increased	3 (10%)	0	0	0
Anemia	4 (13.3%)	0	0	0
Arthralgia	6 (20%)	0	0	0
Aspartate aminotransferase increased	3 (10%)	0	0	0
Central nervous system disorder*	5 (16.7%)	0	0	0
Colitis	0	1 (3.3%)	0	0
Cough	7 (23.3%)	0	0	0
CPK increased	2 (6.7%)	0	1 (3.3%)	0
Creatinin increased	1 (3.3%)	0	0	0
Decreased appetite	6 (20%)	1 (3.3%)	0	0
Diarrhea	18 (60%)	1 (3.3%)	0	0
Dyspnea	11 (36.7%)	2 (6.7%)	0	0
Dysphagia & dyspepsia	3 (10%)	0	0	0
Fatigue	14 (46.7%)	2 (6.7%)	0	0
Fever	6 (20%)	0	0	0
GGT increased	1 (3.3%)	1 (3.3%)	0	0
Hypomagnesemia	5 (16.7%)	0	0	0
Hypothyroidism	4 (13.3%)	0	0	0
Lipase increased	1 (3.3%)	2 (6.7%)	1 (3.3%)	0
Mucositis	1 (3.3%)	0	0	0
Myocarditis & cardiac disorder	1 (3.3%)	1 (3.3%)	0	1 (3.3%)
Nausea	7 (23.3%)	1 (3.3%)	0	0
Peripheral nervous system disorder**	2 (6.7%)	0	0	0
Pneumonitis	3 (10%)	0	0	0
Skin disorder (including rash & pruritis)	6 (20%)	2 (6.7%)	0	0
Vomiting	10 (30%)	0	0	0
Weight loss	3 (10%)	0	0	0

TABLE 7. LISTING OF ADVERSE EVENTS ASSOCIATED WITH TREATMENTS OR NOT OCCURING DURING THE TRIAL (MESOTHELIOMA COHORT).

Median follow-up was 14.8 months (95% confidence interval [95%CI] [9.70:18.2]). Patient's median progression free survival (PFS) was 6.2 months (95%CI [3:8.7]) (**Figure 11A**). One patient could not be evaluated for tumoral response because of early death related to the above-mentioned grade 5 adverse event. Best Objective Responses (BOR) were Partial Response (PR, n=7/29; 24.1%), Stable Disease (SD, n=17/29; 58.6%) and Progressive Disease (n=5/29; 17.2%) (**Figure 11B**). Disease Control Rates (DCR) (defined as PR + SD) were 68.4% (95%IC [43.4:87.4]) and 46.6% at 3 and 6 months, respectively. At database lock, two patients (7%) ended treatment because they completed the 2-year treatment per protocol but 23/30 (79%) had to stop because of cancer progression (**Figure 11C**). Median PFS according to best objective responses were respectively 7.1 months (95% CI [3:9.3]) and 12.9 months (95% CI [1.7: not reached]) for SD and PR patients, respectively (**Supplementary figure 4**).

11A

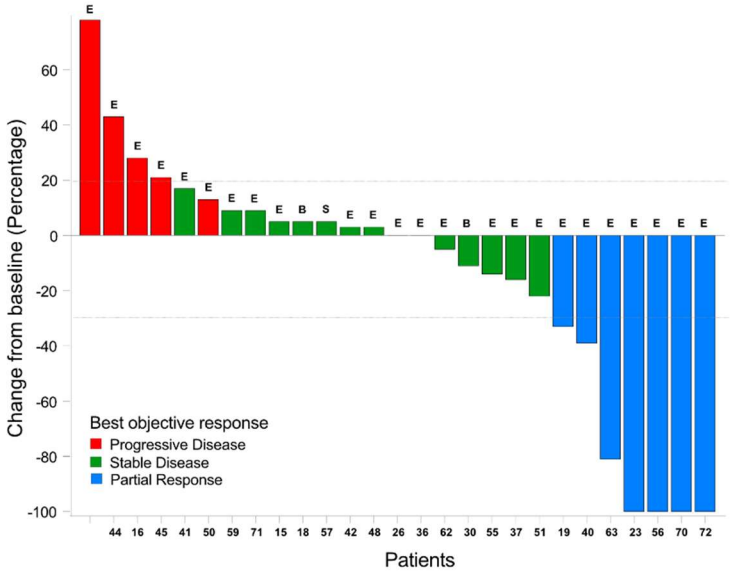

11B

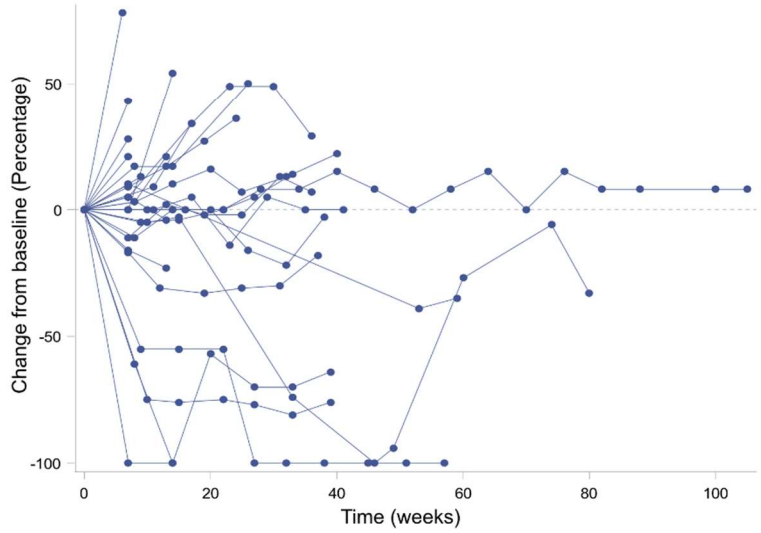

11C

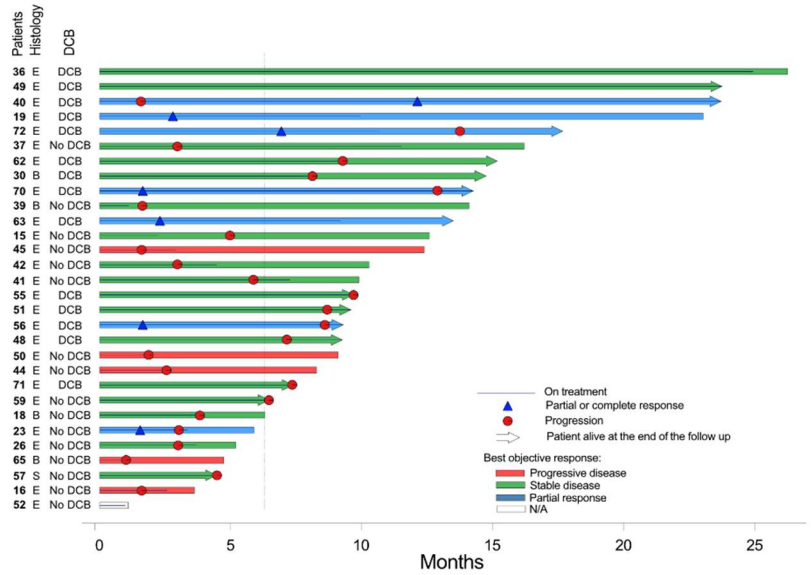

FIGURE 11. EVOLUTION OF PATIENTS DURING TREATMENT WITH NINTEDANIB AND PEMBROLIZUMAB ASSOCIATION (MESOTHELIOMA COHORT). 11A. WATERFALL PLOT. 11B. SPIDER PLOT OF SUM OF TARGET LESIONS DURING FOLLOW-UP. 11C. SWIMMER PLOT.

To determine factors associated with the efficacy of the combination therapy, we defined durable clinical benefit (DCB) as the absence of tumor progression before 6 months of treatment. Fourteen (46.7%) and 16 (53.3%) patients had been considered with and without DCB, respectively. Baseline serum levels of interleukin-6 (IL-6), measured retrospectively at accredited diagnostic laboratory, were significantly higher in patients without DCB (**Supplementary table 1**).

There were no differences between tumor biopsies from patients with or without DCB in terms of biopsy size or percentage of tumor cells (**Supplementary figure 6A**). Also, there were no differences in terms of T cells, B cells neither tertiary lymphoid structure infiltrating baseline tumor biopsies according to IHC scoring (**Supplementary table 2**). However, tumor cells of patients with DCB had significantly higher expression of PD-L1 than patients without DCB (**Figure 12A**). Looking at tumor infiltrating T cells by flow cytometry on fresh tumor biopsies at baseline (**Supplementary figure 7**), we found that patients with DCB had higher percentages of $CD45^+$ immune cells and $CD3^+$ T cells among total cells and more $CD8^+$ T cells among $CD3^+$ T cells than patients without DCB (**Figure 12B**). Because of limited subsets of cells (the mean number of $CD3^+$ T cells in biopsies were 2234 cells (SD [4715]) and 435 cells (SD [546]) for patients with and without DCB, respectively) the comparison of costimulatory molecules expressed by t-cells, such as PD-1 or CTLA-4, could not be done rigorously (as illustrated in **Supplementary figure 7B**). Prospective immuno-monitoring of fresh blood circulating T lymphocytes by flow cytometry allowed to observe that patients with DCB presented at screening with higher percentages of type 1 helper T cells (Th1) among helper $CD4^+$ T cells, and $CD49a^+$ effector memory $CD8^+$ T cells than patients without DCB (**Figure 12C**).

DNA and RNA extracted from frozen tumor biopsies collected at baseline brought information about the molecular differences between tumors sensitive or not to our treatment. Recent molecular deconvolution from transcriptomic analyses of human mesothelioma described gradients of “epithelioid signature” (E-score) and “sarcomatoid signature” (S-score) (114)). Here, there was no difference for E-score between biopsies of patients with or without DCB. Mean S-score tended to be higher in biopsies of patients without DCB (**Supplementary figure 3B**). Whole Exome Sequencing done on DNA from tumor biopsies, considering only those with tumor cells (n=13), losses of tumor suppressor genes by mutations and/or copy number alterations (CNA) were identified in *BAP1* (67%), *EP300* (67%), *NF2* (61%), *SETD2* (61%), *CDKN2A* (56%), *CREBBP* (44%), *TP53* (39%), *MGA* (22%) and *DDX3X* (17%) genes (**Figure 12D**; **Supplementary figure 8**). There were no significant differences between patients with or without DCB considering mutations and CNA (data not shown). Median tumor mutational burden was 0.7 mutations per megabase (0.48 to 2.11). Deconvolution of immune

tumoral infiltration from transcriptomic data highlighted that biopsy from patients without DCB and tumoral progression, presented with lower immune infiltrates, higher percentages of tumor cells, and tended to cluster together (**Figure 12D**). Of note the levels of expression of myeloid dendritic cells score in biopsies at screening were higher in tumors from patients with DCB than without DCB (**Figure 12E**).

Measurement of plasmatic angiogenic factors did not identify clear pre-therapeutic difference between patients with or without DCB (**Supplementary figure 9**). The first 7 days of treatment by nintedanib monotherapy leaded to a significant decrease of plasmatic rates of angiopoietin-2 in patients with or without DCB (**Supplementary figure 10**). Also, several chemokines increased their plasma concentrations upon the first pembrolizumab infusion (**Figure 12F**). CXCL9, CXCL10, CXCL13, CCL19, soluble PD-1 and soluble PD-L1 significantly increased their plasma concentrations one week after the first pembrolizumab infusion in all patients, whatever their clinical course (**Figure 12F & 12G; Supplementary figure 11**). However, plasma concentration of CCL3 (ligand of CCR1/4/5), CCL8 (ligand of CCR1/2/3) CCL17 (ligand of CCR4) and CCL23 (ligand of CCR1) increased significantly between day 1 and day 8 only in patients without DCB (**Supplementary figure 11**). Interestingly, according to transcriptomic deconvolution analysis, these pharmacodynamics effects of the treatment were accompanied by an increase in immune infiltrations in tumor biopsies between screening and C2D1 irrespective of clinical benefit (**Supplementary figure 12A**), but higher immune infiltrate estimation tended to cluster data from patients with DCB (**Supplementary figure 12B**). Moreover, flow cytometry analyses of cycle 2 biopsies did not find differences in terms of global $CD45^+$ immune cells, neither in $CD3^+$ T cells, but the percentage of $CD4^+$ among $CD3^+$ T cells and $CD4^+$ $CD25^+$ cells among $CD4^+$ T cells were higher in patients without DCB, suggesting a greater representation of regulatory T cells in these tumors upon treatment (**Figure 12H**).

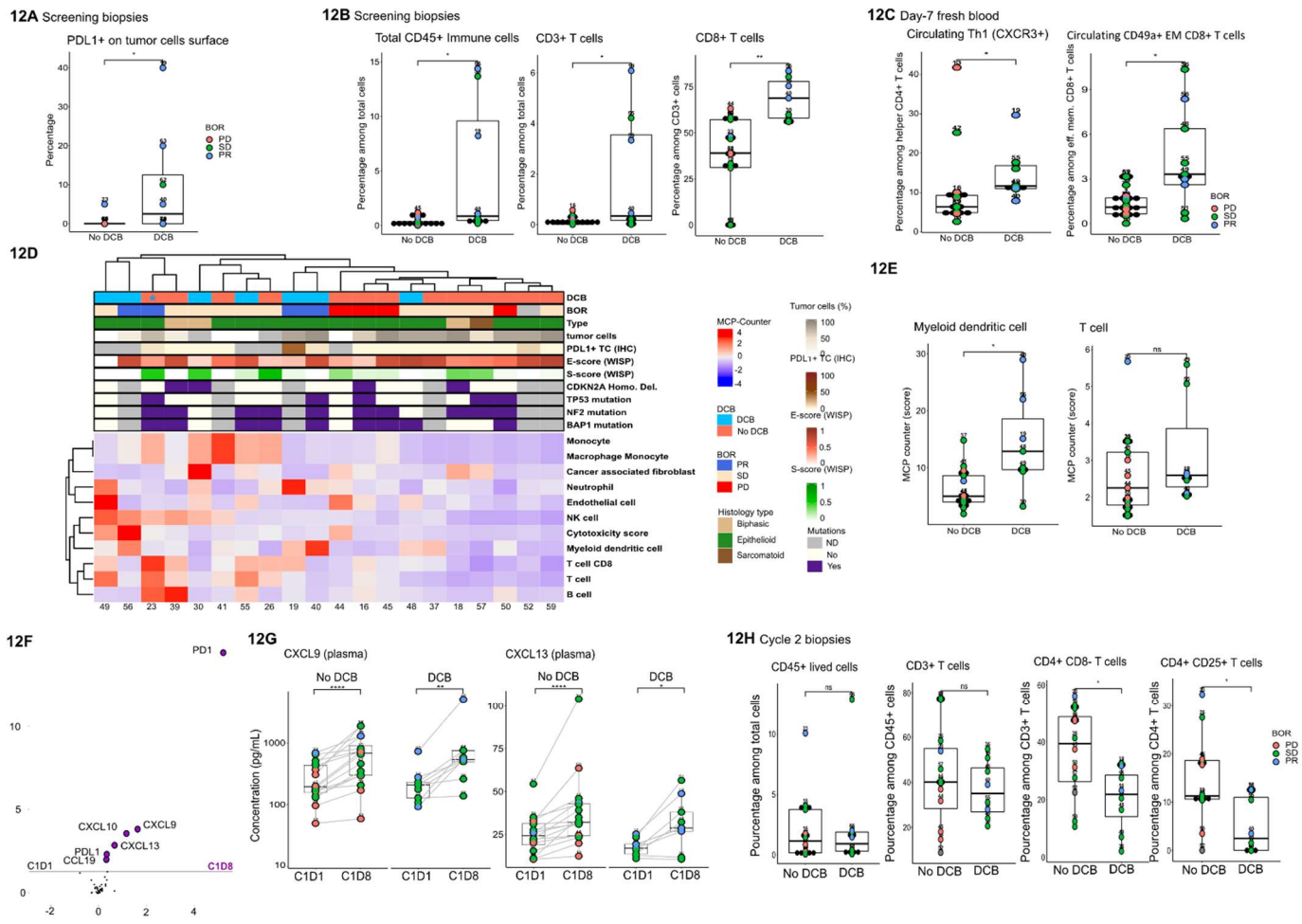

FIGURE 12. PATIENTS WITH BENEFIT TO PEMBROLIZUMAB AND NINTEDANIB HAD TUMORAL AND SYSTEMIC IMMUNE CHARACTERISTICS COMPARED WITH PATIENTS PRIMARY RESISTANT TO TREATMENT (MESOTHELIOMA COHORT).

12A. PD-L1 (CLONE SP263) STAINING OF TUMOR CELLS BY IMMUNE-HISTO-CHEMISTRY ON SCREENING BIOPSIES (N=20). 12B. EVALUATION OF TUMOR IMMUNE INFILTRATE AFTER FRESH TISSUE DISSOCIATION BY FLOW CYTOMETRY (N=22). 12C. ANALYSES OF FRESH BLOOD SAMPLES BY FLOW CYTOMETRY TO PHENOTYPE CIRCULATING T LYMPHOCYTES BEFORE TREATMENT INITIATION, BOXPLOT REPRESENTATION OF PERCENTAGE OF $CXCR3^+$ $CCR4^-$ $CCR6^-$ CELLS AMONG HELPER MEMORY CD4+ T CELLS AND $CD49A^+$ AMONG EFFECTOR MEMORY $CD8^+$ T CELLS (N=25). 12D. HEATMAP REPRESENTATION OF UNSUPERVISED CLUSTERING OF SCREENING TUMOR THROUGH IMMUNE INFILTRATION ESTIMATED BY DECONVOLUTION OF BULK RNA-SEQ DATA (MCP COUNTER) WITH CLINICAL AND MOLECULAR ANNOTATIONS (N=20). 12E. ESTIMATION OF MYELOID DENDRITIC CELLS AND T CELLS INFILTRATION IN TUMOR BY IMMUNE DECONVOLUTION (MCP COUNTER) FROM RNA-SEQ IN SCREENING BIOPSIES FOR PATIENTS WITHOUT AND WITH DCB (N=20). 12F. VOLCANO PLOT REPRESENTATION OF DIFFERENTIAL CONCENTRATION OF PLASMA CHEMOKINES AND SOLUBLE FACTORS MEASURED FOR ALL PATIENTS BETWEEN CYCLE 1 DAY 8 AND DAY 1 BLOOD SAMPLES (N=25). 12G. EVOLUTION OF PAIRED PLASMA CXCL9 AND CXCL13 CONCENTRATION BETWEEN CYCLE 1 DAY 1 AND DAY 8 BLOOD SAMPLES FOR PATIENTS WITHOUT AND WITH DCB (N=25). 12H. COMPARISON OF T CELLS INFILTRATE BETWEEN PATIENTS WITH AND WITHOUT DCB AT CYCLE 2 TUMOR BIOPSIES WITH FLOW CYTOMETRY (N=22). ALL TESTS WERE WILCOXON RANK-SUM TEST (NOT PAIRED SAMPLES) AND PAIRED WILCOXON SIGNED RANK TEST (PAIRED SAMPLES) (REPRESENTATION OF P-VALUE: NS >0.05, * ≤ 0.05, ** ≤ 0.01, *** ≤ 0.001, **** ≤ 0.0001).

To better determine the tumoral characteristics associated with sensitivity to treatment, we performed an unsupervised analysis of genes differentially expressed in screening tumor biopsies by RNA-seq (n=13). This analysis found 115 genes differentially expressed between tumors of patients with and without DCB (log 2-fold change [log2FC] +/-3 and adjusted p-value [padj] < 0.01 with Benjamini-Hochberg method) (**Figure 13A**). Of note, *CCL11* (eotaxin) expression was significantly higher (log2FC = 5.3, padj = 0.0004) and *CXCL8* expression significantly lower (log2FC = -1.93, padj = 0.045) in biopsies of patients with DCB before treatment initiation.

Gene set enrichment analysis (GSEA), with the "Hallmark" panels, identified 11 gene sets which were significantly differentially expressed in biopsies of patients with DCB (**Figure 13B**). Seven gene sets were upregulated and 4 were repressed in tumor biopsies of patients with DCB. Genes significantly upregulated pertained to pathways related to oxidative phosphorylation (OXPHOS) metabolism, interferon alpha (IFNα) pathway, interferon gamma (IFNγ) pathway and "allograft rejection" signature, suggesting an ongoing adaptive immune response in the tumor (**Figure 13C**). Significantly suppressed pathways in tumor from patients with DCB (therefore relatively enriched in tumors primary resistant to treatment), were genes from the epithelial to mesenchymal transition (EMT) pathway, G2M checkpoint, E2F and MYC targets (**Figure 13D**). Those three E2F, MYC and G2M pathways shared several genes downstream expression (**Supplementary figure 13**).

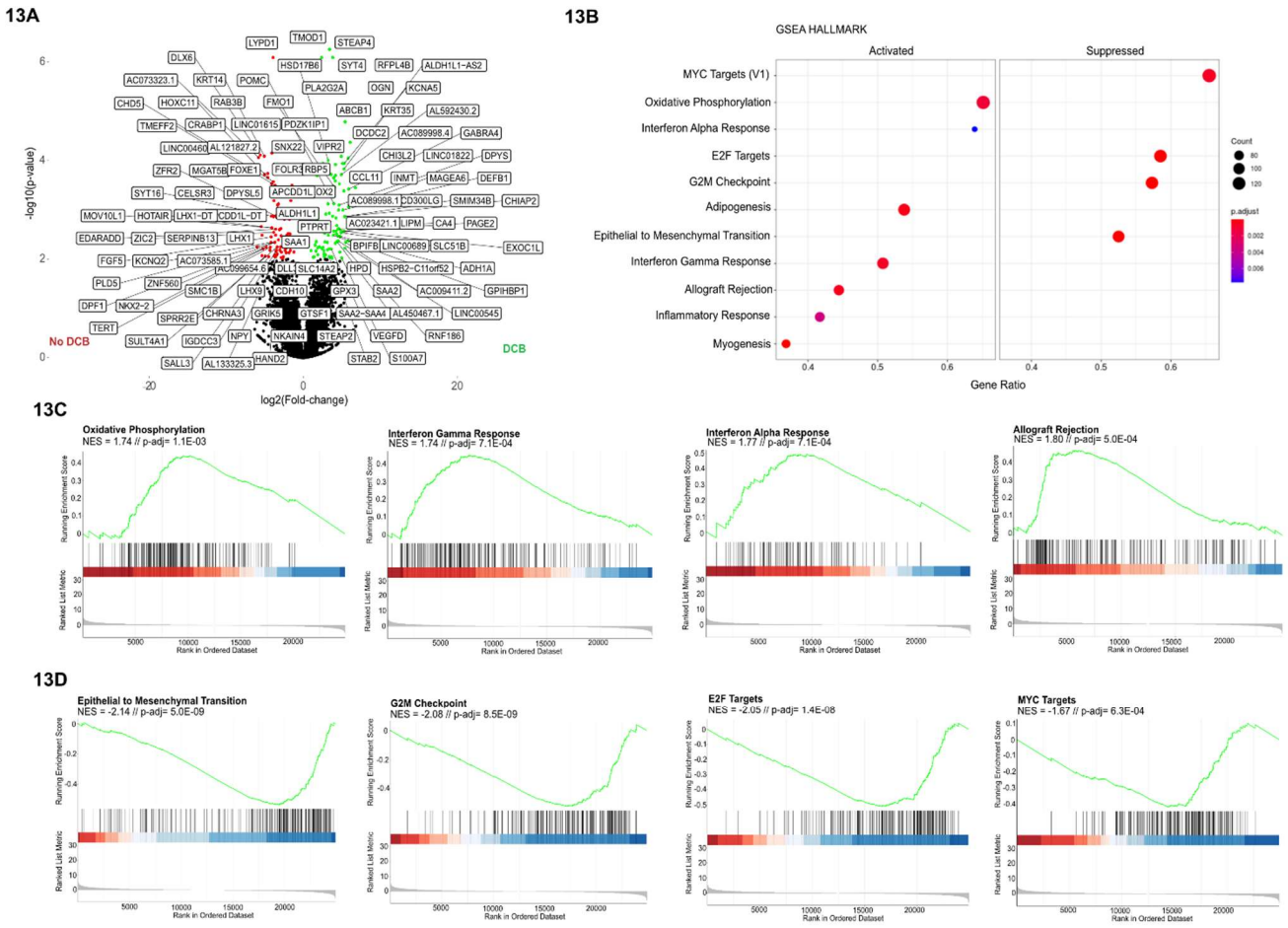

FIGURE 13. DIFFERENTIAL EXPRESSION GENES (DEG) BETWEEN SCREENING TUMOR BIOPSIES HIGHLIGHTED LOW IMMUNE SIGNATURE AND PRO TUMORAL PATHWAYS MOLECULAR ENRICHMENT IN PATIENTS WITH PRIMARY RESISTANCE TO TREATMENT (MESOTHELIOMA COHORT).

13A. VOLCANO PLOT REPRESENTATION OF DEG BETWEEN SCREENING TUMOR BIOPSIES FROM PATIENTS WITH OR WITHOUT DCB (LOG-2 FOLD CHANGE ≤ -3 OR ≥ 1 WITH P-VALUE ≤ 0.01 ADJUSTED WITH BENJAMINI-HOCHBERG METHOD [WALD'S TEST]) (N=13). 13B. DOT PLOT REPRESENTATION OF GENE SET ENRICHMENT ANALYSES ("HALLMARK" PANEL) BETWEEN SCREENING TUMOR BIOPSIES FROM PATIENTS WITH OR WITHOUT DCB (N=13), CONSIDERING ALL GENES DIFFERENTIALLY EXPRESSED (P-VALUE ≤ 0.05 ADJUSTED WITH BENJAMINI-HOCHBERG METHOD [WALD'S TEST]; N=515). GSEA PLOT REPRESENTATIONS OF PATHWAYS SIGNIFICANTLY ENRICHED OR SUPPRESSED IN TUMOR BIOPSIES FROM PATIENTS WITH DCB COMPARED TO THOSE WITHOUT DCB (13C AND 13D, RESPECTIVELY).

Somatic copy number alterations (SCNA), or aneuploidy, estimated by tumoral and constitutive paired WES analyzes, were higher in biopsies from patients without DCB than in patients who benefited from the treatment (**Figure 14A**). SCNA score from all WES data (n=18) correlated positively with serum concentration of IL6 measured from baseline samples and with the concentration of soluble CCL2, present in the supernatant of fresh tumor biopsies done prior treatment initiation (**Figure 14B, 14C**). Median CCL2 concentrations in those tumor supernatants were significantly higher in biopsies of patients without DCB (63.4pg/mL [SD 200.4] versus 18.1pg/mL [SD 48.4], respectively; p=0.027, Wilcoxon rank-sum test) (**Figure 14D**). CCL2 was the only chemokine from tumor biopsy supernatants with significant differences in concentration between patient groups. In blood, the pro-inflammatory cytokines CXCL8 (IL8) were significantly higher before treatment in patients without DCB (**Figure 14E)**. In parallel, prospective immuno-monitoring of circulating immune cells highlighted that percentages of $CD15^+$ polymorphonuclear cells (PMN) among total $CD45^+$ were significantly higher in fresh blood of patients without DCB (**Figure 14F**).

Single cell (n=7239 cells) expression analyses of 400 genes from pre-treatment PBMC of 10 patients (5 patients with DCB and 5 without DCB) and 2 healthy controls were performed to identify preexisting differences between circulating immune cells in patients with or without DCB. Thirteen clusters of cells were identified (**Figure 14G**). The comparison between healthy controls' PBMC (n=1471 cells) to patients with DCB (n=3847 cells) or no DCB (n=1921 cells) allowed to identify a cluster of cells (*Monocyte #1*) which was almost not present in controls but only in MM patients (**Figure 14H**). Top genes those expression defined this cluster were *CD14*, alarmins *S100A12* and *S100A9*, scavenger receptor *CD163*, pattern recognition receptor lectins *CLEC4E* and *FCN1*, nicotinamide transferase *NAMPT*, chemokines *CXCL8*, glutathione transferase *MGST1* and *VEGFA* (**Supplementary figure 14**). Median percentage of cells from cluster *Monocyte #1* among total cells were 3.9% (SD 3.2), 21.6% (SD 21.1) and 39.6% (SD 22.9) in healthy subjects, patients with and without DCB respectively (Kruskal-Wallis test, p=0.12) (**Figure 14I**).

Analyses by flow cytometry of thawed cells from healthy controls and pre-treatment patients' PBMC samples were done to study monocyte's surface proteins presentation, products of these genes (**Figure 14J**). It confirmed that the median percentage of intermediate monocytes among total monocytes were significantly higher in patients than in healthy controls (6.95% [SD 3.1] and 3.95% [SD 1.6], respectively; p=0.028, Wilcoxon rank-sum test) (**Figure 14K;** cf gating strategy in **Supplementary figure 15**). Patients without DCB had significantly higher percentage of intermediate monocytes $CD163^+$ $CCR2^-$ among those HLA-DR^{int}, than patient with DCB (6% [SD 5.8] and 0.8% [SD 0.7], respectively; p=0.013,

Wilcoxon rank-sum test) (**Figure 14K**). In cycle 2 biopsies, *TREM1* expression was higher in biopsies from patients without than with DCB (**Figure 14L**).

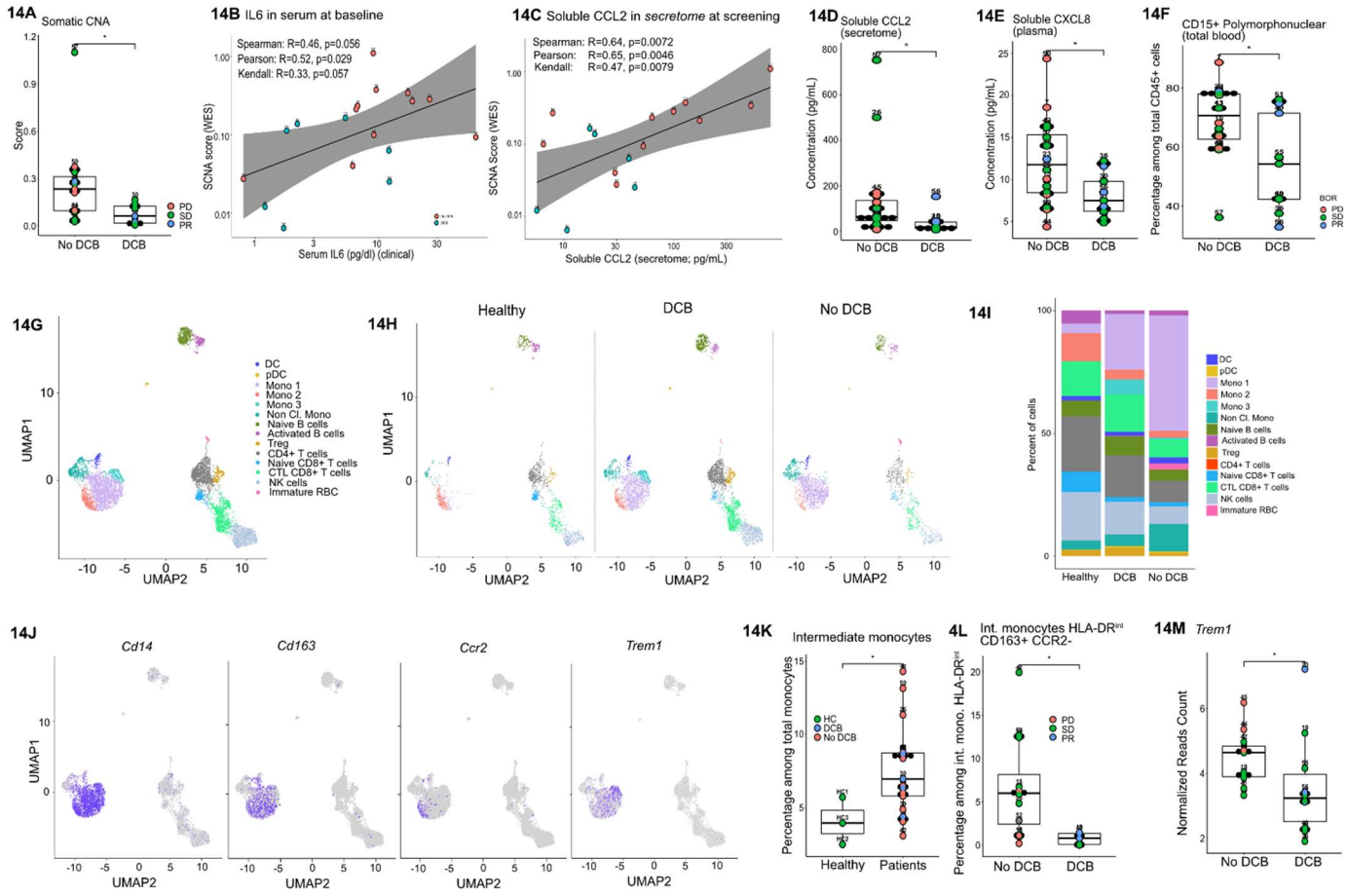

FIGURE 14. ANEUPLOIDY WAS HIGHER IN TUMOR FROM PATIENTS WHO DID NOT BENEFIT TO THE TREATMENT AND WAS POSITIVELY ASSOCIATED WITH CHEMOKINES RECRUITING INFLAMMATORY SUPPRESSIVE INNATE IMMUNE CELLS IN TUMORS (MESOTHELIOMA COHORT).

14A. SOMATIC COPY NUMBER ALTERATION SCORE BETWEEN PATIENTS WITHOUT OR WITH DCB (N=18). 14B. CORRELATION PLOT TO ILLUSTRATE ASSOCIATION BETWEEN SCNA SCORE AND CONCENTRATION OF SERUM IL6 FROM SAMPLES DONE BEFORE TREATMENT INITIATION (DAY -7)(N=18). 14C. CORRELATION PLOT TO ILLUSTRATE ASSOCIATION BETWEEN SCNA SCORE AND CONCENTRATION OF SOLUBLE CCL2 IN SCREENING BIOPSY'S SECRETUM (N=18). 14D. CONCENTRATION OF SOLUBLE CCL2 IN SCREENING BIOPSY'S SECRETUM BETWEEN PATIENTS WITHOUT OR WITH DCB (N=25). 14E. CONCENTRATION OF PLASMATIC CXCL8 (DAY -7) BETWEEN PATIENTS WITHOUT OR WITH DCB (N=25). 14F. PERCENTAGES OF $CD15^+$ POLYMORPHONUCLEAR (PMN) CELLS AMONG TOTAL $CD45^+$ CELLS IN PRE-TREATMENT FRESH BLOOD SAMPLES (DAY -7) (N=25). 14G. REPRESENTATION BY UNIFORM MANIFOLD APPROXIMATION AND PROJECTION (UMAP) OF CONCATENATED CELLS FROM ALL PRE-TREATMENT PBMC OF PATIENTS AND HEALTHY CONTROLS CLUSTERED BY DIFFERENTIAL EXPRESSION OF 400 GENES (N=12). 14H. CLUSTERING OF CONCATENATED SINGLE CELLS RNA-SEQ FROM PRE-TREATMENT PBMC OF HEALTHY CONTROLS (N=2), PATIENTS WITH DCB (N=5) AND WITHOUT DCB (N=5). 14I. BARPLOT REPRESENTING PERCENTAGE OF CELLS FROM EACH CLUSTER FOR HEALTY CONTROLS, PATIENTS WITH OR WITHOUT DCB. 14J. ILLUSTRATION OF SELECTED GENES EXPRESSION AT SINGLE CELLS LEVELS WITH UMAP REPRESENTATION OF ALL CONCATENATED CELLS. 14K. PERCENTAGE OF CIRCULATING INTERMEDIATE MONOCYTES AMONG TOTAL MONOCYTES FROM THAWED PBMC COLLECTED IN HEALTHY CONTROLS (N=3) OR PATIENTS BEFORE INITIATION OF TREATMENT (DAY -7) (N=17). 14L. PERCENTAGE OF CIRCULATING $CD163^+$ $CCR2^-$ CELLS AMONG INTERMEDIATE MONOCYTES $HLA\text{-}DR^{INT}$ MONOCYTES FROM THAWED PBMC COLLECTED IN HEALTHY CONTROLS (N=3) OR PATIENTS BEFORE INITIATION OF TREATMENT (DAY -7) (N=17). 14M. COMPARISON OF *TREM1* NORMALIZED GENE EXPRESSION BETWEEN PATIENTS WITHOUT AND WITH DCB AT CYCLE 2 TUMOR BIOPSIES (N=21). EXCEPT IF DETAILED, ALL TESTS WERE WILCOXON RANK-SUM TEST (NOT PAIRED SAMPLES) AND PAIRED WILCOXON SIGNED RANK TEST (PAIRED SAMPLES) (REPRESENTATION OF P-VALUE: NS >0.05, * ≤ 0.05, ** ≤ 0.01, *** ≤ 0.001, **** ≤ 0.0001).

This expansion cohort of the phase 1b PEMBIB clinical trial, dedicated to patients with advanced mesothelioma naïve to immunotherapy and refractory to first line of platinum-based chemotherapy, showed that the association of pembrolizumab 200mg Q3W with nintedanib 150mg BID has antitumor activities, with manageable toxicities. The disease control rate (DCR) at 12 weeks was 68.4% (95%IC [43.4:87.4]). This is higher than those observed in phase 1 and phase 2 clinical trials which evaluated anti-PD1/PD-L1 monoclonal antibodies monotherapies (79,80,300,365,366), and similar to those with combination of anti PD-1/PD-L1 with anti CTLA-4 monoclonal antibodies (81–83), for patients with advanced mesothelioma refractory to platinum-based chemotherapy.

Our study brought knowledge on mesothelioma characteristics associated with the primary resistance to anti PD-1 monoclonal antibodies combined with an antiangiogenic TKI. First, we observed that after one anti PD-1 infusion, global immune and T cells infiltrates increased in tumors from all patients, but those who did not benefit from treatment presented with higher percentage of $CD4^+$ cells among T cells and $CD25^+$ cells among $CD4^+$ T cells. There results suggest that PD-1 blockade can lead to increase amounts of regulatory T cells in the tumor microenvironment and therefore have pro-tumoral effect. In the TME, PD-1 blockade has been described to release Tregs $PD\text{-}1^+$ immunosuppressive and pro-tumoral abilities (367). These $PD\text{-}1^+$ Tregs expressed high levels of CTLA-4, had important proliferative abilities and had been associated with hyper progressive disease upon anti PD-1 infusion (368,369). Thus, a combination of an Fc competent anti CTLA-4 with an anti PD-1 monoclonal antibodies, for patients with tumors infiltrated by such Tregs, could deplete those Tregs and limit this detrimental phenomenon (241,242). A phase 3 clinical trial (CheckMate743) evaluating the association of an anti PD-1 with an anti CTLA-4 monoclonal antibodies versus standard of care chemotherapy, for untreated unresectable malignant pleural mesothelioma, has shown a significant higher overall survival in patients receiving this combination of immune checkpoint blockade and might therefore support this hypothesis (74).

Our exome analyses did not show significant enrichment of loss of tumor suppressor genes among patients who did not benefit from treatment. However, our transcriptomic analyses highlighted that CDK/E2F and MYC pathways such as G2M checkpoints were enriched in refractory MM tumors. Their upregulation is classically promoted by loss of tumor genes suppressor such as CDKN2A and RB, which are frequently deleted or inactivated in malignant mesothelioma, leading to the deregulation of cyclin D4/6 (CDK4/6) activity, FOXM1 transcriptional activity and cell proliferation. Recent studies have described in different tumor types that those mutations and their downstream pathways lead to

immunosuppressive cancer cells abilities and limit immune infiltrations in tumors (370–376). In mesothelioma such as in other metastatic cancers, TP53 and CDKN2A are somatic genes frequently altered (103,377). CDKN2A homozygous deletion has been associated with low immune infiltrate in TME, and CDK4/6 inhibitors have been shown to increase tumor immune infiltrations and to enhance the efficacy of immune checkpoint blockade (378–381). MYC pathway up-regulation is able to induce an immunosuppressive microenvironment through an upregulation of immune checkpoint expressions by cancer cells and by the recruitment of immunosuppressive immune cells in the tumor stroma (382,383). Moreover, cancer cells proliferation and stemness abilities have been shown to be associated with tumoral immune suppression (384).

Our estimation of aneuploidy from WES, even with a limited number of patients, allowed to highlight that SCNA was higher in pre-treatment tumor biopsies from patients who did not benefit from our treatment. Interestingly, SCNA was positively correlated with the concentration of IL6 and CCL2, respectively in the blood and secretome of tumor biopsies. An association between aneuploidy, low immune tumoral infiltrate and systemic inflammation has been recently observed in different tumor types (385,386). In mesothelioma, a disease with sub clonal evolutions, and in particular, with the late clonal acquisition of deletion of the NF2 genes in addition to BAP1 and CDKN2A, has been associated with this inflammation phenotype (386). The disease evolution of our patient #23 during the treatment, with a dissociated response between his pleural and peritoneal lesions, suggested that an homozygous deletion of CDKN2A could have occurred in his peritoneal cancer cells, hereby promoting an immunosuppressive inflammatory phenotype and a peritoneal progression (**Figure 12D**; **Supplementary figure 8**). The mechanisms leading to the secretion of such chemokines was not determined, but these molecules are known to recruit potential immunosuppressive neutrophils, inflammatory monocytes and recruit macrophages with a high potential to promote tumor metastatic spreading and immune evasion, directly or indirectly, notably through VEGF production and interaction with Tregs in the tumor stroma (342,387–389). Of note, we observed a heterogeneity among circulating monocytes of MM patients, notably among intermediate monocytes which deserve additional analyzes.

The disease control rate at 12 weeks observed in this cohort, close to those observed in early trials evaluating the anti PD-1 + anti CTLA-4 combination, suggest that nintedanib could have a significant effect in combination with pembrolizumab. Of note, bevacizumab proved an antitumoral effect only in association with platinum-based chemotherapy (75,390). Mesothelioma are highly hypoxic tumors and mesothelioma cells are sensitive to VEGF as a growth factor (391). Antiangiogenic drugs should improve tumor endothelial cells and T cells anergy induced by VEGF, and favor tumor infiltrates by efficient anti tumoral cytotoxic T cells (315,392). However, our ancillary analyses did not bring clear

information about differential effects of anti-angiogenics between patients with benefit or not to treatment. Similar decreasing concentrations of angiopoietin-2 in the plasma upon nintedanib should limit the recruitment of inflammatory circulating macrophages expressing Tie2 for every patients receiving the treatment (**Supplementary figure 10**) (128,393–395); but these effects seem insufficient in refractory patients.

Conclusion.

Nintedanib 150mg BID in association with pembrolizumab was well tolerated, although one patient died because of systemic arterial thrombosis with myocardial involvement which seemed related to the combination therapy, but this patient had a history of thrombosis and circulating anti-phospholipid antibodies during her pregnancies decades before her enrollment in the study. A significant antitumor activity has been observed in patients with platinum-based chemotherapy refractory malignant mesothelioma. Ancillary analyses from tumors and circulating factors highlighted that patients with refractory diseases had, before the initiation of treatment, higher aneuploidy, positively associated with inflammatory patterns and recruitment of immunosuppressive inflammatory innate cells in their tumors. The loss of tumor suppressor genes, such as CDKN2A was enriched in malignant pleural mesothelioma, leading to molecular pathway upregulations with pro tumoral inflammatory features. Early identification of patients with such somatic genomic alterations could help to propose new therapeutic associations and treatment stratification strategies in MM.

	DCB (n=14)	No DCB (n=16)	p
Female Male	4 (29%) 10 (71%)	6 (38%) 10 (62%)	0.9
Mean age, years [SD]	70 [8.7	68 [13	0.85
Body mass index, kg/m², mean [SD]	25 [5.4]	25 [4.6]	0.74
ECOG performans status 0 1	 10 (71%) 4 (29%)	 10 (62%) 5 (31%)	0.61
Histology subtypes Epithelioid Biphasic Sarcomatoid	 13 (93%) 1 (7.1%) 0	 12 (75%) 3 (19%) 1 (6.2)	0.38
TNM UICC (v.8) III IV Missing	 6 (43%) 3 (21%) 5 (36%)	 10 (62%) 5 (21%) 1 (6.2%)	0.13
Previous systemic anticancer treatment 1 2 ≥3	 11 (79%) 2 (14%) 1 (7.1%)	 12 (75%) 3 (19%) 1 (6.2%)	0.55
Previous treatment with Bevacizumab No Yes	 8 (57%) 6 (43%)	 10 (62%) 6 (38%)	1
BAP1 expression status (IHC) Loss Normal Not done Missing	 5 (36%) 1 (7.1%) 3 (21%) 5 (36%)	 4 (25%) 2 (12%) 9 (56%) 1 (6.25%)	0.11
PDL1 expression on tumor cells (IHC), mean [SD]	14 [8.3]	3 [1.2]	0.76
Median leucocytes (.10^3/mm^3) (range)	8 (3.6-12.2)	10.1 (4.5-15)	0.58
Neutrophils to lymphocytes ratio, mean [SD]	4.8 [2.1	4.3 [1.8]	0.88
Median LDH (UI/L) (range)	172 (130-266)	197 (132-622)	0.33
Median Albumin (g/L) (range)	39 (29-45)	38 (35-46)	0.99
Median CRP (mg/L) (range)	10.7 (2.4-171.5)	53.4 (4.6-142.5)	0.23
Median IL6 (pg/mL) (range)	5.3 (1.2-12.3)	9.2 (0.8-62)	0.047

SUPPLEMENTARY TABLE 1. BASELINE CHARACTERISTICS OF PATIENTS INCLUDED OF THE EXPANSION COHORT DEDICATED TO NAÏVE OF IMMUNOTHERAPY, REFRACTORY TO PLATINUM-BASED CHEMOTHERAPY, UNRESECTABLE PLEURAL MESOTHELIOMA CONSIDERING PATIENTS WITH AND WITHOUT DCB.

TESTS TO COMPARE NOMINAL AND ORDINAL MEASUREMENT WERE X^2 TEST AND WILCOXON RANK-SUM TEST, RESPECTIVELY.

	DCB (n=8)	No DCB (n=12)	p
$CD8^+$ score			
0	4 (50%)	4 (33%)	0.49
1	3 (38%)	4 (33%)	
2	0	3 (38%)	
3	1 (12%)	1 (8.3%)	
$CD3^+$ $CD8^-$ score			
0	3 (38%)	4 (33%)	0.83
1	3 (38%)	5 (42%)	
2	2 (25%)	2 (17%)	
3	0	1 (8.3%)	
$CD20^+$ score			
0	6 (75%)	6 (50%)	0.5
1	1 (12%)	4 (33%)	
2	0	0	
3	1 (12%)	2 (17%)	
TLS score			
0	7 (88%)	10 (83%)	0.68
1	1 (12%)	1 (8.3%)	
2	0	1 (8.3%)	

SUPPLEMENTARY TABLE 2. STUDY OF IMMUNE INFILTRATION IN SCREENING TUMOR BIOPSIES BY IHC.

THE TEST USED TO COMPARE NOMINAL MEASUREMENTS (SEMI QUANTITATIVE SCORES) WAS X^2 TEST.

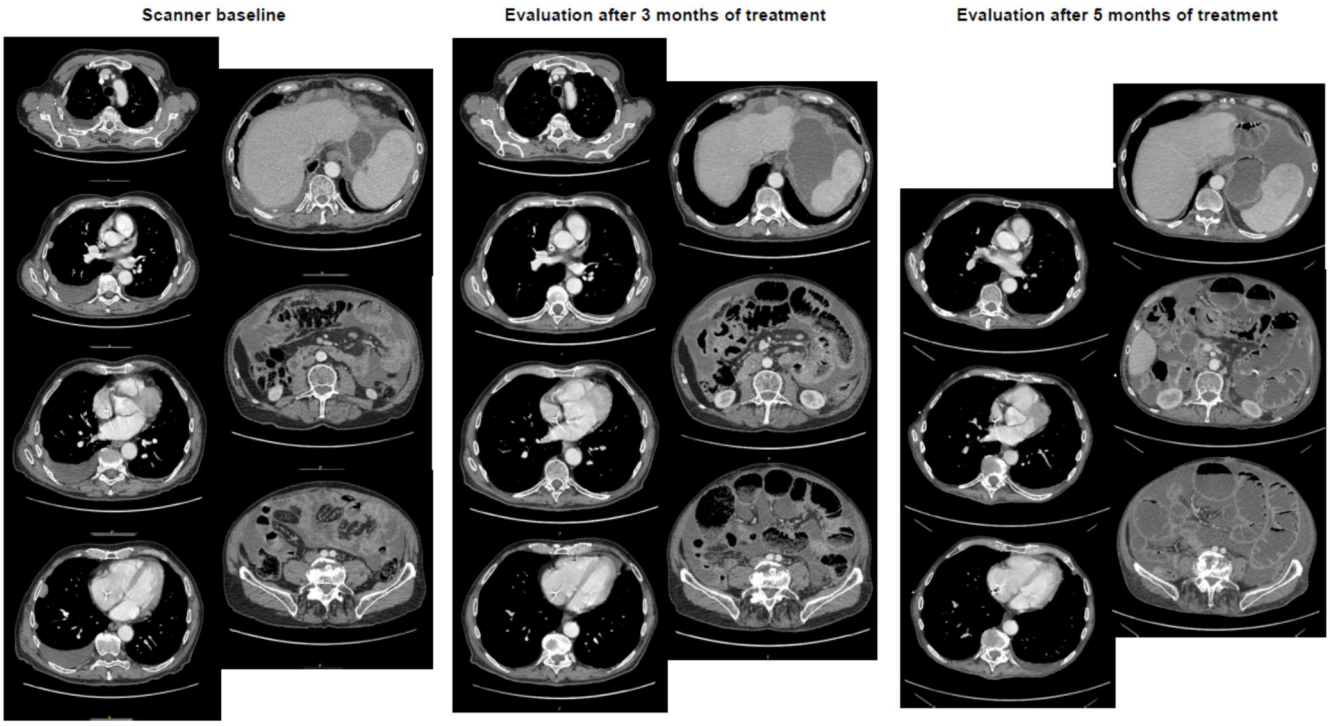

SUPPLEMENTARY FIGURE 4. ILLUSTRATION OF DISSOCIATED RESPONSE BETWEEN PLEURAL AND PERITONEAL LESIONS OF PATIENT #23 BEFORE 6 MONTHS OF TREATMENT.

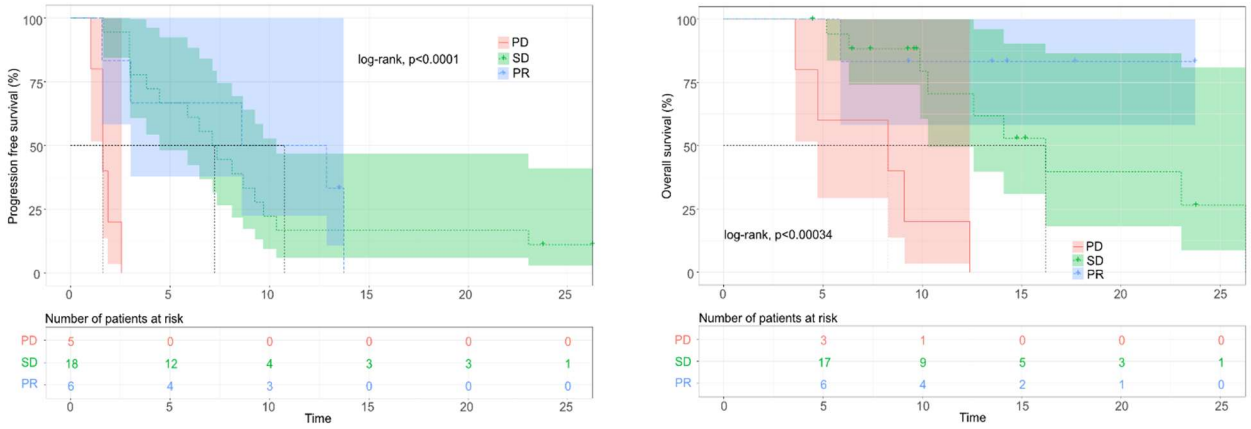

SUPPLEMENTARY FIGURE 5. KAPLAN MEIER SURVIVAL CURVE ILLUSTRATING SIGNIFICANTLY DIFFERENT OUTCOMES OF PATIENTS ACCORDING TO THE BEST OBJECTIVE RESPONSE (MESOTHELIOMA COHORT).

LEFT. PROGRESSION FREE SURVIVAL ACCORDING TO THE BEST OBJECTIVE RESPONSE (RECISTV1.1 DISTINCTION). SUPP. RIGHT. OVERALL SURVIVAL ACCORDING TO BEST OBJECTIVE RESPONSE (RECISTV1.1 DISTINCTION).

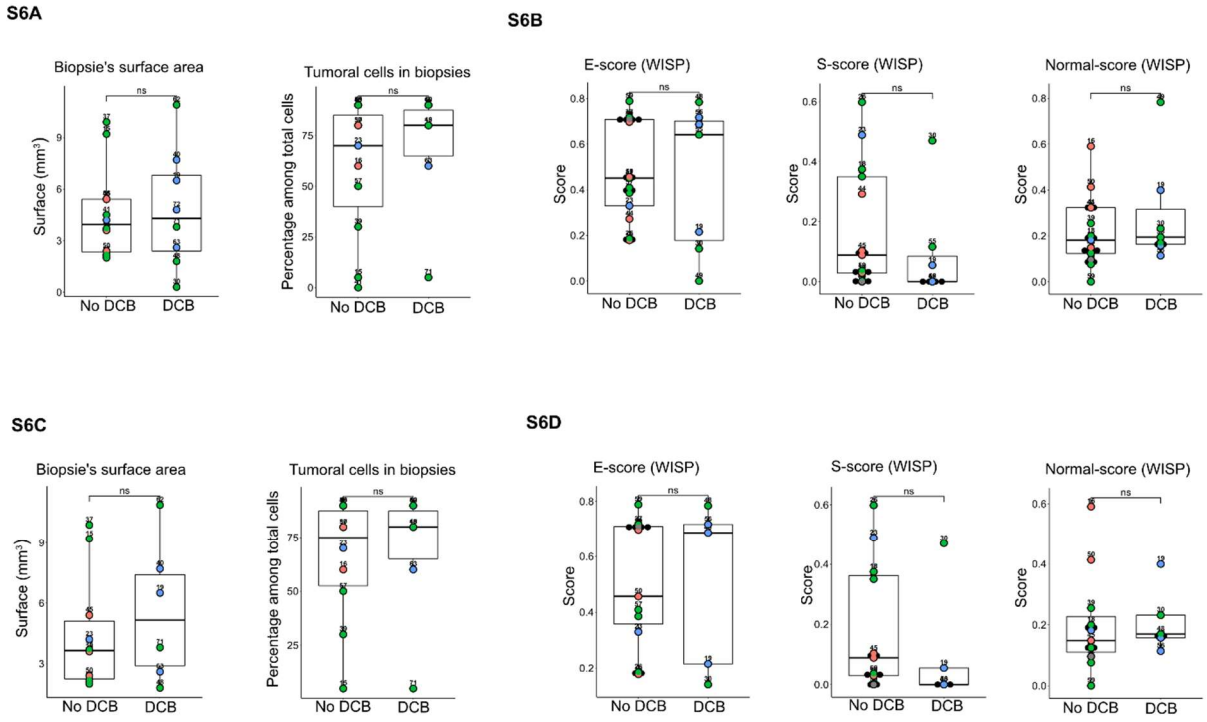

SUPPLEMENTARY FIGURE 6. SUPPLEMENTARY INFORMATION CONCERNING SCREENING TUMORAL BIOPSIES (MESOTHELIOMA COHORT).

SUPP. 6A. SURFACE AREA AND PERCENTAGE OF TUMOR CELLS IN BIOPSIES, INCLUDING BIOPSIES WITHOUT ANY TUMOR CELLS (N=21). SUPP 6B. COMPARISON OF MESOTHELIOMA MOLECULAR SUBTYPE ESTIMATED BY DECONVOLUTION FROM RNA-SEQ WITH WISP ALGORITHM (E-SCORE, S-SCORE AND NORMAL-SCORE), INCLUDING BIOPSIES WITHOUT ANY TUMOR CELLS (N=20). SUPP. 6C. SURFACE AREA AND PERCENTAGE OF TUMOR CELLS IN BIOPSIES, EXCLUDING BIOPSIES WITHOUT ANY TUMOR CELLS (N=17). SUPP 6D. COMPARISON OF MESOTHELIOMA MOLECULAR SUBTYPE ESTIMATED BY DECONVOLUTION FROM RNA-SEQ WITH WISP ALGORITHM (E-SCORE, S-SCORE AND NORMAL-SCORE), EXCLUDING BIOPSIES WITHOUT ANY TUMOR CELLS (N=16). ALL TESTS WERE WILCOXON RANK-SUM TEST (NOT PAIRED SAMPLES) (REPRESENTATION OF P-VALUE: NS >0.05).

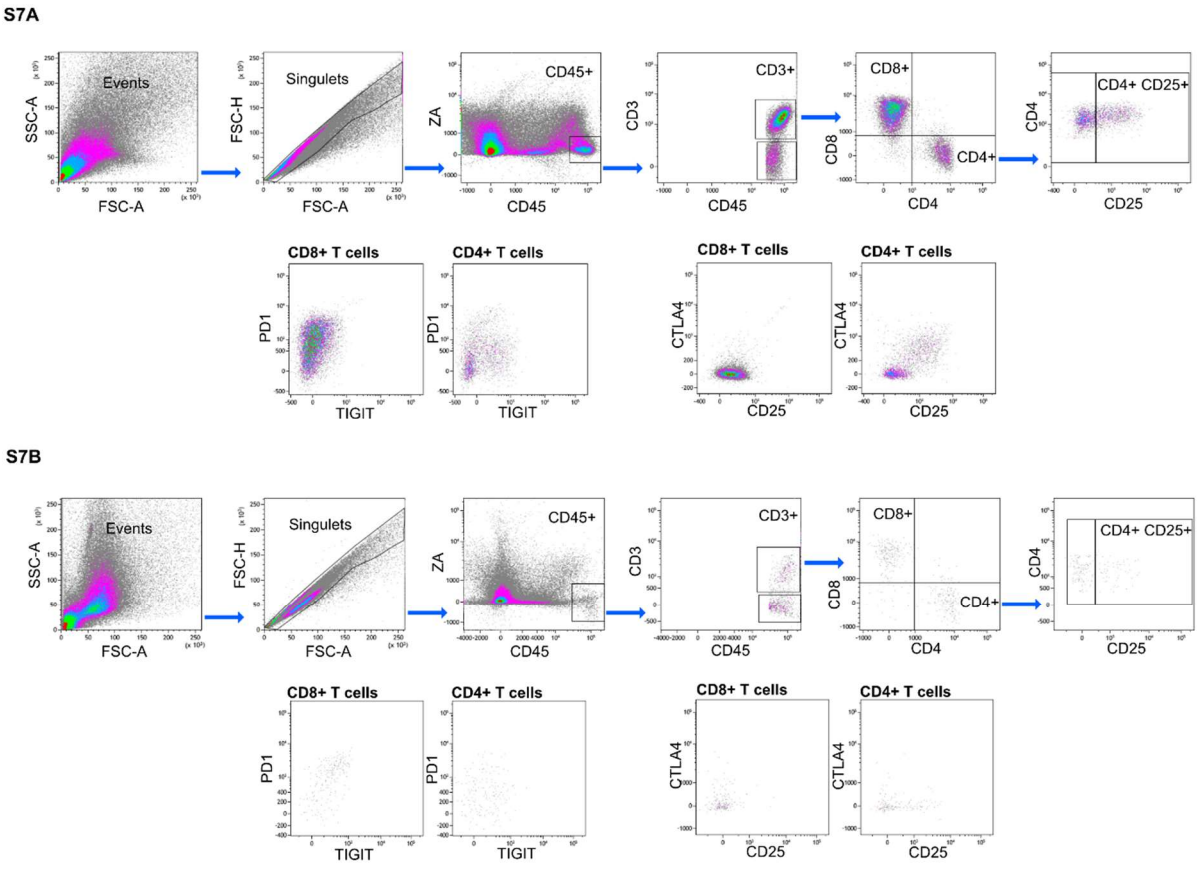

SUPPLEMENTARY FIGURE 7. GATING STRATEGY OF FLOW CYTOMETRY ANALYSES OF T CELLS INFILTRATION FROM TUMOR BIOPSIES (MESOTHELIOMA COHORT).

SUPP. 7A. EXAMPLE OF A PATIENT WITH HIGH IMMUNE INFILTRATE IN TUMOR. SUPP. 7B. EXAMPLE OF A PATIENT WITH LOW IMMUNE INFILTRATE IN TUMOR.

S8

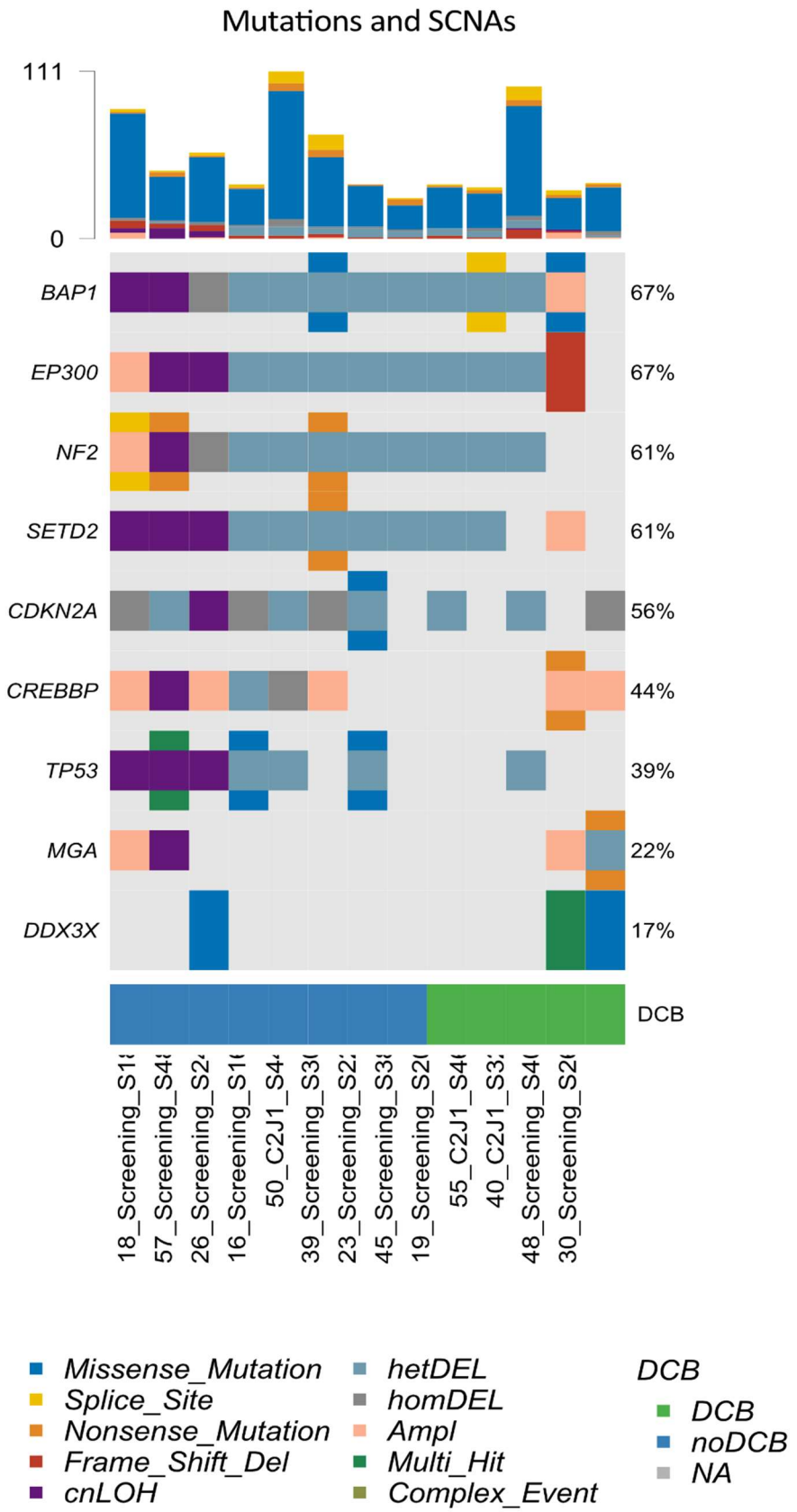

SUPPLEMENTARY FIGURE 8. INDIVIDUAL MUTATIONS AND COPY NUMBER ALTERATION FROM WHOLE EXOME SEQUENCING.

ABBREVIATIONS: DEL = DELETION; CNLOH = COPY NUMBER LOSS OF HETEROZYGOTY; HETDEL = HETEROYZGOUS DELETION; HOMDEL = HOMOZYGOUS DELETION; AMPL = AMPLIFICATION.

S9

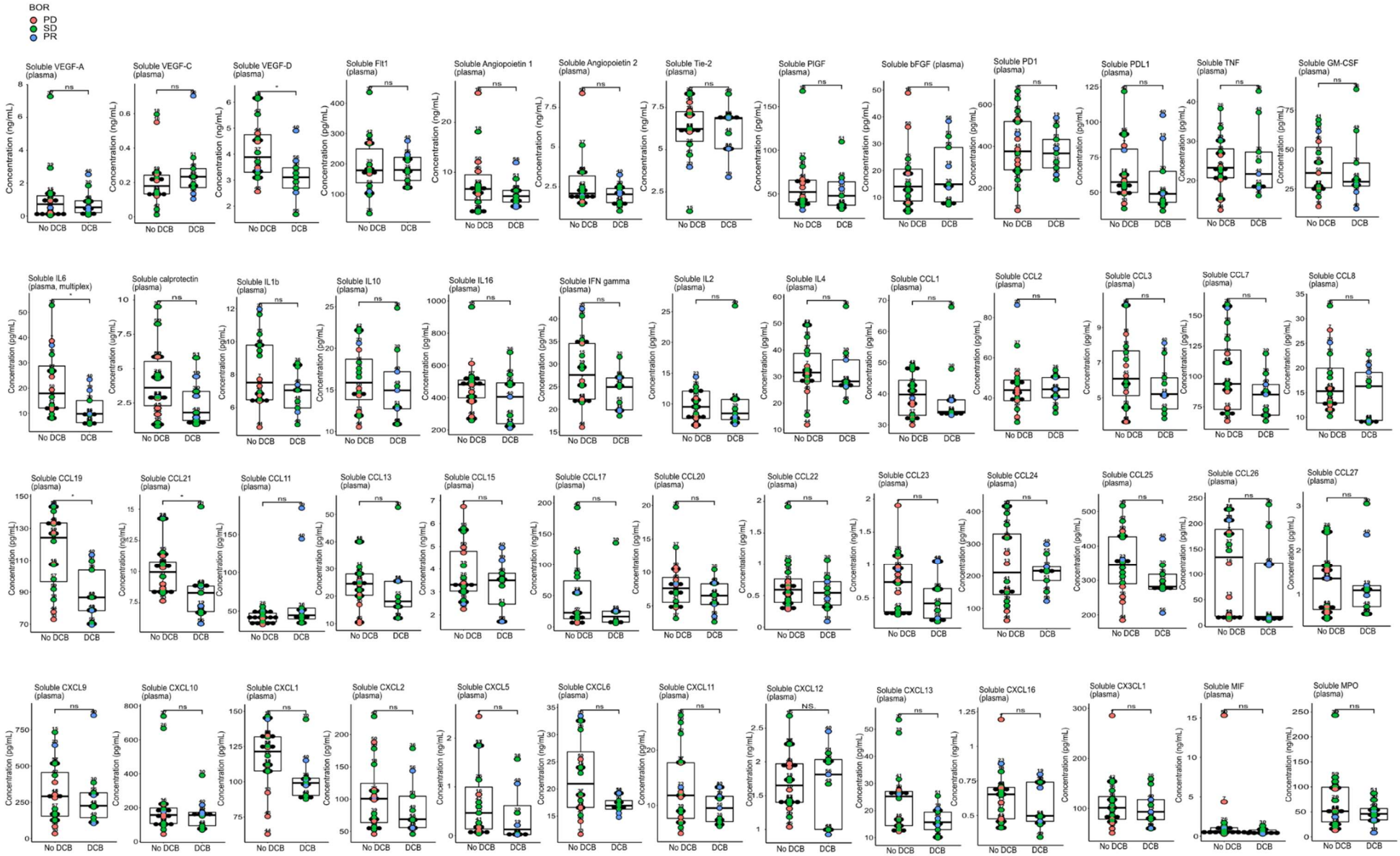

SUPPLEMENTARY FIGURE 9. SOLUBLE ANGIOGENIC FACTORS, CYTOKINES AND CHEMOKINES IN PLASMA AT BASELINE (DAY -7) (MESOTHELIOMA COHORT).

ALL TESTS WERE WILCOXON RANK-SUM TEST (REPRESENTATION OF P-VALUE: NS >0.05, * ≤ 0.05, ** ≤ 0.01, *** ≤ 0.001, **** ≤ 0.0001)

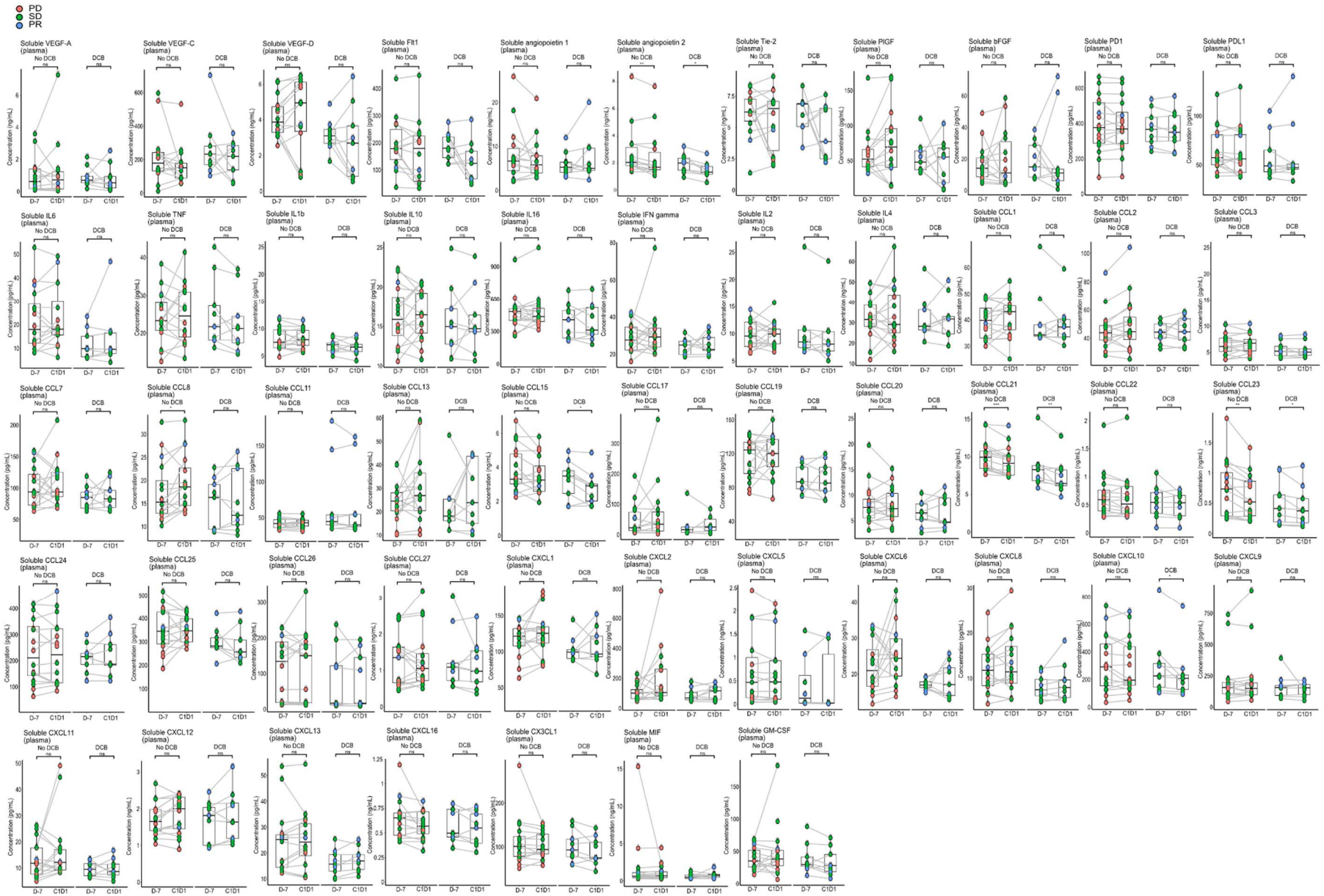

SUPPLEMENTARY FIGURE 10. PLASMA SOLUBLE FACTORS BETWEEN DAY -7 AND CYCLE 1 DAY 1 DURING THE LEAD-IN TREATMENT BY NINTEDANIB MONOTHERAPY (MESOTHELIOMA COHORT).

TESTS WERE PAIRED WILCOXON SIGNED RANK TEST (PAIRED SAMPLES) (REPRESENTATION OF P-VALUE: NS >0.05, * ≤ 0.05, ** ≤ 0.01, *** ≤ 0.001, **** ≤ 0.0001).

S11

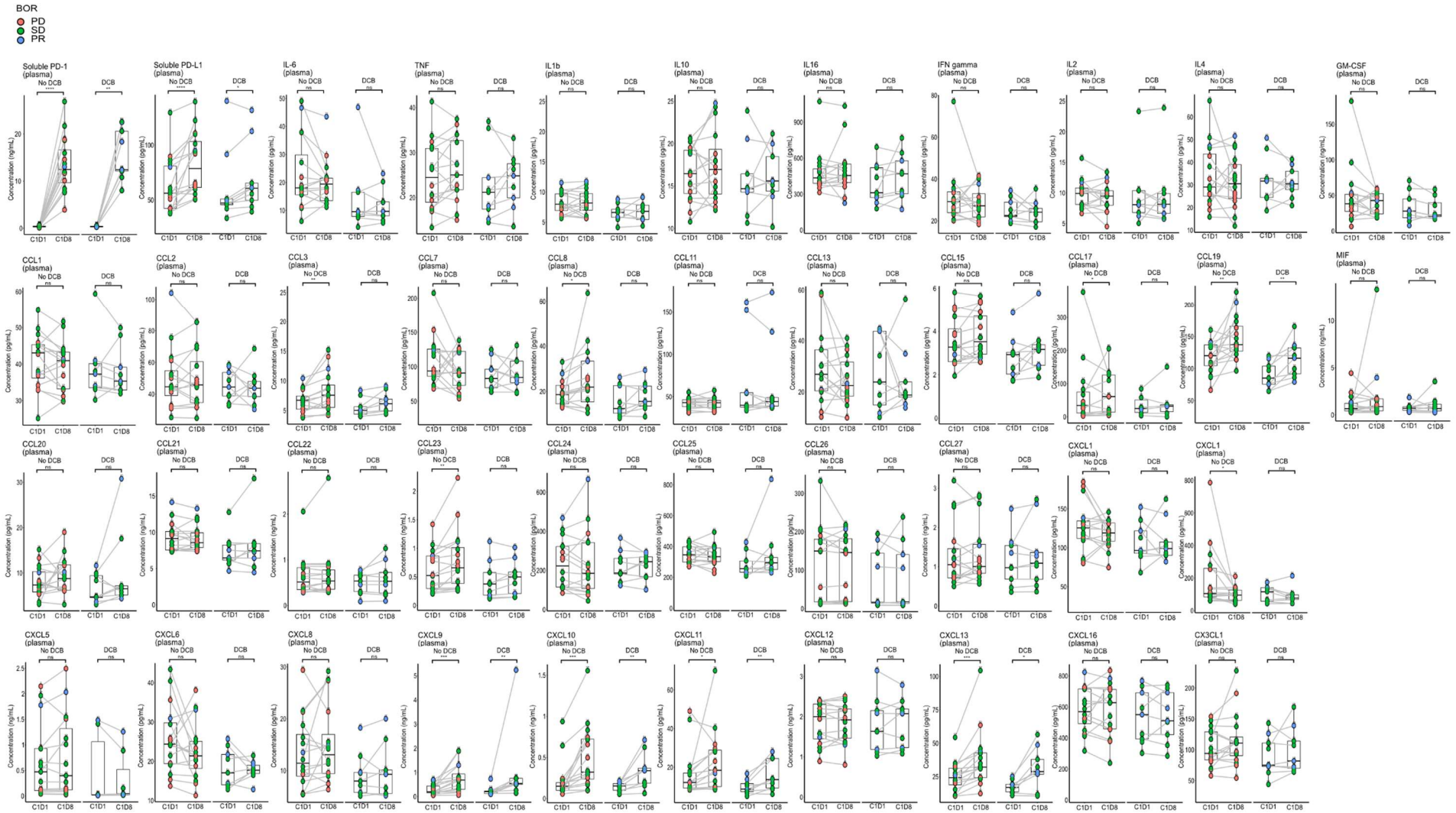

SUPPLEMENTARY FIGURE 11. PLASMA SOLUBLE FACTORS BETWEEN CYCLE 1 DAY 1 AND DAY 8 AFTER THE FIRST INFUSION OF PEMBROLIZUMAB (MESOTHELIOMA COHORT).

TESTS WERE PAIRED WILCOXON SIGNED RANK TEST (PAIRED SAMPLES) (REPRESENTATION OF P-VALUE: NS >0.05, * ≤ 0.05, ** ≤ 0.01, *** ≤ 0.001, **** ≤ 0.0001).

S12A

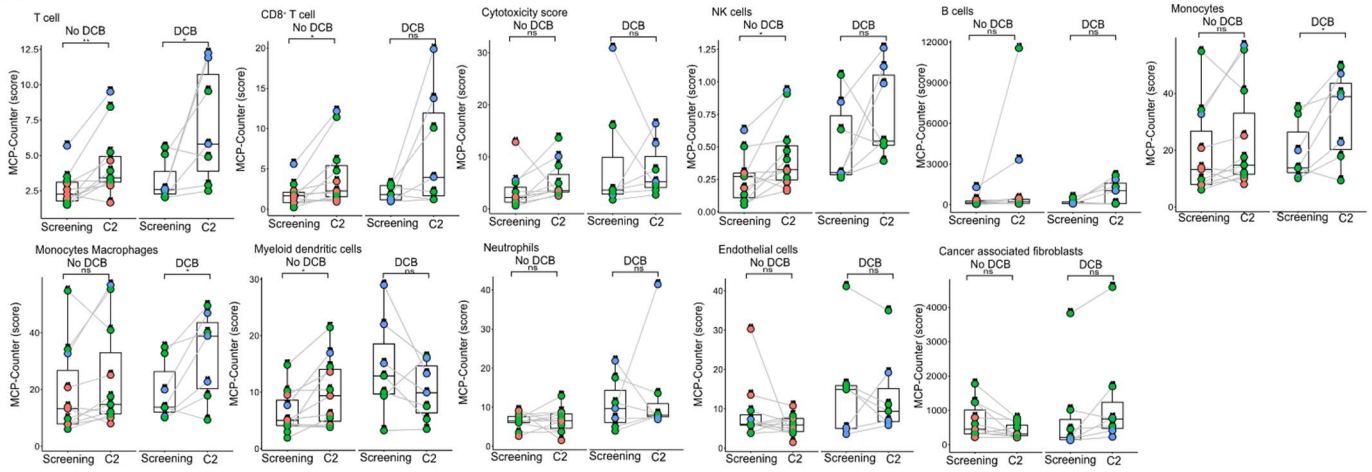

S12B

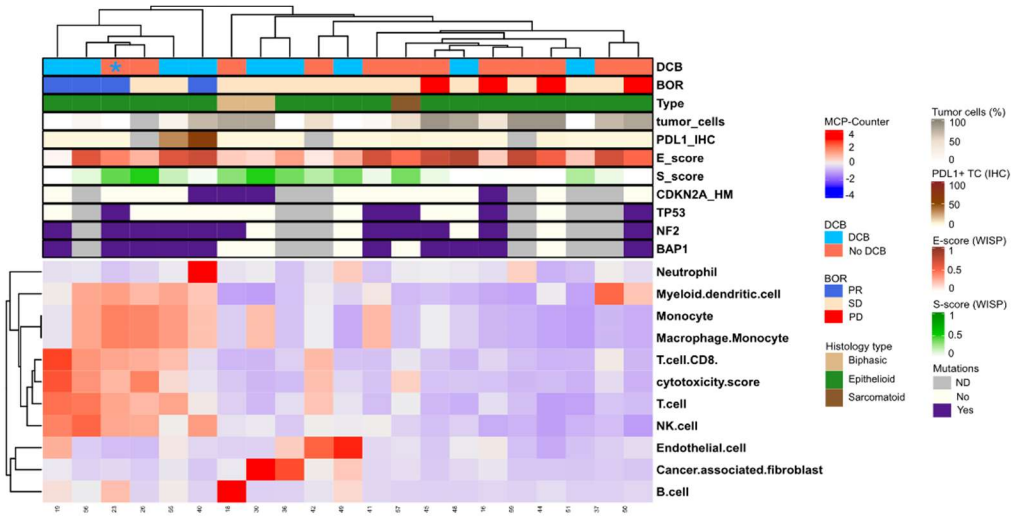

SUPPLEMENTARY FIGURE 12. DYNAMIC OF IMMUNE INFILTRATION IN TUMOR AFTER PEMBROLIZUMAB INFUSION WITH NINTEDANIB (MESOTHELIOMA COHORT).

12A. EVOLUTION OF IMMUNE SUBSETS INFILTRATION IN TUMOR BETWEEN SCREENING AND PRE CYCLE 2 BIOPSIES CONSIDERING PATIENTS WITH AND WITHOUT DCB, BY IMMUNE DECONVOLUTION OF RNA-SEQ (MCP COUNTER). 12B. REPRESENTATION OF UNSUPERVISED CLUSTERING OF PRE CYCLE 2 DAY 1 TUMOR THROUGH IMMUNE INFILTRATION ESTIMATED BY DECONVOLUTION OF BULK RNA-SEQ DATA (MCP COUNTER) WITH CLINICAL AND MOLECULAR ANNOTATIONS (N=21). TESTS WERE PAIRED WILCOXON SIGNED RANK TEST (PAIRED SAMPLES) (REPRESENTATION OF P-VALUE: NS >0.05, * ≤ 0.05, ** ≤ 0.01, *** ≤ 0.001, **** ≤ 0.0001).

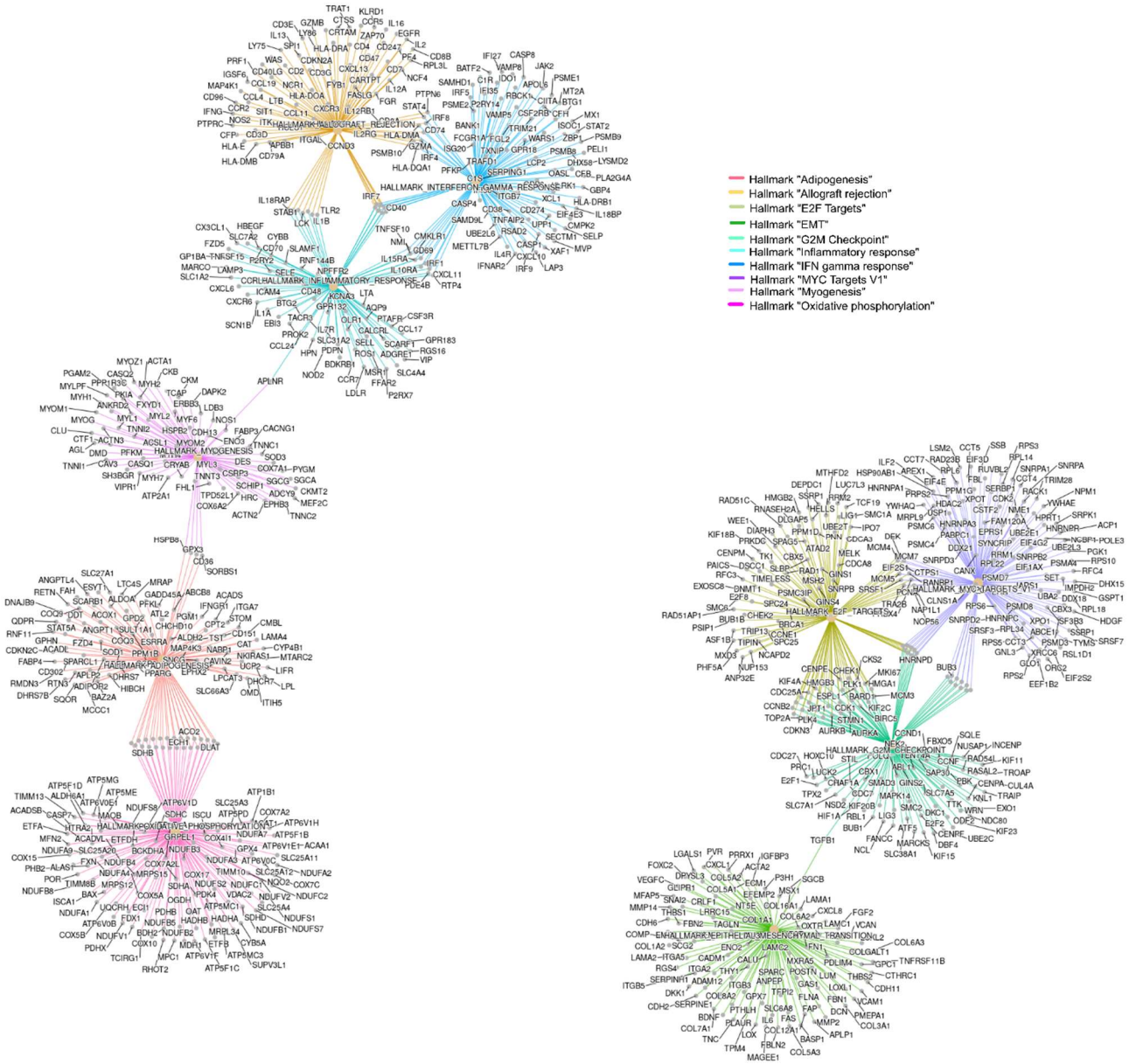

SUPPLEMENTARY FIGURE 13. ILLUSTRATION OF HALLMARKS GSEA NETWORKS FROM DIFFERENTIALLY EXPRESSED GENES IDENTIFIED BETWEEN BASELINE TUMOR BIOPSIES OF PATIENTS WITH AND WITHOUT DCB (N=13) (MESOTHELIOMA COHORT).

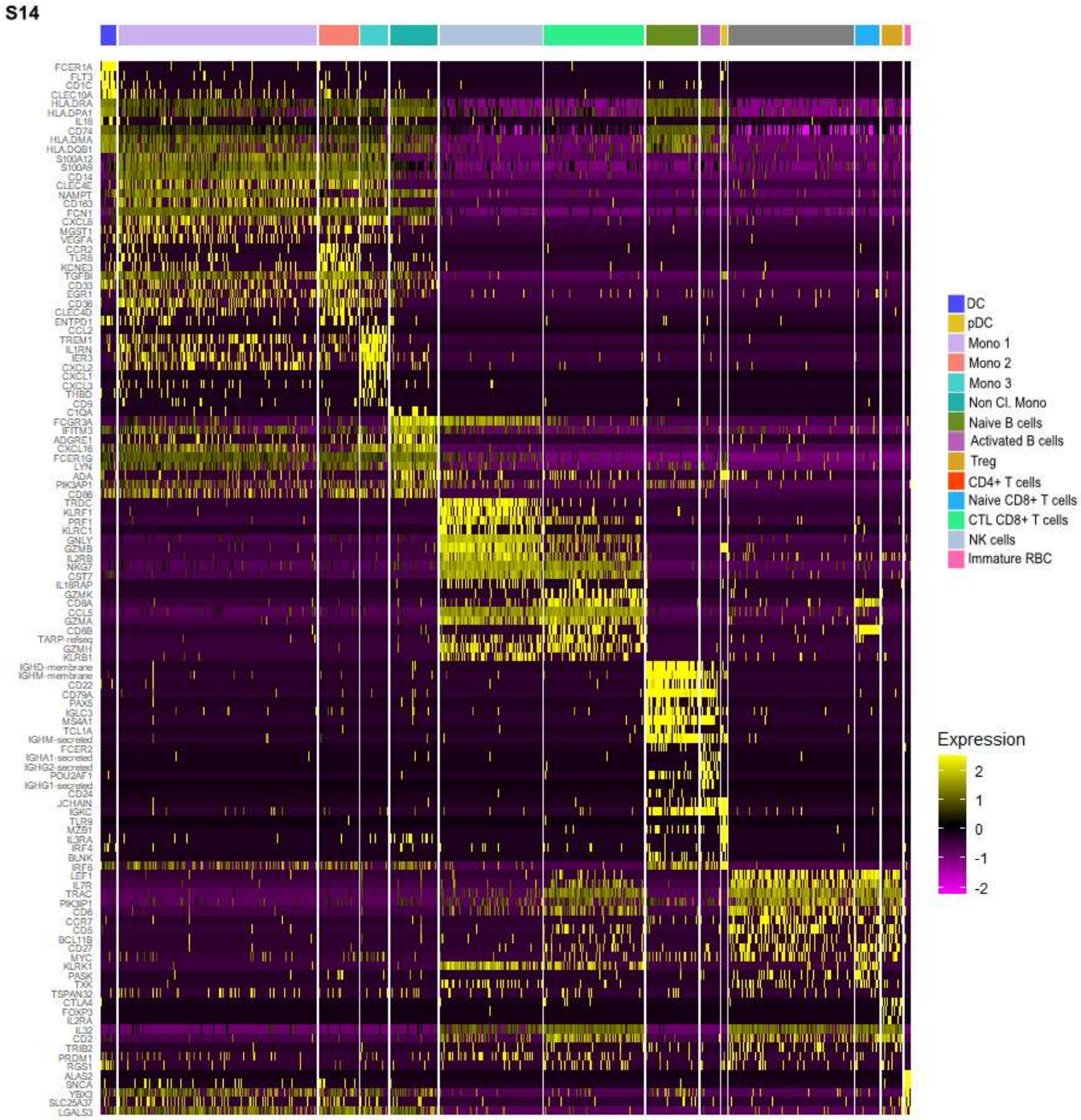

SUPPLEMENTARY FIGURE 14. HEATMAP ILLUSTRATING UNSUPERVISED CLUSTERING OF CELLS FROM THAWED PBMC THROUGH TOP 10 DIFFERENTIALLY EXPRESSED GENES (MESOTHELIOMA COHORT).

S15

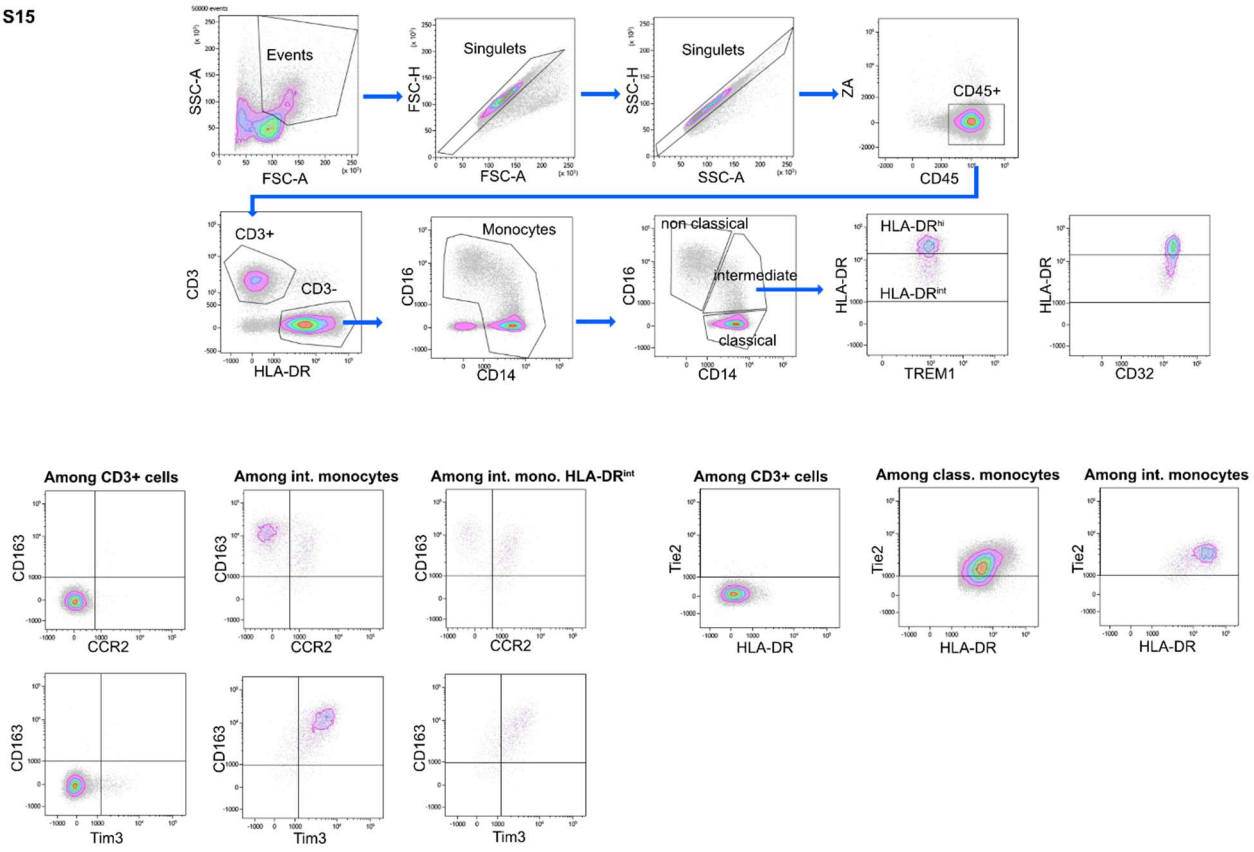

SUPPLEMENTARY FIGURE 15. GATING STRATEGY OF FLOW CYTOMETRY ANALYSES OF CELLS FROM THAWED PBMC OF HEALTHY CONTROLS (N=2) AND PATIENTS WITH DCB (N=5) AND WITHOUT DCB (N=5) (MESOTHELIOMA COHORT).

General discussion.

Many people are implicated to carry out clinical trials, and several years elapse between the preparation of a protocol and the analysis of data resulting from these experiments. The rationales of such trials are built on preclinical knowledges and results of previous trials evaluating therapeutic strategies. Ancillary analyses planned to study the effect of treatments on patients and conversely the patient's characteristics that are affecting the effects of treatments are analyzed through the prism of prior knowledge. Thus, clinical and scientific observations are necessarily guided by pre-conceived ideas. The opportunity of using high throughput tools and unsupervised algorithms, for example on bulk RNA-seq from tumor biopsies and correlate them to the clinical evolution of the patients have allowed us to identify factors that were not previously anticipated to be associated with outcomes to anti-angiogenic & immunotherapy combinations. Such observations can help to carry out additional analyzes, guided by these first results. Also, such results could show us that simple analyses, such as prospective flow cytometry characterization of immune infiltrate in fresh tumors, could bring valuable information which could be simply implemented in clinical practice (if these results can be standardized, replicated, and validated in additional cohorts of patients).

In our work, the number of patients treated remains relatively low, and the number of patient's samples analyzed for each of the experiments is even more limited, because of the difficulties inherent to the conditions of collection and storage, the sometimes-poor quality of the tissues, and the biases related to the techniques and analyzes. Thus, results of ancillary analyses observed from these early trials should be considered with caution, such as clinical results, and need to be reproduced and confirmed in other conditions. However, the limited number of patients is counterbalanced by the number of techniques used here to explore both the blood and the tumor of patients at baseline and upon treatment. Such broad analysis could not be performed on large scale clinical studies. Hence, these observations are important because they provide, at an early stage in the development of a therapeutic strategy, elements associated with the resistance and efficacy of the interventions, in real clinical situations. They enable to anticipate and imagine therapeutic options, which could overcome the resistance of those treatments in patients.

Comparison of results from the dose escalation and the mesothelioma cohorts.

Patients treated with nintedanib and pembrolizumab in both the dose escalation and the mesothelioma cohorts presented with several features which may be important to understand the differences observed between those sets of ancillary analyses. First, these cohorts enrolled patients with different cancer histologies (in dose escalation cohort, they were only two patients with unresectable mesothelioma, those one with a primary peritoneal disease). And the genomic abnormalities associated with cancer types can influence the biology of these tumors and their response to our studied treatments. Second, all the patients did not receive the same dose of nintedanib (in the dose escalation part, patients 7 to 13 received nintedanib at 200mg bid, and all others were at 150mg bid). Although pembrolizumab has not a dose effect pharmacodynamics profile (and all the patients were treated at the approved dose of 200mg Q3W IV), for nintedanib there is a clear dose-efficacy-toxicity relationship which can affect our ancillary biological readouts. For instance, liver toxicities were more frequent when nintedanib was used at 200mg bid instead of 150mg bid with pembrolizumab. But, in the dose escalation cohort, 3/12 patients (25%) presented with an objective partial response and two of them received nintedanib at 150mg bid. These patients were treated for a cervical cancer, an UCNT and a thymic carcinoma, which are very different diseases. The first two are diseases associated with chronic viral infections (HPV and EBV, respectively) and thymic carcinoma is developed from epithelial cells in a primary lymphoid organ. PD-1 blockade was shown to be effective in cancers with oncogenesis promoted by chronic viral infections, such as HNSCC, HCC, cervical carcinoma and maybe UCNT (396). Conversely, mesothelioma are diseases that do not present the usual factors associated with efficacy of immune checkpoint blockade: their mutational burden is typically quite low, and their PD-L1 expression by tumor cells is sparce (except for sarcomatoid subtypes, which were a minority of our patients). These major differences could partly explain the differences observed between both studies.

Differences observed between both studies may also be due to the fact that analyses were not all following the same methods. For example, biopsies in the dose escalation cohort were analyzed with IHC (including a multiplex panel dedicated to analyses of myeloid cells) whereas in the mesothelioma cohort, biopsies were processed for flow cytometry, but had less complete IHC analyses, bulk RNA-seq and WES. Also, the quantification of the immune infiltration by IHC was not evaluated the same way in both cohorts: quantitatively in the escalation cohort (number of cells per HPF or density of cells per mm^2) instead of semi-quantitative scores in the mesothelioma cohort. Another difference concerned post treatment timepoints for measurement of soluble factors in plasma: in escalation cohort, soluble factors were measured at cycle 2 day 1 whereas in the mesothelioma cohort the analysis were performed at cycle 1 day 8. Those differences could also be explained by the fact that those ancillary analysis were not done at the same time and

in a same run. Batch effects could indeed be an important bias that need to be considered for each experiment and requires being cautious to compare results from different experiments.

The pre-treatment observations on tumor biopsies and circulating factors were not exactly similar between both cohorts. For the first 12 patients, even if it was not significant, the immune infiltration estimated by IHC tended to be higher in the tumor microenvironment of patients with benefit to treatment (for CD3+ T cells, FOXP3+ T cells and DC-LAMP+ DC) as opposed to the patients in the mesothelioma cohort (**Figures 8C; Supplementary Table 2**). This point highlights that, in this cohort, the global immune infiltrate, including immunosuppressive regulatory $CD4^+$ T cells, infiltrate more tumors from patients who will benefit to PD-1 blockade combined with anti-angiogenic. The observations that patients with tumor infiltration by Tregs, high plasma rates of CCL22, high percentage of circulating Tregs and $CCR4^+$ $CXCR3^+$ memory $CD4^+$ T helper cells were benefiting from the therapy were surprising because these immune effectors are precisely associated with an immunosuppressive pro-tumoral microenvironment in humans (**Figures 8A, 9C**). This could be explained by the fact that a preexisting immune response, secondary to T cells recognition of type 2 MHC complex with tumor associated antigens, viral associated antigens or neoantigens make those types of tumor to respond to the treatment. Then, the administration of both pembrolizumab and nintedanib may unleash a pre-existing anti-tumor immune response. In addition, if such factors that are typically associated with bad outcomes under conventional therapies become biomarkers of efficacy with those novel treatments they will turn from prognostic to predictive factors.

In the mesothelioma cohort, there was no difference between patients with and without benefit to treatment considering $CD8^+$, $CD3^+$ $CD8^-$, $CD20^+$ cells infiltration and TLS structure (**Supplementary table 2**). Some patients who presented with primary progressive disease had TLS in their tumor microenvironment. This observation highlights that no single factor can simply predict the efficacy of a treatment and that there are other factors limiting their beneficial effect. But flow cytometry analyses of fresh mesothelioma biopsies showed that tumors from patients with clinical benefit had higher $CD45^+$, $CD3^+$ and $CD8^+$ among $CD3^+$ cells than patients without benefit to treatment (**Figure 12B**). This could be concordant with literature but discordant with IHC analyses of paired biopsy samples.

The baseline plasmatic factors, which were identified to differentiate patients with or without clinical benefit in both cohorts, were not identical. First, the plasma rate of CXCL10 was higher in patients with benefits to treatment in the dose escalation cohort (**Figure 8A**). It was also the case in the mesothelioma cohort, but after pembrolizumab infusion, increasing rates of plasma CXCL10 were observed in all patients, independently of their response to treatment (**Supplementary figure 10; Figure 12F/G**). These observations suggest that in some tumor types, the release of CXCL10

by cells in the tumor microenvironment may favor the infiltration of $CXCR3^+$ T cells, and notably specific antitumoral T cells, and not in others. This could explain partly the sensitivity of some tumors to PD-1 blockade and not for others. Also, by disrupting the PD-1/PD-L1 interaction systemically, the PD-1 blockade might let exhausted T cells to produce IFNγ, which in turn could induce the production of CXCL10 by targeted cells and notably macrophages, independently of the sensitivity of the tumor to the treatment. Alternatively, the fact that all patients upregulated CXCL10 could suggest that it is a pharmacodynamics effect of PD1 blockade, and that all patients respond to pembrolizumab and nintedanib but that other downstream mechanisms of resistance limit the efficacy of the treatment in a subgroup of patients.

Common results in both cohorts of the study.

Overall, the clinical results tended to be similar in both cohorts. First, besides conventional immune related adverse events, one patient in the dose escalation cohort and two in the mesothelioma cohort developed unusual vascular adverse events, with mesenteric arterial occlusion in two patients, cardiac involvement with myocarditis in two patients, and one of them died early after the first infusion of pembrolizumab. These were worrying toxicities, rare, and have been related to the treatment. However, the other patients did not present unmanageable adverse events upon combination.

Secondary, even if the disease control rate at 12 weeks in the mesothelioma cohort tended to be slightly higher than in phase 1 clinical trials of PD-1 blockade monotherapies for patients with unresectable mesothelioma refractory to platinum-based chemotherapy, the addition of nintedanib seemed to increase modestly the antitumoral response. PD-1/PD-L1 blockade are now tested in combination with anti-angiogenic TKIs in multiple cancer indications. Early results support that such combination can increase the response rates compared to those obtained with anti-PD1 therapy alone. However, still a majority of patients (>50%) do not respond to such combination treatment (397–399). Anti-angiogenic TKI do not have similar capacities to inhibit kinases pathways: constant of inhibition can be higher or lower depending on the drug, and some of them can inhibit pathways, which are not targeted by others (e.g c-Met, Tie2, and others) (**Table 2; Figure 3**). But maybe, the ideal anti-angiogenic drug for such combination would be a monoclonal antibody. Indeed, the results of a recent phase 1 clinical trial of combination of atezolizumab with bevacizumab for patients with unresectable peritoneal mesothelioma were very impressive, with an objective response rate of 40% (8/20; 95%CI:19.1-64.0) (283).

Several aspects of the observations brought by our ancillary analyses can be considered similar in both cohort studies. With different methods, CD8+ T cells infiltrates in tumors were more abundant in pretreatment biopsies in patients with benefit to treatment. Presence of dendritic cells identified with IHC trough DC-LAMP expression and by expression of some genes using deconvolution of bulk RNA-seq data (MCP-Counter) were higher in tumor infiltrates of patients with benefit to treatment.

We found higher rates of plasma/serum inflammatory cytokines and chemokines, notably IL-6 and CXCL8, in patients without benefit to treatment in the mesothelioma cohort. This was not observed at baseline in the dose escalation cohort (**Supplementary figure 9; Figure 14E**). These observations become to be highly prevalent in the scientific and medical literature, with analyses of large cohort of plasma samples from patients included in phase 3 clinical trials evaluating PD-1 blockade to treat metastatic melanoma or NSCLC (329,330). As presented in our introduction, high levels of IL-6 and CXCL8 have been described as factors associated with tumor resistance to immune checkpoint blockade and anti-angiogenic drugs, when used in monotherapy (384). Combinations of both therapeutic strategies did not allow to overcome these barriers to antitumor efficacy, in our study. However, as opposed to the mesothelioma cohort where concentration of IL6 and CXCL8 stay at the same rate during treatment, patients without benefit to treatment had increasing rates of TNF and higher rates of IL6 and CXCL8 at cycle 2 than patients with benefit to treatment in the dose escalation cohort (**Figure 10**). This could be due to a sampling bias (rates may be higher before initiation of treatment and not only at cycle 2), or secondary to cancer progression or this could be induced by the treatment.

In the dose escalation cohort, after pembrolizumab infusion, plasma rates of CCL3, CCL4, IL18, and IL10 increased significantly only in patients without benefit to treatment between cycle 1 day 1 and cycle 2 day 1 (Supplementary figure 2). In the mesothelioma cohort, plasma rate of CCL3, CCL8, CCL17, CCL19 and CCL23 increased also significantly only in patients without benefit to treatment between cycle 1 day 1 and cycle 1 day 8 (**Supplementary figure 11**). These observations may be compared to those published in relation to the phenomena of tumor hyper-progression (385). A deleterious effect of our treatment on specific cancer subtypes cannot be eliminated. The role played by these chemokines in the biology of the cancers that we treated remain to be determined.

The pathophysiology of the cytokines belonging to the IL-6 family in cancer development is pleiotropic (400). We recently observed that another cytokines of the gp130 family, the leukemia inhibitory factor (LIF,) was also a strong negative predictor of antitumor responses to PD-1 blockade in different tumor types (401) (**Appendix 2**). These cytokines have direct effects on tumor survival, through the induction of cellular growth by amplification of several intracellular kinase pathways (402). They also have effects on innate and adaptive immune cells, promoting immunosuppressive

Treg polarization of $CD4^+$ T cells and impacting the function of monocytes / macrophages toward an immunosuppressive profile (403). IL-6 and cytokines from the gp130 family can be secreted by immune cells, fibroblasts and tumor cells and can shape the tumor microenvironment (404). Interestingly, patients with higher levels of plasma LIF presented with lower immune infiltrates in their tumors (401). Also elevated plasma rate of IL-6 is associated with patients cachexia and systemic manifestations associated with cancer (405–408). Targeting the IL6 pathway with an anti-IL6R could be interesting for such patients with high baseline levels of IL6. However, our experience in Covid-19 patients treated by tocilizumab have suggested that baseline levels of TNF are also important to predict the value of such strategy (409). Hence, blocking TNF could be beneficial for a larger group of patients. Interestingly, this approach of checkpoint blockade plus anti-TNF has recently proved to be safe (410). Also, the targeting of IL-6 cytokines might be insufficient because of the redundancy with other factors, such as LIF, and because of an association with other inflammatory pathways, such as CXCL8 and neutrophils which also can limit the efficacy of PD-1 blockade and anti-angiogenic drugs. Thus, the understanding of mechanisms leading to the production of such cytokines by tumor cells, directly or indirectly, appear essential. Some cancers and molecular alterations were known to produce and promote IL-6 family cytokines, such as pancreatic ductal adenocarcinoma with KRAS mutation (411–414). Senescent associated secretory phenotype was described as the ability of cells with such oncogenic alterations to produce inflammatory cytokines chemokines such as CXCL8 and CCL2, even in different types of diseases (415–417). Last but not least, the link between the level somatic copy number alterations and those pro-tumoral pro-inflammatory profiles remain elusive. More clinical observations and pre-clinical in vitro experiments are needed to decipher if such oncogenic stress directly result into higher secretions of pro-inflammatory cytokines or if those cytokines are secreted by the tumor stroma in reaction to the recognition of these altered-self cancer cells by immune cells in order to protect them.

Perspectives for the next steps: Understanding the genomic alterations of unresectable malignant mesothelioma to overcome the resistance to immune checkpoints blockade.

Impacts of genomic abnormalities on the Immune Microenvironment of Malignant Mesothelioma tumors.

The deletions of tumor suppressor genes identified in mesothelioma might shape the tumor microenvironment and hamper the efficacy of immune checkpoint blockade in patients with advanced malignant mesothelioma (MM). Indeed, *CDKN2A* genomic alterations are associated with lower immune infiltrations in several tumor types and worse outcome upon anti-PD(L)1 immunotherapy for patients with metastatic urothelial carcinoma (418). In murine models of solid cancers, inhibition of CDK4/6 induces an inhibition of tumor cells proliferation and promotes T-cells infiltration in tumors through tumoral expression of endogenous retroviral elements and inhibition of Treg immunosuppressive functions in the tumor stroma, both mediated by control of DNMT1 which is a target of E2F (378). Also, murine models have shown that the hyper activation of the Hippo-YAP pathway induced the recruitment of myeloid derived suppressor cells (MDSC) and immunosuppressive macrophages in the tumor microenvironment and promote tumor growth, notably by production of specific chemokines (419–421). As a consequences of disinhibition of growth factor pathways, cAMP response element binding protein (CREB1) is overexpressed in MM cells and drives to the production of CXCL8 (aka interleukin-8 or IL-8) and CCL2 in the tumor microenvironment (422,423). Interestingly, higher rates of CXCL8 in plasma from cancer patients has been recently associated with resistance to immune checkpoint blockade, and was associated to the recruitment of such polymorphonuclear MDSCs in tumors (342). Also, murine models showed that that the production of CCL2 in breast tumors led to the recruitment of inflammatory monocytes in the tumor microenvironment which favored tumor growth and metastasis spreading (387).

Overexpression of *EZH2* in tumor cells, through *BAP1* loss or upon E2F promotion, leads to H3K27 trimethylation and gene silencing of pathways that are important to coordinate an efficient anti-tumor immunity (191). For instance, a murine model showed that in human ovarian cancer cells, trimethylation of H3K27 and DNA methylation (induced by DNMT1) in the promoter regions of *CXCL9* and *CXCL10* genes led to the downregulation of their expression, a decrease in $CD8^+$ T cells tumor infiltration and in sustained tumor growth (424). Accordingly, in a murine model of melanoma, the presence of TNF in the tumor microenvironment and tumor infiltration by T lymphocytes induced an overexpression of EZH2 in tumor cells, which mediated the silencing of class 1 major histocompatibility complex (MHC-1), *CXCL9* and

CXCL10 genes (425). In both models, Ezh2 blockade restored immune cell infiltrates in tumors, decreased tumor growth and allowed to overcome a mechanism of resistance to anti-tumor immunity.

Biologically driven drug development to overcome immunotherapy resistance in malignant mesothelioma

Targeted therapies to alter immunosuppressive oncogenic pathways

As opposed to oncogenic drivers, loss of tumor suppressor genes has been difficult to target in the past by pharmacological means. But nowadays, novel therapies allow to target those alterations (426). In the context of patients with advanced MM refractory to immune checkpoint blockades, treatments developed to counterbalance *BAP1*, *CDKN2A* or *NF2* somatic loss could be of interest (**Figure 2**). Such drugs are tested in biomarker selected MM patients using FISH to identify *CDKN2A* homozygous deletion, IHC for BAP1 deletion or maybe both for *NF2* deletion and Hippo pathway alterations. Particularly in the mesothelioma cohort of PEMBIB trial, using of FISH for *CDKN2A* (9p21) must be interested because of E2F target gene set was enriched in patients who did not benefit to treatment, in parallel type 1 IFN gene set were decreased in these patients (genes of type 1 IFN are on the same chromosomal region of CDKN2A and are lost by the deletion of 9p21) and all patients who did not benefit to treatment had at least heterozygous deletion of 9p21 instead of patients with benefit (**Figure 13B; Supplementary figure 8**).

To note, ongoing many early clinical trials investigating targeted therapies and cellular immunotherapies in patients with unresectable mesothelioma do not exclude those previously treated by immune checkpoint blockade (**Table 8**).

	Treatment(s)	Phase	Type of treatment	Post-ICB	NCT
Tumor-targeted small molecule therapy	Olaparib	2	PARP inhibitor	Allowed	NCT04515836
	Niraparib	2	PARP inhibitor	Allowed	NCT03207347
	CPI-0209	½	EZH2 inhibitor	Allowed	NCT04104776
	VT3989	2	TEAD inhibitor	Allowed	NCT04665206
	Defactinib	1	FAK inhibitor	Allowed	NCT01870609
	APG-2449	2	FAK, ALK, ROS1 inhibitor	Allowed	NCT03917043
	Vandetanib	2	VEGFR, EGFR, RET inhibitor	Allowed	NCT00597116
	Tivantinib	2	MET inhibitor	Allowed	NCT01861301
	Dovitinib	2	FGFRs, VEGFR, (…) inhibitor	Allowed	NCT03975387
	ASTX295	1/2	MDM2 antagonist	Allowed	NCT04430842
	IOA-244	1	PI3Kδ Inhibitor	Allowed	NCT04328844
	PF-06952229	1	TGFbR1 inhibitor	Allowed	NCT03685591
Tumor-targeted Cellular Immunotherapy	Autologous CAR-T/TCR-T Cell	½	CAR-T-cell anti mesothelin	Allowed	NCT03638206
	Gavo-cel (TC-210)	½	CAR-T-cell anti mesothelin	Allowed	NCT03907852
	huCART-meso cells	1	CAR-T-cell anti mesothelin	Excluded	NCT03054298
	M28z1XXPD1DNR	1	CAR-T-cell anti mesothelin	Allowed	NCT04577326
	αPD1-MSLN-CAR T Cells	1	CAR-T-cell anti mesothelin	Allowed	NCT04489862
	Adoptive Transfer of TIL	2	Tumor infiltrated lymphocytes Tumor infiltrated lymphocytes	Allowed	NCT03935893
	NeoTIL	1		Allowed	NCT04643574
	Allogenic Natural Killer Cells	1	Cord Blood-derived NK	Allowed	NCT03420963
	Autologous Dendritic Cell Vaccination	½	DC-WT1 vaccination	Allowed	NCT02649829
	MesoPher	2/3	DC vaccination	Allowed	NCT03610360
Tumor-targeted protein engineered therapy	LMB-100 with Tofacitinib	1	anti mesothelin ADC + JAKi	Allowed	NCT04034238
	HPN536	½	Trispecific and MSLN/ALB/CD3	Allowed	NCT03872206
	INBRX-109	1	DR5 agonistic antibody	Allowed	NCT03715933
	SCB-313	1	TRAIL-Trimer Fusion Protein	Allowed	NCT03443674
	SGN-CD228A	1	anti-CD228 ADC (MMAE)	Allowed	NCT04042480
	Brentuximab Vedotin	2	anti-CD30 ADC (MMAE)	Allowed	NCT03007030

TABLE 8. ONGOING EARLY CLINICAL TRIALS WITH MONOTHERAPIES FOR MALIGNANT MESOTHELIOMA.

For instance, Poly ADP Ribose Polymerase (PARP) inhibitors have been shown to generate chromatin fragments which activate cyclic GMP-AMP synthase/stimulator of IFN genes (cGAS/STING) pathway, and induce the production of CCL5 and the expression of PD-L1 by tumor cells in cell lines with homologous reparation deficiencies (427,428). Also, as discussed previously, EZH2 inhibition could sensitize tumor cells to specific immune cells. Moreover, it was shown that anti CTLA-4 administration increased EZH2 expression in peripheral T cells from treated patients with cancer receiving ipilimumab (429). EZH2 blockade in Tregs decreased their immunosuppressive functions, increased tumor infiltration by functional effector CD8+ T cells and inhibited tumor growth in a mice model (430).

Considering MM with *BAP1* loss, two phase 2 clinical trials evaluating PARP inhibitor and EZH2 inhibition have been done in patients with MM refractory to platinum-based chemotherapy. In the basket trial MiST1 (for Mesothelioma Stratified Therapy), dedicated to patients with relapsed MM (NCT03654833), treatment by rucaparib monotherapy brought a disease control rate at 12 weeks to 58% (n=15/26; 95% CI 37-77) and was well tolerated (431). Moreover, a phase 2 clinical trial evaluating an EZH2 inhibitor monotherapy for patients with refractory MM reported 51% of patients achieving disease control at 12 weeks (432).

CDK4/6 inhibitors have been shown to decrease tumor cell proliferation, to promote immunogenic cell death through release of factors such as high mobility group box 1 (HMGB1) by tumor cells, to induce T cell infiltration in tumors and to synergize with PD-1 blockade to limit tumor growth (379,433). In a phase 1 clinical trial, patients received anti-aromatase and pembrolizumab with or without palbociclib for positive hormonal receptor breast cancer. The addition of palbociclib induced changed upon treatment in the phenotypes of circulating dendritic cells and monocytes (434).

An Hippo pathway alteration by *NF2* loss leads to YAP/TAZ hyperactivation, to cell survival, proliferation, and to the recruitment of immunosuppressive cells in the tumor microenvironment (435). Therapeutic strategies to inhibit YAP/TAZ signaling is challenging, but recent drugs were shown to directly inhibit their dependent transcription functions through direct inhibition of binding between TEAD and YAP/TAZ, notably in MM cell line with *NF2* loss (436,437). Focal Adhesion Kinase (FAK) inhibition in mouse models limited tumor growth of mesothelioma with loss of *NF2* (438). A phase 2 evaluating a maintenance therapy by defactinib, a FAK inhibitor, versus placebo after a first line of chemotherapy in patients with unresectable mesothelioma, did not shown an improvement of PFS nor OS by defactinib (439). Otherwise, YAP/TAZ interact with the bromodomain-containing protein 4 (BRD4) to recruit RNA polymerase II and regulate downstream genes expression (440). The bromodomain and extra terminal motif (BET) inhibitor JQ1, an established BRD4 inhibitor, was shown to inhibit YAP/TAZ signaling in cell lines with Hippo pathway alterations (441,442). BET inhibition have shown anti-tumoral activities through the modulation of immune infiltrates in the tumor microenvironment by intrinsic tumor effects and regulation of immune cell functions in murine models (443–445).

However, the genomic characterization of human MM highlighted that mesothelioma cells present frequently with several genomic alterations, loss of tumor suppressors and that those alterations are all interconnected (103,113). For instance, loss of *FAT1* or *NF2* genes have been shown to increase *CDK6* expression via the Hippo pathway and to reduce the sensitivity to CDK4/6 inhibitors in a breast tumor model (446). Thus, the alteration of a second tumor suppressor pathway could inhibit the therapeutic intervention against the first targeted pathway. Recent studies have highlighted that human advanced MM present with genomic and epigenetic heterogeneity and sequentially acquired molecular events through cancer cell clonal evolution (386). In this work, BAP1 loss (or 3p21 deletion) were early acquired by MM cancer cells during their phylogenetic evolution, whereas NF2 alterations (or 22q losses), leading to Hippo pathway inactivation, where predominantly late events, positively selected. In this series of human MM, higher number of copy number alterations was associated to high neutrophil to lymphocyte ratios in the blood of patients, a feature strongly associated to resistance to immune checkpoint blockade (447,448). Also, patients with the most genomically unstable MM were presenting with higher CD8+ T-cell infiltration in their tumors and tumors with higher neoantigen burden had HLA loss of heterozygosity, consistent with clonal selection toward immune escape (386,449).

Targeted therapies to modulate the detrimental inflammation and angiogenesis in the microenvironment of mesothelioma tumors

Inflammatory and angiogenic molecules induced by the loss of suppressor tumor genes could be specifically targeted to enhance mesothelioma immunotherapy efficacy (**Figure 15**). Mesothelioma tumor cells can induce, directly or through the recruitment of inflammatory cells, pro-inflammatory cytokines such TNF, IL1β, IL6 and VEGF-A in the tumor milieu. Monoclonal antibodies and small inhibitory molecules targeting those pathways are already available in the clinic (410,450,451). Tumor cells can also secrete chemokines such as CCL2 or CXCL8/IL8 which attract Tregs and MDSCs derived from circulating monocytes and neutrophils; those chemokines could also be therapeutically antagonized (452,453). MDSCs secrete molecules and express soluble factors, such as arginine and leukocyte immunoglobulin-like receptor B4 (LILRB4), which are druggable targets currently tested in oncology clinical trials (454,455). Finally, yet importantly, the anti-angiogenic monoclonal antibody bevacizumab are an important therapeutic options for patients with MM. In a phase 3 clinical trial, the addition of bevacizumab, an anti VEGF-A IgG1 monoclonal antibody, to first line platinum-based chemotherapy with pemetrexed have shown to improve the overall survival of patients with unresectable pleural MM (75). Atezolizumab and bevacizumab showed impressive results for patients with unresectable peritoneal mesothelioma (283). Although bevacizumab is not part of the standard of care, antiangiogenic drugs are efficient

in MM. Interestingly, ongoing trials are currently evaluating the combination of anti-PD1 (pembrolizumab) with the antiangiogenic TKIs lenvatinib and nintedanib (PEMMELA/NCT04287829 and PEMBIB/NCT02856425 respectively).

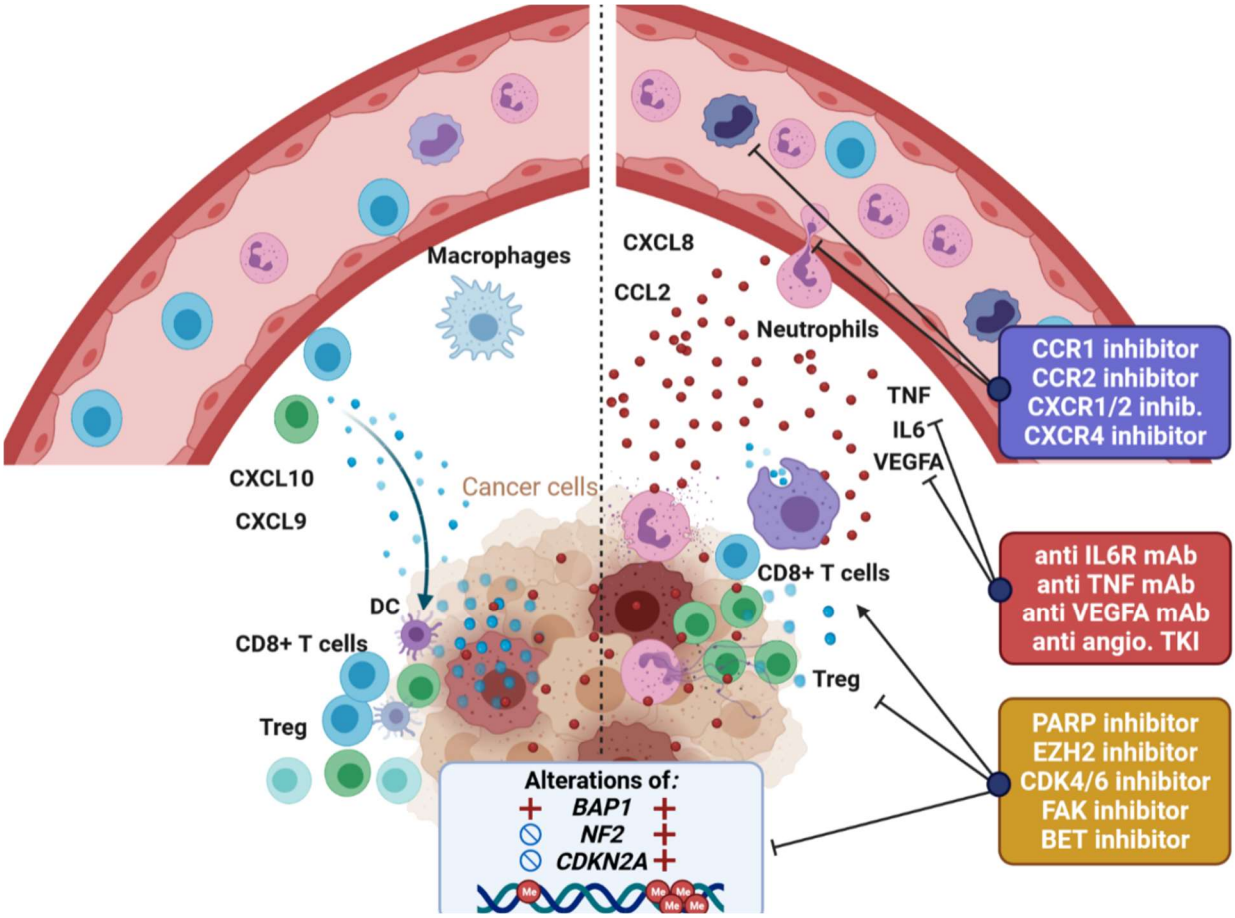

FIGURE 15. TUMOR INFLAMMATORY AND ANGIOGENIC FEATURES ASSOCIATED WITH RESISTANCE TO IMMUNE CHECKPOINT BLOCKADE AND POTENTIAL THERAPEUTIC INTERVENTIONS FOR THE TREATMENT OF PATIENTS WITH MESOTHELIOMA.

LEFT PANEL: SCHEMATIC SITUATION ASSOCIATED WITH EFFICIENCY OF IMMUNE CHECKPOINT BLOCKADE; RIGHT PANEL: SCHEMATIC ILLUSTRATION OF MESOTHELIOMA MOLECULAR AND STROMAL CHARACTERISTICS ASSOCIATED WITH RESISTANCE TO ICB.

Conclusion

The anti PD-1 and anti CTLA-4 immune checkpoint blockade combination has been approved by the FDA to treat patients with unresectable pleural MM, independently of molecular subtypes, genomic or epigenetic alterations, or tumor microenvironment features. Because primary and secondary resistances to those immunotherapies are frequent in MM, novel therapeutic strategies are eagerly awaited for this deadly cancer. The recent discoveries in the pathophysiology of MM and our better understanding of the mechanisms of resistance to immune checkpoint blockade provide now opportunities of patient stratification and biologically driven drug development in future clinical trials.

References.

1. Ribas A, Wolchok JD. Cancer immunotherapy using checkpoint blockade. Science. 23 mars 2018;359(6382):1350-5.

2. Vaddepally RK, Kharel P, Pandey R, Garje R, Chandra AB. Review of Indications of FDA-Approved Immune Checkpoint Inhibitors per NCCN Guidelines with the Level of Evidence. Cancers (Basel). 20 mars 2020;12(3):E738.

3. Wei SC, Levine JH, Cogdill AP, Zhao Y, Anang N-AAS, Andrews MC, et al. Distinct Cellular Mechanisms Underlie Anti-CTLA-4 and Anti-PD-1 Checkpoint Blockade. Cell. 7 sept 2017;170(6):1120-1133.e17.

4. Antonia SJ, López-Martin JA, Bendell J, Ott PA, Taylor M, Eder JP, et al. Nivolumab alone and nivolumab plus ipilimumab in recurrent small-cell lung cancer (CheckMate 032): a multicentre, open-label, phase 1/2 trial. Lancet Oncol. juill 2016;17(7):883-95.

5. Bauml J, Seiwert TY, Pfister DG, Worden F, Liu SV, Gilbert J, et al. Pembrolizumab for Platinum- and Cetuximab-Refractory Head and Neck Cancer: Results From a Single-Arm, Phase II Study. J Clin Oncol. 10 mai 2017;35(14):1542-9.

6. Atkins MB, Plimack ER, Puzanov I, Fishman MN, McDermott DF, Cho DC, et al. Axitinib in combination with pembrolizumab in patients with advanced renal cell cancer: a non-randomised, open-label, dose-finding, and dose-expansion phase 1b trial. Lancet Oncol. mars 2018;19(3):405-15.

7. Reck M, Kaiser R, Mellemgaard A, Douillard J-Y, Orlov S, Krzakowski M, et al. Docetaxel plus nintedanib versus docetaxel plus placebo in patients with previously treated non-small-cell lung cancer (LUME-Lung 1): a phase 3, double-blind, randomised controlled trial. Lancet Oncol. févr 2014;15(2):143-55.

8. Mok TSK, Wu Y-L, Kudaba I, Kowalski DM, Cho BC, Turna HZ, et al. Pembrolizumab versus chemotherapy for previously untreated, PD-L1-expressing, locally advanced or metastatic non-small-cell lung cancer (KEYNOTE-042): a randomised, open-label, controlled, phase 3 trial. Lancet. 4 mai 2019;393(10183):1819-30.

9. Reck M, Rodríguez-Abreu D, Robinson AG, Hui R, Csőszi T, Fülöp A, et al. Pembrolizumab versus Chemotherapy for PD-L1-Positive Non-Small-Cell Lung Cancer. N Engl J Med. 10 2016;375(19):1823-33.

10. Motzer RJ, Escudier B, McDermott DF, George S, Hammers HJ, Srinivas S, et al. Nivolumab versus Everolimus in Advanced Renal-Cell Carcinoma. N Engl J Med. 5 nov 2015;373(19):1803-13.

11. Robert C, Schachter J, Long GV, Arance A, Grob JJ, Mortier L, et al. Pembrolizumab versus Ipilimumab in Advanced Melanoma. N Engl J Med. 25 juin 2015;372(26):2521-32.

12. Tumeh PC, Harview CL, Yearley JH, Shintaku IP, Taylor EJM, Robert L, et al. PD-1 blockade induces responses by inhibiting adaptive immune resistance. Nature. 27 nov 2014;515(7528):568-71.

13. Brahmer JR, Drake CG, Wollner I, Powderly JD, Picus J, Sharfman WH, et al. Phase I study of single-agent anti-programmed death-1 (MDX-1106) in refractory solid tumors: safety, clinical activity, pharmacodynamics, and immunologic correlates. J Clin Oncol. 1 juill 2010;28(19):3167-75.

14. Herbst RS, Soria J-C, Kowanetz M, Fine GD, Hamid O, Gordon MS, et al. Predictive correlates of response to the anti-PD-L1 antibody MPDL3280A in cancer patients. Nature. 27 nov 2014;515(7528):563-7.

15. Keenan TE, Burke KP, Van Allen EM. Genomic correlates of response to immune checkpoint blockade. Nat Med. mars 2019;25(3):389-402.

16. Kalbasi A, Ribas A. Tumour-intrinsic resistance to immune checkpoint blockade. Nat Rev Immunol. janv 2020;20(1):25-39.

17. Schoenfeld AJ, Hellmann MD. Acquired Resistance to Immune Checkpoint Inhibitors. Cancer Cell. 13 avr 2020;37(4):443-55.

18. Aldea M, Andre F, Marabelle A, Dogan S, Barlesi F, Soria J-C. Overcoming Resistance to Tumor-Targeted and Immune-Targeted Therapies. Cancer Discov. avr 2021;11(4):874-99.

19. Fukumura D, Kloepper J, Amoozgar Z, Duda DG, Jain RK. Enhancing cancer immunotherapy using antiangiogenics: opportunities and challenges. Nat Rev Clin Oncol. mai 2018;15(5):325-40.

20. Potente M, Gerhardt H, Carmeliet P. Basic and therapeutic aspects of angiogenesis. Cell. 16 sept 2011;146(6):873-87.

21. Zhao Y, Adjei AA. Targeting Angiogenesis in Cancer Therapy: Moving Beyond Vascular Endothelial Growth Factor. Oncologist. juin 2015;20(6):660-73.

22. Keck PJ, Hauser SD, Krivi G, Sanzo K, Warren T, Feder J, et al. Vascular permeability factor, an endothelial cell mitogen related to PDGF. Science. 8 déc 1989;246(4935):1309-12.

23. Fan F, Wey JS, McCarty MF, Belcheva A, Liu W, Bauer TW, et al. Expression and function of vascular endothelial growth factor receptor-1 on human colorectal cancer cells. Oncogene. 14 avr 2005;24(16):2647-53.

24. Tian X, Song S, Wu J, Meng L, Dong Z, Shou C. Vascular endothelial growth factor: acting as an autocrine growth factor for human gastric adenocarcinoma cell MGC803. Biochem Biophys Res Commun. 24 août 2001;286(3):505-12.

25. Grothey A, Galanis E. Targeting angiogenesis: progress with anti-VEGF treatment with large molecules. Nat Rev Clin Oncol. sept 2009;6(9):507-18.

26. Motzer RJ, Hutson TE, Tomczak P, Michaelson MD, Bukowski RM, Rixe O, et al. Sunitinib versus interferon alfa in metastatic renal-cell carcinoma. N Engl J Med. 11 janv 2007;356(2):115-24.

27. Llovet JM, Ricci S, Mazzaferro V, Hilgard P, Gane E, Blanc J-F, et al. Sorafenib in advanced hepatocellular carcinoma. N Engl J Med. 24 juill 2008;359(4):378-90.

28. Soria J-C, Mauguen A, Reck M, Sandler AB, Saijo N, Johnson DH, et al. Systematic review and meta-analysis of randomised, phase II/III trials adding bevacizumab to platinum-based chemotherapy as first-line treatment in patients with advanced non-small-cell lung cancer. Ann Oncol. janv 2013;24(1):20-30.

29. de Gramont A, Van Cutsem E, Schmoll H-J, Tabernero J, Clarke S, Moore MJ, et al. Bevacizumab plus oxaliplatin-based chemotherapy as adjuvant treatment for colon cancer (AVANT): a phase 3 randomised controlled trial. Lancet Oncol. déc 2012;13(12):1225-33.

30. Perren TJ, Swart AM, Pfisterer J, Ledermann JA, Pujade-Lauraine E, Kristensen G, et al. A phase 3 trial of bevacizumab in ovarian cancer. N Engl J Med. 29 déc 2011;365(26):2484-96.

31. Galateau-Salle F, Churg A, Roggli V, Travis WD, World Health Organization Committee for Tumors of the Pleura. The 2015 World Health Organization Classification of Tumors of the Pleura: Advances since the 2004 Classification. J Thorac Oncol. févr 2016;11(2):142-54.

32. Wagner JC, Sleggs CA, Marchand P. Diffuse pleural mesothelioma and asbestos exposure in the North Western Cape Province. Br J Ind Med. oct 1960;17:260-71.

33. Xu A, Wu LJ, Santella RM, Hei TK. Role of oxyradicals in mutagenicity and DNA damage induced by crocidolite asbestos in mammalian cells. Cancer Res. 1 déc 1999;59(23):5922-6.

34. Hamilton RF, Iyer LL, Holian A. Asbestos induces apoptosis in human alveolar macrophages. Am J Physiol. nov 1996;271(5 Pt 1):L813-819.

35. Lacourt A, Gramond C, Rolland P, Ducamp S, Audignon S, Astoul P, et al. Occupational and non-occupational attributable risk of asbestos exposure for malignant pleural mesothelioma. Thorax. juin 2014;69(6):532-9.

36. Dostert C, Pétrilli V, Van Bruggen R, Steele C, Mossman BT, Tschopp J. Innate immune activation through Nalp3 inflammasome sensing of asbestos and silica. Science. 2 mai 2008;320(5876):674-7.

37. Cassel SL, Eisenbarth SC, Iyer SS, Sadler JJ, Colegio OR, Tephly LA, et al. The Nalp3 inflammasome is essential for the development of silicosis. Proc Natl Acad Sci U S A. 1 juill 2008;105(26):9035-40.

38. Tanaka S, Choe N, Iwagaki A, Hemenway DR, Kagan E. Asbestos exposure induces MCP-1 secretion by pleural mesothelial cells. Exp Lung Res. juin 2000;26(4):241-55.

39. Yang H, Rivera Z, Jube S, Nasu M, Bertino P, Goparaju C, et al. Programmed necrosis induced by asbestos in human mesothelial cells causes high-mobility group box 1 protein release and resultant inflammation. Proc Natl Acad Sci U S A. 13 juill 2010;107(28):12611-6.

40. Yang H, Rivera Z, Jube S, Nasu M, Bertino P, Goparaju C, et al. Programmed necrosis induced by asbestos in human mesothelial cells causes high-mobility group box 1 protein release and resultant inflammation. Proc Natl Acad Sci U S A. 13 juill 2010;107(28):12611-6.

41. Jube S, Rivera ZS, Bianchi ME, Powers A, Wang E, Pagano I, et al. Cancer cell secretion of the DAMP protein HMGB1 supports progression in malignant mesothelioma. Cancer Res. 1 juill 2012;72(13):3290-301.

42. Qi F, Okimoto G, Jube S, Napolitano A, Pass HI, Laczko R, et al. Continuous exposure to chrysotile asbestos can cause transformation of human mesothelial cells via HMGB1 and TNF-α signaling. Am J Pathol. nov 2013;183(5):1654-66.

43. Xue J, Patergnani S, Giorgi C, Suarez J, Goto K, Bononi A, et al. Asbestos induces mesothelial cell transformation via HMGB1-driven autophagy. Proc Natl Acad Sci U S A. 13 oct 2020;117(41):25543-52.

44. Meyerhoff RR, Yang C-FJ, Speicher PJ, Gulack BC, Hartwig MG, D'Amico TA, et al. Impact of mesothelioma histologic subtype on outcomes in the Surveillance, Epidemiology, and End Results database. J Surg Res. 1 juin 2015;196(1):23-32.

45. Saddoughi SA, Abdelsattar ZM, Blackmon SH. National Trends in the Epidemiology of Malignant Pleural Mesothelioma: A National Cancer Data Base Study. Ann Thorac Surg. févr 2018;105(2):432-7.

46. Nicholson AG, Sauter JL, Nowak AK, Kindler HL, Gill RR, Remy-Jardin M, et al. EURACAN/IASLC Proposals for Updating the Histologic Classification of Pleural Mesothelioma: Towards a More Multidisciplinary Approach. J Thorac Oncol. janv 2020;15(1):29-49.

47. Scherpereel A, Opitz I, Berghmans T, Psallidas I, Glatzer M, Rigau D, et al. ERS/ESTS/EACTS/ESTRO guidelines for the management of malignant pleural mesothelioma. Eur Respir J. juin 2020;55(6):1900953.

48. Chevrier M, Monaco SE, Jerome JA, Galateau-Salle F, Churg A, Dacic S. Testing for BAP1 loss and CDKN2A/p16 homozygous deletion improves the accurate diagnosis of mesothelial proliferations in effusion cytology. Cancer Cytopathol. déc 2020;128(12):939-47.

49. Chapel DB, Stewart R, Furtado LV, Husain AN, Krausz T, Deftereos G. Tumor PD-L1 expression in malignant pleural and peritoneal mesothelioma by Dako PD-L1 22C3 pharmDx and Dako PD-L1 28-8 pharmDx assays. Hum Pathol. mai 2019;87:11-7.

50. Rosen LE, Karrison T, Ananthanarayanan V, Gallan AJ, Adusumilli PS, Alchami FS, et al. Nuclear grade and necrosis predict prognosis in malignant epithelioid pleural mesothelioma: a multi-institutional study. Mod Pathol. avr 2018;31(4):598-606.

51. Courtiol P, Maussion C, Moarii M, Pronier E, Pilcer S, Sefta M, et al. Deep learning-based classification of mesothelioma improves prediction of patient outcome. Nat Med. oct 2019;25(10):1519-25.

52. Edwards JG, Cox G, Andi A, Jones JL, Walker RA, Waller DA, et al. Angiogenesis is an independent prognostic factor in malignant mesothelioma. Br J Cancer. 14 sept 2001;85(6):863-8.

53. Edwards JG, Swinson DEB, Jones JL, Muller S, Waller DA, O'Byrne KJ. Tumor necrosis correlates with angiogenesis and is a predictor of poor prognosis in malignant mesothelioma. Chest. nov 2003;124(5):1916-23.

54. Demirag F, Unsal E, Yilmaz A, Caglar A. Prognostic significance of vascular endothelial growth factor, tumor necrosis, and mitotic activity index in malignant pleural mesothelioma. Chest. nov 2005;128(5):3382-7.

55. Antony VB, Hott JW, Godbey SW, Holm K. Angiogenesis in mesotheliomas. Role of mesothelial cell derived IL-8. Chest. mars 1996;109(3 Suppl):21S-22S.

56. Leibovich SJ, Polverini PJ, Shepard HM, Wiseman DM, Shively V, Nuseir N. Macrophage-induced angiogenesis is mediated by tumour necrosis factor-alpha. Nature. 15 oct 1987;329(6140):630-2.

57. Rius J, Guma M, Schachtrup C, Akassoglou K, Zinkernagel AS, Nizet V, et al. NF-kappaB links innate immunity to the hypoxic response through transcriptional regulation of HIF-1alpha. Nature. 5 juin 2008;453(7196):807-11.

58. Ohta Y, Shridhar V, Bright RK, Kalemkerian GP, Du W, Carbone M, et al. VEGF and VEGF type C play an important role in angiogenesis and lymphangiogenesis in human malignant mesothelioma tumours. Br J Cancer. sept 1999;81(1):54-61.

59. König JE, Tolnay E, Wiethege T, Müller KM. Expression of vascular endothelial growth factor in diffuse malignant pleural mesothelioma. Virchows Arch. juill 1999;435(1):8-12.

60. König J, Tolnay E, Wiethege T, Müller K. Co-expression of vascular endothelial growth factor and its receptor flt-1 in malignant pleural mesothelioma. Respiration. 2000;67(1):36-40.

61. Masood R, Kundra A, Zhu S, Xia G, Scalia P, Smith DL, et al. Malignant mesothelioma growth inhibition by agents that target the VEGF and VEGF-C autocrine loops. Int J Cancer. 1 mai 2003;104(5):603-10.

62. Klabatsa A, Sheaff MT, Steele JPC, Evans MT, Rudd RM, Fennell DA. Expression and prognostic significance of hypoxia-inducible factor 1alpha (HIF-1alpha) in malignant pleural mesothelioma (MPM). Lung Cancer. janv 2006;51(1):53-9.

63. Li Q, Wang W, Yamada T, Matsumoto K, Sakai K, Bando Y, et al. Pleural mesothelioma instigates tumor-associated fibroblasts to promote progression via a malignant cytokine network. Am J Pathol. sept 2011;179(3):1483-93.

64. Marek LA, Hinz TK, von Mässenhausen A, Olszewski KA, Kleczko EK, Boehm D, et al. Nonamplified FGFR1 is a growth driver in malignant pleural mesothelioma. Mol Cancer Res. oct 2014;12(10):1460-9.

65. Schelch K, Wagner C, Hager S, Pirker C, Siess K, Lang E, et al. FGF2 and EGF induce epithelial-mesenchymal transition in malignant pleural mesothelioma cells via a MAPKinase/MMP1 signal. Carcinogenesis. 5 avr 2018;39(4):534-45.

66. Hegmans JPJJ, Hemmes A, Hammad H, Boon L, Hoogsteden HC, Lambrecht BN. Mesothelioma environment comprises cytokines and T-regulatory cells that suppress immune responses. Eur Respir J. juin 2006;27(6):1086-95.

67. Combaz-Lair C, Galateau-Sallé F, McLeer-Florin A, Le Stang N, David-Boudet L, Duruisseaux M, et al. Immune biomarkers PD-1/PD-L1 and TLR3 in malignant pleural mesotheliomas. Hum Pathol. juin 2016;52:9-18.

68. Inaguma S, Lasota J, Wang Z, Czapiewski P, Langfort R, Rys J, et al. Expression of ALCAM (CD166) and PD-L1 (CD274) independently predicts shorter survival in malignant pleural mesothelioma. Hum Pathol. janv 2018;71:1-7.

69. Pasello G, Zago G, Lunardi F, Urso L, Kern I, Vlacic G, et al. Malignant pleural mesothelioma immune microenvironment and checkpoint expression: correlation with clinical-pathological features and intratumor heterogeneity over time. Ann Oncol. 1 mai 2018;29(5):1258-65.

70. Brosseau S, Danel C, Scherpereel A, Mazières J, Lantuejoul S, Margery J, et al. Shorter Survival in Malignant Pleural Mesothelioma Patients With High PD-L1 Expression Associated With Sarcomatoid or Biphasic Histology Subtype: A Series of 214 Cases From the Bio-MAPS Cohort. Clin Lung Cancer. sept 2019;20(5):e564-75.

71. Awad MM, Jones RE, Liu H, Lizotte PH, Ivanova EV, Kulkarni M, et al. Cytotoxic T Cells in PD-L1-Positive Malignant Pleural Mesotheliomas Are Counterbalanced by Distinct Immunosuppressive Factors. Cancer Immunol Res. déc 2016;4(12):1038-48.

72. Klampatsa A, O'Brien SM, Thompson JC, Rao AS, Stadanlick JE, Martinez MC, et al. Phenotypic and functional analysis of malignant mesothelioma tumor-infiltrating lymphocytes. Oncoimmunology. 2019;8(9):e1638211.

73. Thapa B, Salcedo A, Lin X, Walkiewicz M, Murone C, Ameratunga M, et al. The Immune Microenvironment, Genome-wide Copy Number Aberrations, and Survival in Mesothelioma. J Thorac Oncol. mai 2017;12(5):850-9.

74. Baas P, Scherpereel A, Nowak AK, Fujimoto N, Peters S, Tsao AS, et al. First-line nivolumab plus ipilimumab in unresectable malignant pleural mesothelioma (CheckMate 743): a multicentre, randomised, open-label, phase 3 trial. Lancet. 30 janv 2021;397(10272):375-86.

75. Zalcman G, Mazieres J, Margery J, Greillier L, Audigier-Valette C, Moro-Sibilot D, et al. Bevacizumab for newly diagnosed pleural mesothelioma in the Mesothelioma Avastin Cisplatin Pemetrexed Study (MAPS): a randomised, controlled, open-label, phase 3 trial. Lancet. 2 avr 2016;387(10026):1405-14.

76. Vogelzang NJ, Rusthoven JJ, Symanowski J, Denham C, Kaukel E, Ruffie P, et al. Phase III study of pemetrexed in combination with cisplatin versus cisplatin alone in patients with malignant pleural mesothelioma. J Clin Oncol. 15 juill 2003;21(14):2636-44.

77. Popat S, Curioni-Fontecedro A, Dafni U, Shah R, O'Brien M, Pope A, et al. A multicentre randomised phase III trial comparing pembrolizumab versus single-agent chemotherapy for advanced pre-treated malignant pleural mesothelioma: the European Thoracic Oncology Platform (ETOP 9-15) PROMISE-meso trial. Ann Oncol. déc 2020;31(12):1734-45.

78. Quispel-Janssen J, van der Noort V, de Vries JF, Zimmerman M, Lalezari F, Thunnissen E, et al. Programmed Death 1 Blockade With Nivolumab in Patients With Recurrent Malignant Pleural Mesothelioma. J Thorac Oncol. oct 2018;13(10):1569-76.

79. Yap TA, Nakagawa K, Fujimoto N, Kuribayashi K, Guren TK, Calabrò L, et al. Efficacy and safety of pembrolizumab in patients with advanced mesothelioma in the open-label, single-arm, phase 2 KEYNOTE-158 study. Lancet Respir Med. juin 2021;9(6):613-21.

80. Hassan R, Thomas A, Nemunaitis JJ, Patel MR, Bennouna J, Chen FL, et al. Efficacy and Safety of Avelumab Treatment in Patients With Advanced Unresectable Mesothelioma: Phase 1b Results From the JAVELIN Solid Tumor Trial. JAMA Oncol. 1 mars 2019;5(3):351-7.

81. Calabrò L, Morra A, Giannarelli D, Amato G, D'Incecco A, Covre A, et al. Tremelimumab combined with durvalumab in patients with mesothelioma (NIBIT-MESO-1): an open-label, non-randomised, phase 2 study. Lancet Respir Med. 2018;6(6):451-60.

82. Disselhorst MJ, Quispel-Janssen J, Lalezari F, Monkhorst K, de Vries JF, van der Noort V, et al. Ipilimumab and nivolumab in the treatment of recurrent malignant pleural mesothelioma (INITIATE): results of a prospective, single-arm, phase 2 trial. Lancet Respir Med. mars 2019;7(3):260-70.

83. Scherpereel A, Mazieres J, Greillier L, Lantuejoul S, Dô P, Bylicki O, et al. Nivolumab or nivolumab plus ipilimumab in patients with relapsed malignant pleural mesothelioma (IFCT-1501 MAPS2): a multicentre, open-label, randomised, non-comparative, phase 2 trial. Lancet Oncol. févr 2019;20(2):239-53.

84. Flejter WL, Li FP, Antman KH, Testa JR. Recurring loss involving chromosomes 1, 3, and 22 in malignant mesothelioma: possible sites of tumor suppressor genes. Genes Chromosomes Cancer. nov 1989;1(2):148-54.

85. Pyrhönen S, Tiainen M, Rautonen J, Tammilehto L, Laasonen A, Mattson K, et al. Comparison of DNA and karyotype ploidy in malignant mesothelioma. Cancer Genet Cytogenet. mai 1992;60(1):8-13.

86. Taguchi T, Jhanwar SC, Siegfried JM, Keller SM, Testa JR. Recurrent deletions of specific chromosomal sites in 1p, 3p, 6q, and 9p in human malignant mesothelioma. Cancer Res. 15 sept 1993;53(18):4349-55.

87. Musti M, Kettunen E, Dragonieri S, Lindholm P, Cavone D, Serio G, et al. Cytogenetic and molecular genetic changes in malignant mesothelioma. Cancer Genet Cytogenet. 1 oct 2006;170(1):9-15.

88. Lindholm PM, Salmenkivi K, Vauhkonen H, Nicholson AG, Anttila S, Kinnula VL, et al. Gene copy number analysis in malignant pleural mesothelioma using oligonucleotide array CGH. Cytogenet Genome Res. 2007;119(1-2):46-52.

89. Serrano M, Hannon GJ, Beach D. A new regulatory motif in cell-cycle control causing specific inhibition of cyclin D/CDK4. Nature. 16 déc 1993;366(6456):704-7.

90. Hannon GJ, Beach D. p15INK4B is a potential effector of TGF-beta-induced cell cycle arrest. Nature. 15 sept 1994;371(6494):257-61.

91. Harvey KF, Zhang X, Thomas DM. The Hippo pathway and human cancer. Nat Rev Cancer. avr 2013;13(4):246-57.

92. Bianchi AB, Mitsunaga SI, Cheng JQ, Klein WM, Jhanwar SC, Seizinger B, et al. High frequency of inactivating mutations in the neurofibromatosis type 2 gene (NF2) in primary malignant mesotheliomas. Proc Natl Acad Sci U S A. 21 nov 1995;92(24):10854-8.

93. Meng Z, Moroishi T, Guan K-L. Mechanisms of Hippo pathway regulation. Genes Dev. 1 janv 2016;30(1):1-17.

94. Huang J, Wu S, Barrera J, Matthews K, Pan D. The Hippo signaling pathway coordinately regulates cell proliferation and apoptosis by inactivating Yorkie, the Drosophila Homolog of YAP. Cell. 12 août 2005;122(3):421-34.

95. Tschöp K, Conery AR, Litovchick L, Decaprio JA, Settleman J, Harlow E, et al. A kinase shRNA screen links LATS2 and the pRB tumor suppressor. Genes Dev. 15 avr 2011;25(8):814-30.

96. Aylon Y, Michael D, Shmueli A, Yabuta N, Nojima H, Oren M. A positive feedback loop between the p53 and Lats2 tumor suppressors prevents tetraploidization. Genes Dev. 1 oct 2006;20(19):2687-700.

97. Aragona M, Panciera T, Manfrin A, Giulitti S, Michielin F, Elvassore N, et al. A mechanical checkpoint controls multicellular growth through YAP/TAZ regulation by actin-processing factors. Cell. 29 août 2013;154(5):1047-59.

98. Testa JR, Cheung M, Pei J, Below JE, Tan Y, Sementino E, et al. Germline BAP1 mutations predispose to malignant mesothelioma. Nat Genet. 28 août 2011;43(10):1022-5.

99. Carbone M, Emri S, Dogan AU, Steele I, Tuncer M, Pass HI, et al. A mesothelioma epidemic in Cappadocia: scientific developments and unexpected social outcomes. Nat Rev Cancer. févr 2007;7(2):147-54.

100. Jensen DE, Proctor M, Marquis ST, Gardner HP, Ha SI, Chodosh LA, et al. BAP1: a novel ubiquitin hydrolase which binds to the BRCA1 RING finger and enhances BRCA1-mediated cell growth suppression. Oncogene. 5 mars 1998;16(9):1097-112.

101. Carbone M, Harbour JW, Brugarolas J, Bononi A, Pagano I, Dey A, et al. Biological Mechanisms and Clinical Significance of BAP1 Mutations in Human Cancer. Cancer Discov. août 2020;10(8):1103-20.

102. Bott M, Brevet M, Taylor BS, Shimizu S, Ito T, Wang L, et al. The nuclear deubiquitinase BAP1 is commonly inactivated by somatic mutations and 3p21.1 losses in malignant pleural mesothelioma. Nat Genet. 5 juin 2011;43(7):668-72.

103. Bueno R, Stawiski EW, Goldstein LD, Durinck S, De Rienzo A, Modrusan Z, et al. Comprehensive genomic analysis of malignant pleural mesothelioma identifies recurrent mutations, gene fusions and splicing alterations. Nat Genet. avr 2016;48(4):407-16.

104. Nishikawa H, Wu W, Koike A, Kojima R, Gomi H, Fukuda M, et al. BRCA1-associated protein 1 interferes with BRCA1/BARD1 RING heterodimer activity. Cancer Res. 1 janv 2009;69(1):111-9.

105. Lee H-S, Lee S-A, Hur S-K, Seo J-W, Kwon J. Stabilization and targeting of INO80 to replication forks by BAP1 during normal DNA synthesis. Nat Commun. 6 oct 2014;5:5128.

106. Machida YJ, Machida Y, Vashisht AA, Wohlschlegel JA, Dutta A. The deubiquitinating enzyme BAP1 regulates cell growth via interaction with HCF-1. J Biol Chem. 4 déc 2009;284(49):34179-88.

107. Yu H, Mashtalir N, Daou S, Hammond-Martel I, Ross J, Sui G, et al. The ubiquitin carboxyl hydrolase BAP1 forms a ternary complex with YY1 and HCF-1 and is a critical regulator of gene expression. Mol Cell Biol. nov 2010;30(21):5071-85.

108. Scheuermann JC, de Ayala Alonso AG, Oktaba K, Ly-Hartig N, McGinty RK, Fraterman S, et al. Histone H2A deubiquitinase activity of the Polycomb repressive complex PR-DUB. Nature. 13 mai 2010;465(7295):243-7.

109. LaFave LM, Béguelin W, Koche R, Teater M, Spitzer B, Chramiec A, et al. Loss of BAP1 function leads to EZH2-dependent transformation. Nat Med. nov 2015;21(11):1344-9.

110. Bracken AP, Kleine-Kohlbrecher D, Dietrich N, Pasini D, Gargiulo G, Beekman C, et al. The Polycomb group proteins bind throughout the INK4A-ARF locus and are disassociated in senescent cells. Genes Dev. 1 mars 2007;21(5):525-30.

111. Bracken AP, Pasini D, Capra M, Prosperini E, Colli E, Helin K. EZH2 is downstream of the pRB-E2F pathway, essential for proliferation and amplified in cancer. EMBO J. 15 oct 2003;22(20):5323-35.

112. Joseph NM, Chen Y-Y, Nasr A, Yeh I, Talevich E, Onodera C, et al. Genomic profiling of malignant peritoneal mesothelioma reveals recurrent alterations in epigenetic regulatory genes BAP1, SETD2, and DDX3X. Mod Pathol. févr 2017;30(2):246-54.

113. Hmeljak J, Sanchez-Vega F, Hoadley KA, Shih J, Stewart C, Heiman D, et al. Integrative Molecular Characterization of Malignant Pleural Mesothelioma. Cancer Discov. déc 2018;8(12):1548-65.

114. Blum Y, Meiller C, Quetel L, Elarouci N, Ayadi M, Tashtanbaeva D, et al. Dissecting heterogeneity in malignant pleural mesothelioma through histo-molecular gradients for clinical applications. Nat Commun. 22 mars 2019;10(1):1333.

115. Hanahan D, Weinberg RA. Hallmarks of cancer: the next generation. Cell. 4 mars 2011;144(5):646-74.

116. Morikawa S, Baluk P, Kaidoh T, Haskell A, Jain RK, McDonald DM. Abnormalities in pericytes on blood vessels and endothelial sprouts in tumors. Am J Pathol. mars 2002;160(3):985-1000.

117. Baluk P, Morikawa S, Haskell A, Mancuso M, McDonald DM. Abnormalities of basement membrane on blood vessels and endothelial sprouts in tumors. Am J Pathol. nov 2003;163(5):1801-15.

118. Bergers G, Benjamin LE. Tumorigenesis and the angiogenic switch. Nat Rev Cancer. juin 2003;3(6):401-10.

119. Hanahan D, Folkman J. Patterns and emerging mechanisms of the angiogenic switch during tumorigenesis. Cell. 9 août 1996;86(3):353-64.

120. Pugh CW, Ratcliffe PJ. Regulation of angiogenesis by hypoxia: role of the HIF system. Nat Med. juin 2003;9(6):677-84.

121. Leung DW, Cachianes G, Kuang WJ, Goeddel DV, Ferrara N. Vascular endothelial growth factor is a secreted angiogenic mitogen. Science. 8 déc 1989;246(4935):1306-9.

122. Matsumoto K, Ema M. Roles of VEGF-A signalling in development, regeneration, and tumours. J Biochem. juill 2014;156(1):1-10.

123. Simons M, Gordon E, Claesson-Welsh L. Mechanisms and regulation of endothelial VEGF receptor signalling. Nat Rev Mol Cell Biol. oct 2016;17(10):611-25.

124. Lewis CE, Harney AS, Pollard JW. The Multifaceted Role of Perivascular Macrophages in Tumors. Cancer Cell. 11 juill 2016;30(1):18-25.

125. Lewis JS, Landers RJ, Underwood JC, Harris AL, Lewis CE. Expression of vascular endothelial growth factor by macrophages is up-regulated in poorly vascularized areas of breast carcinomas. J Pathol. oct 2000;192(2):150-8.

126. Harney AS, Arwert EN, Entenberg D, Wang Y, Guo P, Qian B-Z, et al. Real-Time Imaging Reveals Local, Transient Vascular Permeability, and Tumor Cell Intravasation Stimulated by TIE2hi Macrophage-Derived VEGFA. Cancer Discov. sept 2015;5(9):932-43.

127. Murdoch C, Muthana M, Coffelt SB, Lewis CE. The role of myeloid cells in the promotion of tumour angiogenesis. Nat Rev Cancer. août 2008;8(8):618-31.

128. Venneri MA, De Palma M, Ponzoni M, Pucci F, Scielzo C, Zonari E, et al. Identification of proangiogenic TIE2-expressing monocytes (TEMs) in human peripheral blood and cancer. Blood. 15 juin 2007;109(12):5276-85.

129. De Palma M, Venneri MA, Galli R, Sergi Sergi L, Politi LS, Sampaolesi M, et al. Tie2 identifies a hematopoietic lineage of proangiogenic monocytes required for tumor vessel formation and a mesenchymal population of pericyte progenitors. Cancer Cell. sept 2005;8(3):211-26.

130. Capobianco A, Monno A, Cottone L, Venneri MA, Biziato D, Di Puppo F, et al. Proangiogenic Tie2(+) macrophages infiltrate human and murine endometriotic lesions and dictate their growth in a mouse model of the disease. Am J Pathol. nov 2011;179(5):2651-9.

131. Coffelt SB, Tal AO, Scholz A, De Palma M, Patel S, Urbich C, et al. Angiopoietin-2 regulates gene expression in TIE2-expressing monocytes and augments their inherent proangiogenic functions. Cancer Res. 1 juill 2010;70(13):5270-80.

132. Murdoch C, Tazzyman S, Webster S, Lewis CE. Expression of Tie-2 by human monocytes and their responses to angiopoietin-2. J Immunol. 1 juin 2007;178(11):7405-11.

133. Coffelt SB, Chen Y-Y, Muthana M, Welford AF, Tal AO, Scholz A, et al. Angiopoietin 2 stimulates TIE2-expressing monocytes to suppress T cell activation and to promote regulatory T cell expansion. J Immunol. 1 avr 2011;186(7):4183-90.

134. Georganaki M, van Hooren L, Dimberg A. Vascular Targeting to Increase the Efficiency of Immune Checkpoint Blockade in Cancer. Front Immunol. 2018;9:3081.

135. Dirkx AEM, Oude Egbrink MGA, Kuijpers MJE, van der Niet ST, Heijnen VVT, Bouma-ter Steege JCA, et al. Tumor angiogenesis modulates leukocyte-vessel wall interactions in vivo by reducing endothelial adhesion molecule expression. Cancer Res. 1 mai 2003;63(9):2322-9.

136. Chen DS, Mellman I. Oncology meets immunology: the cancer-immunity cycle. Immunity. 25 juill 2013;39(1):1-10.

137. Huinen ZR, Huijbers EJM, van Beijnum JR, Nowak-Sliwinska P, Griffioen AW. Anti-angiogenic agents - overcoming tumour endothelial cell anergy and improving immunotherapy outcomes. Nat Rev Clin Oncol. 8 avr 2021;

138. Schmittnaegel M, Rigamonti N, Kadioglu E, Cassará A, Wyser Rmili C, Kiialainen A, et al. Dual angiopoietin-2 and VEGFA inhibition elicits antitumor immunity that is enhanced by PD-1 checkpoint blockade. Sci Transl Med. 12 avr 2017;9(385):eaak9670.

139. Facciabene A, Peng X, Hagemann IS, Balint K, Barchetti A, Wang L-P, et al. Tumour hypoxia promotes tolerance and angiogenesis via CCL28 and T(reg) cells. Nature. 13 juill 2011;475(7355):226-30.

140. Palucka AK, Coussens LM. The Basis of Oncoimmunology. Cell. 10 mars 2016;164(6):1233-47.

141. Jain RK. Normalizing tumor microenvironment to treat cancer: bench to bedside to biomarkers. J Clin Oncol. 10 juin 2013;31(17):2205-18.

142. Huang Y, Goel S, Duda DG, Fukumura D, Jain RK. Vascular normalization as an emerging strategy to enhance cancer immunotherapy. Cancer Res. 15 mai 2013;73(10):2943-8.

143. Gabrilovich DI, Chen HL, Girgis KR, Cunningham HT, Meny GM, Nadaf S, et al. Production of vascular endothelial growth factor by human tumors inhibits the functional maturation of dendritic cells. Nat Med. oct 1996;2(10):1096-103.

144. Gabrilovich D, Ishida T, Oyama T, Ran S, Kravtsov V, Nadaf S, et al. Vascular endothelial growth factor inhibits the development of dendritic cells and dramatically affects the differentiation of multiple hematopoietic lineages in vivo. Blood. 1 déc 1998;92(11):4150-66.

145. Voron T, Colussi O, Marcheteau E, Pernot S, Nizard M, Pointet A-L, et al. VEGF-A modulates expression of inhibitory checkpoints on CD8+ T cells in tumors. J Exp Med. 9 févr 2015;212(2):139-48.

146. Scholz A, Lang V, Henschler R, Czabanka M, Vajkoczy P, Chavakis E, et al. Angiopoietin-2 promotes myeloid cell infiltration in a β_2-integrin-dependent manner. Blood. 3 nov 2011;118(18):5050-9.

147. Banchereau J, Steinman RM. Dendritic cells and the control of immunity. Nature. 19 mars 1998;392(6673):245-52.

148. Almand B, Resser JR, Lindman B, Nadaf S, Clark JI, Kwon ED, et al. Clinical significance of defective dendritic cell differentiation in cancer. Clin Cancer Res. mai 2000;6(5):1755-66.

149. Dikov MM, Ohm JE, Ray N, Tchekneva EE, Burlison J, Moghanaki D, et al. Differential roles of vascular endothelial growth factor receptors 1 and 2 in dendritic cell differentiation. J Immunol. 1 janv 2005;174(1):215-22.

150. Alfaro C, Suarez N, Gonzalez A, Solano S, Erro L, Dubrot J, et al. Influence of bevacizumab, sunitinib and sorafenib as single agents or in combination on the inhibitory effects of VEGF on human dendritic cell differentiation from monocytes. Br J Cancer. 7 avr 2009;100(7):1111-9.

151. Almand B, Clark JI, Nikitina E, van Beynen J, English NR, Knight SC, et al. Increased production of immature myeloid cells in cancer patients: a mechanism of immunosuppression in cancer. J Immunol. 1 janv 2001;166(1):678-89.

152. Ghiringhelli F, Puig PE, Roux S, Parcellier A, Schmitt E, Solary E, et al. Tumor cells convert immature myeloid dendritic cells into TGF-beta-secreting cells inducing CD4+CD25+ regulatory T cell proliferation. J Exp Med. 3 oct 2005;202(7):919-29.

153. Serafini P, Mgebroff S, Noonan K, Borrello I. Myeloid-derived suppressor cells promote cross-tolerance in B-cell lymphoma by expanding regulatory T cells. Cancer Res. 1 juill 2008;68(13):5439-49.

154. Suzuki H, Onishi H, Wada J, Yamasaki A, Tanaka H, Nakano K, et al. VEGFR2 is selectively expressed by FOXP3high CD4+ Treg. Eur J Immunol. janv 2010;40(1):197-203.

155. Terme M, Pernot S, Marcheteau E, Sandoval F, Benhamouda N, Colussi O, et al. VEGFA-VEGFR pathway blockade inhibits tumor-induced regulatory T-cell proliferation in colorectal cancer. Cancer Res. 15 janv 2013;73(2):539-49.

156. Tada Y, Togashi Y, Kotani D, Kuwata T, Sato E, Kawazoe A, et al. Targeting VEGFR2 with Ramucirumab strongly impacts effector/ activated regulatory T cells and CD8+ T cells in the tumor microenvironment. J Immunother Cancer. 11 oct 2018;6(1):106.

157. Suzuki H, Onishi H, Morisaki T, Tanaka M, Katano M. Intratumoral FOXP3+VEGFR2+ regulatory T cells are predictive markers for recurrence and survival in patients with colorectal cancer. Clin Immunol. janv 2013;146(1):26-33.

158. Noman MZ, Buart S, Van Pelt J, Richon C, Hasmim M, Leleu N, et al. The cooperative induction of hypoxia-inducible factor-1 alpha and STAT3 during hypoxia induced an impairment of tumor susceptibility to CTL-mediated cell lysis. J Immunol. 15 mars 2009;182(6):3510-21.

159. Motz GT, Santoro SP, Wang L-P, Garrabrant T, Lastra RR, Hagemann IS, et al. Tumor endothelium FasL establishes a selective immune barrier promoting tolerance in tumors. Nat Med. juin 2014;20(6):607-15.

160. Shrimali RK, Yu Z, Theoret MR, Chinnasamy D, Restifo NP, Rosenberg SA. Antiangiogenic agents can increase lymphocyte infiltration into tumor and enhance the effectiveness of adoptive immunotherapy of cancer. Cancer Res. 1 août 2010;70(15):6171-80.

161. Kim CG, Jang M, Kim Y, Leem G, Kim KH, Lee H, et al. VEGF-A drives TOX-dependent T cell exhaustion in anti-PD-1-resistant microsatellite stable colorectal cancers. Sci Immunol. 8 nov 2019;4(41):eaay0555.

162. Gavalas NG, Tsiatas M, Tsitsilonis O, Politi E, Ioannou K, Ziogas AC, et al. VEGF directly suppresses activation of T cells from ascites secondary to ovarian cancer via VEGF receptor type 2. Br J Cancer. 20 nov 2012;107(11):1869-75.

163. Ziogas AC, Gavalas NG, Tsiatas M, Tsitsilonis O, Politi E, Terpos E, et al. VEGF directly suppresses activation of T cells from ovarian cancer patients and healthy individuals via VEGF receptor Type 2. Int J Cancer. 15 févr 2012;130(4):857-64.

164. Gougis P, Wassermann J, Spano JP, Keynan N, Funck-Brentano C, Salem JE. Clinical pharmacology of anti-angiogenic drugs in oncology. Crit Rev Oncol Hematol. nov 2017;119:75-93.

165. Ferrara N, Hillan KJ, Gerber H-P, Novotny W. Discovery and development of bevacizumab, an anti-VEGF antibody for treating cancer. Nat Rev Drug Discov. mai 2004;3(5):391-400.

166. Mancuso MR, Davis R, Norberg SM, O'Brien S, Sennino B, Nakahara T, et al. Rapid vascular regrowth in tumors after reversal of VEGF inhibition. J Clin Invest. oct 2006;116(10):2610-21.

167. Pàez-Ribes M, Allen E, Hudock J, Takeda T, Okuyama H, Viñals F, et al. Antiangiogenic therapy elicits malignant progression of tumors to increased local invasion and distant metastasis. Cancer Cell. 3 mars 2009;15(3):220-31.

168. Izzedine H, Ederhy S, Goldwasser F, Soria JC, Milano G, Cohen A, et al. Management of hypertension in angiogenesis inhibitor-treated patients. Ann Oncol. mai 2009;20(5):807-15.

169. Higa GM, Abraham J. Biological mechanisms of bevacizumab-associated adverse events. Expert Rev Anticancer Ther. juill 2009;9(7):999-1007.

170. Holash J, Davis S, Papadopoulos N, Croll SD, Ho L, Russell M, et al. VEGF-Trap: a VEGF blocker with potent antitumor effects. Proc Natl Acad Sci U S A. 20 août 2002;99(17):11393-8.

171. Van Cutsem E, Prenen H, D'Haens G, Bennouna J, Carrato A, Ducreux M, et al. A phase I/II, open-label, randomised study of nintedanib plus mFOLFOX6 versus bevacizumab plus mFOLFOX6 in first-line metastatic colorectal cancer patients. Ann Oncol. oct 2015;26(10):2085-91.

172. Krupitskaya Y, Wakelee HA. Ramucirumab, a fully human mAb to the transmembrane signaling tyrosine kinase VEGFR-2 for the potential treatment of cancer. Curr Opin Investig Drugs. juin 2009;10(6):597-605.

173. Fuchs CS, Tomasek J, Yong CJ, Dumitru F, Passalacqua R, Goswami C, et al. Ramucirumab monotherapy for previously treated advanced gastric or gastro-oesophageal junction adenocarcinoma (REGARD): an international, randomised, multicentre, placebo-controlled, phase 3 trial. Lancet. 4 janv 2014;383(9911):31-9.

174. Garon EB, Ciuleanu T-E, Arrieta O, Prabhash K, Syrigos KN, Goksel T, et al. Ramucirumab plus docetaxel versus placebo plus docetaxel for second-line treatment of stage IV non-small-cell lung cancer after disease progression on platinum-based therapy (REVEL): a multicentre, double-blind, randomised phase 3 trial. Lancet. 23 août 2014;384(9944):665-73.

175. Mackey JR, Ramos-Vazquez M, Lipatov O, McCarthy N, Krasnozhon D, Semiglazov V, et al. Primary results of ROSE/TRIO-12, a randomized placebo-controlled phase III trial evaluating the addition of ramucirumab to first-line docetaxel chemotherapy in metastatic breast cancer. J Clin Oncol. 10 janv 2015;33(2):141-8.

176. Manning G, Whyte DB, Martinez R, Hunter T, Sudarsanam S. The protein kinase complement of the human genome. Science. 6 déc 2002;298(5600):1912-34.

177. Schlessinger J. Cell signaling by receptor tyrosine kinases. Cell. 13 oct 2000;103(2):211-25.

178. Hubbard SR. Structural analysis of receptor tyrosine kinases. Prog Biophys Mol Biol. 1999;71(3-4):343-58.

179. Andrae J, Gallini R, Betsholtz C. Role of platelet-derived growth factors in physiology and medicine. Genes Dev. 15 mai 2008;22(10):1276-312.

180. Beenken A, Mohammadi M. The FGF family: biology, pathophysiology and therapy. Nat Rev Drug Discov. mars 2009;8(3):235-53.

181. Escudier B, Eisen T, Stadler WM, Szczylik C, Oudard S, Siebels M, et al. Sorafenib in advanced clear-cell renal-cell carcinoma. N Engl J Med. 11 janv 2007;356(2):125-34.

182. Motzer RJ, Escudier B, Gannon A, Figlin RA. Sunitinib: Ten Years of Successful Clinical Use and Study in Advanced Renal Cell Carcinoma. Oncologist. janv 2017;22(1):41-52.

183. Frampton JE. Pazopanib: a Review in Advanced Renal Cell Carcinoma. Target Oncol. août 2017;12(4):543-54.

184. Bellesoeur A, Carton E, Alexandre J, Goldwasser F, Huillard O. Axitinib in the treatment of renal cell carcinoma: design, development, and place in therapy. Drug Des Devel Ther. 2017;11:2801-11.

185. de la Fouchardière C. Regorafenib in the treatment of metastatic colorectal cancer. Future Oncol. sept 2018;14(22):2239-46.

186. Markowitz JN, Fancher KM. Cabozantinib: A Multitargeted Oral Tyrosine Kinase Inhibitor. Pharmacotherapy. mars 2018;38(3):357-69.

187. Roth GJ, Binder R, Colbatzky F, Dallinger C, Schlenker-Herceg R, Hilberg F, et al. Nintedanib: from discovery to the clinic. J Med Chem. 12 févr 2015;58(3):1053-63.

188. Scott LJ. Lenvatinib: first global approval. Drugs. avr 2015;75(5):553-60.

189. Geng R, Li J. Apatinib for the treatment of gastric cancer. Expert Opin Pharmacother. janv 2015;16(1):117-22.

190. Syed YY. Anlotinib: First Global Approval. Drugs. juill 2018;78(10):1057-62.

191. Schreiber RD, Old LJ, Smyth MJ. Cancer immunoediting: integrating immunity's roles in cancer suppression and promotion. Science. 25 mars 2011;331(6024):1565-70.

192. Coley WB. The Treatment of Inoperable Sarcoma by Bacterial Toxins (the Mixed Toxins of the Streptococcus erysipelas and the Bacillus prodigiosus). Proc R Soc Med. 1910;3(Surg Sect):1-48.

193. Atzpodien J, Körfer A, Franks CR, Poliwoda H, Kirchner H. Home therapy with recombinant interleukin-2 and interferon-alpha 2b in advanced human malignancies. Lancet. 23 juin 1990;335(8704):1509-12.

194. Angevin E, Valteau-Couanet D, Farace F, Dietrich PY, Lecesne A, Triebel F, et al. Phase I study of prolonged low-dose subcutaneous recombinant interleukin-2 (IL-2) in patients with advanced cancer. J Immunother Emphasis Tumor Immunol. oct 1995;18(3):188-95.

195. Bajetta E, Del Vecchio M, Nova P, Fusi A, Daponte A, Sertoli MR, et al. Multicenter phase III randomized trial of polychemotherapy (CVD regimen) versus the same chemotherapy (CT) plus subcutaneous interleukin-2 and interferon-alpha2b in metastatic melanoma. Ann Oncol. avr 2006;17(4):571-7.

196. Passalacqua R, Buzio C, Buti S, Porta C, Labianca R, Pezzuolo D, et al. Phase III, randomised, multicentre trial of maintenance immunotherapy with low-dose interleukin-2 and interferon-alpha for metastatic renal cell cancer. Cancer Immunol Immunother. avr 2010;59(4):553-61.

197. Traversari C, van der Bruggen P, Luescher IF, Lurquin C, Chomez P, Van Pel A, et al. A nonapeptide encoded by human gene MAGE-1 is recognized on HLA-A1 by cytolytic T lymphocytes directed against tumor antigen MZ2-E. J Exp Med. 1 nov 1992;176(5):1453-7.

198. Bakker AB, Schreurs MW, de Boer AJ, Kawakami Y, Rosenberg SA, Adema GJ, et al. Melanocyte lineage-specific antigen gp100 is recognized by melanoma-derived tumor-infiltrating lymphocytes. J Exp Med. 1 mars 1994;179(3):1005-9.

199. Gaudin C, Kremer F, Angevin E, Scott V, Triebel F. A hsp70-2 mutation recognized by CTL on a human renal cell carcinoma. J Immunol. 1 févr 1999;162(3):1730-8.

200. Inoue K, Ogawa H, Sonoda Y, Kimura T, Sakabe H, Oka Y, et al. Aberrant overexpression of the Wilms tumor gene (WT1) in human leukemia. Blood. 15 févr 1997;89(4):1405-12.

201. Hellström I, Hellström KE, Pierce GE, Yang JP. Cellular and humoral immunity to different types of human neoplasms. Nature. 28 déc 1968;220(5174):1352-4.

202. Brunet JF, Denizot F, Luciani MF, Roux-Dosseto M, Suzan M, Mattei MG, et al. A new member of the immunoglobulin superfamily--CTLA-4. Nature. 16 juill 1987;328(6127):267-70.

203. Freeman GJ, Lombard DB, Gimmi CD, Brod SA, Lee K, Laning JC, et al. CTLA-4 and CD28 mRNA are coexpressed in most T cells after activation. Expression of CTLA-4 and CD28 mRNA does not correlate with the pattern of lymphokine production. J Immunol. 15 déc 1992;149(12):3795-801.

204. Walunas TL, Lenschow DJ, Bakker CY, Linsley PS, Freeman GJ, Green JM, et al. CTLA-4 can function as a negative regulator of T cell activation. Immunity. août 1994;1(5):405-13.

205. Krummel MF, Sullivan TJ, Allison JP. Superantigen responses and co-stimulation: CD28 and CTLA-4 have opposing effects on T cell expansion in vitro and in vivo. Int Immunol. avr 1996;8(4):519-23.

206. Chambers CA, Kuhns MS, Egen JG, Allison JP. CTLA-4-mediated inhibition in regulation of T cell responses: mechanisms and manipulation in tumor immunotherapy. Annu Rev Immunol. 2001;19:565-94.

207. Ishida Y, Agata Y, Shibahara K, Honjo T. Induced expression of PD-1, a novel member of the immunoglobulin gene superfamily, upon programmed cell death. EMBO J. nov 1992;11(11):3887-95.

208. Freeman GJ, Long AJ, Iwai Y, Bourque K, Chernova T, Nishimura H, et al. Engagement of the PD-1 immunoinhibitory receptor by a novel B7 family member leads to negative regulation of lymphocyte activation. J Exp Med. 2 oct 2000;192(7):1027-34.

209. Baumeister SH, Freeman GJ, Dranoff G, Sharpe AH. Coinhibitory Pathways in Immunotherapy for Cancer. Annu Rev Immunol. 20 mai 2016;34:539-73.

210. Ribas A. Adaptive Immune Resistance: How Cancer Protects from Immune Attack. Cancer Discov. sept 2015;5(9):915-9.

211. Dong H, Strome SE, Salomao DR, Tamura H, Hirano F, Flies DB, et al. Tumor-associated B7-H1 promotes T-cell apoptosis: a potential mechanism of immune evasion. Nat Med. août 2002;8(8):793-800.

212. Sen DR, Kaminski J, Barnitz RA, Kurachi M, Gerdemann U, Yates KB, et al. The epigenetic landscape of T cell exhaustion. Science. 2 déc 2016;354(6316):1165-9.

213. Leach DR, Krummel MF, Allison JP. Enhancement of antitumor immunity by CTLA-4 blockade. Science. 22 mars 1996;271(5256):1734-6.

214. Hodi FS, Mihm MC, Soiffer RJ, Haluska FG, Butler M, Seiden MV, et al. Biologic activity of cytotoxic T lymphocyte-associated antigen 4 antibody blockade in previously vaccinated metastatic melanoma and ovarian carcinoma patients. Proc Natl Acad Sci USA. 15 avr 2003;100(8):4712-7.

215. Ribas A, Camacho LH, Lopez-Berestein G, Pavlov D, Bulanhagui CA, Millham R, et al. Antitumor activity in melanoma and anti-self responses in a phase I trial with the anti-cytotoxic T lymphocyte-associated antigen 4 monoclonal antibody CP-675,206. J Clin Oncol. 10 déc 2005;23(35):8968-77.

216. Brahmer JR, Drake CG, Wollner I, Powderly JD, Picus J, Sharfman WH, et al. Phase I study of single-agent anti-programmed death-1 (MDX-1106) in refractory solid tumors: safety, clinical activity, pharmacodynamics, and immunologic correlates. J Clin Oncol. 1 juill 2010;28(19):3167-75.

217. Garon EB, Rizvi NA, Hui R, Leighl N, Balmanoukian AS, Eder JP, et al. Pembrolizumab for the treatment of non-small-cell lung cancer. N Engl J Med. 21 mai 2015;372(21):2018-28.

218. Ribas A, Hamid O, Daud A, Hodi FS, Wolchok JD, Kefford R, et al. Association of Pembrolizumab With Tumor Response and Survival Among Patients With Advanced Melanoma. JAMA. 19 avr 2016;315(15):1600-9.

219. Gauci M-L, Lanoy E, Champiat S, Caramella C, Ammari S, Aspeslagh S, et al. Long-Term Survival in Patients Responding to Anti-PD-1/PD-L1 Therapy and Disease Outcome upon Treatment Discontinuation. Clin Cancer Res. 8 oct 2018;

220. Michot JM, Bigenwald C, Champiat S, Collins M, Carbonnel F, Postel-Vinay S, et al. Immune-related adverse events with immune checkpoint blockade: a comprehensive review. Eur J Cancer. févr 2016;54:139-48.

221. Wang DY, Salem J-E, Cohen JV, Chandra S, Menzer C, Ye F, et al. Fatal Toxic Effects Associated With Immune Checkpoint Inhibitors: A Systematic Review and Meta-analysis. JAMA Oncol. 13 sept 2018;

222. Blank CU, Haanen JB, Ribas A, Schumacher TN. CANCER IMMUNOLOGY. The « cancer immunogram ». Science. 6 mai 2016;352(6286):658-60.

223. Blank CU, Haining WN, Held W, Hogan PG, Kallies A, Lugli E, et al. Defining « T cell exhaustion ». Nat Rev Immunol. 2019;19(11):665-74.

224. Im SJ, Hashimoto M, Gerner MY, Lee J, Kissick HT, Burger MC, et al. Defining CD8(+) T cells that provide the proliferative burst after PD-1 therapy. Nature. 15 sept 2016;537(7620):417-21.

225. Huang AC, Postow MA, Orlowski RJ, Mick R, Bengsch B, Manne S, et al. T-cell invigoration to tumour burden ratio associated with anti-PD-1 response. Nature. 04 2017;545(7652):60-5.

226. Forde PM, Chaft JE, Smith KN, Anagnostou V, Cottrell TR, Hellmann MD, et al. Neoadjuvant PD-1 Blockade in Resectable Lung Cancer. N Engl J Med. 24 2018;378(21):1976-86.

227. Simoni Y, Becht E, Fehlings M, Loh CY, Koo S-L, Teng KWW, et al. Bystander CD8+ T cells are abundant and phenotypically distinct in human tumour infiltrates. Nature. mai 2018;557(7706):575-9.

228. Caushi JX, Zhang J, Ji Z, Vaghasia A, Zhang B, Hsiue EH-C, et al. Transcriptional programs of neoantigen-specific TIL in anti-PD-1-treated lung cancers. Nature. août 2021;596(7870):126-32.

229. Spitzer MH, Carmi Y, Reticker-Flynn NE, Kwek SS, Madhireddy D, Martins MM, et al. Systemic Immunity Is Required for Effective Cancer Immunotherapy. Cell. 26 janv 2017;168(3):487-502.e15.

230. Nakanishi Y, Lu B, Gerard C, Iwasaki A. CD8(+) T lymphocyte mobilization to virus-infected tissue requires CD4(+) T-cell help. Nature. 26 nov 2009;462(7272):510-3.

231. Iijima N, Iwasaki A. Access of protective antiviral antibody to neuronal tissues requires CD4 T-cell help. Nature. 26 mai 2016;533(7604):552-6.

232. Petitprez F, de Reyniès A, Keung EZ, Chen TW-W, Sun C-M, Calderaro J, et al. B cells are associated with survival and immunotherapy response in sarcoma. Nature. janv 2020;577(7791):556-60.

233. Helmink BA, Reddy SM, Gao J, Zhang S, Basar R, Thakur R, et al. B cells and tertiary lymphoid structures promote immunotherapy response. Nature. 2020;577(7791):549-55.

234. Cabrita R, Lauss M, Sanna A, Donia M, Skaarup Larsen M, Mitra S, et al. Tertiary lymphoid structures improve immunotherapy and survival in melanoma. Nature. 2020;577(7791):561-5.

235. Dahan R, Sega E, Engelhardt J, Selby M, Korman AJ, Ravetch JV. FcγRs Modulate the Anti-tumor Activity of Antibodies Targeting the PD-1/PD-L1 Axis. Cancer Cell. 14 sept 2015;28(3):285-95.

236. Feng Y, Roy A, Masson E, Chen T-T, Humphrey R, Weber JS. Exposure-response relationships of the efficacy and safety of ipilimumab in patients with advanced melanoma. Clin Cancer Res. 15 juill 2013;19(14):3977-86.

237. Desnoyer A, Broutin S, Delahousse J, Maritaz C, Blondel L, Mir O, et al. Pharmacokinetic/pharmacodynamic relationship of therapeutic monoclonal antibodies used in oncology: Part 2, immune checkpoint inhibitor antibodies. Eur J Cancer. mars 2020;128:119-28.

238. Leven C, Padelli M, Carré J-L, Bellissant E, Misery L. Immune Checkpoint Inhibitors in Melanoma: A Review of Pharmacokinetics and Exposure-Response Relationships. Clin Pharmacokinet. nov 2019;58(11):1393-405.

239. Arce Vargas F, Furness AJS, Litchfield K, Joshi K, Rosenthal R, Ghorani E, et al. Fc Effector Function Contributes to the Activity of Human Anti-CTLA-4 Antibodies. Cancer Cell. 9 avr 2018;33(4):649-663.e4.

240. Ingram JR, Blomberg OS, Rashidian M, Ali L, Garforth S, Fedorov E, et al. Anti-CTLA-4 therapy requires an Fc domain for efficacy. Proc Natl Acad Sci U S A. 10 avr 2018;115(15):3912-7.

241. Marabelle A, Kohrt H, Sagiv-Barfi I, Ajami B, Axtell RC, Zhou G, et al. Depleting tumor-specific Tregs at a single site eradicates disseminated tumors. J Clin Invest. juin 2013;123(6):2447-63.

242. Romano E, Kusio-Kobialka M, Foukas PG, Baumgaertner P, Meyer C, Ballabeni P, et al. Ipilimumab-dependent cell-mediated cytotoxicity of regulatory T cells ex vivo by nonclassical monocytes in melanoma patients. Proc Natl Acad Sci USA. 12 mai 2015;112(19):6140-5.

243. Quezada SA, Peggs KS. Lost in Translation: Deciphering the Mechanism of Action of Anti-human CTLA-4. Clin Cancer Res. 15 févr 2019;25(4):1130-2.

244. Ferrara R, Susini S, Marabelle A. Anti-CTLA-4 Immunotherapy Does Not Deplete FOXP3+ Regulatory T Cells (Tregs) in Human Cancers-Letter. Clin Cancer Res. 1 juin 2019;25(11):3468.

245. Zhang T, Song X, Xu L, Ma J, Zhang Y, Gong W, et al. The binding of an anti-PD-1 antibody to FcγRI has a profound impact on its biological functions. Cancer Immunol Immunother. juill 2018;67(7):1079-90.

246. Chen X, Song X, Li K, Zhang T. FcγR-Binding Is an Important Functional Attribute for Immune Checkpoint Antibodies in Cancer Immunotherapy. Front Immunol. 2019;10:292.

247. Fujii R, Friedman ER, Richards J, Tsang KY, Heery CR, Schlom J, et al. Enhanced killing of chordoma cells by antibody-dependent cell-mediated cytotoxicity employing the novel anti-PD-L1 antibody avelumab. Oncotarget. 7 juin 2016;7(23):33498-511.

248. Khanna S, Thomas A, Abate-Daga D, Zhang J, Morrow B, Steinberg SM, et al. Malignant Mesothelioma Effusions Are Infiltrated by CD3+ T Cells Highly Expressing PD-L1 and the PD-L1+ Tumor Cells within These Effusions Are Susceptible to ADCC by the Anti-PD-L1 Antibody Avelumab. J Thorac Oncol. nov 2016;11(11):1993-2005.

249. Boyerinas B, Jochems C, Fantini M, Heery CR, Gulley JL, Tsang KY, et al. Antibody-Dependent Cellular Cytotoxicity Activity of a Novel Anti-PD-L1 Antibody Avelumab (MSB0010718C) on Human Tumor Cells. Cancer Immunol Res. oct 2015;3(10):1148-57.

250. Heery CR, O'Sullivan-Coyne G, Madan RA, Cordes L, Rajan A, Rauckhorst M, et al. Avelumab for metastatic or locally advanced previously treated solid tumours (JAVELIN Solid Tumor): a phase 1a, multicohort, dose-escalation trial. Lancet Oncol. mai 2017;18(5):587-98.

251. Schumacher TN, Schreiber RD. Neoantigens in cancer immunotherapy. Science. 3 avr 2015;348(6230):69-74.

252. McGranahan N, Furness AJS, Rosenthal R, Ramskov S, Lyngaa R, Saini SK, et al. Clonal neoantigens elicit T cell immunoreactivity and sensitivity to immune checkpoint blockade. Science. 25 mars 2016;351(6280):1463-9.

253. Łuksza M, Riaz N, Makarov V, Balachandran VP, Hellmann MD, Solovyov A, et al. A neoantigen fitness model predicts tumour response to checkpoint blockade immunotherapy. Nature. 23 nov 2017;551(7681):517-20.

254. McGranahan N, Rosenthal R, Hiley CT, Rowan AJ, Watkins TBK, Wilson GA, et al. Allele-Specific HLA Loss and Immune Escape in Lung Cancer Evolution. Cell. 30 nov 2017;171(6):1259-1271.e11.

255. Marabelle A, Fakih M, Lopez J, Shah M, Shapira-Frommer R, Nakagawa K, et al. Association of tumour mutational burden with outcomes in patients with advanced solid tumours treated with pembrolizumab: prospective biomarker analysis of the multicohort, open-label, phase 2 KEYNOTE-158 study. Lancet Oncol. oct 2020;21(10):1353-65.

256. Le DT, Uram JN, Wang H, Bartlett BR, Kemberling H, Eyring AD, et al. PD-1 Blockade in Tumors with Mismatch-Repair Deficiency. N Engl J Med. 25 juin 2015;372(26):2509-20.

257. Mehnert JM, Panda A, Zhong H, Hirshfield K, Damare S, Lane K, et al. Immune activation and response to pembrolizumab in POLE-mutant endometrial cancer. J Clin Invest. 01 2016;126(6):2334-40.

258. Eroglu Z, Zaretsky JM, Hu-Lieskovan S, Kim DW, Algazi A, Johnson DB, et al. High response rate to PD-1 blockade in desmoplastic melanomas. Nature. 18 janv 2018;553(7688):347-50.

259. Subbiah V, Solit DB, Chan TA, Kurzrock R. The FDA approval of pembrolizumab for adult and pediatric patients with tumor mutational burden (TMB) ≥10: a decision centered on empowering patients and their physicians. Ann Oncol. sept 2020;31(9):1115-8.

260. Merino DM, McShane LM, Fabrizio D, Funari V, Chen S-J, White JR, et al. Establishing guidelines to harmonize tumor mutational burden (TMB): in silico assessment of variation in TMB quantification across diagnostic platforms: phase I of the Friends of Cancer Research TMB Harmonization Project. J Immunother Cancer. mars 2020;8(1):e000147.

261. Adam J, Le Stang N, Rouquette I, Cazes A, Badoual C, Pinot-Roussel H, et al. Multicenter harmonization study for PD-L1 IHC testing in non-small-cell lung cancer. Ann Oncol. 1 avr 2018;29(4):953-8.

262. Ferris RL, Blumenschein G, Fayette J, Guigay J, Colevas AD, Licitra L, et al. Nivolumab for Recurrent Squamous-Cell Carcinoma of the Head and Neck. N Engl J Med. 10 2016;375(19):1856-67.

263. Galon J, Costes A, Sanchez-Cabo F, Kirilovsky A, Mlecnik B, Lagorce-Pagès C, et al. Type, density, and location of immune cells within human colorectal tumors predict clinical outcome. Science. 29 sept 2006;313(5795):1960-4.

264. Pagès F, Berger A, Camus M, Sanchez-Cabo F, Costes A, Molidor R, et al. Effector memory T cells, early metastasis, and survival in colorectal cancer. N Engl J Med. 22 déc 2005;353(25):2654-66.

265. Fusco N, Vaira V, Righi I, Sajjadi E, Venetis K, Lopez G, et al. Characterization of the immune microenvironment in malignant pleural mesothelioma reveals prognostic subgroups of patients. Lung Cancer. déc 2020;150:53-61.

266. Jiang P, Gu S, Pan D, Fu J, Sahu A, Hu X, et al. Signatures of T cell dysfunction and exclusion predict cancer immunotherapy response. Nat Med. oct 2018;24(10):1550-8.

267. Fridman WH, Galon J, Pagès F, Tartour E, Sautès-Fridman C, Kroemer G. Prognostic and predictive impact of intra- and peritumoral immune infiltrates. Cancer Res. 1 sept 2011;71(17):5601-5.

268. Sautès-Fridman C, Petitprez F, Calderaro J, Fridman WH. Tertiary lymphoid structures in the era of cancer immunotherapy. Nat Rev Cancer. juin 2019;19(6):307-25.

269. Vanhersecke L, Brunet M, Guégan J-P, Rey C, Bougouin A, Cousin S, et al. Mature tertiary lymphoid structures predict immune checkpoint inhibitor efficacy in solid tumors independently of PD-L1 expression. Nat Cancer. août 2021;2(8):794-802.

270. Vétizou M, Pitt JM, Daillère R, Lepage P, Waldschmitt N, Flament C, et al. Anticancer immunotherapy by CTLA-4 blockade relies on the gut microbiota. Science. 27 nov 2015;350(6264):1079-84.

271. Sivan A, Corrales L, Hubert N, Williams JB, Aquino-Michaels K, Earley ZM, et al. Commensal Bifidobacterium promotes antitumor immunity and facilitates anti-PD-L1 efficacy. Science. 27 nov 2015;350(6264):1084-9.

272. Routy B, Le Chatelier E, Derosa L, Duong CPM, Alou MT, Daillère R, et al. Gut microbiome influences efficacy of PD-1-based immunotherapy against epithelial tumors. Science. 5 janv 2018;359(6371):91-7.

273. Matson V, Fessler J, Bao R, Chongsuwat T, Zha Y, Alegre M-L, et al. The commensal microbiome is associated with anti-PD-1 efficacy in metastatic melanoma patients. Science. 5 janv 2018;359(6371):104-8.

274. Gopalakrishnan V, Spencer CN, Nezi L, Reuben A, Andrews MC, Karpinets TV, et al. Gut microbiome modulates response to anti-PD-1 immunotherapy in melanoma patients. Science. 5 janv 2018;359(6371):97-103.

275. Derosa L, Hellmann MD, Spaziano M, Halpenny D, Fidelle M, Rizvi H, et al. Negative association of antibiotics on clinical activity of immune checkpoint inhibitors in patients with advanced renal cell and non-small cell lung cancer. Ann Oncol. 30 mars 2018;

276. Andrews MC, Duong CPM, Gopalakrishnan V, Iebba V, Chen W-S, Derosa L, et al. Gut microbiota signatures are associated with toxicity to combined CTLA-4 and PD-1 blockade. Nat Med. août 2021;27(8):1432-41.

277. Champiat S, Dercle L, Ammari S, Massard C, Hollebecque A, Postel-Vinay S, et al. Hyperprogressive Disease Is a New Pattern of Progression in Cancer Patients Treated by Anti-PD-1/PD-L1. Clin Cancer Res. 15 2017;23(8):1920-8.

278. Yasuda S, Sho M, Yamato I, Yoshiji H, Wakatsuki K, Nishiwada S, et al. Simultaneous blockade of programmed death 1 and vascular endothelial growth factor receptor 2 (VEGFR2) induces synergistic anti-tumour effect in vivo. Clin Exp Immunol. juin 2013;172(3):500-6.

279. Meder L, Schuldt P, Thelen M, Schmitt A, Dietlein F, Klein S, et al. Combined VEGF and PD-L1 Blockade Displays Synergistic Treatment Effects in an Autochthonous Mouse Model of Small Cell Lung Cancer. Cancer Res. 1 août 2018;78(15):4270-81.

280. Läubli H, Müller P, D'Amico L, Buchi M, Kashyap AS, Zippelius A. The multi-receptor inhibitor axitinib reverses tumor-induced immunosuppression and potentiates treatment with immune-modulatory antibodies in preclinical murine models. Cancer Immunol Immunother. mai 2018;67(5):815-24.

281. Wallin JJ, Bendell JC, Funke R, Sznol M, Korski K, Jones S, et al. Atezolizumab in combination with bevacizumab enhances antigen-specific T-cell migration in metastatic renal cell carcinoma. Nat Commun. 30 août 2016;7:12624.

282. McDermott DF, Huseni MA, Atkins MB, Motzer RJ, Rini BI, Escudier B, et al. Clinical activity and molecular correlates of response to atezolizumab alone or in combination with bevacizumab versus sunitinib in renal cell carcinoma. Nat Med. juin 2018;24(6):749-57.

283. Raghav K, Liu S, Overman MJ, Willett AF, Knafl M, Fu S-C, et al. Efficacy, Safety and Biomarker Analysis of Combined PD-L1 (Atezolizumab) and VEGF (Bevacizumab) Blockade in Advanced Malignant Peritoneal Mesothelioma. Cancer Discov. 14 juill 2021;candisc.0331.2021.

284. Kato R, Haratani K, Hayashi H, Sakai K, Sakai H, Kawakami H, et al. Nintedanib promotes antitumour immunity and shows antitumour activity in combination with PD-1 blockade in mice: potential role of cancer-associated fibroblasts. Br J Cancer. mars 2021;124(5):914-24.

285. Hilberg F, Roth GJ, Krssak M, Kautschitsch S, Sommergruber W, Tontsch-Grunt U, et al. BIBF 1120: triple angiokinase inhibitor with sustained receptor blockade and good antitumor efficacy. Cancer Res. 15 juin 2008;68(12):4774-82.

286. Stopfer P, Rathgen K, Bischoff D, Lüdtke S, Marzin K, Kaiser R, et al. Pharmacokinetics and metabolism of BIBF 1120 after oral dosing to healthy male volunteers. Xenobiotica. avr 2011;41(4):297-311.

287. Mross K, Stefanic M, Gmehling D, Frost A, Baas F, Unger C, et al. Phase I study of the angiogenesis inhibitor BIBF 1120 in patients with advanced solid tumors. Clin Cancer Res. 1 janv 2010;16(1):311-9.

288. Doebele RC, Conkling P, Traynor AM, Otterson GA, Zhao Y, Wind S, et al. A phase I, open-label dose-escalation study of continuous treatment with BIBF 1120 in combination with paclitaxel and carboplatin as first-line treatment in patients with advanced non-small-cell lung cancer. Ann Oncol. août 2012;23(8):2094-102.

289. Ellis PM, Kaiser R, Zhao Y, Stopfer P, Gyorffy S, Hanna N. Phase I open-label study of continuous treatment with BIBF 1120, a triple angiokinase inhibitor, and pemetrexed in pretreated non-small cell lung cancer patients. Clin Cancer Res. 15 mai 2010;16(10):2881-9.

290. Vargatef | European Medicines Agency [Internet]. [cité 8 sept 2021]. Disponible sur: https://www.ema.europa.eu/en/medicines/human/EPAR/vargatef#authorisation-details-section

291. Richeldi L, du Bois RM, Raghu G, Azuma A, Brown KK, Costabel U, et al. Efficacy and safety of nintedanib in idiopathic pulmonary fibrosis. N Engl J Med. 29 mai 2014;370(22):2071-82.

292. Hanna NH, Kaiser R, Sullivan RN, Aren OR, Ahn M-J, Tiangco B, et al. Nintedanib plus pemetrexed versus placebo plus pemetrexed in patients with relapsed or refractory, advanced non-small cell lung cancer (LUME-Lung 2): A randomized, double-blind, phase III trial. Lung Cancer. déc 2016;102:65-73.

293. Scapin G, Yang X, Prosise WW, McCoy M, Reichert P, Johnston JM, et al. Structure of full-length human anti-PD1 therapeutic IgG4 antibody pembrolizumab. Nat Struct Mol Biol. déc 2015;22(12):953-8.

294. Hamid O, Robert C, Daud A, Hodi FS, Hwu W-J, Kefford R, et al. Safety and tumor responses with lambrolizumab (anti-PD-1) in melanoma. N Engl J Med. 11 juill 2013;369(2):134-44.

295. Robert C, Ribas A, Wolchok JD, Hodi FS, Hamid O, Kefford R, et al. Anti-programmed-death-receptor-1 treatment with pembrolizumab in ipilimumab-refractory advanced melanoma: a randomised dose-comparison cohort of a phase 1 trial. Lancet. 20 sept 2014;384(9948):1109-17.

296. Ribas A, Puzanov I, Dummer R, Schadendorf D, Hamid O, Robert C, et al. Pembrolizumab versus investigator-choice chemotherapy for ipilimumab-refractory melanoma (KEYNOTE-002): a randomised, controlled, phase 2 trial. Lancet Oncol. août 2015;16(8):908-18.

297. Armand P, Shipp MA, Ribrag V, Michot J-M, Zinzani PL, Kuruvilla J, et al. Programmed Death-1 Blockade With Pembrolizumab in Patients With Classical Hodgkin Lymphoma After Brentuximab Vedotin Failure. J Clin Oncol. 1 nov 2016;34(31):3733-9.

298. Muro K, Chung HC, Shankaran V, Geva R, Catenacci D, Gupta S, et al. Pembrolizumab for patients with PD-L1-positive advanced gastric cancer (KEYNOTE-012): a multicentre, open-label, phase 1b trial. Lancet Oncol. 3 mai 2016;

299. Varga A, Piha-Paul S, Ott PA, Mehnert JM, Berton-Rigaud D, Morosky A, et al. Pembrolizumab in patients with programmed death ligand 1-positive advanced ovarian cancer: Analysis of KEYNOTE-028. Gynecol Oncol. févr 2019;152(2):243-50.

300. Alley EW, Lopez J, Santoro A, Morosky A, Saraf S, Piperdi B, et al. Clinical safety and activity of pembrolizumab in patients with malignant pleural mesothelioma (KEYNOTE-028): preliminary results from a non-randomised, open-label, phase 1b trial. Lancet Oncol. 2017;18(5):623-30.

301. Plimack ER, Bellmunt J, Gupta S, Berger R, Chow LQM, Juco J, et al. Safety and activity of pembrolizumab in patients with locally advanced or metastatic urothelial cancer (KEYNOTE-012): a non-randomised, open-label, phase 1b study. Lancet Oncol. févr 2017;18(2):212-20.

302. El-Khoueiry AB, Sangro B, Yau T, Crocenzi TS, Kudo M, Hsu C, et al. Nivolumab in patients with advanced hepatocellular carcinoma (CheckMate 040): an open-label, non-comparative, phase 1/2 dose escalation and expansion trial. Lancet. 24 juin 2017;389(10088):2492-502.

303. Champiat S, Lambotte O, Barreau E, Belkhir R, Berdelou A, Carbonnel F, et al. Management of immune checkpoint blockade dysimmune toxicities: a collaborative position paper. Ann Oncol. avr 2016;27(4):559-74.

304. Salem J-E, Manouchehri A, Moey M, Lebrun-Vignes B, Bastarache L, Pariente A, et al. Cardiovascular toxicities associated with immune checkpoint inhibitors: an observational, retrospective, pharmacovigilance study. Lancet Oncol. déc 2018;19(12):1579-89.

305. Collins M, Michot JM, Danlos FX, Mussini C, Soularue E, Mateus C, et al. Inflammatory gastrointestinal diseases associated with PD-1 blockade antibodies. Ann Oncol. 1 nov 2017;28(11):2860-5.

306. De Martin E, Michot J-M, Papouin B, Champiat S, Mateus C, Lambotte O, et al. Characterization of liver injury induced by cancer immunotherapy using immune checkpoint inhibitors. J Hepatol. juin 2018;68(6):1181-90.

307. Boutros C, Scoazec J-Y, Mateus C, Routier E, Roy S, Robert C. Arterial thrombosis and anti-PD-1 blockade. Eur J Cancer. mars 2018;91:164-6.

308. O'Connor P, Bhadbhade P, Khan Q, Williamson S. Acral vascular syndrome during an immune checkpoint inhibitor. BMJ Case Rep. 17 mai 2020;13(5):e233463.

309. Thoreau B, Gouaillier-Vulcain F, Machet L, Mateus C, Robert C, Ferreira-Maldent N, et al. Acute Lower Limb Ischaemia and Diabetes in a Patient Treated with Anti-PD1 Monoclonal Antibody for Metastatic Melanoma. Acta Derm Venereol. 10 mars 2017;97(3):408-9.

310. Dall'Olio FG, Sperandi F, Rihawi K, Gargiulo M, Melotti B, Brocchi S, et al. Arterial Embolization During Programmed Death-1 Inhibitor Treatment: An Unexpected Finding. J Thorac Oncol. déc 2018;13(12):e247-8.

311. Xin Yu J, Hubbard-Lucey VM, Tang J. Immuno-oncology drug development goes global. Nat Rev Drug Discov. nov 2019;18(12):899-900.

312. Dugger SA, Platt A, Goldstein DB. Drug development in the era of precision medicine. Nat Rev Drug Discov. mars 2018;17(3):183-96.

313. Pulendran B, Davis MM. The science and medicine of human immunology. Science. 25 sept 2020;369(6511).

314. Vajkoczy P, Farhadi M, Gaumann A, Heidenreich R, Erber R, Wunder A, et al. Microtumor growth initiates angiogenic sprouting with simultaneous expression of VEGF, VEGF receptor-2, and angiopoietin-2. J Clin Invest. mars 2002;109(6):777-85.

315. De Palma M, Biziato D, Petrova TV. Microenvironmental regulation of tumour angiogenesis. Nat Rev Cancer. août 2017;17(8):457-74.

316. Ribas A, Wolchok JD. Cancer immunotherapy using checkpoint blockade. Science. 23 2018;359(6382):1350-5.

317. Hirsch L, Zitvogel L, Eggermont A, Marabelle A. PD-Loma: a cancer entity with a shared sensitivity to the PD-1/PD-L1 pathway blockade. Br J Cancer. janv 2019;120(1):3-5.

318. Finn RS, Qin S, Ikeda M, Galle PR, Ducreux M, Kim T-Y, et al. Atezolizumab plus Bevacizumab in Unresectable Hepatocellular Carcinoma. N Engl J Med. 14 mai 2020;382(20):1894-905.

319. Rini BI, Plimack ER, Stus V, Gafanov R, Hawkins R, Nosov D, et al. Pembrolizumab plus Axitinib versus Sunitinib for Advanced Renal-Cell Carcinoma. N Engl J Med. 21 mars 2019;380(12):1116-27.

320. Motzer RJ, Penkov K, Haanen J, Rini B, Albiges L, Campbell MT, et al. Avelumab plus Axitinib versus Sunitinib for Advanced Renal-Cell Carcinoma. N Engl J Med. 21 mars 2019;380(12):1103-15.

321. Roland CL, Dineen SP, Lynn KD, Sullivan LA, Dellinger MT, Sadegh L, et al. Inhibition of vascular endothelial growth factor reduces angiogenesis and modulates immune cell infiltration of orthotopic breast cancer xenografts. Mol Cancer Ther. juill 2009;8(7):1761-71.

322. Hegde PS, Wallin JJ, Mancao C. Predictive markers of anti-VEGF and emerging role of angiogenesis inhibitors as immunotherapeutics. Semin Cancer Biol. oct 2018;52(Pt 2):117-24.

323. Khan KA, Kerbel RS. Improving immunotherapy outcomes with anti-angiogenic treatments and vice versa. Nat Rev Clin Oncol. mai 2018;15(5):310-24.

324. Amin A, Plimack ER, Ernstoff MS, Lewis LD, Bauer TM, McDermott DF, et al. Safety and efficacy of nivolumab in combination with sunitinib or pazopanib in advanced or metastatic renal cell carcinoma: the CheckMate 016 study. J Immunother Cancer. 22 oct 2018;6(1):109.

325. Qin S, Li A, Yi M, Yu S, Zhang M, Wu K. Recent advances on anti-angiogenesis receptor tyrosine kinase inhibitors in cancer therapy. J Hematol Oncol. 12 mars 2019;12(1):27.

326. Skolnik JM, Barrett JS, Jayaraman B, Patel D, Adamson PC. Shortening the timeline of pediatric phase I trials: the rolling six design. J Clin Oncol. 10 janv 2008;26(2):190-5.

327. Schwartz LH, Litière S, de Vries E, Ford R, Gwyther S, Mandrekar S, et al. RECIST 1.1-Update and clarification: From the RECIST committee. Eur J Cancer. juill 2016;62:132-7.

328. Seymour L, Bogaerts J, Perrone A, Ford R, Schwartz LH, Mandrekar S, et al. iRECIST: guidelines for response criteria for use in trials testing immunotherapeutics. Lancet Oncol. mars 2017;18(3):e143-52.

329. Pitoiset F, Cassard L, El Soufi K, Boselli L, Grivel J, Roux A, et al. Deep phenotyping of immune cell populations by optimized and standardized flow cytometry analyses. Cytometry A. août 2018;93(8):793-802.

330. Chowdhury S, Infante JR, Hawkins R, Voss MH, Perini R, Arkenau T, et al. A Phase I/II Study to Assess the Safety and Efficacy of Pazopanib and Pembrolizumab Combination Therapy in Patients with Advanced Renal Cell Carcinoma. Clin Genitourin Cancer. 20 avr 2021;S1558-7673(21)00092-6.

331. Herbst RS, Soria J-C, Kowanetz M, Fine GD, Hamid O, Gordon MS, et al. Predictive correlates of response to the anti-PD-L1 antibody MPDL3280A in cancer patients. Nature. 27 nov 2014;515(7528):563-7.

332. Lewis CE, De Palma M, Naldini L. Tie2-expressing monocytes and tumor angiogenesis: regulation by hypoxia and angiopoietin-2. Cancer Res. 15 sept 2007;67(18):8429-32.

333. Findley CM, Cudmore MJ, Ahmed A, Kontos CD. VEGF induces Tie2 shedding via a phosphoinositide 3-kinase/Akt dependent pathway to modulate Tie2 signaling. Arterioscler Thromb Vasc Biol. déc 2007;27(12):2619-26.

334. Korbecki J, Kojder K, Kapczuk P, Kupnicka P, Gawrońska-Szklarz B, Gutowska I, et al. The Effect of Hypoxia on the Expression of CXC Chemokines and CXC Chemokine Receptors-A Review of Literature. Int J Mol Sci. 15 janv 2021;22(2):E843.

335. Iellem A, Mariani M, Lang R, Recalde H, Panina-Bordignon P, Sinigaglia F, et al. Unique chemotactic response profile and specific expression of chemokine receptors CCR4 and CCR8 by CD4(+)CD25(+) regulatory T cells. J Exp Med. 17 sept 2001;194(6):847-53.

336. Gobert M, Treilleux I, Bendriss-Vermare N, Bachelot T, Goddard-Leon S, Arfi V, et al. Regulatory T cells recruited through CCL22/CCR4 are selectively activated in lymphoid infiltrates surrounding primary breast tumors and lead to an adverse clinical outcome. Cancer Res. 1 mars 2009;69(5):2000-9.

337. Faget J, Biota C, Bachelot T, Gobert M, Treilleux I, Goutagny N, et al. Early detection of tumor cells by innate immune cells leads to T(reg) recruitment through CCL22 production by tumor cells. Cancer Res. 1 oct 2011;71(19):6143-52.

338. Sun W, Li W-J, Wei F-Q, Wong T-S, Lei W-B, Zhu X-L, et al. Blockade of MCP-1/CCR4 signaling-induced recruitment of activated regulatory cells evokes an antitumor immune response in head and neck squamous cell carcinoma. Oncotarget. 21 juin 2016;7(25):37714-27.

339. Marshall LA, Marubayashi S, Jorapur A, Jacobson S, Zibinsky M, Robles O, et al. Tumors establish resistance to immunotherapy by regulating Treg recruitment via CCR4. J Immunother Cancer. nov 2020;8(2):e000764.

340. Yoo S-A, Kim M, Kang M-C, Kong J-S, Kim K-M, Lee S, et al. Placental growth factor regulates the generation of TH17 cells to link angiogenesis with autoimmunity. Nat Immunol. oct 2019;20(10):1348-59.

341. Laino AS, Woods D, Vassallo M, Qian X, Tang H, Wind-Rotolo M, et al. Serum interleukin-6 and C-reactive protein are associated with survival in melanoma patients receiving immune checkpoint inhibition. J Immunother Cancer. 2020;8(1).

342. Schalper KA, Carleton M, Zhou M, Chen T, Feng Y, Huang S-P, et al. Elevated serum interleukin-8 is associated with enhanced intratumor neutrophils and reduced clinical benefit of immune-checkpoint inhibitors. Nat Med. mai 2020;26(5):688-92.

343. Churg J, Rosen SH, Moolten S. Histological characteristics of mesothelioma associated with asbestos. Ann N Y Acad Sci. 31 déc 1965;132(1):614-22.

344. Yap TA, Aerts JG, Popat S, Fennell DA. Novel insights into mesothelioma biology and implications for therapy. Nat Rev Cancer. 25 juill 2017;17(8):475-88.

345. Jain RK. Antiangiogenesis strategies revisited: from starving tumors to alleviating hypoxia. Cancer Cell. 10 nov 2014;26(5):605-22.

346. Love MI, Soneson C, Patro R. Swimming downstream: statistical analysis of differential transcript usage following Salmon quantification. F1000Res. 2018;7:952.

347. Köster J, Rahmann S. Snakemake--a scalable bioinformatics workflow engine. Bioinformatics. 1 oct 2012;28(19):2520-2.

348. Ewels P, Magnusson M, Lundin S, Käller M. MultiQC: summarize analysis results for multiple tools and samples in a single report. Bioinformatics. 1 oct 2016;32(19):3047-8.

349. Patro R, Duggal G, Love MI, Irizarry RA, Kingsford C. Salmon provides fast and bias-aware quantification of transcript expression. Nat Methods. avr 2017;14(4):417-9.

350. Love MI, Huber W, Anders S. Moderated estimation of fold change and dispersion for RNA-seq data with DESeq2. Genome Biol. 2014;15(12):550.

351. Sturm G, Finotello F, Petitprez F, Zhang JD, Baumbach J, Fridman WH, et al. Comprehensive evaluation of transcriptome-based cell-type quantification methods for immuno-oncology. Bioinformatics. 15 2019;35(14):i436-45.

352. Yu G, Wang L-G, Han Y, He Q-Y. clusterProfiler: an R package for comparing biological themes among gene clusters. OMICS. mai 2012;16(5):284-7.

353. Li H, Durbin R. Fast and accurate short read alignment with Burrows-Wheeler transform. Bioinformatics. 15 juill 2009;25(14):1754-60.

354. Van der Auwera GA, Carneiro MO, Hartl C, Poplin R, Del Angel G, Levy-Moonshine A, et al. GATK Best Practices. Current protocols in bioinformatics / editoral board, Andreas D Baxevanis . [et al]. 2002;

355. DePristo MA, Banks E, Poplin R, Garimella KV, Maguire JR, Hartl C, et al. A framework for variation discovery and genotyping using next-generation DNA sequencing data. Nat Genet. mai 2011;43(5):491-8.

356. Ramos AH, Lichtenstein L, Gupta M, Lawrence MS, Pugh TJ, Saksena G, et al. Oncotator: cancer variant annotation tool. Hum Mutat. avr 2015;36(4):E2423-2429.

357. Shen R, Seshan VE. FACETS: allele-specific copy number and clonal heterogeneity analysis tool for high-throughput DNA sequencing. Nucleic Acids Res. 19 sept 2016;44(16):e131.

358. Andrews S. FASTQC A Quality Control tool for High Throughput Sequence Data. Babraham Institute. 2015;

359. Li H, Handsaker B, Wysoker A, Fennell T, Ruan J, Homer N, et al. The Sequence Alignment/Map format and SAMtools. Bioinformatics. 15 août 2009;25(16):2078-9.

360. Köster J, Rahmann S. Snakemake-a scalable bioinformatics workflow engine. Bioinformatics. 15 oct 2018;34(20):3600.

361. Mayakonda A, Lin D-C, Assenov Y, Plass C, Koeffler HP. Maftools: efficient and comprehensive analysis of somatic variants in cancer. Genome Res. nov 2018;28(11):1747-56.

362. Morgan M, Pagès H, Obenchain V, Hayden N. Rsamtools: Binary alignment (BAM), FASTA, variant call (BCF), and tabix file import [Internet]. Bioconductor version: Release (3.13); 2021 [cité 1 sept 2021]. Disponible sur: https://bioconductor.org/packages/Rsamtools/

363. Van Loo P, Nordgard SH, Lingjærde OC, Russnes HG, Rye IH, Sun W, et al. Allele-specific copy number analysis of tumors. Proc Natl Acad Sci U S A. 28 sept 2010;107(39):16910-5.

364. Hao Y, Hao S, Andersen-Nissen E, Mauck WM, Zheng S, Butler A, et al. Integrated analysis of multimodal single-cell data. Cell. 24 juin 2021;184(13):3573-3587.e29.

365. Quispel-Janssen JM, Badhai J, Schunselaar L, Price S, Brammeld J, Iorio F, et al. Comprehensive Pharmacogenomic Profiling of Malignant Pleural Mesothelioma Identifies a Subgroup Sensitive to FGFR Inhibition. Clin Cancer Res. 1 janv 2018;24(1):84-94.

366. Okada M, Kijima T, Aoe K, Kato T, Fujimoto N, Nakagawa K, et al. Clinical Efficacy and Safety of Nivolumab: Results of a Multicenter, Open-label, Single-arm, Japanese Phase II study in Malignant Pleural Mesothelioma (MERIT). Clin Cancer Res. 15 sept 2019;25(18):5485-92.

367. Kumagai S, Togashi Y, Kamada T, Sugiyama E, Nishinakamura H, Takeuchi Y, et al. The PD-1 expression balance between effector and regulatory T cells predicts the clinical efficacy of PD-1 blockade therapies. Nat Immunol. nov 2020;21(11):1346-58.

368. Kamada T, Togashi Y, Tay C, Ha D, Sasaki A, Nakamura Y, et al. PD-1+ regulatory T cells amplified by PD-1 blockade promote hyperprogression of cancer. Proc Natl Acad Sci U S A. 14 mai 2019;116(20):9999-10008.

369. Rauch DA, Conlon KC, Janakiram M, Brammer JE, Harding JC, Ye BH, et al. Rapid progression of adult T-cell leukemia/lymphoma as tumor-infiltrating Tregs after PD-1 blockade. Blood. 24 oct 2019;134(17):1406-14.

370. Schwitalla S, Ziegler PK, Horst D, Becker V, Kerle I, Begus-Nahrmann Y, et al. Loss of p53 in enterocytes generates an inflammatory microenvironment enabling invasion and lymph node metastasis of carcinogen-induced colorectal tumors. Cancer Cell. 14 janv 2013;23(1):93-106.

371. Guo G, Yu M, Xiao W, Celis E, Cui Y. Local Activation of p53 in the Tumor Microenvironment Overcomes Immune Suppression and Enhances Antitumor Immunity. Cancer Res. 1 mai 2017;77(9):2292-305.

372. Luke JJ, Bao R, Sweis RF, Spranger S, Gajewski TF. WNT/β-catenin Pathway Activation Correlates with Immune Exclusion across Human Cancers. Clin Cancer Res. 15 mai 2019;25(10):3074-83.

373. An Y, Adams JR, Hollern DP, Zhao A, Chang SG, Gams MS, et al. Cdh1 and Pik3ca Mutations Cooperate to Induce Immune-Related Invasive Lobular Carcinoma of the Breast. Cell Rep. 16 oct 2018;25(3):702-714.e6.

374. Lal N, White BS, Goussous G, Pickles O, Mason MJ, Beggs AD, et al. KRAS Mutation and Consensus Molecular Subtypes 2 and 3 Are Independently Associated with Reduced Immune Infiltration and Reactivity in Colorectal Cancer. Clin Cancer Res. 1 janv 2018;24(1):224-33.

375. Koyama S, Akbay EA, Li YY, Aref AR, Skoulidis F, Herter-Sprie GS, et al. STK11/LKB1 Deficiency Promotes Neutrophil Recruitment and Proinflammatory Cytokine Production to Suppress T-cell Activity in the Lung Tumor Microenvironment. Cancer Res. 1 mars 2016;76(5):999-1008.

376. Kumagai S, Togashi Y, Sakai C, Kawazoe A, Kawazu M, Ueno T, et al. An Oncogenic Alteration Creates a Microenvironment that Promotes Tumor Progression by Conferring a Metabolic Advantage to Regulatory T Cells. Immunity. 14 juill 2020;53(1):187-203.e8.

377. Robinson DR, Wu Y-M, Lonigro RJ, Vats P, Cobain E, Everett J, et al. Integrative clinical genomics of metastatic cancer. Nature. 17 août 2017;548(7667):297-303.

378. Goel S, DeCristo MJ, Watt AC, BrinJones H, Sceneay J, Li BB, et al. CDK4/6 inhibition triggers anti-tumour immunity. Nature. 24 août 2017;548(7668):471-5.

379. Schaer DA, Beckmann RP, Dempsey JA, Huber L, Forest A, Amaladas N, et al. The CDK4/6 Inhibitor Abemaciclib Induces a T Cell Inflamed Tumor Microenvironment and Enhances the Efficacy of PD-L1 Checkpoint Blockade. Cell Rep. 13 mars 2018;22(11):2978-94.

380. Lai AY, Sorrentino JA, Dragnev KH, Weiss JM, Owonikoko TK, Rytlewski JA, et al. CDK4/6 inhibition enhances antitumor efficacy of chemotherapy and immune checkpoint inhibitor combinations in preclinical models and enhances T-cell activation in patients with SCLC receiving chemotherapy. J Immunother Cancer. oct 2020;8(2):e000847.

381. Brenner E, Schörg BF, Ahmetlić F, Wieder T, Hilke FJ, Simon N, et al. Cancer immune control needs senescence induction by interferon-dependent cell cycle regulator pathways in tumours. Nat Commun. 12 mars 2020;11(1):1335.

382. Casey SC, Tong L, Li Y, Do R, Walz S, Fitzgerald KN, et al. MYC regulates the antitumor immune response through CD47 and PD-L1. Science. 8 avr 2016;352(6282):227-31.

383. Kortlever RM, Sodir NM, Wilson CH, Burkhart DL, Pellegrinet L, Brown Swigart L, et al. Myc Cooperates with Ras by Programming Inflammation and Immune Suppression. Cell. 30 nov 2017;171(6):1301-1315.e14.

384. Miranda A, Hamilton PT, Zhang AW, Pattnaik S, Becht E, Mezheyeuski A, et al. Cancer stemness, intratumoral heterogeneity, and immune response across cancers. Proc Natl Acad Sci USA. 30 2019;116(18):9020-9.

385. Davoli T, Uno H, Wooten EC, Elledge SJ. Tumor aneuploidy correlates with markers of immune evasion and with reduced response to immunotherapy. Science. 20 janv 2017;355(6322):eaaf8399.

386. Zhang M, Luo J-L, Sun Q, Harber J, Dawson AG, Nakas A, et al. Clonal architecture in mesothelioma is prognostic and shapes the tumour microenvironment. Nat Commun. 19 mars 2021;12(1):1751.

387. Qian B-Z, Li J, Zhang H, Kitamura T, Zhang J, Campion LR, et al. CCL2 recruits inflammatory monocytes to facilitate breast-tumour metastasis. Nature. 8 juin 2011;475(7355):222-5.

388. Geng Y, Fan J, Chen L, Zhang C, Qu C, Qian L, et al. A Notch-Dependent Inflammatory Feedback Circuit between Macrophages and Cancer Cells Regulates Pancreatic Cancer Metastasis. Cancer Res. 1 janv 2021;81(1):64-76.

389. Lee JC, Mehdizadeh S, Smith J, Young A, Mufazalov IA, Mowery CT, et al. Regulatory T cell control of systemic immunity and immunotherapy response in liver metastasis. Sci Immunol. 2 oct 2020;5(52):eaba0759.

390. Scagliotti GV, Gaafar R, Nowak AK, Nakano T, van Meerbeeck J, Popat S, et al. Nintedanib in combination with pemetrexed and cisplatin for chemotherapy-naive patients with advanced malignant pleural mesothelioma (LUME-Meso): a double-blind, randomised, placebo-controlled phase 3 trial. Lancet Respir Med. juill 2019;7(7):569-80.

391. Laszlo V, Valko Z, Kovacs I, Ozsvar J, Hoda MA, Klikovits T, et al. Nintedanib Is Active in Malignant Pleural Mesothelioma Cell Models and Inhibits Angiogenesis and Tumor Growth In Vivo. Clin Cancer Res. 1 août 2018;24(15):3729-40.

392. Huinen ZR, Huijbers EJM, van Beijnum JR, Nowak-Sliwinska P, Griffioen AW. Anti-angiogenic agents - overcoming tumour endothelial cell anergy and improving immunotherapy outcomes. Nat Rev Clin Oncol. août 2021;18(8):527-40.

393. Huang H, Lai J-Y, Do J, Liu D, Li L, Del Rosario J, et al. Specifically targeting angiopoietin-2 inhibits angiogenesis, Tie2-expressing monocyte infiltration, and tumor growth. Clin Cancer Res. 1 mars 2011;17(5):1001-11.

394. Mazzieri R, Pucci F, Moi D, Zonari E, Ranghetti A, Berti A, et al. Targeting the ANG2/TIE2 axis inhibits tumor growth and metastasis by impairing angiogenesis and disabling rebounds of proangiogenic myeloid cells. Cancer Cell. 12 avr 2011;19(4):512-26.

395. Rigamonti N, Kadioglu E, Keklikoglou I, Wyser Rmili C, Leow CC, De Palma M. Role of angiopoietin-2 in adaptive tumor resistance to VEGF signaling blockade. Cell Rep. 7 août 2014;8(3):696-706.

396. Gao P, Lazare C, Cao C, Meng Y, Wu P, Zhi W, et al. Immune checkpoint inhibitors in the treatment of virus-associated cancers. J Hematol Oncol. 10 juin 2019;12(1):58.

397. Cousin S, Cantarel C, Guegan J-P, Gomez-Roca C, Metges J-P, Adenis A, et al. Regorafenib-Avelumab Combination in Patients with Microsatellite Stable Colorectal Cancer (REGOMUNE): A Single-arm, Open-label, Phase II Trial. Clin Cancer Res. 15 avr 2021;27(8):2139-47.

398. Kawazoe A, Fukuoka S, Nakamura Y, Kuboki Y, Wakabayashi M, Nomura S, et al. Lenvatinib plus pembrolizumab in patients with advanced gastric cancer in the first-line or second-line setting (EPOC1706): an open-label, single-arm, phase 2 trial. Lancet Oncol. août 2020;21(8):1057-65.

399. Lee C-H, Shah AY, Rasco D, Rao A, Taylor MH, Di Simone C, et al. Lenvatinib plus pembrolizumab in patients with either treatment-naive or previously treated metastatic renal cell carcinoma (Study 111/KEYNOTE-146): a phase 1b/2 study. Lancet Oncol. juill 2021;22(7):946-58.

400. Jones SA, Jenkins BJ. Recent insights into targeting the IL-6 cytokine family in inflammatory diseases and cancer. Nat Rev Immunol. déc 2018;18(12):773-89.

401. Loriot Y, Marabelle A, Guégan JP, Danlos FX, Besse B, Chaput N, et al. Plasma proteomics identifies Leukemia Inhibitory Factor (LIF) as a novel predictive biomarker of immune-checkpoint blockade resistance. Ann Oncol. 17 août 2021;S0923-7534(21)03978-8.

402. Handle F, Puhr M, Schaefer G, Lorito N, Hoefer J, Gruber M, et al. The STAT3 Inhibitor Galiellalactone Reduces IL6-Mediated AR Activity in Benign and Malignant Prostate Models. Mol Cancer Ther. déc 2018;17(12):2722-31.

403. Johnson DE, O'Keefe RA, Grandis JR. Targeting the IL-6/JAK/STAT3 signalling axis in cancer. Nat Rev Clin Oncol. avr 2018;15(4):234-48.

404. Karakasheva TA, Lin EW, Tang Q, Qiao E, Waldron TJ, Soni M, et al. IL-6 Mediates Cross-Talk between Tumor Cells and Activated Fibroblasts in the Tumor Microenvironment. Cancer Res. 1 sept 2018;78(17):4957-70.

405. Ohira T, Nishio K, Ohe Y, Arioka H, Nishio M, Funayama Y, et al. Improvement by eicosanoids in cancer cachexia induced by LLC-IL6 transplantation. J Cancer Res Clin Oncol. 1996;122(12):711-5.

406. Strassmann G, Fong M, Kenney JS, Jacob CO. Evidence for the involvement of interleukin 6 in experimental cancer cachexia. J Clin Invest. mai 1992;89(5):1681-4.

407. Strassmann G, Jacob CO, Fong M, Bertolini DR. Mechanisms of paraneoplastic syndromes of colon-26: involvement of interleukin 6 in hypercalcemia. Cytokine. sept 1993;5(5):463-8.

408. Pettersen K, Andersen S, Degen S, Tadini V, Grosjean J, Hatakeyama S, et al. Cancer cachexia associates with a systemic autophagy-inducing activity mimicked by cancer cell-derived IL-6 trans-signaling. Sci Rep. 17 2017;7(1):2046.

409. Danlos FX, Ackermann F, Rohmer J, Roumier M, Marabelle A, Michot JM. High levels of TNFα in patients with COVID-19 refractory to tocilizumab. Eur J Cancer. mai 2021;149:102-4.

410. Montfort A, Filleron T, Virazels M, Dufau C, Milhès J, Pagès C, et al. Combining Nivolumab and Ipilimumab with Infliximab or Certolizumab in Patients with Advanced Melanoma: First Results of a Phase Ib Clinical Trial. Clin Cancer Res. 15 févr 2021;27(4):1037-47.

411. Wang M-T, Fer N, Galeas J, Collisson EA, Kim SE, Sharib J, et al. Blockade of leukemia inhibitory factor as a therapeutic approach to KRAS driven pancreatic cancer. Nat Commun. 11 juill 2019;10(1):3055.

412. Mace TA, Shakya R, Pitarresi JR, Swanson B, McQuinn CW, Loftus S, et al. IL-6 and PD-L1 antibody blockade combination therapy reduces tumour progression in murine models of pancreatic cancer. Gut. févr 2018;67(2):320-32.

413. Long KB, Tooker G, Tooker E, Luque SL, Lee JW, Pan X, et al. IL6 Receptor Blockade Enhances Chemotherapy Efficacy in Pancreatic Ductal Adenocarcinoma. Mol Cancer Ther. sept 2017;16(9):1898-908.

414. Corcoran RB, Contino G, Deshpande V, Tzatsos A, Conrad C, Benes CH, et al. STAT3 plays a critical role in KRAS-induced pancreatic tumorigenesis. Cancer Res. 15 juill 2011;71(14):5020-9.

415. Coppé J-P, Desprez P-Y, Krtolica A, Campisi J. The senescence-associated secretory phenotype: the dark side of tumor suppression. Annu Rev Pathol. 2010;5:99-118.

416. Tchkonia T, Zhu Y, van Deursen J, Campisi J, Kirkland JL. Cellular senescence and the senescent secretory phenotype: therapeutic opportunities. J Clin Invest. mars 2013;123(3):966-72.

417. Bigenwald C, Le Berichel J, Wilk CM, Chakraborty R, Chen ST, Tabachnikova A, et al. BRAFV600E-induced senescence drives Langerhans cell histiocytosis pathophysiology. Nat Med. mai 2021;27(5):851-61.

418. Adib E, Nassar AH, Akl EW, Abou Alaiwi S, Nuzzo PV, Mouhieddine TH, et al. CDKN2A Alterations and Response to Immunotherapy in Solid Tumors. Clin Cancer Res. 15 juill 2021;27(14):4025-35.

419. Wang G, Lu X, Dey P, Deng P, Wu CC, Jiang S, et al. Targeting YAP-Dependent MDSC Infiltration Impairs Tumor Progression. Cancer Discov. janv 2016;6(1):80-95.

420. Guo X, Zhao Y, Yan H, Yang Y, Shen S, Dai X, et al. Single tumor-initiating cells evade immune clearance by recruiting type II macrophages. Genes Dev. 1 févr 2017;31(3):247-59.

421. Jia J, Zhang H, He L, Zhang H, Shu M. Cutaneous neurofibroma cells with active YAP promotes proliferation of macrophages resulting in increased accumulation of macrophages by modulating CCL5 and TGF-β1. Oncol Rep. avr 2020;43(4):1319-30.

422. Shukla A, Bosenberg MW, MacPherson MB, Butnor KJ, Heintz NH, Pass HI, et al. Activated cAMP response element binding protein is overexpressed in human mesotheliomas and inhibits apoptosis. Am J Pathol. nov 2009;175(5):2197-206.

423. Westbom CM, Shukla A, MacPherson MB, Yasewicz EC, Miller JM, Beuschel SL, et al. CREB-induced inflammation is important for malignant mesothelioma growth. Am J Pathol. oct 2014;184(10):2816-27.

424. Peng D, Kryczek I, Nagarsheth N, Zhao L, Wei S, Wang W, et al. Epigenetic silencing of TH1-type chemokines shapes tumour immunity and immunotherapy. Nature. 12 nov 2015;527(7577):249-53.

425. Zingg D, Arenas-Ramirez N, Sahin D, Rosalia RA, Antunes AT, Haeusel J, et al. The Histone Methyltransferase Ezh2 Controls Mechanisms of Adaptive Resistance to Tumor Immunotherapy. Cell Rep. 25 juill 2017;20(4):854-67.

426. Morris LGT, Chan TA. Therapeutic targeting of tumor suppressor genes. Cancer. 1 mai 2015;121(9):1357-68.

427. Chabanon RM, Muirhead G, Krastev DB, Adam J, Morel D, Garrido M, et al. PARP inhibition enhances tumor cell-intrinsic immunity in ERCC1-deficient non-small cell lung cancer. J Clin Invest. 1 mars 2019;129(3):1211-28.

428. Jiao S, Xia W, Yamaguchi H, Wei Y, Chen M-K, Hsu J-M, et al. PARP Inhibitor Upregulates PD-L1 Expression and Enhances Cancer-Associated Immunosuppression. Clin Cancer Res. 15 juill 2017;23(14):3711-20.

429. Goswami S, Apostolou I, Zhang J, Skepner J, Anandhan S, Zhang X, et al. Modulation of EZH2 expression in T cells improves efficacy of anti-CTLA-4 therapy. J Clin Invest. 31 août 2018;128(9):3813-8.

430. Wang D, Quiros J, Mahuron K, Pai C-C, Ranzani V, Young A, et al. Targeting EZH2 Reprograms Intratumoral Regulatory T Cells to Enhance Cancer Immunity. Cell Rep. 12 juin 2018;23(11):3262-74.

431. Fennell DA, King A, Mohammed S, Branson A, Brookes C, Darlison L, et al. Rucaparib in patients with BAP1-deficient or BRCA1-deficient mesothelioma (MiST1): an open-label, single-arm, phase 2a clinical trial. Lancet Respir Med. juin 2021;9(6):593-600.

432. Zauderer MG, Szlosarek P, Le Moulec S, Popat S, Taylor P, Planchard D, et al. Phase 2, multicenter study of the EZH2 inhibitor tazemetostat as monotherapy in adults with relapsed or refractory (R/R) malignant mesothelioma (MM) with BAP1 inactivation. JCO. 20 mai 2018;36(15_suppl):8515-8515.

433. Hossain DMS, Javaid S, Cai M, Zhang C, Sawant A, Hinton M, et al. Dinaciclib induces immunogenic cell death and enhances anti-PD1-mediated tumor suppression. J Clin Invest. 1 févr 2018;128(2):644-54.

434. Egelston C, Guo W, Yost S, Lee JS, Rose D, Avalos C, et al. Pre-existing effector T-cell levels and augmented myeloid cell composition denote response to CDK4/6 inhibitor palbociclib and pembrolizumab in hormone receptor-positive metastatic breast cancer. J Immunother Cancer. mars 2021;9(3):e002084.

435. Dey A, Varelas X, Guan K-L. Targeting the Hippo pathway in cancer, fibrosis, wound healing and regenerative medicine. Nat Rev Drug Discov. juill 2020;19(7):480-94.

436. Gibault F, Sturbaut M, Bailly F, Melnyk P, Cotelle P. Targeting Transcriptional Enhanced Associate Domains (TEADs). J Med Chem. 28 juin 2018;61(12):5057-72.

437. Tang TT, Konradi AW, Feng Y, Peng X, Ma M, Li J, et al. Small Molecule Inhibitors of TEAD Auto-palmitoylation Selectively Inhibit Proliferation and Tumor Growth of NF2-deficient Mesothelioma. Mol Cancer Ther. juin 2021;20(6):986-98.

438. Shapiro IM, Kolev VN, Vidal CM, Kadariya Y, Ring JE, Wright Q, et al. Merlin deficiency predicts FAK inhibitor sensitivity: a synthetic lethal relationship. Sci Transl Med. 21 mai 2014;6(237):237ra68.

439. Fennell DA, Baas P, Taylor P, Nowak AK, Gilligan D, Nakano T, et al. Maintenance Defactinib Versus Placebo After First-Line Chemotherapy in Patients With Merlin-Stratified Pleural Mesothelioma: COMMAND-A Double-Blind, Randomized, Phase II Study. J Clin Oncol. 1 avr 2019;37(10):790-8.

440. Zanconato F, Battilana G, Forcato M, Filippi L, Azzolin L, Manfrin A, et al. Transcriptional addiction in cancer cells is mediated by YAP/TAZ through BRD4. Nat Med. oct 2018;24(10):1599-610.

441. Gobbi G, Donati B, Do Valle IF, Reggiani F, Torricelli F, Remondini D, et al. The Hippo pathway modulates resistance to BET proteins inhibitors in lung cancer cells. Oncogene. oct 2019;38(42):6801-17.

442. Song S, Li Y, Xu Y, Ma L, Pool Pizzi M, Jin J, et al. Targeting Hippo coactivator YAP1 through BET bromodomain inhibition in esophageal adenocarcinoma. Mol Oncol. juin 2020;14(6):1410-26.

443. Zhu H, Bengsch F, Svoronos N, Rutkowski MR, Bitler BG, Allegrezza MJ, et al. BET Bromodomain Inhibition Promotes Anti-tumor Immunity by Suppressing PD-L1 Expression. Cell Rep. 13 sept 2016;16(11):2829-37.

444. Hogg SJ, Vervoort SJ, Deswal S, Ott CJ, Li J, Cluse LA, et al. BET-Bromodomain Inhibitors Engage the Host Immune System and Regulate Expression of the Immune Checkpoint Ligand PD-L1. Cell Rep. 28 févr 2017;18(9):2162-74.

445. Kagoya Y, Nakatsugawa M, Yamashita Y, Ochi T, Guo T, Anczurowski M, et al. BET bromodomain inhibition enhances T cell persistence and function in adoptive immunotherapy models. J Clin Invest. 1 sept 2016;126(9):3479-94.

446. Li Z, Razavi P, Li Q, Toy W, Liu B, Ping C, et al. Loss of the FAT1 Tumor Suppressor Promotes Resistance to CDK4/6 Inhibitors via the Hippo Pathway. Cancer Cell. 10 déc 2018;34(6):893-905.e8.

447. Cassidy MR, Wolchok RE, Zheng J, Panageas KS, Wolchok JD, Coit D, et al. Neutrophil to Lymphocyte Ratio is Associated With Outcome During Ipilimumab Treatment. EBioMedicine. avr 2017;18:56-61.

448. Bigot F, Castanon E, Baldini C, Hollebecque A, Carmona A, Postel-Vinay S, et al. Prospective validation of a prognostic score for patients in immunotherapy phase I trials: The Gustave Roussy Immune Score (GRIm-Score). Eur J Cancer. oct 2017;84:212-8.

449. Meiller C, Montagne F, Hirsch TZ, Caruso S, de Wolf J, Bayard Q, et al. Multi-site tumor sampling highlights molecular intra-tumor heterogeneity in malignant pleural mesothelioma. Genome Med. 14 juill 2021;13(1):113.

450. Garrido P, Pujol J-L, Kim ES, Lee JM, Tsuboi M, Gómez-Rueda A, et al. Canakinumab with and without pembrolizumab in patients with resectable non-small-cell lung cancer: CANOPY-N study design. Future Oncol. avr 2021;17(12):1459-72.

451. Dijkgraaf EM, Santegoets SJ a. M, Reyners AKL, Goedemans R, Wouters MCA, Kenter GG, et al. A phase I trial combining carboplatin/doxorubicin with tocilizumab, an anti-IL-6R monoclonal antibody, and interferon-α2b in patients with recurrent epithelial ovarian cancer. Ann Oncol. oct 2015;26(10):2141-9.

452. Nywening TM, Wang-Gillam A, Sanford DE, Belt BA, Panni RZ, Cusworth BM, et al. Targeting tumour-associated macrophages with CCR2 inhibition in combination with FOLFIRINOX in patients with borderline resectable and locally advanced pancreatic cancer: a single-centre, open-label, dose-finding, non-randomised, phase 1b trial. Lancet Oncol. mai 2016;17(5):651-62.

453. Goldstein LJ, Perez RP, Yardley D, Han LK, Reuben JM, Gao H, et al. A window-of-opportunity trial of the CXCR1/2 inhibitor reparixin in operable HER-2-negative breast cancer. Breast Cancer Res. 10 janv 2020;22(1):4.

454. De Santo C, Cheng P, Beggs A, Egan S, Bessudo A, Mussai F. Metabolic therapy with PEG-arginase induces a sustained complete remission in immunotherapy-resistant melanoma. J Hematol Oncol. 18 mai 2018;11(1):68.

455. Deng M, Gui X, Kim J, Xie L, Chen W, Li Z, et al. LILRB4 signalling in leukaemia cells mediates T cell suppression and tumour infiltration. Nature. oct 2018;562(7728):605-9.

Appendices

1. **Chemokine biology on immune checkpoint-targeted therapies**. Letourneur D, Danlos FX, Marabelle A. Eur J Cancer. 2020 Sep;137:260-271. doi: 10.1016/j.ejca.2020.06.009.

2. **Plasma proteomics identifies Leukemia Inhibitory Factor (LIF) as a novel predictive biomarker of immune-checkpoint blockade resistance.** Y Loriot#, A Marabelle# , JP Guégan, FX Danlos et al. Ann Oncol. 2021 Aug 17;S0923--534(21)03978-8. doi: 10.1016/j.annonc.2021.08.1748.

3. **Metabolomic analyses of COVID-19 patients unravel stage-dependent and prognostic biomarkers.** Danlos FX, Grajeda-Iglesias C, Durand S, et al. Cell Death Dis. 2021 Mar 11;12(3):258. doi: 10.1038/s41419-021-03540-y.

4. **High levels of TNFα in patients with COVID-19 refractory to tocilizumab.** Danlos FX, Ackermann F et al. Eur J Cancer. 2021 Mar 20;149:102-104. doi: 10.1016/j.ejca.2021.01.056

5. **Prolonged SARS-CoV-2 RNA virus shedding and lymphopenia are hallmarks of COVID-19 in cancer patients with poor prognosis.** Anne-Gaëlle Goubet#, Agathe Dubuisson#, Arthur Geraud, François-Xavier Danlos et al. Cell Death Differ. 2021 Jul 6;1-19. doi: 10.1038/s41418-021-00817-9.

6. **Repurposing of Anticancer Drugs Expands Possibilities for Antiviral and Anti-Inflammatory Discovery in COVID-19.** Mihaela Aldea, Jean-Marie Michot, Francois-Xavier Danlos et al. Cancer Discov. 2021 Jun;11(6):1336-1344. doi: 10.1158/2159-8290.CD-21-0144.

7. **Applications of single-cell and bulk RNA sequencing in onco-immunology**. Kuksin M, Morel D, Aglave M, Danlos FX, et al. Eur J Cancer. 2021 Apr 15;149:193-210. doi: 10.1016/j.ejca.2021.03.005.

European Journal of Cancer 137 (2020) 260–271

Available online at www.sciencedirect.com

ScienceDirect

journal homepage: www.ejcancer.com

Review

Chemokine biology on immune checkpoint–targeted therapies

Diane Letourneur [a,b], François-Xavier Danlos [a,c], Aurélien Marabelle [a,d,*]

[a] *INSERM U1015, Gustave Roussy, Villejuif, France*
[b] *École normale supérieure de Lyon, Département de biologie, Master biologie, Lyon, France*
[c] *Université Paris-Saclay, France*
[d] *Département D'Innovation Thérapeutique et D'Essais Précoces (DITEP), Gustave Roussy, Université Paris Saclay, Villejuif, France*

Received 28 May 2020; accepted 12 June 2020
Available online 18 August 2020

KEYWORDS
Chemokine;
Immune checkpoint blockade;
Biomarker;
PD-1;
PD-L1;
CTLA-4

Abstract The use of antagonistic immune checkpoint–targeted monoclonal antibodies has profoundly modified the standard of care and significantly increased the survival for many cancers. However, many patients still do not respond to those treatments. Biomarkers predictive for efficacy or failure of such immunotherapies would allow developing treatment stratification strategies which could further increase the survival rates of patients with cancer. Chemokines are a subset of the immune cell messenger molecules known as cytokines. Chemokines are key chemoattractant molecules which are essential for the homing of immune cells, notably within tumours. Therefore, they are good candidates for providing predictive biomarkers of the clinical response to checkpoint blockade immunotherapies. In this review, we summarise the recent advances in our understanding of the role of chemokines and how chemokine concentrations may set the tone for the efficacy of immune checkpoint–targeted immunotherapies.

* *Corresponding author*: Aurélien Marabelle, INSERM U1015, Gustave Roussy, Villejuif, France.
E-mail address: AURELIEN.MARABELLE@gustaveroussy.fr (A. Marabelle).

https://doi.org/10.1016/j.ejca.2020.06.009
0959-8049/

1. Introduction

Cancer is one of the leading causes of mortality worldwide. More than 9.5 million people died from cancer in 2018 [1]. Over the last decade, immunotherapy has taken a significant place within the anticancer armamentarium beside surgery, radiotherapy, cytotoxic chemotherapies, anti-angiogenics and oncogenic tyrosine kinase inhibitors [2]. For the first time, monoclonal antibodies (mAbs) have been designed to target the immune system rather than the tumour itself to boost the anticancer response naturally occurring in patients with cancer. The tumour microenvironment is composed not only of cancer cells but also of stromal cells and immune cell infiltrates such as T cells, B cells, macrophages and dendritic cells (DCs); all these cells can secrete activating or inhibitory messenger molecules, chemoattractants and growth factors of the immune system known as cytokines [3]. The immune response seems to be inefficient in its fight against tumours because of a dysregulated expression of immune checkpoints such as programmed cell death 1 (PD-1)/programmed cell death ligand 1 (PD-L1) and cytotoxic T-lymphocyte–associated protein 4 (CTLA-4) [4,5]. In physiological conditions, these checkpoints can inhibit inflammatory responses and protect organisms against autoimmune diseases. However, PD-1/PD-L1 and CTLA-4 can be overexpressed in the tumour microenvironment and therefore hamper the antitumour immune response. Among the commercially available immunotherapies, immune checkpoint–targeted antibodies are blocking PD-1/PD-L1 and CTLA-4. Durable tumour responses can be obtained in up to 40% of the patients in anti–PD-1 monotherapies and 55% in combination with anti–CTLA-4 [6,7].

Interestingly, the levels of tumour-infiltrating immune cells have been shown to be more accurate predictors of the clinical outcome than the tumour stage [9,10]. Chemokines are the chemotactic cytokines which are essential for the homing of immune cells in specific tissue microenvironment, notably within tumours. Therefore, circulating chemokine concentrations could correlate with the immune profile of a tumour and could be monitored more easily than tumour-infiltrating immune cells during immunotherapy. In this review, we summarise the current knowledge of how chemokines could participate to the cancer spreading or the homing

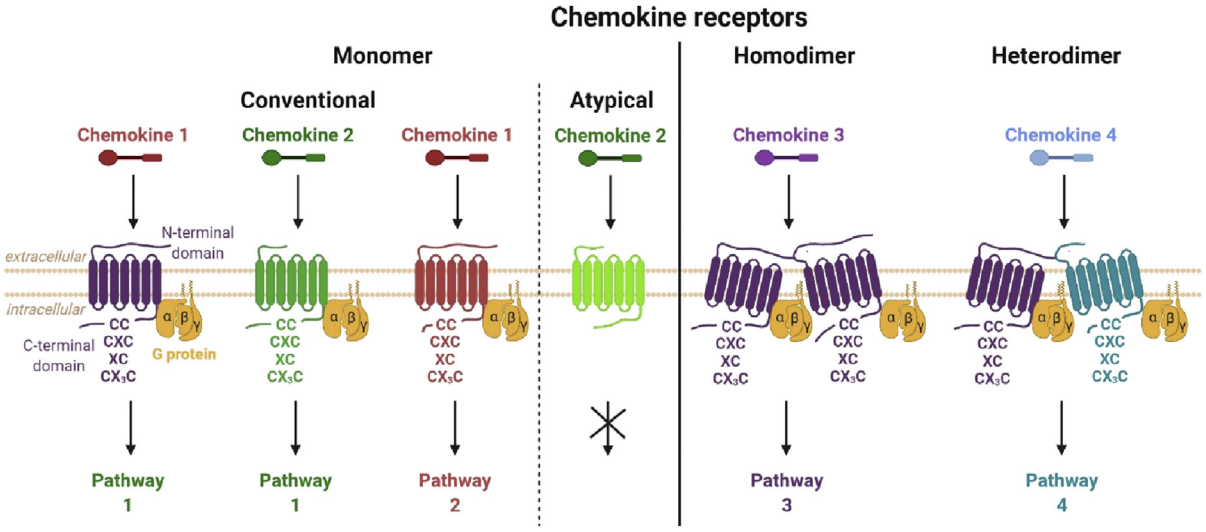

Chemokine	CCL7	CCL21	CCL7	CCL21	CCL2	CCL2 and CCL5
Chemokine Receptor	CCR2	CCR7	CCR1	ACKR4	CCR2	CCR2 and CCR5
Pathway	Monocyte migration	Monocyte migration	Breast cancer cells proliferation	None	Monocyte migration	Cell adhesion
Reference	[11]	[12]	[11]	[12]	[13]	[14]

Fig. 1. **Structure of chemokine receptors.** Chemokine receptors are structured into an extracellular N-terminal domain, an intracellular C-terminal domain and seven transmembrane helices. In conventional receptors, the C-terminal domain is coupled with a G-protein and contains either two adjacent cysteines (CC), two cysteines separated by another amino acid (CXC), one single cysteine (XC) or two cysteines separated by three amino acids (CX_3C). The N-terminal domain determines the affinity of the chemokine receptor for its ligands, while the C-terminal domain triggers the intracellular pathway in response to the binding of the ligand. Chemokine receptors can be biologically functional as monomers, homodimers and heterodimers. An example of each case is provided in the table [11-14].

of immune cells into tumours and how their monitoring could ameliorate immune checkpoint blockade therapy.

1.1. Chemokines are a family of immune-related molecules

1.1.1. Molecular nature of chemokines

Chemokines are small secreted proteins of 8–14 kDa from the cytokine superfamily [15]. They are expressed by a broad variety of immune cell types from the myeloid and lymphoid lineages but can also be expressed by stromal and cancer cells of the tumour microenvironment [16]. They are classified in four subfamilies relatively to the position of one or two conserved cysteines ('C') in the N-terminal domain of each of these proteins: CC, CXC, CX_3C and XC (where 'X' stands for an alternate amino acid) ([17], Fig. 1). Their chemotactic properties allow for the recruitment of leukocytes to the site of inflammation. 48 chemokines and 23 chemokine receptors, among which 5 are atypical receptors, have been described so far in the human species ([12], Table 1). Conventional chemokine receptors are heptahelical G-protein–coupled molecules that activate intracellular pathways. Atypical receptors do not seem to transduce intracellular signals but seem to contribute to the regulation of ligand colocalisation [17].

1.1.2. Chemokine-receptor interaction

The chemokine network is redundant, as different ligands can bind to the same receptor and *vice versa* ([17], Table 1). The ligand-receptor interaction is notably modulated by the nature of the receptor, its glycosylation, the concentration of the ligand and the number of receptors expressed at the cell surface. Moreover, chemokine receptors can form homodimers or heterodimers [17,18]. For example, the CXC motif chemokine receptors 3 and 4 (CXCR3 and CXCR4) can form heterodimers [19]. Agonistic ligands can induce conformational changes of their receptors, leading to the intracellular activation of various pathways including the Janus kinase/signal transducer and activator of transcription (STAT) and mitogen-activated protein kinase pathways [12].

1.1.3. Biological role of the chemokine network

Chemokines are mostly known to form a gradient that can chemoattract leukocytes to the site of damage or infection. Their biological activity relies on the nature of the immune cells that express the chemokine receptor.

Table 1
The human chemokine network: receptors and ligands.

Receptors conventional or '*atypical*'	Chemokines agonist	Antagonist	Main immune functions [12]
CCR1	CCL 2, 3, 5, 7, 8, 13, 14, **15**, **23**	CCL 4, 18	DC and monocytes chemotaxis
CCR2	CCL **2**, 7, 8, 11, 13, 16	CCL 24, 26	T-helper 1 differentiation, DC and monocytes chemotaxis
CCR3	CCL 2, 5, 8, **11**, 13, 15, **24**, **26**, 28	CCL 18	T-helper 2 immunity, mast cells and eosinophils chemotaxis
CCR4	CCL 17, 22		T-helper 2 immunity
CCR5	CCL 2, 3, 4, 5, 8, 11, 13, 14	CCL 7	DC chemotaxis, production of TNF-α
CCR6	CCL 20		DC chemotaxis, T-cell migration
CCR7	CCL 19, 21		DC, monocytes and neutrophils chemotaxis, lymphocytes chemotaxis in lymphoid tissues
CCR8	CCL 21		Monocytes chemotaxis, thymopoiesis
CCR9	CCL 25		Recruitment of leukocytes to the gut
CCR10	CCL 27, 28		Recruitment of T cells to the skin
CXCR1	CXCL 1, 6, **8**		DC and neutrophils chemotaxis
CXCR2	CXCL 1, 2, 3, 5, 6, 7, 8		DC and neutrophils chemotaxis
CXCR3-A, B, Alt	CCL 5, 13, 19, 20		
	CXCL **9**, **10**, **11**, 12α	CCL 7,11	T-helper 1 immunity
CXCR4	CXCL 12α, 12β, 12γ, 12δ, 12ε		Lymphopoiesis, haematopoiesis
CXCR5	CXCL 13		B-cell activation
CXCR6	CXCL 16		T-cell adhesion and migration
CX3CR1	CX3CL 1		Monocytes chemotaxis, microglial cells activation and migration
XCR1	XCL 1, 2		Treg cells differentiation in the thymus
ACKR1	CCL 2, 5, 7, 11, 14, 17		
	CXCL 5, 6, 8, 11		
ACKR2	CCL 2, 3, 4, 5, 7, 8, 11, 13, 14, 17, 22		Regulation of chemokine abundance
ACKR3	CXCL 11, **12α**		
ACKR4	CCL 19, 21, 25		
CCRL2	CCL 19		

The human chemokine receptors are activated by agonistic ligands and inhibited by antagonistic ligands. They display various roles in immunity depending on the type of cells expressing the corresponding chemokine receptors.
In bold are main ligands responsible for the biological activity of the receptor and *in italic* are atypical chemokine receptors. DC: dendritic cell.

For example, CXCR5 is involved in adaptive immunity by activating B cells [12]. More and more studies demonstrate that chemokines are involved in other processes such as cell proliferation and differentiation, apoptosis and embryonic development [12].

1.2. Cancer cells can hijack the chemokine network

1.2.1. Chemokines are reknown to participate to the anticancer immune response

Chemokines counter cancer spreading using various processes. Chemokines can be secreted by either sentinel cells that perform tissue immunosurveillance, stromal cells or cancer cells. They form a gradient from the tumour site to the blood and lymph vessels, thereby recruiting leukocytes expressing the corresponding chemokine receptors. For example, CXCL9/10/11 could chemoattract natural killer cells and T cells to the tumour site [20]. Once activated, DCs can present tumour antigens to naive and memory T cells leading to their priming and their migration throughout the blood, lymphatic vessels and tumours. Eventually, cancer cells can be destroyed by such primed cytotoxic natural killers and CD8+ T lymphocytes ([21], Fig. 2A). Similarly, CXCL13 produced by T follicular helper cells (T_{FH}) could chemoattract B cells and favour their activation in tertiary lymphoid structures (TLSs) [22]. Such B cells could act as antigen-presenting cells or differenciate into plasma cells to produce antibodies and cytokines targeted against the tumour [10].

1.2.2. Chemokines can also have direct inhibitory effects on cancer cells

Interestingly, chemokines can also directly target cancer cells. First, they can inhibit cancer cell proliferation. For example, in hepatocellular carcinoma (HCC), C–C

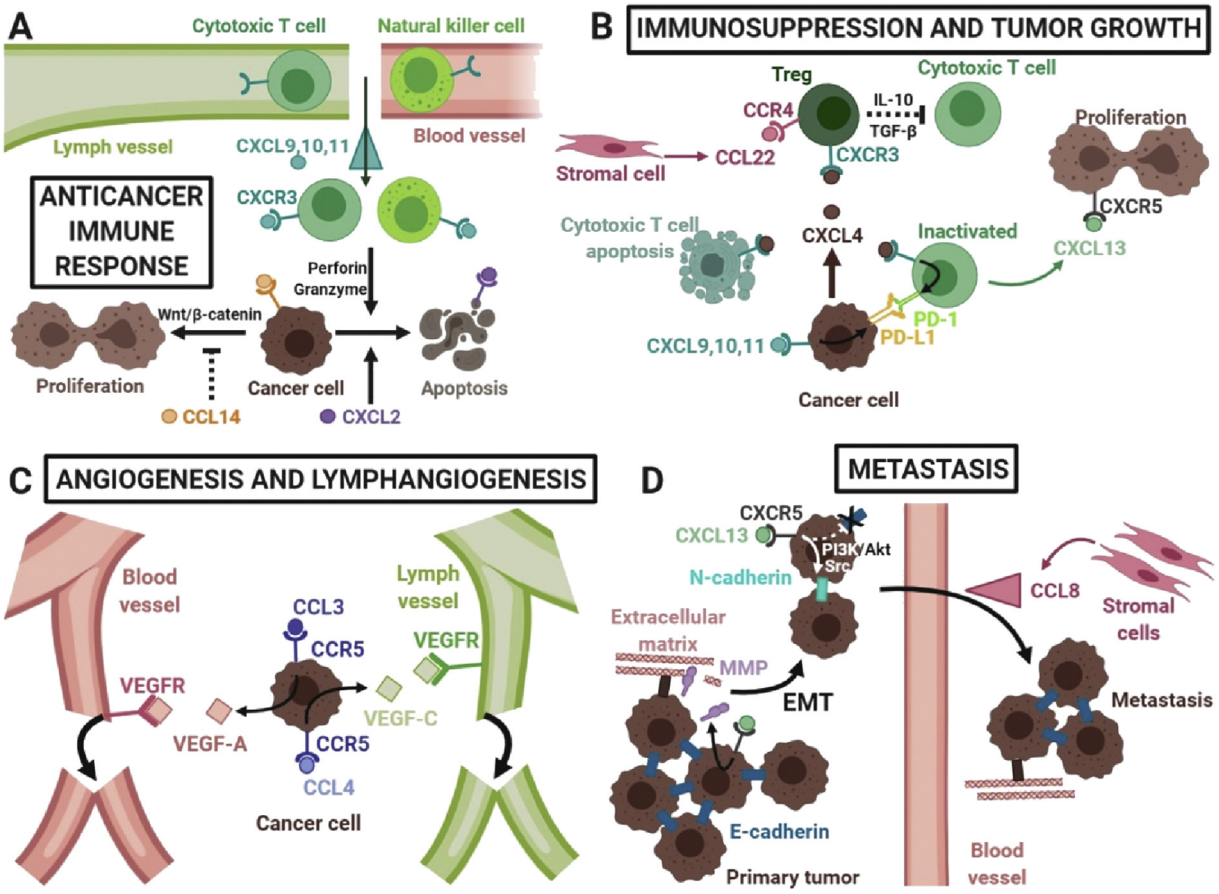

Fig. 2. **Chemokines participate in the tumour microenvironment and can favour cancer spreading.** Chemokines can either promote or inhibit cancer spreading, depending on the type of cancer and on the chemokines and receptors involved. (A) Gradients of chemokines participate in the immune response by chemoattracting natural killer cells and cytotoxic T cells that lyse cancer cells, and chemokines can directly enhance apoptosis and inhibit tumour proliferation. (B) Chemokines can enhance tumour proliferation and suppress the immune response by inactivating cytotoxic T cells *via* their apoptosis, PD-1/PD-L1 upregulation and Tregs chemoattraction. (C) Chemokines can favour angiogenesis and lymphangiogenesis by producing VEGFs that attracts VEGFR-expressing endothelial cells. (D) Chemokines can activate the production of MMP that degrade components of the extracellular matrix and promote EMT. Gradients of chemokines can guide tumour migration to form metastasis. EMT: epithelial-mesenchymal transition, MMP: matrix metalloprotease, PD-1: programmed cell death 1, PD-L1: programmed cell death ligand 1, Treg: regulator T cell, VEGF: vascular endothelial growth factor, VEGFR: vascular endothelial growth factor receptor.

motif chemokine ligand 14 reduces avian myelocytomatosis virus oncogene cellular homologue expression *via* the Wnt/β-catenin pathway [23], and *in vitro* CXCL2 promotes apoptosis and alters the extracellular signal-regulated kinase 1/2 pathway, resulting in cell cycle arrest in cancer cells ([24], Fig. 2A).

Second, chemokines can impair metastasis. For example, the CCL28-CCR10 axis increases the expression of E-cadherin in oral squamous cell carcinoma, favouring cell-to-cell adhesion and reducing epithelial-mesenchymal transition (EMT) [25]. Interestingly, CCL28 and CXCL2 are downregulated in the tumour microenvironment compared with healthy tissues, suggesting that there is an escape mechanism from cancer cells [8,9]. Epigenetic processes could be involved in such escape, as suggested by a recent article showing that the CXCL2 gene is over methylated in HCC cell lines [26].

1.2.3. Chemokines can also favour the tumour immunosuppressive microenvironment

Cancer cells can secrete diverse molecules which impact the tumour tissue microenvironment and counteract the antitumour immune response. Chemokines can participate to this immunosuppression, either indirectly by recruiting and promoting the proliferation of regulatory T cells (Tregs) or directly by impairing the function of cytotoxic T cells (Fig. 2B).

Chemokines can recruit Tregs that inhibit the antitumour effect of cytotoxic T cells by producing anti-inflammatory cytokines such as interleukin 10 (IL-10) and tumour growth factor β (TGF-β). In HCC, histological studies suggest that CCL22 expressed by stromal cells attracts CCR4-expressing immunosuppressive Tregs [27]. The same phenomenon was observed in ovarian and breast cancers [28–30].

In a mouse model, CXCL4 produced by colon cancer cells have been shown to induce Tregs proliferation and to inhibit cytotoxic T-cell proliferation [31]. Moreover, CXCL4 can promote cytotoxic T-cell apoptosis [31]. These processes were not observed anymore in CXCR3−/− mice showing that CXCL4 favours tumour immunosuppressive microenvironment *via* CXCR3 [31]. In addition, the CXCL4-CXCR3 interaction has been shown to reduce the cytotoxic T-cell response and therefore allow for cancer spreading [31].

Chemokines can also manipulate the PD-1/PD-L1 axis. This mechanism will be detailed in The immune checkpoint–targeted therapy paradigm of this review. In brief, PD-1 expressed by T cells interacts with PDL-1 mainly expressed by antigen-presenting cells, leading to T-cell inactivation [4]. CXCL4 produced by cancer cells upregulates PD-1 expression on CXCR3+ cytotoxic T cells and downregulates it on CXCR3+ Tregs [31]. A bioinformatics study has shown that the interaction between the ligands CXCL9/10/11 and the CXCR3 receptor can upregulate PD-L1 expression in gastric cancer cells, *via* the STAT and phosphoinositide 3-kinase (PI3K)/AKT8 virus oncogene cellular homologue (Akt) pathways [32]. Therefore, CXCL9/10/11 *via* CXCR3 signalling may both favour the expression of PD-1 in cytotoxic T cells and PD-L1 in cancer cells, thereby hindering the anticancer immune response.

1.2.4. Chemokines can also directly support cancer cell growth

Growing evidence shows that chemokines can directly bind cancer cells and increase their proliferation. CXCR5 is expressed by different types of cancer cells and its activation by CXCL13 can lead to cancer cell proliferation ([15], Fig. 2B). The downstream pathways comprise PI3K/Akt and extracellular signal-regulated kinase in prostate and clear cell renal cell carcinoma (RCC). Interestingly, in non–small-cell lung cancer (NSCLC), T cells with high PD-1 expression secrete more CXCL13 [15,33]. Therefore, the induction of PD-1 in T cells by cancer cells [31] can not only favour tumour survival but also promote its growth.

1.2.5. Chemokines can support tumour angiogenesis and lymphangiogenesis

The formation of blood (angiogenesis) and lymph vessels (lymphangiogenesis) is crucial for cancer metastasis. Tumour cells are known to produce vascular endothelial growth factors (VEGFs) to promote angiogenesis and/or lymphangiogenesis (Fig. 2C). *In vitro* stimulation of osteosarcoma cells with CCL3 has shown that CCL3 can induce VEGF-A expression [34]. In this work, VEGF-A production was highly reduced in presence of CCR5 antagonists or mAbs, showing that CCL3 activates VEGF-A production *via* CCR5 engagement. VEGF-A and CCL3/CCR5-mediated angiogenesis was also assessed in a mouse model using CCL3-shRNA that downregulates CCL3. CCL3 was overexpressed in osteosarcoma tumours; however, the type of cells expressing CCL3 was not investigated in this work.

CCR5 is also involved in lymphangiogenesis. Oral squamous cell carcinoma has been shown to preferentially spread metastasis *via* lymph vessels [35]. Using *in vitro* studies, these authors have demonstrated that the CCL4-CCR5 axis can activate the VEGF-C pathway. Interestingly, *in vivo*, nude mice grafted with cancer cells expressing CCL4-shRNA displayed less lymph vessels compared with the control without knockdown. Hence, the same receptor seemed to be involved in both angiogenesis and lymphangiogenesis depending on the type of ligand. Altogether, the CCR5-VEGF pathway might be an interesting therapeutic target to counter cancer metastasis.

1.2.6. Chemokines can favour cancer cells metastasis

To metastasise, cancer cells need to dissociate with the primary tumour to reach vessels, circulate and then stick again to an extracellular matrix to form new distant

tumours. Chemokines can play a role in all those steps (Fig. 2D). First, cancer cells can dissociate from the tumour during the EMT [15]. Matrix metalloproteases (MMPs) favour this process by degrading proteins of the extracellular matrix. In breast cancer cells expressing CXCR5, CXCL13 induces the expression of mesenchymal markers such as N-cadherin and MMP9 and downregulates epithelial markers such as E-cadherin [15]. Two main oncogenic pathways seem to be involved in the cancer chemokine expression: the Rous sarcoma oncogene cellular homologue (Src) kinase family and the PI3K/Akt pathway [36,37]. Indeed, human prostate cancer cells expressing CXCR1 and 2 have been shown to present enhanced migration and downregulation of E-cadherin upon CXCL1 stimulation [36]. Analysis of the phosphorylation state of members of the Src pathway demonstrated that this pathway was upregulated in that process. Moreover, the migration of cancer cells was abolished upon their exposure to an inhibitor of the Src pathway. These results suggest that the binding of CXCL1 to its receptors CXCR1 and 2 could lead to the activation of the Src pathway and then engage cancer cells to an EMT. Another study using similar methods in tongue squamous cell carcinoma demonstrated that the CXCL9-CXCR3 axis was associated to the promotion of EMT *via* the Akt pathway stimulation [37]. It remains unknown if both CXCR5 and CXCR3 pathways are activated simultaneously by chemokines or if they are independent ways of triggering an EMT.

After EMT, cancer cells can spread throughout the organism using vasculature and can eventually form metastases. We have previously shown that chemokines can favour metastasis by promoting the formation of blood or lymph vessels [34,35]. Once in the vasculature, chemokine gradients may guide cancer cells to the tissues where they preferentially metastasise. For instance, in human breast cancers, the lung and brain are the most frequent sites for metastases. Interestingly, breast cancer cells injected intravenously in a mouse model formed spontaneously tumours in the mammary glands, the organs where CCL8 was the most abundant [38]. When the experiment was performed with neutralising antibodies against CCL8, less breast tumours were formed. The same tendency was observed in the lung [38].

1.3. Chemokines as biomarkers for the efficacy of the immune checkpoint blockade therapy

1.3.1. The immune checkpoint–targeted therapy paradigm

Immune checkpoint blockade therapy consists in using intravenous administrations of antagonistic mAbs against PD-1 (αPD-1), PD-L1 (αPD-L1) or CTLA-4 (αCTLA-4) to block the corresponding coinhibitory signalling to the T-cell receptor (Fig. 3). αPD-1 and αPD-L1 mAbs prevent the PD-1/PD-L1 interaction and allow for reactivation of the T-cell–mediated antitumour response [39]. Two non-mutually exclusive hypotheses would explain the efficacy/toxicity profile of αCTLA-4 mAbs. One classical and historical mechanism of action relies on the ability of αCTLA-4 mAbs to prevent the interaction of CTLA-

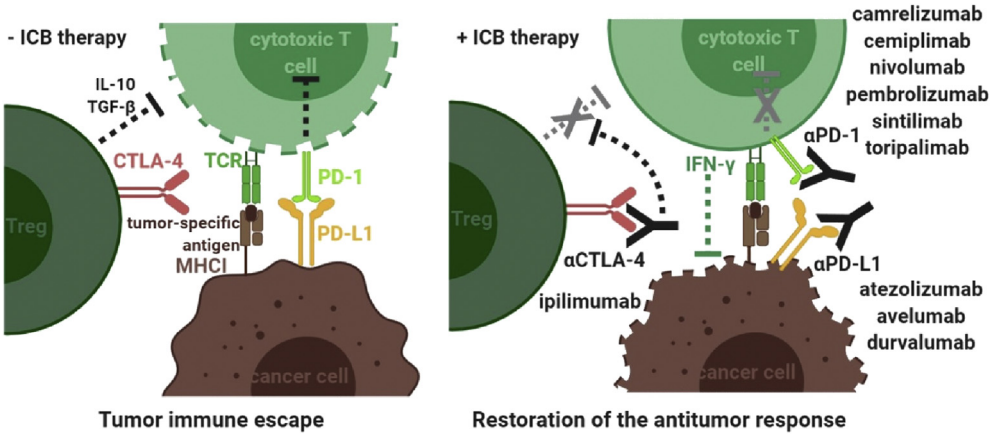

Fig. 3. **Immune checkpoint–targeted antibodies reactivate the immune response within the tumour microenvironment.** The T-cell receptor (TCR) of tumour-specific cytotoxic T cells recognises the antigen presented on the major histocompatibility complex I (MHC I) of cancer cells. The tumour microenvironment is immunosuppressive. Tregs produce cytokines such as IL-10 and TGF-β that inhibit cytotoxic T-cell activation, and cancer cells overexpress PD-L1 that binds to PD-1 exposed at the cytotoxic T-cell membrane. This interaction leads to the inactivation of the latter. Immune checkpoint blockade therapy using αPD-1 or αPD-L1 antibodies prevent PD-1/PD-L1 interaction and restore cytotoxic T-cell function. αCTLA-4 antibodies can either promote T-cell proliferation within the lymph nodes (not shown on this figure) or directly deplete tumour-specific Tregs. αPD-L1: antibody against PD-L1, αCTLA-4: antibody against CTLA-4, αPD-1: antibody against PD-1, CTLA-4: cytotoxic T-lymphocyte–associated protein 4, ICB: immune checkpoint blockade, MHCI: major histocompatibility complex 1, PD-1: programmed cell death 1, PD-L1: programmed cell death ligand 1, TCR: T-cell receptor, Treg: regulator T cell, TGF-β: tumour growth factor β, IL-10: interleukin 10.

Table 2
Critical chemokines in immune checkpoint blockade therapy.

Chemokine	Assay	Material	Therapy	Outcome	Reference
CCL4	Gene expression	Tumour	Ipilimumab (αCTLA-4)	Higher at baseline in responders	[54]
CCL5	Gene expression	Tumour	Ipilimumab (αCTLA-4)	Higher at baseline in responders	[54]
			Pembrolizumab (αPD-1)		[55]
CXCL5	Protein assay	Serum	Nivolumab (αPD-1)	Higher absolute increase in patients who developed adverse events upon treatment	[66]
CXCL9	Gene expression	Tumour	Atezolizumab (αPD-L1)	Higher at baseline in responders	[51]
			Durvalumab (αPD-L1)		[56]
			Ipilimumab (αCTLA-4)		[54]
			Pembrolizumab (αPD-1)		[55]
	Protein assay	Plasma	Pembrolizumab (αPD-1)	Increase in all patients upon treatment	[52]
		Serum	Nivolumab (αPD-1)	Decrease in all patients upon treatment	[53]
CXCL10	Gene expression	Tumour	Ipilimumab (αCTLA-4)	Higher at baseline in responders	[54]
			Pembrolizumab (αPD-1)		[55]
	Protein assay	Serum	Nivolumab (αPD-1)	Decrease in all patients upon treatment	[53]
CXCL11	Gene expression	Tumour	Ipilimumab (αCTLA-4)	Higher at baseline in responders	[54]
			Pembrolizumab (αPD-1)		[55]
	Gene expression	Tumour	Ipilimumab (αCTLA-4)	Higher increase in responders upon treatment	[54]
	Protein assay	Plasma	Atezolizumab (αPD-L1)	Increase in all patients upon treatment	[51]
CXCL13	Gene expression	Tumour	Ipilimumab (αCTLA-4) + nivolumab (αPD-1)	Increase in all patients upon treatment	[59]
			Pembrolizumab (αPD-1)	Higher in responders	[60]
CX3CL1	Gene expression	Tumour	Atezolizumab (αPD-L1)	Higher at baseline in non-responders	[51]
CCR5	Gene expression	Tumour	Pembrolizumab (αPD-1)	Higher at baseline in responders	[55]
CXCR5	IHC	Tumour	Pembrolizumab (αPD-1)	Higher in responders	[60]
			Ipilimumab (αCTLA-4)		[61]
CXCR6	Gene expression	Tumour	Pembrolizumab (αPD-1)	Higher at baseline in responders	[55]
				Higher at baseline in non-responders	[63]

The gene and protein expression of chemokine ligands and receptors have been associated with the effect of the immune checkpoint blockade therapy, dependently or independently of the clinical response. IHC: immunohistochemistry, αCTLA-4: antibody against CTLA-4, αPD-1: antibody against PD-1, αPD-L1: antibody against PD-L1.

4 with CD80 and CD86 [40]. The second mechanism relies on the ability of such antibody-derived cell cytotoxicity (ADCC) competent mAbs to deplete CTLA-4–positive cells, that is, mainly Tregs (mouse and humans αCTLA-4 are ADCC competent and therefore not purely antagonistic) [41–47]. However, this second mechanism of action remains currently controversial [48–50].

1.3.2. Chemokines as pharmacodynamic vs predictive markers of efficacy

Pharmacodynamic (PD) markers are molecules or cells whose presence/expression/concentration is correlated with the bioactivity of a drug and its mechanism of action but independently from the question of its clinical efficacy. They provide information on the drug's bioavailability in tissues and on the target engagement of the drug.

A higher level of baseline *Cxcl9* gene expression prior treatment by atezolizumab (initially called MPDL3280A, an Fc-silent IgG1 αPD-L1 mAb) has been associated to objective tumour responses in multiple tumour types including NSCLC, RCC and melanoma ([51], Table 2). However, the circulating levels of CXCL9 (aka MIG) and CXCL10 (aka IP10) proteins in the blood seem to increase [52] or decrease [53] eventually in all patients upon αPD-1 therapy independently from the tumour response. This would suggest that changes in CXCL9 and CXCL10 levels upon treatment might behave as a good PD marker for αPD-1 therapy, but the higher absolute values at baseline would be associated to a higher chance of αPDL-1 efficacy in patients with cancer.

Indeed, responders have been associated with a high expression of CXCR3 ligands in the tumour before immunotherapy, before αCTLA-4 [54], αPD-1 [55] and αPD-L1 [56] treatment. High levels of CXCL9 in tumours before αPD-L1 treatment were associated with response in melanoma and RCC but not in NSCLC [51]. In addition, in metastatic melanoma, responders displayed higher gene expression of CCL5, CCR5, CXCR6 and CXCL9/10/11 before αPD-1 treatment [55]. The predictive power of this set of genes for diagnosis was assessed in an independent cohort of metastatic melanoma, as well as head and neck squamous cell carcinoma, and gastric cancer. Along with other immune genes, this set was sufficient to discriminate between responders and non-responders, suggesting that mechanisms of response following αPD-1 are shared among different types of cancer.

An immune-active tumour microenvironment may enhance the effect of immune checkpoint inhibitors,

likely *via* T-helper type 1 cells [54]. CXCR3 and its ligands have long been thought to enhance immunotherapy efficacy by recruiting T cells at the tumour site. However, a recent study in mice questions this dogma [57]. There were no differences in CD8+ T-cell populations within tumours between wild-type and *Cxcr3*−/− mice before αPD-1 treatment. Intratumoural CD8+ T-cell populations of wild-type mice expanded after treatment, whereas those of *Cxcr3*−/− mice did not change. Therefore, CXCR3 does not seem to be involved in the recruitment of CD8+ T cells to the tumour site in the context of αPD-1 treatment but rather favours their proliferation within the tumour.

These chemokines have been shown to be produced by myeloid cells within tumour tissues in a neuroblastoma mice model [58]. CXCL9, 10 and 11 guide T cells expressing CXCR3 to the tumour site ([12,58], Fig. 2A), and those results are consistent with the observed increased T-cell infiltration after treatment.

In addition, increase. in CXCL11 (also called ITAC or IP-9) has been seen upon αPD-L1 therapy but did not track significantly with response or progression ([51], Fig. 4)

Most chemokine studies have been initially performed on melanoma, NSCLC and RCC, and it is possible that the response to αPD(L)-1 therapy might vary with the cancer histology. Indeed, a trial of pembrolizumab in HCC did not find any correlation between baseline circulating CXCL9, CCL4 and CCL5 between responders and non-responders, but the baseline levels of TGF-β were significantly associated to disease progression on treatment [52].

Intratumoural levels of chemokine proteins have also been associated with clinical responses. In NSCLC, intratumoural CD8+ T cells expressing high levels of PD-1 constitutively secrete CXCL13 [33]. A chemotaxis assay showed that CXCR5+ cells and especially CD4+ T cells migrate through a CXCL13 gradient, suggesting that CXCL13 mediates the recruitment of immune cells to the tumour microenvironment. Because CD8+ T cells with high PD-1 expression are associated with good prognosis for αPD-1 therapy, CXCL13 could behave as a biomarker for responders as well (Fig. 5).

A recent study by Chalabi *et al.* [59] testing the neoadjuvant combination of nivolumab (αPD-1) and ipilimumab (αCTLA-4) in mismatch repair deficient (dMMR) or mismatch repair proficient (pMMR) colon cancers showed that CXCL13 gene expression was upregulated upon treatment by both dMMR and pMMR tumours but at a much higher level in dMMR (2–3 fold higher) and increased at the same level of magnitude in responding vs non-responding patients. This would suggest that the increase of CXCL13 gene expression behaves as a PD marker of the PD-1/CTLA-4 blockade and not as a biomarker of response. However, the baseline level of CXCL13 and CXCR5 gene and protein expression in tumours correlates with the

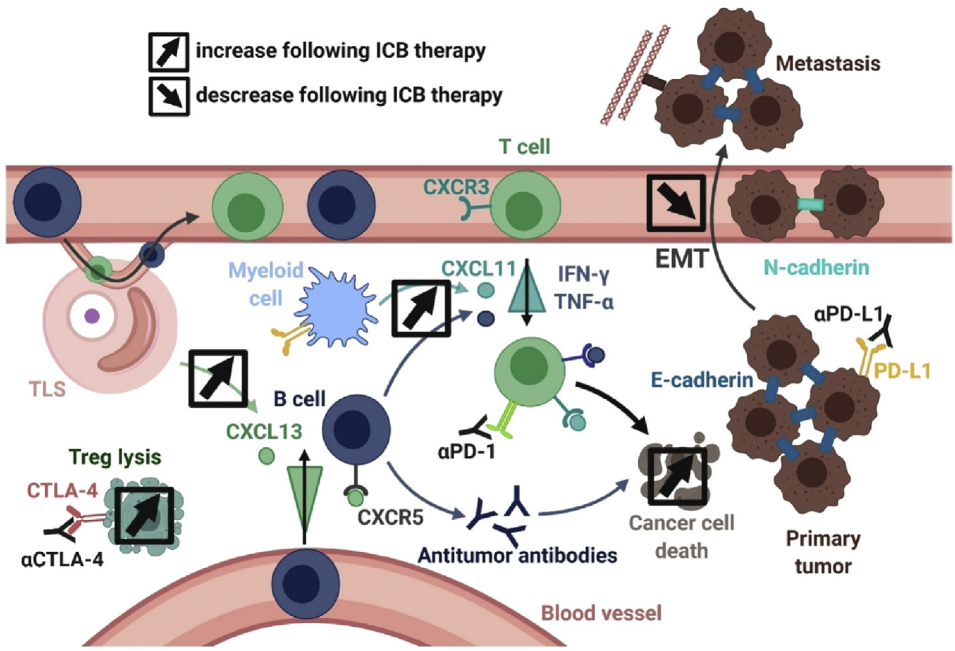

Fig. 4. **Expected effects of immune checkpoint inhibitors.** Within the tumour microenvironment, αPD-1 and αPD-L1 can reactivate cytotoxic T cells that kill cancer cells and thus reduce the number of cells doing EMT. αCTLA-4 depletes Tregs and thereby reduces immunosuppression. Besides, αPD-1 boosts the production of CXCL11 by myeloid cells and favours the recruitment of T cells to the tumour site, whereas αPD-1 and αCTLA-4 boost the production of CXCL13 by CD8+ T cells in the TLS and favour the recruitment of B cells. αCTLA-4: antibody against CTLA-4, αPD-1: antibody against PD-1, αPD-L1: antibody against PD-L1, CTLA-4: cytotoxic T-lymphocyte–associated protein 4, EMT: epithelial-mesenchymal transition, ICB: immune checkpoint blockade, PD-1: programmed cell death 1, PD-L1: programmed cell death ligand 1, TLS: tertiary lymphoid structure, Treg: regulator T cell.

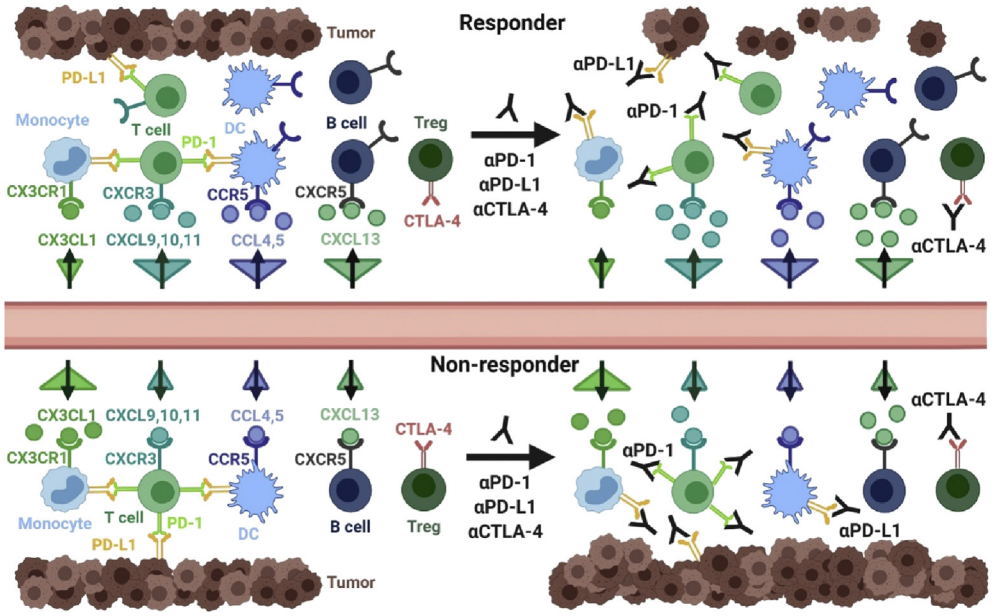

Fig. 5. **Impact of baseline chemokine gene expression on the efficacy of immune checkpoint blockade therapy.** The concentration of CCL4 and 5, CXCL9, 10, 11 and 13 before αPD(L)-1 and αCTLA-4 immunotherapy has been retrospectively shown to be higher in the tumour of responding patients. Moreover, CX3CL1 was more expressed in the tumour microenvironment of patients whose disease progressed and worsened after αPD-L1 therapy, whereas CCR5 and CXCR5 were more expressed in tumours from responders before αPD-1 and αCTLA-4 therapy. αCTLA-4: antibody against CTLA-4, αPD-1: antibody against PD-1, αPD-L1: antibody against PD-L1, CTLA-4: cytotoxic T-lymphocyte–associated protein 4, DC: dendritic cell, EMT: epithelial-mesenchymal transition, PD-1: programmed cell death 1, PD-L1: programmed cell death ligand 1, Treg: regulator T cell.

existence of TLSs and has been shown to correlate with a higher chance of response to αPD-1 in melanoma and sarcoma [10,60,61]. Interestingly, many genes included in the various TLS gene signature identified so far in the literature include predominantly chemokine genes, namely *Ccl19, Ccl21, Cxcl13, Ccr7* and *Cxcr5* [62]. More specifically, CXCL13 has been associated to a strong correlation with baseline TLS in sarcoma [60]. CXCL13 seems to be predominantly expressed by CD8+ T cells, whereas its receptor CXCR5 by B cells and CD4+ T cells (mostly T_{FH}) in the TLS [61]. An important chemokine that seems to be differentially expressed in tumour infiltrative B cells is CXCR3. An increased percentage of CXCR3+ switched memory B cells has been found in melanoma tumours responding to αPD-1 compared with non-responding tumours [10].

On the other hand, some chemokine patterns of expression seem to correlate with non-responders. High tumoural levels of CXCR6 [63] and CX3CL1 [51] before treatment are promising markers of resistance to αPD-1 and αPDL-1, respectively. Some articles have also demonstrated that CX3CL1 enhances the metastatic activity of CX3CR1-expressing cancer cells [64,65]; however, this role has never been investigated in patients after immunotherapy. Whether CX3CL1 hinders immunotherapy efficacy and how are yet to be shown because this chemokine is also known for its antitumour activity *via* the chemoattraction of immune cells [51].

Interestingly, the absolute increase in the serum level of CXCL5 upon nivolumab (αPD-1) treatment has been suggested to be associated to the occurrence of immune-related adverse events [66].

1.3.3. Chemokines associated with resistance to immune checkpoint blockade

Liver kinase B1 (LKB1) mutations and phosphatase and tensin homologue (PTEN) loss have been described as mutations of resistance to αPD(L)-1 therapies in NSCLC and melanoma [67–69]. In a mouse model, the dual loss of both *Lkb1* and *Pten* in tumours led to an activation of the AKT and mechanistic target of rapamycin (mTOR) pathways, pathways classically associated to cancer cell proliferation and tumourigenesis [70]. The co-deletion of these two genes in cancer cells was also associated with the upregulation of expression of specific chemokine genes in mouse tumours. Compared with Kras G12D mutated tumour cells, LKB1/PTEN double negative EpCAM+cell–sorted cancer cells expressed very high levels of the chemokines CXCL3 and CXCL5, high PD-L1 expression and the bronchoalveolar fluid contained elevated CXCL1, CXCL2, CXCL5 and CXCL7.

Immunotherapy using immune checkpoint–targeted antibodies can also lead to a paradoxical acceleration of the disease, an atypical pattern of progression known as hyperprogression [71]. Interestingly, a lower frequency of effector/memory T-cell subsets that are CCR7- and

CD45RA- among the total CD8+ T cells has been associated with hyperprogression and inferior survival rate than with classical progression in NSCLC [72]. This would suggest a potential role for the CCL19/21-CCR7 axis in CD8+ T cells to prevent that phenomenon.

1.3.4. Chemokines as therapeutic targets

So far, few strategies can be described to identify patients that are likely to respond to immune checkpoint blockade immunotherapy. It becomes increasingly clear that a better response is observed when immune checkpoint–targeted antibodies reactivate a pre-existing immunity [51,54]. High intratumoural gene levels or protein expressions of PD-1, PD-L1 and CTLA-4 have been associated to a better outcome for αPD-1 [33], αPD-L1 [51] and αCTLA-4 [73] therapy, respectively.

Some key chemokines appear to play an important role in the antitumour response and the sensitivity to immune checkpoint blockade therapy. Therefore, activators or inhibitors of chemokines could be envisioned as anticancer therapies. Clinical trials have shown promising antitumour effects. In a phase Ib study, 33 patients with metastatic breast cancer were treated three times a day with oral tablets containing 1200 mg of a CXCR1 and 2 antagonist ([74], NCT02001974). Grade III treatment-related adverse events were rare, and 29.6% of patients responded to the treatment. An anti-CXCR4 antibody was even more promising ([75], NCT01359657). Forty six patients with myeloma received 10 mg/kg/dose intravenously on a weekly basis and 72.4% had a clinical benefit. However, grade IV neutropenia was observed for 13 patients. Moreover, anti-CXCR4 therapy combined with chemotherapy led to a higher response rate with acceptable toxicity [75].

Chemokine antagonists might also synergise with immune checkpoint inhibitors to improve their efficacy. Only few clinical trials have combined chemokine antagonists with immunotherapy, with no blatant results. In a phase I/II study in pancreatic adenocarcinoma and small cell lung cancer, 41 patients received intravenously either 200 or 400 mg of an anti-CXCR4 every week in combination with 3 mg/kg of αPD-1 administered every two weeks. All participants presented adverse events, and the trial was terminated because of its inefficiency ([76], Identifier: NCT02472977). Results of the phase I/II study of an anti-CCR4 in hepatocellular carcinoma ([77], Identifier: NCT02705105) or an anti-CCR5 in colorectal cancer ([78], Identifier: NCT03274804) with αPD-1 are yet to be published.

2. Conclusion

Chemokines, similar to most cytokines, have a pleiotropic effect and therefore can be involved in both the anticancer immune response but also in the biology of tumour spreading, by favouring tumour growth, immunosuppression and metastasis. They are likely to be the effectors of the reactivation of the immune response after immune checkpoint blockade therapy. However, the expression of some chemokine receptors or the release of some chemokine ligands such as CXCL5 by cancer cells could be the source of some immune-related adverse events. The level of concentration of the chemokines CXCL9 and CXCL10 before treatment can be correlated with the clinical response according to retrospective studies. Identifying chemokines associated with responders for each immunotherapy may permit to choose the most beneficial treatment for a patient and to increase the survival rate.

Combining immunotherapy with chemotherapy, radiotherapy or chemokine antagonists may increase further the response rate by targeting different pathways and thereby countering cancer resistance. Besides, identifying immune profiles favourable to cancer could permit the diagnosis of cancer at early stages, perhaps before tumours become detectable, and lead to preventive treatments.

Conflict of interest statement

The funding of research on chemokines in the laboratory of A.M. is partly funded by academic grants from Boehringer Ingelheim, Fondation MSD Avenir and CIC BT Inserm 1428. The other authors declare no conflicts of interest.

Acknowledgements

All figures were created with BioRender.com. The authors would like to deeply thank Dr. Déborah PREVOT (École Normale Supérieure de Lyon) for her critical review of the manuscript.

References

[1] IARC – International Agency for Research on Cancer, https://www.iarc.fr/, Accessed December 2, 2019.
[2] Galluzzi L, Vacchelli E, Pedro J-MB-S, Buqué A, Senovilla L, Baracco EE, et al. Classification of current anticancer immunotherapies. Oncotarget 2014;5:12472–508.
[3] Raman D, Baugher PJ, Thu YM, Richmond A. Role OF chemokines IN tumor growth. Canc Lett 2007;256:137–65.
[4] Akinleye A, Rasool Z. Immune checkpoint inhibitors of PD-L1 as cancer therapeutics. J Hematol Oncol 2019;12:92.
[5] Kudo M. Immuno-oncology in hepatocellular carcinoma: 2017 update. OCL 2017;93:147–59.
[6] Larkin J, Chiarion-Sileni V, Gonzalez R, Grob J-J, Rutkowski P, Lao CD, et al. Five-year survival with combined nivolumab and ipilimumab in advanced melanoma. N Engl J Med 2019;381:1535–46.
[7] Overman MJ, Lonardi S, Wong KYM, Lenz H-J, Gelsomino F, Aglietta M, et al. Durable clinical benefit with nivolumab plus ipilimumab in DNA mismatch repair–deficient/microsatellite instability–high metastatic colorectal cancer. J Clin Orthod 2018;36:773–9.
[8] Borcoman E, Nandikolla A, Long G, Goel S, Le Tourneau C. Patterns of response and progression to immunotherapy.

American Society of Clinical Oncology Educational Book; 2018. https://doi.org/10.1200/EDBK_200643.
[9] Fridman WH, Pagès F, Sautès-Fridman C, Galon J. The immune contexture in human tumours: impact on clinical outcome. Nat Rev Canc 2012;12:298–306.
[10] Helmink BA, Reddy SM, Gao J, Zhang S, Basar R, Thakur R, et al. B cells and tertiary lymphoid structures promote immunotherapy response. Nature 2020;577:549–55.
[11] Liu Y, Cai Y, Liu L, Wu Y, Xiong X. Crucial biological functions of CCL7 in cancer. PeerJ 2018;6.
[12] IUPHAR/BPS Guide to Pharmacology, https://guidetopharmacology.org/, Accessed November 11, 2019.
[13] Rodríguez-Frade JM, Vila-Coro AJ, Martín de Ana A, Albar JP, Martínez -AC, Mellado M. The chemokine monocyte chemoattractant protein-1 induces functional responses through dimerization of its receptor CCR2. Proc Natl Acad Sci U S A 1999;96:3628–33.
[14] Mellado M, Rodríguez-Frade JM, Vila-Coro AJ, Fernández S, Martín de Ana A, Jones DR, et al. Chemokine receptor homo- or heterodimerization activates distinct signaling pathways. EMBO J 2001;20:2497–507.
[15] Kazanietz MG, Durando M, Cooke M. CXCL13 and its receptor CXCR5 in cancer: inflammation, immune response, and beyond. Front Endocrinol 2019:10.
[16] Balkwill F. Cancer and the chemokine network. Nat Rev Canc 2004;4:540–50.
[17] Hughes CE, Nibbs RJB. A guide to chemokines and their receptors. FEBS J 2018;285:2944–71.
[18] Jacquelot N, Enot DP, Flament C, Vimond N, Blattner C, Pitt JM, et al. Chemokine receptor patterns in lymphocytes mirror metastatic spreading in melanoma. J Clin Invest 2016;126:921–37.
[19] Watts AO, Lipzig M van, Jaeger WC, Seeber RM, Zwam M van, Vinet J, et al. Identification and profiling of CXCR3–CXCR4 chemokine receptor heteromer complexes. Br J Pharmacol 2013;168:1662–74.
[20] Bronger H, Singer J, Windmüller C, Reuning U, Zech D, Delbridge C, et al. CXCL9 and CXCL10 predict survival and are regulated by cyclooxygenase inhibition in advanced serous ovarian cancer. Br J Canc 2016;115:553–63.
[21] Gonzalez H, Hagerling C, Werb Z. Roles of the immune system in cancer: from tumor initiation to metastatic progression. Genes Dev 2018;32:1267–84.
[22] Sautès-Fridman C, Petitprez F, Calderaro J, Fridman WH. Tertiary lymphoid structures in the era of cancer immunotherapy. Nat Rev Canc 2019;19:307–25.
[23] Zhu M, Xu W, Wei C, Huang J, Xu J, Zhang Y, et al. CCL14 serves as a novel prognostic factor and tumor suppressor of HCC by modulating cell cycle and promoting apoptosis. Cell Death Dis 2019;10.
[24] Ding J, Xu K, Zhang J, Lin B, Wang Y, Yin S, et al. Overexpression of CXCL2 inhibits cell proliferation and promotes apoptosis in hepatocellular carcinoma. BMB Rep 2018;51:630–5.
[25] Park J, Zhang X, Lee SK, Song N-Y, Son SH, Kim KR, et al. CCL28-induced RARβ expression inhibits oral squamous cell carcinoma bone invasion. J Clin Invest 2019;129.
[26] Subat S, Mogushi K, Yasen M, Kohda T, Ishikawa Y, Tanaka H. Identification of genes and pathways, including the CXCL2 axis, altered by DNA methylation in hepatocellular carcinoma. J Canc Res Clin Oncol 2019;145:675–84.
[27] Wiedemann GM, Röhrle N, Makeschin M-C, Fesseler J, Endres S, Mayr D, et al. Peritumoural CCL1 and CCL22 expressing cells in hepatocellular carcinomas shape the tumour immune infiltrate. Pathology 2019;51:586–92.
[28] Curiel TJ, Coukos G, Zou L, Alvarez X, Cheng P, Mottram P, et al. Specific recruitment of regulatory T cells in ovarian carcinoma fosters immune privilege and predicts reduced survival. Nat Med 2004;10:942–9.
[29] Gobert M, Treilleux I, Bendriss-Vermare N, Bachelot T, Goddard-Leon S, Arfi V, et al. Regulatory T cells recruited through CCL22/CCR4 are selectively activated in lymphoid infiltrates surrounding primary breast tumors and lead to an adverse clinical outcome. Cancer Res 2009;69:2000–9.
[30] Faget J, Biota C, Bachelot T, Gobert M, Treilleux I, Goutagny N, et al. Early detection of tumor cells by innate immune cells leads to Treg recruitment through CCL22 production by tumor cells. Cancer Res 2011;71:6143–52.
[31] Deng S, Deng Q, Zhang Y, Ye H, Yu X, Zhang Y, et al. Non-platelet-derived CXCL4 differentially regulates cytotoxic and regulatory T cells through CXCR3 to suppress the immune response to colon cancer. Canc Lett 2019;443:1–12.
[32] Zhang C, Li Z, Xu L, Che X, Wen T, Fan Y, et al. CXCL9/10/11, a regulator of PD-L1 expression in gastric cancer. BMC Canc 2018;18.
[33] Thommen DS, Koelzer VH, Herzig P, Roller A, Trefny M, Dimeloe S, et al. A transcriptionally and functionally distinct PD-1 + CD8 + T cell pool with predictive potential in non-small-cell lung cancer treated with PD-1 blockade. Nat Med 2018;24:994–1004.
[34] Liao Y-Y, Tsai H-C, Chou P-Y, Wang S-W, Chen H-T, Lin Y-M, et al. CCL3 promotes angiogenesis by dysregulation of miR-374b/VEGF-A axis in human osteosarcoma cells. Oncotarget 2015;7:4310–25.
[35] Lien M-Y, Tsai H-C, Chang A-C, Tsai M-H, Hua C-H, Wang S-W, et al. Chemokine CCL4 induces vascular endothelial growth factor C expression and lymphangiogenesis by miR-195-3p in oral squamous cell carcinoma. Front Immunol 2018;9.
[36] Lu Y, Dong B, Xu F, Xu Y, Pan J, Song J, et al. CXCL1-LCN2 paracrine axis promotes progression of prostate cancer via the Src activation and epithelial-mesenchymal transition. Cell Commun Signal 2019;17.
[37] Li Z, Liu J, Li L, Shao S, Wu J, Bian L, et al. Epithelial mesenchymal transition induced by the CXCL9/CXCR3 axis through AKT activation promotes invasion and metastasis in tongue squamous cell carcinoma. Oncol Rep 2018;39:1356–68.
[38] Farmaki E, Chatzistamou I, Kaza V, Kiaris H. A CCL8 gradient drives breast cancer cell dissemination. Oncogene 2016;35:6309–18.
[39] Sharma P, Allison JP. Immune checkpoint targeting in cancer therapy: towards combination strategies with curative potential. Cell 2015;161:205–14.
[40] Sharma P, Allison JP. The future of immune checkpoint therapy. Science 2015;348:56–61.
[41] Marabelle A, Kohrt H, Levy R. New insights into the mechanism of action of immune checkpoint antibodies. OncoImmunology 2014;3.
[42] Vargas FA, Furness AJS, Litchfield K, Joshi K, Rosenthal R, Ghorani E, et al. Fc effector function contributes to the activity of human anti-CTLA-4 antibodies. Canc Cell 2018;33:649–663.e4.
[43] Romano E, Kusio-Kobialka M, Foukas PG, Baumgaertner P, Meyer C, Ballabeni P, et al. Ipilimumab-dependent cell-mediated cytotoxicity of regulatory T cells ex vivo by nonclassical monocytes in melanoma patients. Proc Natl Acad Sci U S A 2015;112:6140–5.
[44] Marabelle A, Kohrt H, Sagiv-Barfi I, Ajami B, Axtell RC, Zhou G, et al. Depleting tumor-specific Tregs at a single site eradicates disseminated tumors. J Clin Invest 2013;123:2447–63.
[45] Simpson TR, Li F, Montalvo-Ortiz W, Sepulveda MA, Bergerhoff K, Arce F, et al. Fc-dependent depletion of tumor-infiltrating regulatory T cells co-defines the efficacy of anti–CTLA-4 therapy against melanoma. J Exp Med 2013;210:1695–710.
[46] Selby MJ, Engelhardt JJ, Quigley M, Henning KA, Chen T, Srinivasan M, et al. Anti-CTLA-4 antibodies of IgG2a isotype enhance antitumor activity through reduction of intratumoral regulatory T cells. Cancer Immunol Res 2013;1:32–42.

[47] Quezada SA, Peggs KS, Simpson TR, Shen Y, Littman DR, Allison JP. Limited tumor infiltration by activated T effector cells restricts the therapeutic activity of regulatory T cell depletion against established melanoma. J Exp Med 2008;205:2125–38.
[48] Quezada SA, Peggs KS. Lost in translation: deciphering the mechanism of action of anti-human CTLA-4. Clin Canc Res 2019;25:1130–2.
[49] Sharma A, Subudhi SK, Blando J, Scutti J, Vence L, Wargo J, et al. Anti–CTLA-4 immunotherapy does not deplete FOXP3+ regulatory T cells (Tregs) in human cancers. Clin Canc Res 2019; 25:1233–8.
[50] Ferrara R, Susini S, Marabelle A. Anti-CTLA-4 immunotherapy does not deplete FOXP3+ regulatory T cells (Tregs) in human cancers-Letter. Clin Canc Res 2018. https://doi.org/10.1158/1078-0432.CCR-18-3740.
[51] Herbst RS, Soria J-C, Kowanetz M, Fine GD, Hamid O, Gordon MS, et al. Predictive correlates of response to the anti-PD-L1 antibody MPDL3280A in cancer patients. Nature 2014; 515:563–7.
[52] Feun LG, Li Y-Y, Wu C, Wangpaichitr M, Jones PD, Richman SP, et al. Phase 2 study of pembrolizumab and circulating biomarkers to predict anticancer response in advanced, unresectable hepatocellular carcinoma. Cancer 2019;125: 3603–14.
[53] Yamazaki N, Kiyohara Y, Uhara H, Iizuka H, Uehara J, Otsuka F, et al. Cytokine biomarkers to predict antitumor responses to nivolumab suggested in a phase 2 study for advanced melanoma. Canc Sci 2017;108:1022–31.
[54] Ji R-R, Chasalow SD, Wang L, Hamid O, Schmidt H, Cogswell J, et al. An immune-active tumor microenvironment favors clinical response to ipilimumab. Cancer Immunol Immunother 2012;61: 1019–31.
[55] Ayers M, Lunceford J, Nebozhyn M, Murphy E, Loboda A, Kaufman DR, et al. IFN-γ–related mRNA profile predicts clinical response to PD-1 blockade. J Clin Invest 2017;127: 2930–40.
[56] Higgs BW, Morehouse CA, Streicher K, Brohawn PZ, Pilataxi F, Gupta A, et al. Interferon gamma messenger RNA signature in tumor biopsies predicts outcomes in patients with non–small cell lung carcinoma or urothelial cancer treated with durvalumab. Clin Canc Res 2018;24:3857–66.
[57] Chow MT, Ozga AJ, Servis RL, Frederick DT, Lo JA, Fisher DE, et al. Intratumoral activity of the CXCR3 chemokine system is required for the efficacy of anti-PD-1 therapy. Immunity 2019;50: 1498–512. e5.
[58] Eissler N, Mao Y, Brodin D, Reuterswärd P, Andersson Svahn H, Johnsen JI, et al. Regulation of myeloid cells by activated T cells determines the efficacy of PD-1 blockade. OncoImmunology 2016;5.
[59] Chalabi M, Fanchi LF, Dijkstra KK, Van den Berg JG, Aalbers AG, Sikorska K, et al. Neoadjuvant immunotherapy leads to pathological responses in MMR-proficient and MMR-deficient early-stage colon cancers. Nat Med 2020;26:566–76.
[60] Petitprez F, de Reyniès A, Keung EZ, Chen TW-W, Sun C-M, Calderaro J, et al. B cells are associated with survival and immunotherapy response in sarcoma. Nature 2020;577: 556–60.
[61] Cabrita R, Lauss M, Sanna A, Donia M, Skaarup Larsen M, Mitra S, et al. Tertiary lymphoid structures improve immunotherapy and survival in melanoma. Nature 2020;577:561–5.
[62] Dieu-Nosjean M-C, Goc J, Giraldo NA, Sautès-Fridman C, Fridman WH. Tertiary lymphoid structures in cancer and beyond. Trends Immunol 2014;35:571–80.
[63] Manasanch EE, Han G, Mathur R, Qing Y, Zhang Z, Lee H, et al. A pilot study of pembrolizumab in smoldering myeloma: report of the clinical, immune, and genomic analysis. Blood Adv 2019;3:2400–8.
[64] Tardáguila M, Mañes S. CX3CL1 at the crossroad of EGF signals. OncoImmunology 2013;2.
[65] Andre F, Cabioglu N, Assi H, Sabourin JC, Delaloge S, Sahin A, et al. Expression of chemokine receptors predicts the site of metastatic relapse in patients with axillary node positive primary breast cancer. Ann Oncol 2006;17:945–51.
[66] Fujimura T, Sato Y, Tanita K, Kambayashi Y, Otsuka A, Fujisawa Y, et al. Serum levels of soluble CD163 and CXCL5 may be predictive markers for immune-related adverse events in patients with advanced melanoma treated with nivolumab: a pilot study. Oncotarget 2018;9:15542–51.
[67] Skoulidis F, Goldberg ME, Greenawalt DM, Hellmann MD, Awad MM, Gainor JF, et al. STK11/LKB1 mutations and PD-1 inhibitor resistance in KRAS-mutant lung adenocarcinoma. Canc Discov 2018;8:822–35.
[68] Parsa AT, Waldron JS, Panner A, Crane CA, Parney IF, Barry JJ, et al. Loss of tumor suppressor PTEN function increases B7-H1 expression and immunoresistance in glioma. Nat Med 2007;13: 84–8.
[69] George S, Miao D, Demetri GD, Adeegbe D, Rodig SJ, Shukla S, et al. Loss of PTEN is associated with resistance to anti-PD-1 checkpoint blockade therapy in metastatic uterine leiomyosarcoma. Immunity 2017;46:197–204.
[70] Xu C, Fillmore CM, Koyama S, Wu H, Zhao Y, Chen Z, et al. Loss of Lkb1 and pten leads to lung squamous cell carcinoma with elevated PD-L1 expression. Canc Cell 2014;25:590–604.
[71] Champiat S, Dercle L, Ammari S, Massard C, Hollebecque A, Postel-Vinay S, et al. Hyperprogressive disease is a new pattern of progression in cancer patients treated by anti-PD-1/PD-L1. Clin Canc Res 2017;23:1920–8.
[72] Kim CG, Kim KH, Pyo K-H, Xin C-F, Hong MH, Ahn B-C, et al. Hyperprogressive disease during PD-1/PD-L1 blockade in patients with non-small-cell lung cancer. Ann Oncol 2019;30: 1104–13.
[73] Boussiotis VA. Somatic mutations and immunotherapy outcome with CTLA-4 blockade in melanoma. N Engl J Med 2014;371: 2230–2.
[74] Schott AF, Goldstein LJ, Cristofanilli M, Ruffini PA, McCanna S, Reuben JM, et al. Phase Ib pilot study to evaluate reparixin in combination with weekly paclitaxel in patients with HER-2 negative metastatic breast cancer (MBC). Clin Canc Res 2017;23:5358–65.
[75] Ghobrial IM, Liu C-J, Redd RA, Perez RP, Baz R, Zavidij O, et al. A phase Ib/II trial of the first-in-class Anti-CXCR4 antibody ulocuplumab in combination with lenalidomide or bortezomib plus dexamethasone in relapsed multiple myeloma. Clin Canc Res 2019. https://doi.org/10.1158/1078-0432.CCR-19-0647.
[76] Safety and efficacy study of ulocuplumab and nivolumab in subjects with solid tumors - ClinicalTrials.gov, Identifier: NCT02472977.
[77] Study of mogamulizumab + nivolumab in subjects w/locally advanced or metastatic solid tumors - ClinicalTrials.gov, Identifier: NCT02705105.
[78] Combined PD-1 and CCR5 inhibition for the treatment of refractory microsatellite stable mCRC - ClinicalTrials.gov, Identifier: NCT03274804.

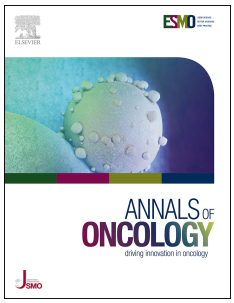

Plasma proteomics identifies Leukemia Inhibitory Factor (LIF) as a novel predictive biomarker of immune-checkpoint blockade resistance

Y. Loriot, A. Marabelle, J.P. Guégan, F.X. Danlos, B. Besse, N. Chaput, C. Massard, D. Planchard, C. Robert, C. Even, M. Khettab, L. Tselika, L. Friboulet, F. André, I. Nafia, F. Le Loarer, J.C. Soria, A. Bessede, A. Italiano

PII: S0923-7534(21)03978-8

DOI: https://doi.org/10.1016/j.annonc.2021.08.1748

Reference: ANNONC 722

To appear in: *Annals of Oncology*

Received Date: 8 June 2021

Revised Date: 23 July 2021

Accepted Date: 6 August 2021

Please cite this article as: Loriot Y, Marabelle A, Guégan J, Danlos F, Besse B, Chaput N, Massard C, Planchard D, Robert C, Even C, Khettab M, Tselika L, Friboulet L, André F, Nafia I, Le Loarer F, Soria J, Bessede A, Italiano A, Plasma proteomics identifies Leukemia Inhibitory Factor (LIF) as a novel predictive biomarker of immune-checkpoint blockade resistance, *Annals of Oncology* (2021), doi: https://doi.org/10.1016/j.annonc.2021.08.1748.

ORIGINAL ARTICLE

Plasma proteomics identifies Leukemia Inhibitory Factor (LIF) as a novel predictive biomarker of immune-checkpoint blockade resistance

Y. Loriot[1*]; A. Marabelle[2*]; JP. Guégan[3] ; FX. Danlos[2] ; B. Besse[1,4] ; N. Chaput[5,6,7] ; C. Massard[2] ; D. Planchard[1] ; C. Robert[1] ; C. Even[1] ; M. Khettab[1] ; L. Tselika[8] ; L. Friboulet[9] ; F. André[14] ; I. Nafia[3] ; F. Le Loarer[10,11] ; JC Soria[1] ; A. Bessede[3¥] ; A. Italiano[¥2,11,12].

**Y.L. and A.M. contributed equally to this work*

[¥]*A.B. and A.I. contributed equally to this work*

1 Cancer Medicine Department, INSERM U981, Gustave Roussy, Université Paris-Saclay, F-94800 Villejuif, France.
2 Département d'Innovation Précoce et d'Essais Thérapeutiques (DITEP), INSERM U1015 & CIC1428, Université Paris Saclay, Gustave Roussy, Villejuif, France
3 Explicyte, 229 cours de l'Argonne, 33000 Bordeaux, France
4 Faculty of Medicine, University Paris-Saclay, F-94276 Le Kremlin Bicêtre, France.
5 Laboratory of Immunomonitoring in Oncology, Gustave Roussy Cancer Campus, CNRS-UMS 3655 and INSERM-US23, F-94805 Villejuif, France.
6 Faculty of Pharmacy, University Paris-Saclay, F-92296 Chatenay-Malabry, France.
7 Laboratory of Genetic Instability and Oncogenesis, UMR CNRS 8200, Gustave Roussy, Université Paris-Saclay, F-94805 Villejuif, France.
8 Interventional Radiology, Gustave Roussy, 94800 Villejuif
9 Université Paris-Saclay, Institut Gustave Roussy, Inserm U981, Biomarqueurs prédictifs et nouvelles stratégies thérapeutiques en oncologie, 94800 Villejuif, France
10 Department of Pathology, Institut Bergonié, Bordeaux, France
11 Faculty of Medicine, University of Bordeaux, Bordeaux, France
12 Department of Medicine, Institut Bergonié, Bordeaux, France

Correspondence to: Pr Antoine ITALIANO, Gustave Roussy, Rue Camille Desmoulins, Villejuif, France

Tel : +33 01 42 11 42 11

Email: antoine.italiano@gustaveroussy.fr

ABSTRACT

Background: Immune checkpoint blockers (ICBs) are now widely used in oncology. However, most patients do not derive benefit from these agents. Therefore, there is a crucial need to identify novel and reliable biomarkers of resistance to such treatments in order to prescribe potentially toxic and costly treatments only to patients with expected therapeutic benefits. In the wake of genomics, the study of proteins is now emerging as the new frontier for understanding real-time human biology.

Methods: We analyzed the proteome of plasma samples, collected before treatment onset, from two independent prospective cohorts of cancer patients treated with ICB (Discovery cohort n= 95, validation cohort n= 292). We then investigated the correlation between protein plasma levels, clinical benefit rate, progression-free survival (PFS) and overall survival (OS) by Cox proportional hazards models.

Results: By using an unbiased proteomics approach, we show that, in both Discovery and Validation cohorts, elevated baseline serum level of Leukemia Inhibitory Factor (LIF) is associated with a poor clinical outcome in cancer patients treated with ICB, independently of other prognostic factors. We also demonstrated that circulating level of LIF is inversely correlated with the presence of Tertiary Lymphoid Structures (TLS) in the tumor microenvironment.

Conclusion: This novel clinical dataset brings strong evidence for the role of LIF as a potential suppressor of anti-tumor immunity and suggest that targeting LIF or its pathway may represent a promising approach to improve efficacy of cancer immunotherapy in combination with ICB.

KEY WORDS: LIF, immunotherapy, biomarkers, resistance

HIGHLIGHTS

- Plasma proteomics identified Leukemia Inhibitory Factor (LIF) as a robust biomarker associated with resistance to immunotherapy
- Plasma levels of LIF are associated with tumor microenvironment features such as the presence of tertiary lymphoid structures
- LIF appears as an important therapeutic target to improve ICB efficacy

INTRODUCTION

The discovery of immune inhibitory checkpoints has revolutionized the systemic approach of the treatment of cancer. Blocking the interaction between the Programmed cell death 1 (PD-1) receptor and its primary ligand Programmed death-ligand 1 (PD-L1) has demonstrated remarkable anti-cancer activity and has led to the recent approval of anti-PD-1/PD-L1 drugs in several solid tumors[1]. However, most patients receiving anti-PD-1/PD-L1 monoclonal antibodies do not derive clinical benefit. Therefore, there is a crucial need to identify reliable predictive biomarkers of response to anti-PD-1/PD-L1 agents, both to develop precision medicine in cancer immunotherapy and to better understand mechanisms of sensitivity and resistance.

PD-L1 expression status as assessed by immunohistochemistry, tumor mutational burden and microsatellite instability status are so far the sole companion diagnostic markers approved to guide for anti-PD(L)1 therapy[2-4]. However, all of them and particularly PD-L1 expression are imperfect predictors of response to immune-checkpoint inhibition as demonstrated by the discordant results reported by multiple studies[2].

While tumor tissue profiling is important for biomarker discovery, this approach has several limitations including limited accessibility and temporal and spatial heterogeneity. Hence, identification of biomarkers than can be readily evaluable through peripheral blood sampling is crucial to allow the easiest implementation in routine clinical practice. To the best of our knowledge, we report here the first large analysis, including discovery and validation cohorts, of plasma proteome from cancer patients treated with immune checkpoint blockers (ICB).

METHODS

Patients (Figure 1)

This study was based on the analysis of two prospective cohorts of advanced cancer patients treated with ICB at Gustave Roussy (Villejuif, France) (Discovery: MATCH-R[5], NCT02517892; Validation cohort: PREMIS, NCT03984318). The inclusion criteria were age ≥ 18 years, histologically proven malignant tumor, unresectable and/or metastatic disease, at least one tumor evaluation by imaging after immunotherapy onset, and, for the MATCH-R study, availability of paraffin-embedded tumor material obtained before immunotherapy onset. Patients treated with combinations of ICB and chemotherapy were excluded from the analysis. Institutional ethics review board approval and patient informed consents were obtained for both studies.

Treatments and evaluation

All patients were treated either with anti-PD(L)1 monotherapies or anti-PD(L)1 based combination therapies. Patients were treated by immunotherapy either within clinical trials, or in the context of EMA-approved indications, or within early access programs. The best response to treatment was evaluated according to Response Evaluation Criteria in Solid Tumors (RECIST)[6] or iRECIST depending on the protocol in which patients were treated. Routine follow-up and treatment beyond progression therapeutic options were similar within the two cohorts. Durable clinical benefit (DCB) was defined as the proportion of patients achieving objective response or stable disease lasting ≥ 12 months. Progression-free survival (PFS) was defined as the time from the start of treatment until disease progression, death, or last patient contact. Overall survival (OS) was defined as the time from the start of treatment until death or last patient contact.

Plasma proteome analysis

Proteome analysis has been performed as previously described[7] thanks to the Olink Proximity Extension Assay (PEA) (Olink Proteomics AB, Uppsala, Sweden). In brief, pairs of oligonucleotide-labeled antibody probes bind to their targeted protein, and if the two probes are brought in proximity the oligonucleotides will hybridize in a pair-wise manner. The addition of a DNA polymerase leads to a proximity-dependent DNA polymerization event, generating a unique target sequence analyzed through either Next Generation Sequencing or Real-Time PCR.

Analysis of baseline samples from the discovery cohort has been performed using the Olink® Explore 1536 library consisting of 1472 proteins and 48 controls assays divided into four 384-plex panels focused on inflammation, oncology, cardiometabolic and neurology proteins. Sequencing was performed on a NovaSeq 6000 system using two S1 flow cells with 2 × 50 base read lengths. Counts of known sequences are thereafter translated into normalized protein expression (NPX) units through a QC and normalization process developed and provided by Olink.

Plasma samples from the validation cohort were assessed using the Olink® Target 96 Inflammation panel (Olink Proteomics AB, Uppsala, Sweden) according to the manufacturer's instructions[8]. In that case, the resulting DNA sequence was subsequently detected and quantified using a microfluidic real-time PCR instrument (Biomark HD, Fluidigm).

Data were quality controlled and normalized using an internal extension control and an inter-plate control, to adjust for intra- and inter-run variation. The final assay read-out is presented in Normalized Protein eXpression (NPX) values, which is an arbitrary unit on a log2-scale where a high value corresponds to a higher protein expression. All

assay validation data (detection limits, intra- and inter-assay precision data, etc.) are available on manufacturer's website (www.olink.com).

Immunohistochemistry stainings

All staining were carried out on 3,5 micrometers paraffin slides using a Ventana Discovery Ultra platform (Ventana, Roche Diagnostics). Double immunohistochemistry was performed on all cases with **i)** CD3 (2GV6, Ventana) combined with CD20 (L26, Ventana) and **ii)** CD8 (C8/144B, Dako) combined to PD-L1 (QR1, Diagomics). Stainings were performed with the protocol RUO discovery universal according to the manufacturer's recommendations with the detection kits OmniMap anti-Rb HRP (760-4311, Ventana) and OmniMap anti-Ms HRP (760-4310, Ventana).

Tumor TLS assessment

All cases were reviewed blindly by a pathologist for the presence of TLS according to the hematoxylin eosin saffron (HES) and the multiplexed immunohistochemistry on serial sections as previously described[9]. TLS were defined as lymphoid aggregates of B lymphocytes (admixed with a variable proportion of plasma cells and T lymphocytes in most cases). Only TLS made up of more than 50 cells and located either among the tumor cells or at the invasive margin (defined as fibrous tissue distant of less than 1mm from tumor cells) were considered. When the TLS status was assessed on lymphoid organs (namely lymph nodes, spleen, tonsils), TLS were only taken into account when admixed to tumor cells and if distant from the residual parenchyma, to exclude pre-existing lymphoid follicles.

Tumor PD-L1 scoring

For all tumors, the PD-L1 status was determined with TPS (tumor positive score) following guidelines. Only viable tumor cells displaying partial or complete staining for

PD-L1 membrane expression were considered relative to the total number of tumor cells. Positive immune cells and neoplastic cells showing only cytoplasmic staining were excluded[10].

Semi-automated and quantitative analysis of T-cell infiltrate

Density of CD8+ T cells within the tumor lesion was obtained by image analysis after slides digitization on a multispectral slide-imaging platform (Vectra Polaris, Akoya Bioscience). Using Inform software (Akoya Bioscience, version 2.4.1), tissue segmentation and cell phenotyping were performed and allowed for CD8+ T cells detection within the tumor lesion previously annotated by an expert pathologist. Combining CD8+ T cell detection and calculation of the tumor lesion surface, density of CD8+ lymphocytes was obtained for each sample.

RNAseq analysis

RNA sequencing was performed as previously described[11]. Reads were aligned to the hg38 human genome assembly using Rsubread (version 2.2.6) without prior trimming[12]. Counts were then summarized at the gene level using FeatureCounts and normalized using Deseq2. Relative abundance of immune cell types was estimated using the ConcensusTME[13] on the CIBERSORT[14] and Bindea[15] gene sets.

Statistical analysis

The cutoff date for statistical analysis of baseline demographic data and clinical outcome was 11/30/2020. Descriptive statistics were used to describe the distribution of variables in the population. Survival rates were estimated using the Kaplan–Meier method. Differences between groups were evaluated by chi-square test or Fisher's exact test for categorical variables and Student's test for continuous variables.

Receiver operating characteristic (ROC) curve analysis was performed using the ROCit R package. Prognostic factors were planned to be identified by univariate and multivariate analyses using a Cox regression model. Variables tested in univariate analysis included age, gender, tumor type, number of metastatic sites, presence of liver metastasis, performance status (PS), number of previous lines of treatment, and LIF plasma levels. Variables associated with PFS and OS with a *P*-value <0.05 in the univariate analysis were planned to be included in the multivariate analysis. Analyses were carried out using SPSS 20.0 statistical software (IPSS Inc., Chicago, IL). All statistical tests were two-sided, and $P < 0.05$ indicated statistical significance.

RESULTS

Unbiased proteomic analysis identifies baseline serum level of Leukemia Inhibitory Factor (LIF) is associated with poor clinical outcome in cancer patients treated with immune-checkpoint blockers

To detect potential peripheral biomarkers of efficacy of ICB, we implemented a proteomics analysis based on the Proximity Extension Assay (PEA) technology and the use of Olink® Explore 1536 panel[7] (1472 proteins and 48 controls) on plasma samples, collected before anti-PD(L)1-based immunotherapy onset, from 95 patients enrolled prospectively in the MATCH-R study (NCT02517892, Discovery cohort) - patient's characteristics are described in Table 1. Proteomic analysis allowed for the detection and quantification of 1463 unique proteins in all plasma samples. We then explored the correlation for each marker –classified as High and Low according to their respective median value - with progression-free survival. Among several cytokines (Supplementary Figure 2) already known to be associated with clinical outcome in cancer patients treated with immunotherapy such as IL6, CXCL8 (IL8) or CXCL1 (**Supp. Fig.2**)[16-17], Leukemia Inhibitory Factor (LIF) was the most significantly associated with outcome (**Fig. 2a**). The median follow-up was 26.4 months. The median PFS of LIF^{Low} patients was 7.4 months (95% CI, 2.9–11.9) versus 1.7 months (95% CI, 1.3–2.1) in the LIF^{High} group, p<0.0001 (**Fig. 2b**). The 6-month, 1-year, and 2-year PFS rates were 55.9%, 41.5%, and 16.2% in LIF^{Low} group and 17%, 6.4% and 0% in the LIF^{High} group, respectively. At the time of analysis, 69 patients (72.6%) had died and 26 (27.4%) were still alive. The median overall survival (OS) was 21.7 months (95% CI, 12–31.4) in the LIF^{Low} group versus 4.3 months (95% CI, 3.4–5.1) in the LIF^{High} group, p<0.0001 (**Fig. 2b**). The 6-month, 1-year, and 2-year OS rates were 81.1%, 67.8%, and 47.2% in the LIF^{Low} group and 40.4%, 29%, and 10.6% in the LIF^{High}

group, respectively. Overall, LIF plasma levels were significantly lower in patients with durable clinical benefit in comparison with other patients (**Fig. 2c**). Indeed, in patients classified as plasma LIF^{High}, the durable clinical benefit rate was 6.4% versus 41.7% in LIF^{Low} patients (NPX value below the median), p<0.0001 (**Fig. 2d**). Also, to analyze the performance of baseline LIF level to predict the clinical benefit, we performed a univariate time-dependent ROC (Receiver Operating Characteristics) curve analysis and found an AUC (Area Under Curve) at 0,735 thus confirming its strong predictive value (**Supp. Fig. 1**).

Leukemia Inhibitory Factor (LIF) predicts outcome in cancer patients treated with immune-checkpoint blockers independently of PD-L1 expression status

We then performed an exploratory analysis investigating association of LIF level with clinical outcome according to PD-L1 expression score (**Fig. 3a**) and CD8+ T-cell infiltration density (**Fig. 3d**) - as assessed by multiplexed immunohistochemistry - in a sub-cohort of 59 patients with available matched-tumor tissue. The PD-L1 tumor proportion score (TPS) was ≥ 1% in 20 patients (33.9%) and < 1% in 39 patients (66,1%). Peripheral level of LIF was similar in patients with PD-L1-positive and negative tumors (**Fig. 3b**). The proportion of PD-L1-positive tumors was similar among tumors with a high level (46.1%) and a low level of circulating LIF (55%) (data not shown). Regardless of the PD-L1 expression status, and despite the limited size of the sub-cohort, we observed that patients with tumors characterized by a low level of circulating LIF had better outcome. Indeed, among patients with a PD-L1 TPS < 1%, the median PFS was 7 months (95% CI, 2.8–11.1) in the LIF^{Low} group versus 1.5 months (95% CI, 0.9–2) in the LIF^{High} group; overall log–rank test p=0.001 (PFS). Among patients with a PD-L1 TPS ≥ 1%, the median PFS was 6.3 months (95% CI,

0–13.5) in the LIF^{Low} group versus 2.2 months (95% CI, 0.6–3.7) in the LIF^{High} group, overall log–rank test p=0.106 (PFS) (**Fig. 3c**).

We then quantified the density of CD8+ T cells within the tumor lesion and considered highly infiltrated tumor when density was above the threshold value of 262.7/mm² (corresponding to the 75th percentile). Interestingly, CD8-infiltrated tumors were characterized by a lower level of peripheral LIF (**Fig. 3e**, p=0,02). Also, whatever the CD8 infiltration density of the tumor, circulating LIF level was significantly associated with an improved PFS in the low CD8+ T-cell density group (p=0,016), and a trend was observed in the high CD8+ T-cell density subgroup (p=0,062) (**Fig. 3f**). The lack of statistical significance in the high CD8+ T-cell density subgroup may be related to the low sample size.

Leukemia Inhibitory Factor (LIF) serum levels are associated with specific tumor microenvironment features and the presence of tertiary lymphoid structures

We then investigated whether circulating LIF level was correlated with the intratumor immune landscape through RNAseq expression data deconvolution with Bindea (**Fig. 4a**) or CIBERSORT (**Supp. Fig.3)** algorithms. A significant inverse correlation between LIF and B cells (**Fig. 4a and b**) as well as with follicular helper T cells (**Fig. 4a**) was observed. These two cell types are major components of the so called tertiary lymphoid structures (TLS)[17], and we therefore decided to assess the presence of TLS in tumor samples by using multiplexed-immunohistochemistry (**Fig. 4c**) as previously described[9]. We observed the presence of TLS in 22 cases (37.3%). The proportion of TLS positive cases was significantly higher in the LIF^{Low} group than in the LIF^{High} group; 50% vs 24.1%, p=0.04 (**Fig. 4d**).

Baseline serum levels of LIF predict outcome independently of other prognostic factors in a validation cohort of cancer patients treated with immune-checkpoint blockers

To confirm the robustness of the predictive value of peripheral LIF level, plasma samples collected from 292 patients enrolled in the PREMIS study (NCT03984318) – serving as a validation cohort – cytokines, including LIF, were measured using the Olink Target 96 inflammation panel. This assay relies on a qPCR readout which was found to be highly similar and correlated with the Olink® Explore 1536 panel[18]. We found improved objective response rate (32.2% vs 16.4%, p=0.002), durable clinical benefit rate (34.2% vs 17.8%, p=0.001) (**Fig. 5c**), PFS (5.1 vs 2.6 months, p<0.0001) (**Fig. 5a**), and OS (not reached vs 8.5 months, p<0.001) (**Fig. 5b**), in the LIF^{Low} group compared with the LIF^{High} group. AUC of the ROC curve analysis was evaluated at 0.622 (**Supp. Fig. 4**) thus confirming the predictive value of LIF in an independent validation cohort. On multivariate analysis, LIF plasma levels remained independently associated with both PFS and OS (table 2).

To confirm that our results were representative of all cancer types, we performed one additional analysis by stratifying patients included in the PREMIS study according to tumor type: non-small-cell lung cancer (NSCLC) or non- NSCLC cases. We observed in each stratum significantly higher objective response rate, durable clinical benefit rate, PFS and OS indicating that the predictive value of circulating LIF level was not solely driven by the NSCLC histology (**Supp. Fig. 5a and 5b)**

DISCUSSION

In the wake of genomics, the study of proteins is now emerging as the new frontier for understanding real-time human biology. Protein biomarker discovery enables identification of signatures with pathophysiological importance, bridging the gap between genomes and phenotypes. This type of data may have a deep impact on improving future healthcare, particularly with respect to precision medicine, but progress has been hampered by the lack of technologies that can provide reliable specificity, high throughput, good precision, and high sensitivity. Here, we used a Proximity Extension Assay (PEA) technology, a unique method where each biomarker is addressed by a matched pair of antibodies, coupled to unique, partially complementary oligonucleotides, and measured by next generation sequencing[7]. This enables a high level of multiplexing while maintaining high-level data quality. To the best of our knowledge, we report here the largest study implementing a comprehensive analysis of the plasma proteome to identify predictive biomarker of efficacy in cancer patients treated with ICB. In comparison with traditional biomarkers such as PD-L1 expression status, circulating biomarkers offer a promising alternative to address the pitfalls associated with analysis of tumor tissue such as temporal and spatial tumor heterogeneity.

Thanks to a robust methodology, we were able to identify, starting from a Discovery cohort, LIF as a predictive factor of objective response rate, PFS and OS in cancer patients treated with ICB. To strengthen this finding, these results have been validated using samples from an independent and large validation cohort. In addition, analysis of the lung adenocarcinoma cohort of the TCGA database (Broad GDAC 1/28/2016) demonstrated that LIF was not associated with prognosis of lung cancer patients thus

highlighting its specific predictive value for patients treated with anti-PD(L)1-based ICB (data not shown).

LIF is a pleiotropic cytokine involved in many physiological and pathological processes (reviewed in ref 19) and is highly expressed in a subset of tumors across multiple tumor types where it has been shown to be associated with poor prognosis. As recently shown by single-cell studies, LIF is mainly expressed by tumor cells[20]. However, the mechanisms involving this cytokine in cancer progression are not well understood. One of the first demonstration of the role of LIF in immunity was reported by Gao et al showing that LIF promotes self-tolerance by stimulating the Treg differentiation and inhibiting T helper type 17 cell differentiation[21]. Moreover, LIF favors the acquisition of an M2 phenotype by macrophages and the recruitment of myeloid-derived suppressor cells into the tumor microenvironment [22-23], all these mechanisms participating in the anti-tumor immune evasion. LIF has also been shown to regulate the maturation of dendritic cells (DCs), leading to the development of tolerogenic DCs, which contribute to an immunosuppressive microenvironment[24]. Interestingly, LIF neutralization was associated with strong inhibition of tumor growth in several preclinical models[25,26]. A recent study has also shown that LIF blockade is associated with an increased production of CXCL9 by macrophages and a concomitant decrease in CD206, CD163 and CCL2[26]. In our study, while baseline plasma LIF was associated with an intratumoral expression of LIF, no correlation was found for either CCL2, CD206 or CXCL9 (**Supp. Fig. 6**) – the same results were observed by analyzing *LIF* gene expression in tumor samples (*data not shown*). In addition, we highlighted that plasma LIF was positively associated with circulating IL6 and CCL2 (**Supp. Fig. 7**).

We therefore assessed whether the peripheral level of LIF was associated with specific tumor microenvironment features. By using both transcriptomic and multiplexed-IHC

analysis, we found that low levels of LIF were strongly associated with the presence of follicular helper T (Tfh) and B cells in the context of TLS. TLS can be likened to micro-secondary lymphoid organs. TLS have been identified in several solid tumor types and are associated with better survival when present in the tumor microenvironment[27-30]. Higher densities of TLS were associated with an increased density of tumor-infiltrating CD8+ T lymphocytes[31-32] and with an activated and cytotoxic immune signature[30]. We have recently reported that the presence of TLS is highly predictive of improved outcomes in cancer patients treated with immune checkpoint inhibitors[11]. Preclinical data have suggested that LIF blockade promotes $CD8^+$ T cell infiltration in several tumors models[26]. In our study, we bring, for the first time, evidence suggesting that low level of LIF is associated with the presence of TLS, which could in turn favor antitumor T-cell immunity induction. The combination of anti-LIF and anti-PD1 antibodies has also been shown to be synergistic in pre-clinical tumor models[26].

Recently, the results of a phase I study investigating the safety and efficacy of MSC-1, a first-in-class humanized IgG1 monoclonal antibody that potently and selectively inhibits LIF, have been reported[33]. Eligible patients had advanced relapsed/refractory solid tumors and received treatment with MSC-1 intravenously (75mg-1500 mg) once every 3-weeks as a single agent until disease progression. Single agent MSC-1 was well tolerated with no dose limiting toxicities observed during the first cycle of treatment. Preliminary signs of activity were observed with disease stabilization in 9 patients out of 41. Interestingly, analysis of paired biopsies (before treatment onset and on treatment) showed increase CD8 T-cell infiltration in a subset of samples.

Our results indicate that LIF could represent a key factor in resistance to cancer immunotherapy and thus suggest that targeting LIF axis may represent a promising

approach to improve efficacy of ICB in cancer patients, and particularly in patients characterized by a high plasma level of LIF.

AUTHOR CONTRIBUTIONS

AI, AB, conceived and designed the study. FLL performed the histological analyses. YL, AM, FXD, BB, NC, CM, DP, CR, CE, MK, LT, LF, FA, JCS provided study material or treated patients. All authors collected and assembled data. AI, and AB developed the tables and figures. AI and AB conducted the literature search and wrote the manuscript. All authors were involved in the critical review of the manuscript and approved the final version.

FUNDING STATEMENT

None

DECLARATION OF INTERESTS

CM, FXD, MK, LT, LF, FLL, FA: Nothing to disclose

AB and JPG: Employees of Explicyte

AI: Received research grants from Astra Zeneca, Bayer, BMS, Chugai, Merck, MSD, Pharmamar, Novartis, Roche, and received personal fees from Epizyme, Bayer, Lilly, Roche, and Springworks

BB: Received grants from AstraZeneca , Pfizer , Eli Lilly , Onxeo , Bristol Myers Squibb, Inivata , Abbvie , Amgen , Blueprint Medicines , Celgene , GlaxoSmithKline , Ignyta , Ipsen , Merck KGaA , MSD Oncology , Nektar , PharmaMar , Sanofi , Spectrum Pharmaceuticals , Takeda , Tiziana Therapeutics , Cristal Therapeutics , Daiichi Sankyo , Janssen Oncology , OSE Immunotherapeutics , BeiGene , Boehringer Ingelheim , Genentech , SERVIER , Tolero Pharmaceuticals

YL: Received grants and personal fees from Janssen, during the conduct of the study; personal fees and non-financial support from Astellas, grants and personal fees from Sanofi, personal fees and non-financial support from Roche, personal fees and non-financial support from AstraZeneca, grants, personal fees and non-financial support from MSD, personal fees and non-financial support from BMS, personal fees from Clovis , personal fees and non-financial support from Seattle Genetics, personal fees from Incyte, personal fees from Pfizer.

AM: Received research grants from Mersu, Bristol-Myers Squibb, Boehringer Ingelheim, Transgene, MSD and received personal fees from Bristol-Myers Squibb, AstraZeneca, MedImmune, Oncovir, Merieux

JCS: Has received consultancy fees from AstraZeneca, Astex, Clovis, GSK, GamaMabs, Lilly, MSD, Mission Therapeutics, Merus, Pfizer, Pharma Mar, Pierre Fabre, Roche/Genentech, Sanofi, Servier, Symphogen, and Takeda.

All remaining authors have declared no conflicts of interest.

DATA SHARING STATEMENT

Individual participant data that underlie the results reported in this article will be available after deidentification beginning 24 months and ending 48 months following article publication to researchers who provide a methodologically sound proposal. Requests should be sent to the corresponding author.

REFERENCES

1. Vaddepally RK, Kharel P, Pandey R, Garje R, Chandra AB. Review of Indications of FDA-Approved Immune Checkpoint Inhibitors per NCCN Guidelines with the Level of Evidence. Cancers (Basel). 2020 Mar 20;12(3).
2. Davis AA, Patel VG. The role of PD-L1 expression as a predictive biomarker: an analysis of all US Food and Drug Administration (FDA) approvals of immune checkpoint inhibitors. J Immunother Cancer. 2019;7(1):278.
3. Marabelle A, Fakih M, Lopez J, Shah M, Shapira-Frommer R, Nakagawa K, Chung HC, Kindler HL, Lopez-Martin JA, Miller WH Jr, Italiano A, Kao S, Piha-Paul SA, Delord JP, McWilliams RR, Fabrizio DA, Aurora-Garg D, Xu L, Jin F, Norwood K, Bang YJ. Association of tumour mutational burden with outcomes in patients with advanced solid tumours treated with pembrolizumab: prospective biomarker analysis of the multicohort, open-label, phase 2 KEYNOTE-158 study. Lancet Oncol. 2020 Oct;21(10):1353-1365.
4. André T, Shiu KK, Kim TW, Jensen BV, Jensen LH, Punt C, Smith D, Garcia-Carbonero R, Benavides M, Gibbs P, de la Fouchardiere C, Rivera F, Elez E, Bendell J, Le DT, Yoshino T, Van Cutsem E, Yang P, Farooqui MZH, Marinello P, Diaz LA Jr; KEYNOTE-177 Investigators. Pembrolizumab in Microsatellite-Instability-High Advanced Colorectal Cancer. N Engl J Med. 2020 Dec 3;383(23):2207-2218.
5. Recondo G, Mahjoubi L, Maillard A, Loriot Y, Bigot L, Facchinetti F, Bahleda R, Gazzah A, Hollebecque A, Mezquita L, Planchard D, Naltet C, Lavaud P, Lacroix L, Richon C, Lovergne AA, De Baere T, Tselikas L, Deas O, Nicotra C, Ngo-Camus M, Frias RL, Solary E, Angevin E, Eggermont A, Olaussen KA, Vassal G, Michiels S, Andre F, Scoazec JY, Massard C, Soria JC, Besse B,

Friboulet L. Feasibility and first reports of the MATCH-R repeated biopsy trial at Gustave Roussy. NPJ Precis Oncol. 2020 Sep 8;4:27.

6. Eisenhauer EA, Therasse P, Bogaerts J, Schwartz LH, Sargent D, Ford R, Dancey J, Arbuck S, Gwyther S, Mooney M, Rubinstein L, Shankar L, Dodd L, Kaplan R, Lacombe D, Verweij J. New response evaluation criteria in solid tumours: revised RECIST guideline (version 1.1). Eur J Cancer. 2009 Jan;45(2):228-47.
7. Michael R. Filbin, Arnav Mehta, Alexis M. Schneider, Kyle R. Kays, Jamey R. Guess, Matteo Gentili, Bánk G. Fenyves, Nicole C. Charland, Anna L.K. Gonye, Irena Gushterova, Hargun K. Khanna, Thomas J. LaSalle, Kendall M. Lavin-Parsons, Brendan M. Lilly, Carl L. Lodenstein, Kasidet Manakongtreecheep, Justin D. Margolin, Brenna N. McKaig, Maricarmen Rojas-Lopez, Brian C. Russo, Nihaarika Sharma, Jessica Tantivit, Molly F. Thomas, Robert E. Gerszten, Graham S. Heimberg, Paul J. Hoover, David J. Lieb, Brian Lin, Debby Ngo, Karin Pelka, Miguel Reyes, Christopher S. Smillie, Avinash Waghray, Thomas E. Wood, Amanda S. Zajac, Lori L. Jennings, Ida Grundberg, Roby P. Bhattacharyya, Blair Alden Parry, Alexandra-Chloé Villani, Moshe Sade-Feldman, Nir Hacohen, Marcia B. Goldberg. Plasma proteomics reveals tissue-specific cell death and mediators of cell-cell interactions in severe COVID-19 patients. bioRxiv 2020.11.02.365536; doi: https://doi.org/10.1101/2020.11.02.365536
8. Assarsson E, Lundberg M, Holmquist G, Björkesten J, Thorsen SB, Ekman D, Eriksson A, Rennel Dickens E, Ohlsson S, Edfeldt G, Andersson AC, Lindstedt P, Stenvang J, Gullberg M, Fredriksson S. Homogenous 96-plex PEA

immunoassay exhibiting high sensitivity, specificity, and excellent scalability. PLoS One. 2014 Apr 22;9(4):e95192.

9. Vanhersecke L, Brunet M, Guégan JP, Rey C, Bougouin A, Cousin S, Le Moulec S, Besse B, Loriot Y, Larroquette M, Soubeyran I, Toulmonde M, Roubaud G, Pernot S, Cabart M, Chomy F, Lefevre C, Bourcier K, Kind M, Giglioli I, Sautès-Fridman C, Velasco V, Courgeon F, Oflazoglu E, Savina A, Marabelle A, Soria JC, Bellera C, Sofeu C, Bessede A, Fridman WH, Le Loarer F, Italiano A. Mature tertiary lymphoid structures predicts immune checkpoint inhibitor efficacy in solid tumors independently of PD-L1 expression. Nat Cancer 2021, In Press
10. Vigliar E, Malapelle U, Iaccarino A, Acanfora G, Pisapia P, Clery E, De Luca C, Bellevicine C, Troncone G. PD-L1 expression on routine samples of non-small cell lung cancer: results and critical issues from a 1-year experience of a centralised laboratory. J Clin Pathol. 2019; 72:412-417
11. Massard C, Michiels S, Ferté C, Le Deley MC, Lacroix L, Hollebecque A, Verlingue L, Ileana E, Rosellini S, Ammari S, Ngo-Camus M, Bahleda R, Gazzah A, Varga A, Postel-Vinay S, Loriot Y, Even C, Breuskin I, Auger N, Job B, De Baere T, Deschamps F, Vielh P, Scoazec JY, Lazar V, Richon C, Ribrag V, Deutsch E, Angevin E, Vassal G, Eggermont A, André F, Soria JC. High-Throughput Genomics and Clinical Outcome in Hard-to-Treat Advanced Cancers: Results of the MOSCATO 01 Trial. Cancer Discov. 2017 Jun;7(6):586-595.
12. Liao Y, Smyth GK, Shi W. The R package Rsubread is easier, faster, cheaper and better for alignment and quantification of RNA sequencing reads. Nucleic Acids Res. 2019 May 7;47(8):e47.

13. Jiménez-Sánchez A, Cast O, Miller ML. Comprehensive Benchmarking and Integration of Tumor Microenvironment Cell Estimation Methods. Cancer Res. 2019 Dec 15;79(24):6238-6246.
14. Newman AM, Liu CL, Green MR, Gentles AJ, Feng W, Xu Y, Hoang CD, Diehn M, Alizadeh AA. Robust enumeration of cell subsets from tissue expression profiles. Nat Methods. 2015 May;12(5):453-7.
15. Bindea G, Mlecnik B, Tosolini M, Kirilovsky A, Waldner M, Obenauf AC, Angell H, Fredriksen T, Lafontaine L, Berger A, Bruneval P, Fridman WH, Becker C, Pagès F, Speicher MR, Trajanoski Z, Galon J. Spatiotemporal dynamics of intratumoral immune cells reveal the immune landscape in human cancer. Immunity. 2013 Oct 17;39(4):782-95.
16. Keegan A, Ricciuti B, Garden P, Cohen L, Nishihara R, Adeni A, Paweletz C, Supplee J, Jänne PA, Severgnini M, Awad MM, Walt DR. Plasma IL-6 changes correlate to PD-1 inhibitor responses in NSCLC. J Immunother Cancer. 2020 Oct;8(2):e000678.
17. Schalper KA, Carleton M, Zhou M, Chen T, Feng Y, Huang SP, Walsh AM, Baxi V, Pandya D, Baradet T, Locke D, Wu Q, Reilly TP, Phillips P, Nagineni V, Gianino N, Gu J, Zhao H, Perez-Gracia JL, Sanmamed MF, Melero I. Elevated serum interleukin-8 is associated with enhanced intratumor neutrophils and reduced clinical benefit of immune-checkpoint inhibitors. Nat Med. 2020 May;26(5):688-692.
18. Sautès-Fridman C, Petitprez F, Calderaro J, Fridman WH. Tertiary lymphoid structures in the era of cancer immunotherapy. Nat Rev Cancer. 2019;19:307-325.

19. Zhong W, Edfors F, Gummesson A, Bergström G, Fagerberg L, Uhlén M. Next generation plasma proteome profiling to monitor health and disease. Nat Commun. 2021 May 3;12(1):2493.
20. Zhang C, Liu J, Wang J, Hu W, Feng Z. The emerging role of leukemia inhibitory factor in cancer and therapy. Pharmacol Ther. 2020 Nov 28:107754.
21. Gao W, Thompson L, Zhou Q, Putheti P, Fahmy TM, Strom TB, Metcalfe SM. Treg versus Th17 lymphocyte lineages are cross-regulated by LIF versus IL-6. Cell Cycle. 2009 May 1;8(9):1444-50.
22. Duluc D, Delneste Y, Tan F, Moles MP, Grimaud L, Lenoir J, Preisser L, Anegon I, Catala L, Ifrah N, Descamps P, Gamelin E, Gascan H, Hebbar M, and Jeannin P. Tumor-associated leukemia inhibitory factor and IL-6 skew monocyte differentiation into tumor-associated macrophage-like cells. Blood 2007; 110: 4319–4330.
23. Won H, Moreira D, Gao C, Duttagupta P, Zhao X, Manuel E, Diamond D, Yuan YC, Liu Z, Jones J, D'Apuzzo M, Pal S, and Kortylewski M. TLR9 expression and secretion of LIF by prostate cancer cells stimulates accumulation and activity of polymorphonuclear MDSCs. J Leukoc Biol 2017; 102: 423–436.
24. Yaftiyan A, Eskandarian M, Jahangiri AH, Kazemi Sefat NA, Moazzeni SM. Leukemia inhibitory factor (LIF) modulates the development of dendritic cells in a dual manner. Immunopharmacol Immunotoxicol. 2019 Jun;41(3):455-462.
25. Ghanei Z, Mehri N, Jamshidizad A, Joupari MD, Shamsara M. Immunization against leukemia inhibitory factor and its receptor suppresses tumor formation of breast cancer initiating cells in BALB/c mouse. Sci Rep. 2020 Jul 10;10(1):11465.

26. Pascual-García M, Bonfill-Teixidor E, Planas-Rigol E, Rubio-Perez C, Iurlaro R, Arias A, Cuartas I, Sala-Hojman A, Escudero L, Martínez-Ricarte F, Huber-Ruano I, Nuciforo P, Pedrosa L, Marques C, Braña I, Garralda E, Vieito M, Squatrito M, Pineda E, Graus F, Espejo C, Sahuquillo J, Tabernero J, Seoane J. LIF regulates CXCL9 in tumor-associated macrophages and prevents CD8+ T cell tumor-infiltration impairing anti-PD1 therapy. Nat Commun. 2019 Jun 11;10(1):2416. doi: 10.1038/s41467-019-10369-9.

27. Sautès-Fridman C, Petitprez F, Calderaro J, Fridman WH. Tertiary lymphoid structures in the era of cancer immunotherapy. Nat Rev Cancer. 2019;19(6):307-325.

28. Ladányi A, Kiss J, Mohos A, Somlai B, Liszkay G, Gilde K, Fejös Z, Gaudi I, Dobos J, Tímár J. Prognostic impact of B-cell density in cutaneous melanoma. Cancer Immunol Immunother. 2011 Dec;60(12):1729-38.4

29. Messina JL, Fenstermacher DA, Eschrich S, Qu X, Berglund AE, Lloyd MC, Schell MJ, Sondak VK, Weber JS, Mulé JJ. 12-Chemokine gene signature identifies lymph node-like structures in melanoma: potential for patient selection for immunotherapy? Sci Rep. 2012;2:765.

30. Goc J, Germain C, Vo-Bourgais TK, Lupo A, Klein C, Knockaert S, de Chaisemartin L, Ouakrim H, Becht E, Alifano M, Validire P, Remark R, Hammond SA, Cremer I, Damotte D, Fridman WH, Sautès-Fridman C, Dieu-Nosjean MC. Dendritic cells in tumor-associated tertiary lymphoid structures signal a Th1 cytotoxic immune contexture and license the positive prognostic value of infiltrating CD8+ T cells. Cancer Res. 2014 Feb 1;74(3):705-15.

31. Behr DS, Peitsch WK, Hametner C, et al. (2014) Prognostic value of immune cell infiltration, tertiary lymphoid structures and PD-L1 expression in Merkel cell carcinomas. Int J Clin Exp Pathol 7:7610–7621.
32. Caro GD, Bergomas F, Grizzi F, et al. (2014) Occurrence of tertiary lymphoid tissue is associated with T-cell infiltration and predicts better prognosis in early-stage colorectal cancers. Clin Cancer Res 20:2147–2158.
33. Schram A, Borazanci E, Brana I, Vieito Villar M, Garralda E, Spreafico A, Oliva M, Lakhani N, Wasserman R, Hoffmann K, Hallett R, Anido J, Maetzel D, Giblin P, Moran E, Kelly A, Seoane J, Von Hoff D, Siu L, Tabernero J. Phase 1 dose escalation of MSC-1, a humanized anti-LIF monoclonal antibody, in patients with advanced solid tumors [abstract]. In: Proceedings of the Annual Meeting of the American Association for Cancer Research 2020; 2020 Apr 27-28 and Jun 22-24. Philadelphia (PA): AACR; Cancer Res 2020;80(16 Suppl):Abstract nr CT147.

FIGURES LEGENDS

Figure 1. Flow chart depicting the identification strategy of a biomarker associated to resistance to anti-PD(L)1 immunotherapy within a discovery cohort and its assessment in an additional validation cohort. Pre-treatment (Pre-Tx) plasma samples and matched tumor biopsies were collected before anti-PD1/PDL1 antibodies-based treatment in cancer patients (see Table 1 for patient details). Plasma samples (n=95 patients) were processed for a comprehensive proteomic analysis allowing the simultaneous detection of 1463 proteins. Tumor biopsies were exploited for **i)** RNA-Sequencing for tumor immune gene expression profile (n=52 patients) and for **ii)** immunohistochemistry in order to assess tumor PDL1 expression (TPS score), CD8 T-cells density and the presence of Tertiary Lymphoid Structures (TLS) (n=59 patients). Computed data were then tested for their association with clinical data including clinical outcome. Durable Clinical Benefit (DCB) was considered for patients deriving complete or partial response but also a stable disease with a progression free survival (PFS) > 12months. Non Durable Benefit (NDB) was considered for patients with a progressive disease or a stable disease with a PFS ≤ 12 months. The best selected biomarker was investigated in an independent validation cohort of 292 patients (see Table 1 for patients' details) receiving PD1 / PDL1 blockade antibodies.

Figure 2. Baseline plasmatic LIF level predicts response to PD1 / PDL1 axis blockade. A Display of the Log Rank p-values for progression-free survival (PFS) (y axis) and of the delta median PFS (y axis) associated with each plasmatic marker. Median value of each plasmatic marker was used to categorize patients with High or Low status. Each dot represents one marker. **B** Kaplan Meier curves of progression-free survival (left) and overall survival (right) according to baseline plasmatic LIF levels. **C** Quantification of baseline plasmatic LIF in NDB (n= 72, blue) and DCB (n= 23, red) patients. p value was calculated using Wilcoxon Rank sum test. **D** Proportion of patients who experienced durable clinical benefit (DCB) or non-clinical benefit (NCB) according to their baseline plasmatic level of LIF classified as High (above median value) and Low (below median value).

Figure 3. LIF is a predictive biomarker independently from PDL1 expression status and tumoral CD8 infiltration level. A PDL1 expression was assessed by immunohistochemistry (PDL1 stained in purple). Illustrations here depict tumor cases with negative (TPS<1%) and positive (TPS ≥ 1%) PDL1 expression. **B** Representation of plasmatic LIF level in patients according to their PDL1 TPS score (TPS<1 vs TPS ≥1). p value was calculated using Wilcoxon Rank sum test. **C** PFS probability according to LIF level (High vs Low) in patients negative (TPS<1, n=39) or positive (TP≥1, n=20) for tumoral PDL1 expression. **D** CD8+ T cell infiltration was assessed through immunohistochemistry staining (CD8 stained in brown). Illustrations highlight tumor cases with low and high CD8 infiltration level. E Plasmatic LIF level in patients according to their CD8 infiltration level. p value was calculated using Wilcoxon Rank sum test. **E** PFS probability according to LIF level (High vs Low) in patients classified as $CD8^{Low}$ (n=44) or $CD8^{High}$ (n=15).

Figure 4. Peripheral LIF level is associated with an intratumoral B cell signature and presence of Tertiary Lymphoid Structures. A Correlation of immune cell lineages - obtained through RNA-sequencing and data deconvolution with Bindea algorithm - and LIF plasma level. Dot size depicts the correlation coefficient while the color is indicative of positive (red) or negative (blue) correlation. The X-axis represents the transformed Log10 pearson p-value. **B** Histogram representation of B cell score (in relative units, RU) according to baseline plasmatic level of LIF classified as High or Low (median value used as a cut-off). p value was calculated using a Wilcoxon Rank sum test. **C** Representative histological images from a patient with squamous cell lung carcinoma showing presence of TLS highlighted through both Hematoxylin Eosin Saffron (HES) staining and double staining of CD3-CD20 (CD3 in brown, CD20 in purple). Left image has been captured at a low magnification – scale bar indicates 400µm size – while the images on the right has been obtained through slide digitization at a higher magnification; scale bar indicates 100µm. Black arrow indicates tumor cells that juxtapose TLS. **D** Proportion of patients with presence or absence of intratumoral TLS according to baseline LIF plasma level. p value was calculated through Chi-squared test.

Figure 5. Baseline circulating LIF level is predictive of outcome of cancer patients treated with anti-PD(L)1 immunotherapy – results from an independent validation cohort. A Probability of PFS for LIF^{High} (median survival = 2,57 mo.) and LIF^{Low} (median survival = 5,07 mo.) patients in the Validation Cohort (n = 292). **B** Probability of OS for LIF^{High} (median survival = 8,53 mo.) and LIF^{Low} (median survival = NA) patients in the same patients cohort. **C** Proportion of patients who experienced DCB or NCB according to their baseline plasmatic level of LIF classified as High (above median value) and Low (below median value). P value was calculated through Chi-squared test.

TABLE 1. Patient characteristics		
Discovery cohort (n=95)		
Age	Median 63 years (range 34-91)	
Gender	N	%
Male	61	64.2
Female	34	35.8
Tumor Type		
Non-small cell lung cancer	71	74.7
Bladder cancer	13	13.7
Others[1]	11	11.6
Performance status		
≤ 1	78	82.1
> 1	17	17.9
Stage IV cancer	95	100
Treatment		
Anti-PD1	66	69.5
Anti-PD-L1	22	23.1
PD1 or anti-PD-L1 + another immunecheckpoint	7	7.4
Validation Cohort (n=292)		
Age	Median 61 years (range 25-97)	
Gender	N	%
Male	173	59.2
Female	119	40.8
Tumor Type		
Non-small cell lung cancer	107	36.6
Melanoma	24	8.2

Soft-tissue sarcoma	22	7.5
Kidney	19	6.5
Bladder	15	5.1
Others[2]	105	36.0
Performance status		
≤ 1	244	83.6
> 1	48	16.4
Previous lines of treatment		
≤ 1	100	34.2
> 1	192	65.8
Treatment		
Anti-PD1	160	54.8
Anti-PD-L1	101	34.6
Combination of Immune Checkpoint	31	10.6

[1]prostate carcinoma, biliary tract cancer, thyroid cancer, prostate carcinoma, uterine carcinoma, [2]cervix carcinoma, colorectal cancer, gastric cancer, head and neck cancer, renal cancer, soft-tissue sarcoma, triple negative breast carcinoma

TABLE 2. Multivariate Analysis for Progression-Free Survival and Overall Survival			
Progression-Free Survival			
Independent Variables		Hazard ratio	P value
ECOG CODE	≤1	0.43 95% CI [0.29-0.65]	<0.001
	≥2	1	
Liver metastasis	Yes	1	0.042
	No	0.67 95% CI [0.46-0.98]	
Number_of_previous lines of treatment	≤1	0.61 95% CI [0.44-0.86]	0.004
	≥2	1	
LIF plasma levels	High	1.51 95% CI [1.1-2.1]	0.013
	Low	1	
Overall Survival			
	B	Hazard ratio	P value
ECOG CODE	≤1	0.21 95% CI [0.13-0.35]	<0.001
	≥2	1	
Liver metastasis	Yes	1	0.008
	No	0.54 95% CI [0.34-0.85]	
Number_of_previous lines of treatment	≤1	0.61 95% CI [0.40-0.94]	0.027
	≥2	1	
LIF plasma levels	High	1.78 95% CI [1.14-2.77]	0.01
	Low	1	

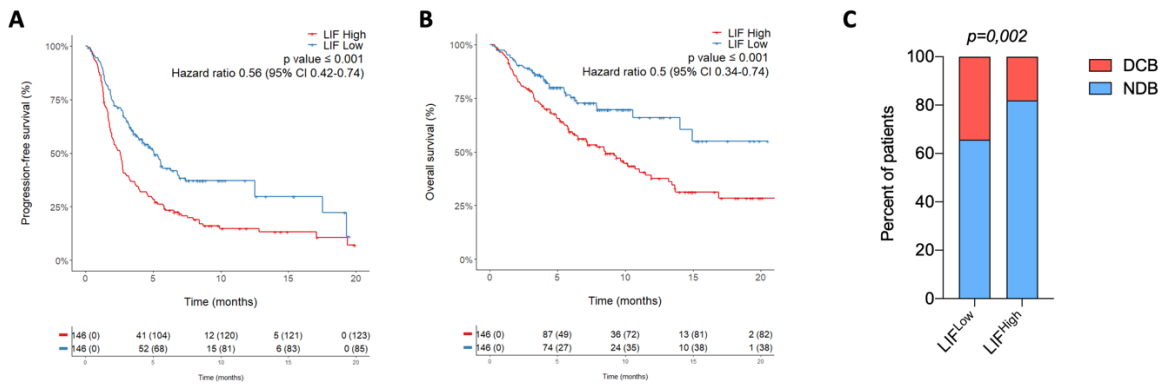

Figure 5. Baseline circulating LIF level is predictive of outcome of cancer patients treated with anti-PD(L)1 immunotherapy – results from an independent validation cohort. A Probability of PFS for LIF ^{High} (median survival = 2,57 mo.) and LIF ^{Low} (median survival = 5,07 mo.) patients in the Validation Cohort (n = 292). **B** Probability of OS for LIF ^{High} (median survival = 8,53 mo.) and LIF ^{Low} (median survival = NA) patients in the same patients cohort. **C** Proportion of patients who experienced DCB or NCB according to their baseline plasmatic level of LIF classified as High (above median value) and Low (below median value). P value was calculated through Chi-squared test.

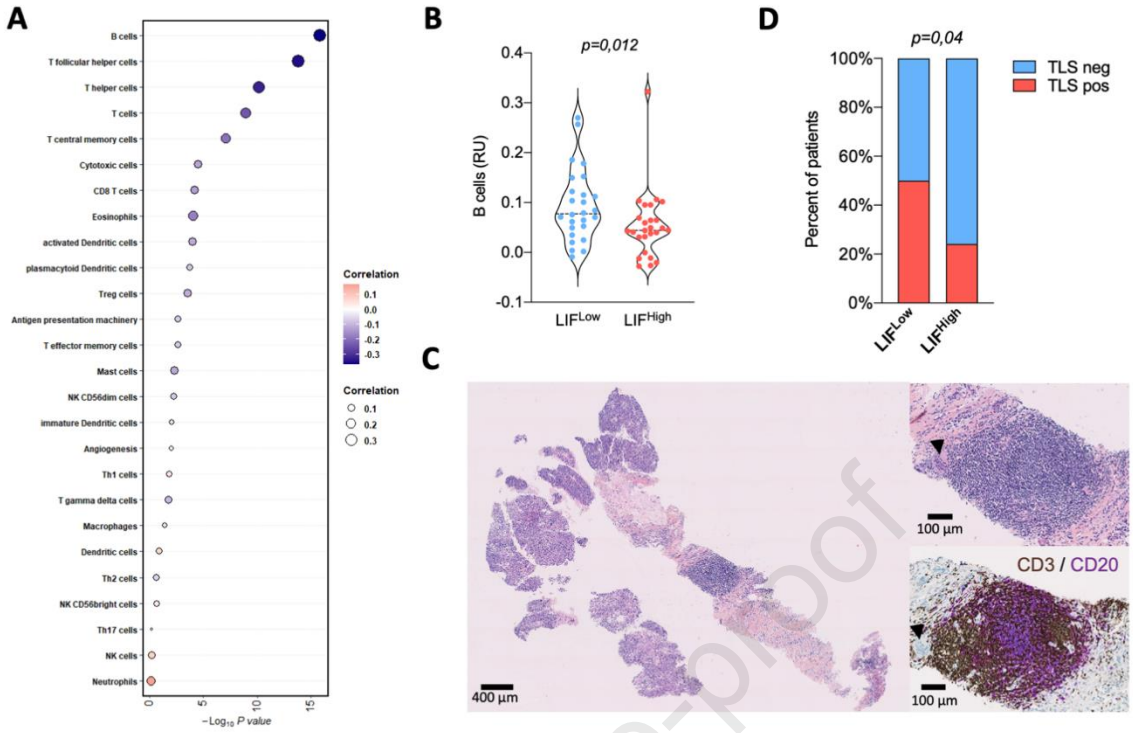

Figure 4. Peripheral LIF level is associated with an intratumoral B cell signature and presence of Tertiary Lymphoid Structures. A Correlation of immune cell lineages - obtained through RNA-sequencing and data deconvolution with Bindea algorithm - and LIF plasma level. Dot size depicts the correlation coefficient while the color is indicative of positive (red) or negative (blue) correlation. The X-axis represents the transformed Log10 pearson p-value. **B** Histogram representation of B cell score (in relative units, RU) according to baseline plasmatic level of LIF classified as High or Low (median value used as a cut-off). p value was calculated using a Wilcoxon Rank sum test. **C** Representative histological images from a patient with squamous cell lung carcinoma showing presence of TLS highlighted through both Hematoxylin Eosin Saffron (HES) staining and double staining of CD3-CD20 (CD3 in brown, CD20 in purple). Left image has been captured at a low magnification – scale bar indicates 400µm size – while the images on the right has been obtained through slide digitization at a higher magnification; scale bar indicates 100µm. Black arrow indicates tumor cells that juxtapose TLS. **D** Proportion of patients with presence or absence of intratumoral TLS according to baseline LIF plasma level. p value was calculated through Chi-squared test.

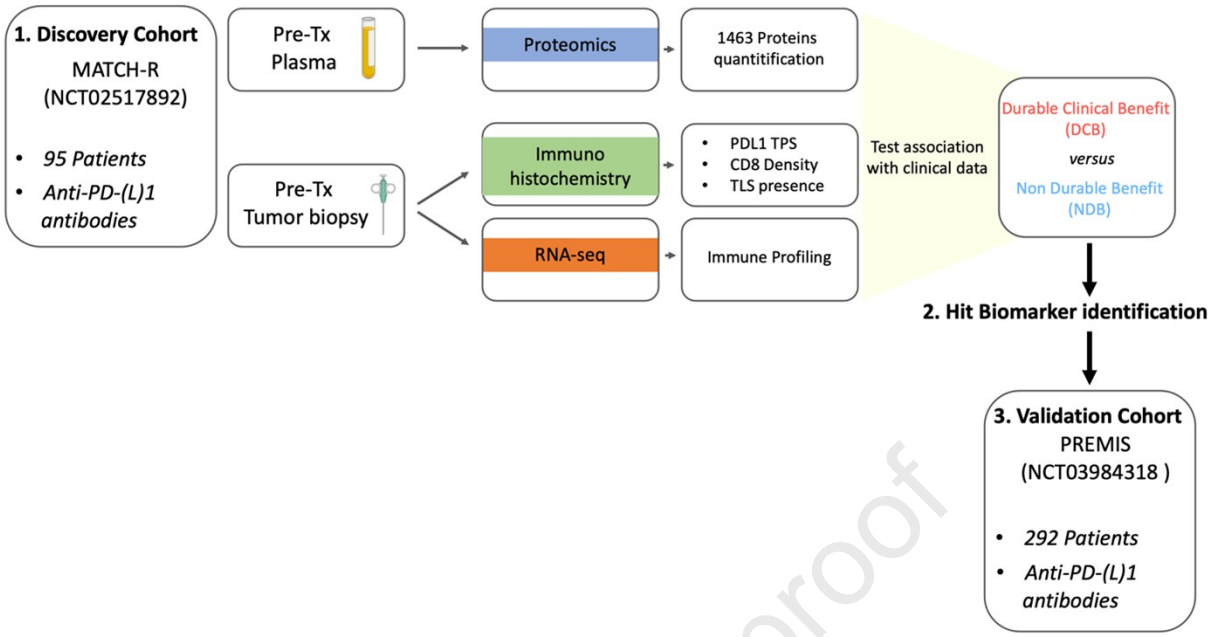

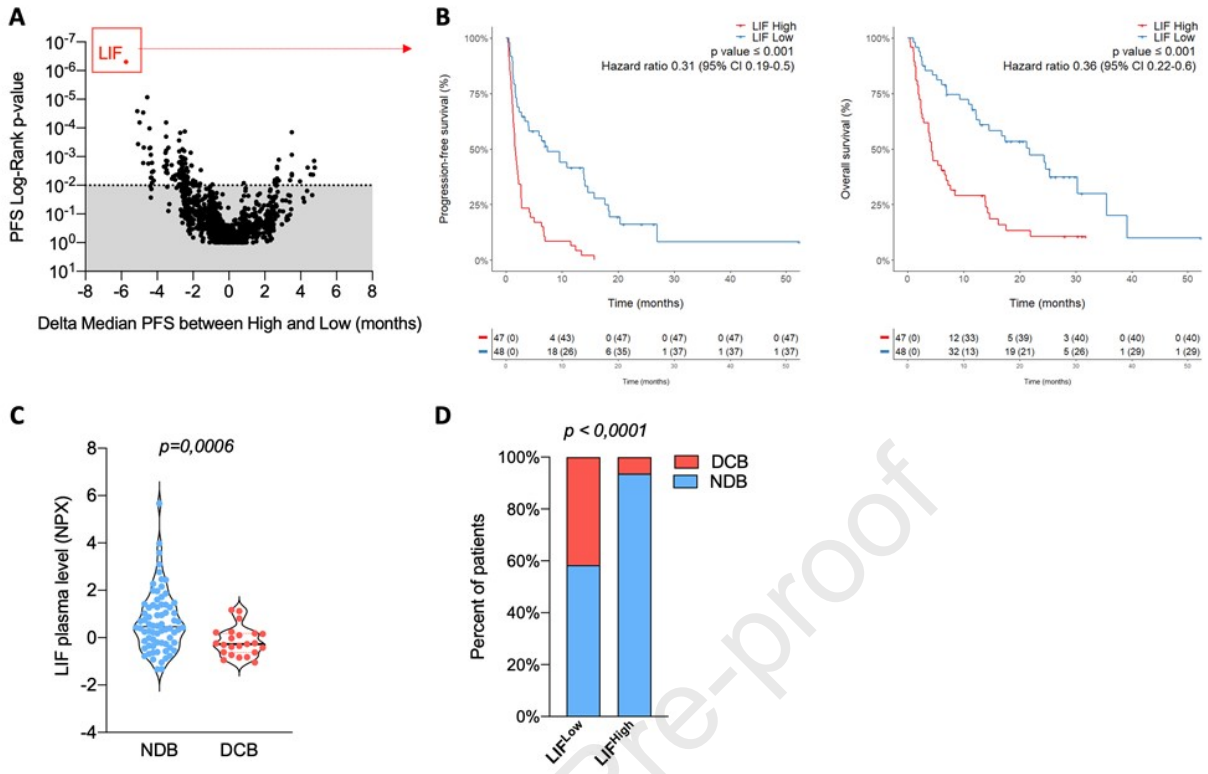

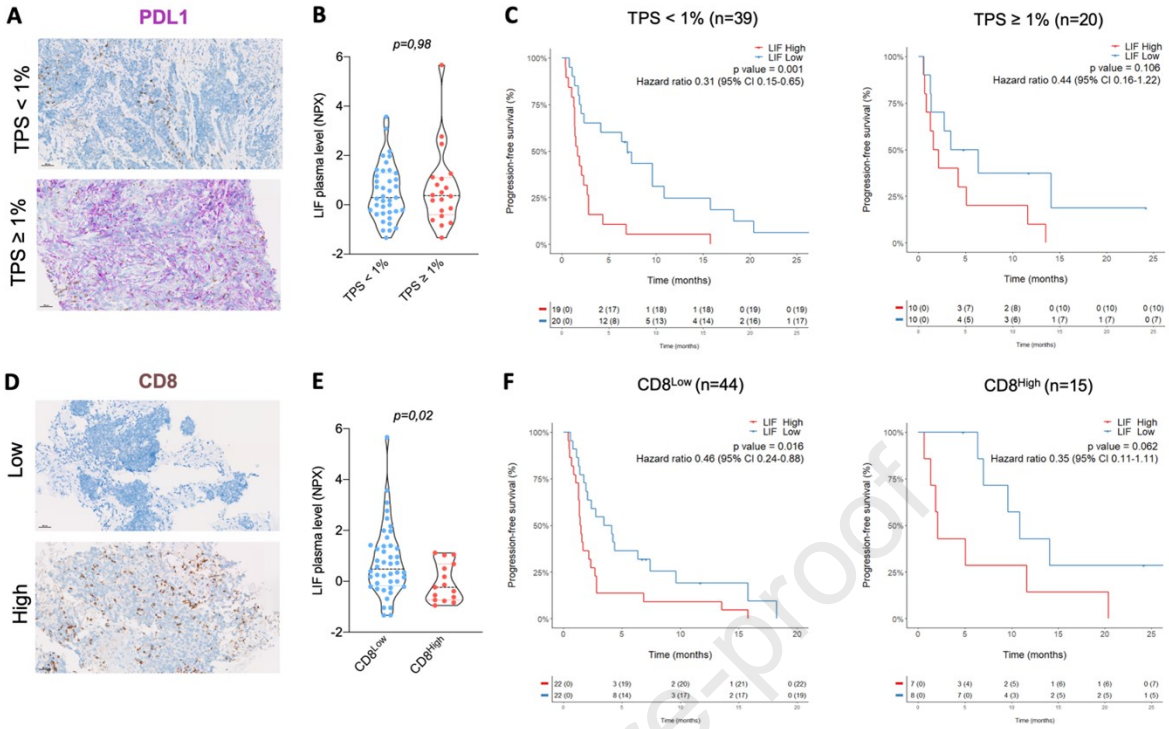

Danlos et al. *Cell Death and Disease* (2021)12:258
https://doi.org/10.1038/s41419-021-03540-y

Cell Death & Disease

ARTICLE Open Access

Metabolomic analyses of COVID-19 patients unravel stage-dependent and prognostic biomarkers

François-Xavier Danlos[1,2], Claudia Grajeda-Iglesias[3,4], Sylvère Durand[3], Allan Sauvat[3], Mathilde Roumier[5], Delphine Cantin[6], Emeline Colomba[7], Julien Rohmer[5], Fanny Pommeret[7], Giulia Baciarello[7], Christophe Willekens[8], Marc Vasse[9], Frank Griscelli[10], Jean-Eudes Fahrner[1,2], Anne-Gaëlle Goubet[1,2], Agathe Dubuisson[1,2], Lisa Derosa[1,7,11], Nitharsshini Nirmalathasan[3], Delphine Bredel[1], Séverine Mouraud[1], Caroline Pradon[12], Annabelle Stoclin[13], Flore Rozenberg[14], Jérôme Duchemin[15], Georges Jourdi[15,16], Syrine Ellouze[15], Françoise Levavasseur[17], Laurence Albigès[7], Jean-Charles Soria[18], Fabrice Barlesi[7,19], Eric Solary[2,8,20], Fabrice André[2,7,21], Frédéric Pène[17,22], Félix Ackerman[5], Luc Mouthon[17,23], Laurence Zitvogel[1,2,11], Aurélien Marabelle[1,2,11,24], Jean-Marie Michot[8,24], Michaela Fontenay[15,17] and Guido Kroemer[3,25,26,27,28]

Abstract

The circulating metabolome provides a snapshot of the physiological state of the organism responding to pathogenic challenges. Here we report alterations in the plasma metabolome reflecting the clinical presentation of COVID-19 patients with mild (ambulatory) diseases, moderate disease (radiologically confirmed pneumonitis, hospitalization and oxygen therapy), and critical disease (in intensive care). This analysis revealed major disease- and stage-associated shifts in the metabolome, meaning that at least 77 metabolites including amino acids, lipids, polyamines and sugars, as well as their derivatives, were altered in critical COVID-19 patient's plasma as compared to mild COVID-19 patients. Among a uniformly moderate cohort of patients who received tocilizumab, only 10 metabolites were different among individuals with a favorable evolution as compared to those who required transfer into the intensive care unit. The elevation of one single metabolite, anthranilic acid, had a poor prognostic value, correlating with the maintenance of high interleukin-10 and -18 levels. Given that products of the kynurenine pathway including anthranilic acid have immunosuppressive properties, we speculate on the therapeutic utility to inhibit the rate-limiting enzymes of this pathway including indoleamine 2,3-dioxygenase and tryptophan 2,3-dioxygenase.

Introduction

The year 2020 has been overshadowed by coronavirus disease-19 (COVID-19) caused by severe acute respiratory syndrome (SARS) coronavirus-2 (SARS-CoV-2), challenging the resilience of public and private health systems[1]. As a result, COVID-19 is mobilizing an unprecedented technological and scientific effort to diagnose, comprehend, and adequately treat the disease. Indeed, contagion by SARS-CoV-2 provokes a silent or pauci-symptomatic infection in at least 80% of patients, not requiring any treatment[2,3]. However, a substantial fraction of patients with pre-existing and often age-associated medical conditions (obesity, diabetes, hypertension, cardiomyopathy, hematological cancers, and general frailty) develop SARS, requiring hospitalization, oxygen supply, and for the most severe cases mechanical ventilation in the intensive care

Correspondence: Guido Kroemer (kroemer@orange.fr)
[1]INSERM U1015, Gustave Roussy Cancer Campus, 94800 Villejuif, France
[2]Université Paris Saclay, Faculté de Médecine, 94270 Le Kremlin-Bicêtre, France
Full list of author information is available at the end of the article
These authors contributed equally: François-Xavier Danlos, Claudia Grajeda-Iglesias
Edited by G. Melino

SPRINGER NATURE
CDDpress

unit[1,4,5]. Nonetheless, there is a substantial 'gray zone', meaning that physically fit and relatively young patients without known pre-existing pathologies may succumb to SARS-CoV-2, calling for the identification of biomarkers that predict COVID-19 severity and help management of patients[1,4,5].

Beyond genomic studies (to find COVID-19 susceptibility genes)[6], single-cell transcriptomics performed on circulating leukocytes (to identify inflammatory/ immune cell subsets involved in, and predictive of, COVID-19 pathogenesis)[7,8] and plasma proteomics (to pinpoint relevant cytokines)[9,10], metabolomics offers a functional, 'post-genomic' characterization of biochemical circuitries influenced by COVID-19 and its treatment. Indeed, a few studies have used mass spectrometric metabolomics to identify COVID-19-induced alterations in circulating metabolites, focusing on the correlation of such parameters with clinical presentation[10], circulating interleukin (IL)-6 concentrations[11] or male sex[12]. Additional studies have revealed a metabolomic signature of COVID-19 infection in circulating exosomes[13] and in the saliva[14].

Here, we report the results of two metabolomic studies, a first one, non-interventional, in which we correlate shifts in circulating metabolites with the severity stage of COVID-19 patients and a second study, interventional, in which we focus on patients with a uniformly moderate clinical presentation to identify metabolites whose alteration predicts clinical evolution. We identified anthranilic acid, a product of the kynurenine pathway, as a potentially prognostic biomarker of the evolution of COVID-19.

Results

COVID-19 stage-dependents shifts in the plasma metabolome

Targeted and untargeted metabolomics were performed using gas chromatography-mass spectrometry (GC-MS) and ultra-high-pressure liquid chromatography-mass spectrometry (UHPLC-MS) on plasma samples retrieved from a total of 72 patients with PCR-verified diagnosis of SARS-CoV-2 infection and compared to 27 ambulatory patients with flu-like symptoms, negative for SARS-CoV-2. Patients with COVID-19 were staged according to their clinical characteristics into mild (confinement at home, no complementary exams), moderate (standard hospitalization with a radiological diagnosis of pneumonitis, oxygen therapy <9 L/min), and critical (intensive care unit, oxygen therapy >9 L/min) cases. Clustering of mass spectrometry-detectable peaks revealed stage-associated shifts in the metabolome (Supplemental Fig. 1) that become clearly visible upon statistical filtering at $p < 0.05$ (Wilcoxon rank-sum test) and application of a false discovery rate of 0.05 following the Benjamini–Hochberg procedure to identify metabolites which were stringently different between critical and mild COVID-19 patients. Thus, 77 metabolites exhibited stage-dependent alterations in their plasma concentration (Fig. 1A). Among these metabolites, 57 were increased in critical care patients. Random forest classification model was built to rank the metabolites the upregulation or downregulation of which distinguished critical from mild patients (Fig. 1B). Among 30 metabolites, 29 were higher (and 1 lower) in critical than in mild cases, indicating a preponderance of upregulation ($p < 0.000044$, χ^2 analysis).

As described in the literature[3,4], critical COVID-19 patients were more overweighted, obese, diabetic, and hypertensive than mild COVID-19 and controls patients (Supplemental Table 1). Linear regression was used to control the differences in mean metabolites concentrations between critical and mild COVID-19 patients after adjustment for such comorbidities (Supplemental Table 2).

Specific changes associated with COVID-19 severity stages

A number of simple sugars including arabinose and ribose (and its reduction product ribitol), sugar alcohols (arabitol, erythritol and xylitol), the disaccharide maltose (which is undistinguishable from trehalose), and the trisaccharide raffinose were increased in critical cases (Figs. 1A and 2A and Supplemental Fig. 1A). Moreover, a series of amino acids were elevated in critical care patients: arginine, aspartic acid, glutamic acid, phenylalanine, and tyrosine. In addition, the methylated derivative of lysine, trimethyl-lysine, the methionine derivative (and methyl group donor) S-adenosylmethionine, and the dipeptide leucylproline were elevated (Figs. 1A and 2B), perhaps resulting from increased proteolysis. In contrast, desaminotyrosine was reduced in critical care patients (Figs. 1A and 2B), likely reflecting the use of antibiotics that inhibit the generation of this bacterial metabolite in the gut[15]. One of the few amino acids that decreased with disease severity is arginine, contrasting with an increase in ornithine, spermine, spermidine, and their mono- or diacetylated derivatives (Figs. 1A and 3A), suggesting enhanced polyamine synthesis from arginine. Moreover, tryptophan tended to diminish, while its immunosuppressive metabolite kynurenine increased in critical care patients as compared to mild cases. The kynurenine metabolite anthranilic acid was higher in critical as compared to moderate and mild COVID-19 patients (Figs. 1A and 3B). Of note, the elevation of anthranilic acid has not been found in another study that actually claimed that anthranilic acid decreased in COVID-19 patients as compared to controls[11]. Indeed, we found that another molecule that shared the same neutral monoisotopic mass (137.04768 Da) as anthranilic acid and that decreased in COVID-19 patients (annotated and validated as trigonelline, Supplemental Table 3), perhaps explaining the difference in the results. Since we compared the gas

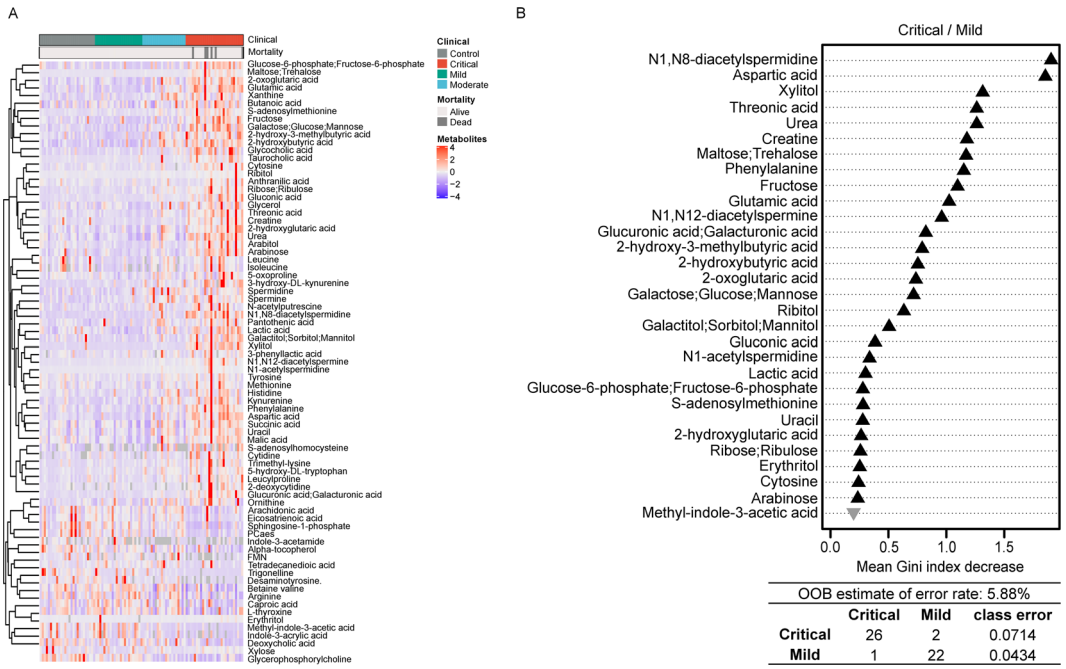

Fig. 1 Profound metabolomics alterations associated with COVID-19 clinical severity. A Heatmap illustrating the changes in metabolite abundance in the plasma from control ($n = 27$), mild ($n = 23$), moderate ($n = 21$), and critical ($n = 28$) COVID-19 patients. Significant metabolites were identified by Wilcoxon rank-sum test and the false discovery rate (FDR) controlled with Benjamini–Hochberg procedure between patients with critical and mild COVID-19. Hierarchical clustering (Euclidean distance, ward linkage method) of the metabolite abundance is shown. PCaes, total abundance of the different phosphatidylcholines identified in the cohort plasma samples. **B**, Random forest classification model was built using main metabolites altered ($p < 0.05$) between critical and mild COVID-19 patients as a predicting tool. The variables importance (as the mean decrease of the Gini index) for building the model is reported in a dot plot, with dots substituted by an up-pointing triangle to indicate metabolites increased in critical vs mild COVID-19 patients, and by a down-pointing triangle in the opposite case (**B**), the confusion matrix (indicating model accuracy) is depicted below. OOB out-of-bag error.

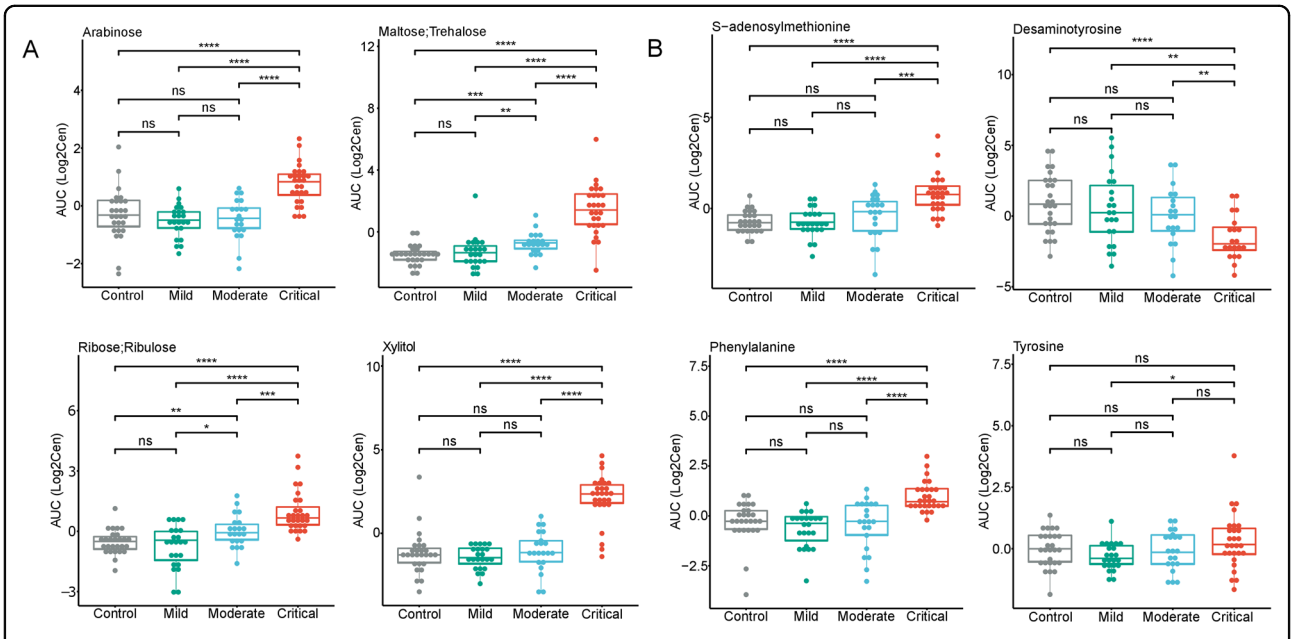

Fig. 2 Effects of COVID-19 on circulating sugars and amino acids. Modified carbohydrates (**A**) and amino acids (**B**) were profoundly altered in patients with the most severe COVID-19. Data in **A** and **B** were analyzed by non-parametric unpaired Wilcoxon test (Mann–Whitney) for each two-group comparison. *$p < 0.05$, **$p < 0.01$, ***$p < 0.001$, ****$p < 0.0001$.

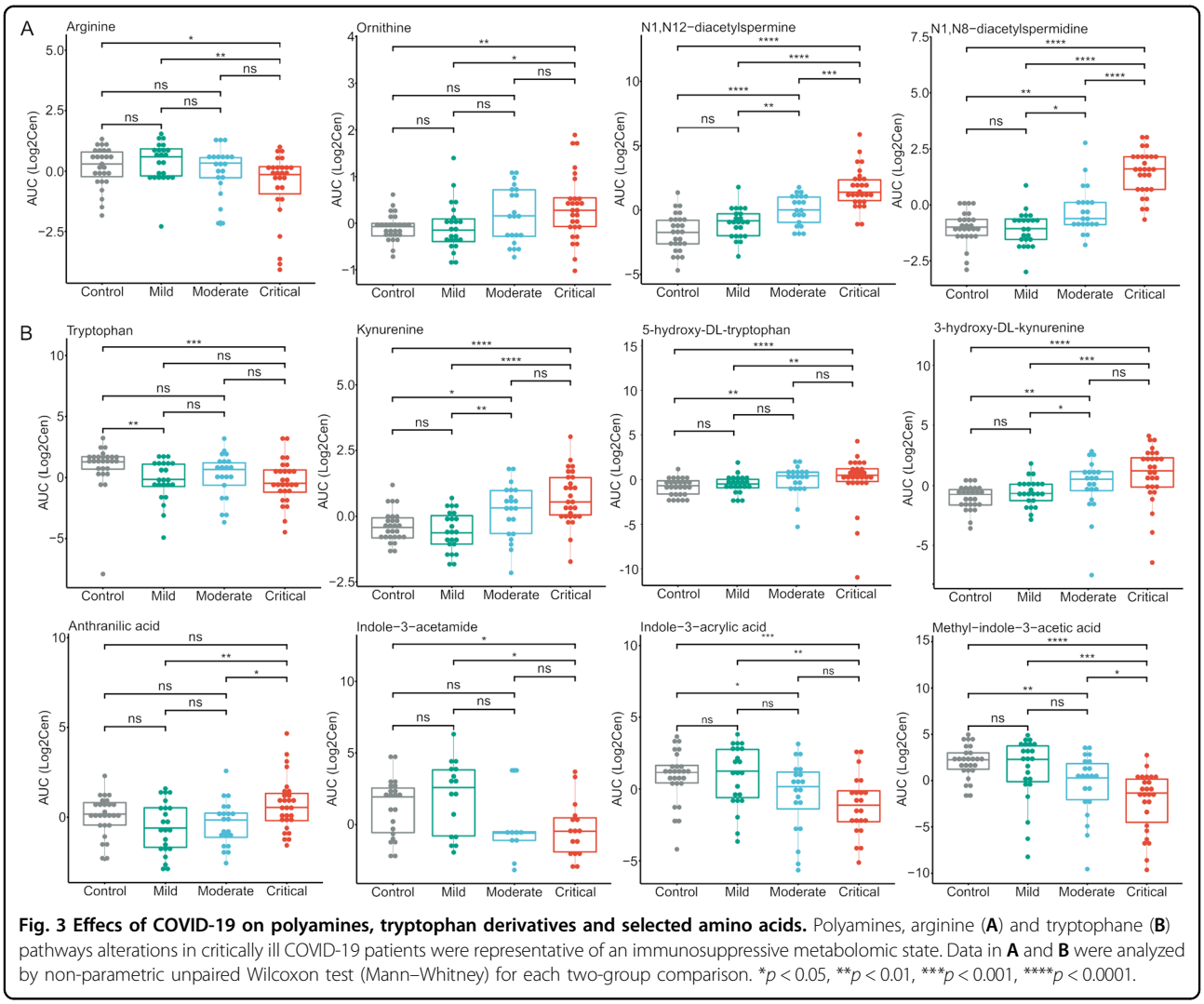

Fig. 3 Effecs of COVID-19 on polyamines, tryptophan derivatives and selected amino acids. Polyamines, arginine (**A**) and tryptophane (**B**) pathways alterations in critically ill COVID-19 patients were representative of an immunosuppressive metabolomic state. Data in **A** and **B** were analyzed by non-parametric unpaired Wilcoxon test (Mann–Whitney) for each two-group comparison. *$p < 0.05$, **$p < 0.01$, ***$p < 0.001$, ****$p < 0.0001$.

chromatographic retention time of the derivatized analytes to standards (Supplemental Fig. 2), we conclude that anthranilic acid is indeed increased in severe COVID-19. We also found that 3-hydroxy-DL-kynurenine, which his produced from kynurenine by the enzyme kynurenine 3-hydroxylase, and 5-hydroxy-DL-tryptophan, which is produced from tryptophan by the enzyme tryptophan 5-monooxygenase, were increased, correlating with the severity of COVID-19 (Fig. 3B).

Bacterial breakdown products of tryptophan, such as indole, indole-acetamide, indole-3-acrylic acid, and methyl-3-indole-acetate were significantly reduced in critical care patients (Figs. 1 and 3B). Other important metabolic changes affected free fatty acids (arachidonic acid) or carnitine esters, phospholipids, the immunomodulator spingosine-1-phosphate, the secondary bile acid deoxycholic acid, as well as the niacin metabolite trigonelline, that all diminish with disease severity, contrasting with markers of reduced renal clearance (creatine, urea) that increase (Fig. 1A). Altogether, a specific pattern of stage-dependent alterations in the metabolome emerges.

Prognostic alterations in the circulating metabolome

The aforementioned results indicate that the progression of COVID-19 is associated with major metabolic shifts, yet do not allow to identify prognostic biomarkers. For this, we recruited a group of 25 patients that were hospitalized in standard conditions (not in the ICU) and were relatively homogeneous in their clinical presentation (Fig. 4A and Supplemental Tables 4 and 5). After the initial determination of their circulating metabolome and the quantitation of serum cytokines ($n = 21$), these patients received standard of care treatments plus tocilizumab. Unfavorable evolution of the COVID-19 (9 out of 21 patients) was defined as a clinical deterioration with WHO progression scale >5,

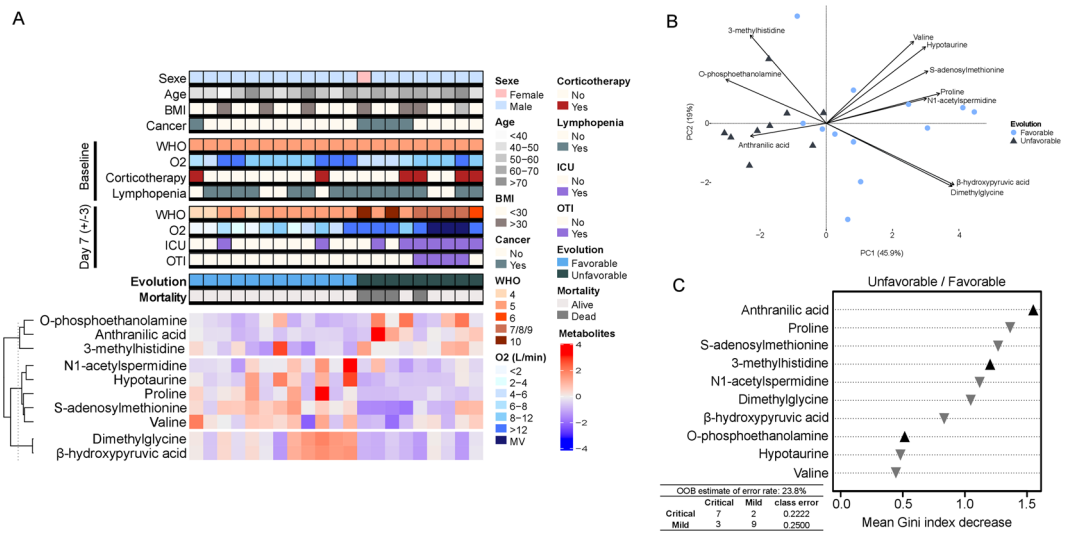

Fig. 4 Patients with unfavorable clinical evolution after tocilizumab, infused for worsening pulmonary involvement of COVID-19, had pre-treatment metabolomics differences compared to patients with favorable outcome. A Heatmap illustrating pre-tocilizumab metabolite abundance in COVID-19 patients evaluable for clinical evolution after treatment ($n = 21$). Significant metabolites were identified by Wilcoxon rank-sum test between patients with favorable and unfavorable evolution after tocilizumab infusion. BMI Body Mass Index, WHO World Health Organization, O2 oxygenotherapy, ICU intensive care unit, OTI orotracheal intubation. **B** Principal component analysis biplot, showing the contribution of the most significant metabolites ($p < 0.05$) to the discrimination (PC1 45.9%) between patients with favorable and unfavorable evolution after tocilizumab infusion. **C** Random forest classification model was built using main metabolites altered ($p < 0.05$) in baseline samples from COVID-19 patients with favorable and unfavorable evolution after tocilizumab treatment as a predicting tool. The variable importance (as the mean decrease of the Gini index) for building the model is reported in a dot plot, with dots substituted by an up-pointing black triangle to indicate metabolites increased in patients who showed unfavorable vs favorable evolution, and by a gray down-pointing triangle in the opposite case. The confusion matrix (indicating model accuracy) is depicted. OOB out-of-bag error.

transfer to ICU, mechanical ventilation, or death[16]. Inspection of the global metabolomic profiles did not revealed any major shift that would distinguish the favorable versus unfavorable evolution of COVID-19 neither at baseline nor at day 7 (Supplemental Fig. 3 and Supplemental Tables 6 and 7). Only 10 metabolites were significantly different between patients that demonstrated favorable versus unfavorable evolution (Fig. 4A). However, they allowed a good discrimination between groups (PC1 45.9%) according to their abundance variation (Fig. 4B and Supplemental Fig. 5). To find out the variable importance of these metabolites, we used a random forest classification model. Although the model was limited because of the reduced number of individuals in the study, it showed that, among the most significant metabolites, the upregulation of anthranilic acid coupled to the diminution of S-adenosylmethionine and proline stood out as parameters that allowed to distinguish the unfavorable and favorable evolution of COVID-19 patients respectively (Fig. 4C). Dimethylglycine, ß-hydroxypyruvate, N1-acetylspermidine, hypotaurine, and valine were significantly lower in patients with an unfavorable evolution, while 3-methylhistidine and O-phosphoethanolamine were higher, but these changes had a lower impact according to the random forest classification (Fig. 4B).

Prognostic immunometabolic correlations

None of the 10 cytokines measured at baseline did exhibit significant differences between the patients with favorable and unfavorable clinical evolution (Supplemental Fig. 4), in line with the similar clinical presentation of the patients. At difference with patients that exhibited an unfavorable evolution, patients who ameliorated their condition exhibited an increase in total lymphocyte counts (Fig. 5A), a decrease in the inflammatory cytokine interleukin (IL)-18 (IL18) (Fig. 5B), a reduction in the immunosuppressive factor IL10 (Fig. 5C) and an increase in circulating tryptophan levels (Fig. 5D). Correlation plots revealed a median correlation (all values positive) among cytokines of 0.1573, between cytokines and metabolites of 0.2116, and among metabolites of 0.3702 (which was significantly higher than the intragroup correlation and the correlation among cytokines, $p < 0.0001$, Mann–Whitney test), suggesting a more robust coordination of metabolic as compared to inflammatory pathways (Fig. 6A). IL8 correlated with N1-acetylspermidine and hypotaurine, tumor necrosis factor-α (TNFα) with O-phosphoethanolamine (Fig. 6A), and anthranilic acid with both IL10 and IL18 (Fig. 6B) at baseline, before the initiation of the treatment. This latter correlation appears particularly intriguing because anthranilic acid is ranked as the best negative

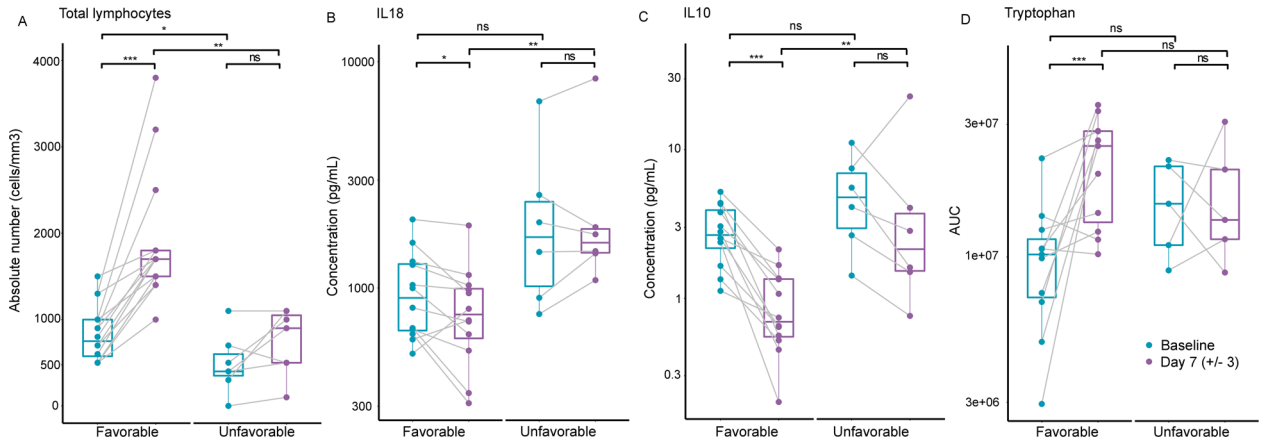

Fig. 5 COVID-19 Patients with unfavorable outcome after tocilizumab infusion did not improved lymphopenia, inflammatory, immunosuppressive, and metabolomic abnormalities instead of patients who evolved towards clinical improvement. Patients with paired baseline and post treatment (day 7 ± 3) serum samples are represented ($n = 18$). The measured parameters include total lymphocyte counts (**A**) as well as the concentrations of IL18 (**B**), IL10 (**C**) and tryptophan (**D**). Wilcoxon signed-rank test was used to compare paired baseline and post treatment measures and Wilcoxon rank-sum test to compare baseline or day 7 (±3) measures between patients with response or no response. *$p < 0.05$, **$p < 0.01$, ***$p < 0.001$, ****$p < 0.0001$.

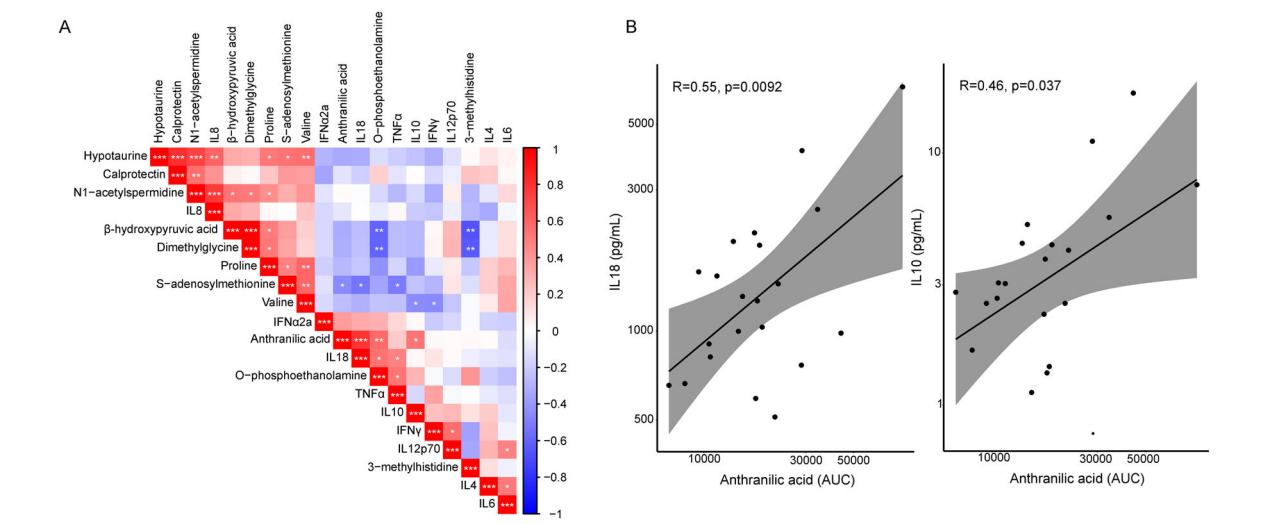

Fig. 6 Correlations between cytokines and metabolites before tocilizumab infusion in patients with worsening COVID-19 highlighted that dysregulated metabolomic and immunologic pathways were closely related to clinical worsening of patients developing critical COVID-19. A Correlation between cytokines and most significant metabolites at baseline was analyzed by Pearson correlation. *$p < 0.05$, **$p < 0.01$, ***$p < 0.001$. **B** Pearson correlations between IL10 and IL18 with anthranilic acid serum levels.

prognostic marker (Fig. 4B) and both IL10 and IL18 remain elevated in the context of an unfavorable evolution (Fig. 5).

Discussion

The present study has been designed to unravel COVID-19 stage-dependent and prognostic alterations in the circulating metabolome. Strong shifts across multiple classes of metabolites were observed among different stages of COVID-19, from mild through moderate to critical disease. These shifts reflect in part iatrogenic effects such as the apparent improvement of the nutritional state (with higher levels of circulating sugars but lower levels of free fatty acids and ketone bodies, which would be indicative of acute undernutrition) in the critical stage and the reduction of bacterial metabolites (such as the tyrosine metabolite desaminotyrosine and the tryptophane metabolites indole, indole-3-acetamide, indole-3-acrylic acid, and methyl-3-indole-acetate), likely resulting

from the administration of broad-spectrum antibiotics. Other metabolomic shifts may reflect proteolysis (with an increase in free amino acids and amino acid derivatives), as well as ongoing organ failure affecting the kidney (enhanced acetyl polyamine, creatine, and urate levels) and the liver (reduced primary bile acid production).

Most intriguingly, however, COVID-19 appears to be associated with metabolic signs of immunosuppression, as indicated by the increase of kynurenic acid and anthranilic acid. Tryptophan was diminished in mild and critical COVID-19 patients compared to uninfected controls, suggesting a disease-associated activation of tryptophan-consuming indoleamine 2,3-dioxygenase (IDO) and tryptophan 2,3-dioxygenase (TDO) that produce the kynurenic acid precursor kynurenine[17]. Anthranilate is a downstream metabolite of kynurenine[18], with marked immunosuppressive effects[19]. Previous work has identified an activation of the kynurenine pathway (though without an elevation of anthranilate) in COVID-19 patients, correlating with an elevation of IL6 levels[11], which in turn are associated with poor prognosis[20–23].

Small, but specific differences were observed in a cohort of patients that demonstrated a similar clinical stage at presentation, but dissimilar evolution during hospitalization. Some metabolites that apparently were not COVID-19 stage-associated were different between patients that demonstrated a favorable or unfavorable evolution. This applies to dimethylglycine, 3-methylhistidine and O-phosphoethanolamine, proline, and valine. Some metabolites exhibited a behavior that can be classified as 'paradoxical'. Thus, N1-acetylspermidine, S-adenosylmethionine, and hypotaurine that are highest among severe COVID-19 patients are associated with favorable prognosis, perhaps because their production reflects an attempt to attenuate the pathogenesis of COVID-19. Indeed, in preclinical models, the N1-acetylspermidine precursor, spermidine, has marked anti-inflammatory and immunostimulatory effects[24–27]. Administration of S-adenosylmethionine attenuates the cytokine storm induced by bacterial sepsis[28] and mediates immunostimulatory effects in a cancer model[29]. Clinical trials have demonstrated that taurine, the downstream metabolite of hypotaurine, decreases serum markers of inflammation including C-reactive protein[30], which is a negative prognostic marker of COVID-19[31].

In sharp contrast to these 'paradoxical' associations, one metabolite exhibited a 'concordant' behavior. This applies to anthranilic acid, the concentration of which increases with disease severity and which also predicts unfavorable prognosis. This observation places the kynurenine pathway in the limelight of this study. Larger prospective studies are required to validate the conjecture that metabolomic profiling and specific measurement of selected metabolites including anthranilic acid may predict the fate of COVID-19 patients. Circulating anthranilic acid levels reportedly correlate with hyperleptinemia in schizophrenia[32] and are increased in the plasma of patients with type-1 (but not type-2) diabetes[33] and subgroups of patients with chronic liver disease[34], calling for additional investigations of possible confounding factors. Irrespective of these considerations, it might be worthwhile to explore the experimental treatment of COVID-19 with IDO and TDO inhibitors that are in clinical development[35–38]. Such inhibitors have been generated as immune checkpoint inhibitors for the treatment of cancer, but have not yet received regulatory approval. The fact that high levels of anthranilic acid predict the maintenance of high levels of IL10 and IL18 suggests (but does not prove) that the kynurenine pathway has an immunomodulatory impact on COVID-19 pathogenesis. However, this speculation should be tested by treating anthranilic acid-high COVID-19 patients with IDO/TDO or other kynurenine pathway inhibitors within a dedicated Phase 2 clinical trial.

Methods

Patients

All patients were recruited by different hospitals of the Assistance Publique Hôpitaux de Paris (AP-HP) network or at Foch Hospital or Gustave Roussy. The non-interventional study was approved by institutional review boards (IRB) of Cochin-Port Royal (Paris, France) hospital and the ethical committee of Cochin-Port Royal Hospital (CLEP Decision N: AAA-2020-08023), and conformed to the principles outlined in the Declaration of Helsinki. Controls ($n = 29$) were symptomatic patients who were seen at the Hôtel-Dieu screening unit and were negative for SARS-CoV-2 RT-PCR on pharyngeal swab. Mild COVID-19 patients ($n = 23$) were defined by having limited clinical symptoms (fever, cough, diarrhea, myalgia, and anosmia/ageusia) that did not require CT scan or hospitalization. Moderate cases ($n = 21$) were defined as symptomatic patients with dyspnea and radiological findings of pneumonia on thoracic CT scan, requiring hospitalization and a maximum of 9 L/min of oxygen. Critical patients ($n = 28$) were those hospitalized in the ICU with respiratory distress requiring 10 L/min of oxygen or more, without or with endotracheal intubation and mechanical ventilation. "Comorbidities" variable for adjustment was considered for patients with obesity or diabetes or chronic kidney disease and hypertension.

The interventional study was approved by the Foch IRB (approval number IRB00012437) and was registered on the National Institute of Health data platform INDS (no 4710280420). Patients received tocilizumab, in an off-label use setting, to treat severe COVID-19, at Gustave Roussy and Foch Hospital, over the period of March 20 and 5 April 2020. Inclusions criteria were: (i) Patients who received at least one dose of tocilizumab, as treatment of

COVID-19. (ii) ≥18 years, informed, and not opposed for retrospective use of their anonymized health care files. (iii) Diagnosis of COVID-19 confirmed by RT-PCR test, with respiratory symptoms, shortness of breath and requirement of oxygen therapy and pulmonary images compatible with COVID-19. (iv) Patients at risk of developing respiratory distress due to COVID-19, with worsening of oxygen therapy supplementation equal or more than 4 L/min and requirement by increase of >50% of the need for supplemental oxygen therapy in the last 24 h before first dose of tocilizumab. Exclusion criteria for evaluable population for the response to tocilizumab were: (i) Patients placed under mechanical ventilation with intubation due to the COVID-19 before the first dose of tocilizumab treatment. (ii) Respiratory failure related to other cause than COVID-19 at tocilizumab initiation. (iii) Patients, who have previously received anti-IL6 receptor therapy in the last 3 weeks before tocilizumab initiation. (iii) Alanine transaminase/aspartate transaminase (ALT/AST) >5 times the upper limit of normal at timing of first dose of tocilizumab. (iv) Absolute neutrophil count $<1.0 \times 10^9$ or platelets $<50 \times 10^9$ at timing of first dose of tocilizumab. Tocilizumab was given intravenously at 8 mg/kg and could be repeated once in the following 48 h if necessary. All patients were followed until day 30 after the first dose of tocilizumab. Patients' sera were collected and stored before and after treatment. Favorable clinical evolution after tocilizumab infusion was retained in patients evaluable for the outcome and fulfilling the following three criteria. Criterion 1: on day 14 post first dose of tocilizumab, the patient has a WHO progression scale ≤ 5[16]. Criterion 2: between days 1 and 14 after the first dose of tocilizumab, the patient is alive and did not need to have at any time recourse to invasive mechanical ventilation (orotracheal intubation) and without any new intention of "non-realization of resuscitation or ventilation". Criterion 3: the respiratory symptoms related to COVID-19 clinically significantly improved with decrease in oxygen requirements after first dose of tocilizumab and the WHO scale did not deteriorate after the administration of the first dose of tocilizumab.

Sampling

Human peripheral blood from the first cohort was collected into sterile dry vacutainer tubes with 3.2% buffered sodium citrate solution. Samples were centrifuged twice (2500 × *g*/20 min), and plasma was collected. Regarding the samples from the interventional study, human peripheral blood was collected into sterile dry vacutainer tubes and centrifuged (1500–2000 × *g*/15 min) for serum collection. Fifty microliters of sample were mixed with 500 µL of a cold solvent mixture (meOH/water, 9/1, −20 °C, with a cocktail of internal standards), vortexed and centrifuged (10 min at 1500 × *g*, 4 °C) for metabolite extraction and protein precipitation. The supernatants were collected, split in 4 fractions, and treated according to the protocols described previously[39]. Briefly, 2 fractions of 120 µL each (1st and 2nd fractions, respectively) of sample extract were transferred to an injection amber glass vial (with fused-in insert) and evaporated to dryness (Techne DB3, Staffordshire, UK) at 40 °C. The 1st dried fraction was solubilized in 50 µL of methoxyamine (CAS 593-56-6; 20 mg/mL in pyridine, Sigma-Aldrich), and left to incubate overnight, at room temperature and protected from light. The next day, derivatization was carried out by adding 80 µL of MSTFA (CAS 24589-78-4; Supelco), followed by 30 min-incubation at 40 °C. Derivatized samples were immediately used for GC/MS injection and analysis. The 2nd dried fraction was recovered with 100 µL of ultra-pure water and kept at −80 °C until injection and analysis by UHPLC/MS. The 3rd fraction consisted of 40 µL of sample extract transferred to an injection amber glass vial (with fused-in insert) for derivatization and SCFA analysis. Sample derivatization was carried out by adding 20 µL of 3-NPH (200 mM in meOH; CAS 636-95-3; Sigma-Aldrich) and 20 µL of EDC (150 mM in meOH; CAS 25952-53-8; Sigma-Aldrich) to the sample. Immediately after incubation (1 h/ 40 °C), 80 µL of water were added, and the derivatized samples were used for UHPLC/MS injection and analysis. Finally, the 4th fraction together with the sample pellet were re-extracted with 80 µL of 2% SSA (in meOH), vortexed and centrifuged (10 min at 15,000 × *g*, 4 °C). The supernatant (200 µl) was transferred to an injection polypropylene vial (with fused-in insert) and evaporated to dryness (Techne DB3, Staffordshire, UK) at 40 °C. Dried samples were recovered with 200 µl of ultra-pure water and kept at −80 °C until injection and analysis by UHPLC/MS for polyamines detection.

Cytokine measurements

Serum samples were monitored using the V-plex Proinflammatory panel 1 Human kit (Meso Scale Discovery, ref: K15049D) according to the manufacturer's instructions, for the measurement of IFNγ, IL1β, IL2, IL4, IL6, IL8, IL10, IL12p70, IL13, and TNFα. Soluble Calprotectin (diluted 1:100), IFNα2a and IL18 were analyzed using a R-plex Human Calprotectin Antibody Set (Meso Scale Discovery, ref: F21YB), the ultra-sensitive assay S-plex Human IFNa2a kit (Meso Scale Discovery, ref: K151P3S) and the U-plex Human IL18 assay (Meso Scale Discovery, ref: K151VJK), respectively, following manufacturer's instructions. Acquisitions and analyses of soluble cytokines and calprotectin were performed on a MESO QuickPlex SQ120 reader and the MSD's Discovery Workbench 4.0. Each serum sample was assayed twice with the average value taken as the result.

Widely targeted analysis of intracellular metabolites

GC/MS

Derivatized samples for GC/MS analysis (1st fraction) were injected (1 µL) into a gas chromatograph (Agilent 7890B; Agilent Technologies, Waldbronn, Germany) coupled to a triple quadrupole mass spectrometer (QQQ/MS; 7000C Agilent Technologies, Waldbronn, Germany), equipped with a high sensitivity electronic impact source (EI) operating in positive mode. Injection was performed in splitless mode. Front inlet temperature was kept at 250 °C, transfer line and ion-source temperature were 250 °C and 230 °C, respectively. Septum purge flow was fixed at 3 mL/min, purge flow to split vent operated at 80 mL/min during 1 min and gas saver mode was set to 15 mL/min after 5 min. Helium gas flowed through column (HP-5MS, 30 m × 0.25 mm, i.d. 0.25 mm, d.f. J&WScientific, Agilent Technologies Inc.) at 1 mL/min. Column temperature was held at 60 °C for 1 min, raised to 210 °C (10 °C/min), then to 230 °C (5 °C/min), to finally reach 325 °C (15 °C/min), and hold at during 5 min. Collision gas was nitrogen.

UHPLC/MS

Targeted UHPLC/MS analyses were performed on a RRLC 1260 system (Agilent Technologies, Waldbronn, Germany), with an autosampler kept at 4 °C, and a peltier oven for rigorous control of the column temperature. The UHPLC was coupled to a QQQ/MS 6410 (Agilent Technologies) equipped with an electrospray source, using nitrogen as collision gas. For bile acids detection, 10 µL from samples recovered in water (2nd fraction) were injected into a Poroshell 120 EC-C8 (100 mm × 2.1 mm particle size 2.7 µm; Agilent technologies) column protected by a guard column (XDB-C18, 5 mm × 2.1 mm particle size 1.8 µm). Mobile phase consisted of 0.2% formic acid (A) and ACN/IPA (1/1; v/v) (B) freshly made. Flow rate was set to 0.3 mL/min, and gradient as follow: 30% B during 1.5 min; increased to 60% B over 9 min; and finally to 98% B for 2 minutes (column washing), followed by 2 min of column equilibration at 30% B (initial conditions). After each injection, needle was washed twice with IPA and thrice with water. The QQQ/MS was operated in negative mode. Gas temperature and flow were set to 325 °C and 12 L/min, respectively. Capillary voltage was set to 4.5 kV.

Derivatized samples for SCFA detection (3rd fraction) were injected (10 µL) into a Zorbax Eclipse XBD C18 (100 mm × 2.1 mm particle size 1.8 µm; Agilent technologies) column, protected by a guard column (XDB-C18, 5 mm × 2.1 mm particle size 1.8 µm). Column oven maintained at 50 °C during analysis. Mobile phase consisted of 0.01% formic acid (A) and ACN (0.01% formic acid) (B). Flow rate was set to 0.4 mL/min, and gradient as follow: 20% B during 6 min; increased to 45% B over 7 min; and finally to 95% B for 5 minutes (column washing), followed by column equilibration phase at 20% B, during 4 min. The QQQ/MS was operated in negative mode. Gas temperature was set to 350 °C with a gas flow of 12 L/min. Capillary voltage was set to 4.0 kV.

Polyamines were detected in the 4th fraction after injection of 10 µL of sample were into a Kinetex C18 (150 mm × 2.1 mm particle size 2.6 µm; Phenomenex) column protected by a guard column C18 (5 mm × 2.1 mm, particle size 1.8 µm). Column oven maintained at 40 °C during analysis. The gradient mobile phase consisted of 0.1% HFBA (Sigma-Aldrich) (A) and ACN (0.1% HFBA) (B) freshly made. The flow rate was set to 0.2 ml/min, and gradient as follow: from 5% (initial conditions) to 40% B in 10 min; then 90% B maintained 2.5 min, and finally equilibration to initial conditions, 5% B, for 4 min. The QQQ/MS was operated in positive mode. The gas temperature was set to 350 °C with a gas flow of 12 l/min. The capillary voltage was set to 3.5 kV. At the end of each UHPLC/MS batch analysis, column was rinsed with 0.3 mL/min of ultra-pure water (A) and ACN (B) as follow: 10% B during 20 min, to 90% B in 20 min, and maintained during 20 min before shutdown. MRM scan mode was used for targeted analysis in both GC and UHPLC/MS. Peak detection and integration were performed using the Agilent Mass Hunter quantitative software (B.07.01).

Pseudo-targeted analysis of intracellular metabolites

The profiling analysis was performed with a Dionex Ultimate 3000 UHPLC system (Thermo Scientific) coupled to an Orbitrap mass spectrometer (q-Exactive, Thermo Fisher Scientific) equipped with an electrospray source operating in both positive and negative mode, and acquired samples in full scan analysis mode, from 100 to 1200 m/z. LC separation was performed on reversed phase (Zorbax Sb-Aq 100 ×2.1 mm × 1.8 µm particle size), with mobile phases: 0.2% acetic acid (A) and ACN (B). Column oven was kept at 40 °C. Ten microliters of aqueous sample (2nd fraction) were injected for metabolite separation with a gradient starting from 2% B, increased to 95% B in 22 min, and maintained during 2 min for column rinsing, followed by column equilibration at 2% B for 4 min. Flow rate was set to 0.3 mL/min. The q-Exactive parameters were: sheath gas flow rate 55 au, auxiliary gas flow rate 15 au, spray voltage 3.3 kV, capillary temperature 300 °C, and S-Lens RF level 55V. The mass spectrometer was calibrated with sodium acetate solution dedicated to low mass calibration. Data were treated by the quantitative node of Thermo Xcalibur™ (version 2.2) in a pseudo-targeted approach with a home-based metabolites list.

Untargeted analysis of intracellular metabolites

Raw data files obtained by the previously described pseudo-targeted analysis were also used to perform unbiased

profiling analysis, using the Thermo Compound Discoverer (3.1.). After sample injection and data acquisition, raw data files were processed following a customized node-based workflow for identifying unknown compounds in metabolomics. Spectra selection and retention time alignment were performed, followed by removal of background noise and baseline correction. Next, the processing workflow found chromatographic peaks for unknown compounds (molecular weight, MW, x retention time, RT) extracting all relevant spectral and chromatographic information, to predict the elemental composition of the unknowns. All data was exported to R software (version 3.4) for data representation.

Statistical analysis

All targeted and pseudo-targeted treated data were merged and cleaned with a dedicated R (version 3.4) package (@Github/Kroemerlab/GRMeta). Calculations and statistical tests were performed using R v3.4. Wilcoxon-Mann–Whitney test was used to assess differences in concentration between two different groups. When indicated, the false discovery rate (FDR, $p > 0.05$) was controlled using the Benjamini–Hochberg procedure. Data representation was performed with softwares R v3.6 and Rstudio v1.2.1335 using tidyverse, dplyr, ggplot2, ggpubr, complexheatmap, and corrplot packages. Principal component analysis biplot was built using FactoMineR and factoextra packages, after selection of the metabolites significantly different ($p < 0.05$) between clinical evolution groups ("unfavorable" and "favorable"), at baseline. Data were scaled unit variance before the analysis.

Determination of most discriminating metabolites with Random Forest Classification Model

Selected metabolites were thereafter used for training a random forest classification model using the R *caret* package. This machine learning tool allowed to classify the relative importance of metabolites for distinguishing COVID-19 stage (here classified in a binary fashion as «critical» and «mild») and clinical evolution ("unfavorable" and "favorable"), by computing the mean decrease of the Gini index (an entropy-like measure of the impurity) over the random forest nodes that were split on them.

Acknowledgements

We thanks Mme Chifaou Mohamed-Djalim (INSERM U1015, Gustave Roussy), Dr Elise Sourdeau (Service d'accueil des urgences, AP-HP, Hôtel Dieu), Dr Tali-Anne Szwebel (Service de Médecine Interne, AP-HP, Hôpital Cochin), and Dr Nathalie Marin (Service de Médecine Intensive et Réanimation, AP-HP, Hôpital Cochin). This study has been supported by CARE network (directed by X. Mariette, Kremlin Bicêtre, AP-HP).

Author details

[1]INSERM U1015, Gustave Roussy Cancer Campus, 94800 Villejuif, France. [2]Université Paris Saclay, Faculté de Médecine, 94270 Le Kremlin-Bicêtre, France. [3]Metabolomics and Cell Biology Platforms, Gustave Roussy Cancer Campus, 94800 Villejuif, France. [4]INSERM U1138, Gustave Roussy Cancer Campus, 94800 Villejuif, France. [5]Service de Médecine Interne, Hôpital Foch, 92150 Suresnes, France. [6]Service d'Accueil des Urgences, AP-HP, Hôpital Hôtel-Dieu, 75004 Paris, France. [7]Département d'Oncologie Médicale, Gustave Roussy Cancer Campus, 94800 Villejuif, France. [8]Département d'Hématologie, Gustave Roussy Cancer Campus, 94800 Villejuif, France. [9]Service de biologie clinique, Hôpital Foch, 92150 Suresnes, France. [10]Service de virologie, Gustave Roussy Cancer Campus, 94800 Villejuif, France. [11]Centre d'Investigation Clinique – Biothérapie, INSERM CICBT1428, 94800 Villejuif, France. [12]Département de Biologie Médicale, Gustave Roussy Cancer Campus, 94800 Villejuif, France. [13]Département de Réanimation, Gustave Roussy Cancer Campus, 94800 Villejuif, France. [14]Service de Virologie, AP-HP. Centre-Université de Paris, Hôpital Cochin, Paris, France. [15]Service d'Hématologie Biologique, AP-HP, Centre-Université de Paris, Hôpital Cochin, 75014 Paris, France. [16]Université de Paris, Innovative Therapies in Haemostasis, INSERM 1140, F-75006 Paris, France. [17]Université de Paris, Institut Cochin, CNRS UMR8104, INSERM U1016, 75006 Paris, France. [18]Gustave Roussy, Paris-Saclay University, Paris, France. [19]Aix Marseille University, CNRS, INSERM, CRCM, Marseille, France. [20]INSERM U1287, Gustave Roussy Cancer Campus, 94800 Villejuif, France. [21]INSERM U981, Gustave Roussy Cancer Campus, 94800 Villejuif, France. [22]Service de Médecine Intensive et Réanimation, AP-HP, Hôpital Cochin, 75014 Paris, France. [23]Service de Médecine Interne, AP-HP, Hôpital Cochin, 75014 Paris, France. [24]Département d'Innovation Thérapeutique et des Essais Précoces, Gustave Roussy Cancer Campus, 94800 Villejuif, France. [25]Centre de Recherche des Cordeliers, Equipe labellisée par la Ligue contre le cancer, Université de Paris, Sorbonne Université, INSERM U1138, Institut Universitaire de France, Paris, France. [26]Pôle de Biologie, Hôpital Européen Georges Pompidou, AP-HP, 75015 Paris, France. [27]Suzhou Institute for Systems Biology, Chinese Academy of Sciences, Suzhou, China. [28]Department of Women's and Children's Health, Karolinska University Hospital, 17176 Stockholm, Sweden

Author contributions

F.-X.D., C.G.-l., J.-M.M., M.F., and G.K. performed study concept and design; F.-X.D., C.G.-l., S.D., A.S., J.-M.M., M.F., and G.K. performed development of methodology and writing, review and revision of the paper; F.-X.D., C.G.-l., S.D., A.S., M.R., D.C., E.C., J.R., F.P., G.B., C.W., M.V., F.G., J.-E.F., A.-G.G., A.D., L.D., N.N., D.B., S.M., C.P., A.S., F.R., J.D., G.J., S.E., F.L., L.A., J.-C.S., F.B., E.S., F.A., F.P., F.A., L.M., L.Z., and A.M. provided acquisition and/or analysis and interpretation of data, and statistical analysis; A.M., L.Z., and G.K. provided technical and material support. All authors read and approved the final paper.

Funding

G.K. is supported by the Ligue contre le Cancer (équipe labellisée); Agence National de la Recherche (ANR) – Projets blancs; AMMICa US23/CNRS UMS3655; Association pour la recherche sur le cancer (ARC); Association "Ruban Rose"; Cancéropôle Ile-de-France; Chancelerie des universités de Paris (Legs Poix), Fondation pour la Recherche Médicale (FRM); a donation by Elior; European Research Area Network on Cardiovascular Diseases (ERA-CVD, MINOTAUR); Gustave Roussy Odyssea, the European Union Horizon 2020 Project Oncobiome; Fondation Carrefour; High-end Foreign Expert Program in China (GDW20171100085), Institut National du Cancer (INCa); Inserm (HTE); Institut Universitaire de France; LeDucq Foundation; the LabEx Immuno-Oncology (ANR-18-IDEX-0001); the RHU Torino Lumière; the Seerave Foundation; the SIRIC Stratified Oncology Cell DNA Repair and Tumor Immune Elimination (SOCRATE); and the SIRIC Cancer Research and Personalized Medicine (CARPEM). This study contributes to the IdEx Université de Paris ANR-18-IDEX-0001. LZ, LD, and the ONCOVID effort have sponsored philantropists (Ralph Lauren, Agnès b. Izipizi, Malakoff Humanis). F.X.D. have been supported by Fondation Philanthropia.

Conflict of interest

G.K. has been holding research contracts with Bayer Healthcare, Daiichi Sankyo, Genentech, Glaxo Smyth Kline, Institut Mérieux, Kaleido, Lytix Pharma, Nucana, Oncolinx, PharmaMar, Samsara, Sotio, and Vasculox. G.K. is on the Board of Directors of the Bristol Myers Squibb Foundation France. G.K. is a scientific co-founder of everImmune, Samsara Therapeutics, and Therafast Bio. L.Z. is a founder of everImmune.

Ethical approval

The non-interventional study was approved by institutional review boards (IRB) of Cochin-Port Royal (Paris, France) hospital and the ethical committee of Cochin-Port Royal Hospital (CLEP Decision N: AAA-2020-08023). The

interventional study was approved by the Foch IRB (approval number IRB00012437) and was registered on the National Institute of Health data platform INDS (n°4710280420). They were conformed to the principles outlined in the Declaration of Helsinki.

Publisher's note
Springer Nature remains neutral with regard to jurisdictional claims in published maps and institutional affiliations.

Supplementary information The online version contains supplementary material available at https://doi.org/10.1038/s41419-021-03540-y.

Received: 24 November 2020 Revised: 9 February 2021 Accepted: 10 February 2021
Published online: 11 March 2021

References

1. Morens, D. M. & Fauci, A. S. Emerging pandemic diseases: how we got to COVID-19. *Cell* **182**, 1077–1092 (2020).
2. Ghinai, I. et al. First known person-to-person transmission of severe acute respiratory syndrome coronavirus 2 (SARS-CoV-2) in the USA. *Lancet* **395**, 1137–1144 (2020). 04.
3. Guan, W.-J. et al. Clinical characteristics of coronavirus disease 2019 in China. *N. Engl. J. Med.* **382**, 1708–1720 (2020).
4. Berlin, D. A., Gulick, R. M. & Martinez, F. J. Severe Covid-19.*New Engl. J. Med.* **383**, 2451–2460 (2020).
5. Petersen, E. et al. Comparing SARS-CoV-2 with SARS-CoV and influenza pandemics. *Lancet Infect. Dis.* **20**, e238–e244 (2020).
6. Ellinghaus, D. et al. Genomewide association study of severe Covid-19 with respiratory failure. *N. Engl. J. Med.* **383**, 1522–1534 (2020).
7. Schulte-Schrepping, J. et al. Severe COVID-19 is marked by a dysregulated myeloid cell compartment. *Cell* **182**, 1419–1440.e23 (2020).
8. Silvin, A. et al. Elevated calprotectin and abnormal myeloid cell subsets discriminate severe from mild COVID-19. *Cell* **182**, 1401–1418.e18 (2020).
9. D'Alessandro, A. et al. Serum proteomics in COVID-19 patients: altered coagulation and complement status as a function of IL-6 level. *J. Proteome Res.* **19**, 4417–4427 (2020).
10. Shen, B. et al. Proteomic and metabolomic characterization of COVID-19 patient sera. *Cell* **182**, 59–72.e15 (2020).
11. Thomas, T. et al. COVID-19 infection alters kynurenine and fatty acid metabolism, correlating with IL-6 levels and renal status. *JCI insight* **23**, 5 (2020).
12. Cai, Y. et al. Kynurenic acid underlies sex-specific immune responses to COVID-19. *medRxiv* https://doi.org/10.1101/2020.09.06.20189159 (2020).
13. Song, J.-W. et al. Omics-driven systems interrogation of metabolic dysregulation in COVID-19 pathogenesis. *Cell Metab.* **32**, 188–202.e5 (2020).
14. Sapkota, D., Søland, T. M., Galtung, H. K., Sand, L. P., Giannecchini, S., To, KKW, et al. COVID-19 salivary signature: diagnostic and research opportunities. *J. Clin. Pathol.* https://doi.org/10.1136/jclinpath-2020-206834 (2020).
15. Steed, A. L. et al. The microbial metabolite desaminotyrosine protects from influenza through type I interferon. *Science* **357**, 498–502 (2017).
16. WHO Working Group on the Clinical Characterisation and Management of COVID-19 infection. A minimal common outcome measure set for COVID-19 clinical research. *Lancet Infect. Dis.* **20**, e192–e197 (2020).
17. Platten, M., Wick, W. & Van den Eynde, B. J. Tryptophan catabolism in cancer: beyond IDO and tryptophan depletion. *Cancer Res.* **72**, 5435–5440 (2012). 1 nov.
18. Aslamkhan, A. G. et al. Characterization of indoleamine-2,3-dioxygenase 1, tryptophan-2,3-dioxygenase, and Ido1/Tdo2 knockout mice. *Toxicol. Appl. Pharmacol.* **406**, 115216 (2020).
19. Platten, M. et al. Treatment of autoimmune neuroinflammation with a synthetic tryptophan metabolite. *Science* **310**, 850–855 (2005).
20. Del Valle, D. M. et al. An inflammatory cytokine signature predicts COVID-19 severity and survival. *Nat. Med.* **26**, 1636–1643 (2020).
21. Grifoni, E. et al. Interleukin-6 as prognosticator in patients with COVID-19. *J. Infect.* **81**, 452–482 (2020).
22. Hadjadj, J. et al. Impaired type I interferon activity and inflammatory responses in severe COVID-19 patients. *Science* **369**, 718–724 (2020).
23. Laing, A. G. et al. A dynamic COVID-19 immune signature includes associations with poor prognosis. *Nat. Med.* **26**, 1623–1635 (2020).
24. Carriche, G. M. et al. Regulating T-cell differentiation through the polyamine spermidine. *J. Allergy Clin. Immunol.* https://doi.org/10.1016/j.jaci.2020.04.037 (2020).
25. Madeo, F., Eisenberg, T., Pietrocola, F. & Kroemer, G. Spermidine in health and disease. *Science* **359**, eaan2788 (2018).
26. Pietrocola, F. et al. Caloric restriction mimetics enhance anticancer immunosurveillance. *Cancer Cell* **30**, 147–160 (2016).
27. Zhang, H. et al. Polyamines control eIF5A hypusination, TFEB translation, and autophagy to reverse B cell senescence. *Mol. Cell* **76**, 110–125.e9 (2019).
28. García-Alvarez, F. et al. S-adenosylmethionine immunomodulator treatment in sepsis. *Int. J. Surg. Investig.* **2**, 9–15 (2000).
29. Mehdi, A. et al. Enhanced anticancer effect of a combination of S-adenosylmethionine (SAM) and immune checkpoint inhibitor (ICPi) in a syngeneic mouse model of advanced melanoma. *Front. Oncol.* **10**, 1361 (2020).
30. Rosa, F. T., Freitas, E. C., Deminice, R., Jordão, A. A. & Marchini, J. S. Oxidative stress and inflammation in obesity after taurine supplementation: a double-blind, placebo-controlled study. *Eur. J. Nutr.* **53**, 823–830 (2014).
31. Zhang, J., Yu, M., Tong, S., Liu, L.-Y. & Tang, L.-V. Predictive factors for disease progression in hospitalized patients with coronavirus disease 2019 in Wuhan. *China J. Clin. Virol.* **127**, 104392 (2020).
32. Steiner, J., Bernstein, H.-G., Guest, P. C., Summergrad, P. & Oxenkrug, G. Plasma leptin correlates with anthranilic acid in schizophrenia but not in major depressive disorder. *Eur. Neuropsychopharmacol.* **41**, 167–168 (2020).
33. Oxenkrug, G., van der Hart, M. & Summergrad, P. Elevated anthranilic acid plasma concentrations in type 1 but not type 2 diabetes mellitus. *Integr. Mol. Med.* **2**, 365–368 (2015).
34. Pawlak, K., Kowalewska, A., Mysliwiec, M. & Pawlak, D. Kynurenine and its metabolites-kynurenic acid and anthranilic acid are associated with soluble endothelial adhesion molecules and oxidative status in patients with chronic kidney disease. *Am. J. Med. Sci.* **338**, 293–300 (2009). oct.
35. Le Naour, J., Galluzzi, L., Zitvogel, L., Kroemer, G. & Vacchelli, E. Trial watch: IDO inhibitors in cancer therapy. *Oncoimmunology* **9**, 1777625 (2020).
36. Liu, Q., Hua, S., Wang, X., Chen, F. & Gou, S. The introduction of immunosuppressor (TDO inhibitor) significantly improved the efficacy of irinotecan in treating hepatocellular carcinoma. *Cancer Immunol. Immunother.* **70**, 497–508 (2021).
37. Pilotte, L. et al. Reversal of tumoral immune resistance by inhibition of tryptophan 2,3-dioxygenase. *Proc. Natl Acad. Sci. USA* **109**, 2497–2502 (2012).
38. Prendergast, G. C., Malachowski, W. P., DuHadaway, J. B. & Muller, A. J. Discovery of IDO1 inhibitors: from bench to bedside. *Cancer Res.* **77**, 6795–6811 (2017).
39. Viltard, M. et al. The metabolomic signature of extreme longevity: naked mole rats versus mice. *Aging* **11**, 4783–4800 (2019).

European Journal of Cancer 149 (2021) 102–104

Available online at www.sciencedirect.com

ScienceDirect

journal homepage: www.ejcancer.com

Letter to the Editor

High levels of TNFα in patients with COVID-19 refractory to tocilizumab

F.X. Danlos [a], F. Ackermann [b], J. Rohmer [b], M. Roumier [b], A. Marabelle [a,c,*], J.M. Michot [c]

[a] *INSERM U1015, Gustave Roussy Villejuif, France*
[b] *Hôpital Foch, Suresnes, France*
[c] *Département D'Innovation Thérapeutique et D'Essais Précoces (DITEP), Gustave Roussy, Université Paris Saclay, Villejuif, France*

Received 25 January 2021; accepted 29 January 2021
Available online 20 March 2021

Recently, Feldmann *et al.* in *Lancet* suggested investigating TNF alpha blocker therapies for patients with COVID-19 at high risk of developing a life-threatening form [1]. The cytokine release syndrome and immunothrombosis induced by Sars-CoV2 mostly explain the severity of coronavirus disease 2019 (COVID-19) [2,3]. In a recent issue of *Nature Medicine*, Del Valle *et al.* reported the plasma levels of IL-6, IL-8, tumour necrosis factor (TNF)-α and IL-1β in patients hospitalised for COVID-19 [7]. They highlighted in a comprehensive multivariate analysis that high plasma levels of IL-6 and TNF-α remained significantly associated with a poor prognosis of patients with COVID-19 [7]. They proposed to measure IL-6 and TNF-α to stratify patients in further prospective clinical trials treating COVID-19 patients [7]. Targeting interleukin-6 (IL6) – one of the more proinflammatory cytokine – with the anti-IL6 receptor (anti-IL6R) have shown encouraging, although controversial, preliminary efficacy in the treatment of severe COVID-19 patients, while definitive results of clinical trials are still pending (COVACTA trial [NCT04320615]; CORIMUNO-TOCI trial [NCT04331808]; RECOVERY trial [NCT04381936] [4–6].

In order to better understand the effects of the anti-IL6R tocilizumab (Roche, Switzerland) on Covid19, we measured the serum cytokines levels before and during the tocilizumab therapy of 25 consecutive patients hospitalised for severe respiratory symptoms of COVID-19 at Gustave Roussy and Foch hospitals in the Paris area in France. Patients received tocilizumab (one infusion 8 mg/kg, intravenously, repeated once 12 h later at the same dose in case of absence of clinical response) in an off-label use between 20th March and 20th April 2020 (i.e. at the time of the first epidemic peak in France). All patients were treated because of worsening of their respiratory symptoms and their increase in oxygen therapy requirements ≥4 L/mn. Cytokine titration was performed on serum samples collected for routine biological assessments. Patients and healthy donors were informed of those analyses, and this project was run in compliance with the French law on human research (Loi Jardé, hors RIPH, conformité MR004). The measurements of serum IL-6 and TNF-α were done at two time points: before tocilizumab infusion 'baseline' and 7 days after tocilizumab. Serum IL-6 and TNF-α titrations were performed with the Meso Scale Discovery® VPlex proinflammatory assay (Meso Scale Diagnostics, USA). The main

* *Corresponding author*: 114, rue Edouard Vaillant, 94805, Villejuif, France.
E-mail address: Aurelien.marabelle@gustaveroussy.fr (A. Marabelle).

https://doi.org/10.1016/j.ejca.2021.01.056
0959-8049/

outcomes were mortality 30 days after treatment and favourable clinical response to tocilizumab. Clinical response was defined by improvement of respiratory symptoms related to COVID-19 and decrease in oxygen requirements and a WHO clinical progression scale [8] $\leq$ 5, following tocilizumab therapy. Patients were mainly men (22/25), median age was 56 [32–77] years old, median body mass index was 27.6 [22.7–39.0] and 13 (25%) patients had at least one comorbidity (cancer [n = 6, 24%], high blood pressure [n = 5, 20%], obesity [n = 4, 16%] or diabetes [n = 4, 16%]). Before tocilizumab, the median [range] of oxygen therapy was 9 [4–15] L/min. The median time between first COVID19 symptoms and tocilizumab infusion was 10 days (3–19). Fourteen patients received one dose of tocilizumab and the 11 other patients were treated with two doses. During follow-up, 16 (64%) patients achieved favourable clinical response to tocilizumab. Four (16%) patients died of COVID-19 in the first 30 days. Before tocilizumab, median C-reactive protein was 186 [26–396] mg/l, procalcitonin 0.15 [0.05–21.27] ng/mL, ferritin 1313 [232–4148] µg/L, d-dimer 858 [232–20,412] µg/L and fibrinogen 6.8 [2.2–8.9] g/L. The baseline serum IL-6 level did not significantly differ between patients who eventually died and those who survived (21.4 [5.1–38.2] pg/mL and 23.0 [5.4–56.7] pg/mL respectively, p = 0.652, Wilcoxon test) as between those with or without response to tocilizumab (19.4 [9.6–45.1] pg/mL and 27.5 [5.1–56.7] pg/mL respectively, p = 0.471, Wilcoxon test). However, the baseline serum TNF-α level was significantly higher in patients who eventually died of COVID-19 within 30 days post-tocilizumab treatment (4.7 [2.5–6.4] pg/mL] and 2.4 [0.9–3.6] pg/mL respectively, p = 0.015, Wilcoxon test). Additionally, 7 days after treatment, serum TNF-α increased from 3.5 [1.7–6.4] pg/mL to 12.1 [2.6–36.1] pg/mL in patients who did not favourably respond to tocilizumab, whereas patients favourably responding to tocilizumab were keeping their serum TNF-α at the same levels than healthy controls (Fig. 1).

Huang and *et al.* reported that COVID-19 patients in the intensive care unit had higher plasma concentrations of TNF-α than non-ICU patients [2]. Del Valle and *et al.* reported serum IL-6 and TNF-alpha as significant predictors of survival [4]. Furthermore, a pivotal role of calprotectin, an inflammation protein upstream of tumour necrosis factor-alpha (TNF-a), has been recently demonstrated in severe forms of COVID-19 [9]. Our results confirm TNF-α as a biomarker of severity in a cohort of patients treated with tocilizumab and support that serum levels of TNF-α should help to stratify patients according to their severity in further prospective clinical trials. These data reinforce Feldmann and *et al.*

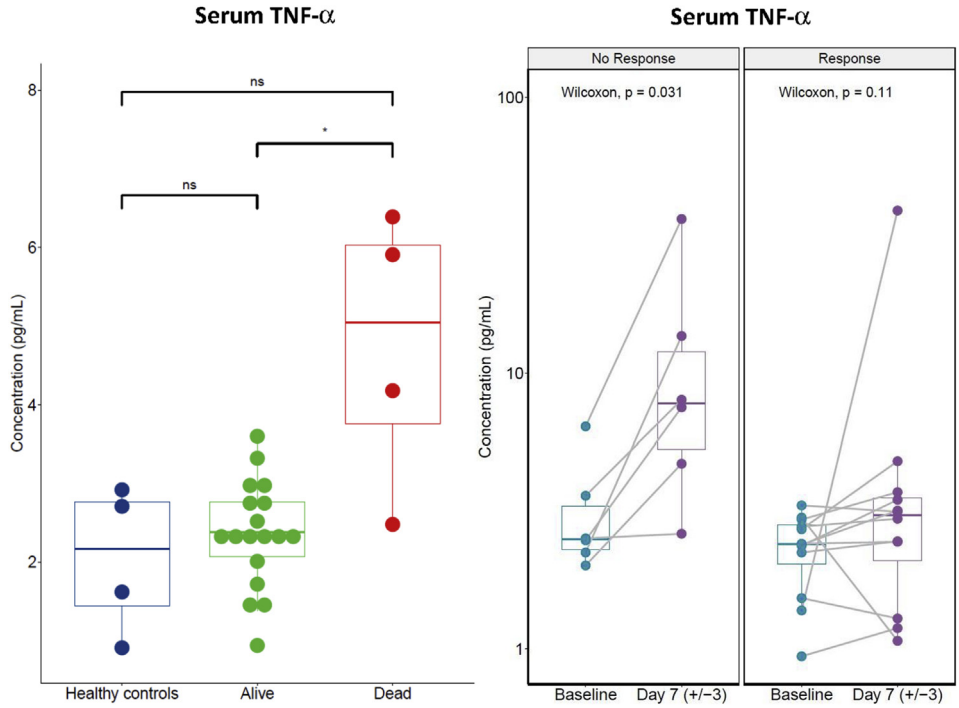

Fig. 1. TNF-α levels were measured in serum collected from Healthy controls and COVID-19 patients before 'baseline' and 7 days after tocilizumab. Data shown are those of all the patients treated with tocilizumab and who were able to provide a pre-treatment (baseline) and post-treatment serum (up-to-date serum +7). Of the 25 patients treated with tocilizumab, pre-treatment and post-treatment serum analyses were available for 18 patients represented according to their outcome; mortality before day 30 (left panel) and response to tocilizumab (right panel). Baseline TNF-α serum levels were significantly higher at baseline in patients who eventually died of Covid19 (left panel). Post-tocilizumab TNF-α serum levels were significantly increasing in patients who did not favourably respond to tocilizumab (right panel).

view [1] supporting further investigations of TNF-α blocking therapies as potential drugs for patients with a severe and life-threatening form of COVID-19 and provide a putative rationale for tocilizumab resistance.

Conflict of interest statement

The authors declare the following financial interests/personal relationships which may be considered as potential competing interests: Over the last 5 years, AM and JMM have participated as principal investigators and sub-investigators of oncology clinical trials sponsored by manufacturers of anti-IL6 and anti-IL6R therapies Roche/Genentech, Sanofi/Regeneron, J&J/Janssen. AM has received honoraria from Roche / Genentech, J&J and Sanofi for consulting in the field of cancer immunotherapy. AM has received grants for oncology research from Sanofi. Gustave Roussy has received funding, grants and drug supply from Roche / Genentech, Sanofi / Regeneron, Janssen for running clinical trials or research projects in oncology. FXD, FA, JR and MR have no conflict of interest to disclose.

Acknowledgements

We would like to thank the following collaborators for their effort during this Covid19 crisis and their contribution to the generation, collection and analysis of our dataset: Dr Laurence Albiges, Dr Fanny Pommeret, Dr Emeline Colomba, Dr Lisa de Rosa, Pr Laurence Zitvogel, Pr Guido Kroemer, Dr Marc Vasse, Dr Christophe Willekens, Dr Antoine Hollebecque, Delphine Bredel, Dr Thomas Hueso, Severine Mouraud, Chifaou Mohamed-Djalim, Dr Giulia Baciarello, Prof Benjamin Besse, Prof Fabrice Barlesi, Prof Fabrice André, Prof Jean-Charles Soria. This work could have been done thanks to the funding support of Fondation Philanthropia, Gustave Roussy Cancer Center and Fondation Gustave Roussy.

References

[1] Feldmann M, Maini RN, Woody JN, et al. Trials of anti-tumour necrosis factor therapy for COVID-19 are urgently needed. Lancet 2020;395:1407–9.
[2] Huang C, Wang Y, Li X, et al. Clinical features of patients infected with 2019 novel coronavirus in Wuhan, China. Lancet 2020;395:497–506.
[3] McGonagle D, O'Donnell JS, Sharif K, Emery P, Bridgewood C. Immune mechanisms of pulmonary intravascular coagulopathy in COVID-19 pneumonia. Lancet Rheumatol 2020;2:e437–45.
[4] Guaraldi G, Meschiari M, Cozzi-Lepri A, et al. Tocilizumab in patients with severe COVID-19: a retrospective cohort study. Lancet Rheumatol 2020;2:e474–84.
[5] Xu X, Han M, Li T, et al. Effective treatment of severe COVID-19 patients with tocilizumab. Proc Natl Acad Sci USA 2020;117:10970–5.
[6] Sciascia S, Aprà F, Baffa A, et al. Pilot prospective open, single-arm multicentre study on off-label use of tocilizumab in patients with severe COVID-19. Clin Exp Rheumatol 2020;38:529–32.
[7] Del Valle DM, Kim-Schulze S, Huang H-H, et al. An inflammatory cytokine signature predicts COVID- 19 severity and survival. Nat Med 2020. https://doi.org/10.1038/s41591-020-1051-9. published online Aug 24.
[8] Marshall JC, Murthy S, Diaz J, et al. A minimal common outcome measure set for COVID-19 clinical research. Lancet Infect Dis 2020;20:e192–7.
[9] Silvin A, Chapuis N, Dunsmore G, et al. Elevated calprotectin and abnormal myeloid cell subsets discriminate severe from mild COVID-19. Cell 2020. https://doi.org/10.1016/j.cell.2020.08.002. published online Aug 5.

CDDpress

www.nature.com/cdd

ARTICLE OPEN

Check for updates

Prolonged SARS-CoV-2 RNA virus shedding and lymphopenia are hallmarks of COVID-19 in cancer patients with poor prognosis

Anne-Gaëlle Goubet[1,2,3,58], Agathe Dubuisson[2,3,58], Arthur Geraud[2,4,5], François-Xavier Danlos[2,3], Safae Terrisse[2,3], Carolina Alves Costa Silva[2,3], Damien Drubay[2,6,7], Lea Touri[2,8], Marion Picard[2,3,9,10,11], Marine Mazzenga[2,3], Aymeric Silvin[2,3], Garett Dunsmore[2,3], Yacine Haddad[2,3], Eugenie Pizzato[2,3], Pierre Ly[2,3], Caroline Flament[2,3], Cléa Melenotte[2,3], Eric Solary[1,2,12,13], Michaela Fontenay[14,15], Gabriel Garcia[2,16], Corinne Balleyguier[2,16], Nathalie Lassau[1,2,16,17], Markus Maeurer[18], Claudia Grajeda-Iglesias[2,3,19,20], Nitharsshini Nirmalathasan[2,19,20], Fanny Aprahamian[2,19,20], Sylvère Durand[2,19,20], Oliver Kepp[19,20], Gladys Ferrere[2,3], Cassandra Thelemaque[2,3], Imran Lahmar[2,3], Jean-Eudes Fahrner[2,3], Lydia Meziani[2,21], Abdelhakim Ahmed-Belkacem[22], Nadia Saïdani[23], Bernard La Scola[24,25], Didier Raoult[24,25], Stéphanie Gentile[26], Sébastien Cortaredona[25,27], Giuseppe Ippolito[28], Benjamin Lelouvier[29], Alain Roulet[29], Fabrice Andre[1,2,4,30], Fabrice Barlesi[2,4,31], Jean-Charles Soria[1,2], Caroline Pradon[2,32,33], Emmanuelle Gallois[2,34], Fanny Pommeret[2,4], Emeline Colomba[2,4], Florent Ginhoux[35,36,37], Suzanne Kazandjian[38], Arielle Elkrief[38,39], Bertrand Routy[39,40], Makoto Miyara[41], Guy Gorochov[41], Eric Deutsch[1,2,21,42], Laurence Albiges[1,2,4], Annabelle Stoclin[2,43], Bertrand Gachot[2,44], Anne Florin[2,8], Mansouria Merad[2,45], Florian Scotte[2,46], Souad Assaad[47,48,49], Guido Kroemer[2,19,20,50,51,52,53], Jean-Yves Blay[47,48,49], Aurélien Marabelle[2,3,4,5,54], Frank Griscelli[2,34,55,56,57], Laurence Zitvogel[1,2,3,54,59]✉ and Lisa Derosa[1,2,3,4,59]✉

Patients with cancer are at higher risk of severe coronavirus infectious disease 2019 (COVID-19), but the mechanisms underlying virus–host interactions during cancer therapies remain elusive. When comparing nasopharyngeal swabs from cancer and noncancer patients for RT-qPCR cycle thresholds measuring acute respiratory syndrome coronavirus-2 (SARS-CoV-2) in 1063 patients (58% with cancer), we found that malignant disease favors the magnitude and duration of viral RNA shedding concomitant with prolonged serum elevations of type 1 IFN that anticorrelated with anti-RBD IgG antibodies. Cancer patients with a prolonged SARS-CoV-2 RNA detection exhibited the typical immunopathology of severe COVID-19 at the early phase of infection including circulation of immature neutrophils, depletion of nonconventional monocytes, and a general lymphopenia that, however, was accompanied by a rise in plasmablasts, activated follicular T-helper cells, and non-naive Granzyme $B^{+}FasL^{+}$, $Eomes^{high}TCF\text{-}1^{high}$, $PD\text{-}1^{+}CD8^{+}$ Tc1 cells. Virus-induced lymphopenia worsened cancer-associated lymphocyte loss, and low lymphocyte counts correlated with chronic SARS-CoV-2 RNA shedding, COVID-19 severity, and a higher risk of cancer-related death in the first and second surge of the pandemic. Lymphocyte loss correlated with significant changes in metabolites from the polyamine and biliary salt pathways as well as increased blood DNA from Enterobacteriaceae and Micrococcaceae gut family members in long-term viral carriers. We surmise that cancer therapies may exacerbate the paradoxical association between lymphopenia and COVID-19-related immunopathology, and that the prevention of COVID-19-induced lymphocyte loss may reduce cancer-associated death.

Cell Death & Differentiation; https://doi.org/10.1038/s41418-021-00817-9

INTRODUCTION

Severe acute respiratory syndrome coronavirus-2 (SARS-CoV-2) is a novel beta-coronavirus that has caused a worldwide pandemic of the human respiratory illness COVID-19, resulting in a severe threat to public health and safety worldwide. Because of age, gender, cancer-associated risk factors, metabolic syndrome, and side effects induced by their specific therapies (such as cardiomyopathy, systemic immunosuppression, and cellular senescence), cancer patients appear more vulnerable to severe infection than individuals without cancer [1]. Indeed, a high hospitalization and mortality rates of SARS-CoV-2 infection were heralded in patients with malignancy in several studies across distinct geographical sites [2–5]. Cancer types, performance status, and stage are additional risk factors for severe COVID-19 in this patient population. Patients with hematological, lung and breast cancer have been reported to be more susceptible to hospitalization or death due to COVID-19 as compared to patients with other malignancies [3, 5–8]. Patients diagnosed with metastatic cancers are more vulnerable to severe forms of COVID-19 than individuals with localized malignancies [9]. Recent (<3 months) cancer

A full list of author affiliations appears at the end of the paper.

Edited by M. Piacentini

Received: 30 January 2021 Revised: 26 May 2021 Accepted: 28 May 2021
Published online: 06 July 2021

treatments including surgery, chemotherapy, and immunotherapy independently contribute to worsening the prognosis of COVID-19 among patients with the malignant disease [2, 5, 7, 9–11].

Here, we explored several independent cohorts of cancer patients diagnosed with COVID-19 (1063 patients, 58% with cancer) during the first surge of the pandemic to analyze the dynamics between host (blood immunology, metabolism, metagenomics) and viral parameters and validated the most clinically relevant findings in the second surge of the pandemic. We concluded that virus-induced or -associated lymphopenia that coincided with T-cell exhaustion, abnormalities in polyamine and biliary salt pathways and circulation of Enterobacteriaceae and Micrococcaceae bacterial DNA, is a dismal prognosis factor in cancer patients, likely participating in the vicious circle of immunosuppression-associated chronic virus shedding.

RESULTS

Prolonged viral shedding and higher viral loads in cancer patients compared with cancer-free COVID-19^{+} patients

To explore the clinical significance of viral and/or immunological parameters in cancer patients, we gathered the data from electronic clinical files from various cancer centers or general hospitals across France and Canada, in order to monitor the magnitude and duration of virus RNA shedding in nasopharyngeal swabs according to cancer (versus healthcare workers (HCW) or COVID-19^{+} cancer-free individuals), tumor types (hematological versus solid malignancies) and staging (localized, locally advanced, metastatic diseases) (Fig. 1A). First, we conducted a prospective epidemiological study named Cancer_FR1_Translational Research (TR) at Gustave Roussy, Villejuif, France, during the first surge of the COVID-19 pandemic (from April 10, 2020 to May 11, 2020, NCT04341207) to evaluate the prevalence and severity of COVID-19 in all adult patients under treatment or recently treated for solid tumors or hematological malignancies (Fig. S1 and Table S1). Our secondary endpoint was the identification of viral, immunological, metabolic, and metagenomics blood predictors of severe complications among cancer patients. Clinical characteristics were collected from electronic medical records (Table S1). Nasopharyngeal samples were serially collected at every hospital visit motivated by the cancer management or any symptomatology related to seasonal flu or COVID-19 and transferred to the virology laboratory for SARS-CoV-2-specific quantitative reverse transcription-PCR (RT-qPCR) testing. Out of 473 patients enrolled in Cancer_FR1_TR, 53 (11%) were diagnosed with COVID-19 by RT-qPCR, and this diagnosis was corroborated by a specific serology in 87% of cases (Fig. S1A). Among the 52 patients evaluable for translational research, 37% were males, 60% suffered from at least one of the comorbidities associated with coronavirus pandemic, such as hypertension (58%) or obesity (21%) (Table S1). Seventy-seven percent had an ECOG performance status of 0–1 at the time of nasopharyngeal sampling. Twenty-one percent of COVID-19-positive cancer patients did not report any symptom of infection, 61% required hospital admission (for any cause or because of COVID-19 aggravation within 28 days after diagnosis) and 11% a transfer to intensive care unit (ICU), culminating with cancer death in 7% of the cases (from an undetermined cause, no systematic necropsy) (Fig. S1B–G and Table S1). Among patients with cancer diagnosed with COVID-19, 20% were followed up for hematological (as opposed to solid) malignancies and developed more severe symptoms of infection (Fig. S1B, G and Table S1). In the Cancer_FR1_TR study, 33%, 21%, and 46% presented with localized, locally advanced, and metastatic disease, respectively, that were equally susceptible to severe COVID-19 (Fig. S1F–G).

Given that cycle threshold (Ct) values of the first RT-qPCR test may be correlated with the clinical characteristics of the patients [12, 13], we performed a longitudinal follow-up of Ct values by RT-qPCR. We targeted several genes coding for the envelope, the nucleocapsid and/or the replication–transcription complex (RdRP, Orf1a, subgenomic RNA of the SARS-CoV-2 [14, 15]) to assess the duration of the nasopharyngeal SARS-CoV-2 RNA shedding, starting at COVID-19 diagnosis for up to 6 months as per-protocol indications (Fig. S2A). The duration of viral shedding was defined as the number of days from the first positive to the first negative RT-qPCR, after longitudinal monitoring with an interval inferior to 40 days, to reduce bias in viral shedding estimation. This time lapse of 40 days corresponded to the median of SARS-CoV-2 virus carriage in the cancer population (Fig. 1B, C and Table S1). In parallel, a similar and systematic COVID-19 protocol with longitudinal RT-qPCR testing was applied to healthcare workers (HCW) at Gustave Roussy. Healthcare workers had a mean age of 35 years (range: 19–61), were mostly females (male versus female: 13% versus 87%), and presented with one or two comorbidities in 27% and 4%, respectively, thereby significantly diverging from the cancer population diagnosed with COVID-19. Starting from 50 COVID-19-positive cancer patients and 100 HCW, we conducted RT-qPCR in 210 and 200 nasopharyngeal swabs, respectively (Fig. S2). However, applying the exclusion criteria detailed in Fig. S2, we could compare the median length of SARS-CoV-2 RNA detection in 35 cancer patients (Cancer_FR1_TR) and 45 HCW using 168 and 118 samples, respectively. Patients with cancer exhibited prolonged nasopharyngeal RNA virus shedding (Fig. 1B, median of 40 days (range: 6–137) for patients with cancer compared to 21 days (range: 7–53) for HCW, Fig. 1C, log-rank test P value < 0.0001). This difference persisted after adjusting for age, gender, and comorbidities (Cox multivariate analysis, adjusted hazard ratio (95% confidence interval) = 2.88 [1.42;5/85], $P = 0.00291$, Fig. 1C). To further validate the differences observed in the duration of viral RNA shedding between Cancer_FR1_TR and HCW, we analyzed another cohort of patients diagnosed with COVID-19 in a general hospital from Southern France and paired—in a case-control study—175 cancer patients (with a history of cancer or currently treated with cancer (Table S1)) with 350 cancer-free individuals based on age, gender, comorbidities, and COVID-19 severity (FR2_Case-Control, Cancer and Non-Cancer) (Fig. 1A and Table S1). Here again, there was a prolonged length of RT-qPCR positivity in cancer individuals compared with cancer-free COVID-19 patients (8 days versus 6 days, log-rank test P value, $P = 0.03$), taking into account that >70% were treated with hydroxychloroquine and azithromycin, a combination regimen reducing viral shedding [16]. Moreover, the proportion of patients with a viral shedding above 16 days (corresponding to the 90th percentile of the viral shedding in cancer-free patients) was higher in cancer patients (Fig. 1D, $P < 0.0015$). A second independent validation was achieved in the third series of 66 patients with cancer extracted from a cohort of 252 cancer individuals living in Canada and diagnosed with COVID-19 (Cancer_CA), for whom a longitudinal SARS-CoV-2-specific RT-qPCR (using *Orf1* and *E* gene probe sets [17]) follow-up had been carried out [18] (Fig. 1A and Table S1). Here again, we observed that 26% of cancer patients were still PCR positive after 40 days from diagnosis by RT-qPCR (Fig. 1E). Such a long-term PCR detection of viral RNA could indicate stable subgenomic RNA contained within double-membrane vesicles or the presence of a replicative mucosal viral strain. Hence, we confirmed in three independent series of cancer patients prolongation of RNA virus shedding previously described in case reports in hematological or immunocompromised patients [19–22].

Hence, we focused on the differential characteristics of cancer patients presenting with long-term viral RNA shedding (LVS), defined by a positive RT-qPCR duration ≥40 days (median of RT-qPCR duration in Cancer_FR1_TR (Fig. 1C)), compared to those experiencing Short term Viral RNA Shedding (SVS), defined by a positive RT-qPCR duration <40 days henceforth (Table S1). The increased susceptibility to develop a LVS was independent of initial symptomatology, observed in 33% of Canadian (CA) to 40% of French (FR1_TR) asymptomatic and 27% (CA) to 56% (FR1_TR) of symptomatic cancer patients (Fig. 1F). There was a higher propensity to LVS in hematological malignancies compared to

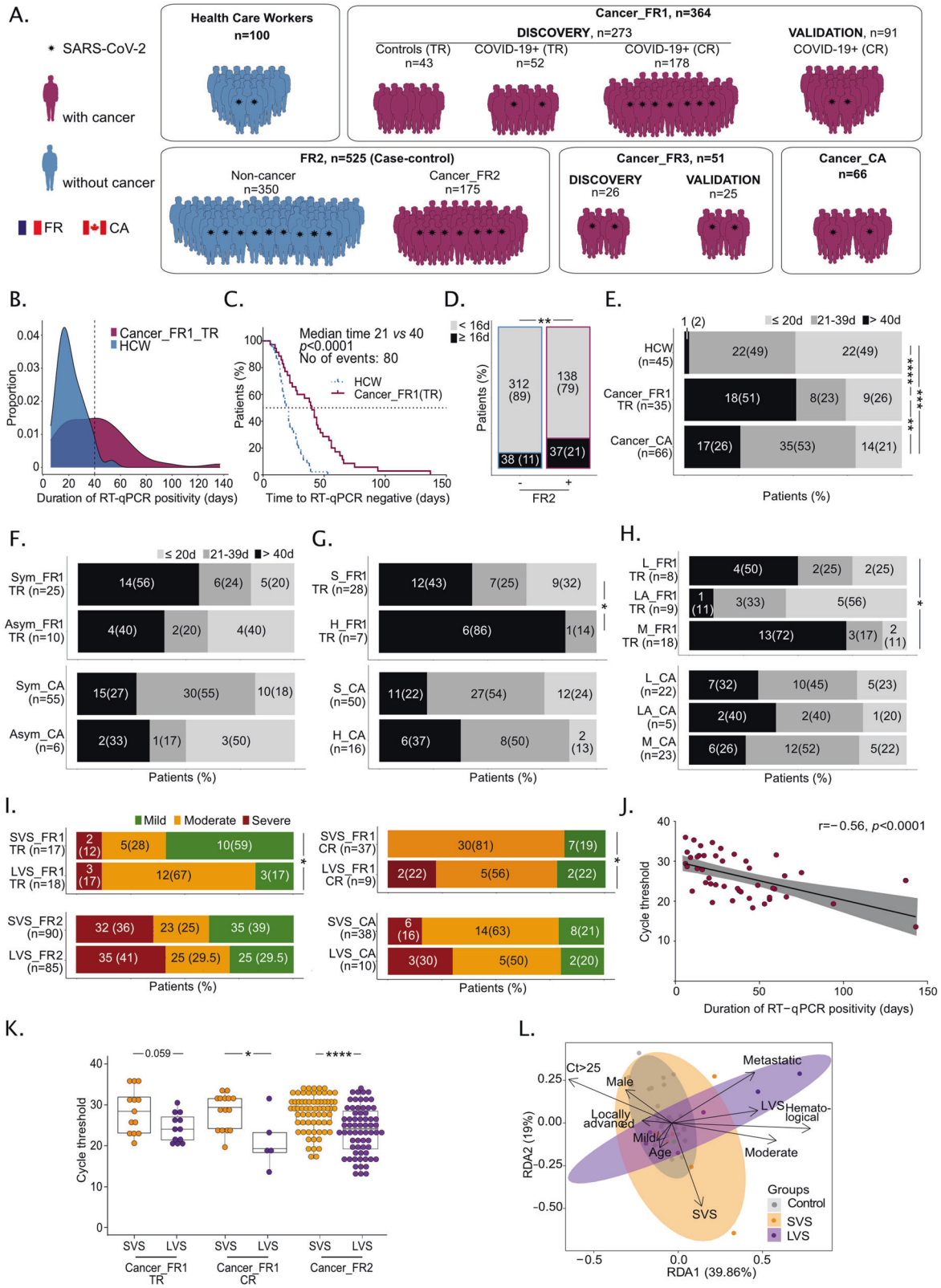

solid cancers (86% versus 43%, respectively ($P = 0.04$, Fig. 1G and Table S1) and in advanced disease ($P = 0.011$) in FR1_TR cohort (Fig. 1H and Table S1) but less so, in the CA cohort. Importantly, the LVS phenotype was associated with an increased risk to develop a moderate form of COVID-19 (defined by thoracic CT scan, hospitalization, and oxygen requirement <9 L/min) in Cancer_FR1_TR ($P = 0.032$) (Fig. 1I). This trend was confirmed in the third series of French patients from the clinical routine (CR) managed outside the translational ancillary study at Gustave Roussy (called henceforth "Cancer_FR1_CR"; Table S1 and Fig. S3),

Fig. 1 Prolonged duration of SARS-CoV-2 RNA shedding correlated with high viral load and COVID-19 severity in patients with cancer. A Graphical schema of cohorts and patients' accrual. **B** Proportion of patients with cancer from translational research (TR) (Cancer_FR1_TR, $n = 35$, magenta area) or healthcare workers (HCW, $n = 45$, blue area) by days of RT-qPCR positivity. Vertical dashed line at 40 days represents the 95th percentile of HCW and the median of positivity of patients with cancer. **C** Kaplan–Meier curves of time to negative RT-qPCR in HCW ($n = 45$, blue dotted lines) and patients with cancer (Cancer_FR1_TR, $n = 35$, magenta continuous lines). **D** COVID-19$^+$ cancer-bearing or history of cancer (+) and cancer-free (−) individuals from FR2 treated with hydroxychloroquine +/− azithromycin: number (percentages) of patients with RT-qPCR positivity beyond 16 days (90th percentile of the cancer-free population of FR2). **E** Number (percentages) of HCW, Cancer_FR1 patients (Cancer_FR1_TR), or Canadian patients with cancer (Cancer_CA) with short, intermediate (grouped in short-term viral RNA shedding, SVS), and prolonged (long-term viral RNA shedding, LVS) viral RNA shedding (**E**), according to the presence/absence of viral symptoms (symptomatic, Sym, vs asymptomatic, Asym) (**F**), diagnosis of hematological (H) versus solid (S) malignancy (**G**), and cancer staging (localized (L), locally advanced (LA), metastatic (M)) (**H**). **I** Number (percentages) of Cancer_FR1 patients (from translational research and clinical routine), Cancer_FR2 patients (Cancer_FR2) or Canadian patients with cancer (Cancer_CA) divided in SVS and LVS and regarding their respective COVID-19 severity. **J** Spearman correlation between Cycle threshold (Ct) for the RT-qPCR amplification of genes encoding proteins of SARS-CoV-2 replication–transcription complex at diagnosis and duration of RT-qPCR positivity for Cancer_FR1 (from translational research and clinical routine), each dot representing one sample/patient. **K** Ct values for the RT-qPCR amplification of genes encoding proteins of SARS-CoV-2 replication–transcription complex in nasopharyngeal swabs performed at diagnosis in SVS versus LVS in Cancer_FR1_TR and CR and Cancer_FR2, and dynamics over time from day 0 up to day 80 after inclusion in SVS ($n = 33$ samples, $n = 28$ patients, orange dots) versus LVS (57 samples, $n = 17$ patients, purple dots) in Cancer_FR1 (from translational research and clinical routine). **L** Redundancy statistical analysis (RDA) of cancer and viral related-clinical factors accounting for the variance of SARS-CoV-2 viral shedding status. Clinical components were influenced by the virus shedding (SVS versus COVID-19-negative, $P = 0.037$; LVS versus COVID-19 negative, $P = 0.0010$), COVID severity (mild versus COVID-19-negative, $P = 0.0030$; moderate versus COVID-19-negative, $P = 0.0574$; severe versus COVID-19-negative, P not computable), age ($P = 0.0514$), hematological rather than solid malignancy (hematological versus solid, $P = 0.001$), metastatic status ($P = 0.0059$), and Ct values at diagnosis (≥25 versus < 25, $P = 0.0738$). Chi-square tests with $^*P < 0.05$, $^{**}P < 0.01$, $^{***}P < 0.001$, $^{****}P < 0.0001$.

where 20% of cancer patients were diagnosed with LVS and exhibited more severe COVID-19 infections (Fig. 1I, $P = 0.011$). Again, the hospitalization rates and transfer to intensive care units were increased in LVS compared with SVS patients in Cancer_FR1_TR ($P = 0.0018$, Table S1) and Cancer_FR2, respectively ($P = 0.02$, Table S1). Finally, the FR2 and Canadian series of LVS cancer patients also tended to exhibit more severe manifestations of COVID-19 compared with SVS Canadian cancer patients (Fig. 1I, bottom).

Of note, the duration of viral RNA shedding correlated with "viral load", i.e., Ct values at diagnosis, in that cancer patient with LVS experienced lower Ct values at diagnosis than SVS cancer patients in most cohorts for which the data were available (Fig. 1J). Importantly, cancer patients doomed to develop LVS presented with lower Ct values at diagnosis than those prone to become SVS in Cancer_FR1 and Cancer_FR2 cohorts (Fig. 1K). Of note, Ct values at disease onset were significantly anticorrelated with duration of viral RNA shedding in cancer patients using either *N* or *Orf1ab/RdRP* gene-specific probe sets (data not shown).

The redundancy analysis (RDA) is an extension of the principal component analysis (PCA) aimed at identifying viral components which depend on other known covariates such as clinical parameters. RDA revealed that, within 30 days from diagnosis, 18% of the variance of the biological parameters are explained by ten components adjusted for the major clinical parameters for COVID-19 in Cancer_FR1_TR (Fig. 1L). These components were mainly influenced by the virus shedding (SVS versus COVID-19-negative, $P = 0.037$; LVS versus COVID-19-negative, $P = 0.0010$), COVID severity (mild versus COVID-19-negative, $P = 0.0030$; moderate versus COVID-19-negative, $P = 0.0574$; severe versus COVID-19-negative, P not computable), age ($P = 0.0514$), hematological rather than solid malignancy (hematological versus solid, $P = 0.001$), metastatic status ($P = 0.0059$), and Ct values at diagnosis (>25 versus < 25, $P = 0.0738$). As outlined in Table S1, LVS patients tended to be older (66 versus 56 years old, $P = 0.08$), more metastatic (72% versus 29%, $P = 0.01$), and experienced increased hospitalization rates (83% versus 23%, $P < 0.001$) than SVS cancer patients in the Cancer_FR1_TR cohort.

Immunological hallmarks of long-term virus carriers at diagnosis

Intrigued by these findings, we addressed the question as to whether and how prolonged viral RNA shedding would impact on Cancer_FR1_TR patients with respect to COVID-19-related immunological alterations previously reported for cancer-free infected individuals [23–29]. More than 80 phenotypic markers were quantified on circulating leukocytes by means of high-dimensional spectral flow cytometry, complemented by multiplex ELISAs to detect serum chemokines, cytokines, and growth factors. These parameters were recorded within or after the first 20 days of inclusion in the Cancer_FR1_TR protocol, for 25 COVID-19$^+$ cancer patients that were divided into LVS versus SVS subgroups, in comparison to 43 COVID-19-negative cancer patients ("controls" or "Ctls") matched for age, gender, comorbidities, cancer types, and tumor extension (Table S2). Asymptomatic individuals and cancer patients enrolled at the recovery phase of COVID-19 (meaning that they became PCR-negative) were analyzed separately. Within the first 20 days from diagnosis, LVS presented increased proportions of monocytes among circulating leukocytes (Fig. S4A, left panel), and a parallel drop in CD169$^-$HLA-DR$^+$ within conventional monocytes (Fig. S4A, middle panel) and in nonconventional monocytes (CD16$^+$CD14$^{low/-}$, Fig. S4A, right panel) compared to SVS, cancer controls, asymptomatic or recovered patients, as reported [23, 30]. Polymorphonuclear cells (PMN) tended to increase in LVS, specifically immature CD101$^{+/-}$CD10$^{+/-}$CD16$^-$ neutrophils, compared with SVS, convalescent, and controls (Fig. 2A, B, upper and lower panels and Fig. S4B).

Importantly, the most significant phenotypic traits distinguishing LVS from SVS featured among the reported hallmarks of severe COVID-19 in cancer-free subjects [23–29] (Fig. 2A). In accordance with the reported defects in germinal center formation in secondary lymphoid organs of severe COVID-19 [28], LVS cancer patients exhibited increased recirculation of activated CXCR5$^+$PD-1^{high} CD4$^+$ follicular T-helper cells (TFH) expressing ICOS and CD38 (Fig. 2C, left panel), as well as a marked rise in plasmablasts (defined as CD19^{low} CD27^{hi} CD38^{hi}) at the expense of transitional B (CD24$^+$CD38^{hi}CD19$^+$) and double-negative B cells (IgD$^-$CD27$^-$CD19$^+$) (Fig. 2C, right panel, Fig. S4C and Fig. 2D). As indicated in the Volcano plot in Fig. 2A, immature PMN and double-negative B cells were among the most significant immunological features, positively and negatively predicting LVS, respectively (Fig. 2B, bottom panel and Fig. 2D, right panel). LVS coincided with the prolonged systemic release of, and exposure to, type 1 IFN above levels measured in SVS, controls, and recovered individuals (Fig. 2E). Type 1 IFN levels anticorrelated with titers of neutralizing anti-S1 RBD antibodies (Fig. 2F). This landscape of immune profiling was corroborated by non-supervised hierarchical clustering of innate and cognate

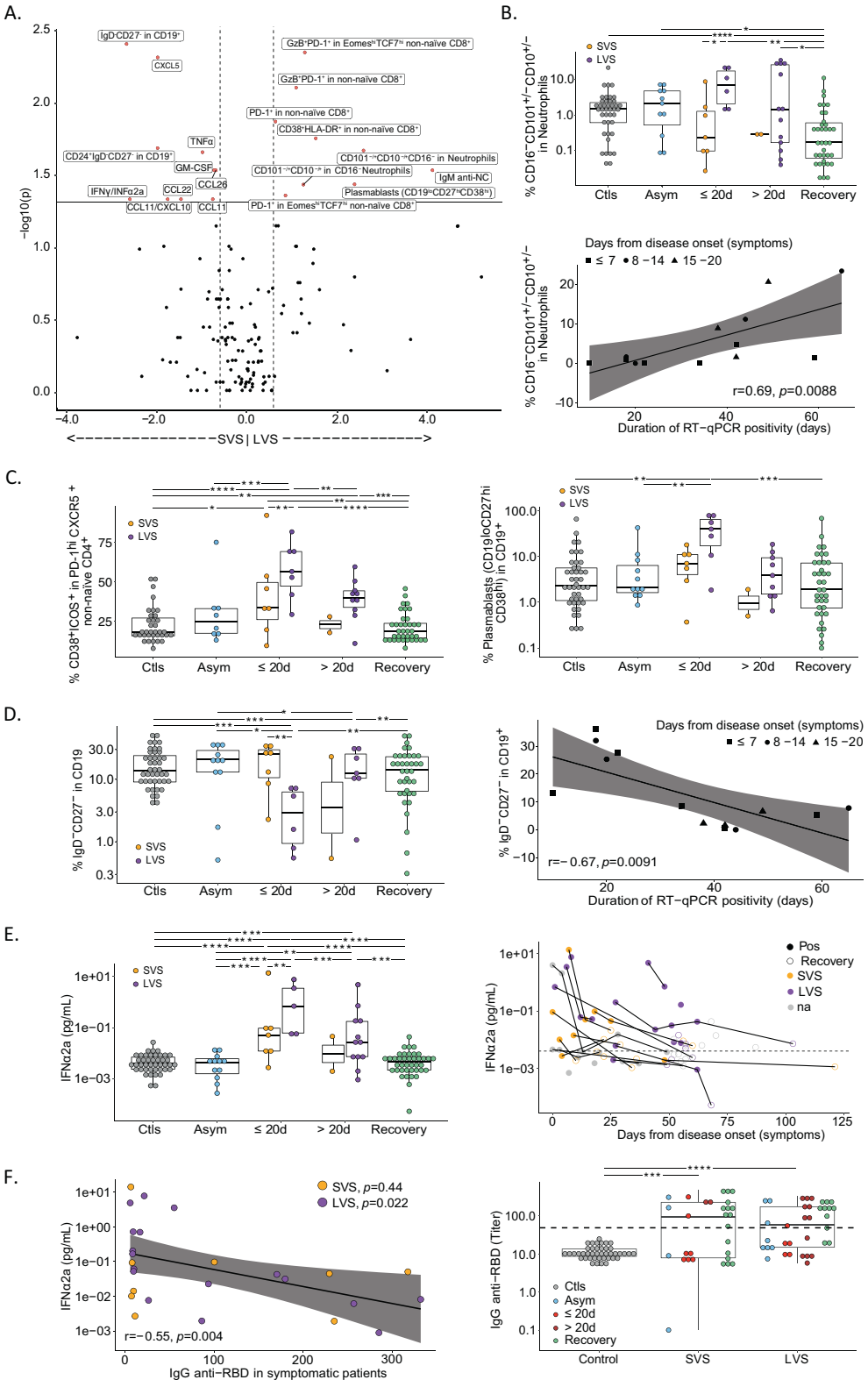

immunotypes and serum cytokine concentrations analyzed within 30 days from diagnosis. This method allowed to segregate a small cluster of individuals characterized by low Ct values (<25), and moderate/severe complications of COVID-19, which included metastatic cancer carriers with LVS or SVS (Fig. S5). This cluster was separated from the others by typical signs of viral infection, including abundant circulating $CD38^{+}HLA\text{-}DR^{+}CD8^{+}$T cells, plasmablasts, activated TFH cells, and high serum IFNα2a levels (Fig. S5). Likewise, while many inflammatory cytokines, chemokines, or alarmins (such as IFNγ, CXCL10, IL-4, IL-6, and

Fig. 2 Immunotypes associated with prolonged viral RNA shedding in patients with cancer. A Volcano plot of the differential cellular and soluble immune parameters contrasting short-term viral RNA shedding (SVS) versus long-term viral RNA shedding (LVS) during the first 20 days of symptoms. Volcano plot was generated computing for each immune factor: (i) the log2 of fold change among the mean relative percentages after normalization in SVS versus LVS (*x* axis); (ii) the log10 of *P* values deriving from Wilcoxon test calculated on relative percentages in absolute values (*y* axis). Black and red dots are considered nonsignificant ($P < 0.05$) or significant ($P > 0.05$), respectively. **B**–**F** Temporal changes and correlation of blood leukocyte parameters measured by high-dimensional spectral flow cytometry (**B**–**D**) and soluble factors IFNα2a and anti-SARS-CoV-2 IgG (**E**, **F**) in various phases of COVID-19 presentation (no virus infection (Ctls, gray dots), asymptomatic viral infection (Asym, light blue dots), symptomatic viral infection examined in the first 20 days (≤20 d) or after 20 days (>20 d) of symptoms with those experiencing short-term viral RNA shedding (SVS, orange dots) or long-term viral RNA shedding (LVS, purple dots) and RT-qPCR-negative COVID-19 patients in the convalescent phase (recovery, green dots, or circled dots). Box plots display a group of numerical data through their 3rd and 1st quartiles (box), mean (central band), minimum and maximum (whiskers). Each dot represents one sample, each patient being drawn one to three times. Statistical analyses used one-way ANOVA with Kenward–Roger method to take into account the number of specimen/patient: $*P < 0.05$, $**P < 0.01$, $***P < 0.001$, $****P < 0.0001$. **B**–**D** Percentages of neutrophils that do not express either CD101 and/or CD10 and lost CD16 within the gate of $CD45^+CD56^-CD3^-CD19^-CD15^+$ cells (**B**, upper panel). Spearman correlation between the percentage of immature neutrophils ($CD10^{+/-}CD101^{+/-}CD16^-$) measured within the first 20 days of symptoms with the duration of SARS-CoV-2 RT-qPCR positivity (**B**, lower panel). **C**, **D** Percentages of $CD38^+ICOS^+$ among $CXCR5^+PD\text{-}1^+$ non-naive $CD4^+$ (**C**, left panel), plasmablasts defined as $CD19^{low}CD38^{high}CD27^+$ within the $CD19^+$ gate (**C**, right panel), double-negative IgD^-CD27^- among $CD19^+$ cells (**D**, left panel) and their Spearman correlation when measured within the first 20 days of symptoms with the duration of SARS-CoV-2 RT-qPCR positivity (**D**, right panel). **E** Ultrasensitive electrochemiluminescence assay to monitor the serum concentrations of IFNα2a (**E**, left panel) in a kinetic fashion (**E**, right panel). Each line and dot represent one patient and one sample, respectively, and the dashed line represents the median value of controls. **F** Spearman correlation between the serum IFNα2a values measured in symptomatic patients with IgG titers against SARS-CoV-2 S1 RBD considered as continuous variables (**F**, left panel). The raw data are represented in the right panel at both time points for each group of patients.

calprotectin) were elevated in symptomatic COVID-19 individuals compared with controls, asymptomatic, and recovered patients, none of them could predict LVS, except a drop in the IFNγ/IFNα2a and CCL11/CXCL10 ratios whose significance remains unclear ($P = 0.016$ and $P = 0.0019$, respectively) (Fig. S4D–I). Interestingly, innate and cognate immunotypes performed in convalescent patients and controls segregated at random in the non-supervised hierarchical clustering (Fig. S6).

Altogether, the high-dimensional flow cytometry of blood immune subsets indicated that LVS cancer patients harbored the immunological hallmarks of severe COVID-19 at diagnosis.

Virus-associated lymphopenia predicted shorter overall survival in the first and second surge of the pandemic

Lymphocyte loss is a feature of severe COVID-19 in noncancer patients [24, 27]. The "FR2" cohort was a case-control study with 175 cancer patients paired with 350 cancer-free individuals based on age, gender, comorbidities, and COVID-19 severity. As observed in Fig. 1J for cancer patients, there was an anti-correlation between Ct values at diagnosis and the duration of viral RNA shedding in cancer-free patients ($r = -0.6$, $P < 0.0001$) (Fig. S7A). Not surprisingly, blood absolute lymphocyte counts (ALC) at diagnosis anticorrelated with the duration of PCR positivity in Cancer_FR1_TR and Cancer_FR1_CR cohorts (Fig. 3A). However, although the ALC before the COVID-19 pandemic (blood drawn from December 2019 to mid-March 2020) were already somewhat lower in LVS than in SVS cancer patients, the ALC during the outbreak dramatically dropped in cancer patients doomed to develop LVS (in both Cancer_FR1_TR and Cancer_FR1_CR cohorts), more so than in individuals prone to SVS (Fig. 3B, left panel). The extent in ALC reduction was more severe in patients presenting LVS than SVS (Fig. 3C). Of note, ALC recovered in both patient groups regardless of the LVS/SVS status. It supports that reduced ALC at COVID-19 diagnosis is induced by the virus rather than by cancer (Fig. 3B, left panel). In accord with the finding that LVS correlates with high viral load at symptom onset (Fig. 1J, K), higher viral loads at diagnosis were associated with a pronounced COVID-19-associated lymphopenia (Fig. 3B, right panel). Contrary to what we observed in cancer patients, there was no correlation between ALC at diagnosis, and duration of RT-qPCR in cancer-free individuals ($r = 0.05$, $P = 0.3$) (Fig. S7B). Comparing ALC at diagnosis to ALC post-hospitalization, we concluded that cancer-free patients presenting with a high viral load (Ct<25) did not harbor lymphopenia at diagnosis or during the acute phase ($P = 0.11$) (Fig. S7C) in contrast with what we observed in cancer patients. So, virus-induced lymphocyte loss occurs in a fraction of individuals with cancer and is detrimental for the prognosis. This phenomenon may be ascribed to cancer-associated chronic inflammation or co-medications.

We next assessed the clinical significance of the interaction between Ct values, ALC, and cancer patient survival in 110 cancer patients with COVID-19 (Discovery cohort (first surge of the pandemic) including 84 patients from Cancer_FR1 treated at Gustave Roussy and 26 patients from Cancer_ FR3 treated at Léon Bérard Cancer Center in Lyon, France) (Fig. 3D and Table 1). Cox logistic regression analyses and Kaplan–Meier survival curves were performed after stratification of the patients according to both, Ct and ALC values at diagnosis. The cutoff for the Ct value was 25 and corresponded to the median of the whole cohort FR1 + FR3, which coincided with the threshold at which live virus particles can be isolated in 70% of the cases [31]. The cut-off value for ALC was the median found in patients with high viral load (Ct <25) at diagnosis ($ALC = 800/mm^3$). ALC combined with Ct values predicted cancer-related overall survival in univariate analyses across all cancer stages (local, locally advanced, or metastatic) (Fig. 3D and Table 1). While patients presenting with $ALC > 800/mm^3$ and low viral load (Ct >25) exhibited prolonged survival, a dismal prognosis affected 21% of them (23/110) who presented both deep lymphopenia ($ALC < 800/mm^3$) and high viral loads (Ct <25) at diagnosis (Fig. 3D) culminating in 40% deaths at 3 months. All four groups were comparable in terms of age, gender, comorbidities, cancer type, or staging (Table 1). Multivariate Cox analysis stratified for the cohort origin and adjusted for age (hazard ratio (95% confidence interval) = 1.042 [1.013; 1.072], $P = 0.0043$), ECOG performance status (4.547 [1.845; 11.206], $P = 0.0001$), gender (1.668 [0.775; 3.588], $P = 0.1907$), and metastatic status and hematological malignancies (2.747 [1.090; 6.923], $P = 0.0322$) confirmed a continuous decrease of risk with the increase of the Ct value (0.841 [0.776; 0.911], $P = 0.00002$) and the increase of the ALC (0.282 [0.119; 0.672], $P = 0.0043$) (Fig. 3E). Of note, treatment retardation could not explain the high mortality of patients presenting with a high viral load and low ALC (Table 1).

We confirmed these predictors (ALC < 800 & Ct <25) of poor survival during the second surge of the pandemic (between May 5, 2020 to November 25, 2020) in 116 new COVID-19 cancer patients ("Validation", Cancer_FR1 and Cancer_FR3, Fig. 1A). Here again, the subset of patients with ALC < 800 & Ct <25 ($n = 38/116$, 32.7%) exhibited the most reduced overall survival compared to

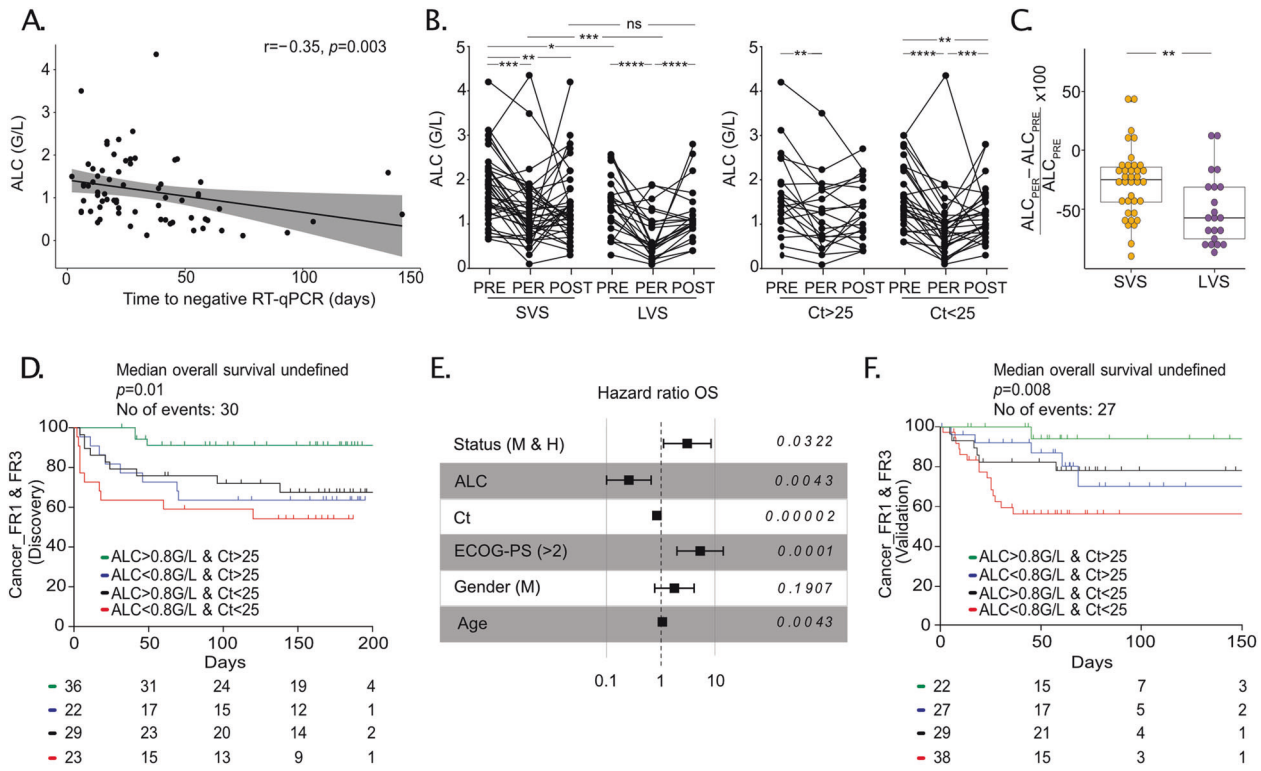

Fig. 3 Lymphopenia and high viral load are dismal prognosis factors for overall survival in cancer patients in the first and second surge of the pandemic. A Spearman correlation between the absolute lymphocyte counts (ALC) of Cancer_FR1 (from translational research and clinical routine), with the duration of SARS-CoV-2 RT-qPCR positivity (only evaluable patients for both factors, $n = 69$ patients). **B**, **C** ALC of Cancer_FR1 (from translational research and clinical routine) in SVS ($n = 37$ patients) versus LVS ($n = 22$ patients) subsets (**B**, left panel) or SARS-CoV-2-cycle threshold (Ct) >25 ($n = 21$ patients) versus Ct <25 ($n = 29$ patients) (**B**, right panel) monitored during the COVID-19 pandemic ("PER", between −4 and +7 days of the disease diagnosis by RT-qPCR), between 210 and 12 days before the symptom onset of COVID-19 ("PRE") or within the recovery period (between 0 and 123 days after negative RT-qPCR) ("POST") at Gustave Roussy, with the calculation of the reduction between "PRE" and during COVID-19 (**C**). One patient defined as an outlier (at 215%) by ROUT method was excluded from the LVS group for the analysis. Each line and dot represents one patient and one sample. Statistical analyses used one-way ANOVA (paired and unpaired) with Kenward–Roger method taking into account the number of specimen/patient (**B**): $^{*}P < 0.05$, $^{**}P < 0.01$, $^{***}P < 0.001$, $^{****}P < 0.0001$, and Mann–Whitney (**C**): $^{**}P < 0.01$. **D** Kaplan–Meier curve and Cox regression analysis of overall survival of cancer patients from the Discovery (1st surge) cohort (Cancer_FR1 + Cancer_FR3), all stages included, according to ALC and Ct value at diagnosis. Refer to Table 1 for patient characteristics. **E** Multivariate Cox regression analysis stratified for the cohort and adjusted for age, ECOG status, gender, and metastatic and/or hematological status of cancer patients from the Discovery (1st surge) cohort (Cancer_FR1 + Cancer_FR3). **F** Kaplan–Meier curve and Cox regression analysis of overall survival of cancer patients from Validation (2nd surge) cohort (Cancer_FR1 + Cancer_FR3), all stages included, according to ALC and Ct value at diagnosis. Refer to Table 1 for patient characteristics.

the other groups with >40% deaths at 50 days (Fig. 3F). Of note, the reduced survival rate in the subset of patients defined by ALC < 800 & Ct <25 was not a peculiarity of hematological malignancies (characterized by therapy-induced B cell depletion) since it was also observed in patients with solid neoplasia (Fig. S7D and S7E).

In conclusion, it appears that uncontrolled viral infection capable of compromising the number and function of circulating lymphocytes predicts the lethal outcome of patients with malignant disease.

Immunological, metabolic, and metagenomic parameters associated with virus-induced lymphocyte loss

Multiple and non-exclusive mechanisms could account for virus-associated lymphopenia [25, 27, 32–35]. To further investigate this deleterious virus-induced lymphocyte loss, we searched for the most robust correlates between ALC and immunological, metabolic, or pathogenic cues in the Cancer_FR_TR cohort as well as noncancer COVID-19 patients that we previously reported [23].

First, the Spearman correlation matrix of the main immunological and serum markers monitored at the peak of disease (within the first 20 days of disease onset) indicated close interconnections between lymphocyte proportions and their subsets within leukocytes (Fig. 4A). Lymphopenia, which is a prominent feature of COVID-19 and a hallmark of severe infection, distinguished LVS from SVS or asymptomatic individuals (Fig. S8A, B), as exemplified for the proportion of B lymphocytes among total $CD45^+$ leukocytes after 20 days of symptoms. As reported [27], the transitional differentiation of naive into effector/memory T cells co-expressing $CD38^+HLA\text{-}DR^+$ among $CD8^+$T cells is a hallmark of COVID-19 that persisted in LVS compared to controls and SVS ($P = 0.002$ and $P = 0.012$) (Fig. S8C, D). In particular, the most compelling LVS-associated T-cell subpopulation that expanded in the context of lymphopenia was the non-naive (non-$CD45RA^+CD27^+$) $CD8^+$ T subset expressing an activation/exhaustion phenotype characterized by early and sustained expression of PD-1 (Fig. 4B), Eomes, Granzyme B, TCF-1 including the pro-apoptotic marker CD95-L (FasL) (Fig. 4C, D, left panel). There was no difference in T-bet^+ (effector) expression within $Eomes^+PD\text{-}1^+$ non-naive $CD8^+$ over the different time courses and compared with controls (6.2 ± 0.74% (mean ± SEM) (data shown). However, COVID-19^+ patients (both asymptomatic and symptomatic ones) exhibited higher proportions of cells co-expressing TOX and Eomes within PD-1^+ non-naive $CD8^+$ compared with patients at recovery or controls (Fig. S8E, left panel). Interestingly, a subset of these exhausted PD-1^+CD8^+ T cells was proliferating while

Table 1. Clinical characteristics of Cancer_FR1 and Cancer_FR3 patients from discovery and validation cohorts presenting cycle threshold below (Ct<25) or above 25 (Ct>25) and with (<800/mm^3) or without (>800/mm^3) lymphopenia at diagnosis (refer Fig. 3D–F).

Discovery cohort							
Cancer patients' characteristics		**Cancer_FR1_TR + Cancer_FR1_CR + Cancer_FR3 (*n* = 110)**	**Ct > 25 & ALC > 800 (*n* = 36)**	**Ct > 25 & ALC < 800 (*n* = 22)**	**Ct < 25 & ALC > 800 (*n* = 29)**	**Ct < 25 & ALC < 800 (*n* = 23)**	***P***
Age (year)	Median (range)	62 (13–95)	62 (13–82)	63 (20–83)	59 (38–95)	60 (21–84)	*0.76*[#]
Gender—no. (%)	Male	46 (42)	18 (50)	9 (41)	13 (45)	6 (26)	*0.33*
	Female	64 (58)	18 (50)	13 (59)	16 (55)	17 (74)	
Number of comorbidities —no. (%)°	0	38 (45)	10 (45)	5 (34)	10 (38)	13 (62)	*0.26*
	1	25 (30)	5 (23)	6 (40)	10 (38)	4 (19)	
	2	16 (19)	4 (18)	2 (13)	6 (24)	4 (19)	
	3	5 (6)	3 (14)	2 (13)	0 (0)	0 (0)	
Comorbidities —no. (%)°	COPD	6 (7)	2 (9)	1 (7)	1 (4)	2 (10)	*0.98*
	BMI ≥ 30	12 (14)	2 (9)	3 (20)	4 (15)	3 (14)	
	Hypertension	32 (38)	11 (50)	7 (47)	8 (31)	6 (29)	
	Congestive heart failure	3 (6)	1 (5)	1 (7)	1 (4)	0 (0)	
	Diabetes mellitus	10 (12)	3 (14)	1 (7)	4 (15)	2 (10)	
Type of malignancy —no. (%)	S	92 (84)	33 (92)	15 (68)	26 (90)	18 (78)	*0.08*
	H	18 (16)	3 (8)	7 (32)	3 (10)	5 (22)	
Cancer spread —no. (%)	Localized	19 (17)	7 (19)	1 (5)	7 (24)	4 (17)	*0.46*
	Locally advanced	24 (22)	9 (25)	6 (27)	3 (10)	6 (26)	
	Metastatic	67 (61)	20 (56)	15 (68)	19 (66)	13 (57)	
Cancer status —no. (%)	Remission or NED	29 (26)	12 (30)	3 (14)	10 (34)	4 (17)	*0.21*
	SD/PD	47 (43)	17 (47)	11 (50)	11 (38)	8 (35)	
	Present or PD	34 (31)	7 (19)	8 (36)	8 (28)	11 (48)	
ECOG PS—no. (%)	0	28 (25)	13 (36)	5 (23)	5 (18)	5 (22)	*0.01*
	1	46 (42)	18 (50)	4 (18)	12 (41)	12 (52)	
	2 or more	36 (33)	5 (14)	13 (59)	12 (41)	6 (26)	
Type of anticancer therapy—no. (%)	None*	53 (48)	20 (56)	8 (36)	14 (48)	10 (43)	*0.53*
	Chemotherapy	47 (43)	4 (11)	12 (55)	11 (38)	14 (61)	*0.19*
	Radiotherapy	8 (7)	2 (6)	3 (14)	1 (3)	2 (9)	
	Surgery	8 (7)	3 (8)	2 (9)	3 (10)	0 (0)	
	Hormonal therapy	11 (10)	4 (11)	0	4 (14)	3 (13)	
	Immunotherapy	12 (11)	4 (11)	1 (5)	4 (14)	3 (13)	
	Others	11 (10)	2 (6)	2 (9)	0 (0)	5 (22)	
Delay of treatment —no. (%)°	Yes (range: 16–170 days)	12 (32)	2 (33)	2 (22)	8 (67)	0 (0)	*<0.01*
	No	26 (68)	4 (67)	7 (78)	4 (33)	11 (100)	
Clinical course —no. (%)°	Day hospital	27 (32)	10 (45)	4 (27)	8 (31)	5 (24)	*0.63*
	Hospitalization	53 (63)	12 (55)	10 (67)	17 (65)	14 (67)	
	Admission to ICU	4 (5)	0	1 (6)	1 (4)	2 (9)	
Death—no. (%)	Yes	31 (28)	4 (11)	7 (32)	9 (31)	11 (48)	*0.02*

Validation cohort							
Cancer patients' characteristics		**Cancer_FR1_CR + Cancer_FR3 (*n* = 116)**	**Ct > 25 & ALC > 800 (*n* = 22)**	**Ct > 25 & ALC < 800 (*n* = 27)**	**Ct < 25 & ALC > 800 (*n* = 29)**	**Ct < 25 & ALC < 800 (*n* = 38)**	***P***
Age (year)	Median (range)	65 (13–91)	55 (13–86)	64 (46–77)	68 (41–84)	66 (18–91)	*0.09*[#]
Gender—no. (%)	Male	71 (61)	9 (41)	14 (52)	17 (59)	23 (61)	*0.48*
	Female	45 (39)	13 (59)	13 (48)	12 (41)	15 (39)	
Type of malignancy —no. (%)	S	85 (73)	19 (86)	19 (70)	22 (76)	25 (66)	*0.36*
	H	31 (27)	3 (14)	8 (30)	7 (24)	13 (34)	
	Localized	9 (8)	3 (14)	1 (4)	3 (10)	2 (5.3)	*0.40*

Table 1 continued

Validation cohort							
Cancer patients' characteristics		**Cancer_FR1_CR + Cancer_FR3 (*n* = 116)**	**Ct > 25 & ALC > 800 (*n* = 22)**	**Ct > 25 & ALC < 800 (*n* = 27)**	**Ct < 25 & ALC > 800 (*n* = 29)**	**Ct < 25 & ALC < 800 (*n* = 38)**	***P***
Cancer spread —no. (%)	Locally advanced	15 (13)	4 (18)	6 (22)	3 (10)	2 (5.3)	
	Metastatic	82 (70)	15 (68)	17 (63)	21 (72)	29 (76.4)	
	Unknown	10 (9)	0 (0)	3 (11)	2 (8)	5 (13)	
Type of anticancer therapy—no. (%)°*	None*	33 (36)	14 (74)	8 (36)	5 (23)	6 (21)	*0.001*
	Chemotherapy	28 (31)	1 (5)	11 (50)	5 (23)	11 (39)	*0.17*
	Radiotherapy	5 (5)	0 (0)	2 (9)	1 (5)	2 (7)	
	Surgery	1 (1)	0 (0)	0 (0)	1 (5)	0 (0)	
	Hormonal therapy	4 (4)	2 (11)	1 (5)	0 (0)	1 (4)	
	Immunotherapy	20 (22)	2 (11)	2 (9)	6 (27)	10 (36)	
	Others	17 (19)	1 (5)	4 (18)	5 (23)	7 (25)	
Death—no. (%)	Yes	27 (23)	1 (4)	5 (18)	6 (21)	15 (39)	*0.016*

P values are in Italic and were analyzed by Chi-Square / Fisher's exact tests.
BMI body mass index, *COPD* Chronic obstructive pulmonary disease, *CR* clinical routine, *Ct* cycle threshold, *DM* diabetes mellitus, *H* hematological malignancies, *ICU* intensive care unit, *n* number, *NED* no evidence of disease, *no.* number, *PD* progressive disease, *PS* performance status, *S* solid tumors, *SD/PR* stable disease/ partial response, *TR* translational research, *in the 4 weeks before inclusion.
Statistical analyses: ANOVA (Kruskal–Wallis)(#), Chi-Square or Fisher's exact tests.
°Unknown for Cancer_FR3_discovery ($n = 26$ patients), calculations with Cancer_FR1_discovery, $n = 84$.
°*Unknown for Cancer_FR3_validation ($n = 25$ patients), calculations with Cancer_FR1_validation, $n = 91$.

undergoing apoptosis during the acute phase compared with patients at recovery (Fig. S8E, right panel). All of these data tend to indicate that circulating PD-1-expressing $CD8^+$ T cells are rather exhausted than activated with a trend toward apoptosis that could participate in the lymphopenia described in COVID-19^+ cancer patients. The abundance of these non-naive exhausted PD-1^+CD8^+ Tc1 cells positively correlated with the duration of SARS-CoV-2-specific RT-qPCR positivity (Fig. 4B, bottom panel and Fig. 4D, right panel) and may explain, at least partly, the reduced fitness and half-life of peripheral lymphocytes.

Second, we performed the serum metabolome determined by untargeted and targeted mass spectrometry-based metabolomics analyzing more than 221 metabolites in 31 cancer patients from Cancer_FR1_TR, as well as in a previously described cohort of 66 cancer-free COVID-19^+ patients for validation [23]. The non-supervised hierarchical clustering of the serum metabolome clearly contrasted LVS from LVS patients (Fig. S9). The Volcano plot aimed at identifying significant differences between LVS and SVS patients pointed out the biliary salt metabolic pathway segregating SVS from LVS serum (Fig. 5A), previously described to have biological significance for lymphocyte fitness and maintenance [32–35]. Secondary biliary acids (such as the murideoxycholic acid (muri-DOC) (Fig. 5B, left panel) and the DOC (Fig. 5C)) were decreased in LVS compared with SVS and controls and correlated with lower ALC in cancer patients (Fig. 5B, right panels) or severe COVID-19 (Fig. 5D). Similarly, two other derivatives of DOC (hyo-DOC, urso-DOC) were decreased in LVS (compared to controls and SVS, Fig. S10A, B, left panels) and were associated with lymphocyte loss (Fig. S10A and S10B, right panels).

Another metabolic pathway pertaining to polyamines with high biological significance for age-related immunosenescence [36–38] was also strongly associated with the duration of RT-qPCR positivity, ALC, and disease severity (Fig. 5E–G and Fig. S9). In particular, the N1, N8 diacetylspermidine that anticorrelated with ALC (Fig. 5F, right panel) increased in the serum of LVS patients (but not SVS, Fig. 5F, left panel), in accordance with its marked rise in severe COVID-19 in cancer-free individuals (Fig. 5G, left panel) where high levels coincided with the lymphocyte drop (Fig. 5G, right panel). Of note, the tryptophane/kynurenine or lactic acid metabolites were not relevant in our study (Fig. 5A and Fig. S9).

Third, endotoxemia was shown to correlate with the cytokine storm during COVID-19 [25] and might cause activation-induced lymphocyte cell death. Assuming that the gut permeability could be altered during COVID-19-associated intestinal dysbiosis [39], we studied the circulating microbial populations associated with whole leukocytes by sequencing blood rDNA using next-generation sequencing of V3–V4 variable regions of the 16S rRNA bacterial gene as previously described [40]. Although we failed to observe significant quantitative differences in blood bacterial load between SVS ($n = 14$) and LVS ($n = 15$) patients, the linear discriminant analysis effect size indicated significant taxonomic differences in the bacteria family members between the two groups (Fig. 6A, B). The DNA from Enterobacteriaceae (mainly composed of *Escherichia Shigella* genus) was overrepresented in leukocytes of LVS compared with SVS patients (Fig. 6A, B, C, left panel). The circulating Enterobacteriaceae-related DNA markedly anticorrelated with CCL22 (a hallmark of SVS, Fig. 2A), but was strongly associated with the increase of exhausted $CD8^+$ T lymphocytes (Fig. 6D, E). There was a trend for an increase in the relative abundance of Micrococcaceae in the blood leukocytes of LVS that was confirmed in cancer patients with dismal prognosis (ALC < 800 & Ct <25) (Fig. 6F, G, H).

Overall, we conclude that virus-associated lymphopenia may result in complementary or coordinated orthogonal disorders.

DISCUSSION

To interrogate viral–host interactions during the COVID-19 pandemic in cancer patients, we studied 1106 patients, among them 59% were cancer bearers (FR1 + FR2 + FR3 + CA), and 1063 COVID-19-positive (Fig. 1A). We used high-dimensional flow cytometry to perform deep immune profiling of innate, B and T cells, and measurements of 51 soluble markers, with temporal analysis of immune changes during infection in one cohort that was further explored by blood metabolomics and metagenomics.

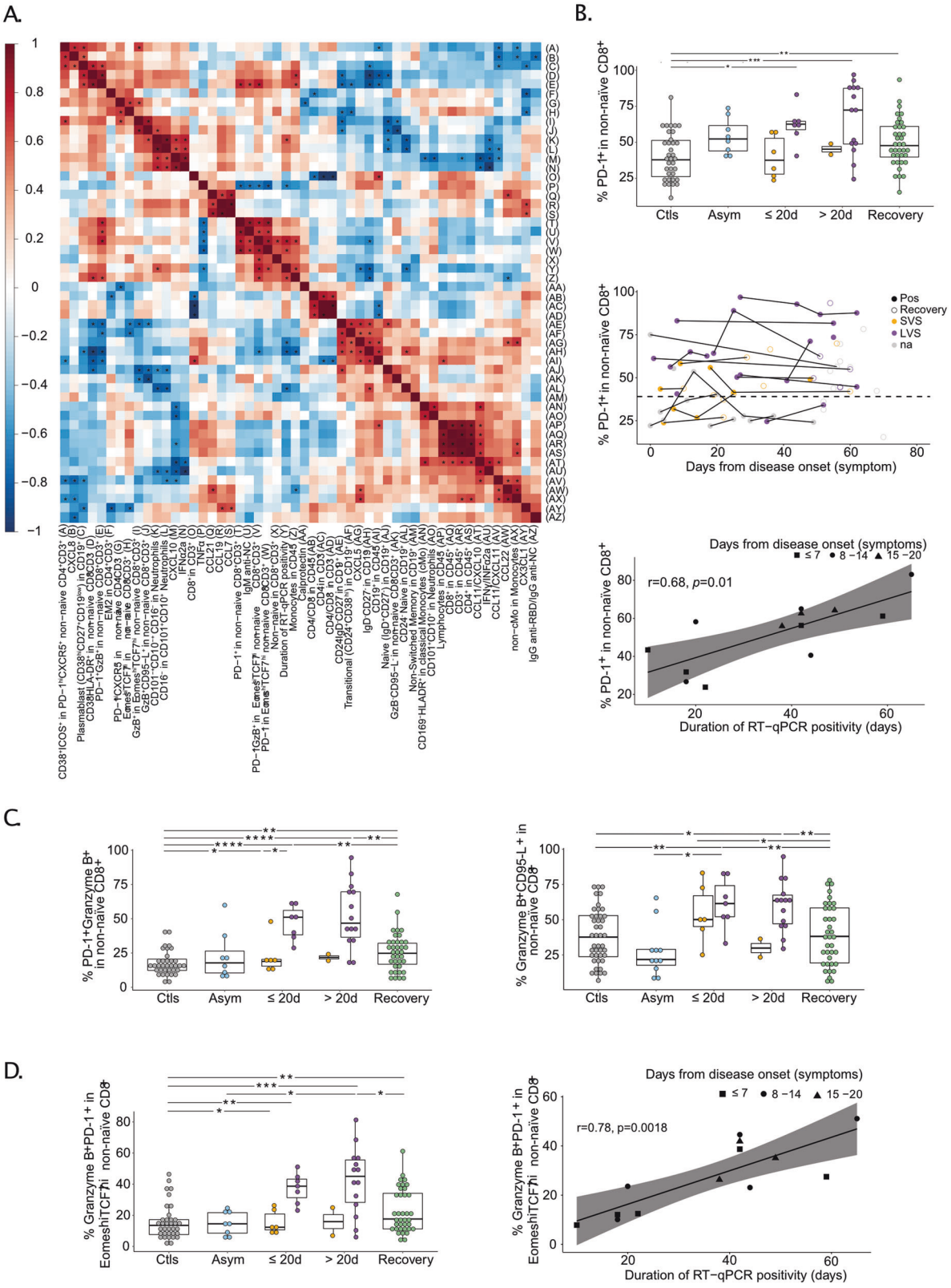

This longitudinal immune analysis was linked to virologic and oncological data (Figs. S5 and S6). Using this approach, we made several intriguing observations.

First, 51%, 20%, and 26% of cancer patients in FR1_TR, FR1_CR, and CA, respectively, still shed SARS-CoV-2 RNA after day 40 from symptoms onset (versus 2% in HCW), correlating with high viral loads (Ct values <25) at diagnosis. Indeed, isolation of replication-competent viral strains between 10 and 20 days after symptom onset has been documented in some persons with severe COVID-19, mostly in immunocompromised

Fig. 4 Prolonged viral shedding is associated with T-cell exhaustion. A Spearman correlation matrix focusing on the most significant immune variables and serum analytes monitored within the first 20 days of symptoms in patients diagnosed with COVID-19 in the Cancer_FR1_TR cohort. Stars indicate significant values ($P < 0.05$) for positive (red) or negative (blue) correlations. **B** Percentages of PD-1 expressing cells within the non-naive $CD8^+CD3^+$ population (**B**, upper panel), monitoring in various phases of COVID-19 presentation (no virus infection (CtIs, gray dots), asymptomatic viral infection (Asym, light blue dots), symptomatic viral infection examined in the first 20 days (≤20 d) or after 20 days (>20 d) of symptoms with those experiencing short-term viral RNA shedding (SVS, orange dots) or long-term viral RNA shedding (LVS, purple dots) and RT-qPCR-negative COVID-19 patients in the convalescent phase (recovery, green dots or circled dots) among Cancer_FR1_TR (**B**, middle panel) and Spearman correlation with the duration of SARS-CoV-2 RT-qPCR positivity measured within the first 20 days of symptoms (**B**, lower panel). **C** Percentages of subsets co-expressing PD-1 and Granzyme B (**C**, left panel) or Granzyme B and FasL (**C**, right panel) in non-naive $CD8^+$. **D** Percentage of PD-1^+ and Granzyme B^+ within the non-naive $CD8^+$ expressing $Eomes^{high}TCF\text{-}1^{high}$ gate (**D**, left panel) and Spearman correlation between this ratio measured within the first 20 days of symptoms with the duration of SARS-CoV-2 RT-qPCR positivity (**D**, right panel). Box plots display a group of numerical data through their 3rd and 1st quartiles (box), mean (central band), minimum, and maximum (whiskers). Each dot represents one sample, each patient being drawn one to three times. Statistical analyses used one-way ANOVA with Kenward–Roger method to take into account the number of specimen/patients: $^*P < 0.05$, $^{**}P < 0.01$, $^{***}P < 0.001$. Each line and dot represents one patient and one sample, respectively (**B**, middle panel).

cases [41]. However, ~90% of their specimens no longer yielded replication-competent viruses after day 15 from symptom onset [42, 43]. Prolonged shedding of influenza, parainfluenza, rhinovirus, seasonal coronavirus, and the respiratory syncytial virus has previously been detected in immunosuppressed patients [44–48]. Cancer dissemination, cancer therapies, and virus-induced lymphopenia might cause an immunodeficiency that eventually jeopardizes virus clearance. The proposed mechanisms by which lymphopenia occurs in COVID-19 (often shared with cancer dissemination) [49] include virus-induced atrophy of secondary lymphoid organs [50–52], the disappearance of germinal centers [28], the direct pro-apoptotic activity of the virus related to ACE2-dependent or ACE2-independent entry into lymphocytes [53], T-cell demise consecutive to activation and exhaustion [54, 55], senescence [1, 56], and antiproliferative effects of lactic acid [57]. However, in our study, we found that lymphocyte loss was correlated with a decrease of secondary biliary salts in LVS patients, most likely associated with increased gut permeability that leads to bacterial translocation, as we observed increased circulating DNA for Micrococcaceae and Enterobacteriaceae family members. Moreover, the transformation of spermidine into N1, N8 diacetylspermidine was linked to decreased ALC, in accordance with the role of spermidine in preventing aging-related loss of lymphocyte fitness [36–38].

Second, prolonged viral RNA carriage was associated with signs of immunopathology (exacerbated T-cell responses, extrafollicular TFH, and plasmablast recirculation, exhausted PD-1^+ Tc1 cells, sustained serum type 1 IFN levels), likely maintaining a positive feedback loop for the expression of the interferon-signaling genes product ACE2 [58] and pro-inflammatory interactions between airway epithelia and immune cells [29].

Third, prolonged SARS-CoV-2 RNA shedding after day 40 might precede the aggravation of both COVID-19 and malignant disease. Indeed, virus and/or cancer-induced lymphopenia and T-cell exhaustion may jointly enfeeble tumor immunosurveillance [59]. Interestingly, SARS-CoV-2 virus-induced immunopathology was accompanied by increased blood levels of IL-8 (Fig. S4G) and VEGF [26], which are well-known pro-angiogenic and pro-tumorigenic growth factors, predicting failure to cancer immunotherapy [60]. Of note, patients with high initial viral loads or LVS tended to accumulate poor prognosis-related parameters than SVS or patients with higher Ct values in both cohorts (Table 1 & Table S1), being older (66 versus 56 years old, $P = 0.08$), more metastatic at diagnosis of infection (72% versus 29%, $P = 0.011$), and increased hospitalization rates (83% versus 23%, $P = 0.001$). As a result, virus-induced lymphopenia markedly predicted early death of patients, within the first 2–3 months post-COVID-19 diagnosis in the first and second surge of the pandemic (in more than 200 patients) and call for caution to administer chemotherapy or steroids at the acute phase of the viral infection that exacerbate immunosuppression.

These observations call for a careful follow-up of cancer patients, in particular those bearing hematological and metastatic malignancies, during the second wave of COVID-19. Given the non-consensual efficacy of vaccines against influenza virus in vulnerable individuals suffering from cancer-, virus-, and age-associated lymphopenia [49, 61], passive immunization of high affinity neutralizing monoclonal antibodies against SARS-CoV-2 at COVID-19 onset might be envisaged. This could be combined with therapeutic stimulation of lymphopoiesis (for instance with rIL-7, G-CSF, inhibitors of indoleamine 2,3 deoxygenase), to achieve immunological tonus that is compatible with anticancer treatments [62–64]. Clinical trials are underway to evaluate rIL-7 against COVID-19, but may benefit from patient stratification based on Ct values, duration of viral RNA shedding, and ALC [65, 65, 66].

MATERIALS AND METHODS

All cohorts (refer to Supplementary Material, Table 1).

Cohorts for the duration of viral PCR positivity

Cancer_FR1_Translational Research (TR) (ONCOVID) clinical trial and regulatory approvals for translational research. *Principles:* Gustave Roussy Cancer Center sponsored the "ONCOVID" trial and collaborated with the academic authors on the design of the trial and on the collection, analysis, and interpretation of the data. Sanofi provided trial drugs. The trial was conducted in accordance with Good Clinical Practice guidelines and the provisions of the Declaration of Helsinki. All patients provided written informed consent. Protocol approval was obtained from an independent ethics committee (ethics protocol number EudraCT No: 2020-001250-21). The protocol is available with the full text of this article at https://clinicaltrials.gov/ct2/show/NCT04341207. *Patients:* ONCOVID eligible patients were adults fitted for, or under, or recently treated by chemotherapy and/or immune-checkpoint blockade for the treatment of solid tumors or hematological malignancies (please refer to Table 1 and Table S1). Patients diagnosed for COVID-19 from April 10, 2020 to May 4, 2020 were included in the Discovery cohort and patients from May 5, 2020 to November 25, 2020 were included in the Validation cohort. *Trial design:* Cancer patients were screened for SARS-CoV-2 virus carriage by nasopharyngeal sampling at every hospital visit. The presence of SARS-CoV-2 RNA was detected by RT-qPCR assay in a BSL-2 laboratory. Asymptomatic and symptomatic patients (i.e., presenting with fever (t° >38 °C) and/or cough and/or shortness of breath and/or headache and/or fatigue and/or runny nose and/or sore throat, anosmy/agueusia) with a positive SARS-CoV-2 RT-qPCR test, shifted to the interventional phase (tailored experimental approach with hydroxychloroquine and azithromycin therapy in symptomatic SARS-CoV-2-positive subjects). Asymptomatic or symptomatic patients with negative SARS-CoV-2 RT-qPCR test continued their standard of care anticancer treatments. Repeated RT-qPCR for SARS-CoV-2 on nasopharyngeal swabs and blood samples were performed to monitor the status for SARS-CoV-2 and the immune response, respectively, in COVID-19-positive and negative patients. The COVID-19 severity was defined based on oxygen, imaging, and hospitalization criteria. Patients with mild COVID-19 disease had limited clinical symptoms not requiring scan or hospitalization; patients with a moderate COVID-19 disease were

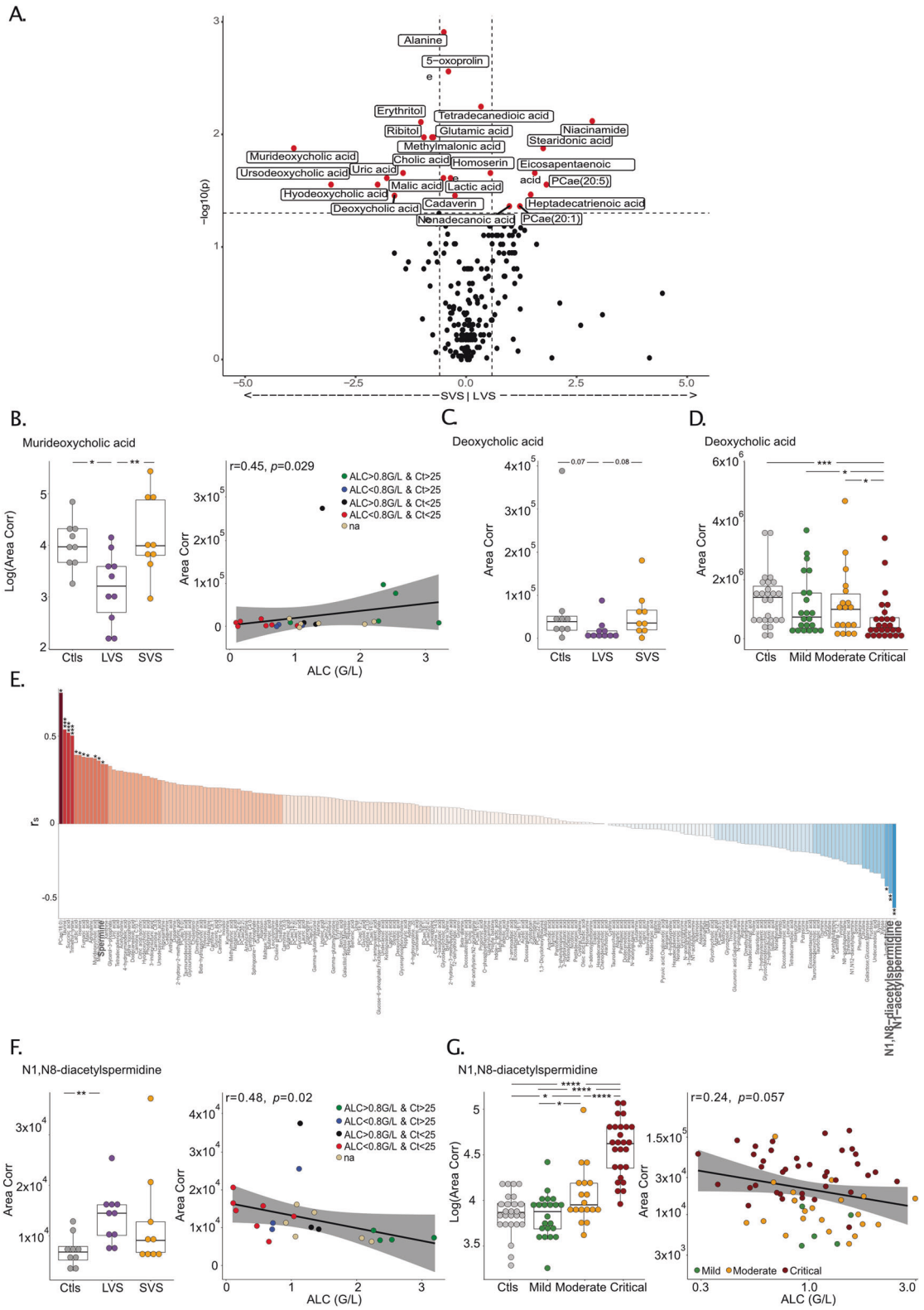

symptomatic with dyspnea and radiological findings of pneumonia on thoracic scan requiring hospitalization and a maximum of 9 L/min of oxygen; severe patients had respiratory distress requiring intensive care and/or more than 9 L/min of oxygen. *Samples for translational research:* Whole blood was used for high-dimensional spectral flow cytometry analyses. Serum samples were used to monitor the concentrations of cytokines and chemokines released and to titer anti-SARS-CoV-2 IgG, M and A antibodies (see "Blood analysis" section) (Supplementary Material Fig. 1).

Healthcare workers (HCW) of Cancer_FR1. The part of the research including healthcare workers was conducted in compliance with General

Fig. 5 Lymphopenia and prolonged viral shedding are associated with perturbations of the polyamine and biliary acid pathways. A Volcano plot identifying statistically different serum metabolites between patients experiencing short-term viral RNA shedding (SVS) and those experiencing long-term viral RNA shedding (LVS) in Cancer_FR1_TR cohort. Metabolites significantly different between both groups are in red and annotated ($P < 0.05$, FC > 0.5). **B** Levels of murideoxycholic acid according to the duration of viral shedding in Cancer_FR1_TR (left panel) and Spearman correlation with absolute lymphocyte count (ALC) (right panel). The color code corresponds to the category of cycle threshold (Ct) and ALC at diagnosis. **C**, **D** Serum concentrations of deoxycholic acid according to the duration of viral shedding in Cancer_FR1_TR (**C**) and the severity of COVID-19 infection in cancer-free individuals (**D**). **E** Waterfall plot of Spearman's correlation coefficient (r_s) between ALC and 221 metabolites in the serum of patients diagnosed positive for COVID-19. **F** N1, N8 diacetylspermidine relative abundance in controls, SVS and LVS patients in the Cancer_FR1 cohort, that is negatively correlated with the ALC. The color code corresponds to the category of cycle threshold (Ct) and ALC at diagnosis. **G** Levels of N1, N8 diacetylspermidine in noncancer COVID-19 patients according to the clinical severity compared to COVID-19-negative controls (Ctls) ($P < 0.0001$) (**G**, left panel), that are negatively correlated with the absolute lymphocyte count (ALC) (**G**, right panel). Box plots display a group of numerical data through their 3rd and 1st quartiles (box), mean (central band), minimum and maximum (whiskers). Each dot represents one sample, each patient being drawn once for cancer-free individuals and one to two times for cancer patients. Statistical analyses used one-way ANOVA with Kenward–Roger method to take into account the number of specimen/patient (**B**, left panel, **C**–**E**, left panel): $*P < 0.05$, $**P < 0.01$), non-parametric unpaired Wilcoxon test (Mann–Whitney) for each two-group comparison: $*P < 0.05$, $**P < 0.01$, $***P < 0.001$, $****P < 0.0001$.

Data Protection Regulation (GDPR) and the French Data Protection Authority's recommendation about Data Protection in clinical researches. Gustave Roussy Data Protection Officer (DPO) has evaluated this project and sent to the principal investigator a formalized operational action plan about data protection compliance: patient's information, security measures, good practices about pseudonymization, etc. All of the DPO's recommendations have been applied by the research team. Healthcare workers diagnosed for COVID-19 between 24 March, 2020 and 24 April, 2020 were included. Results of RT-qPCR, cycle threshold, age, gender, and number of comorbidities were collected. Data from healthcare workers who refused to participate and/or with cancer were excluded. In agreement with MR004 in France, we reported the series to the national information science and liberties commission.

Second series of patients with cancer (Cancer_FR2). CASE-CONTROL study: All comers spontaneously presenting at a general hospital for infectious diseases (IHU Méditerranée Infections, Marseille, FR) (Table S1) from February 27, 2020 to December 15, 2020 composed of 996 COVID-19 patients. We performed a case-control study at a 1:2 paired ratio where the 175 cancer patients (with a currently treated cancer or history of cancer) were matched with 350 cancer-free individuals on age, gender, comorbidities relevant for COVID-19. Of note, >75% received hydroxychloroquine and >96% received azithromycin (Table S1) [16, 67]. This study was approved by the IHU Méditerranée Infections review board committee (Méditerranée Infection N°: 2020-021).

Third series of cancer patients from Canada (Cancer_CA). We used 66 individuals from the clinical cohort previously reported [18] for whom data were available (Table S1). This study was conducted across eight Canadian institutions in Quebec and British Columbia and was approved by the institutional ethics committee at each site (Ethics number: MP-02- 2020-8911 and H20-00892).

Fifth series of cancer patients, Cancer_FR1_Clinical Routine (CR). We used the clinical cohort previously reported [2] (Table S1). In accordance with the French regulations, there was no requirement for ethical approval to be sought for this observational study, based on medical files. Patients diagnosed for COVID-19 from March 14, 2020 to April 29, 2020 were included in the Discovery cohort and from April 29, 20 to November 25, 2020 in the Validation cohort. This study was also declared to the Gustave Roussy Cancer Centre's DPO and registered on the website of the French Healthcare Data Institute (declaration number: MR4911200520).

Cohorts for the ALC and Ct value predictors: first surge and the second surge of the pandemic

Cancer_FR1_Translational Research (TR) (ONCOVID) clinical trial and regulatory approvals for translational research. Among the 52 patients diagnosed for COVID-19 during the first surge (from April 10, 2020 to May 4, 2020), absolute lymphocyte count (ALC) and cycle threshold (Ct) were available for 34 patients whom were included in this cohort.

Then, among the 18 patients included in ONCOVID during the second surge (from May 5, 2020 to November 25, 2020), absolute lymphocyte count (ALC) and cycle threshold (Ct) were available for nine patients who were included in this cohort

Cancer patients referred to the clinical routine (Cancer_FR1_CR). In accordance with the French regulations, there was no requirement for ethical approval to be sought for this observational study, based on medical files. Among the 178 patients diagnosed for COVID-19 during the first surge (March 14, 2020 to April 29, 2020), ALC and Ct were available for 50 patients who were included in this cohort. Then, among 170 patients with cancer diagnosed for COVID-19 during the second surge (from May 5, 2020 to November 25, 2020), ALC and cycle threshold Ct were available for 82 patients who were included in this cohort.

Cancer patients referred to the Centre Léon Bérard, Lyon, France (Cancer_FR3). The PRE-ONCOVID-19 study was approved by the Institutional review board of the Centre Leon Bérard on March 12, 2020 (ET20-069). We used a subset of 25 patients included during the first surge from March 5, 2020 to May 4, 2020 with available ALC and Ct values. We used 26 patients included during the second surge from October 1, 2020 to December 5, 2020 with available data.

Patients from each cohort were classified using the same criteria.

RT-qPCR analysis

SARS-CoV-2 diagnostic testing of clinical nasopharyngeal swabs or other samples by RT-qPCR was conducted from March 14, 2020 to March 23, 2020 at an outside facility using the Charité protocol. From March 23, 2020 testing was performed internally at the Gustave Roussy. The cycle thresholds were collected only for assays performed at Gustave Roussy. Nasopharyngeal swab samples were collected using flocked swabs (Sigma Virocult) and placed in viral transport media. SARS-CoV-2 RNA was detected using one of two available technics at Gustave Roussy: the GeneFinder COVID-19 Plus Real*Amp* kit (ELITech Group) targeting three regions (*RdRp* gene, nucleocapsid, and envelope genes) on the ELITe InGenius (ELITech Group) or the multiplex real-time RT-PCR diagnostic kit (the Applied Biosystems TaqPath COVID-19 CE-IVD RT-PCR Kit) targeting three regions (*ORF1ab*, nucleocapsid and spike genes) with the following modifications. Nucleic acids were extracted from specimens using automated Maxwell instruments following the manufacturer's instructions (Maxwell RSC simply RNA Blood Kit; AS1380; Promega). Real-time RT-PCR was performed on the QuantiStudio 5 Dx Real-Time PCR System (Thermo Fisher Scientific) in a final reaction volume of 20 µl, including 5 µl of extracted nucleic acids according to the manufacturer instruction.

The cut-off value of 25 for the cycle threshold was based on the median calculated on Cancer_FR1_TR and the mean calculated on Cancer_FR1_TR + CR.

RT-PCR for subgenomic RNA (sgRNA) for SARS-CoV-2

We used the protocol previously described by Wölfel et al. [15]. Briefly, the oligonucleotide sequence of the leader-specific primer was as follows: sgLeadSARSCoV2-F; CGATCTCTTGTAGATCTGTTCTC, and the oligonucleotide sequence of the E primer was as follows: E_Sarbeco_R; ATATTGCAGCAGTACGCACACA. Briefly, 5 uL of RNA (>21 ng) were used for the sgRNA RT-PCR assay with Superscript III one-step RT-PCR system with Platinum Taq Polymerase (Invitrogen, Darmstadt, Germany) with 400 nM concentration of each primer. Thermal cycling was set up as described. Finally, RT-PCR products for sgRNAs were analyzed on agarose gel 2%.

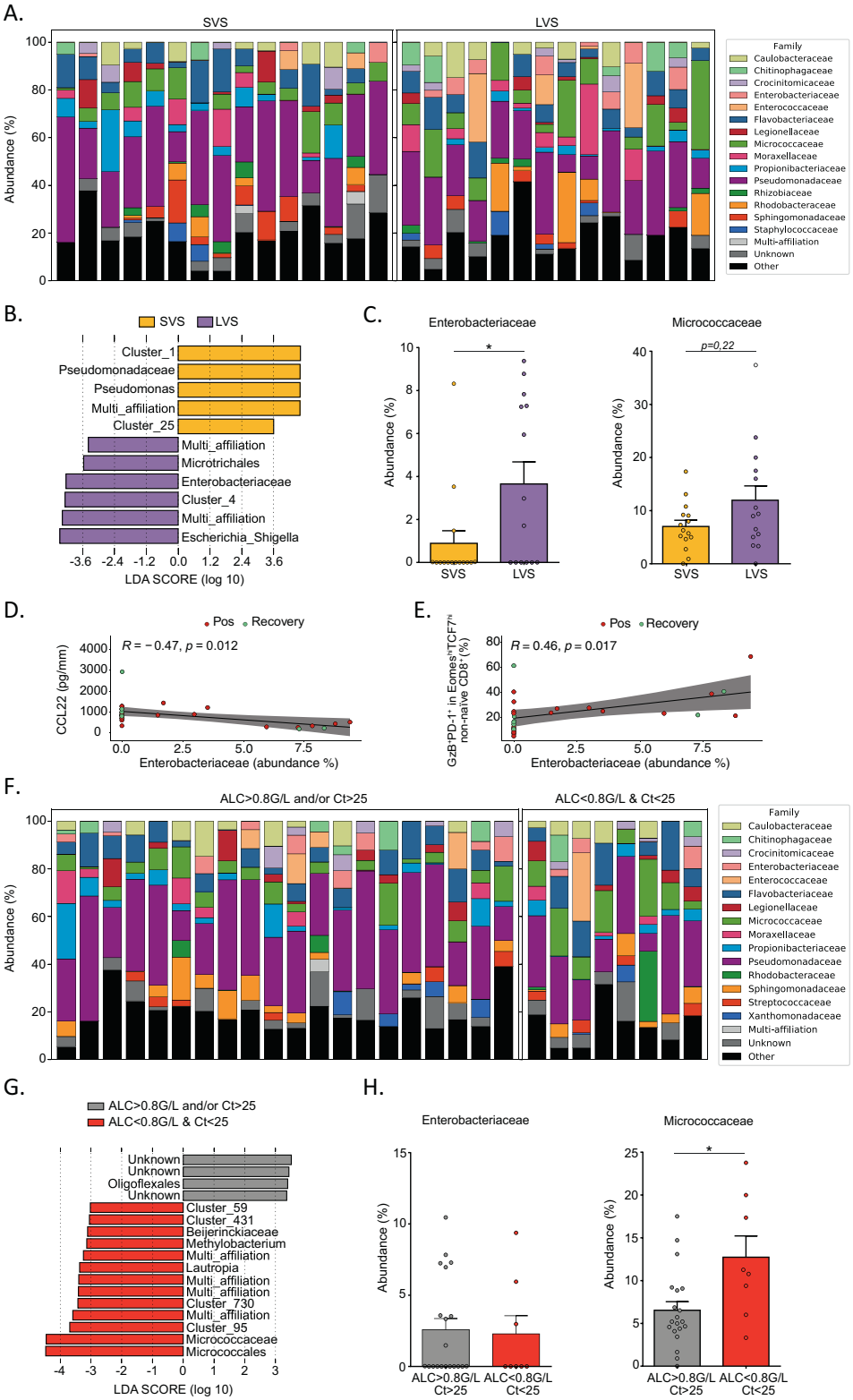

Evaluation of SARS-CoV-2 RNA shedding

The duration of viral shedding was defined as the number of days from the first positive to the first negative RT-qPCR, after longitudinal monitoring. In order to prevent an overvaluation of this duration, we considered in this analysis only patients with an interval below 40 days between the last positive RT-qPCR and the first negative RT-qPCR. Six patients had one negative RT-qPCR followed by positive RT-qPCR. We extend the duration to the second negative RT-qPCR for three patients with a cycle threshold below 35 for the gene coding replication–transcription complex and within 6 days after the first negative result.

Fig. 6 Lymphopenia and prolonged viral shedding are associated with blood recirculation of Enterobacteriaceae and Micrococcaceae DNA. A Stacked bar charts showing the relative abundance of bacterial families obtained by 16S sequencing of the whole-blood samples in patients experiencing short-term viral RNA shedding (SVS) and long-term viral RNA shedding (LVS) among Cancer_FR1_TR. Only the top 15 most abundant bacterial families are represented (the others are in the category "Other"). **B** Linear discriminant analysis effect size (LEfSe) analysis displaying linear discriminant analysis score (LDA) of the blood bacterial taxa differentially recovered from SVS (orange) versus LVS (purple) patients (*$P < 0.05$ with Mann–Whitney test between the two groups of patients). **C** Mean (bar plots, +/− SEM) and individual values (dot plots) of relative proportions of Enterobacteriaceae (**C**, left panel) and Micrococcaceae (**C**, right panel) family members in SARS-CoV-2-positive and recovered patients. Significance between SVS and LVS patients was evaluated using Mann–Whitney test (*$P < 0.05$). **D**, **E** Spearman correlations between the relative proportions of Enterobacteriaceae with paired concentrations of CCL22 in serum (**D**) and with paired percentages of Granzyme B (GzB)$^{+}$PD-1^{+} in Eomes^{hi}TCF-1^{hi} non-naive CD8^{+} measured in blood (**E**). **F** Idem as in **A**. considering segregating the cohort in two groups; ALC > 0.8 G/L and/or Ct >25 patients versus ALC < 0.8 G/L & Ct <25 patients. **G** LEfSe analysis displaying LDA score of the blood bacterial taxa significantly increased in ALC > 0.8 G/L and/or Ct >25 patients (gray) and ALC < 0.8 G/L & Ct <25 patients (red). The displayed bacterial taxa are significantly different (*$P < 0.05$ with Mann–Whitney test) between the two groups of patients. **H** Idem as in C segregating the cohort into the same two groups as in **F**. Significance between ALC > 0.8 G/L and/or Ct >25 patients and ALC < 0.8 G/L & Ct <25 patients was evaluated using the Mann–Whitney test (*$P < 0.05$).

Absolute lymphocyte count (ALC)

The absolute lymphocyte count was measured for the clinical routine using the Sysmex XN (Sysmex, Belgium). Values "PRE" were collected between 210 and 12 days before the symptom onset of COVID-19, values at diagnosis of the infection were collected between −4 and +7 days of the disease diagnosis by RT-qPCR, values "POST" were collected at the recovery time or later, meaning between 0 and 123 days after the first negative RT-qPCR. For the interpretation, the cut-off value for ALC was the median found in patients with high viral load at diagnosis (ALC = 800/mm^3). In parallel, we considered this value as relevant according to the common terminology criteria for adverse events where grades of lymphopenia were assigned as follows: grade 1 ALC < lower limit of normal to 800/mm^3, grade 2 ALC < 800–500/mm^3, and grade 3 ALC < 500–200/mm^3.

Blood tests

Sampling. Blood samples were drawn from patients enrolled in ONCOVID at Gustave Roussy Cancer Campus (Villejuif, France). Whole human peripheral blood was collected into sterile vacutainer tubes.

Spectral flow cytometry. One hundred and twenty-one whole-blood samples from 88 patients (Supplementary Material Fig. 1) were mixed at a 1:1 ratio with Whole Blood Cell Stabilizer (Cytodelics), incubated at room temperature for 10 min and transferred to −80 °C freezer to await analysis. These samples were secondarily thawed in a water bath set to +37 °C. Cells were fixed at a ratio 1:1 with Fixation Buffer (Cytodelics, ratio 1:1) and incubated for 10 min at room temperature. Red blood cells were lysed by the addition of 2 mL of Lysis Buffer (Cytodelics, ratio 1:4) at room temperature for 10 min. White blood cells were washed with 2 mL of Wash Buffer (Cytodelics, ratio 1:5). Cells were resuspended in 100 µL extracellular antibody cocktail and incubated at room temperature for 15 min, then washed in Flow Cytometry Buffer (PBS containing 2% of fetal bovine serum and 2 mM EDTA). For intracellular labeling, a step of permeabilization was performed using 200 µL of eBioscience Foxp3 kit (ThermoFischer); cells were then incubated for 40 min at +4 °C, washed in Perm Buffer (ThermoFischer) and resuspended in an intracellular antibody cocktail. After incubation, cells were washed in Flow Cytometry Buffer and resuspended to proceed to the acquisition. All antibodies used are listed in Supplemental Material Table 2. Samples were acquired on CyTEK Aurora flow cytometer (Cytek Biosciences)(Cytek Biosciences) (T cell, B cell and myeloid cell/global panels) or BD LSR Fortessa X20 Flow cytometer (BD Biosciences-US)(apoptosis and exhaustion panel).

Data analysis

16S rDNA metagenomic profiling DNA from 100 µL of whole blood (from 5 mL EDTA sampling tube) was isolated and amplified in a strictly controlled environment at Vaiomer SAS (Labège, France) using a stringent contamination-aware approach, as discussed previously [40, 68–70]. The microbial populations based on rDNA present in whole blood were determined using next-generation sequencing of V3–V4 variable regions of the 16S rRNA bacterial gene as previously described [69]. For each sample, a sequencing library was generated by the addition of sequencing adapters. The joint pair length was set to encompass a 467 base pairs amplicon (using Escherichia coli 16S as a reference) with a 2 × 300 paired-end MiSeq kit V3 (Illumina, San Diego, CA, USA). The detection of the sequencing fragments was performed using the MiSeq Illumina® technology. Targeted metagenomic sequences from microbiota were analyzed using the bioinformatic pipeline from the FROGS guideline [71]. Briefly, the cleaning was done by removing amplicons without the two PCR primers (10% of mismatches were authorized), amplicons with at least one ambiguous nucleotide ("N"), amplicons identified as chimera (with vsearch v1.9.5), and amplicons with a strong similarity (coverage and identity ≥80%) with the phiX (library used as a control for Illumina sequencing runs). Clustering was produced in two passes of the swarm algorithm v2.1.6. The first pass was a clustering with an aggregation distance equal to 1. The second pass was a clustering with an aggregation distance equal to 3. Taxonomic assignment of amplicons into operational taxonomic units (OTUs) was produced by Blast+ v2.2.30+ with the Silva 134 Parc databank. To assess if the richness of microbiota was adequately captured by metagenomic sequencing, a rarefaction analysis was performed. To ensure a low background signal from bacterial contamination of reagents and consumables, two types of negative controls consisting of molecular grade water were added in an empty tube separately at the DNA extraction step and at the PCR steps and amplified and sequenced at the same time as the extracted DNA of the blood samples. The controls confirm that bacterial contamination was well contained in our pipeline and had a negligible impact on the taxonomic profiles of the samples of this study as published before [40, 68–70]. One sample has been excluded from the analyses for the aberrant profile.

Serum tests

Serums from 120 samples corresponding to 88 patients (Supplementary Material Fig. 1) were collected from whole blood after centrifugation at 600 × *g* for 10 min at room temperature and transferred to −80 °C freezer to await analysis.

Multiplex cytokine and chemokine measurements. Serum samples were centrifuged for 15 min at 1000 × *g*, diluted 1:4, then monitored using the Bio-Plex ProTM Human Chemokine Panel 40-plex Assay (Bio-rad, ref: 171AK99MR2) according to the manufacturer's instructions. 40-plex cytokines and chemokines provided are CCL1, CCL11, CCL13, CCL15, CCL17, CCL19, CCL2, CCL20, CCL21, CCL22, CCL23, CCL24, CCL25, CCL26, CCL27, CCL3, CCL7, CCL8, CX3CL1, CXCL1, CXCL10, CXCL11, CXCL12, CXCL13, CXCL16, CXCL2, CXCL5, CXCL6, CXCL8, CXCL9, GM-CSF, IFN-γ, IL-10, IL-16, IL-1β, IL-2, IL-4, IL-6, MIF, TNF- α. Acquisitions and analyses were performed on a Bio-Plex 200 system (Bio-rad) and a Bio-Plex Manager 6.1 Software (Bio-rad), respectively. Soluble Calprotectin (diluted 1:100) and IFN-α2a were analyzed using a R-plex Human Calprotectin Antibody Set (Meso Scale Discovery, ref: F21YB-3) and the ultrasensitive assay S-plex Human IFN-α2a kit (Meso Scale Discovery, ref: K151P3S-1), respectively, following manufacturer's instructions. Acquisitions and analyses of soluble Calprotectin and IFN-α2a were performed on a MESO™ QuickPlex SQ120 reader and the MSD's Discovery Workbench 4.0. Each serum sample was assayed twice with the average value taken as the final result.

Serology: anti-SARS-CoV-2 immunoglobulins. Serum was collected from whole blood after centrifugation at 600 × *g* for 10 min at room temperature and transferred to −80 °C freezer to await analysis. Serological analysis SARS-CoV-2-specific IgA, IgM, and IgG antibodies were measured in 119 serum samples from 87 patients (Supplementary Material Fig. 1) with The Maverick ™ SARS-CoV-2 Multi-Antigen Serology Panel (Genalyte Inc. USA) according to the manufacturer's instructions. The Maverick™ SARS-CoV-2 Multi-Antigen Serology Panel (Genalyte Inc) is designed to detect antibodies to five SARS-CoV-2 antigens: nucleocapsid, Spike S1 RBD,

Spike S1S2, Spike S2, and Spike S1 with in a multiplex format based on photonic ring resonance technology [72]. This system detects and measures with good reproducibility changes in resonance when antibodies bind to their respective antigens in the chip. The instrument automates the assay. Briefly, 10 µl of each serum sample were added to a sample well plate array containing required diluents and buffers. The plate and chip are loaded into the instrument. First, the chip is equilibrated with the diluent buffer to get baseline resonance. The serum sample is then charged over the chip to bind specific antibodies to antigens present on the chip. Next, chip is washed to remove low-affinity binders. Finally, specific antibodies of patients are detected with anti-IgG or -IgA or -IgM secondary antibodies.

Metabolomics analysis. Samples were prepared as previously described [73]. Briefly, serum samples were mixed with ice-cold extraction mixture (methanol/water, 9/1, v/v, with a mixture of internal standards), then centrifugated. Supernatants were collected for widely-targeted analysis of intracellular metabolites. *GC/MS analysis:* GC-MS/MS method was performed on a 7890B gas chromatography (Agilent Technologies, Waldbronn, Germany) coupled to a triple quadrupole 7000 C (Agilent Technologies, Waldbronn, Germany) equipped with a high sensitivity electronic impact source (EI) operating in positive mode. *Targeted analysis of bile acids:* Targeted analysis was performed on a RRLC 1260 system (Agilent Technologies, Waldbronn, Germany) coupled to a QTRAP 6500 + (Sciex) equipped with an electrospray source operating in negative mode. Gas temperature was set to 450 °C, with ion source gas 1 and 2 set to 30 and 70, respectively. *Targeted analysis of polyamines:* Targeted analysis was performed on a RRLC 1260 system (Agilent Technologies, Waldbronn, Germany) coupled to a QQQ 6410 (Agilent Technologies) equipped with an electrospray source operating in positive mode. The gas temperature was set to 350 °C with a gas flow of 12 l/min. The capillary voltage was set to 3.5 kV. *Targeted analysis of SCFA:* Targeted analysis was performed on a RRLC 1260 system (Agilent Technologies, Waldbronn, Germany) coupled to a QQQ 6410 (Agilent Technologies) equipped with an electrospray source operating in negative mode. Gas temperature was set to 350 °C with a gas flow of 12 L/min. The capillary voltage was set to 4.0 kV. *Pseudo-targeted analysis of intracellular metabolites:* The profiling experiment was performed with a Dionex Ultimate 3000 UHPLC system (Thermo Scientific) coupled to a Q-Exactive (Thermo Scientific) equipped with an electrospray source operating in both positive and negative mode and full scan mode from 100 to 1200 m/z. The Q-Exactive parameters were: sheath gas flow rate 55 au, auxiliary gas flow rate 15 au, spray voltage 3.3 kV, capillary temperature 300 °C, S-Lens RF level 55 V. The mass spectrometer was calibrated with sodium acetate solution dedicated to low mass calibration.

Data analysis

Spectral flow cytometry. Fcs files were exported and analyzed using FlowJo software using the gating strategy showed in Supplementary Material, Fig. 2. Briefly, gates on $CD45^+$, $CD3^+$, or $CD19^+$ from the myeloid, T cell and B panels, respectively, were exported in an fcs file. All exported gate**s** from one panel were used to generate an UMAP [74]. As shown on Supplementary Material Figs. 3 and 4, we used relative expression and manual gating strategy. For patients treated by anti-PD-1 monoclonal antibody, the gates including PD-1 were excluded of the analysis. For patients treated by anti-CD38 monoclonal antibody, the gates including CD38 were excluded of the analysis.

Representation of the results. Data representation was performed with software R v3.3.3 using tidyverse, dplyr, ggplot2, ggpubr, pheatmap, corrplot or Hmisc packages, or GraphPad Prism 7.

Statistical analyses

Calculations and statistical tests were performed either with R v3.3.3 or Prism 7 (GraphPad, San Diego, CA, USA). Unless stated, *P* values are two-sided with 95% confidence intervals for the reported statistic of interest. Individual data points representing the measurement from one patient are systematically calculated from the corresponding distribution. Biological parameters associated to statistically significant differences between groups were considered for the data visualization described below. Group comparison was performed using one-way ANOVA with the lmer function of the lme4 R package. The p-values were computed with the Kenward–Roger method, available in the lmertest R package. Spearman correlations were computed using Hmisc and Pheatmap R package. Hierarchical clustering of the patient's factors was performed using the hclust R package. The redundancy analysis (RDA) was performed using the vegan R package to explore the association between the clinical variables and the biological parameter correlation latent structure. The RDA performs variance decomposition such as principal component analysis, but including additional supervised components depending on the explanatory variables (e.g., clinical factors). The association of the clinical factors with the biological parameter correlation latent structure was tested using a permutation test. Kaplan–Meier methodology was used to estimate the probability of overall survival as well as to visualize the median time of SARS-CoV-2 RNA shedding for each group (HCW and Cancer). One-way ANOVA (paired and unpaired) with Kenward–Roger method was used to calculate *P* value between ALC among groups of viral RNA shedding and Ct values. Chi-Square, Fischer test were used `to calculate the differences in proportion between groups. Comparing two groups, Mann–Whitney test was used. Univariate analyses were performed with the Cox regression model. $P < 0.05$ was considered significant. Multivariate Cox analysis was performed using the survival R package stratified for the cohort and adjusted for the age, ECOG performance status, gender and metastatic status and hematological malignancy.

REFERENCES

1. Derosa L, Melenotte C, Griscelli F, Gachot B, Marabelle A, Kroemer G, et al. The immuno-oncological challenge of COVID-19. Nat Cancer. 2020;1:946–64.
2. Albiges L, Foulon S, Bayle A, Gachot B, Pommeret F, Willekens C, et al. Determinants of the outcomes of patients with cancer infected with SARS-CoV-2: results from the Gustave Roussy cohort. Nat Cancer. 2020;1:965–75.
3. Rugge M, Zorzi M, Guzzinati S. SARS-CoV-2 infection in the Italian Veneto region: adverse outcomes in patients with cancer. Nat Cancer. 2020;1:784–8.
4. Assaad S, Avrillon V, Fournier M-L, Mastroianni B, Russias B, Swalduz A, et al. High mortality rate in cancer patients with symptoms of COVID-19 with or without detectable SARS-COV-2 on RT-PCR. Eur J Cancer. 2020;135:251–9.
5. Luo J, Rizvi H, Preeshagul IR, Egger JV, Hoyos D, Bandlamudi C, et al. COVID-19 in patients with lung cancer. Ann Oncol. 2020;31:1386–96.
6. Garassino MC, Whisenant JG, Huang L-C, Trama A, Torri V, Agustoni F, et al. COVID-19 in patients with thoracic malignancies (TERAVOLT): first results of an international, registry-based, cohort study. Lancet Oncol. 2020;21:914–22.
7. Passamonti F, Cattaneo C, Arcaini L, Bruna R, Cavo M, Merli F, et al. Clinical characteristics and risk factors associated with COVID-19 severity in patients with haematological malignancies in Italy: a retrospective, multicentre, cohort study. Lancet Haematol. 2020;7:e737–45.
8. Martín-Moro F, Marquet J, Piris M, Michael BM, Sáez AJ, Corona M, et al. Survival study of hospitalised patients with concurrent COVID-19 and haematological malignancies. Br J Haematol. 2020;190:e16–20.
9. Robilotti EV, Babady NE, Mead PA, Rolling T, Perez-Johnston R, Bernardes M, et al. Determinants of COVID-19 disease severity in patients with cancer. Nat Med. 2020;26:1218–23.
10. Dai M, Liu D, Liu M, Zhou F, Li G, Chen Z, et al. Patients with cancer appear more vulnerable to SARS-CoV-2: a multicenter study during the COVID-19 outbreak. Cancer Discov. 2020;10:783–91.
11. Q W, Q C, H Z, B Y, X H, Y Z, et al. Clinical outcomes of coronavirus disease 2019 (COVID-19) in cancer patients with prior exposure to immune checkpoint inhibitors. Cancer Commun. 2020;40:374–9.
12. Shlomai A, Ben-Zvi H, Glusman Bendersky A, Shafran N, Goldberg E, Sklan EH. Nasopharyngeal viral load predicts hypoxemia and disease outcome in admitted COVID-19 patients. Crit Care. 2020;24:539.
13. Westblade LF, Brar G, Pinheiro LC, Paidoussis D, Rajan M, Martin P, et al. SARS-CoV-2 viral load predicts mortality in patients with and without cancer who are hospitalized with COVID-19. Cancer Cell. 2020;38:661–71.
14. Corman VM, Landt O, Kaiser M, Molenkamp R, Meijer A, Chu DK, et al. Detection of 2019 novel coronavirus (2019-nCoV) by real-time RT-PCR. Euro Surveill. 2020;25:2000045.
15. Wölfel R, Corman VM, Guggemos W, Seilmaier M, Zange S, Müller MA, et al. Virological assessment of hospitalized patients with COVID-2019. Nature. 2020;581:465–9.
16. Lagier J-C, Million M, Gautret P, Colson P, Cortaredona S, Giraud-Gatineau A, et al. Outcomes of 3,737 COVID-19 patients treated with hydroxychloroquine/azithromycin and other regimens in Marseille, France: a retrospective analysis. Travel Med Infect Dis. 2020;36:101791.
17. Boutin C-A, Grandjean-Lapierre S, Gagnon S, Labbé A-C, Charest H, Roger M, et al. Comparison of SARS-CoV-2 detection from combined nasopharyngeal/oropharyngeal swab samples by a laboratory-developed real-time RT-PCR test and the Roche SARS-CoV-2 assay on a cobas 8800 instrument. J Clin Virol. 2020;132:104615.

18. Elkrief A, Desilets A, Papneja N, Cvetkovic L, Groleau C, Lakehal YA, et al. High mortality among hospital-acquired COVID-19 infection in patients with cancer: a multicentre observational cohort study. Eur J Cancer. 2020;139:181–7.
19. Avanzato VA, Matson MJ, Seifert SN, Pryce R, Williamson BN, Anzick SL, et al. Case study: prolonged infectious SARS-CoV-2 shedding from an asymptomatic immunocompromised individual with cancer. Cell. 2020;183:1901. e9
20. Aydillo T, Gonzalez-Reiche AS, Aslam S, van de Guchte A, Khan Z, Obla A, et al. Shedding of viable SARS-CoV-2 after immunosuppressive therapy for cancer. N. Engl J Med. 2020;383:2586–8.
21. Choi B, Choudhary MC, Regan J, Sparks JA, Padera RF, Qiu X, et al. Persistence and evolution of SARS-CoV-2 in an immunocompromised host. N Engl J Med. 2020;383:2291–3.
22. Helleberg M, Niemann CU, Moestrup KS, Kirk O, Lebech A-M, Lane C, et al. Persistent COVID-19 in an immunocompromised patient temporarily responsive to two courses of remdesivir therapy. J Infect Dis. 2020;222:1103–7.
23. Silvin A, Chapuis N, Dunsmore G, Goubet A-G, Dubuisson A, Derosa L, et al. Elevated calprotectin and abnormal myeloid cell subsets discriminate severe from mild COVID-19. Cell 2020;182:1401. e18
24. Laing AG, Lorenc A, del Molino del Barrio I, Das A, Fish M, Monin L, et al. A dynamic COVID-19 immune signature includes associations with poor prognosis. Nat Med. 2020;26:1623–35.
25. Arunachalam PS, Wimmers F, Mok CKP, Perera RAPM, Scott M, Hagan T, et al. Systems biological assessment of immunity to mild versus severe COVID-19 infection in humans. Science. 2020;369:1210–20.
26. Takahashi T, Ellingson MK, Wong P, Israelow B, Lucas C, Klein J, et al. Sex differences in immune responses that underlie COVID-19 disease outcomes. Nature 2020;26:1–6.
27. Mathew D, Giles JR, Baxter AE, Oldridge DA, Greenplate AR, Wu JE, et al. Deep immune profiling of COVID-19 patients reveals distinct immunotypes with therapeutic implications. Science. 2020;369(6508). https://science.sciencemag.org/content/369/6508/eabc8511.
28. Kaneko N, Kuo H-H, Boucau J, Farmer JR, Allard-Chamard H, Mahajan VS, et al. Loss of Bcl-6-expressing T follicular helper cells and germinal centers in COVID-19. Cell. 2020;183:143–.e13.
29. Chua RL, Lukassen S, Trump S, Hennig BP, Wendisch D, Pott F, et al. COVID-19 severity correlates with airway epithelium–immune cell interactions identified by single-cell analysis. Nat Biotechnol. 2020;38:970–9.
30. Carvelli J, Demaria O, Vély F, Batista L, Benmansour NC, Fares J, et al. Association of COVID-19 inflammation with activation of the C5a–C5aR1 axis. Nature 2020;29:1–5.
31. Jaafar R, Aherfi S, Wurtz N, Grimaldier C, Hoang VT, Colson P, et al. Correlation between 3790 qPCR positives samples and positive cell cultures including 1941 SARS-CoV-2 isolates. Clin Infect Dis. 2020. https://www.ncbi.nlm.nih.gov/pmc/articles/PMC7543373/.
32. Campbell C, McKenney PT, Konstantinovsky D, Isaeva OI, Schizas M, Verter J, et al. Bacterial metabolism of bile acids promotes generation of peripheral regulatory T cells. Nature. 2020;581:475–9.
33. Moole PKR, Papireddypalli JMR. Effect of deoxycholic acid on immune cells—an immunophenotyping analysis of peripheral blood and splenic lymphocytes in CD57 female mice. Int J Pharm Investig. 2020;10:548–52.
34. Sheng L, Jena PK, Hu Y, Liu H-X, Nagar N, Kalanetra KM, et al. Hepatic inflammation caused by dysregulated bile acid synthesis is reversible by butyrate supplementation. J Pathol. 2017;243:431–41.
35. Song X, Sun X, Oh SF, Wu M, Zhang Y, Zheng W, et al. Microbial bile acid metabolites modulate gut RORγ+ regulatory T cell homeostasis. Nature. 2020;577:410–5.
36. Alsaleh G, Panse I, Swadling L, Zhang H, Richter FC, Meyer A, et al. Autophagy in T cells from aged donors is maintained by spermidine and correlates with function and vaccine responses. eLife 2020;15:9.
37. Puleston DJ, Zhang H, Powell TJ, Lipina E, Sims S, Panse I, et al. Autophagy is a critical regulator of memory CD8(+) T cell formation. eLife 2014;11:3.
38. Zhang H, Alsaleh G, Feltham J, Sun Y, Napolitano G, Riffelmacher T, et al. Polyamines control eIF5A hypusination, TFEB translation, and autophagy to reverse B cell senescence. Mol Cell. 2019;76:110–.e9. 3
39. Yeoh YK, Zuo T, Lui GC-Y, Zhang F, Liu Q, Li AY, et al. Gut microbiota composition reflects disease severity and dysfunctional immune responses in patients with COVID-19. Gut. 2021;70:698–706.
40. Païssé S, Valle C, Servant F, Courtney M, Burcelin R, Amar J, et al. Comprehensive description of blood microbiome from healthy donors assessed by 16S targeted metagenomic sequencing. Transfusion. 2016;56:1138–47.
41. van Kampen JJA, van de Vijver DAMC, Fraaij PLA, Haagmans BL, Lamers MM, Okba N, et al. Duration and key determinants of infectious virus shedding in hospitalized patients with coronavirus disease-2019 (COVID-19). Nat Commun. 2021;12:267.
42. Li Q, Guan X, Wu P, Wang X, Zhou L, Tong Y, et al. Early transmission dynamics in Wuhan, China, of novel coronavirus–infected pneumonia. N. Engl J Med. 2020;382:1199–207.
43. Ge H, Wang X, Yuan X, Xiao G, Wang C, Deng T, et al. The epidemiology and clinical information about COVID-19. Eur J Clin Microbiol Infect Dis. 2020;39:1011–9.
44. Lehners N, Tabatabai J, Prifert C, Wedde M, Puthenparambil J, Weissbrich B, et al. Long-term shedding of influenza virus, parainfluenza virus, respiratory syncytial virus and nosocomial epidemiology in patients with hematological disorders. PLoS ONE. 2016;11:e0148258.
45. Geis S, Prifert C, Weissbrich B, Lehners N, Egerer G, Eisenbach C, et al. Molecular characterization of a respiratory syncytial virus outbreak in a hematology unit in Heidelberg, Germany. J Clin Microbiol. 2013;51:155–62.
46. Lehners N, Schnitzler P, Geis S, Puthenparambil J, Benz MA, Alber B, et al. Risk factors and containment of respiratory syncytial virus outbreak in a hematology and transplant unit. Bone Marrow Transplant. 2013;48:1548–53.
47. Milano F, Campbell AP, Guthrie KA, Kuypers J, Englund JA, Corey L, et al. Human rhinovirus and coronavirus detection among allogeneic hematopoietic stem cell transplantation recipients. Blood. 2010;115:2088–94.
48. El Ramahi R, Freifeld A. Epidemiology, diagnosis, treatment, and prevention of influenza infection in oncology patients. JOP. 2019;15:177–84.
49. Péron J, Cropet C, Tredan O, Bachelot T, Ray-Coquard I, Clapisson G, et al. CD4 lymphopenia to identify end-of-life metastatic cancer patients. Eur J Cancer. 2013;49:1080–9.
50. Xu X, Chang XN, Pan HX, Su H, Huang B, Yang M, et al. [Pathological changes of the spleen in ten patients with coronavirus disease 2019(COVID-19) by postmortem needle autopsy]. Zhonghua Bing Li Xue Za Zhi. 2020;49:576–82.
51. Buja LM, Wolf DA, Zhao B, Akkanti B, McDonald M, Lelenwa L, et al. The emerging spectrum of cardiopulmonary pathology of the coronavirus disease 2019 (COVID-19): Report of 3 autopsies from Houston, Texas, and review of autopsy findings from other United States cities. Cardiovasc Pathol. 2020;48:107233.
52. Lax SF, Skok K, Zechner P, Kessler HH, Kaufmann N, Koelblinger C, et al. Pulmonary arterial thrombosis in COVID-19 with fatal outcome: results from a prospective, single-center, clinicopathologic case series. Ann Intern. 2020;173:350–61.
53. Pontelli MC, Castro IA, Martins RB, Veras FP, Serra LL, Nascimento DC, et al. Infection of human lymphomononuclear cells by SARS-CoV-2. bioRxiv.2020;2020.07.28.225912. https://doi.org/10.1101/2020.07.28.225912.
54. Park MD. Macrophages: a Trojan horse in COVID-19? Nat Rev Immunol. 2020;20:351–351.
55. Channappanavar R, Perlman S. Pathogenic human coronavirus infections: causes and consequences of cytokine storm and immunopathology. Semin Immunopathol. 2017;39:529–39.
56. Westmeier J, Paniskaki K, Karaköse Z, Werner T, Sutter K, Dolff S, et al. Impaired cytotoxic CD8+ T cell response in elderly COVID-19 patients. mBio. 2020;11. https://mbio.asm.org/content/11/5/e02243-20
57. Fischer K, Hoffmann P, Voelkl S, Meidenbauer N, Ammer J, Edinger M, et al. Inhibitory effect of tumor cell-derived lactic acid on human T cells. Blood. 2007;109:3812–9.
58. Ziegler CGK, Allon SJ, Nyquist SK, Mbano IM, Miao VN, Tzouanas CN, et al. SARS-CoV-2 receptor ACE2 is an interferon-stimulated gene in human airway epithelial cells and is detected in specific cell subsets across tissues. Cell. 2020;181:1016. e19
59. Schreiber RD, Old LJ, Smyth MJ. Cancer immunoediting: integrating immunity's roles in cancer suppression and promotion. Science. 2011;331:1565–70.
60. Sanmamed MF, Perez-Gracia JL, Schalper KA, Fusco JP, Gonzalez A, Rodriguez-Ruiz ME, et al. Changes in serum interleukin-8 (IL-8) levels reflect and predict response to anti-PD-1 treatment in melanoma and non-small-cell lung cancer patients. Ann Oncol. 2017;28:1988–95.
61. Bitterman R, Eliakim-Raz N, Vinograd I, Trestioreanu AZ, Leibovici L, Paul M. Influenza vaccines in immunosuppressed adults with cancer. Cochrane Database of Systematic Rev. 2018;(2). https://www.cochranelibrary.com/cdsr/doi/10.1002/14651858.CD008983.pub3/full.
62. Francois B, Jeannet R, Daix T, Walton AH, Shotwell MS, Unsinger J, et al. Interleukin-7 restores lymphocytes in septic shock: the IRIS-7 randomized clinical trial. JCI Insight. 2018;3(5). https://insight.jci.org/articles/view/98960.
63. Laterre PF, François B, Collienne C, Hantson P, Jeannet R, Remy KE, et al. Association of interleukin 7 immunotherapy with lymphocyte counts among patients with severe coronavirus disease 2019 (COVID-19). JAMA Netw Open. 2020;3(7):e2016485-e2016485.
64. Cheng L-L, Guan W-J, Duan C-Y, Zhang N-F, Lei C-L, Hu Y, et al. Effect of recombinant human granulocyte colony-stimulating factor for patients with coronavirus disease 2019 (COVID-19) and lymphopenia: a randomized clinical trial. JAMA Intern Med. 2021;181:71–78.

65. NCT04407689. A Multicenter, Randomized, Double-blinded Placebo-controlled Study of Recombinant Interleukin-7 (CYT107) for Immune Restoration of Hospitalized Lymphopenic Patients With Coronavirus COVID-19 Infection in France and Belgium [Internet]. clinicaltrials.gov; [cité 21 janv 2021]. Report No.: NCT04407689. https://clinicaltrials.gov/ct2/show/NCT04407689.
66. NCT04426201. A Multicenter, Randomized, Double-blinded Placebo-controlled Study of Recombinant Interleukin-7 (CYT107) for Immune Restoration of Hospitalized Lymphopenic Patients With Coronavirus COVID-19 Infection. US Oncology Cohort [Internet]. clinicaltrials.gov; [cité 21 janv 2021]. Report No.: NCT04426201. https://clinicaltrials.gov/ct2/show/NCT04426201.
67. Amrane S, Tissot-Dupont H, Doudier B, Eldin C, Hocquart M, Mailhe M, et al. Rapid viral diagnosis and ambulatory management of suspected COVID-19 cases presenting at the infectious diseases referral hospital in Marseille, France, - January 31st to March 1st, 2020: a respiratory virus snapshot. Travel Med Infect Dis. 2020;36:101632.
68. Anhê FF, Jensen BAH, Varin TV, Servant F, Van Blerk S, Richard D, et al. Type 2 diabetes influences bacterial tissue compartmentalisation in human obesity. Nat Metab. 2020;2:233–42.
69. Lluch J, Servant F, Païssé S, Valle C, Valière S, Kuchly C, et al. The characterization of novel tissue microbiota using an optimized 16S metagenomic sequencing pipeline. PLoS ONE. 2015;10:e0142334.
70. Schierwagen R, Alvarez-Silva C, Servant F, Trebicka J, Lelouvier B, Arumugam M. Trust is good, control is better: technical considerations in blood microbiome analysis. Gut 2020;69:1362–3.
71. Escudié F, Auer L, Bernard M, Mariadassou M, Cauquil L, Vidal K, et al. FROGS: find, rapidly, OTUs with galaxy solution. Bioinformatics 2018;34:1287–94.
72. Sterlin D, Mathian A, Miyara M, Mohr A, Anna F, Claer L, et al. IgA dominates the early neutralizing antibody response to SARS-CoV-2. Sci Transl Med. 2021;13:eabd2223.
73. Danlos F-X, Grajeda-Iglesias C, Durand S, Sauvat A, Roumier M, Cantin D, et al. Metabolomic analyses of COVID-19 patients unravel stage-dependent and prognostic biomarkers. Cell Death Dis. 2021;12:258. https://doi.org/10.1038/s41419-021-03540-y.
74. Becht E, McInnes L, Healy J, Dutertre C-A, Kwok IWH, Ng LG, et al. Dimensionality reduction for visualizing single-cell data using UMAP. Nat Biotechnol. 2019;37:38–44.

ACKNOWLEDGEMENTS

We are thankful to the Spectral flow cytometry facility team of Gustave Roussy. We thank the ET-EXTRA team (Biological Resource Center (NF 96-600) and the microbiology team for technical help. We thank Dr. Aude Jary for helping to set up the subgenomic RNA analysis. We thank the staff from the health and safety of Gustave Roussy Cancer Campus for helping to set up the translational research studies. We are thankful to the Genalyte for their supportive help.

AUTHOR CONTRIBUTIONS

LD, LZ, AM, and FB conceived and designed the clinical trial. A-GG, LD, and LZ conceived and designed the translational research trial. AG, F-XD, ST, CM, FP, EC, LA, ASt, BG, MMer, FS, AM, and LD included patients in the clinical trial. A-GG, AD, F-XD, MP, MMaz, ASi, GD carried out all the experiments. A-GG, AD, F-XD, ASi, and GD performed all the biological analyses. DD performed the non-supervised analysis and gave advices for statistical analyses. LD and CA-C-S collected and analyzed the clinical data. LT and AF provided the information from the HCW series. AE, SK, and BR analyzed and provided the clinical data from the Canadian series. BLS, DR, SG, and SC analyzed and provided the clinical data from the IHU series. GG, CB, and NL analyzed CT scan. EG and FGr performed the RT-qPCR. A-GG, CA-C-S, and MMaz collected the biological data (ALC and Ct values). CP collected the samples. MMaz, YH, EP, CF, PL, GF, CT, IL, and J-EF prepared the biological samples and provided some help for the experiments. A-GG, AD, LZ, and LD interpreted data. performed the viral cultures. MMy and GGo performed the dosages of antibodies. A-GG, F-XD, CG-D, SD, NN, FAp, and GK performed the metabolomic experiments and analyses. BL, AR, and AD performed metagenomic analyses of blood microbiota. All the authors advised for the interpretation of the data. OK gave advices on the design of the figures. LZ and LD wrote the manuscript, with all authors contributing to the writing and providing feedback.

FUNDING

A-GG was supported by Fondation pour la Recherche Médicale (FRM). LD has received support by the Philanthropia Fondation Gustave Roussy. The Gustave Roussy sponsored clinical study on COVID-19 (ONCOVID; NCT NCT04341207 has been supported by the Fondation Gustave Roussy, the Dassault family, Malakoff Humanis, Agnès b., Izipizi, Ralph Lauren and Sanofi). LZ and GK were supported by RHU Torino Lumière (ANR-16-RHUS-0008), ONCOBIOME H2020 network, the Seerave Foundation, the Ligue contre le Cancer (équipe labelisée); Agence Nationale de la Recherche (ANR)—Projets blancs; ANR under the frame of E-Rare-2, the ERA-Net for Research on Rare Diseases; Association pour la recherche sur le cancer (ARC); Cancéropôle Ile-de-France; FRM; a donation by Elior; the European Research Council (ERC); Fondation Carrefour; High-end Foreign Expert Program in China (GDW20171100085 and GDW20181100051), Institut National du Cancer (INCa); Inserm (HTE); Institut Universitaire de France; LeDucq Foundation; the LabEx Immuno-Oncology; the SIRIC Stratified Oncology Cell DNA Repair and Tumor Immune Elimination (SOCRATE); CARE network (directed by Prof. Mariette, Kremlin Bicêtre AP-HP), and the SIRIC Cancer Research and Personalized Medicine (CARPEM). GI was supported by Italian Ministry of Health (grants Ricerca CorrenteLinea 1, 1 "Infezioni Emergenti e Riemergenti", projects COVID-2020-12371675 and COVID-2020-12371817). MMy and GG were supported by ANR Flash COVID-19 program and ARS-CoV-2 Program of the Faculty of Medicine from Sorbonne University ICOViD programs (PI: GG).

CONFLICT OF INTEREST

LZ and GK are cofounders of everImmune, a biotech company devoted to the use of commensal microbes for the treatment of cancers. AG and AM as part of the Drug Development Department (DITEP) are Principal/sub-Investigator of Clinical Trials for Abbvie, Adaptimmune, Aduro Biotech, Agios Pharmaceuticals, Amgen, Argen-X Bvba, Arno Therapeutics, Astex Pharmaceuticals, Astra Zeneca, Astra Zeneca Ab, Aveo, Bayer Healthcare Ag, Bbb Technologies Bv, Beigene, Bioalliance Pharma, Biontech Ag, Blueprint Medicines, Boehringer Ingelheim, Boston Pharmaceuticals, Bristol-Myers Squibb, Bristol-Myers Squibb International Corporation, Ca, Celgene Corporation, Cephalon, Chugai Pharmaceutical Co., Clovis Oncology, Cullinan-Apollo, Daiichi-Sankyo, Debiopharm S.A., Eisai, Eisai Limited, Eli Lilly, Exelixis, Forma Tharapeutics, Gamamabs, Genentech, Gilead Sciences, Glaxosmithkline, Glenmark Pharmaceuticals, H3 Biomedicine, Hoffmann-La Roche Ag, Incyte Corporation, Innate Pharma, Institut De Recherche Pierre Fabre, Iris Servier, Janssen Cilag, Janssen Research Foundation, Kura Oncology, Kyowa Kirin Pharm. Dev., Lilly France, Loxo Oncology, Lytix Biopharma As, Medimmune, Menarini Ricerche, Merck Kgaa, Merck Sharp & Dohme Chibret, Merrimack Pharmaceuticals, Merus, Millennium Pharmaceuticals, Molecular Partners Ag, Nanobiotix, Nektar Therapeutics, Nerviano Medical Sciences, Novartis Pharma, Octimet Oncology Nv, Oncoethix, Oncomed, Oncopeptides, Onyx Therapeutics, Orion Pharma, Oryzon Genomics, Ose Pharma, Pfizer, Pharma Mar, Philogen S.P.A., Pierre Fabre Medicament, Plexxikon, Rigontec Gmbh, Roche, Sanofi Aventis, Sierra Oncology, Sotio A.S, Syros Pharmaceuticals, Taiho Pharma, Tesaro, Tioma Therapeutics, Wyeth Pharmaceuticals France, Xencor, Y's Therapeutics, Research Grants from Astrazeneca, BMS, Boehringer Ingelheim, Janssen Cilag, Merck, Novartis, Pfizer, Roche, Sanofi. Non-financial support (drug supplied) from Astrazeneca, Bayer, BMS, Boringher Ingelheim, Johnson & Johnson, Lilly, Medimmune, Merck, NH TherAGuiX, Pfizer, Roche. NL reports to be a Speaker at Jazz Pharmaceutical E.D. reports grants and personal fees from ROCHE GENENTECH, grants from SERVIER, grants from ASTRAZENECA, grants and personal fees from MERCK SERONO, grants from BMS, grants from MSD, outside the submitted work. OK is a cofounder of Samsara Therapeutics. F.B. reports personal fees from Astra Zeneca, Bayer, Bristol-Myers Squibb, Boehringer Ingelheim, Eli Lilly Oncology,ß. Hoffmann-La Roche Ltd, Novartis, Merck, MSD, Pierre Fabre, Pfizer and Takeda, outside the submitted work. J-CS was a full-time employee of Astra Zeneca between September 2017 and December 2019, he reports consultancy: Relay Therapeutics, Gritstone Oncology and shares: Gritstone, Astra Zeneca, Daiichi-Sankyo, outside the submitted work. LA reports consulting fees compensated to institution for Pfizer, Novartis, Bristol Myer Squibb, Ipsen, Roche, MSD, Astra Zeneca, Merck, Amgen, Astellas, Exelixis, Corvus Pharmaceuticals, Peloton Therapeutics, outside the submitted work. FS reports consulting fees from AMGEN, Roche, Chugai, Mylan, Mundi Pharma, Leo Pharma, Pierre Fabre Oncology, Helsinn, MSD, Pfizer, BMS, outside the submitted work.

ETHICAL APPROVAL AND CONSENT TO PARTICIPATE

The ONCOVID trial was conducted in accordance with Good Clinical Practice guidelines and the provisions of the Declaration of Helsinki. All patients provided written informed consent. Protocol approval was obtained from an independent ethics committee (ethics protocol number EudraCT No: 2020-001250-21). The protocol is available with the full text of this article at https://clinicaltrials.gov/ct2/show/NCT04341207. The part of the research including healthcare workers was conducted in compliance with General Data Protection Regulation (GDPR) and the French Data Protection Authority's recommendation about Data Protection in clinical researches. Gustave Roussy Data Protection Officer (DPO) has evaluated this project and sent to the principal investigator a formalized operational action plan about data protection compliance. The Cancer_FR2 cohort used individuals from a clinical study approved by the IHU Méditerranée Infections review board committee (Méditerranée Infection No.: 2020-021). The Cancer_CA cohort used individuals from a clinical study approved by the institutional ethics committee at each site (Ethics number: MP-02-2020-8911 and H20-00892). The Cancer_FR1_CR was also declared to the Gustave

Roussy Cancer Centre's DPO and registered on the website of the French Healthcare Data Institute (declaration number: MR4911200520).

ADDITIONAL INFORMATION

Supplementary information The online version contains supplementary material available at https://doi.org/10.1038/s41418-021-00817-9.

Correspondence and requests for materials should be addressed to L.Z. or L.D.

Reprints and permission information is available at http://www.nature.com/reprints

Publisher's note Springer Nature remains neutral with regard to jurisdictional claims in published maps and institutional affiliations.

[1]Université Paris-Saclay, Faculté de Médecine, Le Kremlin-Bicêtre, France. [2]Gustave Roussy Cancer Campus, Villejuif, France. [3]Institut National de la Santé et de la Recherche Médicale, UMR1015, Gustave Roussy, Villejuif, France. [4]Département d'Oncologie Médicale, Gustave Roussy, Villejuif, France. [5]Département d'Innovation Thérapeutique et d'Essais Précoces, Gustave Roussy, Villejuif, France. [6]Département de Biostatistique et d'Epidémiologie, Gustave Roussy, Université Paris-Saclay, Villejuif, France. [7]Institut National de la Santé et de la Recherche Médicale Oncostat, U1018, Equipe labellisée par la Ligue Contre le Cancer, Gustave Roussy, Villejuif, France. [8]Médecine du travail, Gustave Roussy, Villejuif, France. [9]Institut Pasteur, Unit Biology and Genetics of the Bacterial Cell Wall, Paris, France. [10]CNRS UMR2001, Paris, France. [11]INSERM, Equipe Avenir, Paris, France. [12]Institut National de la Santé et de la Recherche Médicale, U1287, Gustave Roussy, Villejuif, France. [13]Département d'Hématologie, Gustave Roussy, Villejuif, France. [14]Université de Paris, Institut Cochin, Centre National de la Recherche Scientifique UMR8104, Institut National de la Santé et de la Recherche Médicale, Paris, France. [15]Service d'hématologie biologique, Hôpital Cochin, Assistance Publique—Hôpitaux de Paris.Centre-Université de Paris, Paris, France. [16]Département d'Imagerie Médicale, Gustave Roussy, Villejuif, France. [17]Biomaps, UMR1281, INSERM, CNRS, CEA, Université Paris Saclay, Paris, France. [18]Immunotherapy/Immunosurgery, Champalimaud foundation, Lisboa, Portugal. [19]Centre de Recherche des Cordeliers, Equipe labellisée par la Ligue contre le cancer, Université de Paris, Sorbonne Université, Inserm U1138, Institut Universitaire de France, Paris, France. [20]Metabolomics and Cell Biology Platforms, Gustave Roussy Cancer Center, Université Paris Saclay, Villejuif, France. [21]Institut National de la Santé et de la Recherche Médicale, U1030, Gustave Roussy, Villejuif, France. [22]Univ Paris Est Creteil, INSERM U955, IMRB, Creteil, France. [23]Service de maladies infectieuses, Centre Hospitalier de Cornouaille, Quimper, France. [24]Aix-Marseille Université, Institut de Recherche pour le Développement, Assistance Publique – Hôpitaux de Marseille, Microbes Evolution Phylogeny and Infections, Marseille, France. [25]Institut Hospitalo-Universitaire Méditerranée Infection, Marseille, France. [26]Aix Marseille Univ, School of medicine—La Timone Medical Campus, EA 3279: CEReSS—Health Service Research and Quality of life Center, Marseille, France. [27]Aix Marseille Université, IRD, AP-HM, SSA, VITROME, Marseille, France. [28]Scientific Direction, National Institute for Infectious Diseases Lazzaro Spallanzani, Rome, Italy. [29]Vaiomer, Labège, France. [30]Institut National de la Santé et de la Recherche Médicale, U981, Gustave Roussy, Villejuif, France. [31]Aix Marseille University, CNRS, INSERM, CRCM, Marseille, France. [32]Centre de ressources biologiques, ET-EXTRA, Gustave Roussy, Villejuif, France. [33]Département de Biologie Médicale et Pathologie Médicales, service de biochimie, Gustave Roussy, Villejuif, France. [34]Département de Biologie Médicale et Pathologie Médicales, service de microbiologie, Gustave Roussy, Villejuif, France. [35]Singapore Immunology Network, Agency for Science, Technology and Research (A*STAR), Singapore, Singapore. [36]Shanghai Institute of Immunology, Shangai, China. [37]Translational Immunology Institute, SingHealth Duke-NUS Academic Medical Center, Singapore, Singapore. [38]Cedar's Cancer Center, McGill University Healthcare Centre, Montreal, QC, Canada. [39]Centre de recherche du Centre hospitalier de l'Université de Montréal (CRCHUM), Montreal, QC, Canada. [40]Department of Hematology-Oncology, Centre hospitalier de l'Université de Montréal, Montreal, QC, Canada. [41]Institut National de la Santé et de la Recherche Médicale, U1135, Centre d'Immunologie et des Maladies Infectieuses, Hôpital Pitié-Salpêtrière, Assistance Publique—Hôpitaux de Paris, Paris, France. [42]Département de Radiothérapie, Gustave Roussy, Villejuif, France. [43]Service de Réanimation Médicale, Gustave Roussy, Villejuif, France. [44]Service de Pathologie Infectieuse, Gustave Roussy, Villejuif, France. [45]Service de médecine aigue d'urgence en cancérologie, Gustave Roussy, Villejuif, France. [46]Département Interdisciplinaire d'Organisation des Parcours Patients, Gustave Roussy, Villejuif, France. [47]Centre Léon Bérard, Lyon, France. [48]Université Claude Bernard, Lyon, France. [49]Unicancer, Paris, France. [50]Université de Paris, Paris, France. [51]Department of Women's and Children's Health, Karolinska Institute, Karolinska University Hospital, Stockholm, Sweden. [52]Pôle de Biologie, Hôpital Européen George Pompidou, Assistance Publique—Hôpitaux de Paris, Paris, France. [53]Suzhou Institute for Systems Biology, Chinese Academy of Medical Sciences, Suzhou, China. [54]Center of Clinical Investigations BIOTHERIS, Gustave Roussy, Villejuif, France. [55]Institut National de la Santé et de la Recherche Médicale—UMR935/UA9, Université Paris-Saclay, Villejuif, France. [56]INGESTEM National IPSC Infrastructure, Université de Paris-Saclay, Villejuif, France. [57]Université de Paris, Faculté des Sciences Pharmaceutiques et Biologiques, Paris, France. [58]These authors contributed equally: Anne-Gaëlle Goubet, Agathe Dubuisson. [59]These authors contributed equally: Laurence Zitvogel, Lisa Derosa. ✉email: laurence.zitvogel@gustaveroussy.fr; lisa.derosa@gustaveroussy.fr

Published OnlineFirst April 12, 2021; DOI: 10.1158/2159-8290.CD-21-0144

REVIEW

Repurposing of Anticancer Drugs Expands Possibilities for Antiviral and Anti-Inflammatory Discovery in COVID-19

Mihaela Aldea[1], Jean-Marie Michot[2], Francois-Xavier Danlos[3,4], Antoni Ribas[5], and Jean-Charles Soria[2,4]

ABSTRACT In 2020, the COVID-19 pandemic led to an unprecedented destabilization of the world's health and economic systems. The rapid spread and life-threatening consequences of COVID-19 have imposed testing of repurposed drugs, by investigating interventions already used in other indications, including anticancer drugs. The contours of anticancer drug repurposing have been shaped by similarities between the pathogenesis of COVID-19 and malignancies, including abnormal inflammatory and immunologic responses. In this review, we discuss the salient positive and negative points of repurposing anticancer drugs to advance treatments for COVID-19.

Significance: Targeting anti-inflammatory pathways with JAK/STAT inhibitors or anticytokine therapies aiming to curb COVID-19–related cytokine storm, using antiangiogenic drugs to reduce vascular abnormalities or immune-checkpoint inhibitors to improve antiviral defenses, could be of value in COVID-19. However, conflicting data on drug efficacy point to the need for better patient selection and biomarker studies.

INTRODUCTION

A huge international effort has been made in the last 50 years to highlight cancer's mechanisms of proliferation and dissemination (1). Beyond chemotherapy, new drugs such as targeted therapy, immunotherapy, epigenetic modifiers, and more recently cellular therapies have been approved and have succeeded in improving lifetime expectancy and quality of life of patients living with cancer (2). Apart from their antitumor effects, anticancer drugs also increased knowledge about physiologic pathways in healthy tissues. Outside of cancer indication, some anticancer agents were then developed in extended indications. For example, JAK inhibitors, first approved to treat myeloproliferative neoplasia with activating JAK2 mutations, have now extended indications in rheumatologic diseases and are under development for several dysimmune diseases.

At the end of 2019, the world was destabilized by the emergence of a new coronavirus called SARS-CoV-2 and the coronavirus disease 2019 (COVID-19) pandemic (3). International relationships were greatly affected by the virus dissemination and government interventions to limit its spread (4, 5). A huge effort by the scientific and biomedical community has sought to understand the pathophysiology and clinical manifestations of COVID-19. The full RNA sequence of the new coronavirus was identified with unprecedented speed, and insights into how it interacts with human cells quickly followed (6–8). Concomitantly, clinical studies worldwide revealed the different clinical aspects of severe COVID-19 manifestations characterized by brutal cytokine release syndrome (CRS) and visceral inflammatory involvement, particularly pneumonitis (9).

The main risk factors for developing severe COVID-19 are age, male sex, obesity, cardiovascular comorbidities, and diabetes (9, 10). Laboratory science has shown that severe COVID-19 infection is driven mainly by immunopathologic inflammatory pathways mediated by IL6, IL8, tumor necrosis factor alpha (TNFα), and IFNγ (8). Large clinical trials have since evaluated antiviral drugs such as remdesivir (11), anticytokine approaches with anti-IL6 (12) and dexamethasone (13), and passive immunotherapy such as patient convalescent plasmatherapy or recombinant cocktail antibodies against anti-spike antibody (14).

COVID-19 Pathologic Mechanisms

COVID-19 is a human infectious and inflammatory disease related to SARS-CoV-2 infection. A large number of individuals infected with SARS-CoV-2 do not develop symptoms or develop mild manifestations characteristic of flu-like

[1]Department of Medical Oncology, Gustave Roussy, Villejuif, France. [2]Drug Development Department, Gustave Roussy, Villejuif, France. [3]INSERM U1015, Gustave Roussy, Villejuif, France. [4]Paris Saclay University, Saint-Aubin, France. [5]Division of Hematology/Oncology, Department of Medicine, University of California, Los Angles, Los Angeles, California.

Corresponding Author: Jean-Charles Soria, Gustave Roussy Cancer Campus, 114 Rue Edouard Vaillant, Villejuif 94805, France. Phone: 33-0-14211-4016; E-mail: Jean-Charles.Soria@gustaveroussy.fr

Cancer Discov 2021;11:1336–44

doi: 10.1158/2159-8290.CD-21-0144

Published OnlineFirst April 12, 2021; DOI: 10.1158/2159-8290.CD-21-0144

syndrome and acquired immunity directed against the new betacoronavirus (15). However, about 10% to 15% of patients progress to severe pneumonia and respiratory distress and eventually require admission in the intensive care unit (ICU). Nearly 25% to 30% of patients admitted to the ICU will ultimately die. After an incubation phase and 7 to 10 days of symptoms, a sudden viral pneumonia characterized by profound hypoxemia and interstitial lung disease may occur, related not only to virus infection but also to cytokine storm and immunothrombosis phenomenon (15).

Angiotensin-converting enzyme 2 (ACE2) and the transmembrane serine protease TMPRSS2, expressed by human alveolar and endothelial cells, participate in the virus cell internalization and activate the spike (S) protein of SARS-CoV-2 into the human cells (16). Obesity is associated with ACE2 and TMPRSS2 overexpression at the surface of endothelial cells through dysregulation of the leptin pathway (17). Also, TMPRSS2 is an androgen-regulated protein, which could explain male sex predisposition to develop severe forms of COVID-19 (18). *Primum movens* to severe COVID-19 seems to be the immunothrombosis phenomenon, characterized by small blood vessel thrombosis associated with microangiopathy and inflammatory infiltration in alveolar capillary, which leads to alveolar edema and associated systemic cytokine storm (19, 20). Patients with severe COVID-19 develop an inflammatory state characterized by increased concentrations of plasmatic cytokines, chemokines, and alarmins related to activation and recruitment of inflammatory cells, such as IL1β, IL6, IL8, TNF, granulocyte-colony stimulating factor, chemokine ligand 2, and calprotectin (S100A8 and S100A9; refs. 21, 22). The most severe COVID-19 infections correlate with low type 1 IFN concentration in blood and transcriptomic signature in peripheral blood mononuclear cells (23). Defects in type 1 IFN can be related to functional genetic polymorphisms or autoimmunity directed against type 1 IFN (24, 25). Besides soluble inflammatory and immune factors, patients who develop the most severe forms of COVID-19 present with pathologic hematologic and immunologic features, such as increased neutrophilia, monocytopenia (with loss of nonconventional monocytes), and lymphocytopenia (22, 26). Patients with severe COVID-19 have profound lymphocytopenia with low, but activated and exhausted, $CD4^+$ and $CD8^+$ T cells such as $CD19^+$ B cells and particularly early plasmablasts, which do not succeed in establishing effective antiviral immunity (27–29). Finally, patients with severe COVID-19 are also characterized in their blood and lungs by an emergency myelopoiesis with immature neutrophils and monocytes with deleterious proinflammatory abilities and immunosuppressive function, which can limit the development of effective adaptive immunity (22).

Patients living with cancer are exposed to a significantly higher risk of severe SARS-CoV-2 infection and higher risk of death (30). Particularly, patients with hematologic malignancies have a higher mortality rate related to COVID-19 than patients with solid tumors (31, 32). Among patients with cancer, patients with more recent, disseminated, and symptomatic diseases undergoing chemotherapy are generally those with the most severe infections (33). The explanation for these increased risks remains unclear, such as the amplitude of viral load that could independently predict mortality in both patient populations, which certainly reflects that immunosuppression related to cancer predisposes to a more intense viral replication (34). These data provide a basis for priority for COVID-19 vaccination in patients living with cancer (35).

Administration of anticancer treatments is also an important factor that influences the risks of infectivity and severity of COVID-19 (36, 37). Although chemotherapy was shown to be associated with a higher risk of COVID-19 worsening, interestingly, patients treated with immune-checkpoint immunotherapies or targeted anticancer therapies were not at higher risk (33, 34, 36–38). Other studies suggested that patients treated for cancer and receiving antiandrogenic treatments or antiangiogenic drugs could have improved outcomes (39–41). As these treatments do not seem to increase COVID-19 severity and might improve outcomes for patients, the discussion of repurposing anticancer drugs for COVID-19 began (Fig. 1). Anticancer drugs currently undergoing investigation in clinical trials for the treatment of COVID-19 are depicted in Table 1.

REPURPOSING DRUGS FROM ONCOLOGY

Anti-Inflammatory Drugs

Dexamethasone

Corticosteroids, in particular dexamethasone, are drugs commonly used to treat hematologic malignancies such as multiple myeloma, non-Hodgkin lymphoma, or acute lymphoblastic leukemia. For the treatment of severe COVID-19 with viral pneumonia, the British Recovery study has shown that dexamethasone improves the overall survival of patients needing respiratory support (either invasive mechanical ventilation or oxygen alone; ref. 13). Dexamethasone then became the standard of care for patients hospitalized with COVID-19 with viral pneumonia requiring oxygen support.

Other anti-inflammatory drugs targeting new molecular pathways may be tested for patients with severe COVID-19. Biological studies have shown that calprotectin is one of the key molecules implicated in the inflammatory cascade leading to severe forms of COVID-19 (22), suggesting calprotectin as a potential new therapeutic target.

Anti–Cytokine IL6

In hematology oncology, CRS is known as a frequent complication associated with chimeric antigen receptor-T (CAR-T) cells or bispecific antitumor antibodies. CRS is characterized by fever, hypotension, and eventually hypoxemia or biological abnormalities including coagulopathy (42), related to a sudden release of cytokines by the immune system when the latter encounters the tumor antigen under the effect of anticancer treatment (43). CRS is dominated by high levels of IL6 in serum, which led to anti-IL6 receptor therapies being proposed to control CRS (43). The respiratory distress and high fever during COVID-19 viral pneumonia may share similarities with CRS (44).

The cytokine storm induced by the SARS-CoV-2 virus is becoming better understood. Cytokines such as IL6, IL10, and TNFα, and the overactivation of the systemic complement pathways, namely substrates C5b-9 and C4d, are correlated with the severity of COVID-19 (45). This systemic inflammation and complement activation are also associated with the phenomenon of immunothrombosis, a hypercoagulopathy

Published OnlineFirst April 12, 2021; DOI: 10.1158/2159-8290.CD-21-0144

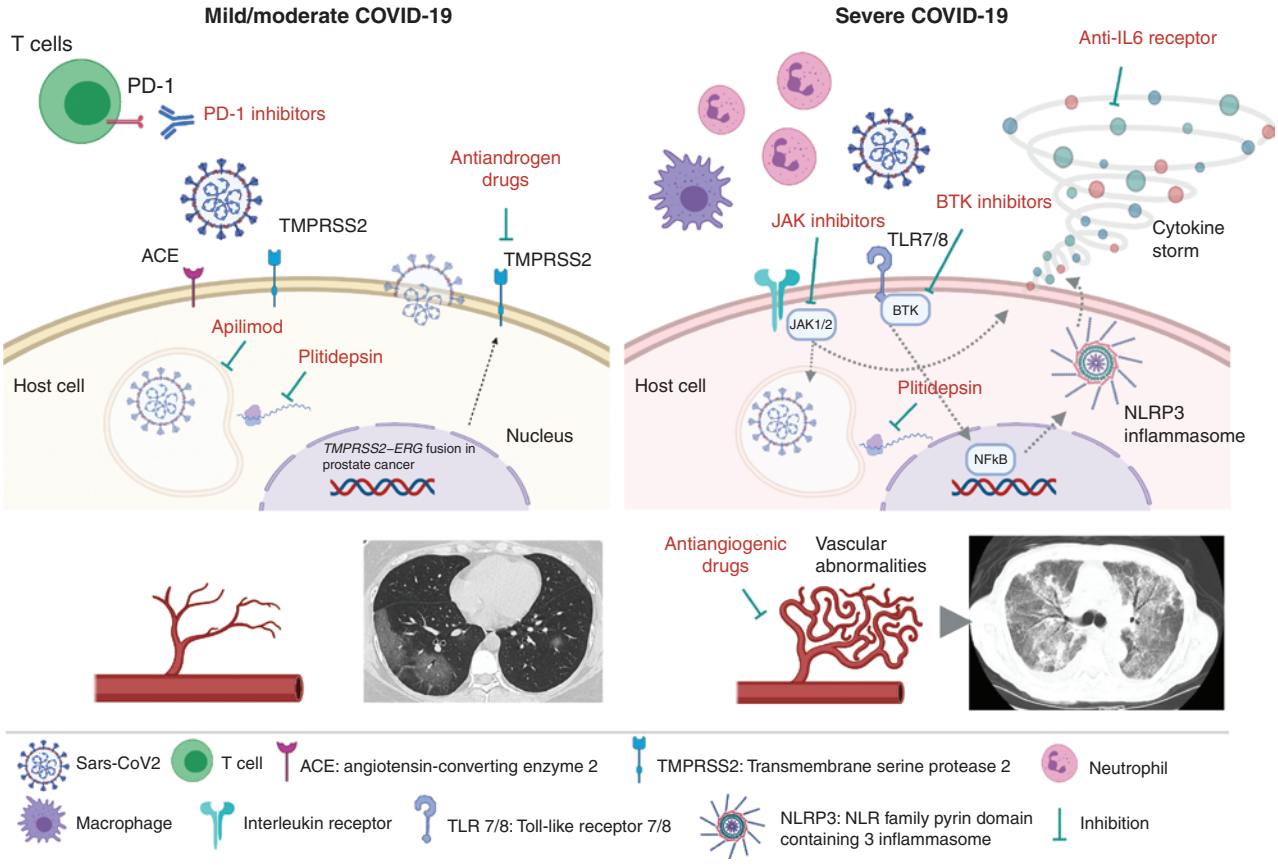

Figure 1. Anticancer drugs proposed for drug repurposing in COVID-19 infection and presented according to their potential therapeutic targets. In mild to moderate COVID-19, anti–PD-1 reinforces the T-cell immune system and may improve viral clearance. Antiandrogen drugs block the TMPRSS2 receptor used by the virus for entry into the cell. In severe COVID-19, JAK/STAT or BTK inhibitors mitigate the inflammatory signaling cascade into the cell and help control the cytokine storm. Anticytokines (anti-IL6 receptor) directly reduce the cytokine storm by blocking the IL6 receptor on the cell surface. Antiangiogenic drugs could limit vascular abnormalities induced by the virus in endothelium. Other anticancer drugs, such as plitidepsin and apilimod, have antiviral activity against SARS-CoV-2 by targeting the host protein eEF1A or by affecting endosomal homeostasis, respectively.

state affecting up to 16% of patients hospitalized for COVID-19 (46). Dysregulated neutrophil extracellular traps in the endothelium of patients also contribute to immunothrombosis in patients with severe COVID-19, by propagating inflammation and microvascular thrombosis (46).

Several anticytokine therapeutics aiming to curb COVID-19–related cytokine storm have been investigated. Retrospective studies and randomized clinical trials evaluating the most used anti-IL6 receptor blocker tocilizumab antibody suggested a therapeutic effect of the drug (47–49), while other clinical trials failed to complete their efficacy endpoints (50–52). Overall, the results of additional clinical trials with longer follow-up of enrolled patients are needed to better understand the magnitude of the therapeutic effect of anti-IL6 receptor therapy in patients with COVID-19. A more precise, and probably more selective, definition of the patient population with COVID-19 who may or may not benefit from anti-IL6 receptor therapy remains to be clarified in future studies.

Targeting the BTK Signaling Pathway

Bruton tyrosine kinase (BTK) inhibitors are approved therapies for treating lymphoid blood disorders such as chronic lymphocytic leukemia (CLL), mantle cell lymphoma (MCL), or Waldenstrom disease (53). The SARS-CoV-2 virus can generate an overactivation of immune cells, including both B and T cells, leading to a "cytokine storm," thus contributing to acute lung injury and respiratory distress (21). BTK pathway effector molecules contribute to the cytokine storm and are potential targets for the drug therapy of COVID-19 (41). An observational study evaluating the use of acalabrutinib in 19 patients with COVID-19 hospitalized and requiring oxygen supplementation suggested potential efficacy. However, the BTK inhibition hypothesis must be interpreted with caution, because of the concomitant use of dexamethasone in initial studies. Definitive results of a randomized controlled clinical trial investigating acalabrutinib for patients with COVID-19 (CALAVI phase II trial: NCT04380688 and NCT04346199) are pending, but a recent press communication reported that the study did not reach its primary endpoint as compared with best supportive care alone.

Implications of JAK/STAT Inhibitors to Treat COVID-19

JAK is a family of intracellular, non–receptor tyrosine kinases that transduce signals transferred by the cytokines

Published OnlineFirst April 12, 2021; DOI: 10.1158/2159-8290.CD-21-0144

Table 1. Examples of cancer drugs currently tested for COVID-19

Targeted pathway	Drug	MoA related to Covid pathogenesis	COVID-19 severity	Clinical trial
Anticytokines				
IL6	Tocilizumab	Prevents the "cytokine storm"	Severe	NCT04377659 Phase II
			Severe	NCT04363853 Phase II
			Requiring hospitalization	NCT04317092 (TOCIVID-19)
			Requiring hospitalization	NCT04372186 (EMPACTA) Phase III
IL8	BMS-986253	Prevents the "cytokine storm"	Severe	NCT04347226 Phase II
JAK inhibitors	Pacritinib (JAK2i)	Blocks multiple, proinflammatory cytokines; antiviral effects by impeding cellular viral endocytosis	Severe	NCT04404361 (PRE-VENT) Phase III
	Baricitinib (JAK1/2i) + antiviral therapy		Moderate and severe	NCT04373044, Phase II
	Baricitinib		Moderate and severe	NCT04346147, Phase II
				NCT04390464, Phase IV
	Ruxolitinib (JAK1/2i)		Severe	NCT04331665
BTK	Ibrutinib	Abrogation of pulmonary inflammatory cytokines, lung injury	Requiring hospitalization	NCT04439006 Phase II
			Severe	NCT04375397 (iNSPIRE) Phase II
	Acalabrutinib		Requiring hospitalization	NCT04346199 (CALAVI) Phase II
	TL-895		Requiring hospitalization	NCT04419623 Phase I/II
Antiangiogenics	Bevacizumab	Inhibits VEGF, a key factor to increase vascular permeability and induce pulmonary edema caused by inflammatory exudation in COVID-19 infection	Severe	NCT04305106 (BEST-RCT)
			Severe	NCT04275414 (BEST-CP) Phase II
			Requiring more than 3 L of oxygen	NCT04344782 (CORIMMUNO-BEVA) Phase II
Androgen blockade	Bicalutamide	Blocks TMPRSS2	Mild/moderate COVID-19 requiring hospitalization	NCT04374279 (RECOVER) Phase II
			Symptomatic	NCT04509999 Phase III
	Degarelix	Suppresses androgens, which might regulate TMPRSS2 expression in lung tissue	Veterans hospitalized for COVID-19 (severity 3, 4, 5 on the influenza scale)	NCT04397718 (HITCH) Phase II
	Enzalutamide	Antiandrogen inhibiting the expression of androgen-regulated proteins, such as TMPRSS2	High-risk male COVID-19 patients, mild symptoms, not requiring hospitalization	NCT04456049 Phase II
			Mild/severe COVID-19 requiring hospitalization	NCT04475601 (COVIDENZA) Phase II
Other				
Proinflammatory	IFNα	Abrogates type I IFN deficiency in severe COVID-19	Severe	NCT04534725 (C-SMART)
	IMM-101	Stimulates dendritic cells	Prevention of severe COVID-19	NCT04442048 (COV-IMMUNO)

(*continued*)

Published OnlineFirst April 12, 2021; DOI: 10.1158/2159-8290.CD-21-0144

Table 1. Examples of cancer drugs currently tested for COVID-19 (*Continued*)

Targeted pathway	Drug	MoA related to Covid pathogenesis	COVID-19 severity	Clinical trial
NK cells	FT516	Engineered NK cells expressing CD16, which destroy antibody-coated target cells	Hospitalized COVID-19 patients with hypoxia	NCT04363346 Phase I
Double-stranded RNA	Rintatolimod ± IFN alpha	Mimics viral infection, stimulates the immune system to limit viral replication	Mild/moderate	NCT04379518 Phase I/II
PI3K–AKT	Duvelisib (PI3K inhibitor)	Inhibits aberrant hyperactivation of the innate immune system	Severe Severe	NCT04487886 (DAMPEN-CI) Phase II NCT04372602 Phase II
MAPKAPK2 (MK2) inhibitor	(ATI)-450	Inhibits multiple inflammatory cytokines	Moderate or severe	NCT04481685 Phase II
HSP	MPT0B640 (HSP inhibitor)	Inhibits defective HSP in COVID-19, to avoid the "cytokine storm"	Requiring hospitalization	NCT04526717 Phase I
SK2	Opaganib (SK2-selective inhibitor)	Anti-inflammatory and antiviral activity	Requiring supplemental oxygen at baseline	NCT04414618 Phase II
Nucleo-cytoplasmic transport inhibitor	Selinexor (selective inhibitor of XPO1)	Anti-inflammatory activity, reduction of proinflammatory cytokines levels	Severe Severe	NCT04534725 (C-SMART) Phase III NCT04349098 Phase II
SUMO	TAK-981	Inhibits SUMOnylation, a process involved in the post-translational modification of the coronavirus N protein	Moderately severe	NCT03648372 Phase I
eEF1A inhibition	Plitidepsin	Antiviral activity by the inhibition of eEF1A, identified in SARS-CoV-2 virions	Requiring hospitalization	NCT04382066 (APLICOV-PC) Phase I
eEF4A inhibition	Zotatifin	Antiviral activity by impairing the cap-dependent mRNA translation of SARS-CoV-2	Mild or moderate	NCT04632381 (PROPEL) Phase I
CK2 inhibition	Silmitasertib	Antiviral activity by inhibiting CK2, involved in viral replication and virus-induced cytoskeleton organization	Moderate Severe	NCT04663737 Phase II NCT04668209 Phase II

Abbreviations: ALI, acute lung injury; ARDS, acute respiratory distress syndrome; CK2, casein kinase 2; eEF1A, Eukaryotic translation elongation factor 1 alpha 1; GM-CSF, granulocyte macrophage–colony stimulating factor; HSP, heat shock protein; IFN, interferon; MoA, mechanism of action; MoAb, monoclonal antibody; NFkB, nuclear factor kB; NK, natural killer; SK2, sphingosine kinase-2; TMPRSS2, transmembrane protease, serine 2; VEGF, vascular endothelial growth factor.

via the JAK–STAT signaling pathway. The JAK–STAT pathway is overactivated by activating mutations in JAK2 hematologic malignancies (54) such as myeloproliferative syndromes including myelofibrosis or polycythemia vera. The JAK–STAT pathway was recently highlighted as an important inflammatory signaling pathway in inflammatory diseases, and JAK inhibitors are approved drugs in rheumatoid arthritis. JAK inhibitors are expected to reduce cytokine storms (55); therefore, they were suggested as a promising therapy to mitigate the inflammatory cascade generated by COVID-19 (56). Preclinical studies in humans suggest that JAK inhibitors may restrict the expression of the ACE2 receptor—necessary for the entry of the SARS-CoV-2 virus—into human cells (57, 58). A clinical study of 601 patients suggests that baricitinib, a JAK1/2 inhibitor, could improve the outcome of patients with severe COVID-19, primarily by reducing the rampant immune inflammation (58). A double-blind, randomized, placebo-controlled trial evaluating baricitinib plus remdesivir in hospitalized adults with COVID-19 concluded that baricitinib plus remdesivir was superior to remdesivir alone in reducing recovery time and accelerating improvement in clinical status among patients with COVID-19 (59). Data from

Published OnlineFirst April 12, 2021; DOI: 10.1158/2159-8290.CD-21-0144

randomized trials with a JAK inhibitor alone versus placebo for the treatment of COVID-19 are still pending (Table 1), while one trial was terminated early for futility (NCT04377620). In light of the hypercoagulability state of COVID-19, vigilance is recommended given the potentially increased risk of thrombosis reported with some JAK inhibitors (60).

Antiangiogenics

The immunothrombosis phenomenon is associated with upregulation of macrophages, complement substrates, platelet activation, thrombosis, and proinflammatory markers (61, 62). Moreover, proangiogenic factors, such as VEGF and angiopoetin 2, are crucial factors implicated in vascular permeability and pulmonary edema of patients with COVID-19 (63). In an autopsy study performed on lungs from people who died from viral infections, the amount of new vessel growth associated with COVID-19 was 2.7 times higher compared with that found in patients with H1N1 influenza virus. Pathologic findings in patients with COVID-19 indicate severe endothelial injury, disruptive cell membranes, and widespread thrombosis (20). In severe forms of COVID-19, some researchers suggest antiangiogenic drugs may suppress pulmonary edema by inhibiting proangiogenic factors and by promoting a vascular normalization. In a single-arm trial investigating bevacizumab plus standard of care in 26 patients with severe COVID-19 infection (NCT04275414), a single dose of 7.5 mg/kg of bevacizumab was associated with rapid improvement in PaO2/FiO2 ratios, improved oxygen support status in 92% of patients by day 28 (versus 62% in the external comparison cohort treated with standard of care only), and significant radiologic reduction of pneumonia lesions within seven days. Of note, no drug-related serious adverse effects were reported (64). However, in this study, patients were excluded if they had received full-dose anticoagulant within 10 days before enrollment or had thrombosis within 6 months before enrollment, criteria that apply to a significant proportion of patients with cancer. Other ongoing clinical trials are investigating bevacizumab, and results are pending (Table 1). A clinical trial (NCT04342897) evaluating the effect of targeting angiopoietin 2 in patients with COVID-19 was terminated early for futility. Further trials evaluating antiangiogenics should carefully assess the risk of thrombosis and probably offer concomitant anticoagulation treatments to control this risk of thrombosis.

Immune-Checkpoint Blockade

An effective immune response against viral infections depends on the activation of host $CD8^+$ T cells expected to eliminate cells containing the SARS-CoV-2 virus (65, 66). In patients with severe COVID-19, there is a reduced number of $CD4^+$ and $CD8^+$ T cells, while the surviving T cells exhibit an exhausted phenotype, with a higher level of PD-1 expression (67, 68). The reduced T-cell counts (total T cells < 800/μL, $CD8^+$ cells < 300/μL and $CD4^+$ cells < 400/μL) in the blood of patients with COVID-19 were negatively correlated with the levels of TNFα, IL6, and IL10 (68). In an observational clinical study of 113 patients with cancer and laboratory confirmed COVID-19 while on treatment with immune-checkpoint inhibitors (ICI) without chemotherapy, the mortality by COVID-19 in patients under ICI did not seem to be higher compared with rates reported in the general cancer population (69). Another observational study conducted in 178 patients with cancer managed for COVID-19 did not identify increased risk of clinical worsening or death in patients treated with ICI for cancer. Conversely, patients receiving cytotoxic chemotherapy had an increased risk of clinical worsening and death in the univariable analysis and a trend toward a higher risk of death in the multivariable analysis, after adjusting for ECOG performance status and cancer status (33). Similarly, chemotherapy negatively affected survival outcomes in patients with thoracic cancer and COVID-19 in the TERAVOLT cohort, as opposed to immunotherapy and targeted therapy (70, 71). However, in another observational study including 423 patients with cancer with symptomatic COVID-19, treatment with ICI ($N = 31$) was a predictor for hospitalization and severe disease, while treatment with chemotherapy was not (72). Overall, these data are limited and their conflicting interpretation imposes caution about potential interest in repurposing ICI for COVID-19. ICI might have a dual effect: it might enhance T cell–mediated viral clearance in the early phase, but it has been suggested to also facilitate late-inflammatory states by promoting T regulatory cell activation and the exacerbation of the cytokine storm (73, 74). The sum of these data suggests that future trials evaluating the potential interest of ICI for COVID-19 should select the patient population to be treated, most likely considering treatment in the early phase of the disease and without a cytokine storm.

Antiandrogenic Treatment

SARS-CoV-2 virus harnesses the TMPRSS2 receptors to enter within the host human cell, and these receptors are regulated by the androgen receptor (16). The TMPRSS2 gene is strongly upregulated in prostate cancer cells, and it has a testosterone-activated response element, suggesting potential antiandrogenic treatment in patients with COVID-19. In a cohort of men with prostate cancer, COVID-19 infection was less likely to be reported in patients treated with androgen deprivation therapy (ADT) as compared with those without (ADT 4/5,273 cases versus 114/37, odds ratio 4.05, 95% confidence interval 1.55–10.59, $P = 0.00043$; ref. 39). However, ADT effect seems to be modest, as the number of patients needed to treat with ADT for the prevention of one case of COVID-19 was 434. This minimal potential therapeutic effect makes ADT a less appealing option in the case of patients without prostate cancer, also considering the associated side effects of ADT (75). Moreover, preliminary data from multicenter registries do not support a decrease in COVID-related mortality with antiandrogenic drugs (76). Ongoing trials testing bicalutamide, enzalutamide, or GnRH antagonists are ongoing (Table 1). Also, camostat mesylate, a direct TMPRSS2 inhibitor, is currently being investigated in several clinical trials for COVID-19 as monotherapy or in combination with bicalutamide, with the aim of reducing the SARS-CoV-2 viral burden and forestalling complications of COVID-19 (NCT0435328, NCT04583592, NCT04608266, NCT04524663, and NCT04652765).

Published OnlineFirst April 12, 2021; DOI: 10.1158/2159-8290.CD-21-0144

The Targeting of Host-Interacting Proteins and Kinases Dysregulated during Infection

Recent preclinical studies on SARS-CoV-2–infected cells found important interactions between human proteins and SARS-CoV-2, and a dramatic rewiring of phosphorylation on host and viral proteins, highlighting how the virus uses the host's posttranslational regulatory systems to induce rapid signaling changes (77–79). The mapping of proteomic changes to pharmacologic modulators identified promising target–drug pairs that might trigger robust antiviral effects (77, 78). For instance, eEF1A was identified in SARS-CoV virions (80, 81), and plitidepsin, an eEF1A inhibitor approved in Australia for the treatment of multiple myeloma, was shown to have a potent anti–SARS-CoV-2 antiviral activity in preclinical studies (IC_{90} = 0.88 nmol/L; ref. 81). Plitidepsin was 27.5-fold more potent than remdesivir *in vitro*, while having limited toxicity (81). These data indicated promising therapeutic repurposing for plitidepsin as antiviral therapy for COVID-19, and phase II/III trials are pending.

Another target is the virus-induced upregulation of casein kinase 2 (CK2), which might facilitate cell-to-cell spread by driving actin polymerization. CK2 inhibition with silmitasertib, currently being tested in recurrent medulloblastoma (NCT03904862), showed robust antiviral activity in SARS-CoV-2–infected cells (77). Phosphatidylinositol-3-Phosphate/Phosphatidylinositol 5-Kinase (PIKfyve) is a protein that resides in early endosomes, being involved in endomembrane homeostasis. Its inhibition has the potential to inhibit viral entry, making it a promising target for the treatment of early COVID-19 infection. *In vitro* experiments showed that apilimod, a specific PIKfyve kinase inhibitor investigated in early-phase clinical trials for the treatment of non-Hodgkin lymphoma, successfully inhibited viral replication during entry (82). Apilimod is currently being evaluated for its impact on SARS-CoV-2 viral load in patients with confirmed COVID-19 infection treated in an outpatient setting (NCT04446377). SARS-CoV-2 also increases the phosphorylation of cyclin-dependent kinase 2 (CDK2) and promotes cell-cycle arrest in the S–G_2 phase, which may facilitate viral replication (77, 83). Accordingly, strong antiviral activity for the CDK inhibitor dinaciclib was observed across two SARS-CoV-2–infected cell lines (77). Other examples of promising target–drug pairs include AXL and gilteritinib (approved by the FDA for relapsed or refractory acute myeloid leukemia with FLT3 mutations) or p38 and p38 inhibitors, such as ralimetinib (undergoing development in ovarian cancer; ref. 77).

CONCLUSION

A better understanding of molecular mechanisms associated with COVID-19 as well as clinical observations from patients with COVID-19 concomitantly treated for cancer generates various hypotheses concerning potential anticancer drug repositioning. Although strong clinical evidence is still lacking, the sum of these data suggests anticancer drugs could be regarded as potent antiviral therapies, with both direct antiviral effects and indirect effects by blocking signaling pathways such as JAK/STAT or abnormal angiogenesis. Clinical trials for hypothesis testing of anticancer drugs are an encouraging strategy for discovering new possible therapies for COVID-19.

Authors' Disclosures

J.-M. Michot reports being Principal/sub-Investigator of Clinical Trials for AbbVie, Aduro, Agios, Amgen, Argen-x, Astex, AstraZeneca, Aveo Pharmaceuticals, Bayer, Beigene, Blueprint, BMS, Boehringer Ingelheim, Celgene, Chugai, Clovis, Daiichi Sankyo, Debiopharm, Eisai, Eos, Exelixis, Forma, Gamamabs, Genentech, Gortec, GSK, H3 Biomedicine, Incyte, Innate Pharma, Janssen, Kura Oncology, Kyowa, Lilly, Loxo, Lysarc, Lytix Biopharma, Medimmune, Menarini, Merus, MSD, Nanobiotix, Nektar Therapeutics, Novartis, Octimet, Oncoethix, Oncopeptides AB, Orion, Pfizer, Pharmamar, Pierre Fabre, Roche, Sanofi, Seattle Genetics, Servier, Sierra Oncology, Taiho, Takeda, Tesaro, and Xencor. A. Ribas reports personal fees from Amgen, Chugai, Genentech, Merck, Novartis, Roche, Sanofi, Vedanta, 4C Biomed, Apricity, Arcus, Highlight, Compugen, ImaginAb, MapKure, Merus, Rgenix, Lutris, PACT Pharma, Tango, Advaxis, CytomX, Five Prime, RAPT, Isoplexis, and Kite-Gilead, and grants from Agilent and Bristol-Myers Squibb outside the submitted work. J. Soria reports other support from Gritstone Oncology, Relay Therapeutics, Hookipa Pharmaceuticals, and AstraZeneca during the conduct of the study. No disclosures were reported by the other authors.

Acknowledgments

We kindly thank the AACR COVID-19 and Cancer Task Force members for their suggestions for this manuscript. The figure is an unpublished original work, created by Mihaela Aldea with BioRender.com, for the express purpose of publication in this *Cancer Discovery* article.

Received February 1, 2021; revised March 22, 2021; accepted April 12, 2021; published first April 12, 2021.

REFERENCES

1. Hanahan D, Weinberg RA. Hallmarks of cancer: the next generation. Cell 2011;144:646–74.
2. Moffat JG, Rudolph J, Bailey D. Phenotypic screening in cancer drug discovery – past, present and future. Nat Rev Drug Discov 2014;13:588–602.
3. Guan WJ, Ni ZY, Hu Y, Liang WH, Ou CQ, He JX, et al. Clinical characteristics of coronavirus disease 2019 in China. N Engl J Med 2020;382:1708–20.
4. Chinazzi M, Davis JT, Ajelli M, Gioannini C, Litvinova M, Merler S, et al. The effect of travel restrictions on the spread of the 2019 novel coronavirus (COVID-19) outbreak. Science 2020;368:395–400.
5. Brauner JM, Mindermann S, Sharma M, Johnston D, Salvatier J, Gavenciak T, et al. Inferring the effectiveness of government interventions against COVID-19. Science 2021;371:eabd9338.
6. Zhou P, Yang XL, Wang XG, Hu B, Zhang L, Zhang W, et al. A pneumonia outbreak associated with a new coronavirus of probable bat origin. Nature 2020;579:270–3.
7. Lan J, Ge J, Yu J, Shan S, Zhou H, Fan S, et al. Structure of the SARS-CoV-2 spike receptor-binding domain bound to the ACE2 receptor. Nature 2020;581:215–20.
8. Vabret N, Britton GJ, Gruber C, Hegde S, Kim J, Kuksin M, et al. Immunology of COVID-19: current state of the science. Immunity 2020;52:910–41.
9. Zhou F, Yu T, Du R, Fan G, Liu Y, Liu Z, et al. Clinical course and risk factors for mortality of adult inpatients with COVID-19 in Wuhan, China: a retrospective cohort study. Lancet 2020;395:1054–62.
10. Nishiga M, Wang DW, Han Y, Lewis DB, Wu JC. COVID-19 and cardiovascular disease: from basic mechanisms to clinical perspectives. Nat Rev Cardiol 2020;17:543–58.
11. Beigel JH, Tomashek KM, Dodd LE, Mehta AK, Zingman BS, Kalil AC, et al. Remdesivir for the treatment of Covid-19 – final report. N Engl J Med 2020;383:1813–26.

Published OnlineFirst April 12, 2021; DOI: 10.1158/2159-8290.CD-21-0144

12. Guillen L, Padilla S, Fernandez M, Agullo V, Garcia JA, Telenti G, et al. Preemptive interleukin-6 blockade in patients with COVID-19. Sci Rep 2020;10:16826.
13. Group RC, Horby P, Lim WS, Emberson JR, Mafham M, Bell JL, et al. Dexamethasone in hospitalized patients with Covid-19. N Engl J Med 2021;384:693–704.
14. Sanders JM, Monogue ML, Jodlowski TZ, Cutrell JB. Pharmacologic treatments for coronavirus disease 2019 (COVID-19): a review. JAMA 2020;323:1824–36.
15. Wiersinga WJ, Rhodes A, Cheng AC, Peacock SJ, Prescott HC. Pathophysiology, transmission, diagnosis, and treatment of coronavirus disease 2019 (COVID-19): a review. JAMA 2020;324:782–93.
16. Hoffmann M, Kleine-Weber H, Schroeder S, Kruger N, Herrler T, Erichsen S, et al. SARS-CoV-2 cell entry depends on ACE2 and TMPRSS2 and is blocked by a clinically proven protease inhibitor. Cell 2020;181:271–80.
17. Ayres JS. A metabolic handbook for the COVID-19 pandemic. Nat Metab 2020;2:572–85.
18. Mani RS, Tomlins SA, Callahan K, Ghosh A, Nyati MK, Varambally S, et al. Induced chromosomal proximity and gene fusions in prostate cancer. Science 2009;326:1230.
19. Wichmann D, Sperhake JP, Lutgehetmann M, Steurer S, Edler C, Heinemann A, et al. Autopsy findings and venous thromboembolism in patients with COVID-19: a prospective cohort study. Ann Intern Med 2020;173:268–77.
20. Ackermann M, Verleden SE, Kuehnel M, Haverich A, Welte T, Laenger F, et al. Pulmonary vascular endothelialitis, thrombosis, and angiogenesis in Covid-19. N Engl J Med 2020;383:120–8.
21. Del Valle DM, Kim-Schulze S, Huang HH, Beckmann ND, Nirenberg S, Wang B, et al. An inflammatory cytokine signature predicts COVID-19 severity and survival. Nat Med 2020;26:1636–43.
22. Silvin A, Chapuis N, Dunsmore G, Goubet AG, Dubuisson A, Derosa L, et al. Elevated calprotectin and abnormal myeloid cell subsets discriminate severe from mild COVID-19. Cell 2020;182:1401–18.
23. Hadjadj J, Yatim N, Barnabei L, Corneau A, Boussier J, Smith N, et al. Impaired type I interferon activity and inflammatory responses in severe COVID-19 patients. Science 2020;369:718–24.
24. Zhang Q, Bastard P, Liu Z, Le Pen J, Moncada-Velez M, Chen J, et al. Inborn errors of type I IFN immunity in patients with life-threatening COVID-19. Science 2020;370:eabd4570.
25. Bastard P, Rosen LB, Zhang Q, Michailidis E, Hoffmann HH, Zhang Y, et al. Autoantibodies against type I IFNs in patients with life-threatening COVID-19. Science 2020;370:eabd4585.
26. Melenotte C, Silvin A, Goubet AG, Lahmar I, Dubuisson A, Zumla A, et al. Immune responses during COVID-19 infection. Oncoimmunology 2020;9:1807836.
27. Mathew D, Giles JR, Baxter AE, Oldridge DA, Greenplate AR, Wu JE, et al. Deep immune profiling of COVID-19 patients reveals distinct immunotypes with therapeutic implications. Science 2020;369:eabc8511.
28. Zhang JY, Wang XM, Xing X, Xu Z, Zhang C, Song JW, et al. Single-cell landscape of immunological responses in patients with COVID-19. Nat Immunol 2020;21:1107–18.
29. Robbiani DF, Gaebler C, Muecksch F, Lorenzi JCC, Wang Z, Cho A, et al. Convergent antibody responses to SARS-CoV-2 in convalescent individuals. Nature 2020;584:437–42.
30. Wang Q, Berger NA, Xu R. Analyses of risk, racial disparity, and outcomes among US patients with cancer and COVID-19 infection. JAMA Oncol 2021;7:220–7.
31. Kuderer NM, Choueiri TK, Shah DP, Shyr Y, Rubinstein SM, Rivera DR, et al. Clinical impact of COVID-19 on patients with cancer (CCC19): a cohort study. Lancet 2020;395:1907–18.
32. Lee LYW, Cazier JB, Starkey T, Briggs SEW, Arnold R, Bisht V, et al. COVID-19 prevalence and mortality in patients with cancer and the effect of primary tumour subtype and patient demographics: a prospective cohort study. Lancet Oncol 2020;21:1309–16.
33. Albiges L, Foulon S, Bayle A, Gachot B, Pommeret F, Willekens C, et al. Determinants of the outcomes of patients with cancer infected with SARS-CoV-2: results from the Gustave Roussy cohort. Nat Cancer 2020;1:965–75.
34. Ekue FN, Nfi AN, Tsangue P, Taylor WP, Gumm ID. Prevalence of bluetongue virus and antibodies in ruminants in Cameroon. Trop Anim Health Prod 1985;17:189.
35. Ribas A, Sengupta R, Locke T, Zaidi SK, Campbell KM, Carethers JM, et al. Priority COVID-19 vaccination for patients with cancer while vaccine supply is limited. Cancer Discov 2021;11:233–6.
36. Sng CCT, Wong YNS, Wu A, Ottaviani D, Chopra N, Galazi M, et al. Cancer history and systemic anti-cancer therapy independently predict COVID-19 mortality: a UK Tertiary Hospital Experience. Front Oncol 2020;10:595804.
37. Jee J, Foote MB, Lumish M, Stonestrom AJ, Wills B, Narendra V, et al. Chemotherapy and COVID-19 outcomes in patients with cancer. J Clin Oncol 2020;38:3538–46.
38. Lee LY, Cazier JB, Angelis V, Arnold R, Bisht V, Campton NA, et al. COVID-19 mortality in patients with cancer on chemotherapy or other anticancer treatments: a prospective cohort study. Lancet 2020;395:1919–26.
39. Montopoli M, Zumerle S, Vettor R, Rugge M, Zorzi M, Catapano CV, et al. Androgen-deprivation therapies for prostate cancer and risk of infection by SARS-CoV-2: a population-based study (N = 4532). Ann Oncol 2020;31:1040–5.
40. Luo J, Rizvi H, Egger JV, Preeshagul IR, Wolchok JD, Hellmann MD. Impact of PD-1 blockade on severity of COVID-19 in patients with lung cancers. Cancer Discov 2020;10:1121–8.
41. Roschewski M, Lionakis MS, Sharman JP, Roswarski J, Goy A, Monticelli MA, et al. Inhibition of Bruton tyrosine kinase in patients with severe COVID-19. Sci Immunol 2020;5:eabd0110.
42. Kotch C, Barrett D, Teachey DT. Tocilizumab for the treatment of chimeric antigen receptor T cell-induced cytokine release syndrome. Expert Rev Clin Immunol 2019;15:813–22.
43. Pennisi M, Jain T, Santomasso BD, Mead E, Wudhikarn K, Silverberg ML, et al. Comparing CAR T-cell toxicity grading systems: application of the ASTCT grading system and implications for management. Blood Adv 2020;4:676–86.
44. England JT, Abdulla A, Biggs CM, Lee AYY, Hay KA, Hoiland RL, et al. Weathering the COVID-19 storm: lessons from hematologic cytokine syndromes. Blood Rev 2021;45:100707.
45. Holter JC, Pischke SE, de Boer E, Lind A, Jenum S, Holten AR, et al. Systemic complement activation is associated with respiratory failure in COVID-19 hospitalized patients. Proc Natl Acad Sci U S A 2020;117:25018–25.
46. Bilaloglu S, Aphinyanaphongs Y, Jones S, Iturrate E, Hochman J, Berger JS. Thrombosis in hospitalized patients with COVID-19 in a New York City Health System. JAMA 2020;324:799–801.
47. Salama C, Han J, Yau L, Reiss WG, Kramer B, Neidhart JD, et al. Tocilizumab in patients hospitalized with Covid-19 pneumonia. N Engl J Med 2021;384:20–30.
48. Gupta S, Wang W, Hayek SS, Chan L, Mathews KS, Melamed ML, et al. Association between early treatment with tocilizumab and mortality among critically ill patients with COVID-19. JAMA Intern Med 2021;181:41–51.
49. Hermine O, Mariette X, Tharaux PL, Resche-Rigon M, Porcher R, Ravaud P, et al. Effect of tocilizumab vs usual care in adults hospitalized with COVID-19 and moderate or severe pneumonia: a randomized clinical trial. JAMA Intern Med 2021;181:32–40.
50. Stone JH, Frigault MJ, Serling-Boyd NJ, Fernandes AD, Harvey L, Foulkes AS, et al. Efficacy of tocilizumab in patients hospitalized with Covid-19. N Engl J Med 2020;383:2333–44.
51. Rosas IO, Brau N, Waters M, Go RC, Hunter BD, Bhagani S, et al. Tocilizumab in hospitalized patients with severe Covid-19 pneumonia. N Engl J Med 2021. doi 10.1056/NEJMoa2028700.
52. Salvarani C, Dolci G, Massari M, Merlo DF, Cavuto S, Savoldi L, et al. Effect of tocilizumab vs standard care on clinical worsening in patients hospitalized with COVID-19 pneumonia: a randomized clinical trial. JAMA Intern Med 2021;181:24–31.
53. Wen T, Wang J, Shi Y, Qian H, Liu P. Inhibitors targeting Bruton's tyrosine kinase in cancers: drug development advances. Leukemia 2021;35:312–32.

Published OnlineFirst April 12, 2021; DOI: 10.1158/2159-8290.CD-21-0144

54. Dupont S, Masse A, James C, Teyssandier I, Lecluse Y, Larbret F, et al. The JAK2 617V>F mutation triggers erythropoietin hypersensitivity and terminal erythroid amplification in primary cells from patients with polycythemia vera. Blood 2007;110:1013–21.
55. Lacy P, Stow JL. Cytokine release from innate immune cells: association with diverse membrane trafficking pathways. Blood 2011;118:9–18.
56. Meletiadis J, Tsiodras S, Tsirigotis P. Interleukin-6 blocking vs. JAK-STAT inhibition for prevention of lung injury in patients with COVID-19. Infect Dis Ther 2020;9:707–13.
57. Hennighausen L, Lee HK. Activation of the SARS-CoV-2 receptor Ace2 by cytokines through pan JAK-STAT enhancers. bioRxiv 2020.
58. Stebbing J, Sanchez Nievas G, Falcone M, Youhanna S, Richardson P, Ottaviani S, et al. JAK inhibition reduces SARS-CoV-2 liver infectivity and modulates inflammatory responses to reduce morbidity and mortality. Sci Adv 2021;7:eabe4724.
59. Kalil AC, Patterson TF, Mehta AK, Tomashek KM, Wolfe CR, Ghazaryan V, et al. Baricitinib plus remdesivir for hospitalized adults with Covid-19. N Engl J Med 2021;384:795–807.
60. Mehta P, Ciurtin C, Scully M, Levi M, Chambers RC. JAK inhibitors in COVID-19: the need for vigilance regarding increased inherent thrombotic risk. Eur Respir J 2020;56:2001919.
61. Varga Z, Flammer AJ, Steiger P, Haberecker M, Andermatt R, Zinkernagel AS, et al. Endothelial cell infection and endotheliitis in COVID-19. Lancet 2020;395:1417–8.
62. Aid M, Busman-Sahay K, Vidal SJ, Maliga Z, Bondoc S, Starke C, et al. Vascular disease and thrombosis in SARS-CoV-2-infected rhesus macaques. Cell 2020;183:1354–66.
63. Teuwen LA, Geldhof V, Pasut A, Carmeliet P. COVID-19: the vasculature unleashed. Nat Rev Immunol 2020;20:389–91.
64. Pang J, Xu F, Aondio G, Li Y, Fumagalli A, Lu M, et al. Efficacy and tolerability of bevacizumab in patients with severe Covid-19. Nat Commun 2021;12:814.
65. Le Bert N, Tan AT, Kunasegaran K, Tham CYL, Hafezi M, Chia A, et al. SARS-CoV-2-specific T cell immunity in cases of COVID-19 and SARS, and uninfected controls. Nature 2020;584:457–62.
66. Peng Y, Mentzer AJ, Liu G, Yao X, Yin Z, Dong D, et al. Broad and strong memory CD4(+) and CD8(+) T cells induced by SARS-CoV-2 in UK convalescent individuals following COVID-19. Nat Immunol 2020;21:1336–45.
67. Diao B, Wang C, Tan Y, Chen X, Liu Y, Ning L, et al. Reduction and functional exhaustion of T cells in patients with coronavirus disease 2019 (COVID-19). Front Immunol 2020;11:827.
68. Zheng M, Gao Y, Wang G, Song G, Liu S, Sun D, et al. Functional exhaustion of antiviral lymphocytes in COVID-19 patients. Cell Mol Immunol 2020;17:533–5.
69. Rogiers A, Tondini C, Grimes JM, Trager MH, Nahm S, Zubiri L, et al. Abstract S02-01: clinical characteristics and outcomes of coronavirus 2019 disease (COVID-19) in cancer patients treated with immune checkpoint inhibitors (ICI). Clin Cancer Res 2020;26:S02-1-S-1.
70. Garassino MC, Whisenant JG, Huang LC, Trama A, Torri V, Agustoni F, et al. COVID-19 in patients with thoracic malignancies (TERAVOLT): first results of an international, registry-based, cohort study. Lancet Oncol 2020;21:914–22.
71. Trama A, Proto C, Whisenant JG, Torri V, Cortellini A, Michielin O, et al. Supporting clinical decision-making during the SARS-CoV-2 pandemic through a global research commitment: the TERAVOLT experience. Cancer Cell 2020;38:602–4.
72. Robilotti EV, Babady NE, Mead PA, Rolling T, Perez-Johnston R, Bernardes M, et al. Determinants of COVID-19 disease severity in patients with cancer. Nat Med 2020;26:1218–23.
73. Maio M, Hamid O, Larkin J, Covre A, Altomonte M, Calabro L, et al. Immune checkpoint inhibitors for cancer therapy in the COVID-19 era. Clin Cancer Res 2020;26:4201–5.
74. Garassino MC, Ribas A. At the crossroads: COVID-19 and immune-checkpoint blockade for cancer. Cancer Immunol Res 2021;9:261–4.
75. O'Callaghan ME, Jay A, Kichenadasse G, Moretti KL. Androgen deprivation therapy in unlikely to be effective for treatment of COVID-19. Ann Oncol 2020;31:1780–2.
76. Tucker MD, Schmidt AL, Hsu C-Y, Shyr Y, Armstrong AJ, Bakouny Z, et al. Severe-COVID-19 and mortality among patients (pts) with prostate cancer (PCa) receiving androgen deprivation therapy (ADT). J Clin Oncol 2021;39:39.
77. Bouhaddou M, Memon D, Meyer B, White KM, Rezelj VV, Correa Marrero M, et al. The global phosphorylation landscape of SARS-CoV-2 infection. Cell 2020;182:685–712.
78. Gordon DE, Jang GM, Bouhaddou M, Xu J, Obernier K, White KM, et al. A SARS-CoV-2 protein interaction map reveals targets for drug repurposing. Nature 2020;583:459–68.
79. Gordon DE, Hiatt J, Bouhaddou M, Rezelj VV, Ulferts S, Braberg H, et al. Comparative host-coronavirus protein interaction networks reveal pan-viral disease mechanisms. Science 2020;370:eabe9403.
80. Neuman BW, Joseph JS, Saikatendu KS, Serrano P, Chatterjee A, Johnson MA, et al. Proteomics analysis unravels the functional repertoire of coronavirus nonstructural protein 3. J Virol 2008;82:5279–94.
81. White KM, Rosales R, Yildiz S, Kehrer T, Miorin L, Moreno E, et al. Plitidepsin has potent preclinical efficacy against SARS-CoV-2 by targeting the host protein eEF1A. Science 2021;371:926–31.
82. Riva L, Yuan S, Yin X, Martin-Sancho L, Matsunaga N, Pache L, et al. Discovery of SARS-CoV-2 antiviral drugs through large-scale compound repurposing. Nature 2020;586:113–9.
83. Schang LM. Effects of pharmacological cyclin-dependent kinase inhibitors on viral transcription and replication. Biochim Biophys Acta 2004;1697:197–209.

AACR American Association for Cancer Research

CANCER DISCOVERY

Repurposing of Anticancer Drugs Expands Possibilities for Antiviral and Anti-Inflammatory Discovery in COVID-19

Mihaela Aldea, Jean-Marie Michot, Francois-Xavier Danlos, et al.

Cancer Discov 2021;11:1336-1344. Published OnlineFirst April 12, 2021.

European Journal of Cancer 149 (2021) 193–210

Available online at www.sciencedirect.com

ScienceDirect

journal homepage: www.ejcancer.com

Original Research

Applications of single-cell and bulk RNA sequencing in onco-immunology

Maria Kuksin [a,b,1], Daphné Morel [b,c,d,1], Marine Aglave [e], François-Xavier Danlos [f], Aurélien Marabelle [b,f], Andrei Zinovyev [g,h,i,j], Daniel Gautheret [k,l,m], Loïc Verlingue [b,d,g,m,*]

[a] *ENS de Lyon, 15 Parvis René Descartes, 69007, Lyon, France*
[b] *Département d'Innovations Thérapeutiques et Essais Précoces (DITEP), Gustave Roussy Cancer Campus, 114 rue Edouard Vaillant, 94800, Villejuif, France*
[c] *Département de Radiothérapie, Gustave Roussy Cancer Campus, Gustave Roussy, 114 rue Edouard Vaillant, 94800, Villejuif, France*
[d] *INSERM UMR1030, Molecular Radiotherapy and Therapeutic Innovations, Gustave Roussy, 114 rue Edouard Vaillant, 94800, Villejuif, France*
[e] *INSERM US23, CNRS UMS 3655, Gustave Roussy Cancer Campus, 114 rue Edouard Vaillant, 94800, Villejuif, France*
[f] *INSERM U1015, Gustave Roussy, Université Paris Saclay, France*
[g] *Institut Curie, PSL Research University, F-75005, Paris, France*
[h] *INSERM, U900, F-75005, Paris, France*
[i] *MINES ParisTech, PSL Research University, CBIO-Centre for Computational Biology, F-75006, Paris, France*
[j] *Laboratory of Advanced Methods for High-dimensional Data Analysis, Lobachevsky University, 603000, Nizhny Novgorod, Russia*
[k] *Institute for Integrative Biology of the Cell, UMR 9198, CEA, CNRS, Université Paris-Saclay, Gif-Sur-Yvette, France*
[l] *IHU PRISM, Gustave Roussy Cancer Campus, Gustave Roussy, 114 Rue Edouard Vaillant, 94800, Villejuif, France*
[m] *Université Paris-Saclay, France*

Received 22 December 2020; received in revised form 26 February 2021; accepted 4 March 2021
Available online 15 April 2021

KEYWORDS
Immunotherapy;
Single-cell RNA-seq;
Bulk RNA-seq;
Tumour microenvironment;
Cancer;

Abstract The rising interest for precise characterization of the tumour immune contexture has recently brought forward the high potential of RNA sequencing (RNA-seq) in identifying molecular mechanisms engaged in the response to immunotherapy. In this review, we provide an overview of the major principles of single-cell and conventional (bulk) RNA-seq applied to onco-immunology. We describe standard preprocessing and statistical analyses of data obtained from such techniques and highlight some computational challenges relative to the sequencing of individual cells. We notably provide examples of gene expression analyses such

* *Corresponding author*: Département d'Innovations Thérapeutiques et Essais Précoces (DITEP), Gustave Roussy Cancer Campus, 114 rue Edouard Vaillant, 94800, Villejuif, France.
E-mail address: loic.verlingue@gustaveroussy.fr (L. Verlingue).
[1] These authors contributed equally to the work.

https://doi.org/10.1016/j.ejca.2021.03.005

Precision medicine

as differential expression analysis, dimensionality reduction, clustering and enrichment analysis. Additionally, we used public data sets to exemplify how deconvolution algorithms can identify and quantify multiple immune subpopulations from either bulk or single-cell RNA-seq. We give examples of machine and deep learning models used to predict patient outcomes and treatment effect from high-dimensional data. Finally, we balance the strengths and weaknesses of single-cell and bulk RNA-seq regarding their applications in the clinic.

1. Introduction

Tumour samples always contain heterogeneous cell populations that comprise—beyond malignant cells—-stromal and immune tumour-associated cells (Fig. 1) [1]. After a long period of focusing on the tumour's genetic alterations, we have slightly entered an era in which the behaviour of non-tumoural cells becomes as meaningful as the tumour itself. Immunotherapy guidance for first-line treatment and beyond still lacks reliable biomarkers, yet accumulating evidence point towards the importance of studying a tumour tissue as a whole to better capture its potential of response to immune-checkpoint blockers: exhaustive composition, density, functional state, organization and interaction between cellular subtypes, including tumour cells [2,3].

Tumour immune infiltrates can associate CD8+ cytotoxic T cells, CD4+ helper cells (T_H1 cells), dendritic cells, CD25+/FOXP3+ regulatory T cells, myeloid-derived suppressor cells (MDSCs), natural-killer cells, B lymphocytes, tumour-associated macrophages, among others. Some of those promote immune escape of the tumour (e.g. MDSCs), some elicit antitumoural actions (e.g. dendritic cells), others can either promote or prevent immune escape depending on their activation status (e.g. CD8+ T cells) [4,5]. For example, the presence and proportion of M1 macrophages, B cells and T_H1 lymphocytes within the immune infiltrate almost always correlates with good prognosis, whereas the presence of regulatory T cells or M2 macrophages usually associates with bad prognosis [3]. Even though their cellular behavior may be influenced by the tumour, it is expected that those non-tumoural immune cells share the same DNA sequence, which is specific to the host (with the exceptions of rearranged immunoglobulin and TCR loci). However, they significantly vary phenotypically and harbor separate mRNA expression profiles, which makes them identifiable by gene expression analysis.

Among various techniques deployed to assess gene expression [6], RNA sequencing (RNA-seq) can provide qualitative (RNA sequence) and quantitative (RNA abundance) analyses of either targeted mRNA transcripts or the complete transcriptome of a particular tissue [7–9]. Two methods of RNA-seq are henceforth commonly considered for onco-immunology studies: standard bulk RNA-seq and single-cell RNA-seq (scRNA-seq). Standard bulk RNA-seq started replacing microarray techniques in the late 2000s and is now widely used in translational research. For each transcript, it provides an average expression level in the sample, which may comprise different cell types [10]. Conversely, scRNA-seq is a relatively new technology that measures the gene expression levels for each transcript within each individual cell of the sample and allows a representation of the distribution of this expression in each subpopulation of cells [11,12]. Therefore, scRNA-seq rather aims to study a particular cell or cell type behavior in the specific context of its microenvironment, while bulk RNA-seq was not primarily designed for the precise characterization of a tumour composition [13].

At first glance, one could believe that scRNA-seq represents the most suited method to draw a complete picture of a tumour and thus, may be a method of choice to study the immune tumour-related features that could be predictive of response to immunotherapy. Yet, the initial substantial excitement regarding scRNA-seq theoretical promises has historically faced technical limitations [13]. In addition, it is now technically possible to extrapolate the cellular composition of a tumour sample from bulk analysis, which at least partially alleviates the conceptual frontier between bulk and scRNA-seq full potentials.

Here, we give an overview of some standard methods used for processing single-cell or bulk RNA-seq data. We describe how scRNA-seq and bulk methods can share several computational analysis concepts (reads quality control, mapping or quasi-mapping, differential expression analysis, dimensionality reduction, clustering, etc.)—sometimes with the same objectives, sometimes with very distinct outputs—bearing in mind that for every task, scRNA-seq analysis will often imply additional dimensionalities to estimate one complete gene expression profile per individual cell.

We notably emphasise the statistical approaches that can be used to study the tumour microenvironment

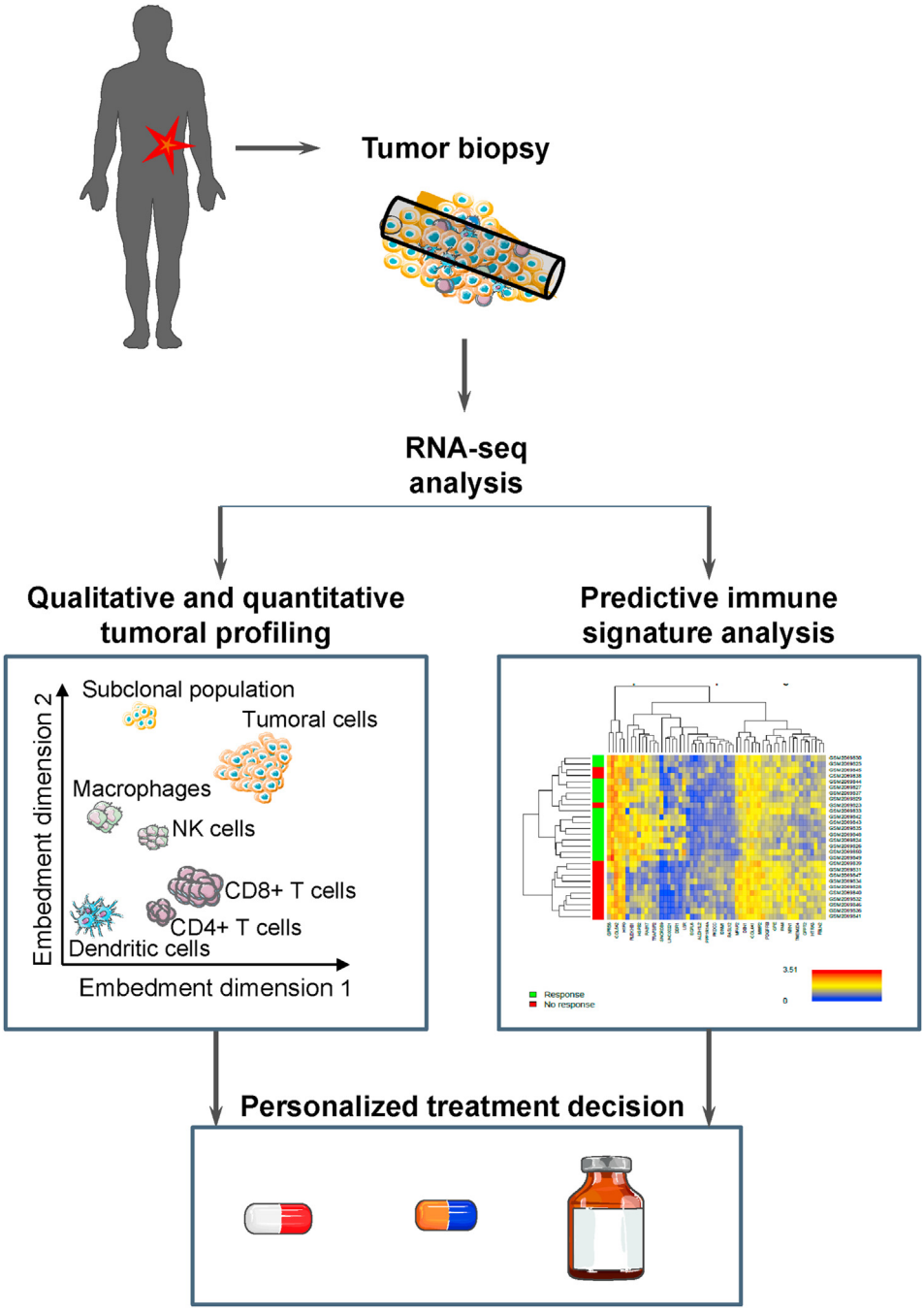

Fig. 1. **Graphical abstract**. Clinical positioning of RNA sequencing to personalise onco-immunotherapy treatments from the analysis of a patient's tumour biopsy. The tumour and its microenvironment can be analysed using gene expression signatures, deconvolution and modeling methods to predict tumour sensitivity to therapies.

composition—including from bulk analysis—in a qualitative and quantitative manner. We also describe machine learning tools that aim at predicting survival or tumour response following treatment with immune-checkpoint blockers. Finally, we depict the recent evolution in the clinical development field of onco-immunology that increasingly integrates RNA-seq in clinical trial designs, reflecting the growing interest in this approach for multiple purposes.

2. Single-cell and bulk RNA-seq processing: basic clues to appreciate the differences

2.1. Collecting, storing, and processing RNA

Unlike DNA, which is a stable structure, RNA is highly sensitive to oxidation and hydrolytic cleavage of its phosphodiester bonds by nucleases, and therefore requires conscientious storage to prevent rapid

degradation [14]. Bulk RNA-seq can be performed on human tumour samples obtained from surgical resection or biopsies, preserved in formalin-fixed and paraffin embedded (FFPE) or freshly frozen [15–17]. Thus, all the samples can be collected in due course and processed at the same time.

Additional facts to consider for scRNA-seq

On the other hand, scRNA-seq analysis requires viable cells suspension to allow robust cell isolation, which contraindicates any fixation of freezing steps. ScRNA-seq therefore requires processing the samples quite promptly—within a few days—after the time of collection. Another important point to consider is that during that process, the cellular viability of each subpopulation of cells can be differently affected, leading to some cell types being over- or under-represented in the final dataset (source of interpretation bias). Therefore, before planning a scRNA-seq analysis, several questions need to be addressed, including: (i) which and how many cell types are to be analysed (for example, only tumour cells, all stromal immune cells or only a subset of immune cells such as memory CD4+ T cells or sparse population of a subset of dendritic cells), (ii) which method is used to prepare cell suspension (tissue dissociation, selected cells enrichment and cells conservation), (iii) which single-cell technology (droplet- or plate-based; short or long reads; Unique Molecular Identifiers or not) and (iv) which library and other RNA-seq parameters to use [18–21].

2.2. Sequencing and basic bias correction

The following steps of single-cell and bulk RNA-seq usually comprise reverse transcription, reads sequencing, mapping or quasi-mapping, data format transformation, count table generation and inference, such as the exploration of gene expression and/or transcript fusions (Fig. 2).

Additional facts to consider for scRNA-seq

As compared to bulk, scRNA-seq comprises additional steps, including: (i) keeping information of unique molecular identifiers (UMI) to further identify mRNA molecules, and barcodes to identify which mRNA belongs to which single cell, and (ii) reduce experimental biases often triggered by the sequencing of single cells (Table 1). Those biases—mainly known as batch effect and dropout effect—exist for both single-cell and bulk RNA-seq, but are exacerbated by the processing of single cells.

Batch effect encompasses various causes of variation in gene expression estimation, related to technical bias or other independent factors such as variations in sampling, library preparation and sequencing platform, or variations inherent to the origin of the sample (different tumour types). Hence, a frequent challenge is to analyse combined data from various tumour types or from various centers. Batch effect can be corrected *a posteriori* with computational methods, such as Mutual Nearest Neighbors [22] and Canonical Correlation Analysis [23]. Several tools using these and other methods exist, such as ComBat-seq [24], RUVseq [25] and svaseq [26] for bulk RNA-seq, and kBET [27], Harmony [28], Conos [29] and Seurat [30] for scRNA-seq.

ScRNA-seq, much more than bulk RNA-seq, generates sparse matrices filled with many zeros, corresponding either to a biological feature (truly silent gene) or to a technical artifact, called "dropout effect" and referring to a statistical observation called zero-inflated distribution. The "dropout effect" refers to the limited sampling of RNA content in single-cell wet protocols (falsely silent gene). Indeed, the expression of only 10% of total genes tends to be effectively measured in scRNA-seq experiments [31,32]. Zero-inflated scRNA-seq data can be processed by imputation methods, in order to reduce the impact of the dropout effects, before using pipelines designed for bulk RNA-seq [33,34]. Although deep learning has contributed to significant improvement on this task, the imputation step is rarely performed due to its highly data-dependent efficiency [34,35].

3. Letting the data speak using statistical analyses of gene expression

Once RNA-seq data are ripe for further analysis, statistical methods are applied to answer different biological questions. Selecting the most appropriate requires bearing in mind the objective of the analysis, the magnitude of the above-cited batch effect and potential statistical biases.

Expression values from bulk RNA-seq can generally be approximated by Poisson, negative-binomial or log-normal distributions and from scRNA-seq by zero-inflated distribution. This limits the use of statistics based on a Gaussian distribution. In practice, simple (log+1)-transformation and expression matrix scaling are often performed, negative-binomial model (adjusted by a regression of bias) [36] can be used, and an increasing number of models now intend to handle zero-inflation in scRNA-seq [37,38]. In the next sections, we review the most common methods used, in a non-exhaustive manner. To illustrate the most common outputs of RNA-seq analysis (Fig. 3), such as volcano plots, we used the published data set from Hugo et al. [39], which comprises bulk RNA-seq data of patients with metastatic melanoma obtained prior to treatment with immune-checkpoint blockers, together with the clinical information of whether or not they responded to treatment. This data set was primarily used to build an immune signature associated with the response to immune-checkpoint blockers.

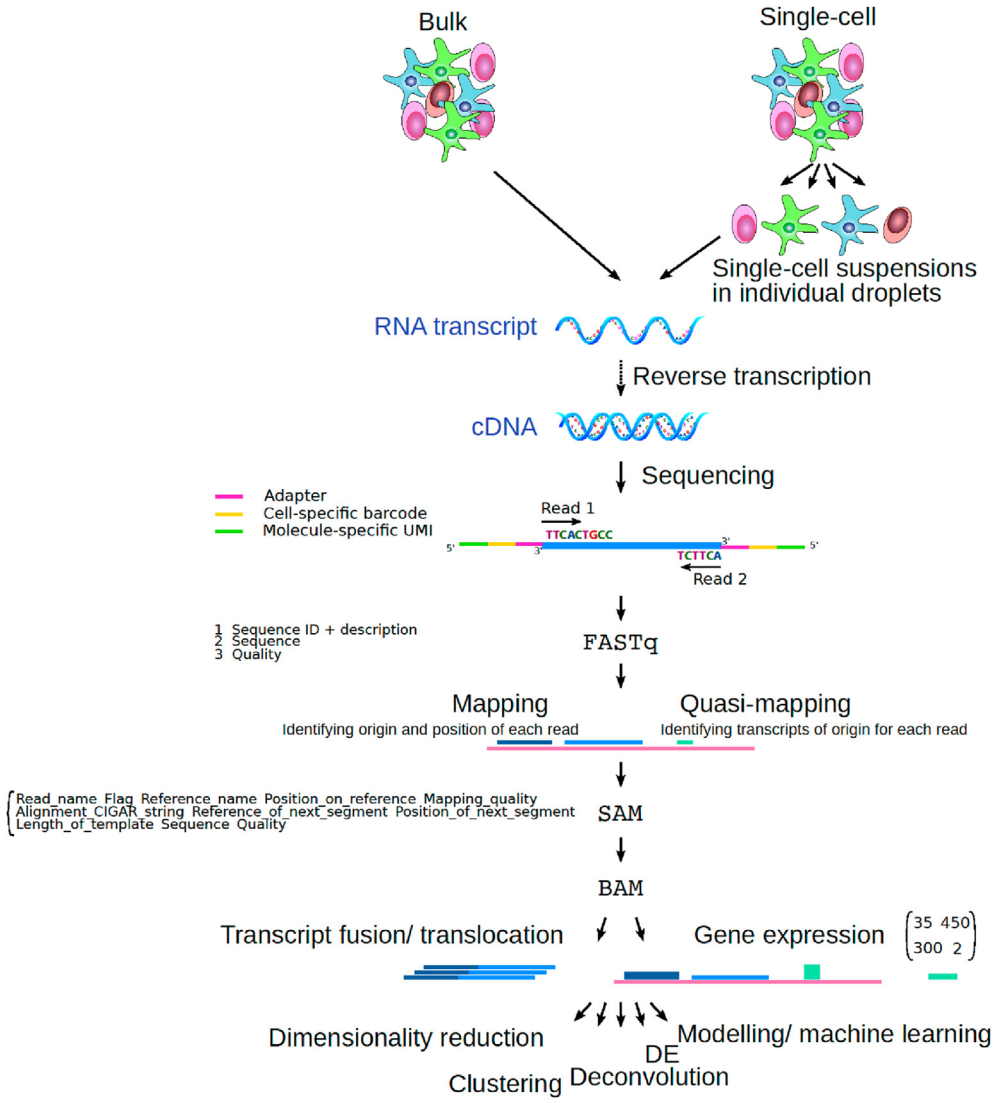

Fig. 2. **Processing pipelines of bulk and single-cell RNA-seq experiments**. RNA transcripts are reverse-transcribed into complementary DNA (cDNA), the cDNA second strand is synthesised and then amplified, before being sequenced by a next-generation sequencing (NGS) machine. In the case of scRNA-seq, the reverse transcription step includes the incorporation of UMI to identify mRNA molecules, and barcodes to identify single cells. RNA-seq generates 100 nucleotide long reads. A FASTQ file stores all the reads of one sample, in an arbitrary order, together with one quality score per sequenced nucleotide. Mapping (or alignment) refers to finding the position of a read on a reference genome or transcriptome. Quasi-mapping (or pseudo-mapping) aligns reads to a pre-indexed transcriptome rather than to a reference genome and is thus faster. A SAM file stores the information relevant to each read. This information, compressed in binary, is known as a BAM file. Expression estimation relates to counting every read using various normalization methods, and producing gene- or transcript-based quantification fitted for further analysis. Other analyses concerns detection of transcript fusions, splicing variants, or estimate genomic variations, which we do not detail in this review.

3.1. Additional facts to consider for scRNA-seq

Expression values from bulk RNA-seq can generally be approximated by Poisson, negative-binomial or log-normal distributions, whereas expression values from scRNA-seq follows a zero-inflated distribution. This limits the use of statistics based on a Gaussian distribution. In practice, simple (log+1)-transformation and expression matrix scaling are often performed, although negative-binomial model (adjusted by a regression of bias) [36] can be used, and an increasing number of models now intend to handle zero-inflation in scRNA-seq [37,38].

3.2. Statistics for high-dimensional data: why do we "adjust" the p-value?

RNA-seq data often display a greater number of variables than observations (i.e. more genes than samples analysed). This high-dimensionality implies a high risk of false discovery. For example, if a statistical test is

Table 1
Comparison of bulk and single-cell RNA-seq for clinical translation, specifically in onco-immunology. The advantages and limitations of combining both techniques were also explored.

	RNA-sequencing		
	Conventional bulk	Single-cell	Joint use of single-cell and bulk data
Experimental and general aspects			
Cost	+	+++	++++
Size of sample (minimal amount of RNA required)	+++	+	+++
Batch effect	+	++	+++
Dropout amplification/coverage bias	+	+++	++
Computational aspects			
Storage capacity	+	++++	++++
Handling sparsity	+	+++	++
Differentiating complex expression patterns from noise	++	+++	++
Dealing with missing data	++	+++	++
Deconvolution requirement to characterise immune infiltrate	++++	+	+
Acquired information			
Appreciating tissue heterogeneity at the cell level	+	++++	++++
Analysing specific populations (T cells, B cells …)	+	+++	++++
Describing populations as a whole	++	++	++++
Accuracy of the final analysis	++	+++	++++

performed iteratively for each individual gene, and considered significant if p-value <0.05, the user will potentially obtain five false-positive results every 100 tested genes. Thus, for 20,000 tested genes, the false-positive signals may reach up to 1000 genes, so the p-values must be adjusted according to the number of tests performed. Multiple methods have been proposed to control this "multiple testing error" as Bonferroni or Benjamini and Hochberg's false discovery rate [40–42].

3.3. Differential expression analysis

Differential expression (DE) analysis aims at identifying significant gene expression variations between two or more experimental groups. For example, DE analysis can be used to uncover genes that are the most differentially expressed in RNA-seq of patients who responded to immune-checkpoint blockers compared to RNA-seq of patients who did not [25]. DESeq2 [43] and EdgeR [44] are two popular R packages for DE analysis from gene expression data.

Outputs of DE are fold-change of expressions between the different groups, associated with a corrected p-value. The results can be represented using a volcano plot (Fig. 3A) or a heatmap (Fig. 3B), which highlight the genes that are significantly overexpressed or underexpressed between two or several groups. Volcano plots display the magnitude of both the difference (x-axis) and its statistical meaning (y-axis), while heatmaps use colour gradients.

Special aspects of differential expression for scRNA-seq analysis

In scRNA-seq, DE analysis can be used to compare subpopulations of cells or several treatment conditions within a peculiar cell type [45]. Some methods have been developed specifically for scRNA-seq, although their performances are often similar to naive methods or methods originally developed for bulk RNA-seq [46].

3.4. Dimensionality reduction

Dimension reduction consists in projecting data from a large space (with many dimensions—for example, each gene being a dimension) into a smaller space (with fewer dimensions—for example, by focusing on genes of interest). Basically, it consists in drastically "summarising" a data set to make it more understandable, ideally while retaining most of its intrinsic properties of interest.

Dimension reduction can be carried out using two ways through either feature selection or feature engineering. Eventually, one can apply both approaches sequentially or even iteratively. Feature selection consists in selecting automatically the most important genes for the analysis (for example, the most differentially expressed genes between two conditions, or variable selection with lasso regression, further detailed in Box 1). Feature engineering, or projection, aims at separating samples according to relevant properties in the data. It can consist in either linear methods—meaning that it preserves all differences between samples—such as Principal Component Analysis (PCA) [47] or Independent Component Analysis (ICA), or non-linear methods such as t-distributed Stochastic Neighbor Embedding (t-SNE) or Uniform Manifold Approximation and Projection (UMAP) (Box 1).

In our example, we used PCA (the most famous linear feature engineering technique) on DE genes (adding feature selection), which reduced the gene list and clearly outlined the two groups of patients,

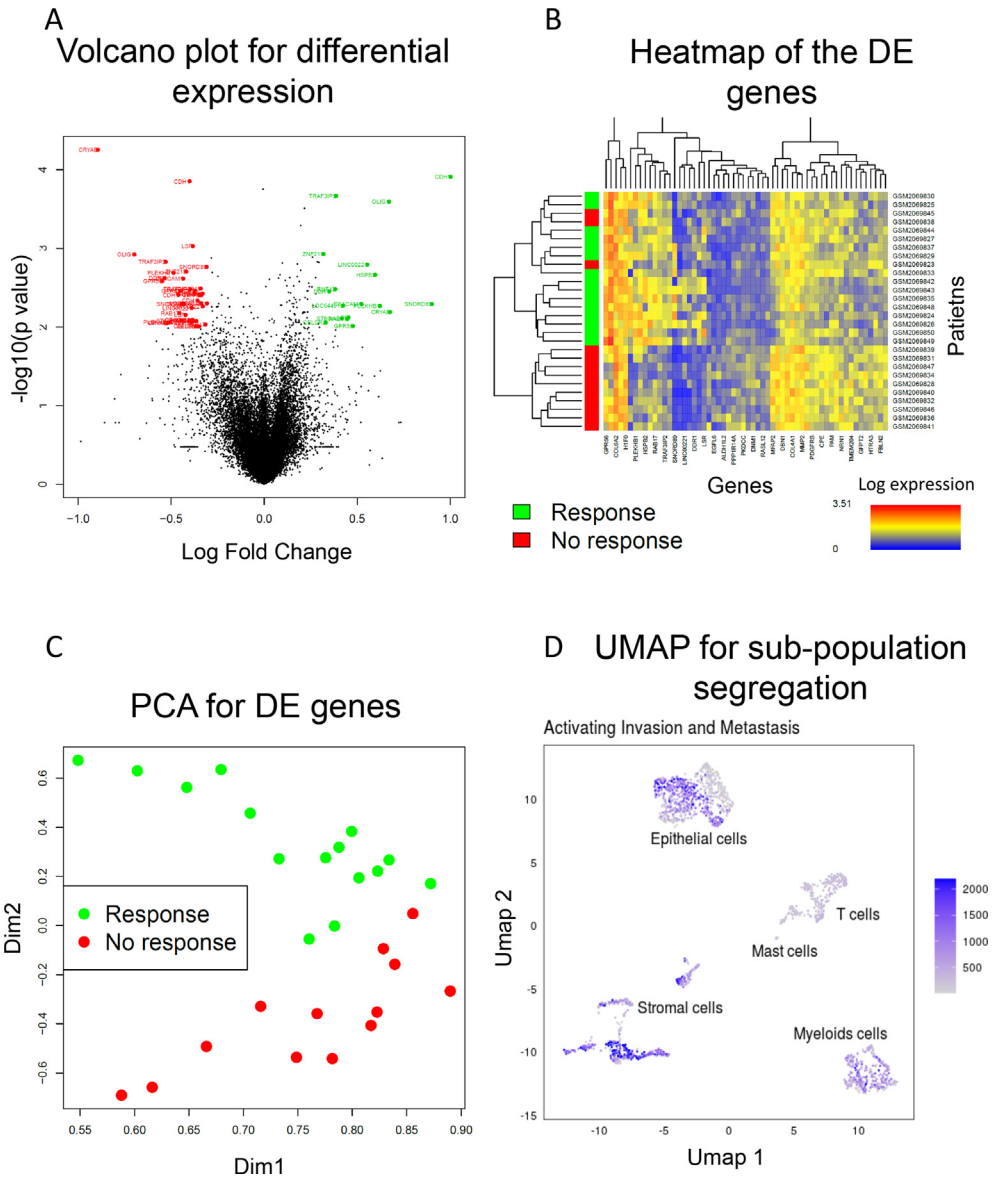

Fig. 3. **Illustration of popular methods used to analyse bulk and single-cell RNA-seq in the field of immune-oncology**. For (A) to (C), we used the public GSE78220 data set of bulk RNA-seq performed on 38 melanoma patients before treatment with immune-checkpoint inhibitors (either pembrolizumab or nivolumab) described in the study by *Hugo et al., Cell (2016)* [25]. (**A**) Volcano plot for differential expression analysis comparing responder and non-responder patients. Gene names are represented in colours for differentially expressed genes with absolute fold change >0.3 and p-values < 0.01. (**B**) Heatmap organised by hierarchical clustering of the log-transformed gene expression for the differentially expressed genes (defined in A). The row side bar represents responder and non-responder patients. (**C**) PCA of the differentially expressed genes separates responder and non-responder patients in the two first dimensions of the PCA (Dim1 and Dim2). (**D**) UMAP representation of the single-cell RNA-seq analysis of the KUL01-T sample retrieved from the publicly available GSE144735 project (*Ho et al., Nat Genet (2020)*). The sample comprised 1.922 cells analysed and pre-filtered and 51.292 genes or genomic loci. Expression values have been normalised by an improved negative binomial model. Dimensionality reduction was performed using PCA and then UMAP on the first 30 dimensions, using R Seurat version 3.2.0. The UMAP plot displays the cells (1 point = 1 cell). UMAP efficiently depict the clusters of immune cell types. A gene list of 1149 genes related to activation of invasion and metastasis processes were retrieved (gene list from *Zhang et al., Front Genet (2020)*). Colouring intensity represents the sum of the expressions in the list of genes. (For interpretation of the references to colour in this figure legend, the reader is referred to the Web version of this article.)

responding or not to immune-checkpoint blockers (Fig. 3C). An example of application of non-linear dimensionality reduction is also shown in Fig. 3D, using the UMAP method.

Special aspect of dimension reduction for scRNA-seq analysis: trajectory inference

In addition, a rapidly advancing field called "cellular trajectory inference", which uses single cell data, can be considered as a special type of non-linear dimensionality

Box 1. To go deeper into dimensionality reduction

Feature selection can consist in the selection of genes from DE analysis by setting thresholds of fold-change and false discovery rate. A reduced gene list comprising only the most differently expressed genes can then be visualised, for example using a heatmap (Fig. 3B). Many other approaches of feature selection exist. For example, in the field of supervised machine learning, regularised and/or sparse linear regression (e.g. based on lasso) forces certain coefficients to zero, resulting in genes not used by the model. Non-zero genes are therefore selected as important for the predictions. Unsupervised methods of feature selection can be used by selecting the most fluctuating genes (from estimation of the variance), genes whose dispersion strongly deviates from what would be expected based on their mean expression level (so-called over-dispersed genes) [114], or genes strongly contributing to the distinction between data clusters or linear components (see below).

The feature engineering approach to dimensionality reduction consists in transforming the initial data variables, such as gene expression, into a relatively small number of linear or non-linear combinations. In the case of linearly constructed features, they are frequently referred to as components or meta-genes. The oldest and most widely used linear method for dimensionality reduction is Principal Component Analysis (PCA) [47], which constructs orthogonal sets of vectors in the data space, corresponding to the directions of maximal variance. The classical PCA is a deterministic method while some of its later modifications are probabilistic, e.g. in the case of large single-cell data sets. Independent Component Analysis (ICA) is another popular linear method which is usually applied on top of PCA and creates the most statistically independent features as possible [115]. Both PCA and ICA components can be interpreted either by considering the weights associated to genes (by applying functional enrichment tests) or to samples (confronting with their annotations). In these analyses, ICA components are systematically characterised by improved biological or clinical interpretation [115]. Thus, individual independent components can emerge from the presence of distinct cell types within a tumour sample: as such, ICA can be used as an unsupervised cell type deconvolution technique [116].

T-distributed Stochastic Neighbor Embedding (t-SNE) [117], and Uniform Manifold Approximation and Projection (UMAP) [118] are non-linear dimensionality reduction methods, based on constructing a pairwise distance similarity graph between data points and representing its structure as faithfully as possible in the reduced 2D or 3D space. t-SNE and UMAP are non-deterministic methods and the resulting axes cannot be directly interpreted. As a matter of fact, t-SNE and UMAP projections can be rotated without their meaning being changed. They can perform significantly better than PCA in grouping on the map points that are close in the large dimensional space, while PCA is more faithful in representing large distances between data points. Compared to t-SNE, the UMAP algorithm better preserves the global structure of the data. Both methods successfully deal with large data sets and are therefore relevant for visualizing scRNA-seq datasets and the results of their analyses. Moderate dimensionality reduction by applying PCA (with 10–50 dimensions being retained) is usually advised before application of t-SNE, which reduces the computational cost and de-noises the single cell profiles to some extent. By contrast, this step is not always mandatory in the case of UMAP, which can be directly applied to large dimensional data.

reduction, with the goal to study cellular dynamic processes such as cell cycle, cell differentiation or cell activation. This method—which cannot be applied to bulk data—is based on the assumption that cells that differentiate display a continuous spectrum of states because individual cells will differentiate in an unsynchronised manner (each cell is a snapshot of differentiation time). Tools are therefore used to order the cells along a trajectory based on similarities in their expression patterns, where the "pseudotime" is the unit allowing representing each cell's transcriptional progression toward the terminal state of its trajectory. There are over 75 existing tools for trajectory inference; most of which can be found in the dynverse wrapper [48]. More details regarding trajectory inference are depicted in Box 2.

3.5. Clustering

Clustering defines a way to simplify and interpret gene expression data by classifying (or, partitioning) the samples (for bulk RNA-seq) or cells (for scRNA-seq), into groups with gene expression profiles more similar within the group rather than between the groups. Clustering belongs to the family of unsupervised machine learning methods: groups are inferred by the data themselves, their distribution and their multidimensional geometry (and not by predefined classes), among other possible characteristics. Interpretation of the resulting clusters often requires other variables to correlate with, such as phenotypic (type of cancer, toxic exposures, clinical outcome or other continuous data), genetic (for e.g. cluster of gene co-expression with HER2 status in breast cancers), cell types/states (for single-cell data) or technical bias to correct (batch effect). More details are provided in Box 3.

In our RNA-seq example, we have clustered samples based on differentially expressed genes and visualised their relation to response to immunotherapy (Fig. 3B, clustering on the left). A second clustering was performed on the same differentially expressed genes in order to identify co/anti-regulated modules (Fig. 3B, clustering on the top).

Box 2. To go deeper into trajectory inference

Trajectory inference is applicable in the case when a population of cells represents a snapshot of an actively developing dynamic process, such as differentiation. In this case, the geometrical structure of the data is recapitulated as a bouquet of diverging and branching trajectories, where branching points represent important cell fate decisions. Each individual cell can be attributed to one or several trajectories and characterised by the value of pseudotime, which reflects the accumulated number of molecular changes as the total path length along the trajectory measured from some root state. The relation between pseudotime and physical time can be highly non-trivial. Dozens of trajectory inference methods such as Monocle [119], STREAM [120], PAGA [121] have been suggested and systematically benchmarked [48]. Interestingly, trajectory-based analysis can be applied to bulk tumoural transcriptomic profiles, too [122]. The usefulness of trajectory inference approaches in onco-immunology is yet to be fully demonstrated.

The trajectory inference is often accompanied by the dynamic network inference whose goal is to discover the gene regulatory networks that drive transitions from one cell type or state to another. Dynamic network inference analysis uses cell ordering from trajectory analysis and co-occurring or correlated genes. Several tools exist (SCENIC [123], GRISLI [124], LEAP [125] and PIDC [126], for example), but the quality of results strongly depends on the data set.

Special aspects of clustering for scRNA-seq analysis

Clustering is a crucial step in single cell data analyses with the objective to characterise the cellular heterogeneity by defining cell types and states. Clustering (or like other dimension reduction methods such as PCA, t-SNE or UMAP) can also be used for data analysis and quality control. For example, clustering of a scRNA-seq gene expression matrix may output clusters corresponding to the origin of each cell types identified. In this case, it might be (at least in part) sufficient to characterise the cellular heterogeneity within a sample, for example, to appreciate the immune infiltrate composition. Other algorithms such as deconvolution or mixture model-based approach adapted to single-cell data can help adjusting on confounding factors [33,49].

Box 3. To go deeper into clustering

Clustering based on the transcriptome is attractive given the wide and unbiased nature of the output. However, clustering algorithms contain a crucial parameter that directly or indirectly defines the number of generated clusters—and thus, the resolution or granularity of the analysis. This parameter has a huge impact on downstream conclusions, although it is usually difficult to define before the interpretation step. Thus, underestimating the number of clusters leads to merging important cellular phenotypes together, while overestimating it might make it impossible to identify statistically significant features distinguishing cell states. Therefore, a pragmatic strategy frequently used is to generate several data partitions into clusters at several scales, and develop a multiscale data analysis strategy.

The most commonly used algorithms for clustering bulk transcriptomic profiles are hierarchical clustering, k-means and density-based clustering such as DBSCAN [127], and graph-based clustering algorithms also exist such as general-purpose Louvain [128] and Leiden [129]. PhenoGraph [130] approach gained popularity in the single-cell data analysis field. These algorithms are based on finding tight communities in point neighborhood graphs which makes them highly scalable and sensitive to relatively fine-grained dissimilarities between cellular transcriptomes [131]. Clustering methods have notably sparked several atlas projects such as the Human Cell Atlas [132].

Using clustering, it is also possible to identify the genes that drive the most the differences between clusters—named "marker genes"—that further reduce the information and help interpretation [50]. In the case of bulk RNA-seq, clustering can output clusters corresponding to tumour types, or to different sequencing techniques. In this case, such analysis can be used as a quality control. If technical (or undesired biological) factors correlate with clusters, additional correction of the batch effect can be considered.

4. Describing the cancer immune contexture from bulk RNA-sequencing

As we just mentioned, when applied to scRNA-seq data, clustering methods might be sufficient to identify the various immune subpopulations that compose a tumour sample. Thus, the scRNA-seq technique is probably the most suited for this purpose. However, it is also possible to describe the immune contexture from bulk RNA-seq, and multiple approaches have become available to extrapolate the qualitative and relatively quantitative compositions of tumour-infiltrating immune cells from bulk data [50,51].

Those methods often rely on prior knowledge of biological processes or cell type specificities. Such information is usually obtained from independent data sets that were established upon purified cell cultures or single-cell experiments.

4.1. Enrichment analysis and gene lists applied to immune infiltrate description

Enrichment analysis provides higher level information compared to gene expression-based analysis. Basically, it enables to identify known biological processes that may be upregulated or downregulated within a sample or a population of cells (cluster). Enrichment analysis

can therefore also be used to identify and quantify cell type-specific signals, for example, to depict whether an identified cluster within a bulk sample is more likely to be CD8+ T cells, macrophages or tumour cells.

Enrichment analysis requires *a-priori* defined sets of genes that are specific to cell types or biological processes. These gene sets are often valid across many biological conditions [52]. For example, ImmuneSigDB is a collection of ~5000 gene lists derived from ~400 immunological studies, which can be completed with other sources of gene lists [53–56]. Depending on the question in hand, the user may also choose other gene set collections such as MsigDB (Molecular Signatures Database) [57] and KEGG (Kyoto Encyclopedia of Genes and Genomes containing pathways) [58].

Scoring methods are often used to design higher-level variables from the gene expression related to gene sets. Among many scoring methods, Gene Set Enrichment Analysis (GSEA) is the most widely used [57]. GSEA-based approaches rank genes according to their expression variation and then evaluate the enrichment of a particular cell type in a sample, using a semiquantitative score. For example, GSEA on bulk RNA-seq data was used to characterise the immune phenotypes of tumour-infiltrating lymphocytes enriched in 598 colorectal cancers [59]. It was also used to build the Cancer Immunome Atlas (https://tcia.at/home) from more than 9000 samples covering 20 different solid cancers [60]. Enrichment analyses are still under development and recent R packages, such as GAGE [61] and topGO [62], that provide access to several methods in a user-friendly manner.

4.2. Deconvolution methods

Deconvolution refers to breaking data up into its various composing elements. Basically, in RNA-seq analysis, the goal of deconvolution is to estimate the relative fractions of individual cell types from a bulk analysis, as a surrogate of what scRNA-seq analysis can produce [50,63]. More than 50 deconvolution algorithms for bulk RNA-seq data are published, with various methods explored, either supervised (the algorithm learns to predict labels from biological measurements) or unsupervised (from the unlabeled data, the algorithm extracts novel features and patterns). Some deconvolution methods assume that each gene expression in a heterogeneous sample is a linear combination of the expression levels of this gene across all the cell types within the sample, weighted by the relative cell fractions [63]. More details are provided in Box 4.

In an alternative approach, scRNA-seq can help deconvolution models applied to bulk RNA-seq: a model can be trained to predict proportions of the different cell types quantified from scRNA-seq, from bulk RNA-seq [64]. This method is notably used by CIBERSORTx [65], an improved version of CIBERSORT, which allows a research of cell signatures, and notably, signatures associated with response to immunotherapy. The joint use of single-cell and bulk RNA-seq for the analysis of a particular tissue or disease can therefore maximise the accuracy and the thoroughness of the final analysis (Table 1).

Box 4. To go deeper into deconvolution methods

Recent popular supervised deconvolution algorithms include CIBERSORT [133], MCP-counter [56], TIMER2.0 [134], xCell [135], ESTIMATE [136], csSAM [137], BSEQ-sc [138], EPIC [139] and ABIS [140], among other tools, which focuses on immune-infiltration quantification. A global approach of immune deconvolution could integrate several of these tools to estimate immune cell fractions from bulk RNA-seq data, as proposed by immunedeconv [141]. Although most of these tools only work for human data, some of them, such as mMCP counter, also offer a version for murine data [142] (adapted from MCP-counter) and ImmuCC [143] (derived from CIBERSORT).

Unsupervised deconvolution algorithms, often based on matrix factorisation methods [116,144–146], work without predefined reference cell type signatures. Recent unsupervised methods have used neural networks in the form of auto-encoders, where the thinnest hidden layer of the neural network is extracted to represent a lower dimension of the data [147,148].

5. Clinical considerations, applications and current limitations of RNA-seq

In the era of cancer immunotherapy, RNA-seq technologies can help addressing major biological questions, such as how does the immune system evolve along with cancer progression, how drugs impact antitumour immunity and how clinicians can anticipate patients' outcomes and treatment effect, and so forth (Fig. 1). Using a rigorously selected pipeline (from wet to dry lab) among the aforementioned overall methods, one could theoretically answer a wide variety of biological questions from analysis of either bulk or single cell data, albeit with fluctuating performances. With this in mind, we reviewed in the next sections the actual landscape of bulk and scRNA-seq usages in translational and clinical practice.

5.1. Predictive biomarkers for immune-checkpoint blockers

Programmed death-ligand 1 (PD-L1) tumoural expression was the first biomarker approved as a companion test for the prescription of the immune-checkpoint inhibitors targeted toward PD-1, such as pembrolizumab. It remains, however, an imperfect biomarker for several

reasons, including high rates of false negatives and false positives [66,67], technical issues despite the standardization of immunohistochemistry assays [68,69] and the absence of consensus regarding the relevant staining threshold that should define a PD-L1–positive or PD-L1–negative tumour [70]. Additionally, tumour mutational load (i.e. the number of mutations per megabase) has been shown to be related to immune-checkpoint blockers efficacy, notably in microsatellite instability-high (MSI-H) tumours [71–78]. In addition to PD-L1 expression, MSI status and tumour mutational burden, an increasing number of immune gene expression signatures are emerging across cancer types, together with methods that aim to estimate neoantigen presentation level, often with the intent to better characterise tumour immune response [39,53,79–81]. Notably, each of these approaches could be addressed using RNA-seq methods. For example, PD-L1 mRNA expression has been shown to correlate both with immunohistochemistry assessment of PD-L1 expression and clinical prediction of response to immune-checkpoint blockade [82,83].

The broad effect of most immunotherapies, including immune-checkpoint blockers, is tempered by the modest proportion of patients who derive a prolonged benefit from it. Up to 30% of patients with commonly sensitive solid tumours (such as melanoma or lung cancer) may in fact be primary refractory to immune-checkpoint blockers [84]. Secondary resistance—a mechanism whereby patient initially responding to a treatment cease to do so—additionally affects up to 20% of patients with melanomas treated in first-line and 30% of patients with lung adenocarcinomas [85]. Finally, about 20% of patients harbour prolonged responses [86]. The type and quantity of immune cells found within the tumour microenvironment influence tumour development and can impact the prognosis of patients [2,87]. The immune infiltrate composition was also shown to be predictive of clinical response to immune-checkpoint blockers [2,88–90]. However, no perfect predictive biomarker has been identified so far and emerging immune signatures often lack validation on independent cohorts, such as in our example. Marker combinations may improve clinical utility. For example, a highly immunogenic tumour—with high PD-L1 expression, CD8+ T cell and dendritic cell infiltration—is more likely to respond to immune-checkpoint blockers than a non-immunogenic tumour [91].

5.2. Machine learning for prediction modeling

Machine learning is a branch of artificial intelligence that exploits a large number of statistical techniques to allow mathematical functions to "learn" from experience acquired from similar examples (training). Deep learning is a branch of machine learning stacking several statistical models together to increase nonlinearity between input data and predictions. Machine learning methods are increasingly used in cancer diagnosis, prognosis and treatment guidance; especially with RNA-seq data as inputs to feed linear models (such as shallow Cox regression) or nonlinear models (such as neural networks). Recent adaptations of neural networks have also integrated methods to learn on survival data (comprising censored values), for example by using a Cox-loss function [92,93].

5.2.1. Prognostic models

Some machine learning approaches have led to clinical applications such as estimating patients' outcome from gene expression values in breast cancers [92,94,95]. Nevertheless, overfitting and poor generalization inherent of high-dimensional data with a small number of examples have limited the success of such methods so far [96,97]. Several teams have developed pan-cancer prognosis predictors by feeding deep learning models with RNA-seq data from the TCGA project [92,93,98,99]. In these studies, concordance indexes (C-indexes)—which provide a global assessment of the model's ability to predict survival—ranged from 0.59 to 0.75, which correspond to modest performance values (0.50 corresponding to random prediction, and 1 to perfect prediction). Limiting overfitting during models training is a very active field of research in machine learning. Several methods exist, that are beyond the spectrum of this review, except for automatic input variable selection such as lasso penalization, which are close to dimension reduction technics detailed above and in Box 1.

5.2.2. Prediction of treatment effect

Evaluation of the effect of treatments has been mostly explored in cell lines [100]. An early study showed that gene expression data were the most efficient data type to predict drug sensitivity, across multi-omics data [100]. Recently, a deep learning-based model based on prior knowledge showed impressive results for the prediction of tumour sensitivity to anticancer compounds [101]. Additionally, Hwang et al. recently reported that they were able to accurately predict the response to anti-PD1 treatment in patients with non-small cell lung cancer (with sensitivity, specificity and accuracy of 0.89, 1.0 and 0.95, respectively), by applying a random forest classifier using immune gene signature scores obtained from single-sample GSEA (ssGSEA) [81]. Altogether, an increasing number of gene expression signatures related to response to immunotherapy are emerging from deep and machine learning analyses of RNA-seq data [102,103].

5.3. RNA-seq in clinical trials in onco-immunology

Recently, an increasing number of clinical trials have been integrating RNA-seq in their design with various objectives; either biological description of the effect of

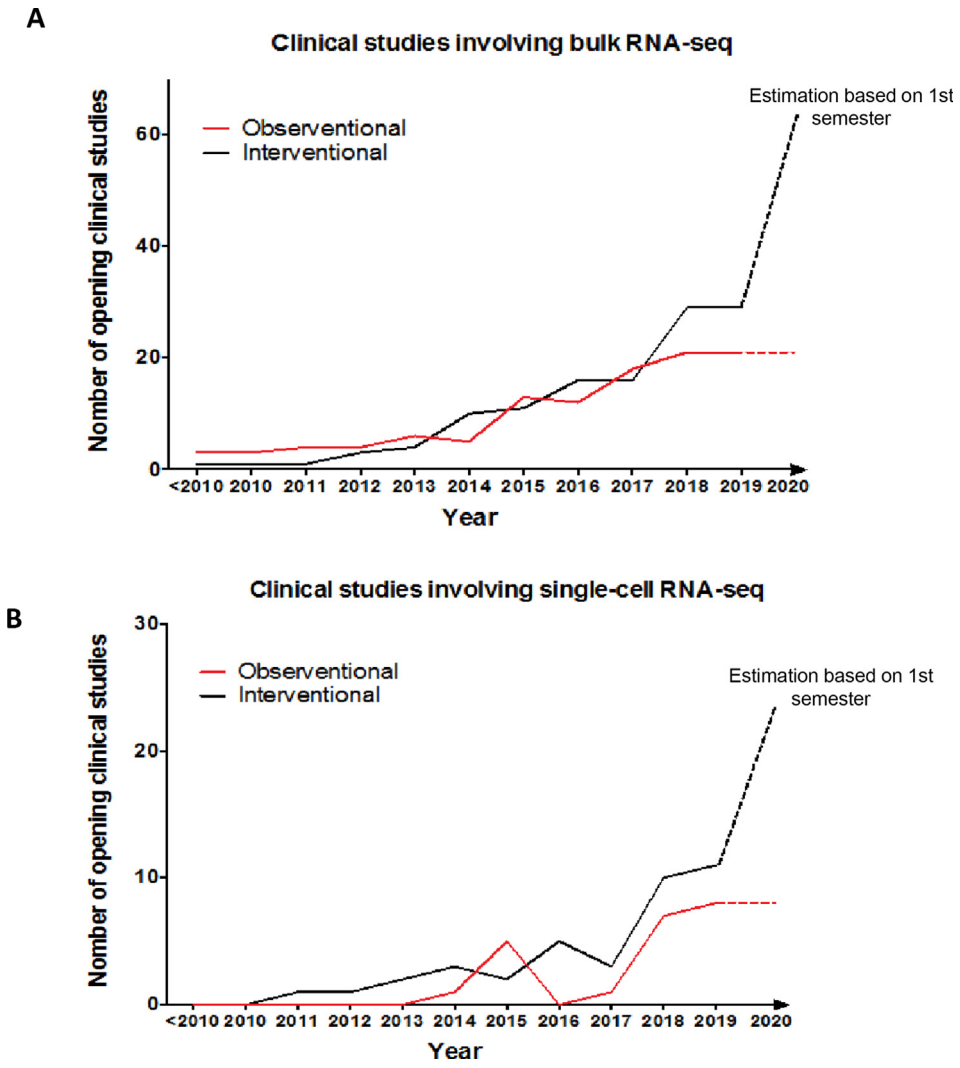

Fig. 4. **Evolution of the number of opening clinical studies that integrated conventional (A) or single-cell (B) RNA-seq analyses in their designs between 2010 and 2019, according to *clinicaltrials.gov***. Only studies related to cancer were considered. Non-interventional studies are shown in red, interventional studies are shown in black. Dotted lines correspond to estimations based on the number of clinical trials fulfilling the criteria that opened between January 1, 2020 and July 1, 2020. (For interpretation of the references to colour in this figure legend, the reader is referred to the Web version of this article.)

treatments or with the intent to treat patients (Fig. 4). This illustrates the growing interest of clinicians in whole transcriptome profiling. Examples of interventional studies using RNA-seq to guide treatment decisions concerned children with high-grade gliomas (NCT03739372), or adult patients with biliary tract cancers (NCT04318834) or soft-tissue sarcomas (NCT03784014, NCT03375437). Recent evaluations of the use of RNA-seq to orient patients with refractory cancers to targeted treatments demonstrated the feasibility of such an approach in routine; however, it failed to improve patients' outcomes so far [104,105]. Other studies used RNA-seq to evaluate the immune transcriptome profiles of tumours receiving immune-checkpoint blockers, some using immune gene expression signatures (for example in trials NCT03978624, NCT04326257 and NCT03673787).

Studies using scRNA-seq often investigate the changes in tumour immune cell population rates in response to treatments. For example, this has been done in patients receiving endocrine therapy and a CDK4/6 inhibitor for advanced or metastatic breast cancer (NCT04352777), and in patients receiving pembrolizumab with or without chemotherapy for non-small cell lung cancer (NCT04061590).

Yet, the feasibility of the translation of RNA-seq methods into the clinical routine raises many questions, such as the lack of gold-standard technical and computational methods. For example, if we consider five types of sequencing libraries, times three different mapping techniques, four imputations, seven

normalization processes and four differential expression testings, this leads to 1680 ways to differentially interpret one data set. This is largely underestimated if we take into account every parameter that could be manually set at each step. Therefore, standardised pipelines need to be developed to allow reproducibility between centers. Awareness is increasing regarding this aspect, and efforts are being made in this direction [106].

5.4. Cost

Another important component for evaluating the implementation of RNA-seq into the routine clinical care is cost. The budget for performing RNA-seq depends on many factors, including sequencing depth (average number or reads per transcript), type of library used (rRNA-depleted, poly(A)-enriched RNA, whole RNA sequencing, small RNA sequencing, etc.), type of sequencing (single-end or paired-end), sample size and quality (number of cells to sequence for single-cell), and, if appropriate, cell isolation method (droplet-based, micro-fluidics and so forth). Bulk RNA-seq usually requires at least 100–2000 ng of total good-quality RNA. This corresponds to 2–10 mg of fresh-frozen tissue or 2–4 FFPE slides; although a few companies propose ultra-low input sequencing from 10 pg of high-quality total RNA, at higher costs. Regarding all these parameters, in 2020, a "typical" experiment of bulk RNA-seq may cost between 150€ and 1500€ per sample; while scRNA-seq still scales between 1000€ and 9000€ per sample (Table 1). These costs do not include bioinformatics services.

Low-cost alternatives are exponentially emerging and intend to reduce the average expense for a whole transcriptome profiling to less than 30€ per sample, mostly by using specific libraries and extensively optimised sequencing techniques [35,107,108]. Additionally, targeted RNA-seq represents an attractive cheaper alternative in case specific transcripts of interest are known beforehand, for example, once a particular immune signature has been built from whole transcriptome analyses and is related to a specific treatment effect. For example, restricting the systematic sequencing to a panel of 500 relevant transcripts could reduce the cost to 10–15€ per sample.

6. Conclusion

After almost a decade of intensive clinical and translational research in the field on onco-immunology, major questions remain, and notably: can we, should we—and how to—anticipate resistance phenomenon upon immune blockade? Those questions are still pending, yet RNA-seq technologies are on a clear positive path regarding technical feasibility, affordability, the vast number of computational tools associated with an active user community engaged in offering free-access to user-friendly tools. RNA-seq is expected to become a cornerstone of personalised care in onco-immunology. The increasing availability and popularity of innovative techniques further scales up the challenges connected to the analysis of molecular data. Bringing scRNA-seq to the clinic may be challenging, although an increasing number of translational studies should contribute to define its position in cancer treatment personalization.

ScRNA-seq analysis provides expressions of the genes within each cell studied, although recent technological advances allow carrying out several measurements on the same cells. For example, for lymphocytes, the complete variable sequences of the TCR/Ig of each cell can be obtained (Single Cell Immune Profiling). Similarly, the presence of target proteins on the surface of cells can be assessed by CITE-seq [109]. Yet, the major innovation remains the association between gene expression and the location of cell groups in a tissue section, so called the "spatially-resolved transcriptomics" [110,111]. In addition, the single-cell technologies are not restricted to transcriptomics. Single-cell ATAC-seq is well established, and single-cell proteomics are actively under development. Great efforts are being made to integrate "multi-omics" from one cell.

Despite great improvement of the techniques, important issues regarding application of the computational and machine learning-based methods for the analysis of both bulk and scRNA-seq data are emerging. Mainly, it affects reproducibility and interpretability of their results and thus, limits their translationality to the clinic. The most technically advanced approaches, such as artificial neural network-based methods, even if they are very tempting to use, frequently produce results with limited generalization performance. Also, poor human interpretability keeps on being a limitation, even if no human can interpret clinically the data from a full cancer transcriptome, and while many methods are developed to decipher neural networks decisions. Also, gaining insights into these methods should improve the way we may use it in the clinic. In this context, clinical guidelines for the redaction of clinical trials protocols (SPIRIT-AI) [112] and final reports (CONSORT-AI) [113] of interventions involving artificial intelligence have very recently evolved to take account of these advances.

Finally, single-cell and bulk RNA-seq would both benefit from being developed as complementary techniques (Table 1). In the context of immune therapy, clinical translation of RNA-seq will require consolidating the robustness of predictive features associated with response/resistance to immune-checkpoint blockers. Ultimately, defining standardised analysis pipelines among thousands available will be essential

and should benefit to reproducibility and gradual generalization of the practice.

Author contributions

Maria Kuksin: Conceptualization, Formal analysis, Writing – original draft, Writing – review & editing; Daphné Morel: Conceptualization, Writing – original draft, Writing – review & editing; Marine Aglave: Data curation, Formal analysis, Writing – review & editing; François-Xavier Danlos: Writing – review & editing; Aurélien Marabelle: Supervision; Andrei Zinovyev: Writing – review & editing; Daniel Gautheret: Writing – review & editing; Loïc Verlingue: Conceptualization, Data curation, Formal analysis, Supervision, Writing – original draft, Writing – review & editing.

Funding

Publication of this review has been funded by ARC foundation for cancer research: Fondation ARC pour la recherche clinique - 9 rue Guy Môquet 94803 Villejuif - France. Grant number SIGNIT201901302.

Conflict of interest statement

M.K., D.M., M.A., F.X.D. and A.Z. have no conflict of interest to declare. L.V. reports personal fees from Adaptherapy, non-personal fees from Pierre-Fabre and Servier, grants from Bristol-Myers Squibb, all outside the submitted work. As part of the Drug Development Department (DITEP), A.M. and L.V. report being: Principal/sub-Investigator of Clinical Trials for Abbvie, Adaptimmune, Aduro Biotech, Agios Pharmaceuticals, Amgen, Argen-X Bvba, Arno Therapeutics, Astex Pharmaceuticals, AstraZeneca Ab, Aveo, Basilea Pharmaceutica International Ltd, Bayer Healthcare Ag, Bbb Technologies Bv, Beigene, Blueprint Medicines, Boehringer Ingelheim, Boston Pharmaceuticals, Bristol Myers Squibb, Ca, Celgene Corporation, Chugai Pharmaceutical Co, Clovis Oncology, Cullinan-Apollo, Daiichi Sankyo, Debiopharm, Eisai, Eisai Limited, Eli Lilly, Exelixis, Faron Pharmaceuticals Ltd, Forma Therapeutics, Gamamabs, Genentech, Glaxosmithkline, H3 Biomedicine, Hoffmann La Roche Ag, Imcheck Therapeutics, Innate Pharma, Institut De Recherche Pierre Fabre, Iris Servier, Janssen Cilag, Janssen Research Foundation, Kura Oncology, Kyowa Kirin Pharm. Dev, Lilly France, Loxo Oncology, Lytix Biopharma As, Medimmune, Menarini Ricerche, Merck Sharp & Dohme Chibret, Merrimack Pharmaceuticals, Merus, Millennium Pharmaceuticals, Molecular Partners Ag, Nanobiotix, Nektar Therapeutics, Novartis Pharma, Octimet Oncology Nv, Oncoethix, Oncopeptides, Orion Pharma, Ose Pharma, Pfizer, Pharma Mar, Pierre Fabre, Medicament, Roche, Sanofi Aventis, Seattle Genetics, Sotio A.S, Syros Pharmaceuticals, Taiho Pharma, Tesaro, Xencor. Research Grants from AstraZeneca, BMS, Boehringer Ingelheim, Janssen Cilag, Merck, Novartis, Onxeo, Pfizer, Roche, Sanofi. Non-financial support (drug supplied) from AstraZeneca, Bayer, BMS, Boehringer Ingelheim, Medimmune, Merck, NH TherAGuiX, Onxeo, Pfizer, Roche. A.Z. was supported by the Ministry of Science and Higher Education of the Russian Federation (Project No. 075-15-2020-808) and by European Union's Horizon 2020 program (grant No. 826121, iPC project).

Acknowledgment

The authors would like to thank colleagues involved in RNA-seq analysis and molecular analysis of tumour immunity for inspiring talks on this topic, including: Guillaume Meurice, Urszula Czerwinska, Nicolas Sompairac, Laurence Zitvogel, Christophe Massard, Antoine Hollebecque.

References

[1] Schreiber RD, Old LJ, Smyth MJ. Cancer immunoediting: integrating immunity's roles in cancer suppression and promotion. Science 2011;331:1565–70.
[2] Fridman WH, Zitvogel L, Sautès–Fridman C, Kroemer G. The immune contexture in cancer prognosis and treatment. Nat Rev Clin Oncol 2017;14:717–34.
[3] Bruni D, Angell HK, Galon J. The immune contexture and Immunoscore in cancer prognosis and therapeutic efficacy. Nat Rev Canc 2020;20:662–80.
[4] Barnes TA, Amir E. HYPE or HOPE: the prognostic value of infiltrating immune cells in cancer. Br J Canc 2017;117:451–60.
[5] Makkouk A, Weiner GJ. Cancer immunotherapy and breaking immune tolerance: new approaches to an old challenge. Cancer Res 2015;75:5–10.
[6] Teo ZL, Savas P, Loi S. Gene expression analysis: current methods. In: Lakhani SR, Fox SB, editors. Molecular pathology in cancer research. Springer; 2016. p. 107–36. https://doi.org/10.1007/978-1-4939-6643-1_6.
[7] Miller DFB, Yan P, Fang F, Buechlein A, Kroll K, Frankhouser D, et al. Complete transcriptome RNA-seq. In: Cancer gene networks. New York, NY: Humana Press; 2017. p. 141–62. https://doi.org/10.1007/978-1-4939-6539-7_10.
[8] Stark R, Grzelak M, Hadfield J. RNA sequencing: the teenage years. Nat Rev Genet 2019:1–26. https://doi.org/10.1038/s41576-019-0150-2.
[9] Heyer EE, Deveson IW, Wooi D, Selinger CI, Lyons RJ, Hayes VM, et al. Diagnosis of fusion genes using targeted RNA sequencing. Nat Commun 2019;10:1388.
[10] Mortazavi A, Williams BA, McCue K, Schaeffer L, Wold B. Mapping and quantifying mammalian transcriptomes by RNA-Seq. Nat Methods 2008;5:621–8.
[11] Tang F, Barbacioru C, Wang Y, Nordman E, Lee C, Xu N, et al. mRNA-Seq whole-transcriptome analysis of a single cell. Nat Methods 2009;6:377–82.
[12] Lähnemann D, Köster J, Szczurek E, McCarthy DJ, Hicks SC, Robinson MD, et al. Eleven grand challenges in single-cell data science. Genome Biol 2020;21:31.
[13] Eberwine J, Sul J-Y, Bartfai T, Kim J. The promise of single-cell sequencing. Nat Methods 2014;11:25–7.

[14] Fabre A-L, Colotte M, Luis A, Tuffet S, Bonnet J. An efficient method for long-term room temperature storage of RNA. Eur J Hum Genet 2014;22:379–85.
[15] Lähnemann D, Köster J, Szczurek E, McCarthy DJ, Hicks SC, Robinson MD, et al. mRNA-seq whole transcriptome profiling of fresh frozen versus archived fixed tissues. BMC Genom 2018; 19:419.
[16] Marczyk M, Fu C, Lau R, Du L, Trevarton AJ, Sinn BV, et al. The impact of RNA extraction method on accurate RNA sequencing from formalin-fixed paraffin-embedded tissues. BMC Canc 2019;19:1189.
[17] Turnbull AK, Selli C, Martinez-Perez C, Fernando A, Renshaw L, Keys J, et al. Unlocking the transcriptomic potential of formalin-fixed paraffin embedded clinical tissues: comparison of gene expression profiling approaches. BMC Bioinf 2020;21:30.
[18] Lafzi A, Moutinho C, Picelli S, Heyn H. Tutorial: guidelines for the experimental design of single-cell RNA sequencing studies. Nat Protoc 2018;13:2742–57.
[19] See P, Lum J, Chen J, Ginhoux F. A single-cell sequencing guide for immunologists. Front Immunol 2018;9:2425.
[20] Andrews TS, Hemberg M. Identifying cell populations with scRNASeq. Mol. Aspects Med 2018;59:114–22.
[21] Fung CW, Chan SN, Wu AR. Microfluidic single-cell analysis—toward integration and total on-chip analysis. Biomicrofluidics 2020;14:021502.
[22] Haghverdi L, Lun ATL, Morgan MD, Marioni JC. Batch effects in single-cell RNA-sequencing data are corrected by matching mutual nearest neighbors. Nat Biotechnol 2018;36: 421–7.
[23] Canonical correlation analysis. In: Härdle W, Simar L, editors. Applied multivariate statistical analysis. Springer; 2007. p. 321–30. https://doi.org/10.1007/978-3-540-72244-1_14.
[24] Zhang Y, Parmigiani G, Johnson WE. ComBat-seq: batch effect adjustment for RNA-seq count data. NAR Genomics Bioinforma 2020;2.
[25] Risso D, Ngai J, Speed TP, Dudoit S. Normalization of RNA-seq data using factor analysis of control genes or samples. Nat Biotechnol 2014;32:896–902.
[26] Leek JT. Svaseq: Removing batch effects and other unwanted noise from sequencing data. Nucleic Acids Res 2014;42.
[27] Büttner M, Miao Z, Wolf FA, Teichmann SA, Theis FJ. A test metric for assessing single-cell RNA-seq batch correction. Nat Methods 2019;16:43–9.
[28] Korsunsky I, Millard N, Fan J, Slowikowski K, Zhang F, Wei K, et al. Fast, sensitive and accurate integration of single-cell data with Harmony. Nat Methods 2019;16:1289–96.
[29] Barkas N, Petukhov V, Nikolaeva D, Lozinsky Y, Demharter S, Khodosevich K, et al. Joint analysis of heterogeneous single-cell RNA-seq dataset collections. Nat Methods 2019;16:695–8.
[30] Butler A, Hoffman P, Smibert P, Papalexi E, Satija R. Integrating single-cell transcriptomic data across different conditions, technologies, and species. Nat Biotechnol 2018;36:411–20.
[31] Kolodziejczyk AA, Kim JK, Svensson V, Marioni JC, Teichmann SA. The technology and biology of single-cell RNA sequencing. Mol Cell 2015;58:610–20.
[32] Ilicic T, Kim JK, Kolodziejczyk AA, Bagger FO, McCarthy DJ, Marioni JC, et al. Classification of low quality cells from single-cell RNA-seq data. Genome Biol 2016;17:29.
[33] Hwang B, Lee JH, Bang D. Single-cell RNA sequencing technologies and bioinformatics pipelines. Exp Mol Med 2018;50: 1–14.
[34] Hou W, Ji Z, Ji H, Hicks SC. A systematic evaluation of single-cell RNA-sequencing imputation methods. Genome Biol 2020; 21:218.
[35] Vieth B, Parekh S, Ziegenhain C, Enard W, Hellmann I. A systematic evaluation of single cell RNA-seq analysis pipelines. Nat Commun 2019;10:4667.
[36] Hafemeister C, Satija R. Normalization and variance stabilization of single-cell RNA-seq data using regularized negative binomial regression. Genome Biol 2019;20:296.
[37] Choi K, Chen Y, Skelly DA, Churchill GA. Bayesian model selection reveals biological origins of zero inflation in single-cell transcriptomics. Genome Biol 2020;21.
[38] McDavid A, Gottardo R, Simon N, Drton M. Graphical models for zero-inflated single cell gene expression. Ann Appl Stat 2019; 13:848–73.
[39] Hugo W, Zaretsky JM, Sun L, Song C, Moreno BH, Hu-Lieskovan S, et al. Genomic and transcriptomic features of response to anti-PD-1 therapy in metastatic melanoma. Cell 2016; 165:35–44.
[40] Hochberg Y. A sharper Bonferroni procedure for multiple tests of significance. Biometrika 1988;75:800–2.
[41] Hochberg Y, Benjamini Y. More powerful procedures for multiple significance testing. Stat Med 1990;9:811–8.
[42] Holm SA. Simple sequentially rejective multiple test procedure. Scand J Stat 1979;6:65–70.
[43] Love MI, Huber W, Anders S. Moderated estimation of fold change and dispersion for RNA-seq data with DESeq2. Genome Biol 2014;15:550.
[44] Robinson MD, McCarthy DJ, Smyth GK. edgeR: A Bioconductor package for differential expression analysis of digital gene expression data. Bioinformatics 2010;26:139–40.
[45] Sandberg R. Entering the era of single-cell transcriptomics in biology and medicine. Nat Methods 2014;11:22–4.
[46] Soneson C, Robinson MD. Bias, robustness and scalability in single-cell differential expression analysis. Nat Methods 2018;15: 255–61.
[47] Abdi H, Williams LJ. Principal component analysis. WIREs Comput Stat 2010;2:433–59.
[48] Saelens W, Cannoodt R, Todorov H, Saeys Y. A comparison of single-cell trajectory inference methods. Nat Biotechnol 2019;37: 547–54.
[49] Huh R, Yang Y, Jiang Y, Shen Y, Li Y. SAME-clustering: single-cell aggregated clustering via mixture model ensemble. Nucleic Acids Res 2020;48:86–95.
[50] Finotello F, Trajanoski Z. Quantifying tumor-infiltrating immune cells from transcriptomics data. Cancer Immunol Immunother 2018;67:1031–40.
[51] Avila Cobos F, Vandesompele J, Mestdagh P, De Preter K. Computational deconvolution of transcriptomics data from mixed cell populations. Bioinformatics 2018;34:1969–79.
[52] Hoffmann M, Pohlers D, Koczan D, Thiesen H-J, Wölfl S, Kinne RW. Robust computational reconstitution – a new method for the comparative analysis of gene expression in tissues and isolated cell fractions. BMC Bioinf 2006;7:369.
[53] Nirmal AJ, Regan T, Shih BB, Hume DA, Sims AH, Freeman TC. Immune cell gene signatures for profiling the microenvironment of solid tumors. Cancer Immunol Res 2018;6: 1388–400.
[54] Bard J, Rhee SY, Ashburner M. An ontology for cell types. Genome Biol 2005;6:R21.
[55] Godec J, Tan Y, Liberzon A, Tamayo P, Bhattacharya S, Butte AJ, et al. Compendium of immune signatures identifies conserved and species-specific biology in response to inflammation. Immunity 2016;44:194–206.
[56] Becht E, Giraldo NA, Lacroix L, Buttard B, Elarouci N, Petitprez F, et al. Estimating the population abundance of tissue-infiltrating immune and stromal cell populations using gene expression. Genome Biol 2016;17:218.
[57] Subramanian A, Tamayo P, Mootha VK, Mukherjee S, Ebert BL, Gillette MA, et al. Gene set enrichment analysis: a knowledge-based approach for interpreting genome-wide expression profiles. Proc Natl Acad Sci USA 2005;102: 15545–50.

[58] Kanehisa M, Goto S. KEGG: kyoto Encyclopedia of genes and genomes. Nucleic Acids Res 2000;28:27–30.
[59] Angelova M, Charoentong P, Hackl H, Fischer ML, Snajder R, Krogsdam AM, et al. Characterization of the immunophenotypes and antigenomes of colorectal cancers reveals distinct tumor escape mechanisms and novel targets for immunotherapy. Genome Biol 2015;16:64.
[60] Re3data.Org. The cancer Immunome atlas. 2016. https://doi.org/10.17616/R37D2V.
[61] Luo W, Friedman MS, Shedden K, Hankenson KD, Woolf PJ. GAGE: generally applicable gene set enrichment for pathway analysis. BMC Bioinf 2009;10:161.
[62] Alexa A, Rahnenfuhrer J. Gene set enrichment analysis with topGO. Bioconductor Improv 2009;vol. 26.
[63] Shen-Orr SS, Gaujoux R. Computational deconvolution: extracting cell type-specific information from heterogeneous samples. Curr Opin Immunol 2013;25:571–8.
[64] Wang X, Park J, Susztak K, Zhang NR, Li M. Bulk tissue cell type deconvolution with multi-subject single-cell expression reference. Nat Commun 2019;10.
[65] Newman AM, Steen CB, Liu CL, Gentles AJ, Chaudhuri AA, Scherer F, et al. Determining cell type abundance and expression from bulk tissues with digital cytometry. Nat Biotechnol 2019;37:773–82.
[66] Ribas A, Hamid O, Daud A, Hodi FS, Wolchok JD, Kefford R, et al. Association of pembrolizumab with tumor response and survival among patients with advanced melanoma. J Am Med Assoc 2016;315:1600.
[67] Reck M, Rodríguez-Abreu D, Robinson AG, Hui R, Csőszi T, Fülöp A, et al. Pembrolizumab versus chemotherapy for PD-L1–positive non–small-cell lung cancer. N Engl J Med 2016;375:1823–33.
[68] Ilie M, Hofman V, Dietel M, Soria J-C, Hofman P. Assessment of the PD-L1 status by immunohistochemistry: challenges and perspectives for therapeutic strategies in lung cancer patients. Virchows Arch Int J Pathol 2016;468:511–25.
[69] Ribas A, Tumeh PC. The future of cancer therapy: selecting patients likely to respond to PD1/L1 blockade. Clin Canc Res 2014;20:4982–4.
[70] Aguilar EJ, Ricciuti B, Gainor JF, Kehl KL, Kravets S, Dahlberg S, et al. Outcomes to first-line pembrolizumab in patients with non-small-cell lung cancer and very high PD-L1 expression. Ann Oncol 2019;30:1653–9.
[71] Rizvi NA, Hellmann MD, Snyder A, Kvistborg P, Makarov V, Havel JJ, et al. Cancer immunology. Mutational landscape determines sensitivity to PD-1 blockade in non-small cell lung cancer. Science 2015;348:124–8.
[72] Van Allen EM, Miao D, Schilling B, Shukla SA, Blank C, Zimmer L, et al. Genomic correlates of response to CTLA-4 blockade in metastatic melanoma. Science 2015;350:207–11.
[73] Snyder A, Makarov V, Merghoub T, Yuan J, Zaretsky JM, Desrichard A, et al. Genetic basis for clinical response to CTLA-4 blockade in melanoma. N Engl J Med 2014;371:2189–99.
[74] McGranahan N, Furness AJS, Rosenthal R, Ramskov S, Lyngaa R, Saini SK, et al. Clonal neoantigens elicit T cell immunoreactivity and sensitivity to immune checkpoint blockade. Science 2016;351:1463–9.
[75] Samstein RM, Lee C-H, Shoushtari AN, Hellmann MD, Shen R, Janjigian YY, et al. Tumor mutational load predicts survival after immunotherapy across multiple cancer types. Nat Genet 2019;51:202–6.
[76] Nebot-Bral L, Brandao D, Verlingue L, Rouleau E, Caron O, Despras E, et al. Hypermutated tumours in the era of immunotherapy: the paradigm of personalised medicine. Eur J Canc 2017;84:290–303.
[77] Lee V, Murphy A, Le DT, Diaz LA. Mismatch repair deficiency and response to immune checkpoint blockade. Oncol 2016;21:1200–11.
[78] Lemery S, Keegan P, Pazdur R. First FDA approval agnostic of cancer site — when a biomarker defines the indication. N Engl J Med 2017;377:1409–12.
[79] Galon J, Bruni D. Approaches to treat immune hot, altered and cold tumours with combination immunotherapies. Nat Rev Drug Discov 2019;18:197–218.
[80] Wang B, Liu M, Ran Z, Li X, Li J, Ou Y. Analysis of genetic signatures of tumor microenvironment yields insight into mechanisms of resistance to immunotherapy. bioRxiv 2020. https://doi.org/10.1101/2020.03.17.980789. 03.17.980789 (2020).
[81] Hwang S, Kwon A-Y, Jeong J-Y, Kim S, Kang H, Park J, et al. Immune gene signatures for predicting durable clinical benefit of anti-PD-1 immunotherapy in patients with non-small cell lung cancer. Sci Rep 2020;10:643.
[82] Lau D, Bobe AM, Khan AA. RNA sequencing of the tumor microenvironment in precision cancer immunotherapy. Trends Cancer 2019;5:149–56.
[83] Conroy JM, Pabla S, Nesline MK, Glenn ST, Papanicolau-Sengos A, Burgher B, et al. Next generation sequencing of PD-L1 for predicting response to immune checkpoint inhibitors. J Immunother Cancer 2019;7:18.
[84] Hirsch L, Zitvogel L, Eggermont A, Marabelle A. PD-Loma: a cancer entity with a shared sensitivity to the PD-1/PD-L1 pathway blockade. Br J Canc 2019;120:3–5.
[85] Larkin J, Chiarion-Sileni V, Gonzalez R, Grob JJ, Cowey CL, Lao CD, et al. Combined nivolumab and ipilimumab or monotherapy in untreated melanoma. N Engl J Med 2015;373:23–34.
[86] Robert C, Ribas A, Hamid O, Daud A, Wolchok JD, Joshua AM, et al. Three-year overall survival for patients with advanced melanoma treated with pembrolizumab in KEYNOTE-001. J Clin Oncol 2016;34.
[87] Iglesia MD, Parker JS, Hoadley KA, Serody JS, Perou CM, Vincent BG. Genomic analysis of immune cell infiltrates across 11 tumor types. J Natl Cancer Inst 2016;108.
[88] Fehrenbacher L, Spira A, Ballinger M, Kowanetz M, Vansteenkiste J, Mazieres J, et al. Atezolizumab versus docetaxel for patients with previously treated non-small-cell lung cancer (POPLAR): a multicentre, open-label, phase 2 randomised controlled trial. Lancet 2016;387:1837–46.
[89] Teixidó C, González-Cao M, Karachaliou N, Rosell R. Predictive factors for immunotherapy in melanoma. Ann Transl Med 2015;3.
[90] Herbst RS, Soria J-C, Kowanetz M, Fine GD, Hamid O, Gordon MS, et al. Predictive correlates of response to the anti-PD-L1 antibody MPDL3280A in cancer patients. Nature 2014;515:563–7.
[91] Sharma P, Allison JP. The future of immune checkpoint therapy. Science 2015;348:56–61.
[92] Ching T, Zhu X, Garmire L. Cox-nnet: an artificial neural network method for prognosis prediction of high-throughput omics data. PLoS Comput Biol 2018;14. e1006076–e1006076.
[93] Cheerla A, Gevaert O. Deep learning with multimodal representation for pancancer prognosis prediction. Bioinforma Oxf Engl 2019;35:i446–54.
[94] Cardoso F, van't Veer LJ, Bogaerts J, Slaets L, Viale G, Delaloge S, et al. 70-Gene signature as an aid to treatment decisions in early-stage breast cancer. N Engl J Med 2016;375:717–29.
[95] Huang Z, Johnson TS, Han Z, Helm B, Cao S, Zhang C, et al. Deep learning-based cancer survival prognosis from RNA-seq data: approaches and evaluations. BMC Med Genom 2020;13:41.
[96] Sestak I, Buus R, Cuzick J, Dubsky P, Kronenwett R, Denkert C, et al. Comparison of the performance of 6 prognostic signatures for estrogen receptor-positive breast cancer: a secondary analysis of a randomized clinical trial. JAMA Oncol 2018;4:545–53.

[97] Michiels S, Koscielny S, Hill C. Prediction of cancer outcome with microarrays: a multiple random validation strategy. Lancet Lond Engl 2005;365:488–92.
[98] Yuan Y, Van Allen EM, Omberg L, Wagle N, Amin-Mansour A, Sokolov A, et al. Assessing the clinical utility of cancer genomic and proteomic data across tumor types. Nat Biotechnol 2014;32:644–52.
[99] Ramazzotti D, Lal A, Wang B, Batzoglou S, Sidow A. Multi-omic tumor data reveal diversity of molecular mechanisms that correlate with survival. Nat Commun 2018;9:4453.
[100] Costello JC, Heiser LM, Georgii E, Gönen M, Menden MP, Wang NJ, et al. A community effort to assess and improve drug sensitivity prediction algorithms. Nat Biotechnol 2014;32:1202–12.
[101] Manica M, Oskooei A, Born J, Subramanian V, Sáez-Rodríguez J, Rodríguez Martínez M. Toward explainable anticancer compound sensitivity prediction via multimodal attention-based convolutional encoders. Mol Pharm 2019;16:4797–806.
[102] Mösch A, Raffegerst S, Weis M, Schendel DJ, Frishman D. Machine learning for cancer immunotherapies based on epitope recognition by T cell receptors. Front Genet 2019;10.1141–1141.
[103] Jamieson NB, Maker AV. Gene-expression profiling to predict responsiveness to immunotherapy. Canc Gene Ther 2016;24:134–40.
[104] Tuxen IV, Rohrberg KS, Oestrup O, Ahlborn LB, Schmidt AY, Spanggaard I, et al. Copenhagen prospective personalized oncology (CoPPO)—clinical utility of using molecular profiling to select patients to phase I trials. Clin Canc Res 2019;25:1239–47.
[105] Rodon J, Soria J-C, Berger R, Miller WH, Rubin E, Kugel A, et al. Genomic and transcriptomic profiling expands precision cancer medicine: the WINTHER trial. Nat Med 2019;25:751–8.
[106] Tanjo T, Kawai Y, Tokunaga K, Ogasawara O, Nagasaki M. Practical guide for managing large-scale human genome data in research. J Hum Genet 2020:1–14. https://doi.org/10.1038/s10038-020-00862-1.
[107] Alpern D, Gardeux V, Russeil J, Mangeat B, Meireles-Filho ACA, Breysse R, et al. BRB-seq: ultra-affordable high-throughput transcriptomics enabled by bulk RNA barcoding and sequencing. Genome Biol 2019;20:71.
[108] Mai Z, Xiao C, Jin J, Zhang G. Low-cost, low-bias and low-input RNA-seq with high experimental verifiability based on semiconductor sequencing. Sci Rep 2017;7:1053.
[109] Stoeckius M, Hafemeister C, Stephenson W, Houck-Loomis B, Chattopadhyay PK, Swerdlow H, et al. Simultaneous epitope and transcriptome measurement in single cells. Nat Methods 2017;14:865–8.
[110] Marx V. Method of the Year: spatially resolved transcriptomics. Nat Methods 2021;18:9–14.
[111] Larsson L, Frisén J, Lundeberg J. Spatially resolved transcriptomics adds a new dimension to genomics. Nat Methods 2021;18:15–8.
[112] Rivera SC. Guidelines for clinical trial protocols for interventions involving artificial intelligence: the SPIRIT-AI extension. Nat Med 2020;26:13.
[113] Liu X, Cruz Rivera S, Moher D, Calvert MJ, Denniston AK. Reporting guidelines for clinical trial reports for interventions involving artificial intelligence: the CONSORT-AI extension. Nat Med 2020;26:1364–74.
[114] Kharchenko PV, Silberstein L, Scadden DT. Bayesian approach to single-cell differential expression analysis. Nat Methods 2014;11:740–2.
[115] Sompairac N, Nazarov PV, Czerwinska U, Cantini L, Biton A, Molkenov A, et al. Independent component analysis for unraveling the complexity of cancer omics datasets. Int J Mol Sci 2019;20.
[116] Nazarov PV, Wienecke-Baldacchino AK, Zinovyev A, Czerwińska U, Muller A, Nashan D, et al. Deconvolution of transcriptomes and miRNomes by independent component analysis provides insights into biological processes and clinical outcomes of melanoma patients. BMC Med Genom 2019;12:132.
[117] Maaten L van der, Hinton G. Visualizing Data using t-SNE. J Mach Learn Res 2008;9:2579–605.
[118] Becht E, McInnes L, Healy J, Dutertre C-A, Kwok IWH, Ng LG, et al. Dimensionality reduction for visualizing single-cell data using UMAP. Nat Biotechnol 2018. https://doi.org/10.1038/nbt.4314.
[119] Qiu X, Mao Q, Tang Y, Wang L, Chawla R, Pliner HA, et al. Reversed graph embedding resolves complex single-cell trajectories. Nat Methods 2017;14:979–82.
[120] Chen H, Albergante L, Hsu JY, Lareau CA, Lo Bosco G, Guan J, et al. Single-cell trajectories reconstruction, exploration and mapping of omics data with STREAM. Nat Commun 2019;10:1903.
[121] Wolf FA, Hamey FK, Plass M, Solana J, Dahlin JS, Göttgens B, et al. PAGA: graph abstraction reconciles clustering with trajectory inference through a topology preserving map of single cells. Genome Biol 2019;20:59.
[122] Sun Y, Yao J, Nowak NJ, Goodison S. Cancer progression modeling using static sample data. Genome Biol 2014;15:440.
[123] Aibar S, González-Blas CB, Moerman T, Huynh-Thu VA, Imrichova H, Hulselmans G, et al. SCENIC: single-cell regulatory network inference and clustering. Nat Methods 2017;14:1083–6.
[124] Aubin-Frankowski P-C, Vert J-P. Gene regulation inference from single-cell RNA-seq data with linear differential equations and velocity inference. Bioinformatics 2020;36:4774–80.
[125] Specht AT, Li J. LEAP: Constructing gene co-expression networks for single-cell RNA-sequencing data using pseudotime ordering. Bioinforma. Oxf. Engl. 2017;33:764–6.
[126] Chan TE, Stumpf MPH, Babtie AC. Gene regulatory network inference from single-cell data using multivariate information measures. Cell Syst 2017;5:251–67. e3.
[127] Xu Rui, Wunsch DC. Clustering. 2008.
[128] Blondel VD, Guillaume J-L, Lambiotte R, Lefebvre E. Fast unfolding of communities in large networks. J Stat Mech Theor Exp 2008;2008:P10008.
[129] Traag VA, Waltman L, van Eck NJ. From Louvain to Leiden: guaranteeing well-connected communities. Sci Rep 2019;9:5233.
[130] Levine JH, Simonds EF, Bendall SC, Davis KL, Amir ED, Tadmor MD, et al. Data-driven phenotypic dissection of AML reveals progenitor-like cells that correlate with prognosis. Cell 2015;162:184–97.
[131] Stuart T, Butler A, Hoffman P, Hafemeister C, Papalexi E, Mauck WM, et al. Comprehensive integration of single-cell data. Cell 2019;177:1888–902. e21.
[132] Regev A, Teichmann S, Rozenblatt-Rosen O, Stubbington M, Ardlie K, Amit I, et al. The human cell atlas white paper. 2018.
[133] Newman AM, Liu CL, Green MR, Gentles AJ, Feng W, Xu Y, et al. Robust enumeration of cell subsets from tissue expression profiles. Nat Methods 2015;12:453–7.
[134] Li T, Fu J, Zeng Z, Cohen D, Li J, Chen Q, et al. TIMER2.0 for analysis of tumor-infiltrating immune cells. Nucleic Acids Res 2020;48:W509–14.
[135] Aran D, Hu Z, Butte AJ. xCell: digitally portraying the tissue cellular heterogeneity landscape. Genome Biol 2017;18:220.
[136] Yoshihara K, Shahmoradgoli M, Martínez E, Vegesna R, Kim H, Torres-Garcia W, et al. Inferring tumour purity and stromal and immune cell admixture from expression data. Nat Commun 2013;4:2612.
[137] Shen-Orr SS, Tibshirani R, Khatri P, Bodian DL, Staedtler F, Perry NM, et al. Cell type-specific gene expression differences in complex tissues. Nat Methods 2010;7:287–9.

[138] Baron M, Veres A, Wolock SL, Faust AL, Gaujoux R, Vetere A, et al. A single-cell transcriptomic map of the human and mouse pancreas reveals inter- and intra-cell population structure. Cell Syst 2016;3:346–60. e4.
[139] Racle J, de Jonge K, Baumgaertner P, Speiser DE, Gfeller D. Simultaneous enumeration of cancer and immune cell types from bulk tumor gene expression data. eLife 2017; 6:e26476.
[140] Monaco G, Lee B, Xu W, Mustafah S, Hwang YY, Carré C, et al. RNA-seq signatures normalized by mRNA abundance allow absolute deconvolution of human immune cell types. Cell Rep 2019;26:1627–40. e7.
[141] Sturm G, Finotello F, Petitprez F, Zhang JD, Baumbach J, Fridman WH, et al. Comprehensive evaluation of transcriptome-based cell-type quantification methods for immuno-oncology. Bioinformatics 2019;35:i436–45.
[142] Petitprez F, Levy S, Sun C-M, Meylan M, Linhard C, Becht E, et al. The murine Microenvironment Cell Population counter method to estimate abundance of tissue-infiltrating immune and stromal cell populations in murine samples using gene expression. Genome Med 2020;12:86.
[143] Chen Z, Huang A, Sun J, Jiang T, Qin FX-F, Wu A. Inference of immune cell composition on the expression profiles of mouse tissue. Sci Rep 2017;7:40508.
[144] Repsilber D, Kern S, Telaar A, Walzl G, Black G, Selbig J, et al. Biomarker discovery in heterogeneous tissue samples. 2020.
[145] Lähdesmäki H, Dunmire V, Yli-Harja O, Zhang W. In silico microdissection of microarray data from heterogeneous cell populations. BMC Bioinf 2005;6. 54–54.
[146] Gaujoux R, Seoighe C. Semi-supervised Nonnegative Matrix Factorization for gene expression deconvolution: a case study. Infect Genet Evol 2012;12:913–21.
[147] Xie R, Wen J, Quitadamo A, Cheng J, Shi X. A deep auto-encoder model for gene expression prediction. BMC Genom 2017;18:845.
[148] Dincer AB, Janizek JD, Lee S-I. Adversarial deconfounding autoencoder for learning robust gene expression embeddings. bioRxiv 2020. https://doi.org/10.1101/2020.04.28.065052. 04.28.065052 (2020).

université PARIS-SACLAY | ÉCOLE DOCTORALE Cancérologie : biologie - médecine - santé (CBMS)

Titre : Identification de biomarqueurs associés à la combinaison d'immunothérapie et d'anti-angiogéniques dans le traitement des mésothéliomes. Analyses translationnelles de l'essai clinique PEMBIB combinant l'anticorps monoclonal anti-PD1 pembrolizumab et l'inhibiteur de tyrosine kinase anti-angiogénique nintedanib

Mots clés : Immunothérapie, anti-angiogénique, cancer, recherche translationnelle

En oncologie, l'efficacité des immunothérapies par anticorps monoclonaux anti Programmed Death 1 (PD1) reste insuffisante pour de nombreux patients. L'association de ces traitements avec une molécule anti-angiogénique pourrait permettre d'en améliorer leur efficacité, par des effets directs anti-tumoraux et en contribuant au développement d'une réponse immunitaire anti-tumorale.

En oncologie, l'efficacité des immunothérapies par anticorps monoclonaux anti Programmed Death 1 (PD1) reste insuffisante pour de nombreux patients. L'association de ces traitements avec une molécule anti-angiogénique pourrait permettre d'en améliorer leur efficacité, par des effets directs anti-tumoraux et en contribuant au développement d'une réponse immunitaire anti-tumorale.

Title: Identification of biomarkers associated with the combination of immunotherapy and anti-angiogenic drugs in the treatment of mesothelioma. Translational analyses of the PEMBIB clinical trial combining the anti-PD1 monoclonal antibody pembrolizumab and the anti-angiogenic tyrosine kinase inhibitor nintedanib.

Keywords : Immune checkpoint blockade, anti-angiogenic drug, cancer, translational research.

In oncology, the efficacy of monoclonal anti-programmed death 1 (PD1) antibody immunotherapies remains insufficient for many patients. The association of these treatments with an anti-angiogenic molecule could improve their efficacy, by direct anti-tumor effects and by contributing to the development of an anti-tumor immune response.

In oncology, the efficacy of monoclonal anti-programmed death 1 (PD1) antibody immunotherapies remains insufficient for many patients. The association of these treatments with an anti-angiogenic molecule could improve their efficacy, by direct anti-tumor effects and by contributing to the development of an anti-tumor immune response.

Maison du doctorat de l'Université Paris-Saclay
2ème étage aile ouest, Ecole normale supérieure Paris-Saclay
4 avenue des Sciences,
91190 Gif sur Yvette, France